

Sheffield Hallam University

A study of fretting fatigue incorporating sharp corner contact geometry.

GREEN, Richard.

Available from the Sheffield Hallam University Research Archive (SHURA) at:

<http://shura.shu.ac.uk/19720/>

A Sheffield Hallam University thesis

This thesis is protected by copyright which belongs to the author.

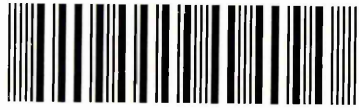
The content must not be changed in any way or sold commercially in any format or medium without the formal permission of the author.

When referring to this work, full bibliographic details including the author, title, awarding institution and date of the thesis must be given.

Please visit <http://shura.shu.ac.uk/19720/> and <http://shura.shu.ac.uk/information.html> for further details about copyright and re-use permissions.

LEARNING CENTRE
CITY CAMPUS, HOWARD STREET
SHEFFIELD S1 1WB

101 715 656 5



REFERENCE

ProQuest Number: 10697022

All rights reserved

INFORMATION TO ALL USERS

The quality of this reproduction is dependent upon the quality of the copy submitted.

In the unlikely event that the author did not send a complete manuscript and there are missing pages, these will be noted. Also, if material had to be removed, a note will indicate the deletion.



ProQuest 10697022

Published by ProQuest LLC (2017). Copyright of the Dissertation is held by the Author.

All rights reserved.

This work is protected against unauthorized copying under Title 17, United States Code
Microform Edition © ProQuest LLC.

ProQuest LLC.
789 East Eisenhower Parkway
P.O. Box 1346
Ann Arbor, MI 48106 – 1346

**A STUDY OF FRETTING FATIGUE
INCORPORATING SHARP CORNER
CONTACT GEOMETRY**

Richard Green

A thesis submitted in partial fulfilment of the requirements of

Sheffield Hallam University

for the degree of

Doctor of Philosophy

January 2003

Collaborating Organisation: EPSRC

PREFACE

This Thesis describes the work carried out in the School of Engineering at Sheffield Hallam University between September 1998 and December 2001.

The submission of this Thesis is in accordance with the requirements for the award of PhD, under the auspices of the University.

ACKNOWLEDGEMENT

I would like to acknowledge and thank my supervisor, Dr. U S Fernando for his guidance help and friendship, without which I could not have completed the research.

I would also like to acknowledge and thank my secondary supervisors, Dr M Islam and Prof. J D Atkinson for their help and guidance.

I would like to thank Mr. D Eaton and Sheffield Hallam University for the use of their facilities and providing an environment within which I could conduct my research.

I would like to thank the workshop technicians Brian and Roger for their help in constructing my experimental test rig and John Stanley for his constant technical assistance and support.

I would like to thank the EPSRC for the funding, which paid for my research.

I would also like to thank my family and friends for their support and understanding particularly Gemma, whose help, motivation and kindness proved inspirational.

ABSTRACT

Fretting fatigue occurs when components are in contact and subjected to cyclic loads or vibrations. The following research programme investigates the fretting fatigue phenomenon using a specific flat contact geometry encompassing sharp corners. The pressure distribution at the contact interface is fundamentally important in the understanding of fretting fatigue problems. In the case of sharp corner contacts, the analysis of the pressure distribution results in an infinite gradient occurring at the edges of the contact. The infinite gradients generate deformation singularities and closed form solutions are not available for this contact geometry. The specific contact pressure generates friction forces, which affect the nucleation and growth of dominant fretting cracks by influencing the stress distributions in the region of the contact.

The current research programme presents a method of analysing flat contacts containing sharp corners. The method includes the development of a finite element solution capable of accurately predicting the friction force behaviour observed in fretting fatigue. The subsequent numerically determined stress distributions in the contact region are then used to generate a multiaxial stress concentration factor, which provide the basis for a fretting fatigue life prediction method. Furthermore, the research programme investigates the phenomenological effects observed during fretting fatigue. The study investigates friction behaviour and its effects on the initiation of fretting cracks and fretting fatigue lives.

LIST OF FIGURES

CHAPTER 2

- Figure 2.1a Gas Turbine Compressor Rotor
- Figure 2.1b Fir tree and dove tail blade root configurations that fit into compressor disc
- Figure 2.2 Cross Section of a Riveted Lap Joint
- Figure 2.3 Schematic of contact surfaces showing microscopic detail of stick and slip behaviour
- Figure 2.4 Types of incomplete and complete contact geometries
- Figure 2.5 Pressure distribution profiles for (a) incomplete geometry and (b) complete geometry

CHAPTER 3

- Figure 3.1 Testing facility with details of specimen and contact
- Figure 3.2 Fretting Fatigue Test Rig Design
- Figure 3.3 Position of specimen and clamping arrangement
- Figure 3.4 Contact load arrangement
- Figure 3.5 Design of the lower actuator beam to attain controlled slip displacement
- Figure 3.6 Contact assembly illustrating the position of the Wheatstone bridge strain gauge arrangement for measuring friction
- Figure 3.7 Friction Calibration Chart
- Figure 3.8 Specimen
- Figure 3.9 Contact pads
- Figure 3.10 Material Test Data Aluminium Alloy 2024-T315
- Figure 3.11 The effects of controlled contact pad displacement of friction
- Figure 3.12 Slip Displacement Calibration Chart



CHAPTER 4

Figure 4.1 A finite element representation of a contact surface, requiring a master and slave surface

Figure 4.2 Finite element load arrangement to simulate contact and axial load

Figure 4.3 Detail of mesh deformation in contact corner region

Figure 4.4 The results of the peak friction force and contact pressure values with element size

Figure 4.5 Illustrates the boundaries used to create the first sub model, this then provides the second boundary to create the next sub model.

Figure 4.6 Location of boundary for sub model illustrating the required reduction ratio of 2:1

Figure 4.7 Contact node pair definition at the corners of the contact pad exhibiting anomalous tangential plane

Figure 4.8 1.27mm pad size finite global element model

Figure 4.9 3mm model geometry and mesh diagram for global model

CHAPTER 5

Figure 5.1 Typical frictional hysteresis response during fretting fatigue lives

Figure 5.2a Variations in the friction amplitudes during the fatigue life for the 500 test series

Figure 5.2b Variations in the friction amplitudes during the fatigue life for the 600 test series

Figure 5.2c Variations in the friction amplitudes during the fatigue life for the 700 test series

- Figure 5.3a Friction response for the 3mm contact pad size experiments with 80MPa contact pressure
- Figure 5.3b Friction response for the 3mm contact pad size experiments with 100MPa contact pressure
- Figure 5.3c Friction response for the 3mm contact pad size experiments with 120MPa contact pressure
- Figure 5.4 Fretting fatigue lives for the 800 series experiments
- Figure 5.5a Friction force response during the fatigue life for experiments with a slip displacement of 70 μm applied in phase with the axial load ($\phi = 0^\circ$)
- Figure 5.5b Friction force response during the fatigue life for experiments with a slip displacement of 10 μm applied in phase with the axial load ($\phi = 0^\circ$)
- Figure 5.5c Friction force response during the fatigue life for experiments with a slip displacement of 20 μm applied out of phase with the axial load ($\phi = 90^\circ$)
- Figure 5.6 Fretting fatigue lives for the controlled slip experiments, 900 series.

CHAPTER 6

- Figure 6.1 A schematic representation of the effects of hysteresis on friction force
- Figure 6.2 Example of the transition from macro to micro slip contact interaction due to the effects of fretting and wear. (Friction results taken from experiment 503 Appendix C)
- Figure 6.3 Typical fretting fatigue scars showing two distinct regions of surface damage, which verifies the presence of debris acting as a third body solid lubricant
- Figure 6.4 Average friction force amplitudes for both the initial (a) and maximum (b) friction conditions

- Figure 6.5 Comparison of both the initial and maximum friction force amplitudes, measured during the experimental crack initiation study.
- Figure 6.6 Comparison of the equivalent friction coefficients for both the initial and fretting conditions
- Figure 6.7 An example (Test 803) of the peak friction response during a fretting fatigue experiment
- Figure 6.8 The average friction force amplitudes for both the initial (a) and maximum (b) friction condition
- Figure 6.9 Comparison of both the initial friction forces with the maximum fretting friction forces measured during the size effect study.
- Figure 6.10 Comparison of the equivalent friction coefficient for the initial and maximum fretting condition.
- Figure 6.11 Comparison of the equivalent friction coefficient for the initial and maximum fretting condition.
- Figure 6.12 Fretting fatigue lives from the 1.27mm pad size experimental study conducted by Fernando *et al* [75]
- Figure 6.13 Comparison of the peak friction forces measured during the fretting period for both the 1.27mm and 3mm pad size experiments
- Figure 6.14 Comparison of the numerically predicted friction hysteresis loop with the experimentally recorded friction hysteresis loop for the 1.27mm contact pad size (test 133) demonstrating the numerical capability to predict macro slip
- Figure 6.15 Comparison of the numerically predicted friction hysteresis loop with the experimentally recorded friction hysteresis loop for the 1.27mm contact pad size (test 128) demonstrating the numerical capability to predict micro slip

- Figure 6.16 Demonstrates non-symmetrical behaviour in the friction loop response, where the friction force does not return to zero when the axial load completes the cycle
- Figure 6.17 Numerically predicted friction force amplitudes for the 1.27mm pad size experiments performed by Fernando *et al* [75]
- Figure 6.18 Comparison of the experimental cyclic friction response with the numerically prediction (test 803)
- Figure 6.19 Numerically predicted friction force amplitudes for the 3mm contact pad size
- Figure 6.20 Comparison of the numerically predicted friction force amplitudes for both the 3mm and 1.27mm contact pad size results with the experimentally recorded friction
- Figure 6.21 Illustrates the location of the leading edge and trailing edge of the contact pads where dominant fretting cracks initiated
- Figure 6.22 Comparison of the fretting scars for tests 501 and 504. Test 504 demonstrates the type of surface damage caused for the 80MPa contact pressure results. Test 501 demonstrates that the contact was not distributed across the entire contact surface.
- Figure 6.23 A typical fretting scar for the 80MPa axial stress and 80MPa contact pressure. The scar shows the two distinct regions of damage, a smooth inner region and a more heavily damaged outer region
- Figure 6.24a Test 504 (20% of fatigue life) showing a dominant fretting crack has initiated at the edge of the fretting scar in both the secondary electron and electron back scatter modes of imaging.

- Figure 6.24b Test 505 (40% of fatigue life) showing detail of the dominant fretting crack in both the secondary electron and electron backscatter modes of imaging.
- Figure 6.25 Test 507 (20% of fatigue life) shows major damage is not confined to the outer region of the fretting scar
- Figure 6.26 Test 509 (60% of fatigue life) both the secondary electron and backscatter modes of imaging show no evidence of a dominate fretting fatigue crack
- Figure 6.27 Test 601 (20%of fatigue life) typical fretting scar for the 80MPa axial stress and 100MPa contact pressure experiments. Image shows distinct boundary between the relatively smooth inner region and heavily damaged outer region of the fretting scar
- Figure 6.28 Test 601(20% of the fatigue life) images showing the presence of a dominant fretting crack in both secondary electron and electron backscatter modes of imaging
- Figure 6.29 Test 603 (60% of the fatigue life) evidence of dominant fretting cracks, which have propagated from a surface crack along the edge of the fretting scar
- Figure 6.30 Test 604 (20% of fatigue life) shows the fretting scar exhibits the two distinct regions of scaring.
- Figure 6.31 Test 601 (20% of fatigue life) shows the type of dominant fretting fatigue crack observed in all test run with 100MPa axial stress and contact pressure
- Figure 6.32 Test 607 (20% of fatigue life) shows the type of surface damage observed for experiments run at 120MPa axial stress with 100MPa contact pressure

- Figure 6.33 Images of the fretting scars for the tests run with 120MPa contact pressure
- Figure 6.34a Test 701 (20%of the fatigue life) shows the presence of a dominant crack at the edge of the fretting scar
- Figure 6.34b Test 704 (20%of the fatigue life) shows two dominant cracks at the edge of the fretting scar
- Figure 6.34c Test 707 (20%of the fatigue life) shows a dominant crack at the edge of the fretting scar
- Figure 6.35a Comparison of friction force and fatigue life for the 3mm contact pad size experiments run with 80MPa contact pressure and three axial stress values
- Figure 6.35b Comparison of friction force and fatigue life for the 3mm contact pad size experiments run with 100MPa contact pressure and three axial stress values
- Figure 6.35c Comparison of friction force and fatigue life for the 3mm contact pad size experiments run with 120MPa contact pressure and three axial stress values
- Figure 6.36 Comparison of the fretting fatigue lives for the 1.27mm [75] and 3mm contact pad size experiments
- Figure 6.37 Comparison of fretting fatigue lives with friction force for experiments run with a 70 μ m slip displacement in phase ($\theta = 0$) with the axial load generating almost no friction
- Figure 6.38 Comparison of fretting fatigue lives with friction force for experiments run with a 10 μ m slip displacement in phase ($\theta = 0$) with the axial load
- Figure 6.39 Comparison of fretting fatigue lives with friction force for experiments run at 10 μ m and 70 μ m slip displacements in phase ($\theta = 0$) with the axial load

- Figure 6.40 Comparison of fretting fatigue lives with friction force for experiments run at $20\mu\text{m}$ slip displacement out of phase ($\theta = 90^0$) with the axial load
- Figure 6.41 The multiaxial stress system in the fretting fatigue specimen
- Figure 6.42 Example from Appendix F (Test 124) demonstrating the shear and axial stress distributions at the contact surface
- Figure 6.43 Demonstrates the effects of increasing contact pressure on the axial (a) and shear (b) stress distributions at the 1.27mm contact surface
- Figure 6.44 Demonstrates the effects of increasing axial load on the axial (a) and shear (b) stress distributions at the 3mm contact surface
- Figure 6.45 Schematic of sub surface planes where stress was measured
- Figure 6.46 Shows how stresses vary as the depth increases through the fretting region at the edge of the contact area (Test 124)
- Figure 6.47 The depths at which the magnitude of the axial stress becomes larger than the shear stress for the 3mm contact pad size results. The results are taken at the critical location.
- Figure 6.48 The multiaxial and uniaxial stress system in the fretting specimen
- Figure 6.49 Method of determining values for both the shear and axial stress concentrations for each analysis
- Figure 6.50a Comparison of numerically predicted fatigue lives with experimentally recorded fatigue lives for 3mm pad size results with 80 MPa contact pressure
- Figure 6.50b Comparison of numerically predicted fatigue lives with experimentally recorded fatigue lives for 3mm pad size results with 100 MPa contact pressure

Figure 6.50c Comparison of numerically predicted fatigue lives with experimentally recorded fatigue lives for 3mm pad size results with 120 MPa contact pressure

Figure 6.51 Comparison of numerically predicted life to experimentally acquired fatigue life for 3mm pad size

Figure 6.52 Comparison of numerically predicted life to experimentally recorded life for 1.27mm pad size experiments with 100MPa contact load

LIST OF TABLES

CHAPTER 3

Table 3.1	Material Composition for 2024-T351 Aluminium alloy
Table 3.2	Material Properties for 2024-T351 Aluminium alloy
Table 3.3	Details of Experimental Program for 500 Test Series
Table 3.4	Details of Experimental Program for 600 Test Series
Table 3.5	Details of Experimental Program for 700 Test Series
Table 3.6	Details of Experimental Program for 800 Test Series
Table 3.7	Details of Experimental Program for 900 Test Series

CHAPTER 4

Table 4.1	Load and material data for 1.27mm pad size models
Table 4.2	Model data for 1.27mm pad size models
Table 4.3	Load and material data for 3mm pad size models
Table 4.4	Model data for 3mm pad size models

CHAPTER 5

Table 5.1	Results of the friction response for 500-700 series experiments
Table 5.2	Fretting fatigue information for the 500-700 series experiments
Table 5.3	Table of friction data for the 800 series experiments
Table 5.4	Friction coefficients determined for the friction force results of the 800 series experiments
Table 5.5	Fretting fatigue information for the 800 series experiments
Table 5.6	Table of friction data for the 900 series experiments
Table 5.7	The effects of fretting on the friction coefficient for the 900 series experiments

- Table 5.8 Fretting fatigue information for the 900 series experiments
- Table 5.9 Friction force amplitudes for 1.27mm pad size
- Table 5.10 Friction force amplitudes for 3mm pad size
- Table 5.11 Location and magnitude of peak stresses for the 1.27mm pad size models
- Table 5.12 Location and magnitude of peak stresses for the 3mm pad size models

CHAPTER 6

- Table 6.1 80MPa Contact Pressure
- Table 6.2 100MPa Contact Pressure
- Table 6.3 120MPa Contact Pressure

CONTENTS

1	INTRODUCTION	1
2	LITERATURE REVIEW	5
2.1	INTRODUCTION TO FRETTING FATIGUE	5
2.2	MECHANICS OF FRETTING FATIGUE AND ACCEPTED IDEOLOGIES	7
2.2.1	Friction	
2.3	INVESTIGATIVE METHODS AND AREAS OF CURRENT RESEARCH	18
2.3.1	Experimental Methods	
2.3.2	Numerical Methods	
2.3.3	Analytical Solutions	
3	EXPERIMENTAL INVESTIGATION INTO FRETTING FATIGUE	28
3.1	INTRODUCTION	28
3.2	EXPERIMENTAL TEST RIG DESIGN	29
3.2.1	Test Arrangement and Design	
3.2.2	Specimen Loading Arrangement	
3.2.3	Contact Loading Arrangement	
3.2.4	Slip Control Arrangement	
3.2.5	The Measurement of Friction Force	
3.3	THE SPECIMEN AND CONTACT PAD	37
3.3.1	Material Data	
3.4	METHODOLOGY AND TESTING PROCEDURES	40
3.4.1	Experimental Procedure	

3.4.2	Study of the Initiation of Fretting Fatigue Cracks	
3.4.2.1	Experimental Programme No. 1 - 500, 600 & 700 Test Series	
3.4.3	The Effects of Contact Zone Size	
3.4.3.1	Experimental Programme No.2 - 800 Test Series	
3.4.4	Controlling Slip and Friction	
3.4.4.1	Experimental Programme No. 3 - 900 Tests Series	
4	NUMERICAL ANALYSIS	52
4.1	INTRODUCTION	52
4.2	APPLICATION OF FINITE ELEMENT METHOD TO FRETTING FATIGUE	54
4.3	DEVELOPMENT OF FINITE ELEMENT MODEL	59
4.3.1	Mesh Design and Element Type	
4.3.2	Elastic Material Properties	
4.3.3	Load Cases	
4.4	FINITE ELEMENT MODEL REFINEMENTS	62
4.4.1	Element Sizing	
4.4.2	Sub Modelling to Increase Accuracy	
4.4.3	Sharp Corner Contact Modelling	
4.5	MODELLING OF THE 1.27MM PAD SIZE EXPERIMENTAL ARRANGEMENT	68
4.5.1	Symmetry and Boundary Conditions for the 1.27mm Pad Size	
4.6	MODELLING OF THE 3MM PAD SIZE EXPERIMENTAL ARRANGEMENT	72
4.6.1	Symmetry and Boundary Conditions for the 3mm Pad Size	

5	RESULTS	76
5.1	INTRODUCTION	76
5.2	EXPERIMENTAL RESULTS	77
5.2.1	The Results of the Fretting Fatigue Crack Initiation Study	
5.2.1.1	Frictional Hysteresis Results (500-700 Experimental Series)	
5.2.1.2	The Response of the Friction Force Amplitude during Tests	
5.2.1.3	Evidence of Fretting Fatigue Crack Initiation	
5.2.2	The Results of the Contact Pad Size Study	
5.2.2.1	Frictional Hysteresis Results (800 Test Series)	
5.2.2.2	The Response of the Friction Force Amplitude during Tests	
5.2.2.3	Fretting Fatigue Lives (800 Test Series)	
5.2.3	The Results of Controlling Slip Displacements	
5.2.3.1	Frictional Hysteresis Results (900 Test Series)	
5.2.3.2	The Response of the Friction Force Amplitude during Tests	
5.2.3.3	Fretting Fatigue Lives (900 Test Series)	
5.3	NUMERICAL RESULTS	94
5.3.1	Numerical Frictional Results	
5.3.1.1	Localised Friction Response during the Load Cycle	
5.3.2	Numerical Elastic Surface Stress Distributions	
5.3.3	Numerical Elastic Subsurface Stress Distributions	
6	DISCUSSION	100
6.1	INTRODUCTION	100
6.2	FRICION BEHAVIOUR IN FRETTING FATIGUE	101

6.2.1	Frictional Hysteresis	
6.2.2	The Response of The Peak Friction Force during the Fatigue Life	
6.2.3	The Behaviour of Friction during the Experimental Program	
6.2.3.1	Friction Force during the Initial Crack Growth Phase	
6.2.3.2	The Effects of Contact Size on Friction Force	
6.2.4	The Effects of Controlled Slip on Friction Force	
6.2.5	Validation of the 1.27mm Pad Size Experimental Friction Results	
6.2.6	Comparison of Friction Force for Different Contact Pad Sizes	
6.2.7	Numerically Predicted Friction Behaviour	
6.2.7.1	Numerically Predicted Friction Force	
6.2.7.2	The Numerically Predicted Friction for the 1.27mm Contact Pad Size	
6.2.7.3	The Numerically Predicted Friction for the 3mm Contact Pad Size	
6.2.8	Validation of the Numerically Predicted Friction Results	
6.3	THE EFFECTS OF FLAT CONTACT ON INITIAL CRACK GROWTH	136
6.3.1	The Study of Initial Crack Growth	
6.3.1.1	Initial Crack Growth for 80MPa Contact Pressure (500 test series)	
6.3.1.2	Initial Crack Growth for 100MPa Contact Pressure (600 test series)	
6.3.1.3	Initial Crack Growth for 120MPa Contact Pressure (700 test series)	
6.3.1.4	Summary of Initial Crack Growth Study	
6.4	THE STUDY OF FRETTING FATIGUE LIVES	152
6.4.1	Fretting Fatigue lives for the 3mm Contact Pad Experiments (800 Series)	
6.4.1.1	Comparison of Fretting Fatigue Lives for the of 1.27mm and 3mm Contact Pad Experiments	
6.4.2	The Effects of Controlled Slip on Fretting Fatigue Lives	
6.5	ANALYSIS OF THE NUMERICALLY PREDICTED STRESSES FOR FLAT CONTACTS	162

6.5.1	The Distribution of Stresses at the Contact Surface	
6.5.2	The Distribution of Sub Surface Stresses	
6.6	THE USE OF NUMERICAL STRESSES FOR FATIGUE LIFE PREDICTION	173
6.6.1	Notch Root Hypothesis	
6.6.2	Neuber's Analysis	
6.6.3	Equivalent Stress Concentration Factor (K_{equ})	
6.6.4	Results of Fretting Fatigue Life Predictions	
7	CONCLUSIONS	186

7.1 FURTHER WORK

REFERENCES

BIBLIOGRAPHY

APPENDICES

A ENGINEERING DRAWINGS OF TEST RIG AND SAMPLE

B SAMPLE ABAQUS INPUT FILES

1.27mm Pad Size Input Files for 124 Test

3mm Pad Size Input Files for 801 Test

C EXPERIMENTAL FRICTION HYSTERESIS LOOPS

500 Test Series Friction Hysteresis Loops

600 Test Series Friction Hysteresis Loops

700 Test Series Friction Hysteresis Loops

800 Test Series Friction Hysteresis Loops

900 Test Series Friction Hysteresis Loops

D NUMERICAL FRICTION HYSTERESIS LOOPS

1.27mm Pad Size Numerical Friction Hysteresis Loops [75]

3mm Pad Size Numerical Friction Hysteresis Loops (800 Test Series)

E LOCALISED FRICTIONAL SHEAR STRESS MAPS

1.27mm Numerical Friction Maps [75]

3mm Numerical Friction Maps (800 Test Series)

F AXIAL AND SHEAR STRESS DISTRIBUTIONS AT THE CONTACT SURFACE

1.27mm Contact Pad Size Results [75]

3mm Contact Pad Size Results (800 Test Series)

G AXIAL AND SHEAR SUB SURFACE STRESS DISTRIBUTIONS THROUGH THE
FRETTING REGION

1.27mm Contact Pad Size Results [75]

3mm Contact Pad Size Results (800 Test Series)

H AXIAL AND SHEAR STRESS VARIATIONS THROUGH THE DEPTH OF THE FRETTING
REGION AT THE CRITICAL LOCATION

1.27mm Contact Pad Size Results [75]

3mm Contact Pad Size Results (800 Test Series)

CHAPTER 1

INTRODUCTION

Fretting fatigue occurs when components are in contact and subjected to cyclic loads or vibrations. The occurrence of cyclic loads induces fatigue in the assembly, which can lead to catastrophic failure. The study of fatigue is well established and there are currently many methods of assessing fatigue damage. However, in fretting fatigue the effects of fatigue are combined with contact, which accentuates the process and significantly reduces component life. Fretting fatigue is dependent on the geometry of the contact and previous studies have focused on those configurations, which can be analysed with a closed form solution. Analysis of flat contacts with sharp edges is difficult and closed form solutions are not available for this configuration. However, engineering structures such as riveted lap joints in aircraft fuselages, gas turbine compressor blade roots and discs as well as many other assemblies have contacts, which

can be defined as flat or containing sharp corners. Therefore it is important to assess fretting fatigue with this specific geometric configuration and attempt to provide an effective analysis method capable of accurately predicting the life.

The following research programme investigates the fretting fatigue phenomenon using a specific flat contact geometry encompassing sharp corners. The pressure distribution at the contact interface is fundamentally important in the understanding of fretting fatigue problems. The presence of sharp corners in contact analysis leads to difficulties in the determination of an accurate pressure distribution profile. Due to limitations in the analytical process, as a result of the geometry, an engineering solution is proposed to account for the affects of this specific geometry and for the fatigue life prediction of fretting fatigue in a flat contact situations. Furthermore, this investigation has provided insights into the characteristics of the fretting fatigue process and methodologies are presented to explain the phenomenological effects observed during fretting fatigue tests.

The basis of the solution focuses on the friction force response during micro slip, which is generated as a result of relative displacements at the interface due to the application of cyclic loading. Friction force is a function of pressure and is an influential parameter in the nucleation and initiation of fretting fatigue cracks. An experimental testing facility and programme was developed to determine the friction response of various sized sharp corner contact geometries on 2024-T351 aluminium alloy specimens subjected to dynamic loading. The current work studied the friction response and the influence friction had on the initiation of dominant fretting cracks. The load range ensured that the relative contact displacement did not occur across the entire contact surface and therefore avoided gross sliding. The loads used induced only partial surface displacement and micro slip. Further studies were conducted to control contact surface

slip displacements, which affected the friction force. The controlled slip studies were performed to determine the effects of varying friction on the fretting fatigue lives.

A hypothesis is proposed, based on experimental observation, to account for the characteristic behaviour of fretting fatigue lives, which at high load cases, exhibit either a stabilisation or increase in the number of cycles to failure. A numerical method has been used to obtain the stress response under micro slip conditions. Finite element models were constructed to simulate the experimental test arrangements by generating comparable friction forces, which allowed the analysis of the specific sharp corner contact geometry. Through the prediction of numerical friction forces, which are compatible with an equivalent experimental arrangement, it is proposed that the finite element solution is an acceptable representation of a sharp corner fretting fatigue problem.

Numerical solutions are provided for a range of experimental test configurations and the surface and subsurface stresses were investigated. A hypothesis is presented, which identifies the peak shear stress location at the contact surface as a probable crack initiation site. This hypothesis is in agreement with experimental observations. The analysis of the sub surface stresses at this location has revealed a depth where the influence of contact on the stresses diminishes and the bulk stress induced by the axial load becomes dominant.

The numerical study, using the simulated fretting test arrangement, has led to a life prediction model based on the elastic stress concentration factor (K_t). Through the determination of an equivalent multiaxial stress concentration factor and Neuber's analysis, an analytical method has been used to predict fretting fatigue lives.

Comparisons between the experimental and predicted fretting fatigue life results provide a validation of the methods used.

Chapter 2 contains a review of the literature on the subject of fretting fatigue and considers the various methods used by others to quantify the phenomenon. Chapter 3, provides the details of the experimental testing facility and describes the three experimental programmes used to investigate the initiation of fretting fatigue cracks, the effects of contact size on sharp corner contact geometries and the effects of controlled slip displacements, on friction and fatigue lives. Chapter 4 describes the numerical method used to simulate sharp corner contact geometries using ABAQUS 5.7 [1] and predict both the friction force response during fretting and the subsequent stress distributions. The results of both the numerical and experimental work are presented in Chapter 5. Chapter 6 discusses both the experimental and numerical friction results and determines the validity of the numerical solution. The study of initial crack growth in fretting fatigue is discussed along with the fretting fatigue lives determined from the experimental programme. A method is proposed to predict fretting fatigue lives using a numerically determined stress concentration factor. The analytically predicted fretting fatigue lives are compared with the experimentally recorded fretting fatigue lives to determine the validity of the analytical method. The conclusions of the work are presented in Chapter 7 with recommendations for further work.

CHAPTER 2

LITERATURE REVIEW

2.1 INTRODUCTION TO FRETTING FATIGUE

The term '*fretting fatigue*' is derived from many sources and has been recognised as the most accurate description of a phenomenon that includes both wear, which is referred to as fretting [2, 3] and fatigue damage due to the application of a cyclic bulk stress. The conjoint contribution of both these processes results in an impact upon component life that is more severe than the isolated influence of both processes. Some researchers have discovered large reductions in overall component fatigue life to those found under non-fretting conditions [2, 4-8]. Therefore, it is imperative that a distinction is made between the phenomena of fretting, fatigue, and fretting fatigue [2, 4, 9-11]. Fretting can be summarised as the degradation of a contact surface through the

oscillatory motion of one or more of the contacts that does not necessarily require the presence of an oscillatory bulk load, as in the case of vibration, which may be the result of an external forcing frequency. Fatigue is defined as changes in the material property of a component, which can occur due to the repeated application of stresses and strains, which is usually applicable for those changes, which induce cracking or failure. [12]. Therefore, fretting fatigue incorporates the effects of fretting with the presence of an oscillatory bulk load bringing about fatigue, which leads to cracking and potential failure of the component.

Originally discovered in the grips of fatigue machines, fretting fatigue has been discovered throughout a range of engineering applications and consequently many studies have focussed on the investigation of fretting fatigue. However, two areas of concern are persistently repeated in the literature; the effects of fretting fatigue at the compressor stage of gas turbine engines particularly at the blade root and disk interface and the riveted lap joints in aircraft structures. In the case of compressor disc and blades the use of coatings are designed to reduce the effects of friction. However, metal to metal contact occurs when the coating has been removed through operation. The result is a rapid increase in friction with detrimental effects to the contacting surfaces, which gives rise to fretting fatigue. Fretting fatigue in the structural lap joints of aircraft [13,14] occurs at the riveted joints, which exhibit fretting between the rivet and rivet hole. The loading originates from the fuselage, which is subjected to cyclic loads either from vibration or bulk loads due to pressurisation and stresses induced by flight manoeuvres.

Many researchers have studied fretting fatigue over the past 90 years with the hope of understanding the relevant processes in order to eradicate component failure in service.

As a range of engineering structures involve joints and mating surfaces that are subjected to loads, or vibrations, which induce oscillatory bulk loads, the phenomena known as fretting fatigue is considered a significant problem. It is interesting to note that some early works refer to fretting fatigue using terms such as fretting wear, fretting corrosion, friction oxidation, wear oxidation and false brinelling [10]. This reflects the complexity and diversity of the subject, and demonstrates that until relatively recently there existed a fundamental lack of knowledge in the area. The epistemology of fretting fatigue has been explored to varying degrees by many *viz.* Waterhouse [2] thoughtfully arranged a concise review of the salient works, which have contributed to the subject since its inception; there is also the work of Suresh [12], Hoepfner [10] and others [15].

2.2 MECHANICS OF FRETTING FATIGUE AND ACCEPTED IDEOLOGIES

Fretting fatigue occurs in contacting bodies when they are subjected to dynamic loads, which produce contact pressure profiles, bulk stress distributions and friction force. This is emphasised when loads parallel to the contacts, such as surface tractions or the application of a bulk stress, cause surfaces to slide in a cyclic manner. Figure 2.1a illustrates a simple schematic of a compressor [16] and figure 2.1b demonstrates the location where fretting fatigue occurs between the disc and blade root for fir tree and dove tail type roots. Figure 22 illustrates where fretting can occur in a typical riveted lap joint.

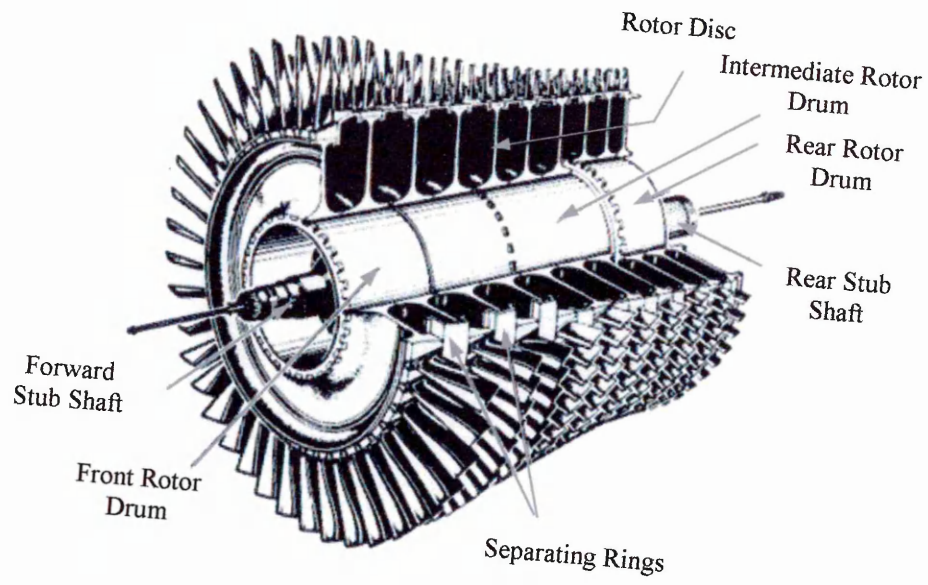


Figure 2.1a Gas Turbine Compressor Rotor

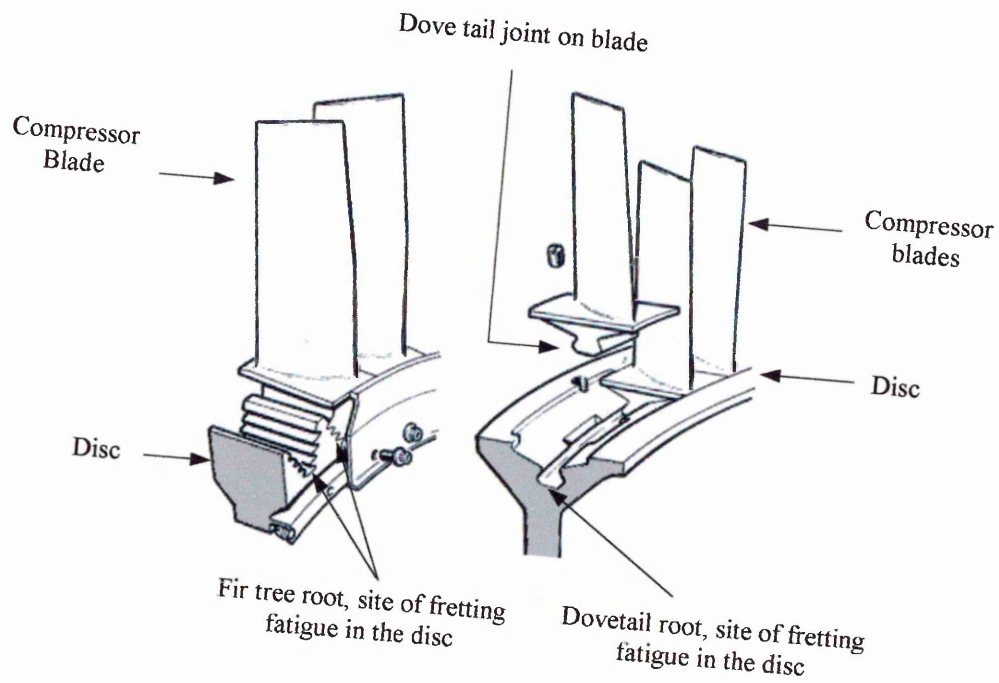


Figure 2.1b Fir tree and dove tail blade root configurations that fit into compressor disc

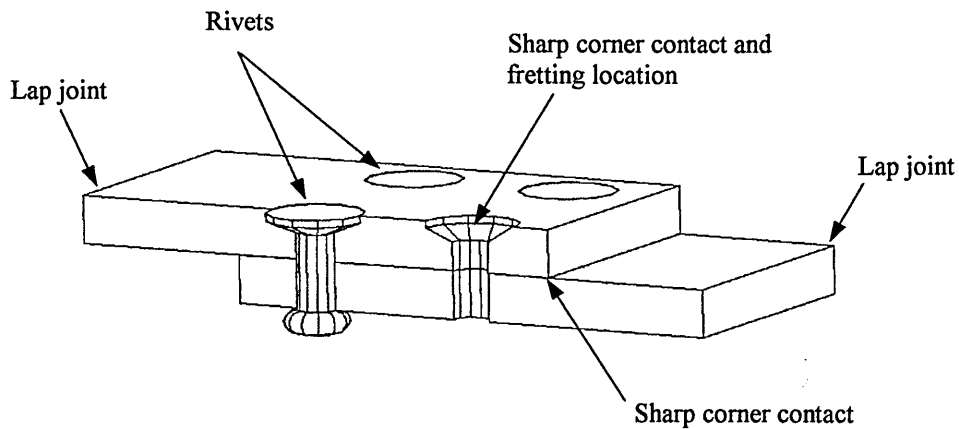


Figure 2.2 Cross Section of a Riveted Lap Joint

The cyclic sliding of the contacting surfaces results in surface degradation, and the production of third bodies through the formation of debris. The overall process is accentuated through cyclic loading and the subsequent nucleation of dominant fatigue cracks [2]. The application of multiple loads introduces multiaxial stresses that result in mixed mode cracks initiating oblique to the contact surface [2]. Cyclic multiaxial stresses that result in fatigue are defined by Bannantine [17] as *“fatigue due to complex stress states in which the three principal stresses are either non-proportional or whose directions change during the loading cycle”*. Influenced by the complexity of the stress fields the preliminary crack propagation, driven initially by mixed mode loading, eventually alters direction. This is due to the depreciative effects of the surface contact and the dominating influence of the bulk stress as the crack length increases [18, 19]. The remaining crack propagation is driven by the bulk stress until critical failure occurs [20]. Many variables affect the fretting fatigue process, Dobromirski [21] suggests there may be as many as fifty variables influencing fretting damage, encompassing contact configurations, temperature and material condition.

The study of the fretting fatigue process involves two aspects; first, the external loading and subsequent mechanical effects, such as friction, can be referred to as the *macro*

mechanics. The first acknowledged macro model was that proposed by Ruiz [22]. The second aspect is considered as *micro mechanics*, which is mainly concerned with material response on a microscopic scale involving the effects of grain boundaries, dislocations and slip planes [23]. The advantage of a macro mechanics solution lies in its generality, whereas micro mechanics is material and process dependent. Therefore, a micro mechanic solution is localised and it is difficult to apply to more generalised problems due to the availability of relevant information [5]. Research in both areas of study is currently ongoing.

Any potential global solution for fretting fatigue should initially consider a macro mechanics model. Previous studies show that the critical parameters involved in fretting are controlled by the external loading and contact geometry. With respect to external loading, past investigations have been primarily concerned with the effect on surface motion in contact. The movement between surfaces in contact is typically called '*slip*' [6][24]. The type of slip is dependent on the magnitude of the surface motion. In fretting, global or macro slip [25-27] occurs when the surfaces are in complete relative motion. Although this is not considered a predominant influence on fretting fatigue, the effects associated with macro slip are still damaging and result in wear, which can rub away micro cracks [2]. However, the level of contribution that micro slip influences fretting fatigue remains largely unclear. The predominant fretting damage comes from partial or micro slip, which occurs only when part of the contact surfaces are in relative motion (*slip*) and the remaining surface does not move relative to the opposing surface (*stick*). Although under *stick* conditions the surfaces may move elastically at the contact (*elastic slip*). Investigations have indicated that micro slip is an important factor in fretting damage as visible damage can occur for slip amplitudes as little as $1\mu\text{m}$ and fretting cracks are observed to nucleate at the slip boundary [28]. Therefore, micro slip

is often considered a primary indicator of the presence of fretting in a system. Figure 2.3 illustrates the types of surface displacements induced during a micro slip condition where the contact surfaces may experience both a stick and slip regime.

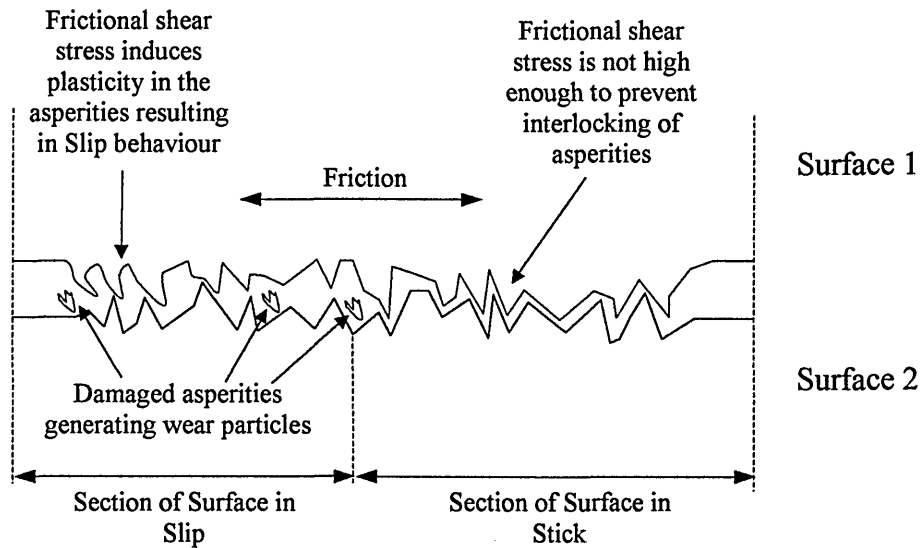


Figure 2.3 Schematic of contact surfaces showing microscopic detail of stick and slip behaviour

Contact geometry is also an important factor when considering fretting fatigue. Hutson *et al* [28] confirms that the majority of research in fretting fatigue has been conducted on Hertzian or punch on flat geometries. This is because of the availability of closed form analytical solutions capable of determining the resulting stress distributions. Although the concept of an ideal contact geometry for fretting fatigue investigation has been the cause for debate in recent years most researchers have concentrated on one of two basic forms. Contact is seen as either, complete (a geometry that has a constant contact area irrespective of load, such as a flat contact) or incomplete (a geometry that has a variable contact area which is dependant on load, such as a spherical or cylindrical contact), the former being defined as a surface containing an edge or sharp corner [29]. Although some research has involved variations on these themes [30] the majority of the work thus far has been concerned with any one of these two categories. The incomplete spherical contact geometry can be analysed mathematically using Hertzian

or Mindlin contact equations. Harish and Farris [31] found that the Mindlin method gave good solutions for the contact of two cylinders with tangential forces as well as normal loads. Due to the fact that contact pressure is fundamental to the analysis of any fretting problem, an accurate contact stress analysis is required.

The problem of utilising incomplete geometries comes in the form of its potential application. Since the shape of the pressure distribution affects the fretting mechanisms, the geometry of the contact must represent that of the intended problem. Due to the limited situations in which incomplete geometry can be considered, its potential application is restricted. This was considered by Kim and Lee [32] and was recently echoed by one of the partisans of spherical geometry, Hills [30] who reviewed the potential for incomplete geometry. Hills [30] concluded that an alternative geometry is necessary to advance the understanding in this area. The alternative suggested was an incomplete contact that is a combination of the flat and spherical geometry, where the geometry alters from a typical Hertzian sphere to a flat surface with radii edges as shown in figure 2.4.

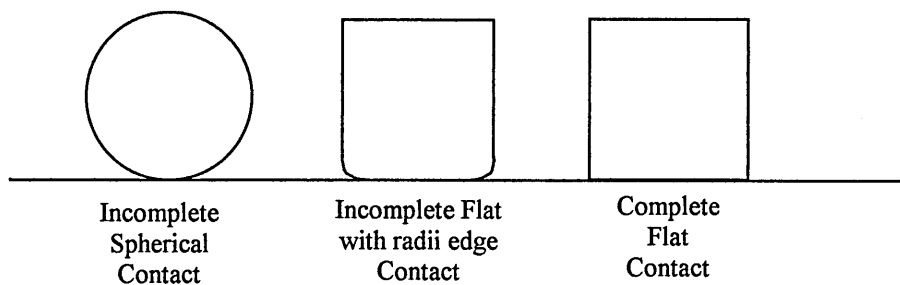


Figure 2.4 Types of incomplete and complete contact geometries

In contrast, the problem with investigating complete flat contact becomes apparent in the analytical phase. Due to the presence of sharp corners, the analytical representation results in an anomaly in the form of a mathematical singularity [29, 30, 33-35]. These

singularities arise because of the discontinuity in the pressure distribution. Unlike the Hertzian contact pressure, which exhibits peak stresses at the geometric centre, the flat contact exhibits peak stresses at the corners. These peaks progress towards infinity, ostensibly indicating an infinite deformation, or stress singularity as shown in figure 2.5.

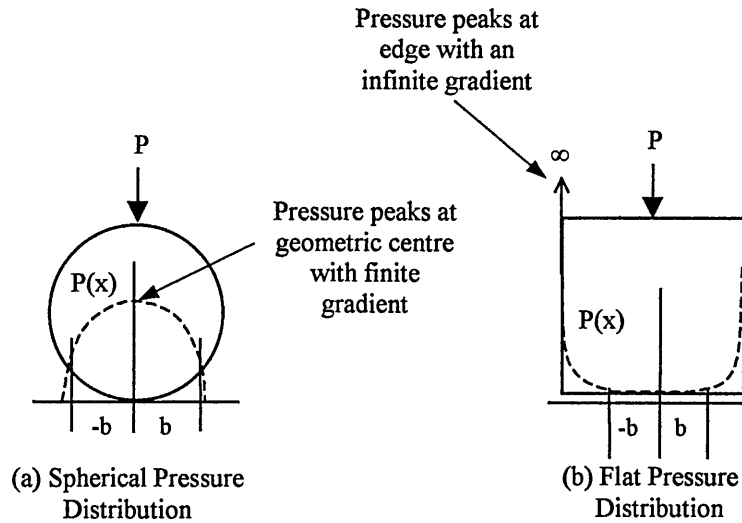


Figure 2.5 Pressure distribution profiles for (a) incomplete geometry and (b) complete geometry

The presence of this singularity in the analysis of complete contacts prevents the formulation of a closed form solution, thereby rendering the geometry incapable of being represented analytically. However, due to its universal shape, the flat geometry has the potential to be used in a wider range of industrial situations. It is this potential which drives researchers [3, 9, 11, 18, 20, 36, 37] to investigate flat contact geometries despite the ambiguity generated by the singularity problem and determine methodologies which are capable of providing a solution. Whatever the geometry or loading conditions used to create fretting fatigue, the primary response of the material is the formation of cracks manifested by surface damage and scarring. The nucleation of these micro cracks within the damaged region is a complex process and the mechanisms of crack initiation and propagation have been examined by many. Fellows *et al* [38]

proposed the process of crack initiation or nucleation is associated with very localised plasticity in the areas of some stress raiser. In further work, Fellows *et al* [23] postulated that once cracks reach grain size they stop initiating and propagate as normal. On a microscopic scale, fretting fatigue crack growth can be considered in terms of dislocations and slip bands. The dislocations form due to shear stress concentrations in the material and move in the direction of the applied load. This mechanism can be defined as the effective accumulation of damage through shear stress to initiate a crack.

Kim and Lee [32] suggested that cracks either initiate at the edges of the contact zone or at the stick slip boundary. From an experimental fretting fatigue programme, they concluded that cracks initiated exactly at the stick slip boundary when the test was performed in the partial slip regime. However, when the tests were conducted in gross slip the cracks initiated at the leading edge of the pad. This observation on the location of the fretting fatigue crack initiation is typical. Study of the continued crack growth revealed that the crack growth process could be represented in two stages. The first stage refers to the short crack region where a decrease in growth is due to a decrease in the contact stresses as the distance from the contact surface increases and the second stage is driven by the bulk axial stress. Sato and Fujii [39] observed that as cracks propagate the fretting effects become weaker because of lower subsurface stresses due to contact pressure at the crack tip and of the decreasing stiffness of the specimen. Others have observed this distinction between crack initiation and propagation, Sato *et al* [40] determined that crack initiation is not affected by the stress ratio (R) unlike crack propagation. Therefore, the number of cycles to initiate a fretting fatigue crack is not affected by the stress ratio. Also, short cracks experience a decrease in the propagation rate, because of a decrease in fretting and increase of crack closure. Cook and Edwards

[41] suggested that at short crack lengths the cracks remain open below zero stress, due to the relatively large plastic zone.

The reduction of fatigue lives due to fretting can be associated to the accelerated initiation of cracks. Lykins *et al* [42] considered that 90% of the fretting fatigue life can be attributed to crack initiation. This observation was confirmed by Araujo and Nowell [8] in their study of contact pad size effects on fretting fatigue in which experiments run at varying frequencies showed that the majority of life was attributed to crack initiation. Therefore, the understanding of the crack initiation process is an important aspect in the assessment of fretting fatigue.

2.2.1 Friction

Friction is considered an important parameter in the initiation of fretting fatigue cracks because of the influence on the stress distributions in the contact region. Friction is intrinsically linked to surface damage, scarring, and wear, which have been considered in the study of fretting fatigue damage [3, 43, 44]. The impact friction has on fretting fatigue lives has not adequately been defined. However, Jaffar [45] considers that friction significantly influences the normal pressure, which is an influential parameter in the assessment of fretting fatigue damage. Friction has also been considered to perform a critical role in the complex and often accelerated crack initiation period [8, 18, 37], which is believed to be the principal difference between fretting fatigue and plain fatigue, in terms of life prediction. Friction force at the contact surface varies throughout fretting fatigue life, typically increasing within the first few hundred cycles to a peak value, which then either stabilises at that peak value or reduces marginally and then stabilise for the remainder of the life [6, 28, 31]. The rapid increase in friction can

be attributed to the degradation of the contact surface in response to the onset of wear and damage. The friction force at the fretted surface can no longer be represented with the typical friction coefficient determined from simple sliding tests and the friction coefficient must increase if Coulomb's relationship (between friction force and contact load) is to be maintained. Therefore, increases in friction force are typically associated with increases in the coefficient of friction [28]. The increase in the friction coefficient can alter the state of the contact surface displacement, changing from global or macro slip during the initial stages of the experiment to partial or micro slip as fretting develops. Ciavarella *et al* [13] observed this phenomena and reported that even if an experiment is started under sliding conditions the rise in the coefficient of friction typically leads to a steady-state operation under partial slip conditions.

The microscopic mechanism of friction has been defined by Fernando *et al* [20] in terms of interlocking asperities and debris. The motion of the surface at this level can be considered as a series of contacts as the asperities move past each other. Friction can then be considered as a function of this very localised elastic plastic behaviour. When the asperities plastically deform, they can detach and form debris. The debris then becomes a third body, which can act as a lubricant [53]. The significance of this contact definition is in the application of the idealised Coulomb friction law, which is often applied to contact situations. This law assumes a global friction value that is applicable to the entire contact surface, which, as mention by Hoepfner *et al* [46], may not be adequate, as it is possible for this very localised friction to alter not only across the contact surface, but also throughout the load cycle.

The study of friction behaviour in fretting fatigue has provided some interesting works [46-52]. These investigations have attempted to include friction in varying ways in an

attempt to provide a more accurate definition of the phenomenon. Due to the fact that friction is an intrinsic response to contacting bodies, its definition has varied from the adaptation of analytical solutions, to the inclusion of friction into numerical models. When friction is included in numerical models, the solutions provide a suitably modified stress in the contact region for the purpose of life prediction. Hills *et al* [19] considered the rapid development of the interfacial friction for the Mindlin - Cattaneo solution to determine stress concentrations. Sellgren and Olofsson [24] developed a micro slip friction law suitable for finite element analysis, which was dependent on asperity deformation. Hills and Nowell [29] proposed that the shearing force at the contact surface is a function of the interfacial friction coefficient, which is almost certain to change during the fretting fatigue life. They also developed a solution using a Mindlin - Cattaneo model with an absolute slip friction coefficient for all points in the slip zone. Johansson [44] presented a frictional contact algorithm for two elastic bodies in contact. The algorithm includes the evolution of the contact pressure and accounts for loss of material due to Archard's Law of wear. The Archard's law is applied locally, where wear rate is proportional to contact pressure and relative tangential displacement. Avitzur [51] considered friction as a function of surface roughness, pressure, local friction factor and the Somerfield number (critical speed of surface to surface motion) and Coulomb's view of surface interaction was replaced with a mobile ridge mechanism.

Ouyang *et al* [48] proposed that the friction coefficient is a variable rather than a constant value. Typically, friction force is determined from the friction coefficient, which has been considered as a constant or as two separate constants to represent the stick and slip behaviour. However, the dynamic friction coefficient (determined by this work) showed that there was little difference in resultant stresses when compared with a

constant friction coefficient. Similar observations were made by Vingsbo and Schon [49], who analysed the stick and slip conditions characterised by low amplitude fretting with respect to the friction coefficient. The work considered variation in the normally static friction coefficient with location and time for the Mindlins model of fretting. The authors observed that the Mindlins model did not differentiate between static and kinetic friction and assumed that the kinetic friction coefficient was equal to the maximum static friction coefficient. Therefore, these works would suggest that the friction force induced by fretting could be accounted for by a single global friction coefficient obtained from a maximum friction condition.

2.3 INVESTIGATIVE METHODS AND AREAS OF CURRENT RESEARCH

Studies of fretting fatigue have typically included an experimental investigation to attain data intrinsically influenced by the fretting fatigue process. The experimental results are then used as a basis or a comparison, for the intended analytical solution to predict cycles to initiation or failure. The analytical solutions are varied and have included numerical simulations and adaptations to account for the phenomenological effects of fretting fatigue. Several methodologies are reviewed, to demonstrate the various approaches taken by researchers in order to determine a greater understanding of the fretting fatigue process and use that understanding to predict fatigue lives.

2.3.1 Experimental Methods

Experimental testing facilities are derived from the intended experimental methodology and have included relatively simple single actuator to more complex multiaxial actuator load rig assemblies. It is important to acknowledge that the testing facility does not

necessarily reflect the research methodology and results. Despite relatively simple testing arrangement Hills *et al* [19, 23, 29, 30, 54-57] and Farris *et al* [9, 14, 31,58-61] have based much of their seminal works on single or dual actuator testing facilities. The test rigs incorporate the use of the one or more actuators to apply the bulk load and surface tractions with a static structure such as a proving ring, employed to apply and control the contact loads. Swalla and Neu [28] devised a similar experimental arrangement to validate their finite element analysis and determine the role of the friction coefficient. Pape and Neu [7] also employed a proving ring arrangement in their assessment of the influence of contact configurations in fretting fatigue testing, in which both cylindrical and flat pads were tested. The results of this study revealed that cylindrical pads resulted in shorter lives than flat pad geometries subjected to equivalent loads, which would suggest that Hertzian contact arrangements yield conservative results.

Although the single and dual actuator arrangements have been employed in relatively successful research programmes, a continued analysis of the fretting fatigue process requires the application of more dedicated and specific machines capable of quantifying the complex relationships in the fretting fatigue process. Gerdes *et al* [6] developed a complex test rig to study turbine fretting fatigue at elevated temperatures. The experimental programme also included the study of friction force during the tests. Fernando *et al* [20, 37] developed a fretting fatigue experimental arrangement based on four independent actuators capable of applying variable normal loads in and out of phase with axial load. Fellows *et al* [23] discussed the problems associated with physically viewing the crack initiation process and identified that a two axis experimental test rig can isolate the initiation phase. Malkin *et al* [15] conducted an experimental study with a test rig, which allowed the control of both contact load and

relative slip amplitude. This arrangement provided a means of measuring friction force and contact resistance at the fretting interface.

The use of more complex testing facilities developed around a multiaxial loading facility provides the opportunity to study the interaction of multiaxial effects of fretting fatigue with greater precision and control.

2.3.2 Numerical Methods

The application of numerical methods to the problem of fretting fatigue has typically focussed on the simulation of an existing experimental arrangement. The advantage of experimentation is the generation of results from an actual physical system, and therefore, the results act as a control by which further numerical and analytical solutions may be measured against. However, experimentation is limited in the data it can record and it is often necessary to resort to numerical methods to simulate the necessary data to further assess the fretting fatigue process. Consequently, many investigations of fretting fatigue incorporate the use of numerical analyses such as finite element method to gain a further understanding of the fretting fatigue process [16, 42]. Continued improvements in the finite element analysis codes have provided a means to study increasingly complex contact configurations with improved accuracy.

Despite variations in the application of finite element method to the simulation and analysis of fretting fatigue, the fundamental principles of application remain consistent. Models typically generated from first or second order elements are constructed to represent an existing experimental specimen and contact arrangement. The use of symmetry in the representation of the geometry is often applied to reduce the

computational effort of the analysis and specific contact elements or nodes are used to characterise the contact surface. The solutions provide a range of results on the contact condition, friction behaviour, and fundamentally, the resultant stress fields. The acquisition of stress fields has typically been performed by complex analytical methods. Hills [19, 56, 57] adapted a variety of analytical models for incomplete or Hertzian contact geometries. Faanes [62] developed a complex analytical solution for flat contact geometries. Manipulation of these methods has led to increasingly more complex contact solutions. Although these works have provided a valuable method of analysing the fretting fatigue problem the use of purely analytical contact analysis methods are typically limited by the geometries capable of providing closed form solutions [7].

Finite element solutions can be generated for highly complex geometries and contact arrangements, which are difficult to obtain analytically. The numerical results can then be compared against experimental data to ascertain the validity of the finite element solution and ensure that the assumptions made during the analysis are correct. Once validated, the solution can then be applied to similar fretting fatigue problems to attain a wider range of results without the further use of experimentation.

Despite the increasing application of finite element method to the fretting fatigue problem, certain researchers, *viz.* Hills *et al* [10, 23, 54] prefer to avoid the use of finite element models and determine the necessary data analytically with the use of a Fourier transform method to calculate the stress field. As previously stated, purely analytical methods of analyses are restricted to closed form solutions, which limits the application of this method and prevents it from being used for more complex and demanding geometries ever present in actual engineering problems. However, numerical techniques such as finite element method provide only part of the solution to the problem of

analysing fretting fatigue. In order to demonstrate an understanding of the fretting fatigue process, it is necessary to develop an analytical model capable of predicting the fretting fatigue life of a component from a numerically determined stress field.

2.3.3 Analytical Solutions

The purpose of quantifying fretting fatigue in terms of an analytical model is to identify the relationship between the fundamental parameters, which influence the fretting fatigue process and in so doing provide a general solution applicable to fretting fatigue configurations outside the scope of the research study. Due to the complex nature of fretting fatigue, the determination of a general mathematical solution capable of predicting the effects of fretting fatigue is a difficult process. An accurate analytical solution is dependant on the geometric configuration of the contact as well as the multi-axial arrangement of the loading mechanisms, coupled with the resultant effects of friction and surface damage, which is influenced further by the material properties of the contacting bodies. The results are often solutions that are restricted to particular geometries and material configurations and as such analytical models exist for very specific fretting fatigue conditions. Typically, solutions have either been adapted from existing analytical models devised for similar fatigue conditions or generated based on observations of the fretting fatigue process. Ruiz [22] studied the fretting problem, at the dove tail joint, between a blade and a disk, in a typical gas turbine configuration. He proposed a parameter (κ) that attempted to include the effects of the localised stresses and the slip amplitude induced by fretting contact. Further adaptations to the Ruiz model [22] included a frictional work parameter ($\tau\delta$) and the effects of the tangential stresses. The Ruiz model has been adapted by others, Ciavarella *et al* [13] developed a hybrid Ruiz parameter in their assessment of damage parameters. Nowell and Hills [55]

also extended the Ruiz parameter by proposing an asperity sized contact theory involving incremental plastic shear strain.

Fellows *et al* [38, 54] used Bueckner's theorem and the dislocation method to evaluate stress intensity factors for fretting fatigue cracks. Hills *et al* [19, 56, 57] addressed the Mindlin-Cattaneo solution for incomplete contact geometries and considered the rapid development of interfacial friction that gives rise to stress concentrations. The bulk stress and contact stress fields were determined using classical Hertzian contact equations. Ganapathy and Farris [58] considered the Mindlin solution in their study of riveted skins. The solution showed a good correlation with Mindlin theory and the finite element model results.

Other successful methodologies have included the critical plane approach, first proposed and developed by Findley *et al* [63], the critical plane approach, which states, for a given material and known stress state, the critical plane is the plane on which cracks were observed to nucleate. Adaptations of this methodology have been employed by Swall and Neu [28] who determined an approach based on the critical plane theory and the accumulation of critical damage, dependant on a range of normal or shear loads on a specific plane. Araujo and Nowell [64] applied the critical plane approach to the multiaxial models proposed by Smith-Watson-Topper (SWT) and Fatemi-Socie-Kurath (FSK) to predict fretting initiation lives. In this work, it is the opinion of the authors that models based on the critical plane approach yield over conservative lives for rapidly varying stress fields, and so their solution incorporated both multiaxial fatigue theory and the critical plane approach. The solution requires all possible planes to be examined in order to identify the critical one at each location. The analysis of each plane is a complex and time consuming process and is considered a drawback in the methodology.

The application of multiaxial stress theory is considered a valid approach to the fretting fatigue problems. The combined effects of the shear and axial stresses can be incorporated into multiaxial fatigue models. Swalla and Neu [28] suggest that due to the configuration and number of influential variables, fretting fatigue can be considered with multiaxial fatigue theory and both the FSK and SWT multiaxial fatigue models were evaluated using the cyclic stress/strain results from finite element analysis. Socie [65] correlated the non-proportional life data with SWT expression, and determined that the SWT equation can be used to predict crack nucleation in the case of tensile crack growth under multiaxial loading conditions. Szolwinski and Farris [14] attempted to predict fretting crack nucleation based on multiaxial fatigue theory with some success.

Lykins *et al* [66] assessed the application of the critical plane approach for both the SWT multiaxial model and a model based on maximum shear stress to the fretting fatigue problem in a study of crack initiation. The work concluded that the SWT critical plane parameter was effective in predicting the cycles to crack initiation and crack location. However, the parameter was not effective in predicting the orientation angle of crack along the contact surface. The shear stress range critical plane parameter was also effective in predicting the cycles to crack initiation and crack location as well as predicting crack orientation angles along the contact surface which were in agreement with experimental observations. This work suggests that shear stress influenced by contact and friction is a suitable parameter to assess fretting fatigue crack initiation. Szolwinski and Farris [60] proposed a mechanics based approach for predicting fretting fatigue crack nucleation by juxtaposing an accurate characterisation of the near surface cyclic stress and strain fields with a critical plane fatigue crack nucleation parameter. This complete characterisation of the surface tractions associated with low-cycle and

high-cycle tangential waveforms enables determination of the near surface stress field by application of appropriate Westergaard functions.

The orientation of the crack growth is an important parameter to consider as it is indicative of the crack driving forces. Nishioka and Hirakawa [66] established a correlation between the orientation of the fretting cracks and the direction of the principal stresses at that orientation site. Furthermore, study of the orientation of the crack path as it grows indicates the influence the contact exerts of the sub surface stress fields. Alic *et al* [67] studied fretting in aircraft aluminium and postulated that a change in crack orientation occurred, which can be attributed to a point where the fretting stresses became negligible.

Other approaches to the fretting fatigue problem have included the application of the cumulative damage rule (Palmgren-Miner) applied by Szolwinski and Farris [60] to assess quantitatively the impact of low and high cycle fatigue interaction on fretting fatigue crack nucleation. This analysis identified the plane perpendicular to the surface at the trailing edge of the contact, as the critical location for crack nucleation. A design approach has also been considered by Hutson *et al* [28] where the use of a step loading procedure allowed the determination of a fretting fatigue limit to generate S-N curves. The design stress or Goodman stress was then interpolated from a failure stress, the number of cycles at failure and the stress from the previous step.

Experimental results have shown that cracks initiate either at the slip stick boundary or in the case of flat contacts relatively close to the leading edge of the contact pad [32, 46]. Interpretation of crack initiation and propagation can be defined in terms of fracture mechanics. The complexity of the fretting fatigue problem has resulted in the

assessment of an additional mode of fracture, which is introduced at the early stage of crack development [9]. The addition of an in plane sliding (mode II) stress intensity factor to the tensile opening (mode I) stress intensity factor has resulted in the formation of a mixed mode response [18, 19]. The mixed mode initiation induces an inclined crack path, oblique to the contact surface [2] and results in a high initial crack growth rate.

The application of fracture mechanics to this area has involved both the linear elastic models [69, 70], as well as adapted models. The application of these models has emphasised the complexity of early crack growth, as these models are only capable of representing '*long cracks*', and not accurately representing '*short cracks*,' in the initial crack growth period. Candidates attempting to address this vital early period range from exponents of the damage threshold concept [68], to all encompassing fretting fatigue solutions based on finite element method [46], as well as short crack modified linear solutions [71]. The theories discussed thus far have been dependant on specific geometry types and boundary conditions or have had a complex solution process, which introduces difficulties with wide spread application to actual engineering problems. A fatigue theory, which has had few applications to fretting fatigue, is the concept of stress concentrations. The method was originally developed for the assessment of discontinuities and notches on the fatigue lives of specific geometries. Peterson [72] provided a range of stress concentration factors for various geometries. A stress concentration is the ratio of the peak stress at the notch, or discontinuity and the nominal stress. The stress concentration factor can then be used to assess fatigue life by employing a strain life approach, such as Nuebers analysis. This method has the potential of incorporating both shear stress and axial stress concentrations, which can be used to determine the multiaxial contact stress field. Taylor [73] used stress

concentrations in an attempt to predict the fatigue limit or high-cycle endurance limit of contacting bodies, irrespective of shape and size. This effective and relatively simple method can be used as a basis for the assessment of fretting fatigue damage and provide the necessary reduction factor required to accurately predict fretting fatigue lives.

The study of fretting fatigue has provided various methodologies developed to determine the effects of fretting and predict the fatigue lives under these conditions. The review of these works has identified several areas, which could be combined to develop a new methodology for sharp corner contact arrangements. The study of sharp corner contact geometry is fundamental to the assessment of fretting fatigue in actual engineering applications. The methodology incorporates the development of a multiaxial experimental arrangement and testing programme, which controls the fundamental aspects of the fretting process to assess the effects of friction force on crack nucleation and fatigue lives. Furthermore, a solution is presented based on the accurate simulation of sharp corner contact arrangement using finite element method and the strain life approach developed by Neuber to predict fretting fatigue lives. The solution is intended to simplify the complex fretting fatigue behaviour with a stress concentration factor based on the multiaxial combination of shear and axial bulk stresses. With the equivalent stress concentration factor and Neubers method it is then possible to predict the fretting fatigue lives for any engineering problem in which fretting fatigue is a concern.

CHAPTER 3

EXPERIMENTAL INVESTIGATION INTO FRETTING

FATIGUE

3.1 INTRODUCTION

The use of experiments is considered a reliable method of obtaining a realistic representation of the fretting process; as many of the effects of fretting, often difficult to represent analytically or numerically, are inherently present in the physical process of experimentation. In order to achieve fretting in a fatigue experiment it is necessary to have a reliable contact with a known load transfer, and avoid unintended pressure distributions caused by uneven contact alignment. The inducement of relative surface

displacements or slip, of the mating surfaces can be achieved through the application of an oscillatory axial load. This ensures the generation of a cyclic friction force, which is a fundamental aspect of the fretting fatigue process.

3.2 EXPERIMENTAL TEST RIG DESIGN

A proper fretting fatigue experimental facility requires an environment within which the contributing factors can be controlled and so through a process of elimination provide an explanation of fretting fatigue [56]. Therefore, the effectiveness and validity of the work depends greatly on the design, performance and accuracy of the experimental apparatus.

In a previous design Hills *et al* [23, 55, 57] developed a simple test rig, the theory behind which was to provide the basic fretting function for analysis of Hertzian, or Hertzian type contacts. Szolwinski *et al* [9] developed several variations around a similar design which provided a means of testing various contact types, focusing primarily on spherical geometry. The purpose of these works was to provide experimental data to support the investigation of riveted lap joints. Other testing facilities considered during the design were those experimental systems developed by Malkin *et al* [15], Fernando *et al* [20][37] and, Kim and Lee [32].

Consideration of the above experimental facilities lead to the design of the current experimental arrangement, which required the test rig to control the fundamental contributory factors involved in the fretting process. In particular, the control of contact pressure, axial load, friction, and slip. Figure 3.1 shows the experimental facility with detailed inserts.

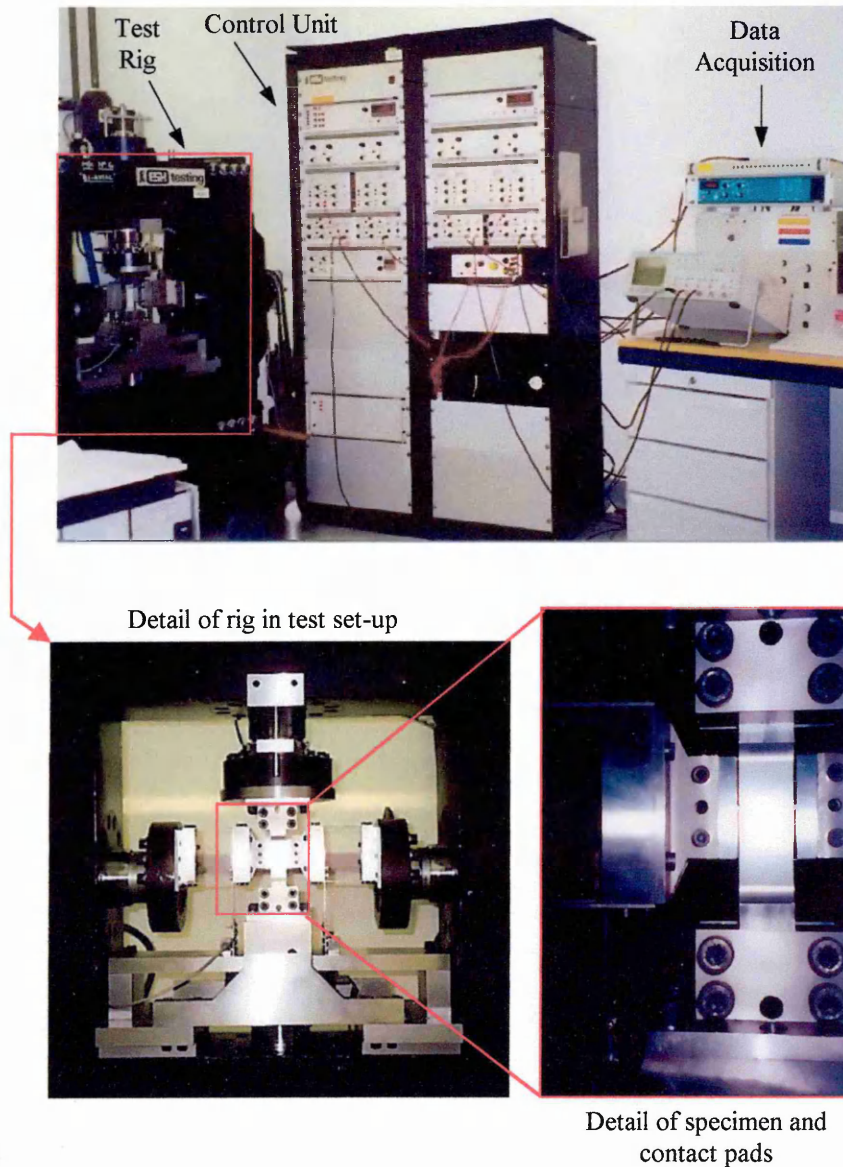


Figure 3.1 Testing facility with details of specimen and contact

3.2.1 Test Arrangement and Design

The present test arrangement is positioned between four servo hydraulic actuators. With the availability of four independently controllable actuators, it was possible to apply the axial load to the specimen, as well as control contact pressure on the contact pads. The design on the rig also allowed the contact pads to be displaced parallel to the specimen

surface. Figure 3.2 illustrates the tooling arrangement used in the test programme.

Detailed engineering drawings of each component are presented in Appendix A.

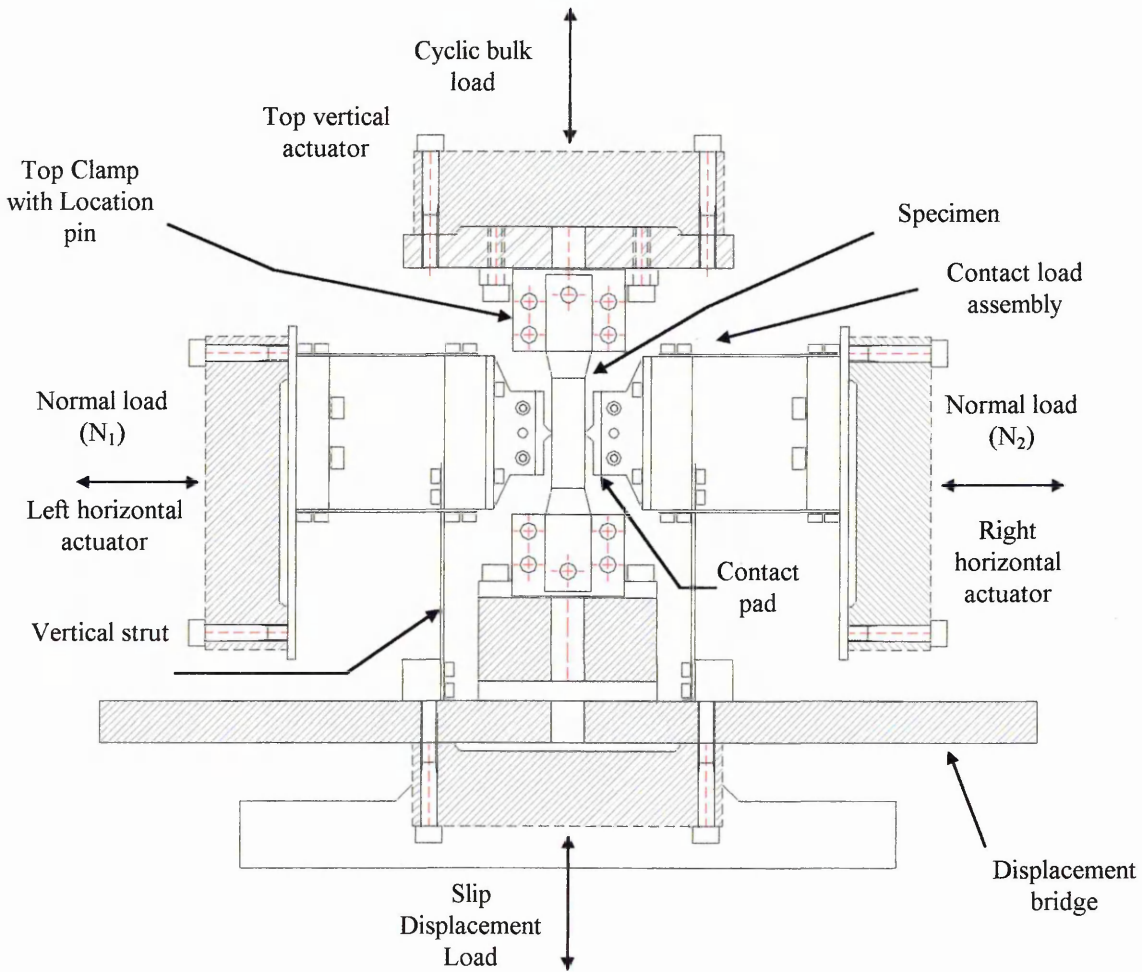


Figure 3.2 Fretting Fatigue Test Rig Design

3.2.2 Specimen Loading Arrangement

The main design feature of the new system was the utilisation of all four of the independent actuators available on the test rig. To make the most efficient use of the loading system the specimen was positioned vertically with the top actuator used to apply an oscillatory axial load to the specimen. A part of the top clamp is a circular flat plate bolted to the load cell, with the specimen held in place by two clamps designed to provide adequate clamping, to apply the intended axial loads without inducing slip. To

ensure repeatable specimen alignment to the loading axis a guiding rod was employed to position the specimen. Correct alignment ensured no bending was induced in the specimen during the assembly process. In case of excessive wear, two removable plates were included, designed to fit between the specimen and the clamps, for simple replacement. The thickness of the plates could also be changed to encompass varying specimen thickness as a result of machining tolerances.

The bottom end of the specimen was clamped using the same method as the top clamp, to a static bridge attached to the machine frame. The bridge was designed so that the displacement of the bottom actuator was limited to less than $15\mu\text{m}$ for the maximum intended axial load. The bridge was secured to the machine frame via a fixing plate, which provided a stable self-aligning platform. Figure 3.3 illustrates the top and bottom clamp assembly.

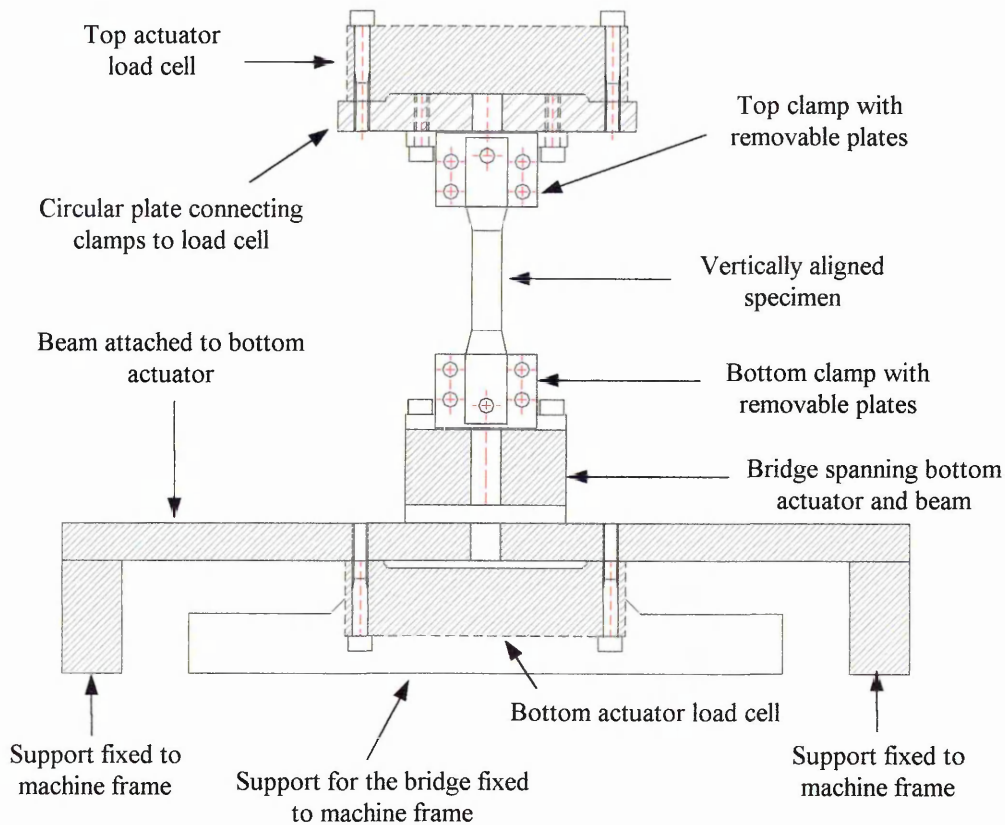


Figure 3.3 Position of specimen and clamping arrangement

3.2.3 Contact Loading Arrangement

The contact loading arrangement is such that the contact position and loads applied through the contact pad align parallel to the surface of the specimen. The horizontal actuators were utilised to apply the contact loads. Accurate positioning of the contact pads was considered particularly important for flat contact geometry to ensure surface parallelism. Figure 3.4 illustrates the contact load arrangement.

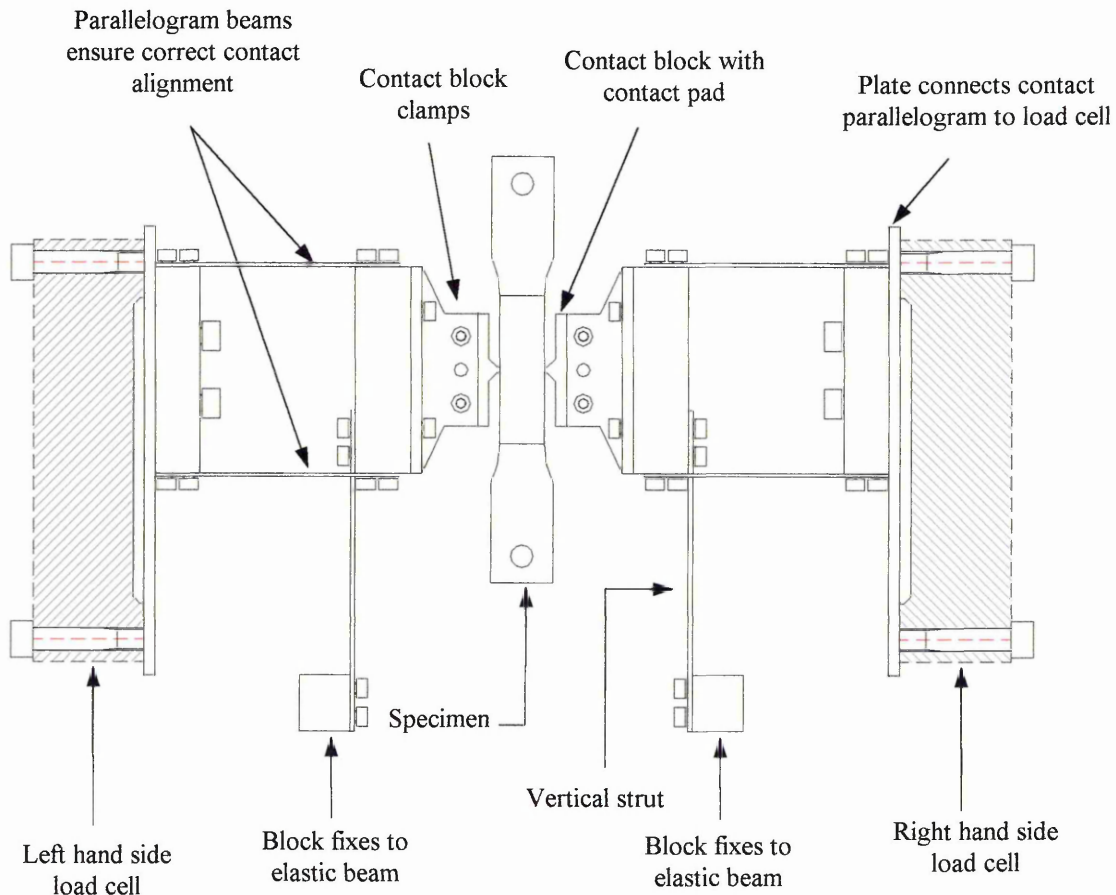


Figure 3.4 Contact load arrangement

In the case of flat contact situations various methods have previously been employed to ensure the contacting surfaces are parallel. Sato *et al* [39] employed pressure sensitive film, where pressure maps were made of the contact surface to provide alignment data. Whereas in the case of Fernando *et al* [20,37] the problem was addressed by introducing

a bridge system, which eliminated pad misalignment due to the self adjusting properties of the bridge. However, other researchers such as Kim and Lee [32] considered the bridge system and identified problems that may occur due to the presence of a number of contact areas and therefore, many crack initiation sites. Therefore, for the present application only a single contact site was located at each side of the specimen. To enable the correct movement of the contact pads, a parallelogram structure was developed, which provided the necessary stiffness needed to ensure alignment. As a result of the parallelogram structure any deviation of the contact pad would still provide the correct contact. The contact pads were fixed to the parallelogram structure with clamps, which were located with the use of pins.

3.2.4 Slip Control Arrangement

The controlling of slip required the contact pads to be moved relative to the specimen by an order of microns to achieve the actual micro and macro slip behaviour, which occurs during fretting fatigue. Due to the precision required in moving the pads it was necessary to devise a method of controlling the pad position whilst under load. A design was developed that allowed the contact pads to be moved in microscopic levels by using the deflection of a large beam. This arrangement was able to maintain the necessary deflection under relatively large load magnitudes. The slip control arrangement is shown in figure 3.5.

Slip control is accomplished through the use of an elastic beam structure that is directly connected to the lower actuator and is supported by the machine frame. The beam is

considered to be elastic and the stiffness of the beam was such that large loads induced only small displacement so that:

$$1.25KN \cong 12\mu m$$

The contact pad assemblies were attached to the elastic beam so that the vertical displacement of the beam was proportional to the vertical displacement of the contact pads. The parallelogram structure ensured that contact pads displaced with the elastic beam and did not rotate, maintaining the required contact alignment and provided a precise vertical displacement, which allows the contact pads to be moved relative to the contact surface by an order of microns.

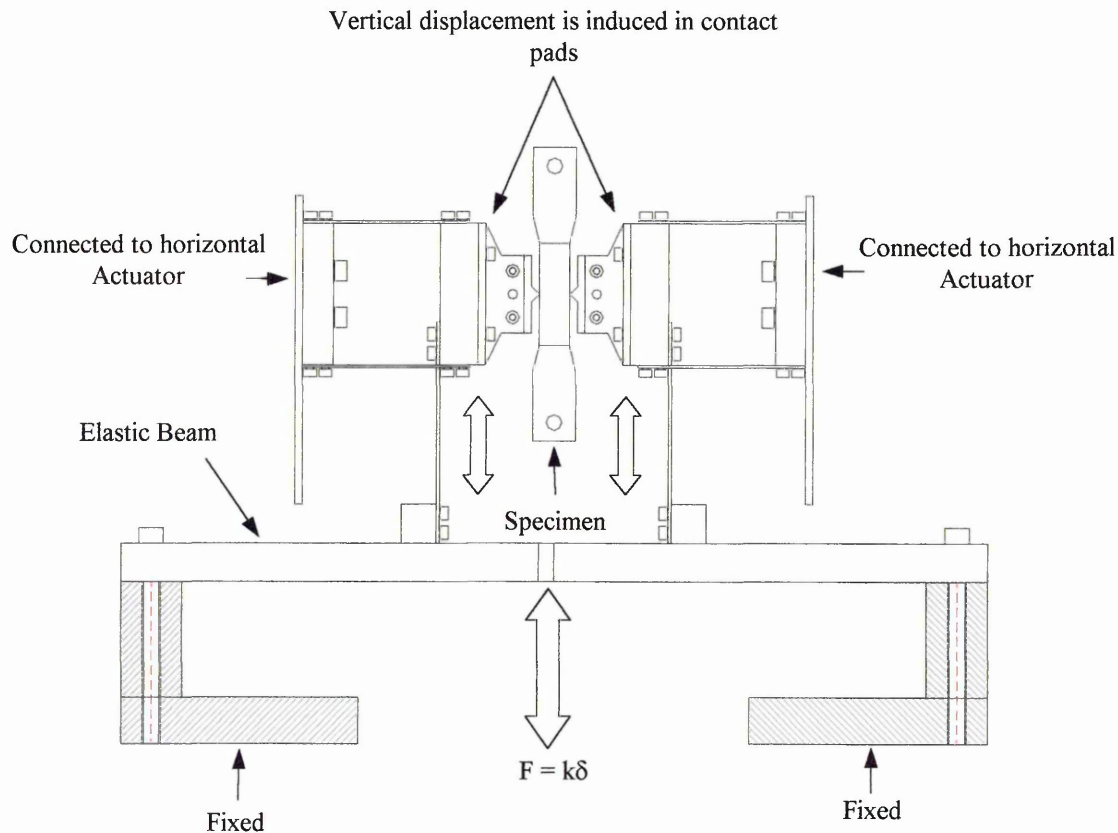


Figure 3.5 Design of the lower actuator beam to attain controlled slip displacement

The slip control arrangement was capable of displacing the contact pads during the set up process prior to testing or cyclically during testing either in or out of phase with the

specimen axial load. This provided the necessary means of controlling the magnitude of slip required in the tests (i.e. 10 – 70 μ m).

3.2.5 The Measurement of Friction Force

To examine the effects of friction on fretting fatigue it was necessary to measure and record the frictional response at the contact surfaces. The test rig was designed to provide friction measurements and this was achieved by including a vertical strut attached to the pads, see figure 3.5. The strain in the struts was directly proportional to the frictional resistance force generated at the contact surfaces. Friction was therefore measured by attaching strain gauges to the struts with a Wheatstone bridge arrangement. Figure 3.6 illustrates the location of the strain gauges on a contact assembly.

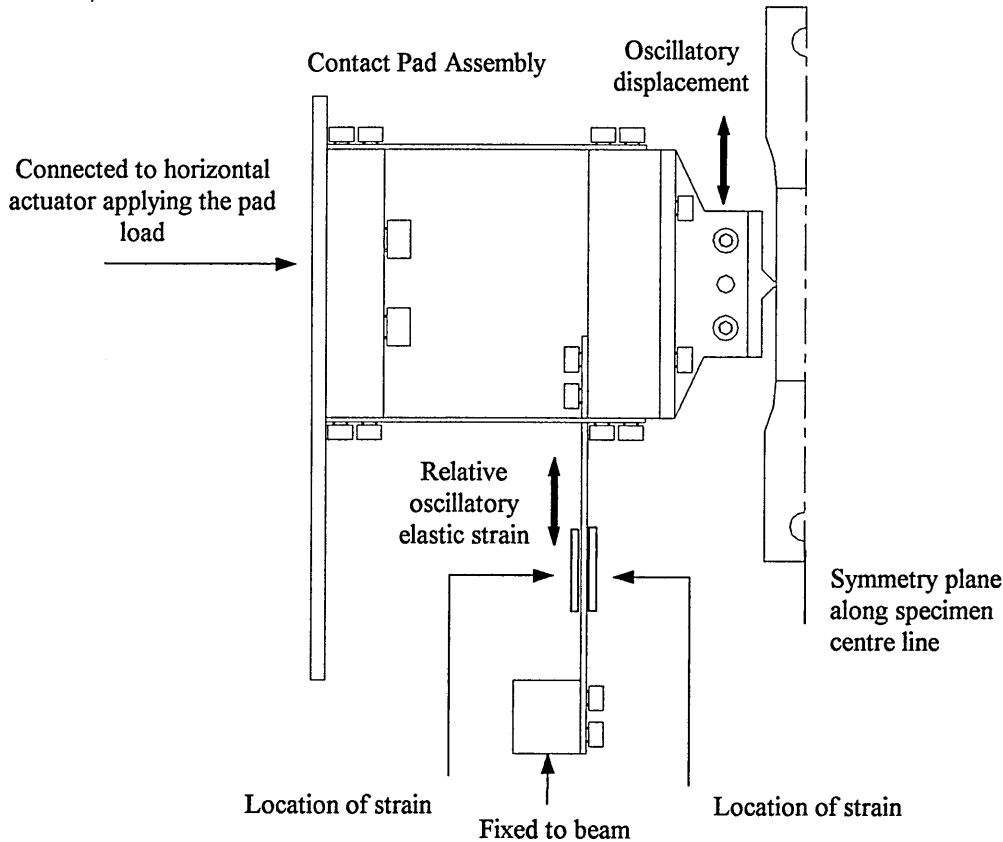


Figure 3.6 Contact assembly illustrating the position of the Wheatstone bridge strain gauge arrangement for measuring friction

During test set-up, the vertical strut was expected to bend as a result of the travel of the horizontal actuator from the initial assembly position to the specimen surface. To isolate the friction induced strain a full bridge strain gauge arrangement was wired to eliminate bending strain from the input signal.

The strain gauges were calibrated under static loads with the use of a *Fylde* modular amplifier to obtain a calibrated friction force curve. Figure 3.7 illustrates the friction force calibration results.

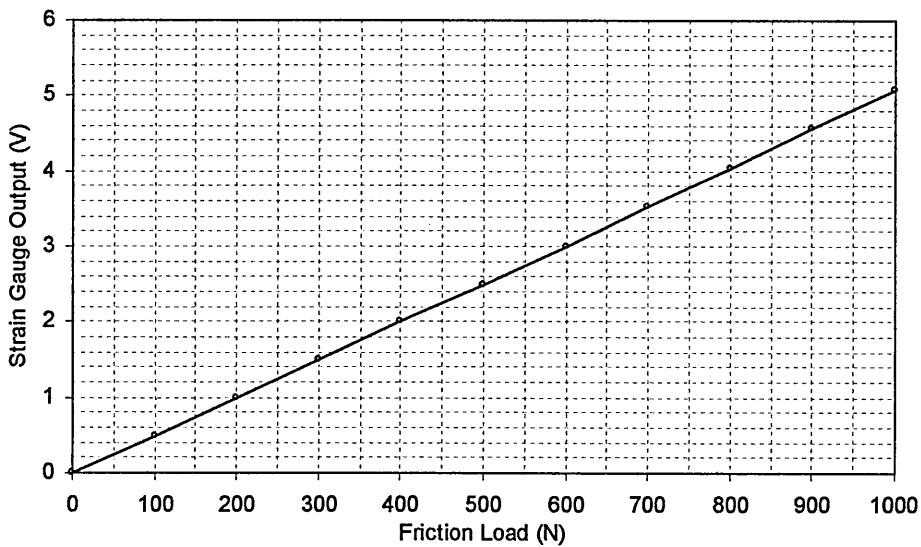


Figure 3.7 Friction Calibration Chart

3.3 THE SPECIMEN & CONTACT PAD

The specimens were manufactured from aerospace aluminium, grade 2024 - T351 (BS L65 4% Copper). The material is a high strength alloy typically used for aerospace structural applications. The design was based on the specimens used by Fernando *et al* [20][37]. The specimen is of rectangular cross section, which consists of a reduced section test area that is blended into gripping areas for the clamps. The change in cross

section is filleted at each end to reduce the risk of fatigue failure at the clamping face cross section. Two holes were provided to locate the specimen in the clamps. Figure 3.8 shows the location of the holes and filleted cross sections of the specimens.

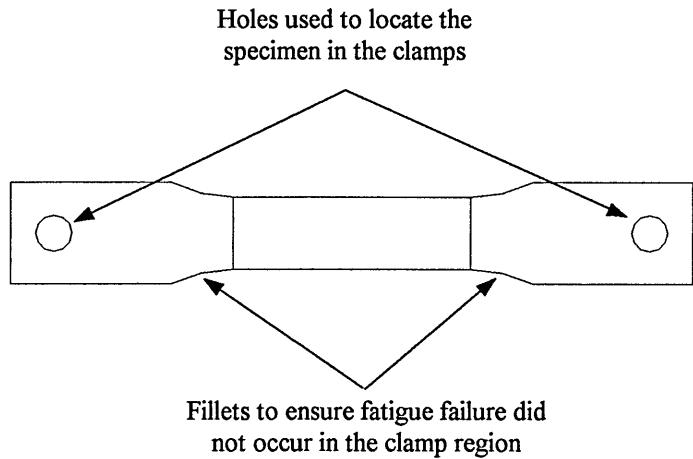


Figure 3.8 Specimen

The contact pads were constructed from low carbon mild steel in the annealed condition. Contact blocks were used so that the required contact area could be machined to achieve the 1.27mm and 3mm pad sizes necessary for the intended experimental programme. Holes were provided to locate the contact pads in the contact assembly structure. Figure 3.9 shows the location holes in the contact pad blocks.

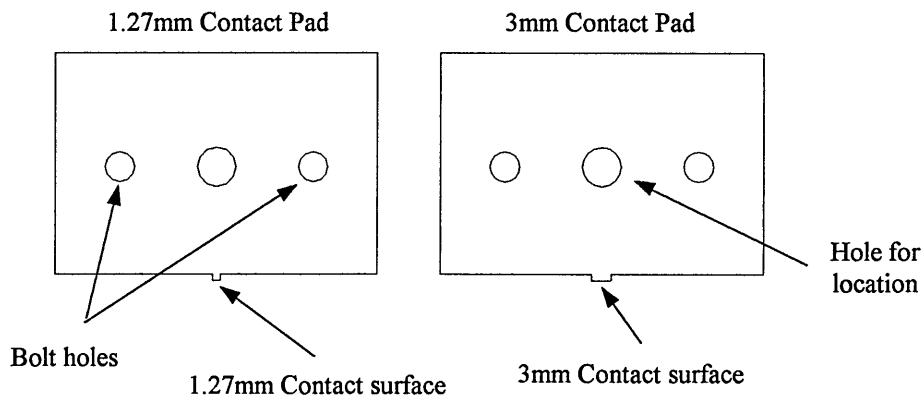


Figure 3.9 Contact pads

The dimensions of the specimens and contact pads are provided in Appendix A.

3.3.1 Material Data

Material data was obtained for 2024-T351 Aluminium alloy [12][74]. Table 3.1 shows the material composition of the alloy and table 3.2 lists the material properties. To validate the specimen material, with the material properties listed in table 3.2, standard tensile tests were conducted on six samples until failure occurred. Figure 3.10 presents the average stress strain curve for the six tests. The results from the tensile tests also include the yield stress (σ_y) and the ultimate tensile stress (σ_{UTS}) which are provided in the figure. As can be seen from the results, the tensile tests conducted on the specimen material agree well with the material data in table 3.2.

Table 3.1 Material Composition for 2024-T351 Aluminium alloy

Component	Wt. %	Component	Wt. %	Component	Wt. %
Al	93.5	Fe	Max 0.5	Si	Max 0.5
Cr	Max 0.1	Mg	1.2 - 1.8	Ti	Max 0.15
Cu	3.8 - 4.9	Mn	0.3 - 0.9	Zn	Max 0.25

Table 3.2 Material Properties for 2024-T351 Aluminium alloy

E (GPa)	ν	σ_{UTS} (MPa)	σ_y (MPa)	σ_r (MPa)	σ_r' (MPa)	ϵ_r'	b	c
72.4	0.33	470	379	140	1103	0.22	-0.124	-0.59

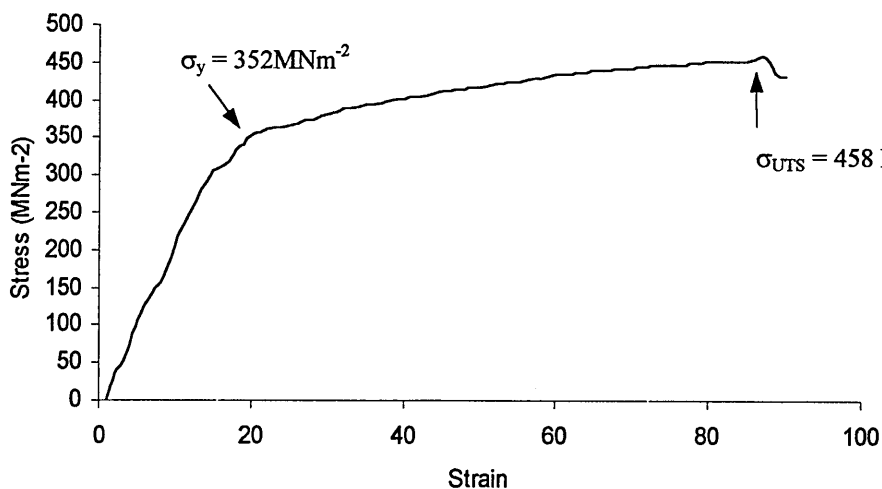


Figure 3.10 Material Test Data for Aluminium Alloy 2024-T315

3.4 METHODOLOGY & TESTING PROCEDURES

The experimental programme was developed to evaluate the fundamental fretting fatigue parameters, such as friction and slip, on the nucleation and initiation of fretting fatigue cracks. Study of fretting fatigue crack initiation of the 1.27mm contact pads size involved the examination of the fretting scar at varying stages of the test prior to critical failure. The intention was to identify the percentage of fatigue life in which cracks would be observed.

The effects of the contact area were examined by increasing the contact pad size to 3mm and conducting fretting fatigue experiments to failure.

An investigation into the effects of slip was conducted using the 3mm pads; whereby the contact pad was oscillated both in and out of phase with the axial load. The intent was to alter the slip behaviour at the contact surface, and determining the effects on fatigue lives.

Friction was observed in all the above cases to ascertain the influence of friction on the nucleation and initiation of fretting fatigue cracks and how friction develops through the fatigue life for the loads and geometry used in the test programme.

3.4.1 Experimental Procedure

The experimental study of fretting fatigue was separated into three programmes and five test series. Each series was composed of nine experiments. The study of crack

initiation incorporated three test series resulting in a total of twenty seven experiments. The study of contact size on the fretting fatigue lives was conducted in a single test series of nine experiments and the effects of controlled slip on friction and fretting fatigue lives was accomplished in the final test series of nine experiments. Although each experimental programme focused on different aspects of the fretting fatigue process, the subsequent procedure was followed in each experiment.

The specimens were mounted in the vertical clamping arrangement allowing the guiding pins to locate the specimen vertically and clamped to prevent the specimen from slipping under the intended axial load. The experiments were conducted in load control and the pre-load was set to zero, therefore setting the mean stress at zero, resulting in an axial stress ratio of $R = -1$. The contact pads were located in the clamps using the guiding pins and then manually travelled to the specimen surface prior to the pads being clamped. This allowed the pads to align to the specimen surface and ensured an even contact pressure distribution. *Pressurex*® pressure sensitive film was used to verify that the contact was aligned correctly. The film was placed between the mating surfaces before contact and the pressure was applied. The film provided a pressure map detailing the pressure distribution across the contact surface. The film holds small corpuscles of ink that rupture under set pressures, the result is a single colour gradient, which can be measured against a colour chart provided with the product.

Analysis of the pressure maps identified any misalignment problems, which were then rectified, and the process repeated to ensure the correct contact pressure was achieved. Once aligned, the clamps were tightened to fix the contact pads in that position and the actuator moved the contact structure and pad mating face into position on the specimen

surface. The vertical strut was then fixed to the lower actuator beam used to measure friction.

The predetermined load was set to achieve the required contact pressure value. Once all loads and positional checks were made, the oscillatory axial load frequency was set at 20Hz. The axial load and strain gauge readings were recorded to measure the friction response using 8 channels of the 16 channel data recorder. The recorder was set to collect 125 data points in a single sweep. This data was then down loaded by the data acquisition software and copied to files at different load cycles. A cycle counter was used to trip the control rig on completion of the total number of cycles per test or failure depending on the requirements of the test.

3.4.2 Study of the Initiation of Fretting Fatigue Cracks

The study of crack initiation is inherently difficult due to the complexity of the crack forming process. The transition from initiation to propagation is difficult to quantify. However, as fretting fatigue is influenced by the conditions at the contact surface, and fretting significantly reduces fatigue lives, it is believed that the effects of fretting are proportional to the effects of contact on the sub surface stress field. As the influence of the surface contact on the sub surface stresses diminish with depth, so the effects of fretting are also expected to diminish until a depth at which the effects of fretting are considered negligible. Therefore, for failure to occur continued crack growth is driven by axial stresses which are not significantly influenced by fretting. Consequently, fretting can be considered as influencing the initial stage of crack growth or crack initiation.

To ascertain the controlling factors of the nucleation of a fretting fatigue crack the following experimental programme was developed to examine the influence of fretting on the crack under different loads. In the experiments, friction was measured, since it was considered influential in the development of subsurface stresses and severity of surface damage.

3.4.2.1 Experimental Programme No. 1 - 500, 600 & 700 Test Series

To study the development of the fretting fatigue crack initiation the experiments were run to a percentage of the total estimated fatigue life. This provided information on how quickly cracks initiated and how extensive the crack growth was at varying stages of the fatigue life.

Each test series considered a single constant contact pressure combined with three axial loads (applied as stresses). The range of axial loads ensured that crack initiation and friction behaviour could be studied in micro slip. No additional fretting fatigue parameters were influenced for this experimental programme, as this would have inhibited the findings of the current investigation. Details of the each test series are presented in the tables 3.3-3.5

Table 3.3 Details of Experimental Program for 500 Test Series

Test No.	Contact Pressure (MPa)	Axial Stress (MPa)	Test Duration (Cycles x10 ³)	Percentage of Estimated life	Estimated Life (Cycles x10 ³)
501	80	60	200	20	1000
502	80	60	400	40	1000
503	80	60	600	60	1000
504	80	80	80	20	400
505	80	80	160	40	400
506	80	80	240	60	400
507	80	100	20	20	100
508	80	100	40	40	100
509	80	100	60	60	100

Table 3.4 Details of Experimental Program for 600 Test Series

Test No.	Contact Pressure (MPa)	Axial Stress (MPa)	Test Duration (Cycles x10 ³)	Percentage of Estimated life	Estimated Life (Cycles x10 ³)
601	100	80	120	20	600
602	100	80	240	40	600
603	100	80	360	60	600
604	100	100	40	20	400
605	100	100	160	40	400
606	100	100	240	60	400
607	100	120	20	20	100
608	100	120	40	40	100
609	100	120	60	60	100

Table 3.5 Details of Experimental Program for 700 Test Series

Test No.	Contact Pressure (MPa)	Axial Stress (MPa)	Test Duration (Cycles x10 ³)	Percentage of Estimated life	Estimated Life (Cycles x10 ³)
701	120	100	120	20	600
702	120	100	240	40	600
703	120	100	360	60	600
704	120	120	80	20	400
705	120	120	160	40	400
706	120	120	240	60	400
707	120	140	20	20	100
708	120	140	40	40	100
709	120	140	60	60	100

Analysis of the surface scars of the fretted specimens was conducted using SEM imaging techniques to identify cracks. This technique has been successfully employed by Pape and Neu [7] to determine some of the characteristics of the fretting fatigue process. The results of the crack initiation study and the friction forces, recorded during the experiments are presented in Chapter 5.

3.4.3 The Effects of Contact Zone Size

For Hertzian type contact geometries the development of friction is influenced by the size of the contact area [38]. However, the effects of increasing the pad size for sharp corner contact geometries were not apparent, the friction model used to calculate an experimentally based friction coefficient does not take true area into account. Area is only considered when the surface load is a pressure and pressure is a function of area. Therefore, if the total contact load is determined as a pressure at the surface, then the area the pressure is acting over becomes a consideration. In the case of a single contact load applied to two different contact areas, the pressure at the surface will be dependent on the area and result in two different friction forces. However, if the contact load is recalculated for each area then the theoretical model should predict the same friction response.

This may not be the case as studies of fretting fatigue often take into account the dynamic slip/stick boundaries, and consider friction on a local, as opposed to a global basis. Therefore, larger contact zones may influence the location of the slip/stick boundary, which will affect the friction response. Furthermore, the contact stiffness influences the partial slip hysteresis loop by affecting the friction range values, as

friction has a direct influence on fretting, the size effect may well affect the crack growth process for partial slip friction conditions.

Consequently, the friction response may vary for identical contact pressures applied to different contact zone sizes. Conversely, as friction is a function of contact pressure and the contact pressure for sharp corner geometries focuses towards the edges of the contact region, larger contact zones may not necessarily induce variations in the friction response. The presence of the pressure concentration at the edges dictates the peak friction response and not the central contact area between the edges. Therefore, the size of the central area may not have an effect on the peak friction condition. The affects of contact zone size on friction response and fatigue lives is studied in the second experimental programme.

3.4.3.1 Experimental Programme No.2 - 800 Test Series

The contact pad size was increased to 3mm and the experiments were run until the specimen failed. Failure was achieved when the crack growth resulted in a catastrophic break through the entire cross section of the specimen, which provided fretting fatigue lives. The test series was conducted with three contact pressures and five axial stresses. The experiments were arranged so that each contact load was repeated for three axial stresses. The details of the loading configurations are summarised in table 3.6.

Table 3.6 Details of Experimental Program for 800 Test Series

Test No.	Contact Pressure (MPa)	Axial Stress (MPa)
801	80	80
802	80	60
803	80	100
804	100	80
805	100	100
806	100	120
807	120	100
808	120	120
809	120	140

The fatigue lives were recorded on the cycle counter, which was set to trip if the axial displacement of the top actuator achieved a specific magnitude. This displacement coincided with the failure of the specimen, therefore halting the test and the counter, which logged the cycle number at which the displacement and failure occurred.

The fatigue lives and friction forces recorded during the experiments are presented in Chapter 5.

3.4.4 Controlling Slip and Friction

The experimental programmes 1 and 2 have focused on the initiation of fretting fatigue cracks and the development of friction, as well as the effects of geometry on friction and total fatigue life. The study of friction has therefore been based on the response of the applied loading conditions. As the test rig was designed with the capability of controlling slip displacement at the contact surface, some investigations were conducted into the effects of controlling slip and examining the effects of slip amplitude on friction.

By controlling the vertical displacement of the contact pads it was possible to control the magnitude of the slip, which has a direct influence on the friction force, generated at the contact surface. When the contact pad is displaced in phase with the same magnitude as the specimen then the relative motion between the surfaces is zero, and there is no friction. If the contact pad is displaced either out of phase or at a different magnitude to the specimen surface then both surfaces will move relative to each other and a friction force will be generated. Figure 3.11 illustrates the relationship between contact pad displacement and the generation of friction forces.

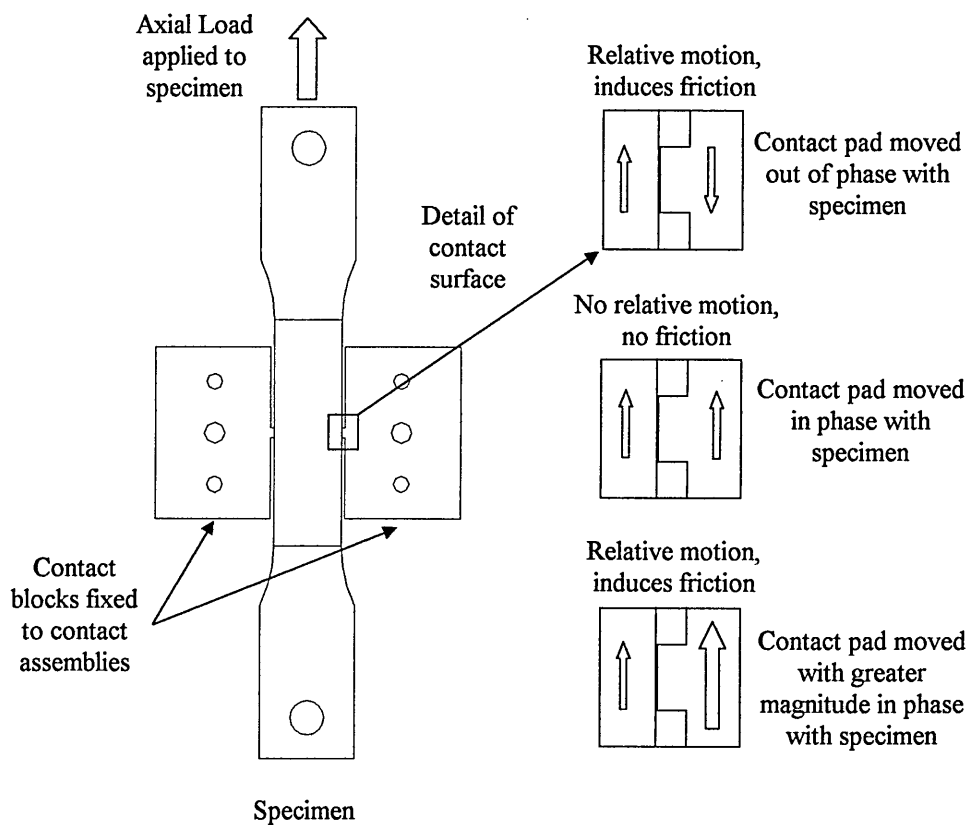


Figure 3.11 The effects of controlled contact pad displacement of friction

Therefore, varying both the phase angle and magnitude of slip it was possible to isolate friction and study the effects on the fatigue lives of the specimen in the third experimental programme.

3.4.4.1 Experimental Programme No. 3 - 900 Tests Series

The elastic beam was displaced both in phase and 90° out of phase with the specimens oscillatory axial load. This was achieved using the second input of the function generator, which allowed the axial load signal to be altered in both magnitude and phase angle. The magnitude of slip at the contact pads was calibrated with the lower actuator input load signal. Figure 3.12 presents the calibration results for the lower actuator load and the slip displacement at the contact pads.

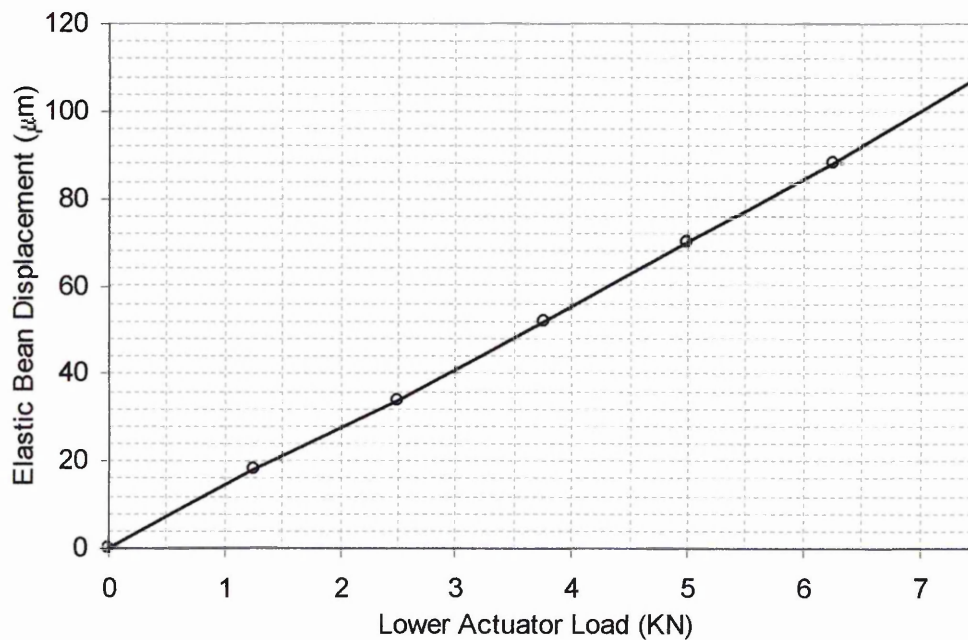


Figure 3.12 Slip Displacement Calibration Chart

Of the nine experiments in the test series, three were run with a zero phase angle, and an equivalent slip magnitude to the specimen, this resulted in the contact pad moving relative to the specimen surface under load and generated a near zero friction condition. Three experiments were set at a zero phase angle with a greater magnitude of slip displacement than the specimen surface under load and the final three experiments were

set to run out of phase by 90° with an intermediate slip displacement magnitude. Figure

3.13 illustrates the two phase angles used in the test series.

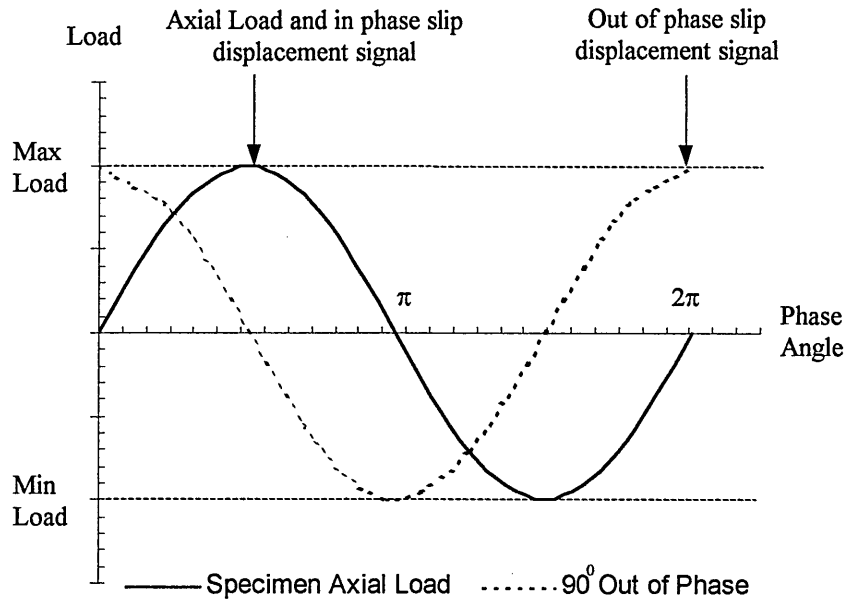


Figure 3.13 Load Signal Arrangement

All experiments were run until failure of the specimen occurred to obtain the fatigue lives under these controlled slip conditions. Table 3.7 lists the experiments with the applied loads, phase angles and controlled slip displacements. .

Table 3.7 Details of Experimental Program for 900 Test Series

Test No.	Contact Pressure (MPa)	Axial Stress (MPa)	Phase angles (degrees)	Slip Displacement (μm)
901	100	100	0	70
902	100	100	0	10
903	100	100	90	20
904	80	100	0	70
905	80	100	0	10
906	80	100	90	20
907	120	100	0	70
908	120	100	0	10
909	120	100	90	20

The fretting fatigue lives were recorded with the use of the cycle counter. The axial load signal and friction strain gauge readings were also recorded at set intervals; the results are presented in Chapter 5.

CHAPTER 4

NUMERICAL ANALYSIS

4.1 INTRODUCTION

The study of fretting fatigue requires many analytical tools in the pursuit of further understanding this phenomenon. Finite element method is a technique, which has been used to study fretting fatigue with varying levels of complexity. The level of complexity is dependent on the requirements of the respective research programme. The application of finite element method, to the fretting fatigue problem, has focused on the determination of stress fields in the vicinity of the contact and the accurate depiction of load transfers and friction force profiles. The collective analysis of these parameters provides a method of understanding and predicting the effects of fretting fatigue.

An advantage of using finite element method is that it provides the opportunity to study relatively complex geometries. It provides a method of analysing engineering arrangements, which have previously been difficult using analytical techniques alone. The accurate use of analytical techniques is limited to Hertzian and Hertzian derived structures. The potential to study difficult contact arrangement justifies the use of finite element method despite the limitation generally associated with this technique.

The finite element code used to perform the fretting fatigue analyses was ABAQUS Standard 5.7, developed by Hibbitt Karlson and Sorenson [1]. This programme offers a powerful contact modelling facility, which provides the tools capable of modelling sharp corner fretting fatigue geometry. Contact models have been developed based on the sharp corner fretting fatigue experiments performed by Fernando *et al* [75] for the 1.27mm contact pad size. Models have also been developed for the 3mm pad size contact pads used for the current experimental programme. The two pad sizes have been modelled as having geometrically sharp corners and the development of the models has focussed on the accurate prediction of frictional shear stress distribution across the contact surface. As the experiments do not provide stress results directly, friction provides the only comparable parameter between experimental and numerical analyses. Therefore, compatibility of the numerically determined friction and the friction generated as a result of experimentation for the same geometry and loading conditions, would suggest that the stress fields are also comparable. The development of numerical contact models capable of accurately predicting friction and stresses in the contact region is detailed in this chapter.

FATIGUE

Fretting fatigue occurs when contacting bodies are subjected to an oscillatory tangential load. The load results in a dynamic slip system at the contact surface, which generates a specific frictional shear stress profile. The continued application of this load system induces a wear rate that alters the contact surface, which in turn affects the friction shear stress profile. This dynamic situation leads to the formation of micro-cracks at the surface, typically at the slip/stick boundaries, and in the case of sharp corner contact, at or near, the edges of the contact pad. This multi-axial stress system at the contact is highly complex and dependant not only on the magnitude and frequency of the applied loads, but also on the geometry, relative stiffness between the contacting bodies and rate of surface wear. Typical analyses have focused on the Hertzian and Hertzian type contact [9, 14, 19, 23, 29-31, 54-61, 64, 76], that can be analysed considering the pressure distribution that can be obtained by Hertzian analysis. However, relatively few works [20, 37, 62] attempted to analyse flat on flat contact arrangements involving sharp corners due to the difficulties in predicting the pressure distribution. Sharp corner contacts generate a stress singularity because of the infinite pressure gradient at the edges.

Due to the stress singularity, all stresses at the sharp corners are infinite, thereby producing anomalous results. Investigation of this particular fretting phenomenon requires an accurate method of analysing sharp corner contact geometry as well as simulating the complex load and surface interactions exhibited under fretting fatigue. Finite element method offers a technique of simulating this condition whilst operating with assumptions that result in an approximate solution. The accuracy of this solution

can be improved to create a method of effectively simulating a fretting fatigue system. The finite element solution affords the opportunity to study the sub surface stress field generated as a result of contact and fretting, which may be used to predict fatigue lives for those geometries that prove difficult to analyse using conventional methods. Swalla and Neu [28] postulated that the nucleation regime is located within approximately 50 μm of the contact surface. This is followed by a secondary regime where the continued crack growth is influenced by sub surface stresses and friction forces between 50 – 200 μm .

The finite element code ABAQUS [1] offers a series of functions for modelling contacting surfaces. Based on element or node pairs, the contact functions vary with the intended application. The element option is primarily suited to three-dimensional application, where relative displacement occurs in two dimensions. In the case of plane stress or plane strain problems, the analysis can be simplified to a two-dimensional model, where the relative displacements occur in only one dimension. Contact node pairs are considerably more effective in terms of computational efficiency and functionality. The contact node pair option has both a *slave* and *master* surface, which is defined by the stiffness of each contacting body. Stiffness is a function of both the material property and geometry of each body. The contacting body that has the highest stiffness is classified as the *master* surface, with the less stiff contacting body classified as the *slave*. This contact arrangement can be applied in three variants (finite sliding, small sliding and infinitesimal sliding) depending on the relative and rigid body displacements of the intended problem.

In the case of the experimental fretting fatigue assemblies, the contact displacements are small (in the order of microns) and relative to the size of the contacting surfaces and as

such, the rigid body displacements are often negligible. For this case, the *small sliding* option provides the most efficient contact solution based on no rigid body displacement and small relative displacements. Figure 4.1 illustrates the relationship between the *slave* and *master* surfaces of a contact problem using contact node pairs.

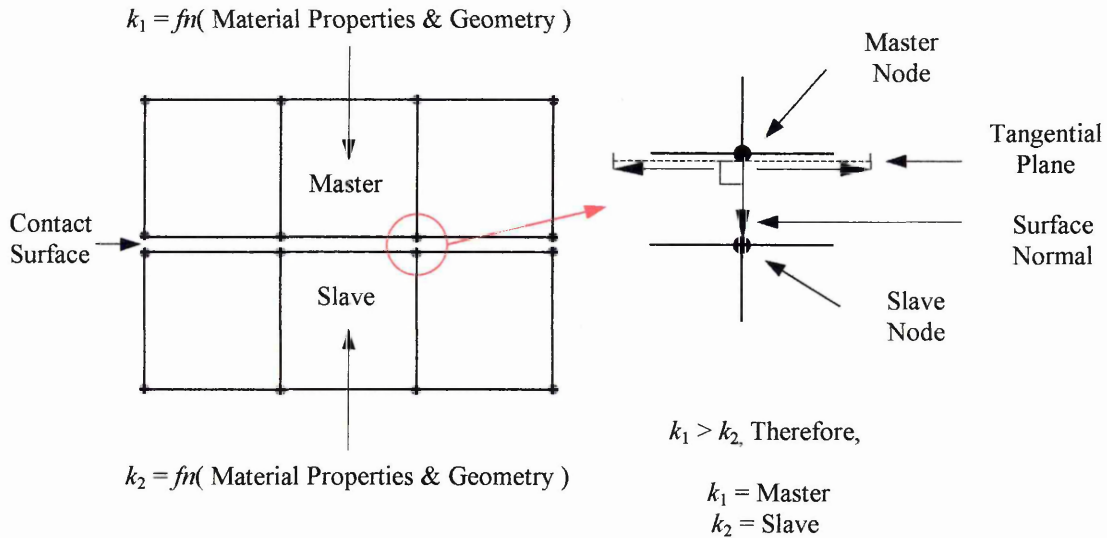


Figure 4.1 A finite element representation of a contact surface, requiring a master and slave surface

Displacements are relative to each contact pair, so that during the analysis the contact nodes on the *slave* surface identify with the closest node on the *master* surface. These pairings result in a calculated normal from the *master* surface to the *slave* surface. The maximum tangential displacement of each node on the *slave* surface is then determined from a relative tangential plane. This plane is based upon the average element length across the *master* surface and the centre occurs at the normal generated between the contacting surfaces for each node pair. This is repeated for each node on the *slave* surface and provides contact results for friction and slip displacements at each *slave* node position. This simulation of contact allows ABAQUS [1] to interpret the friction forces generated at each node position along the contacting surfaces and as such, provide an accurate representation of surface and sub surface stress fields.

Analysis of the stress fields provides the opportunity to determine the effects of contact and friction on the sub surface stresses. Sub surface stresses are useful to predict fretting fatigue lives. A localised maximum stress is insufficient and high values of stress must be sustained over a characteristic volume in order for initiation to take place. Araujo and Nowell [64] discussed the definition of a critical layer for characterising the microstructural state of materials. They suggested that this critical layer is a constant for a specific material and could be related to microstructural dimensions such as grain boundaries. In order to achieve this, the stresses generated from the finite element model need to reflect the most severe fretting situation. Therefore, it is only necessary to analyse the load cycle at the peak stress condition.

Friction is considered as a principal contributor to the nucleation of fretting cracks, and therefore, friction is considered to significantly influence fatigue life. Extreme fretting is attributed to high friction forces. Consequently, simulations based on a single cycle of the most severe friction generated during a fretting fatigue life will produce the most probable sub surface stress fields for nucleating cracks. ABAQUS [1] operates on the classical Coulomb's friction theory in which friction is determined as a function of pressure (or loads normal to the contacting surface) and a coefficient (μ). This coefficient is typically determined through simple experiments. However, as the initial fretting period is transient and surface degradation is dynamic, the friction coefficients obtained from simple tests are no longer applicable. Swalla and Neu [28] observed a higher friction coefficient during partial slip than during gross sliding. Furthermore, the friction coefficient is the result of tests conducted in global sliding and as previously discussed (Chapter 1) fretting can occur during partial sliding, which is the focus of this study. Harish and Farris [31] observed an increase in the friction coefficient during the first few hundred cycles, which then reached a stable value for the remainder of the

experiment. Therefore, a fretting friction coefficient (μ_f) is required that accounts for the changes between the contact surfaces during fretting fatigue and is applicable for partial sliding problems. As the finite element models need to simulate the most severe friction condition, a friction coefficient determined from fretting fatigue experiments was used to generate a true fretting friction. The current analyses were performed with a value of $\mu = 1.5$ as this represented the maximum μ achieved in fretting experiments. This value of μ was also confirmed by Swalla and Neu [28].

ABAQUS [1] applies the Coulomb friction law at each contact node pair. Therefore, friction force is determined as a function of the global fretting μ and the local surface pressure at that point. Sliding occurs for each pair only when equilibrium and the limiting friction are satisfied. This results in a localised friction response with the opportunity to study slip behaviour across the contact surface even under a micro slip condition.

Based on the above assumptions it was necessary to develop a finite element model capable of analysing a sharp corner contact geometry subjected to micro slip to investigate the sub surface stress distributions.

4.3.1 Mesh Design and Element Type

The finite element models were based on the experimental sharp corner contact arrangements. The models were developed using two dimensional plane strain theory and were constructed using linear four-noded elements, for computational efficiency as well as accuracy. A linear shape function provided the necessary geometric shape to represent the sharp corner.

Several mesh configurations were attempted to generate elements that were small enough to accurately represent the contact surface. Due to the number of elements required in the contact region and the size of the structure, which needed to be modelled, attempts to bias the mesh (gradually reducing the element size with distance focusing on the contact area) proved ineffectual. The resultant mesh was composed of either too many elements to effectively run the analysis, or resulted in element aspect ratios that reduced the accuracy of the model. Therefore, an alternative modelling method was required to achieve a suitable mesh density with an aspect ratio, which did not affect the accuracy of the results. A description of the mesh is presented in section 4.5 and 4.6.

The linear elements chosen for the mesh were run with full integration. Although ABAQUS [1] provides the option of reduced integration, which generates a single interpolated result acting at the centre of each element and reduces the computational effort, full integration was necessary due to the versatility offered by this method. Full integration provides results for all integration points of each element, in the case of

linear elements four results were generated for each of the four integration points. These additional result locations provided improved accuracy when interpolating near the micro slip/stick boundaries at the sharp contact corners. Furthermore, analyses of the stress fields around these areas were improved, as significantly large variations between element stresses would have resulted in unacceptable inaccuracies.

4.3.2 Elastic Material Properties

Although fretting fatigue generates highly localised plasticity at the sharp corner regions [28], due to the stress singularity caused by the theoretical infinite pressure distribution gradient, the general state of stress throughout the majority of the model is elastic. Therefore the influence of plasticity was considered negligible for analysis purposes. This was confirmed when the results of models run with elastic/plastic properties were compared with the results of models run with elastic properties. The study showed little difference in the general stress state throughout the majority of the model. Therefore, the models were run with linear elastic material properties and interpreted using Neuber's analysis [77]. The material properties used for the analysis are presented in section 3.3.1.

4.3.3 Load Cases

To effectively simulate the multiaxial load system that occurs during fretting fatigue, both the normal load (which applies the contact pressure) and the oscillatory specimen stress, applied by the axial load (which controls slip and friction) were applied in two steps. The load steps were arranged sequentially so that the sinusoidal axial load (applied in the second step) was initiated when the contact pressure was applied

(through a ramp input in the first step). This ensured that the contact pressure remained constant throughout the cyclic axial load step. The contact force was applied to the elements along the top edge (AB , figure 4.2) to simulate the steel contact pad loading. The mesh density, in this case, controls the contact pressure distribution. The axial load was applied uniformly to the elements along the specimen surface (PQ , figure 4.2). Figure 4.2 illustrates the load locations and load steps.

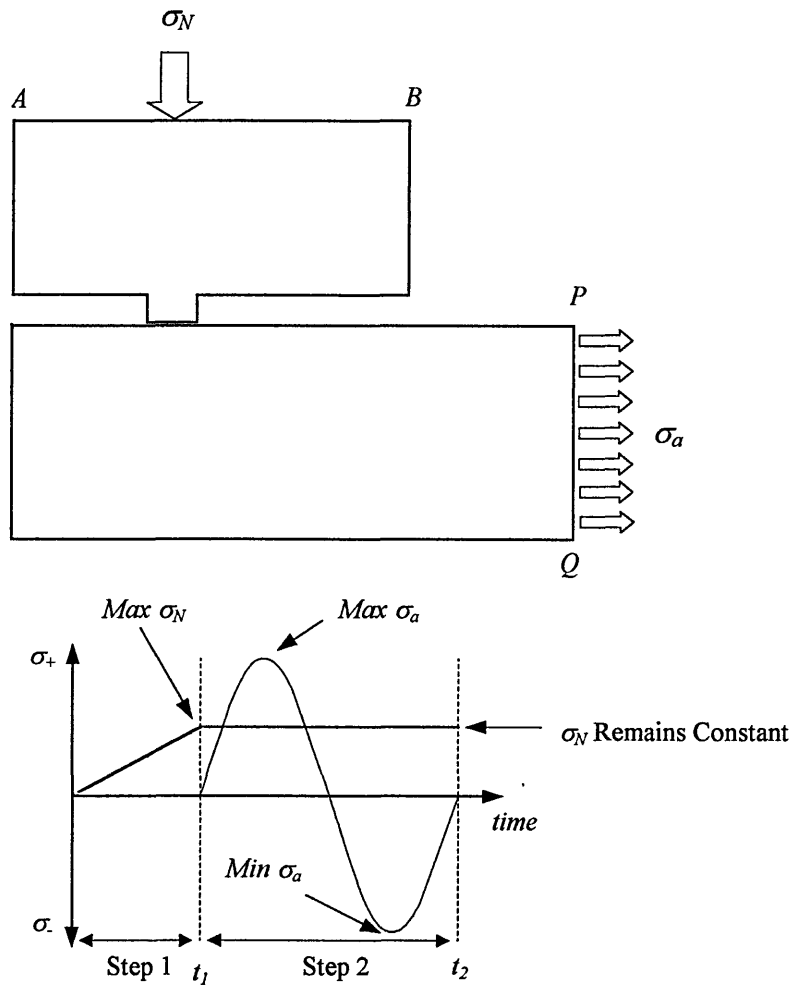


Figure 4.2 Finite element load arrangement to simulate contact and axial load

The current model simulated the fretting fatigue configuration used in experiments. However, the models often failed to achieve equilibrium and resulted in solution divergence, which lead to severe discontinuities. Study of the solution anomaly,

suggested that the reason for the severe discontinuities was due to the interpretation of the contact surface at the sharp corners at the contact pad. The mesh in the region of the contact corners responded uncharacteristically, often leading to the separation of the surfaces and severe deformation. Figure 4.3 illustrates the deformation at the contact corner region using conventional modelling techniques.

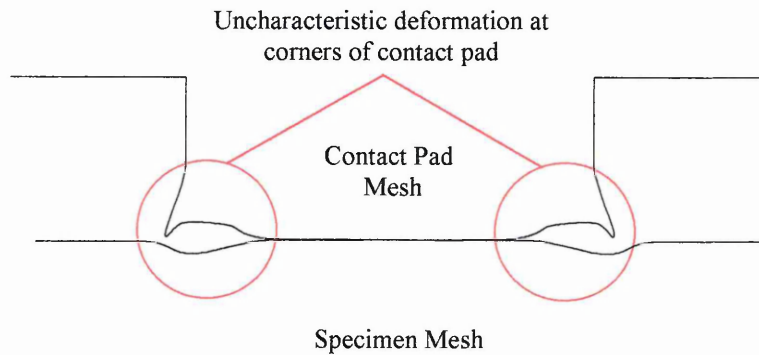


Figure 4.3 Detail of mesh deformation in contact corner region

Furthermore, limitations on the model mesh densities generated results that were inaccurate and attempts to improve accuracy by increasing the density resulted in analyses requiring high computational effort. Therefore, the finite element models were refined to improve accuracy and a method was developed to overcome difficulties associated with the sharp corners at the contact surface.

4.4 FINITE ELEMENT MODEL REFINEMENTS

The finite element models were improved by increasing the mesh density at the contact surface, while maintaining computational efficiency as well as implementing a method of controlling the contact surface to account for the sharp corners of the contact pad.

4.4.1 Element Sizing

In finite element method, it is important to clarify the distinction between an accurate model and the accuracy of the results. A model may be correct in terms of the applied assumptions and modelling criteria, but the results may be inaccurate due to mesh over simplification. It is therefore crucial to the accuracy of the results that the correct element size is used. In the case of the initial fretting fatigue models developed here, over simplifications of the mesh resulted in an inaccurate representation of surface pressure and the friction and stress results were affected.

An element size was required to accurately represent the pressure distribution observed from sharp corner contact. Studies conducted on varying mesh sizes suggested that elements approaching grain size (approximately 12-16 μm) generated accurate contact stress fields. Furthermore, since the stresses are not considered to vary through the grain an element threshold size was established based on the average grain size for the material. An Investigation of element size in contact analysis was performed by Sawalla and Neu [28] the conclusions from this work confirm the observations with element size and accuracy. Figure 4.4 illustrates the relationship between element size and accuracy. As the element size decreases the values of peak pressure and friction force increase. This continues until the peak pressure and friction force reach values that do not significantly change with further reductions in element size. Figure 4.4 shows that this occurs when the element size is reduced to approximately 15 μm , which coincides with the material grain size. Therefore, the mesh was designed to provide an element size at the contact surface that was equivalent to the grain size of 2024 - T351 aluminium alloy.

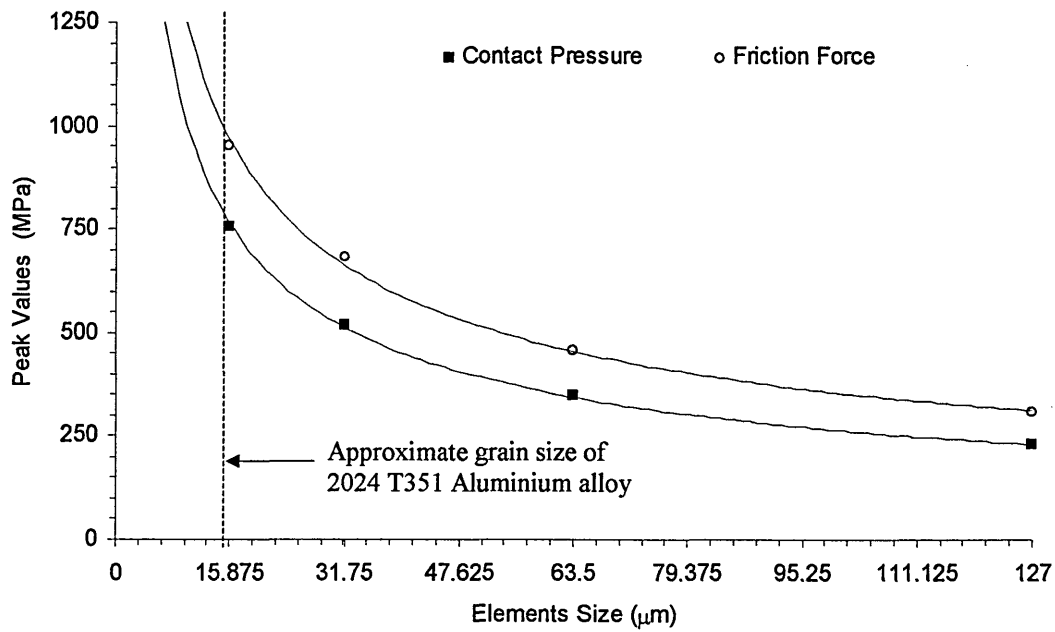


Figure 4.4 The results of the peak friction force and contact pressure values with element size

4.4.2 Sub Modelling to Increase Accuracy

Sub modelling was used to increase the accuracy of the models and attain the required element size at the contact surface without significantly increasing the computational effort. Sub modelling is a technique used in finite element method to improve computational efficiency by running relatively coarse mesh models of the full geometry, which then provide the nodal displacement results necessary to drive the boundary of a sub model. This offers the opportunity to determine a second boundary closer to areas of interest within the full model. The sub model can then be run with an increased mesh density to acquire results that are more accurate. Also, this can be implemented more than once so that multiple sub models can be generated to ensure the required accuracy. This is achieved by increasing the mesh density of each subsequent sub model and reducing the geometric area. Figure 4.5 illustrates the original geometry and the first sub

model used in the analysis. This method was repeated several times to create new sub models until the required element sizes were achieved.

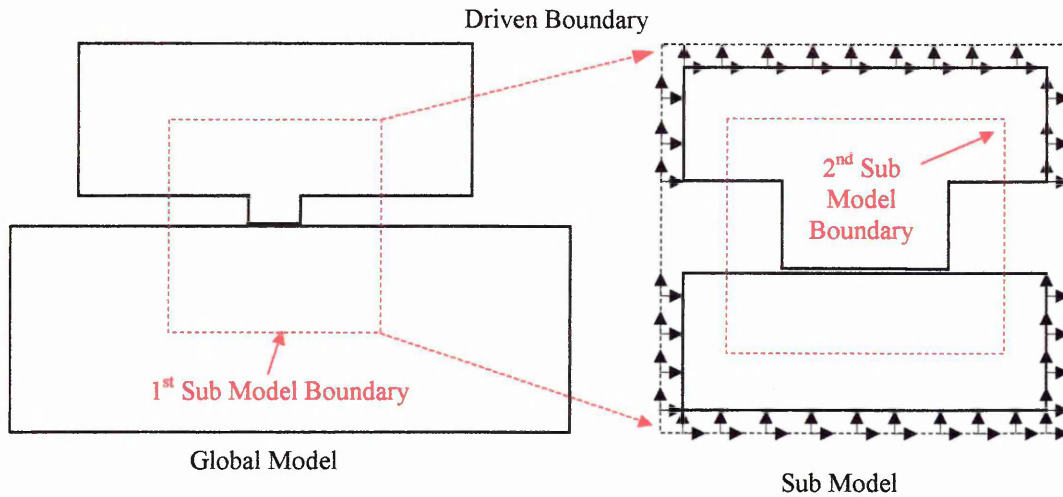


Figure 4.5 Illustrates the boundaries used to create the first sub model, this then provides the second boundary to create the next sub model.

The sub model boundary nodes are assigned interpolated displacements based on the polynomial shape function of the global analysis. Due to this interpolation, it is important to ensure that there is a 2:1 ratio of sub model nodes to global model nodes. A larger ratio generates inaccuracies in the interpolation and solution convergence is affected. This limitation on mesh density improvement was reflected in the choice of boundary position to ensure the correct element size was achievable. Each sub model used contained approximately 23 – 25 thousand elements, over half the area focusing around the contact surface. This resulted in a series of models that sequentially reduced the element size by 50% to achieve a general element size which approximated to an average estimated grain size of the 2024 - T351 aluminium specimen. Figure 4.6 illustrates the location of the sub model driven boundary and the reduction ratio required to achieve solution convergence.

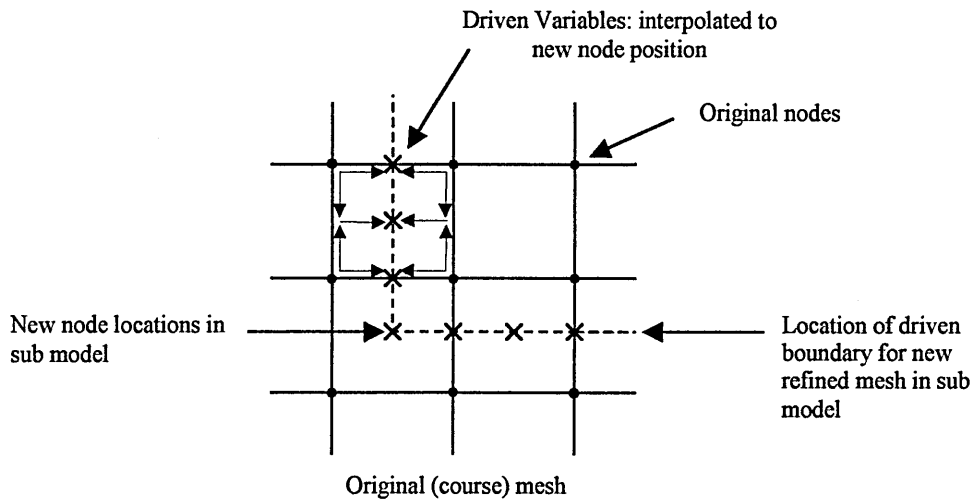


Figure 4.6 Location of boundary for sub model illustrating the required reduction ratio of 2:1

4.4.3 Sharp Corner Contact Modelling

The influence the contact pressure distribution has on fretting fatigue is evident in the friction profile generated at the contact surface. Geometries incorporating flat contacts with sharp corners generate pressure distributions with infinite stress gradients at the contact edges. These singularities do not occur in a real system and as such the finite element model is required to simulate the real conditions.

In real contact stress singularities do not occur because the material yields at the edges of the contact with highly localised areas of plasticity. However, because these regions of plasticity are small in comparison to the surrounding geometry the general state of the geometry is elastic. Therefore, a method was required to represent the contact elastically with sharp corners but without generating a stress singularity. Initial sharp corner contact modelling attempts resulted in severe anomalies when modelling with conventional techniques. The contact surfaces deformed uncharacteristically at the corners, leading to inaccurate results and in many cases the analysis failed to converge

in equilibrium. Many variants were attempted to overcome the sharp corner problem with varying degrees of success.

The difficulty was associated with the way ABAQUS [1] modelled the contact interface, in that the nodes of the contact pair at the corners of the contact pad generated a surface normal with a resultant vector at 45° . The subsequent vector did not align well with the orthogonal surface and as such the *slave* nodes were displacing in an uncharacteristic manner. Figure 4.7 illustrates the contact node pair definition at the corners of the contact pad.

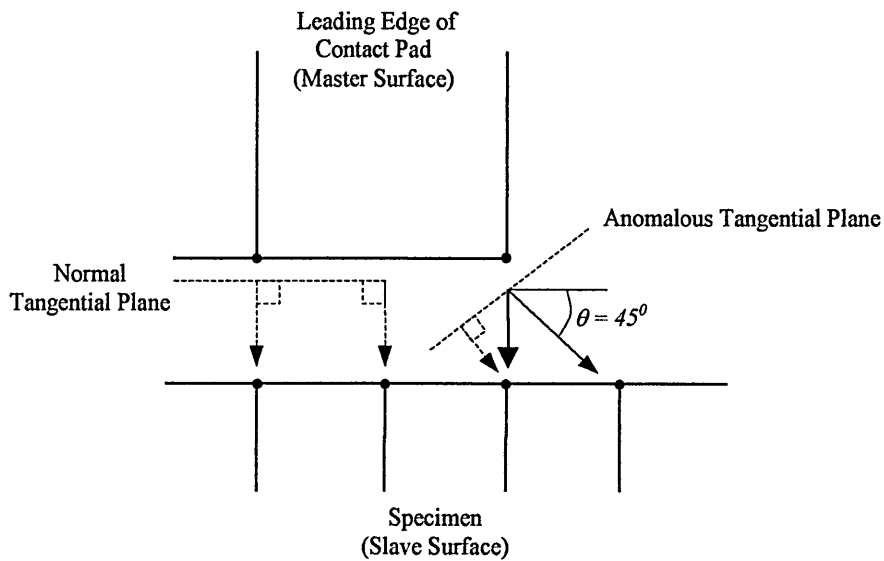


Figure 4.7 Contact node pair definition at the corners of the contact pad exhibiting anomalous tangential plane.

Improvements to the models contact surface definition yielded a method of modelling the sharp corner problem. A symmetry command available to contact modelling provided a way of manually adjusting the normal vector for each node pair. The command was intended for use with contact at symmetry planes to ensure that the contact surface recognised the symmetry and operated as a continuous surface. With the

aid of direction cosines it was possible to realign the normal vector to coincide with the relevant *slave* nodes, thus solving the anomalous contact surface behaviour. Studies of models run with corrected normal vectors resulted in significant improvement in the model response during loading. The solutions achieved convergence and the severe deformation observed in the conventional contact models was absent in the corrected vector models.

4.5 MODELLING OF THE 1.27MM PAD SIZE EXPERIMENTAL ARRANGEMENT

The refined finite element models were capable of representing the sharp corner contact geometry and provide accurate friction and stress results. In order to ascertain the validity of the models it was necessary to simulate an existing experimental arrangement. Consequently, a finite element model was developed to represent the experimental arrangement conducted by Fernando *et al* [75]. The experimental programme was conducted with a 1.27mm steel contact pad arranged in a bridge configuration on either side of a 2024 - T351 aluminium specimen. The programme covered several pad spans at different contact pressures and axial loads. To determine the validity of the numerical solution, the contact geometry for the 16.5mm pad spans was recreated and subjected to a selection of load combinations. Table 4.1 shows the chosen load cases for the finite element model and the elastic material modulus used for the analysis.

Table 4.1 Load and material data for 1.27mm pad size models

Test No.	Contact Pressure (MPa)	Axial Stress (MPa)	Aluminium Properties (GPa)	Steel Properties (GPa)
126	20	70	72.4	209
127	80	70	72.4	209
134	120	70	72.4	209
133	40	100	72.4	209
122	60	100	72.4	209
124	80	100	72.4	209
132	100	100	72.4	209
125	120	100	72.4	209
148	20	125	72.4	209
128	80	125	72.4	209
130	120	125	72.4	209

4.5.1 Symmetry and Boundary Conditions for the 1.27mm Pad Size

To model the experimental arrangement, symmetry was utilised to reduce the computational effort. The model was sectioned in two planes; the first plane was created along the specimen's neutral axis due to the symmetrical position of both contact pad bridges. This assumed identical loading for both contact bridge assemblies, which conformed to the requirements of the original experimental program [75]. The second plane sectioned the geometry through the centre of the contact bridge, perpendicular to the first symmetry plane, with the assumption that the pad symmetrically distributed the contact load, thereby resulting in identical pressure distributions for each pad. This effectively quartered the geometry that needed to be modelled. Figure 4.8 illustrates the geometry, mesh density and loading locations for the global model. The sub models reduced the geometric area by 50% and focused on the contact region

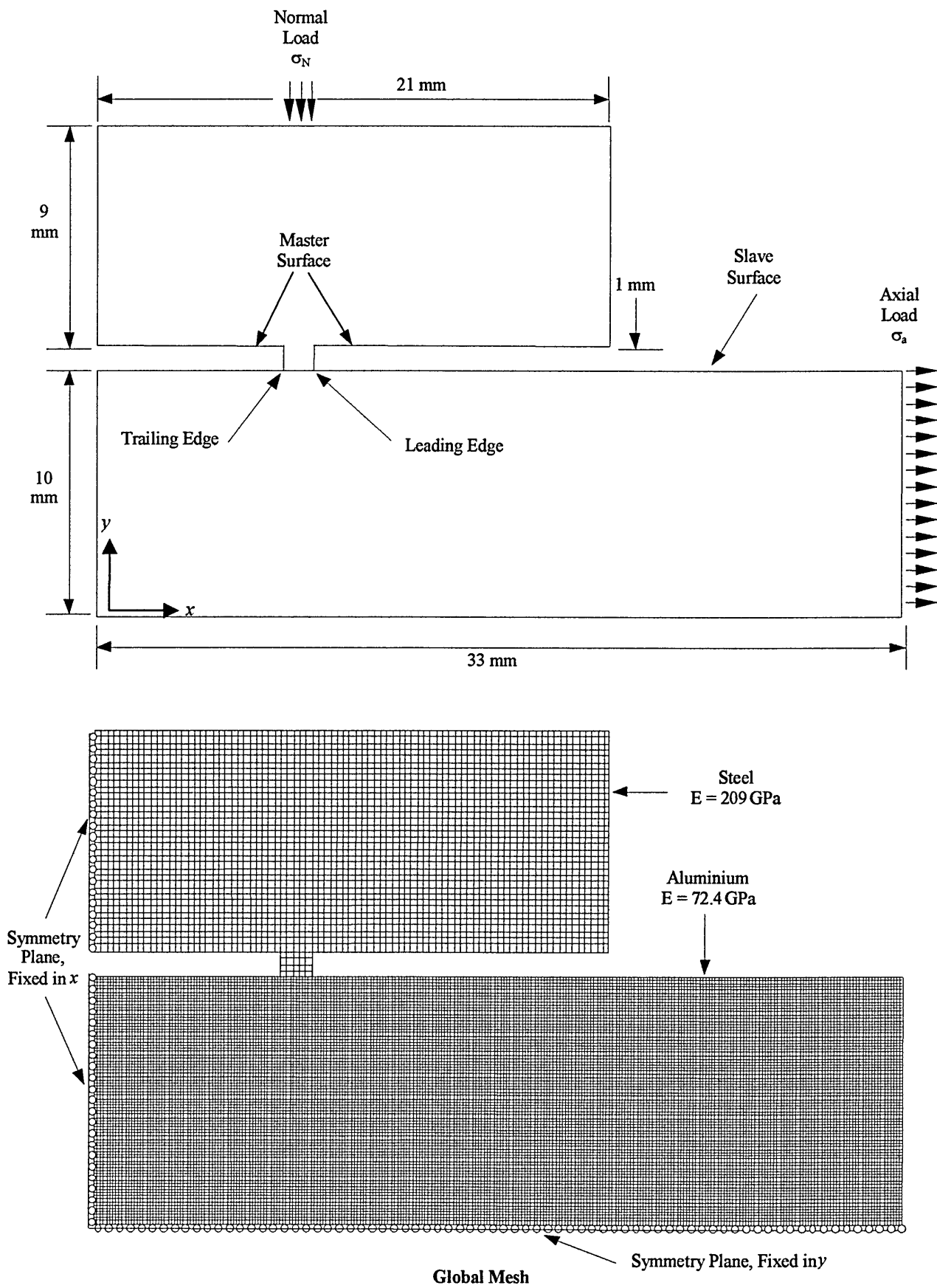


Figure 4.8 1.27mm pad size finite global element model

Boundary conditions were set along the symmetry planes with fixed displacements perpendicular to the plane of symmetry. This condition then simulated the remaining geometric sections of the model providing the relevant stiffness for an accurate model response. The load magnitudes were recalculated for symmetry and positioned to reflect the experimental set-up. The material properties were chosen to represent the experimental arrangement and are presented in Chapter 3. A sample program is provided in Appendix B. The partitioned geometry was modelled using a total of 23465 elements with a ratio of 2:1 at the contact surface in favour of the aluminium. This resulted in a relatively coarse mesh with an average element size at the contact surface of 0.127 mm or 127 μm . Therefore, sub modelling was employed to generate a new model with a refined mesh based on the half dimensions about the contact region. This process was repeated three times until the elements representing the aluminium specimen approached the approximate grain size. Table 4.2 lists model data for each analysis.

Table 4.2 Model data for 1.27mm pad size models

Model	Number of Elements	Element Size at Contact Surface (mm)
Global	23465	0.127
Sub Model 1	23525	0.0635
Sub Model 2	23765	0.03175
Sub Model 3	24725	0.01587

The results of the analyses are presented in Chapter 5 and Appendix D.

4.6 MODELLING OF THE 3MM PAD SIZE EXPERIMENTAL ARRANGEMENT

Models were also constructed for the larger 3mm pad size experimental arrangement. The results from the large contact pad models offered the opportunity to determine the effects of size on the friction forces and sub surface stresses by comparing the results for both pad sizes. Therefore, finite element models were created to simulate the experimental test series 800. However, due to differences in the experimental assembly between the 1.27mm pads size results obtained by Fernando *et al* [75] and the current experimental set-up used for the 3mm pad size results, new boundary conditions were required. Table 4.3 lists the load and material data used in each analysis, were the specimens were modelled with the aluminium properties and the contact pad was modelled with the steel properties.

Table 4.3 Load and material data for 3mm pad size models

Test No.	Contact Pressure (MPa)	Axial Stress (MPa)	Aluminium Properties (GPa)	Steel Properties (GPa)
801	80	80	72.4	209
802	80	60	72.4	209
803	80	100	72.4	209
804	100	80	72.4	209
805	100	100	72.4	209
806	100	120	72.4	209
807	120	100	72.4	209
808	120	120	72.4	209
809	120	140	72.4	209

4.6.1 Symmetry and Boundary Conditions for the 3mm Pad Size

The modelling of the 3mm pad size experimental arrangement used only a single symmetry plane along the specimen's neutral axis. Due to the position of the contact pads and that both pads exerted the same load, the assumption that both contact

conditions were identical in terms of magnitude and position was valid. However, because of the single contact pad configuration used during these tests the contact block assembly was modelled without symmetry and so an alternative boundary condition was required to accurately account for the stiffness of the contact assembly. The actual experimental structure located the contact pad by a vertical strut, which was in turn attached to a beam that was stationary. For the purpose of the finite element models, the structure was assumed to be fixed. Furthermore, each contact pad block was attached to four horizontal beams, which carried the contact load. Both beams and strut displaced to provide contact pressure and friction force generated at the contact interface.

The entire assembly could have been modelled at additional computational expense. However, to avoid this additional modelling, spring elements were used to simulate the stiffness of the contact assembly. Each element operates as an elastic linear spring with a user defined stiffness value. The elements displace when loaded with a force acting along the plane of the spring's orientation. In the case of the fretting fatigue model it is the reaction force generated by friction at the contact surface. Therefore, controlling the spring stiffness controls the frictional response of the model. Consequently, the contact assembly has been modelled with a series of spring elements along the edge of the contact block (figure 4.9). Each element was defined with a linear elastic stiffness value that was validated by comparing the numerical friction response of a single load case with the corresponding experimental friction force. As the contact assembly did not change during testing, the spring element stiffness was set for all the models. Figure 4.9 illustrates the 3mm pad size models, mesh, boundary conditions and load locations

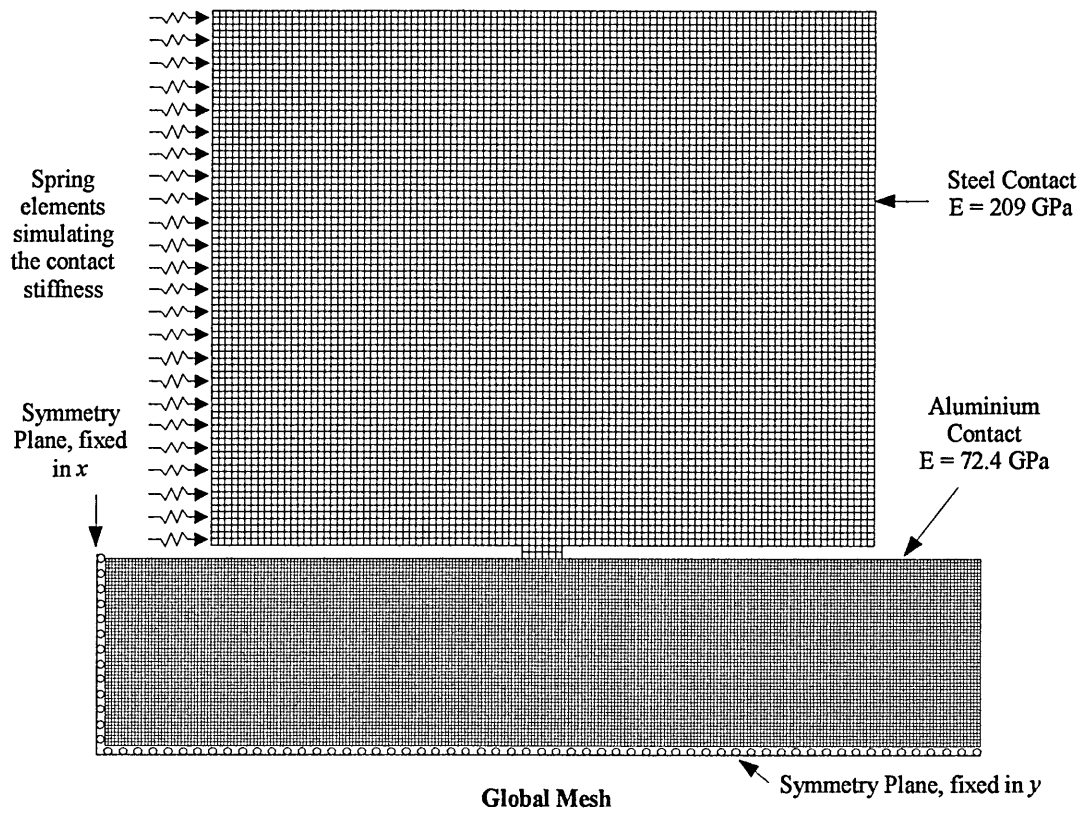
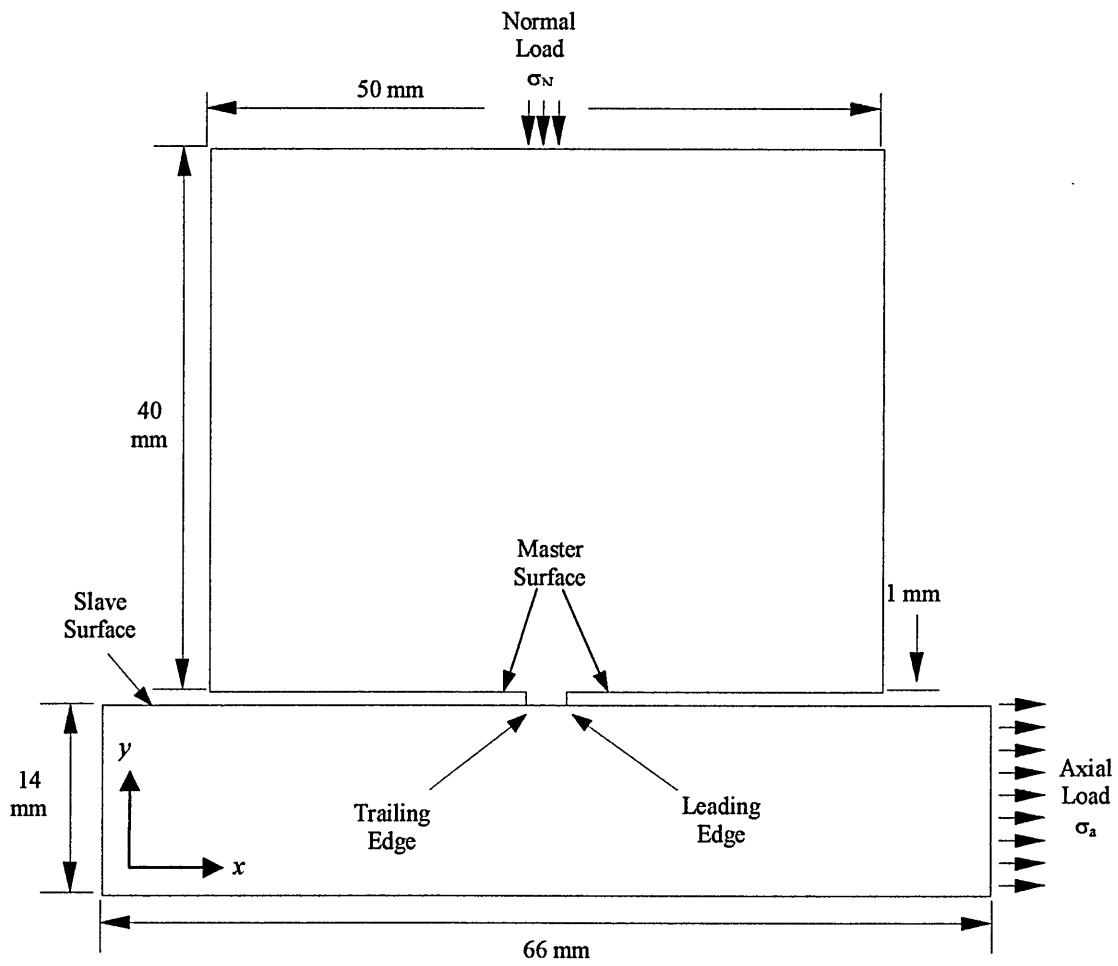


Figure 4.9 3mm model geometry and mesh diagram for global model

The same material data was used from the previous analyses and the loads were recalculated for symmetry. The contact load was calculated as a pressure to simulate the loading between the contact block and contact pad interface. An example program is presented in Appendix B.

The geometry was modelled with 22796 elements adhering to the stipulation of a ratio of 2:1 at the contact surface in favour of the aluminium specimen elements. This produced a global model with an average element size at the contact surface of 0.25mm or 250 μ m. Therefore, four sub models were required to achieve elements that approached the approximate grain size of 2024-T351 aluminium alloy at the contact surface. Table 4.4 lists the number of elements and size for the aluminium specimen mesh for each model.

Table 4.4 Model data for 3mm pad size models

Model	Number of Elements	Element Size at Contact Surface (mm)
Global	22796	0.25
Sub Model 1	22832	0.125
Sub Model 2	22976	0.0625
Sub Model 3	23552	0.03125
Sub Model 4	25856	0.015625

The friction force and stress results for the final sub model are presented in Chapter 5 and Appendix D.

CHAPTER 5

RESULTS

5.1 INTRODUCTION

The results from the experimental and numerical programmes are presented for both the 1.27mm and 3mm contact pad sizes. The experimental results include the recorded friction forces, measured at set intervals during the test, as well as the study of initial crack growth and fretting fatigue lives. The numerical results include the predicted friction forces and stress distributions in the region of the flat contact. The predicted friction forces are compared with the experimentally recorded friction results to determine the accuracy of the numerical solutions.

5.2 EXPERIMENTAL RESULTS

The experimental programme has included the study of fretting fatigue crack initiation as well as the effects of altering the contact zone size on the friction force and fatigue lives. The programme also included the study of controlling slip displacements on friction force and fatigue life. The results of the experimental programmes are presented in the following sections

5.2.1 The Results of the Fretting Fatigue Crack Initiation Study

The experimental study of fretting fatigue crack initiation has provided results on the behaviour of friction during the initial crack growth period, as well as visual evidence of dominant fretting cracks. The friction results include the cyclic friction force measured in response to the axial load at set intervals during the test (frictional hysteresis loops) and the friction force amplitudes measured throughout the duration of the tests. An examination of the fretting scar was conducted to determine at what percentage of the fatigue life dominant fretting cracks could be visually identified.

5.2.1.1 Frictional Hysteresis Results (500-700 Experimental Series)

The cyclic friction responses measured during axial load have resulted in frictional hysteresis loops in all tests. The extent of the hysteresis is dependent on the type of contact interaction (micro slip or macro slip) and the magnitudes of the contact pressure and axial loads. The friction hysteresis loops were assessed by certain criteria to determine the influence contact pressure and axial load had on the development of

friction during different periods of the fretting fatigue life. The friction hysteresis loops were assessed on three criteria:

- The maximum and minimum friction force achieved during each load cycle.
- The rate of change in friction force with changes in axial load. This provides the gradient of the hysteresis loop, which is an influential factor in the determination of the peak friction values.
- The type of contact interaction can be determined from the shape of the hysteresis loop. In macro slip, the peak friction forces occur before the peaks in the axial load cycle. Therefore, the hysteresis loops exhibit a gradient change, which results in a near constant friction force during the peak periods of the load cycle (figure 5.1). This gradient change signifies the maximum and minimum achievable friction for that particular load combination. Hysteresis loops in micro slip do not exhibit this sudden gradient change and although the contact surface does not achieve global relative motion, local relative displacements are present. The extent of the areas of local slip is associated with the width of the micro slip hysteresis loops. The wider the hysteresis loop in micro slip, the larger the area of slip at the contact surface. Figure 5.1 illustrates the types of hysteresis observed during fretting fatigue lives.

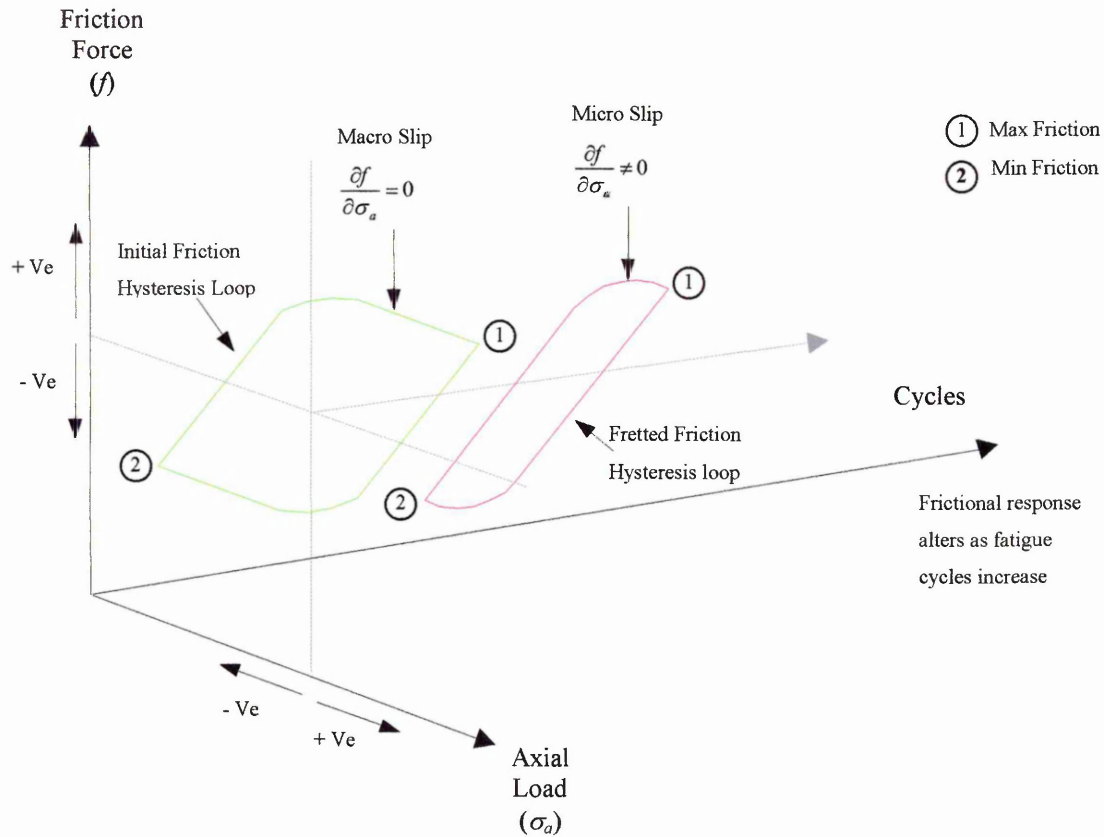


Figure 5.1 Typical frictional hysteresis response during fretting fatigue lives

The friction hysteresis results for the 1.27mm contact pad size arrangement are presented in Appendix C. Each test result includes the hystereses recorded at set intervals during the test. In the case of the 1.27mm results, the total test period represents the percentage of the estimated fatigue life for that load case.

The response of the strain gauges was measured in voltage and is proportional to the friction force at the contact surface. The friction force voltage is plotted on the y-axis against the axial load voltage, which is plotted on the x-axis.

5.2.1.2 The Response of the Friction Force Amplitude during Tests

The development of friction force during the test period is presented in figures 5.2a to 5.2c for the 1.27m contact pad size arrangement.

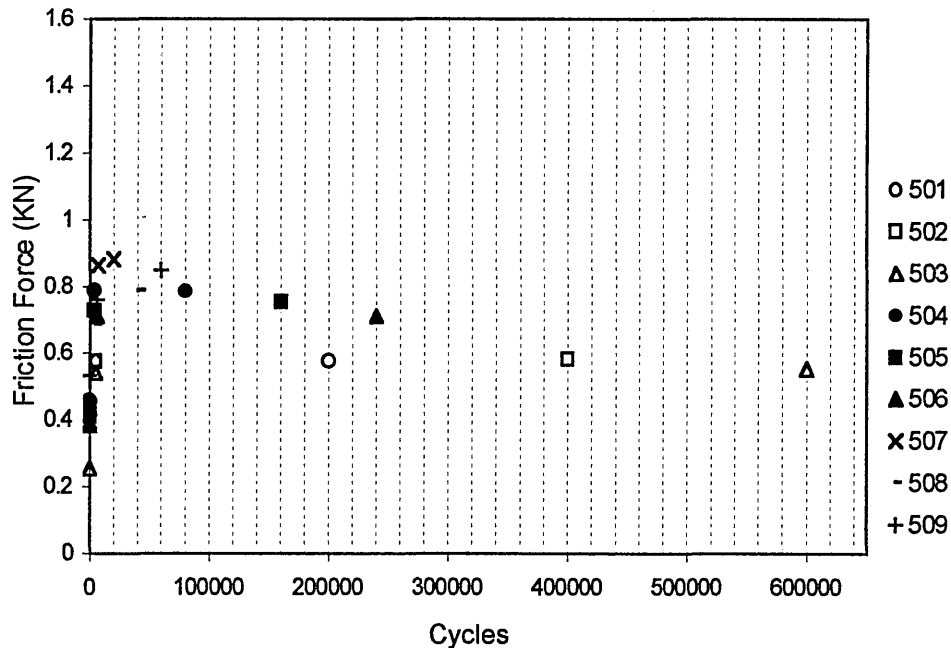


Figure 5.2a Variations in the friction amplitudes during the fatigue life for the 500 test series

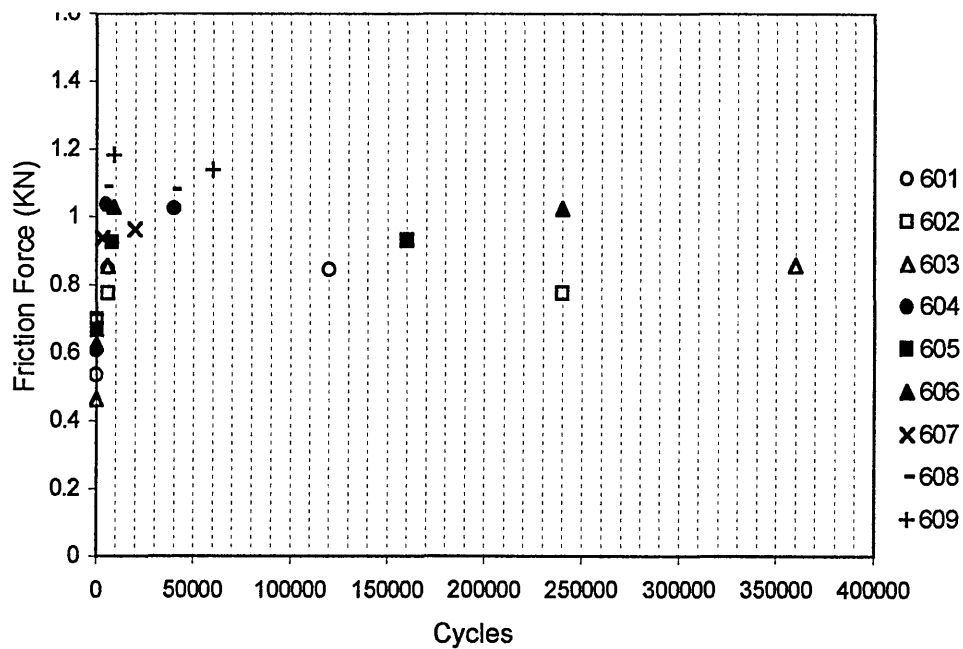


Figure 5.2b Variations in the friction amplitudes during the fatigue life for the 600 test series

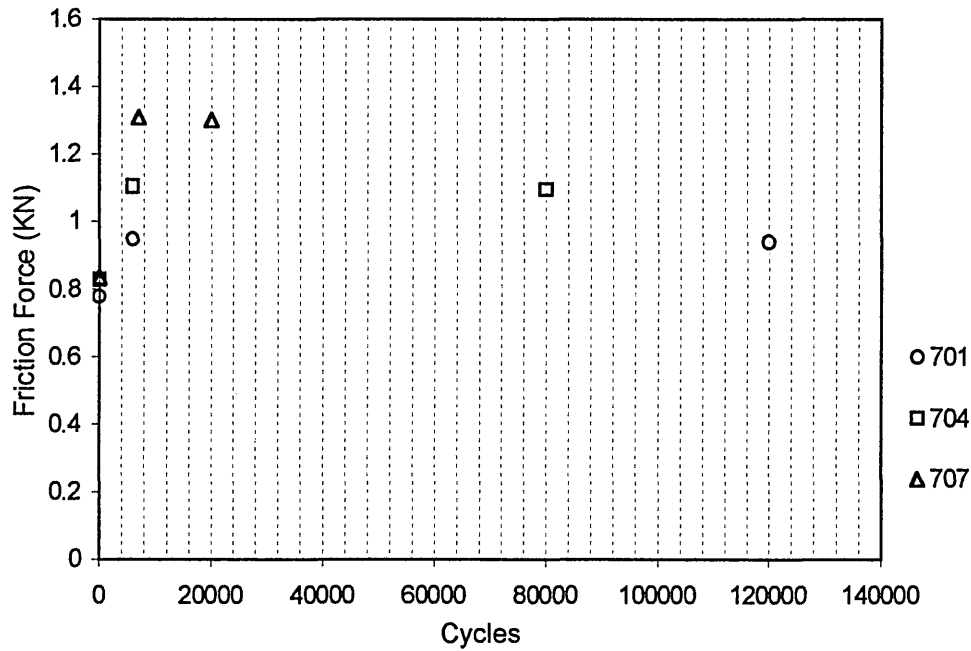


Figure 5.2c Variations in the friction amplitudes during the fatigue life for the 700 test series

The friction force amplitudes represent average values from both contact pads positioned at either side of the specimen. The friction force results for each test were taken at three points during the test period. The first friction force amplitude was obtained during the initial contact period and represents the initial friction response or the friction prior to the onset of wear. The second friction force amplitude is the maximum friction force measured during the experiment and represents the friction response during fretting. The third and final friction force amplitude represents the last recorded friction result during the test period. The friction force amplitudes are plotted against the number of cycle in each test. The number of cycles in each test is determined from a percentage of the estimated fatigue life for each load combination.

A summary of the friction force amplitudes recorded for each load case is presented in table 5.1. The table includes the friction force amplitudes at the initial, peak and final periods of the test, with the load magnitudes and test duration.

Table 5.1 Results of the friction response for 500-700 series experiments

Test No	Axial Stress (MPa)	Contact Pressure (MPa)	% of Estimated Fatigue Life	Initial Friction (KN)	Peak Friction (KN)	Final Friction (KN)
501	60	80	20	0.45005	0.57850	0.57805
502	60	80	40	0.41945	0.58285	0.58240
503	60	80	60	0.37420	0.55420	0.55370
504	80	80	20	0.46010	0.78915	0.78335
505	80	80	40	0.41305	0.75750	0.75390
506	80	80	60	0.38500	0.71735	0.71045
507	100	80	20	0.39720	0.88275	0.88210
508	100	80	40	0.45280	0.78575	0.78575
509	100	80	60	0.53495	0.87210	0.84845
601	80	100	20	0.53395	0.84775	0.84525
602	80	100	40	0.69925	0.78175	0.77535
603	80	100	60	0.46320	0.85970	0.85675
604	100	100	10	0.60725	1.03645	1.02595
605	100	100	40	0.66750	0.93295	0.92845
606	100	100	60	0.62575	1.03310	1.02455
607	120	100	20	0.66970	0.96415	0.96415
608	120	100	40	0.68945	1.08985	1.08120
609	120	100	60	0.71205	1.18335	1.13900
701	100	120	20	0.77895	0.95045	0.93920
704	120	120	20	0.82665	1.10645	1.09395
707	140	120	20	0.83510	1.31010	1.30130

Only three out of the intended nine results are presented for test series 700, due to the presence of severe fretting cracks at 20% of the estimated fatigue life, therefore, no further tests were required.

5.2.1.3 Evidence of Fretting Fatigue Crack Initiation

The visual imaging method used to identify fretting fatigue cracks has been successful in providing evidence of dominant fretting crack growth for a range of contact pressures and axial loads. The Philips XL40 scanning electron microscope was used in both the secondary electron and electron backscatter modes of imaging. By comparing both types of images, it was possible to identify cracks and distinguish between surface cracking and dominant fretting cracks.

The secondary imaging technique provided the necessary detail of the fretting scar to determine the severity of the crack relative to the surrounding surface damage. Dominant fretting cracks typically grew through the depth of the fretting scar into the specimen and the crack path was identified as growing perpendicular to the contact surface. This type of crack path has been observed in other fretting experiments [8]. To distinguish between actual dominant fretting cracks and severe surface cracks, the backscatter imaging technique provided conformation of crack depth by generating a topographical image of the scarred surface.

Due to the extensive study of the fretted specimens and the large amount of visual data generated, the results have been summarised in table 5.2. Images of the damaged surfaces are presented and discussed in Chapter 6. Table 5.2 presents the imaging data in terms of the number of cracks generated and the location of the cracks in relation to the fretting scar for each test.

Table 5.2 Fretting fatigue information for the 500-700 series experiments

Test No.	Axial Stress (MPa)	Contact Pressure (MPa)	% of Estimated Fatigue Life	No. of Fretting Cracks	Location of Fretting Cracks
501	60	80	20	1	LE
502	60	80	40	-	-
503	60	80	60	-	-
504	80	80	20	1	LE
505	80	80	40	1	LE
506	80	80	60	1	LE
507	100	80	20	-	-
508	100	80	40	-	-
509	100	80	60	-	-
601	80	100	20	2	LE
602	80	100	40	2	LE
603	80	100	60	2	LE
604	100	100	10	2	LE
605	100	100	40	2	LE
606	100	100	60	2	LE
607	120	100	20	-	-
608	120	100	40	-	-
609	120	100	60	-	-
701	100	120	20	2	LE
704	120	120	20	2	LE
707	140	120	20	2	LE

The location of the crack is denoted by the suffix, LE for the leading edge, TE for the trailing Edge of the contact pad.

5.2.2 The Results of the Contact Pad Size Study

Changing the contact pad size from 1.27mm to 3mm has provided friction force results for the larger pad size experiments as well as fretting fatigue lives. The friction results include the cyclic friction force measured in response to the axial load at set intervals during the test (frictional hysteresis loops) and the friction force amplitudes measured throughout the duration of the tests. The number of cycles to failure provides the fretting fatigue lives

5.2.2.1 Frictional Hysteresis Results (800 Test Series)

The frictional hysteresis responses for the 3mm contact pad size results are presented for each load case. The hysteresis loops are presented for the following three categories:

- The initial frictional hysteresis measured at the start of the test. The initial friction hysteresis response represents the friction response for undamaged contacts.
- The fretting friction hysteresis measured during the peak fretting period. The fretting friction hysteresis represents the friction response during fretting and includes several loops, which start as early as a few thousand cycles and continue for the majority of the fatigue life.
- The failure friction hysteresis measured at the end of the fatigue life. The failure friction hysteresis represents the friction response either proceeding or during failure.

The friction hysteresis loops are presented in Appendix C for both contact positions at either side of the specimen. The strain gauge voltage readings, which represent the friction response, are plotted against the axial load output voltage. A summary of the friction results are presented in table 5.3.

Table 5.3 Table of friction data for the 800 series experiments

Test No.	Axial Stress (MPa)	Contact Pressure (MPa)	Initial ½ Range Friction (KN)	Fretting ½ Range Friction (KN)	Failure ½ Range Friction (KN)
801	80	80	0.38485	0.91235	0.87260
802	60	80	0.58020	0.63330	0.62955
803	100	80	1.05385	1.16835	1.09230
804	80	100	0.97350	0.97350	0.89350
805	100	100	1.01020	1.16120	0.45775
806	120	100	0.83055	1.35115	0.49560
807	100	120	0.84540	1.17585	1.10550
808	120	120	1.28830	1.38465	1.38465
809	140	120	0.81280	1.62990	1.56745

5.2.2.2 The Response of the Friction Force Amplitude during Tests

The friction response during fretting fatigue lives for the 800 series experiments is presented for each load case. Figure 5.3a presents the tests conducted with a contact pressure of 80MPa. Figure 5.3b presents the tests conducted with a contact pressure of 100MPa. Figure 5.3c presents the tests conducted with a contact pressure of 120MPa. The results demonstrate the effects of fretting and wear on the average friction force amplitude measured during the fatigue life.

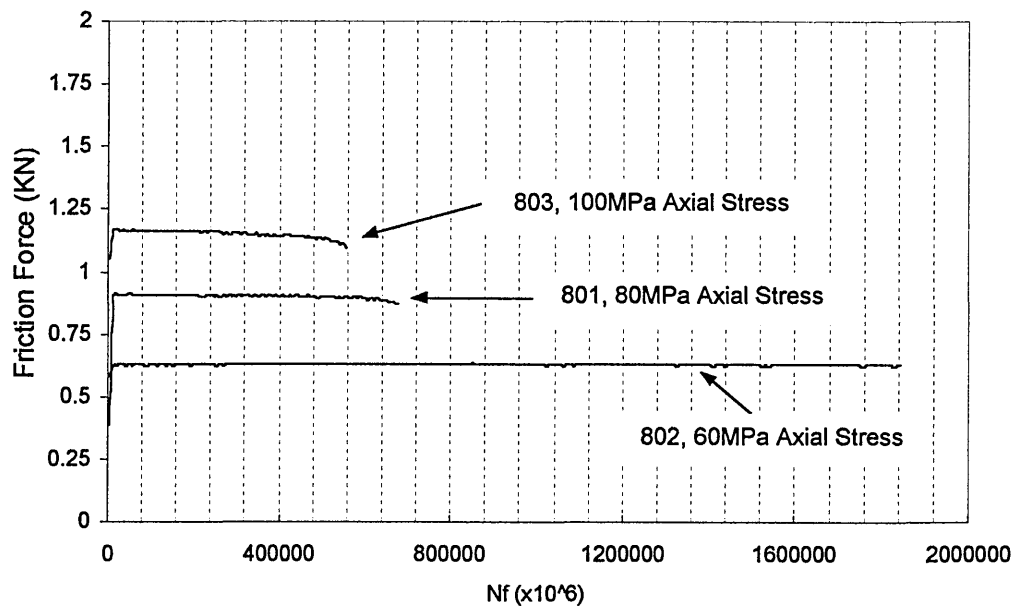


Figure 5.3a Friction response for the 3mm contact pad size experiments with 80MPa contact pressure

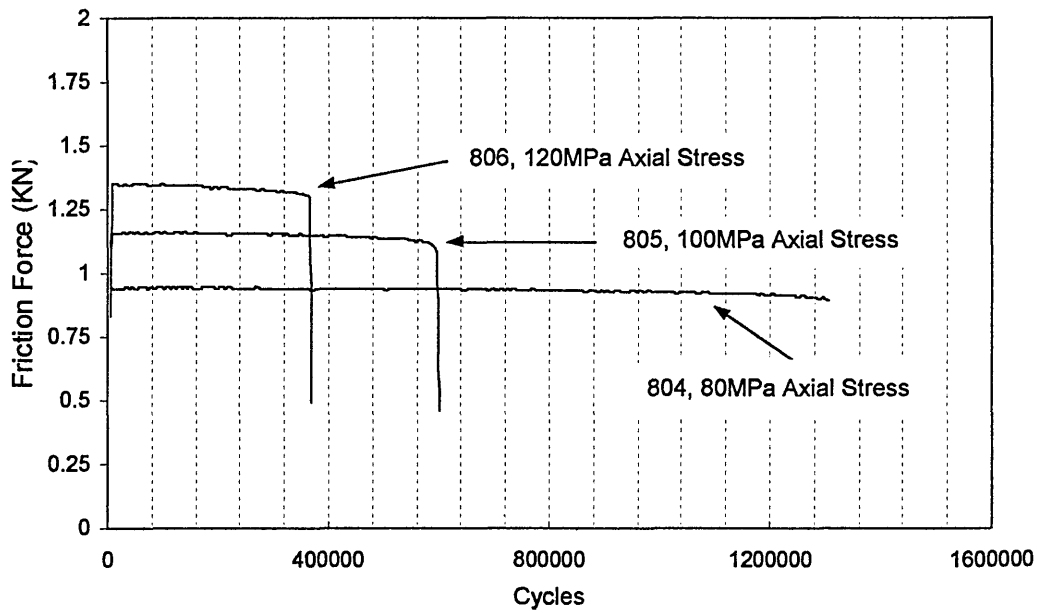


Figure 5.3b Friction response for the 3mm contact pad size experiments with 100MPa contact pressure

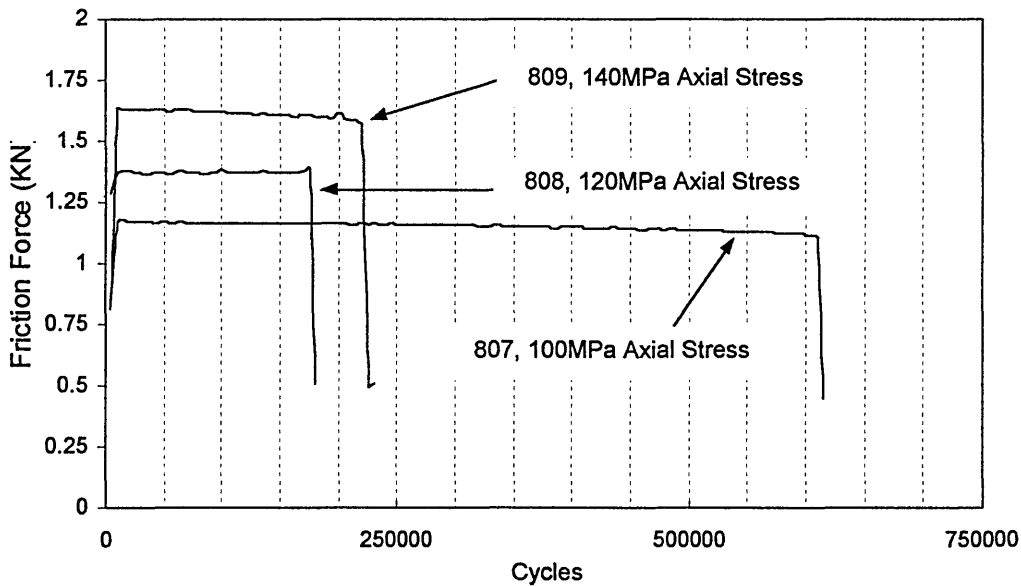


Figure 5.3c Friction response for the 3mm contact pad size experiments with 120MPa contact pressure

Table 5.4 provides a summary of the equivalent friction force coefficients determined from classical Coulomb's friction theory. The table presents the calculated friction coefficients determined at the start of each test. The initial friction coefficients represent

the non-fretting condition. (μ_{initial}). The table also includes the calculated friction coefficient during the fretting period (μ_{fretting}). The fretting friction coefficient represents the increase observed during fretting fatigue. However, the contact interactions change from macro slip at the start of the tests to micro slip during the fretting period. Therefore, the fretting friction coefficients are determined from a micro slip contact interaction and subsequently do not represent the maximum value, which can only be achieved under macro slip. The results are summarised to demonstrate the increase in the friction coefficient during fretting fatigue.

Table 5.4 Friction coefficients determined for the friction force results of the 800 series experiments

Test No.	Axial Stress (MPa)	Contact Pressure (MPa)	Initial Friction Coefficient (μ_{initial})	Fretting Friction Coefficient (μ_{fretting})
801	80	80	0.206	0.456
802	60	80	0.255	0.258
803	100	80	0.530	0.583
804	80	100	0.391	0.378
805	100	100	0.413	0.462
806	120	100	0.344	0.533
807	100	120	0.293	0.390
808	120	120	0.438	0.460
809	140	120	0.281	0.530

5.2.2.3 Fretting Fatigue Lives (800 Test Series)

The fretting fatigue lives for the 800 series experiments are defined as the number of fully reversed axial load cycles required to initiate a crack from the contact area, which achieves a sufficient size to cause failure of the specimen.

The number of cycles used to record the fatigue life is also dependent on the recording interval. Therefore, the fretting fatigue lives are accurate to within 5×10^3 cycles. The

results have been segregated based on the three contact pressures (80MPa, 100MPa and 120MPa). Each contact pressure was combined with three axial loads, resulting in a total of nine fatigue lives, presented in Figure 5.4.

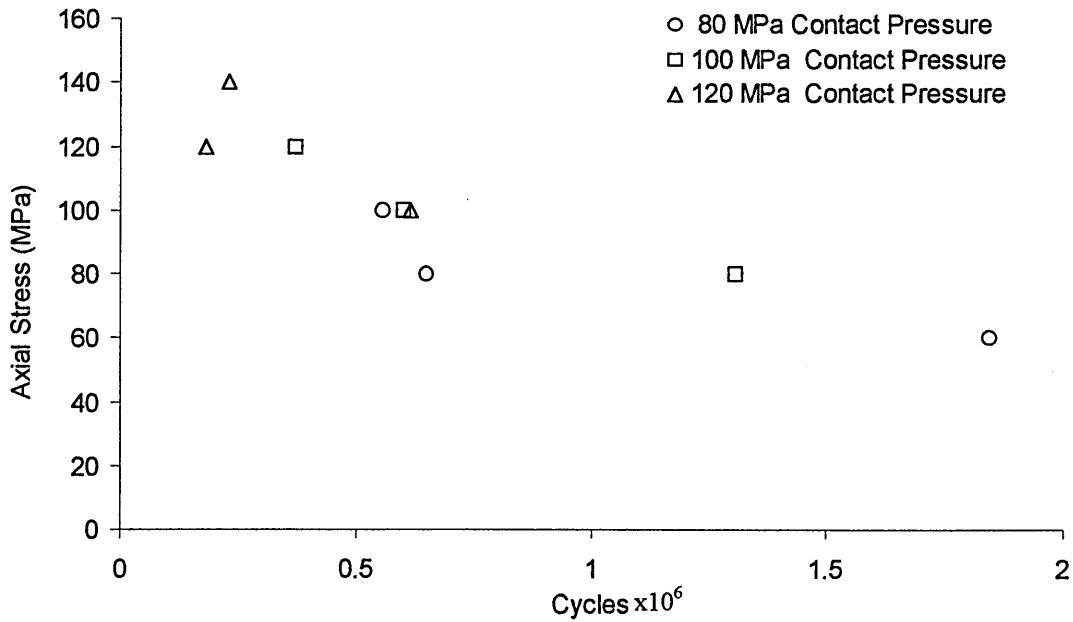


Figure 5.4 Fretting fatigue lives for the 800 series experiments

Table 5.5 provides a summary of the fatigue lives for the 800 series experiments and information on the location of the fretting cracks.

Table 5.5 Fretting fatigue information for the 800 series experiments

Test No.	Axial Stress (MPa)	Contact Pressure (MPa)	Cycles (x10 ⁶)	No. of Fretting Cracks	Location of Fretting Crack
801	80	80	0.650	1	LE
802	60	80	1.845	-	-
803	100	80	0.555	2	LE
804	80	100	1.305	2	LE
805	100	100	0.600	2	LE
806	120	100	0.370	2	LE
807	100	120	0.615	2	TE
808	120	120	0.180	2	LE
809	140	120	0.230	2	LE

5.2.3 The Results of Controlling Slip Displacements

The controlled slip displacement study has provided friction force results as well as fretting fatigue lives. The friction results include the cyclic friction force measured in response to the axial load at set intervals during the test (frictional hysteresis loops) and the friction force amplitudes measured throughout the duration of the tests. The number of cycles to failure provides the fretting fatigue lives

5.2.3.1 Frictional Hysteresis Results (900 Test Series)

Altering the slip magnitude at the contact surface in and out of phase with the axial load signal has generated the hysteresis loops presented in Appendix C. The results are presented in the revised format used in section 5.3 to provide a comprehensive review of the frictional response during the fatigue life of the experiments.

Table 5.6 presents a summary of the initial, peak and failure friction results for each load case, with the corresponding slip displacement magnitude and phase angle. All friction results represent the average friction force of both contact positions at either side of the specimen.

Table 5.6 Table of friction data for the 900 series experiments

Test No.	Axial Stress (MPa)	Contact Pressure (MPa)	Slip Magnitude (δ) (micron)	Phase Angle (ϕ) (degrees)	Initial ½ Range Friction (KN)	Fretting ½ Range Friction (KN)	Failure ½ Range Friction (KN)
901	100	100	70	0	-0.16615	-0.16615	-0.08910
902	100	100	10	0	0.70585	0.81525	0.76725
903	100	100	20	90	0.69980	1.38175	0.76725
904	100	80	70	0	-0.10645	0.12125	0.14490
905	100	80	10	0	0.78600	0.80240	0.75415
906	100	80	20	90	0.91405	1.36590	1.31660
907	100	120	70	0	-0.16330	-0.16330	-0.19485
908	100	120	10	0	0.59930	0.84375	0.81180
909	100	120	20	90	0.63345	1.41885	1.33355

5.2.3.2 The Response of the Friction Force Amplitude during Tests

The friction force amplitudes recorded during the fatigue life of the experiments have been plotted against the recorded number of cycles to failure. The results are categorised by the slip displacements and the phase angle, which is either in phase ($\phi = 0^0$) or out of phase ($\phi = 90^0$) with the axial load cycle. Figure 5.5a to 5.5c presents the friction force amplitudes for each contact pressure used.

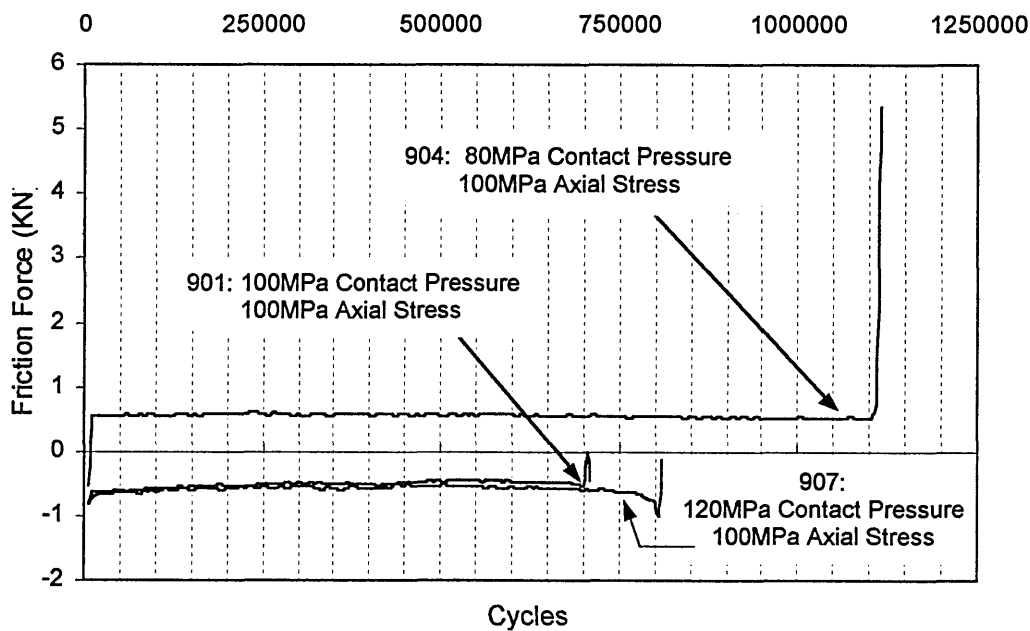


Figure 5.5a Friction force response during the fatigue life for experiments with a slip displacement of 70 μm applied in phase with the axial load ($\phi = 0^0$)

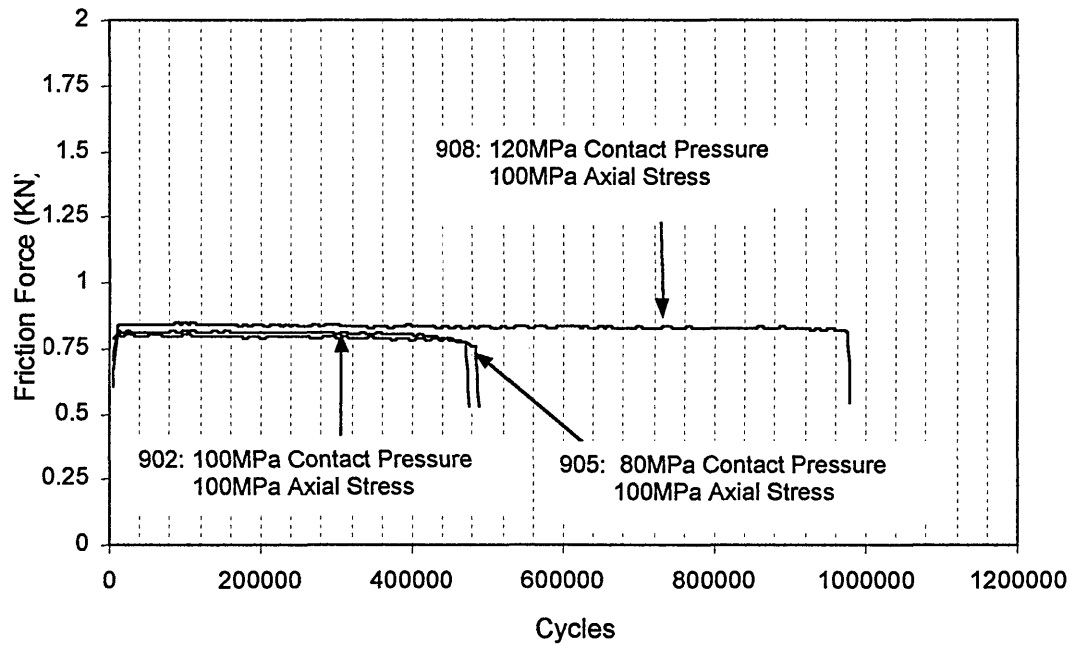


Figure 5.5b Friction force response during the fatigue life for experiments with a slip displacement of 10 μm applied in phase with the axial load ($\phi = 0^\circ$)

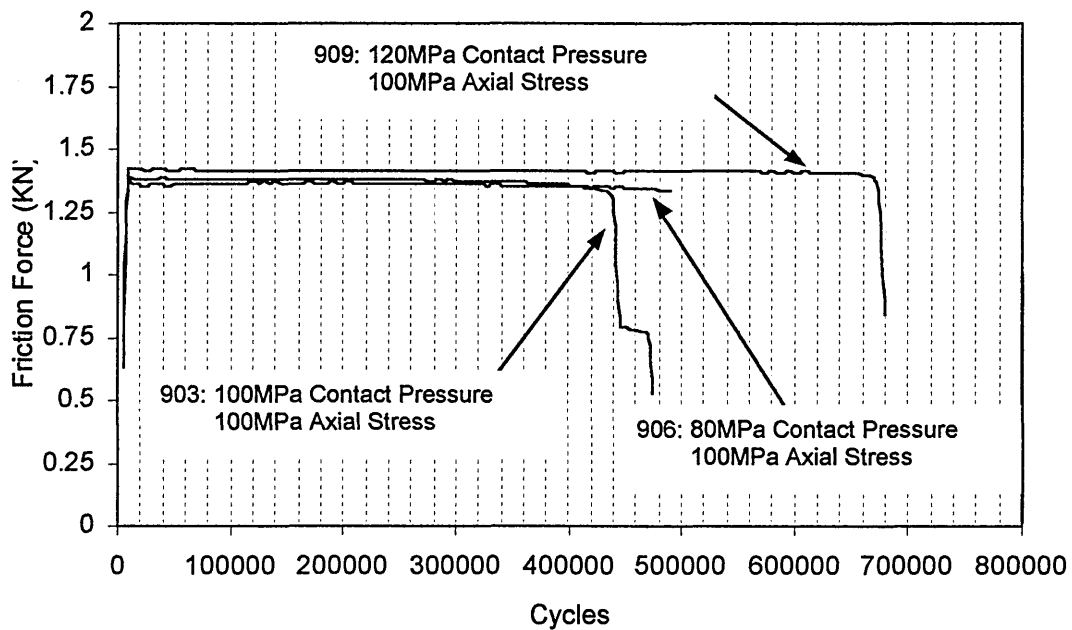


Figure 5.5c Friction force response during the fatigue life for experiments with a slip displacement of 20 μm applied out of phase with the axial load ($\phi = 90^\circ$)

Table 5.7 presents the effective fretting friction coefficients determined from Coulomb's classical theory. The table compares the initial friction coefficient (μ_{Initial}), with the fretting friction coefficient (μ_{Fretting}).

Table 5.7 The effects of fretting on the friction coefficient for the 900 series experiments

Test No.	Axial Stress (MPa)	Contact Pressure (MPa)	Slip Magnitude (δ) (micron)	Phase Angle (ϕ) (degrees)	Initial Friction Coefficient (μ_{Initial})	Fretting Friction Coefficient (μ_{fretting})
901	100	100	70	0	0.038971	0.039273
902	100	100	10	0	0.291294	0.328264
903	100	100	20	90	0.287318	0.560531
904	100	80	70	0	0.034233	0.036234
905	100	80	10	0	0.398174	0.399712
906	100	80	20	90	0.455015	0.681763
907	100	120	70	0	0.026552	0.024285
908	100	120	10	0	0.209267	0.284132
909	100	120	20	90	0.215147	0.484328

5.2.3.3 Fretting Fatigue Lives (900 Test Series)

The fretting fatigue lives from the controlled slip experiments are presented in figure 5.6. Only those tests, which failed within the agreed contact region, are presented and the fretting fatigue lives are accurate to within the recording interval (5×10^3 cycles). The fatigue lives are presented for each slip displacement and phase angle (ϕ) used.

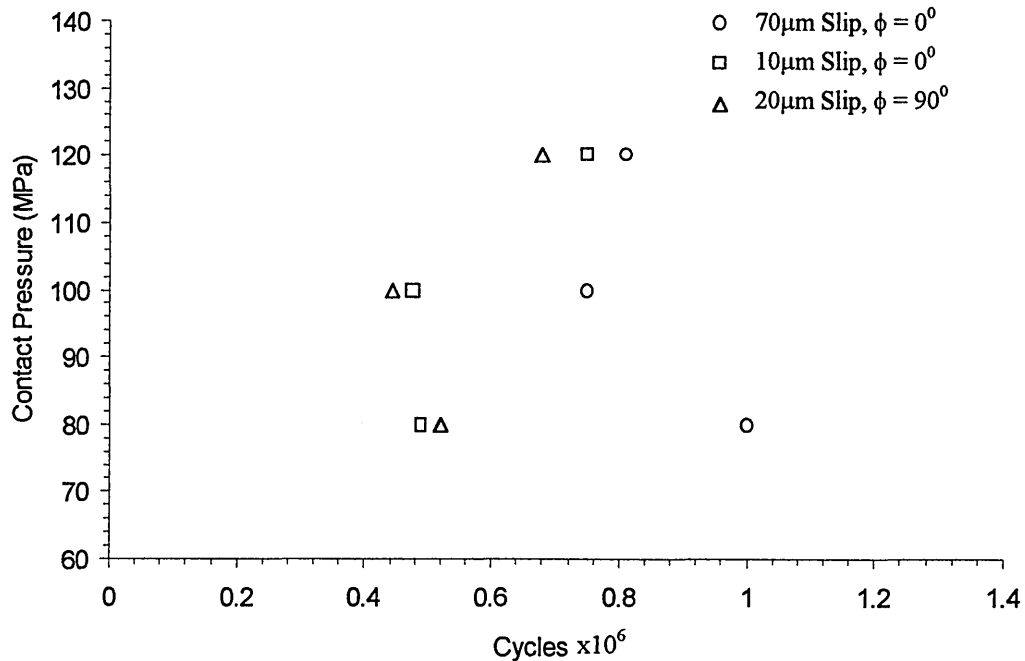


Figure 5.6 Fretting fatigue lives for the controlled slip experiments, 900 series.

A summary of the fretting fatigue results are presented in Table 5.8. The table provides information on the location and number of cracks involved in the failure as well as the fatigue lives for each load case, slip displacement and phase angle used

Table 5.8 Fretting fatigue information for the 900 series experiments

Test No.	Axial Stress (MPa)	Contact Pressure (MPa)	Slip Magnitude (δ) (microns)	Phase Angle (ϕ) (degrees)	Fatigue Life ($\times 10^6$)	Number of Fretting Cracks	Location of Fretting Cracks
901	100	100	70	0	0.750	1	LE
902	100	100	10	0	0.475	2	LE
903	100	100	20	90	0.445	2	LE
904	100	80	70	0	1.001	-	-
905	100	80	10	0	0.490	2	LE
906	100	80	20	90	0.520	2	LE
907	100	120	70	0	0.810	-	-
908	100	120	10	0	0.750	2	LE
909	100	120	20	90	0.680	2	LE

5.3 NUMERICAL RESULTS

The numerical analysis section has produced results for both contact pad sizes. Due to the absence of actual fretting fatigue life data, for the 1.27mm contact pad size experiments (experimental series 500 to 700), the numerical models have been based on the 1.27mm contact pad size experiments conducted by Fernando *et al* [75]. Sufficient data was available to develop numerical models based on the 3mm contact pad size experiments (experimental series 800).

The results were obtained from the data output files generated by ABAQUS 5.7 [1]. The output option list was used to acquire elastic stress data for the elements in the contact region. The output stresses at each integration point were averaged to generate a single stress to represent each element in the contact region. In addition to the stress data, the models also generated contact information at the surface. Each contact node pair

provided localised data on the pressure, slip displacement, contact status and friction force. The latter, was calculated from a Coulomb's friction coefficient, ($\mu = 1.5$), which was used for analyses. The numerical output data was analysed to provide comprehensive results without loss of accuracy. To ascertain the validity of the numerical results it was necessary to present the experimental friction results with the numerical predicted friction.

5.3.1 Numerical Frictional Results

Each contact node pair generated a frictional shear stress at each time increment. The number of time increments in the axial load step was controlled to ensure friction was generated at the peak axial stress points during the load cycle. Therefore, the peak friction forces were acquired for each load combination analysed.

The friction shear stress results at the contact surface were averaged and converted into an equivalent friction force. The friction forces were plotted against the axial loads to produce the numerically predicted friction hysteresis loops, which are presented for both the 1.27mm and 3mm pad sizes in Appendix D. Table 5.9 summarises the 1.27mm pad size numerically predicted friction force amplitudes. Table 5.10 summaries the 3mm pad numerically predicted friction force amplitudes. The experimental equivalent is provided for comparative reference.

Table 5.9 Friction force amplitudes for 1.27mm pad size

Test No.	Axial Stress (MPa)	Contact Pressure (MPa)	Experimental Friction Amplitude (KN)	Numerical Friction Amplitude (KN)	% Difference
126	70	20	0.37	0.308	-16.7
127	70	80	0.75	0.683	-8.9
134	70	120	0.78	0.685	-12.1
133	100	40	0.67	0.607	-9.4
122	100	60	0.70	0.846	20.8
124	100	80	0.85	0.964	13.4
132	100	100	0.90	0.973	8.1
125	100	120	0.80	0.977	22.1
128	125	80	1.00	1.107	10.7
130	125	120	1.20	1.216	1.3

Table 5.10 Friction force amplitudes for 3mm pad size

Test No.	Axial Stress (MPa)	Contact Pressure (MPa)	Experimental Friction Amplitude (KN)	Numerical Friction Amplitude (KN)	% Difference
801	80	80	0.912	1.026	12.4
802	60	80	0.633	0.738	16.4
803	100	80	1.168	1.284	9.9
804	80	100	0.974	1.026	5.3
805	100	100	1.161	1.282	10.4
806	120	100	1.351	1.540	13.9
807	100	120	1.175	1.282	9.1
808	120	120	1.385	1.539	11.1
809	140	120	1.630	1.796	10.2

5.3.1.1 Localised Friction Response during the Load Cycle

The numerical models provided a means of investigating the local distribution of friction force at the contact surface during the load cycle. Therefore, results are presented for the 1.27mm and 3mm pad sizes, which demonstrate the distribution of friction at each increment in the load step, where contact distance, friction force and axial load correspond to the global axis respectively. The resultant graphs provide a topographical image, or map, of the friction response during a single axial load cycle. Friction is presented in terms of magnitude only, providing a comprehensive

comparison throughout the load cycle where the direction of the friction force has been omitted for clarity. The local friction maps for both the 1.27mm and 3mm contact pad sizes are presented in Appendix E.

5.3.2 Numerical Elastic Surface Stress Distributions

The elastic surface stresses are presented for both the 1.27mm and 3mm contact pad sizes models in Appendix F. The stresses are plotted against position at the contact surface where the start position (0mm) represents the trailing edge of the contact pad and the final position (either 1.27mm or 3mm) represents the leading edge of the contact pad. The stresses have been determined from the peak axial load condition and therefore represent the most severe state of stress during the load cycle. The results for the 1.27mm pad size models are provided for the 100MPa axial stress case only. The shear stresses are determined from the minimum and maximum values at each node location and are presented as range magnitudes. The axial stress values represent the maximum values generated during the tensile component of the load cycle. Table 5.11 provides a summary of the location and magnitude of the peak stresses for each load case.

Table 5.11 Location and magnitude of peak stresses for the 1.27mm pad size models

Test No.	Axial Stress (MPa)	Contact Pressure (MPa)	Frictional Shear Stress (MPa)	τ_{xy} (MPa)	σ_{xx} (MPa)	Peak Friction / τ_{xy} Location
133	100	40	898.2	647.23	1096.4	LE
122	100	60	1288.0	936.77	1562.6	LE
124	100	80	1171.0	855.88	1502.0	LE
132	100	100	1204.0	877.82	1528.9	LE
125	100	120	1213.0	893.39	1593.2	LE

LE: leading edge of contact, or nodes > 76 < 82

The elastic axial and shear surface stresses are presented for the 3mm pad size results in table 5.12.

Table 5.12 Location and magnitude of peak stresses for the 3mm pad size models

Test No.	Axial Stress (MPa)	Contact Pressure (MPa)	Frictional Shear Stress (MPa)	τ_{xy} (MPa)	σ_{xx} (MPa)	Peak Friction / τ_{xy} Location
801	80	80	0.912	0.626	0.249	LE
802	60	80	0.633	0.480	0.238	LE
803	100	80	1.168	0.746	0.257	LE
804	80	100	0.974	0.638	0.299	LE
805	100	100	1.161	0.779	0.311	LE
806	120	100	1.351	0.895	0.320	LE
807	100	120	1.175	0.795	0.365	LE
808	120	120	1.385	0.931	0.373	LE
809	140	120	1.630	1.045	0.376	LE

LE: leading edge of contact, or nodes > 192 < 198

5.3.3 Numerical Elastic Subsurface Stress Distributions

As the result of further investigation into the effects of contact on the distribution of stresses, the region beneath the contact area has been analysed. The volume of the material beneath the contact is defined as the fretting region and is considered as the volume of material in which the stresses are influenced by contact. The fretting region is considered to extend to a depth of 0.5mm and stresses on planes parallel to the contact surface at set depth through the fretting region are analysed. Appendix G presents the sub surface axial and shear stresses for both the 1.27mm and 3mm contact pad size models. The subs surface stresses are plotted against the position at the contact surface. The initial position (0mm) represents the trailing edge and the final position (either 1.27mm or 3mm) represents the leading edge of the contact pad. The initial contact

depth ($\delta = 0$) represents the stresses at the surface, with each corresponding series providing the stress distributions through the depth of the fretting region.

The subsurface stress distribution through the depth of the fretting region is considered at the leading edge of the contact pad, or critical location. The results are presented in Appendix H, for both the 1.27mm and 3mm contact pad size models. The axial and shear stresses are plotted against the depth through the fretting region.

CHAPTER 6

DISCUSSION

6.1 INTRODUCTION

The results from the experimental and numerical programmes were analysed and the observed fretting fatigue friction behaviour is discussed. The analyses of the results include comparisons between the friction forces, generated from the different experimental procedures and the numerically predicted friction force from the finite element models. The numerically predicted friction force is compared against the experimentally recorded friction force to validate the numerical solution. The validated numerical solution has then been used to determine the influence of friction force on the sub surface and surface stresses in the sharp corner contact region. These stresses

obtained from the numerical analyses were used to determine an equivalent stress concentration factor for flat contacts. The stress concentration factor was used to predict fretting fatigue lives based on Neuber's analysis. The predicted fretting fatigue lives are compared with the experimental fretting fatigue lives for both the 1.27mm and 3mm contact pad sizes analysed.

6.2 FRICTION BEHAVIOUR IN FRETTING FATIGUE

The experimental study focused on the measurement of friction force during the loading cycles throughout the lifetime of the test, to determine the effects of friction force on the initial phase of fretting fatigue crack growth. The study also included two different contact pad sizes (1.27mm and 3mm) to determine the influence of contact area on the friction force and subsequently the fretting fatigue life. Furthermore, the study included the effects of controlling the slip amplitude and phase angle on the friction force. To determine the accuracy of the experimental results, the friction results were compared with the friction results from the work conducted by Fernando *et al* [75]. The friction forces from both experimental programmes were compared with the numerically predicted friction forces, to determine the accuracy of the assumptions used in the finite element models.

The friction force measured during a load cycle was evaluated by the criteria developed previously in Chapter 5. The cyclic axial loads introduce a frictional hysteresis at the contact surface, which is assessed on three basic criteria;

- The peak friction forces
- The rate of change of friction with axial load (providing the gradient of the loop)
- The shape of the hysteresis loop

The later is used to identify the type of contact interaction and determines if the friction response is in macro or micro slip.

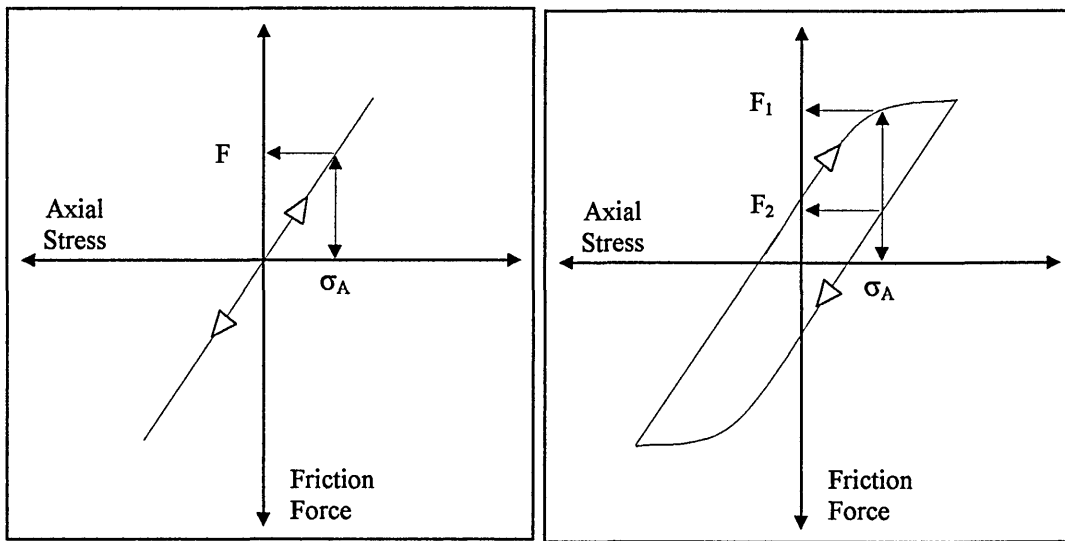
The development of friction during the fatigue life of the tests was observed by recording the peak friction forces at different intervals during the experiment (for all tests the recording increments were approximately 500 – 1000 cycles). The total test period was either a set percentage of the estimated fatigue life (this method was used in the study of crack initiation for the 1.27mm pad size) or in the case of the larger pad size experiments (the 3mm pad size) the number of cycles to failure. The peak friction forces recorded during the experiment offered the opportunity to study the rate of change of friction during the fretting fatigue life. This was in turn used with other features of the hysteresis to identify the role of friction in crack growth.

6.2.1 Frictional Hysteresis

The variation of friction force during a load cycle reveals that hysteresis occurs in all the experimental results. This demonstrates that both micro and macro slip are present in all the test results. During the load cycle, the friction force increases in response to the tangential force induced by the axial load. If the surfaces did not slip the relationship between axial load and friction force is linear and an identical friction force would be measured for the same axial load value during the load cycle (no hysteresis occurs as shown in figure 6.1a). However, when slip occurs the relationship is no longer linear and the hysteresis behaviour is shown in figure 6.1b

Irrespective of the magnitude of either the axial load or contact pressure, micro slip occurred in all the fretting fatigue tests conducted during the current experimental

programme. The greater the area of slip, the greater the difference between the friction forces for the same axial load during the load cycle. This behaviour continues until macro slip occurs, which signifies that the total area of slip is equal to the contact area and the maximum friction force is achieved. Further application of a tangential load during macro slip will result in continued sliding with no subsequent increase in friction force. Figure 6.1 illustrates the effects of hysteresis on friction force during the axial load cycle.



6.1a Without hysteresis only one value of friction force can be measured for the same axial load value during the cycle, indicating no slip has occurred

6.1b During hysteresis, two friction forces can be recorded for the same axial load value during the cycle, indicating slip has occurred

Figure 6.1 A schematic representation of the effects of hysteresis on friction force

Therefore, the presence of hysteresis in the cyclic friction response is indicative of either micro or macro slip. Analysis of the friction results reveals that both macro and micro slip occurs in all the load cases considered. The cyclic friction force results demonstrate this behaviour to varying extents. The friction responses observed in the tests exhibit two distinct loop shapes, a macro slip loop recorded at the start of the test followed by a transition to a micro slip loop, recorded during the fretting period. Once the transition has occurred the micro slip condition is maintained for the remainder of

the test. The friction response at the start of the test achieves a maximum friction force before the axial load achieves the peak values in the cycle. This induces macro slip and results in a constant maximum friction force, which does not change with increasing axial load (zero gradient). The friction response recorded during the fretting period exhibits elongated loops with no such significant gradient change. In such cases the friction force does not reach a maximum value before the peak in the axial load cycle and macro slip does not occur. However, micro slip is present and the level of micro slip is dependent on the contact pressure and axial load. Frictional hysteresis loops during the micro slip condition are described by Pape and Neu [7] as “needle like”. Figure 6.2 presents a typical example from the results in Appendix C, the graph shows the two distinct friction responses, the macro slip loop (measured at the start of the experiment) and the micro slip loop (measured during the fretting period).

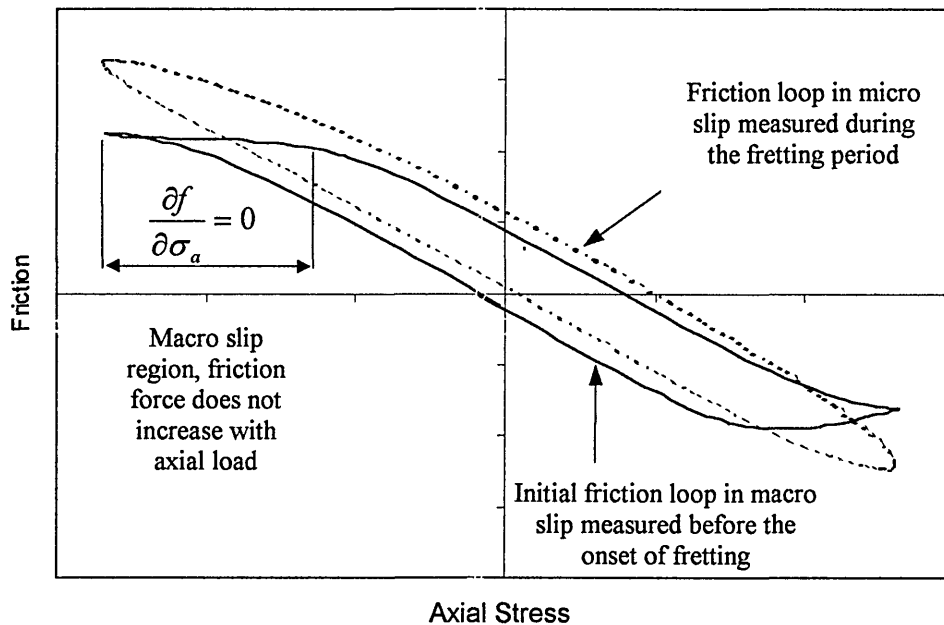


Figure 6.2 Example of the transition from macro to micro slip contact interaction due to the effects of fretting and wear. (Friction results taken from experiment 503 Appendix C)

The transition from macro to micro slip occurs within the first few hundred cycle of the experiment and can be attributed to wear as a result of the fretting process. In the case of

the initial macro slip friction hysteresis loops, the contacting surfaces are undamaged and wear has not yet affected the surface roughness. Therefore, the friction coefficient μ is best represented by the typical value obtained from simple sliding tests. The friction coefficient at this stage is considered as a material constant and is defined by Coulomb's classic friction theory. This theory does not account for dynamic changes in surface roughness. The friction force is therefore a function of the typical undamaged contact surface. However, as surface damage is introduced due to wear from the fretting process, the coefficient of friction changes. The surface damage is a function of wear and the coefficient of friction increases with wear. Subsequently, the friction force increases and the macro slip condition changes to micro slip as the interaction of the contact surfaces change.

The increase in surface roughness causes localised changes in the contact interaction (by decreasing the areas of slip and increasing the areas of stick) and partial slip occurs. The process of surface wear varies with cycle number and therefore time and the friction coefficient becomes transient and dependant on surface damage and wear. The process of wear generates debris, which then acts as a third body solid lubricant that eventually stabilises the process. This phenomenon has been observed by others [53, 76, 78]. As a result of this stability both the friction force response and the rate of wear changes from transient to steady state. The continued steady state fretting process was observed in the stabilised hysteresis results measured after this initial period. This behaviour was apparent in all the fretting fatigue experiments (variations in load magnitudes result in variations in the severity of the transition between macro and micro slip).

The gradient of the hysteresis loop represents the rate of change in friction force with respect to the axial load. All the hysteresis loops exhibited the same gradient regardless of whether the eventual contact interaction was in macro or micro slip. The change in the gradient occurred when the contact pad size changed. This was due to a change in the combined stiffness of the contacting bodies. This can be observed from the results in Appendices C and D, which present the cyclic friction force response for both the experimental programme and the numerical predictions

6.2.2 The Response of the Peak Friction Force during the Fatigue Life

From the friction force amplitudes recorded during the test period it was possible to identify a common trend for all the experimental results. The friction force amplitude increases from the initial undamaged contact condition to achieve a maximum value within a few hundred cycles (as discussed in section 6.2.1). The transition has been attributed to the introduction of wear and surface damage, which has increased the coefficient of friction at the contact surface. The stabilisation observed in the study of the cyclic friction response is also apparent in the friction force amplitudes results. The introduction of debris acts as a third body lubricant and alters the friction force response from transient to steady state. This trend in the development of friction in response to fretting fatigue has been observed by other [7][28].

Once the peak friction force value is achieved within the first few hundred cycles, the friction force magnitude is either maintained or reduces slightly in response to the solid lubrication and remains constant for the duration of the life. For those experimental results that experience a slight drop in friction force after the peak value, it can be seen from images of the fretting scar that the debris acts to smooth the contact surface.

Evidence of this behaviour can be seen in figure 6.3 which shows the inner section of the scarred surface exhibits a smooth almost polished appearance relative to the heavily damaged region at the edge of the contact.

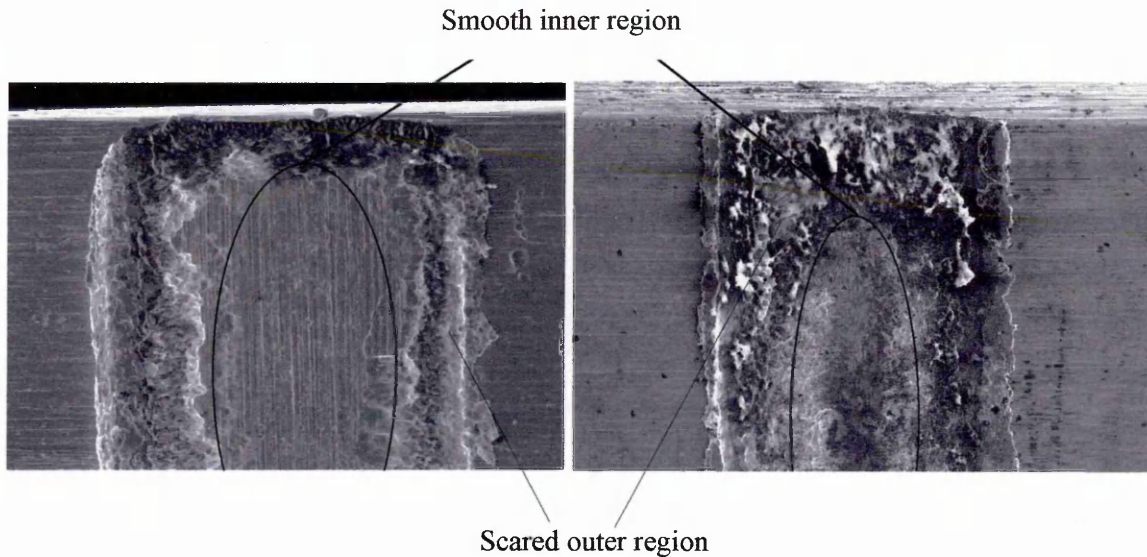


Figure 6.3 Typical fretting fatigue scars showing two distinct regions of surface damage, which verifies the presence of debris acting as a third body solid lubricant

Study of the friction force amplitudes throughout the test period provided no evidence to suggest that the presence of small cracks influenced the magnitude of friction force. The magnitude of the friction force amplitude remains unaffected by the presence of fretting cracks and only began to alter as the specimen approached failure. Study of friction preceding the final stage of failure suggests that although some load cases demonstrate a slight oscillation in the peak friction force prior to failure, the majority of results show no significant indication of failure. This behaviour suggests that as friction remains unaffected by the presence of cracks for the majority of the fatigue life, the crack length has not achieved a size that will affect the stiffness of the specimen. Therefore, the majority of life is taken up in the initiation of cracks and propagation of the dominant crack occurs rapidly within the final phase of the fatigue life.

6.2.3 The Behaviour of Friction during the Experimental Program

The following sections discuss the friction results from the three experimental studies. The programme includes a study of the friction force during the initial stages of crack growth for the 1.27mm contact pad size experiments. The pad size was then changed to 3mm and the experimental programme continued the study of friction to ascertain the effects of contact zone size on friction force. The programme also includes an investigation into the effects of controlling the slip displacement on the friction force.

6.2.3.1 Friction Force during the Initial Crack Growth Phase

The experimental crack initiation study was developed to isolate the initial crack growth within a set percentage of the overall estimated fretting fatigue life, for a range of axial loads and contact pressures. The analysis provides an insight into the development of friction force during the initial fatigue period and the potential influence of the friction force on crack growth.

To assess the potential influence of the friction force on crack growth, the friction results for each load combination were averaged to provide single friction force amplitudes at both the initial friction condition and maximum friction condition during the initial crack growth period. The initial results represent the friction condition before the onset of surface damage. The maximum friction results represent the friction, which occurs during the peak fretting period after several hundred cycles. Figure 6.4 presents the average friction amplitude for each load combination so that a comparison can be made between load magnitude and friction force at the initial and peak fretting conditions.

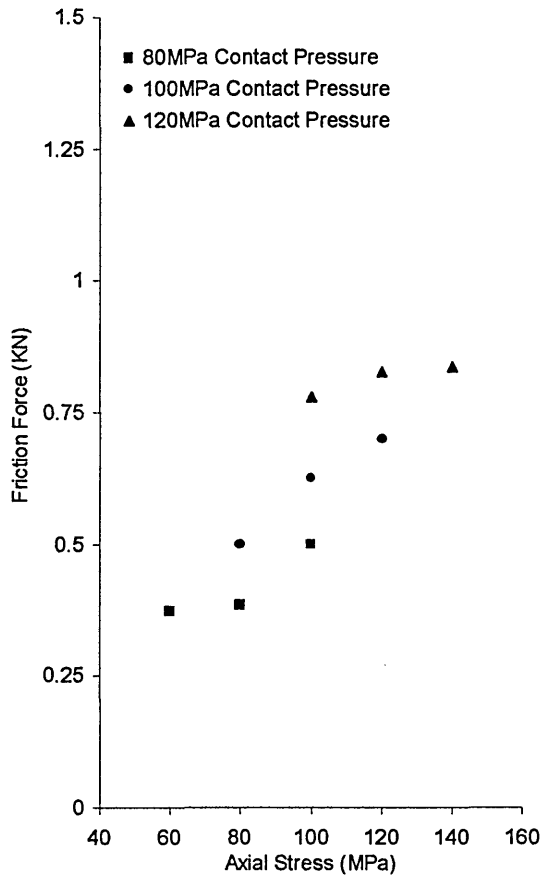


Figure 6.4a

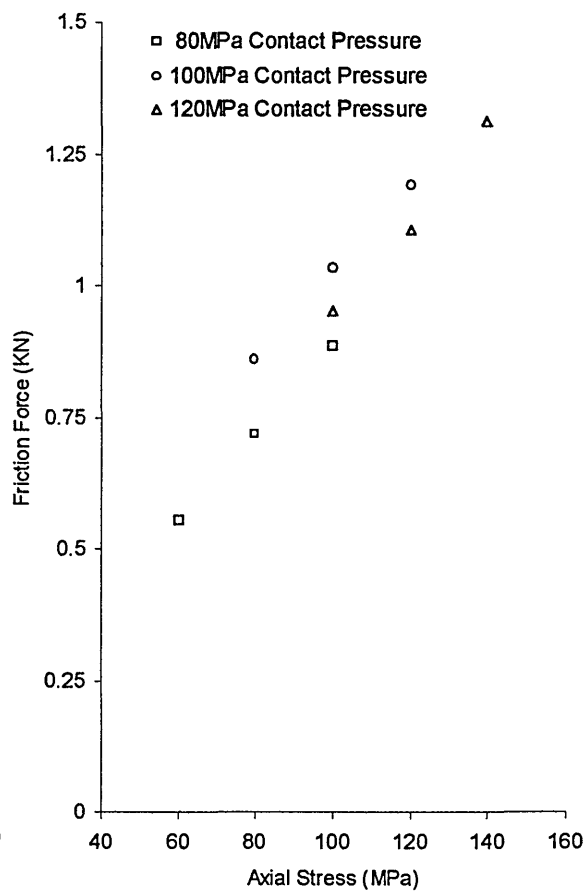


Figure 6.4b

Figure 6.4 Average friction force amplitudes for both the initial (a) and maximum (b) friction conditions

The initial friction response at the undamaged surface (figure 6.4a) shows the average friction forces measured at varying axial loads for each of the three contact pressures. The results show that for an increase in contact pressure there is a subsequent increase in friction force. Although the friction force varies with axial stress, there are three distinct regimes corresponding to the three contact pressures. The most noticeable occurs for the highest contact pressure (120MPa) which reports a constant friction force, despite increases in axial stress. Friction force is a function of the contact pressure induced by the normal load. Therefore, according to Coulomb's law, increases in contact pressure will result in increases in friction force when the friction coefficient is constant (at the start of the experiment). Variations in the peak friction force only occur

with axial stress when the contact surfaces are in micro slip. Therefore, variation in the friction force at the lower contact pressures, suggest that the friction results were in micro slip. This phenomena is due to either the load combination not inducing macro slip or wear occurring either prior to, or during the recording increment. If wear occurs during the initial recording increment the friction coefficient will vary and the friction force will increase. It is this process which has resulted in variations in the friction force with axial stress for the initial friction condition. The higher contact pressures were expected to induce wear within only a few cycles and as such the recording increment was adjusted to account for this. The result is a constant friction force, which does not increases with axial load and these results are considered to be indicative of the friction force during the initial period prior to fretting.

The study of the friction measured during the fretting period (figure 6.4b), reveals an increase in the overall friction amplitudes. This increase in friction force indicates that the friction coefficient has changed due to wear caused by the fretting process. The maximum fretting condition results also show a change in the relationship between friction force and axial stress. During micro slip all increases in axial stress result in an increase in friction force. This confirms that the contact interaction has changed from macro to micro slip and friction force is primarily influenced by the axial stress. The effects of contact pressure are less apparent, as the three distinct friction regimes observed in the initial friction condition are less noticeable. This is partially apparent for the 100MPa contact pressure, which exhibit higher friction forces than the 120MPa contact pressure results at the same axial stress.

Comparison of both the initial and maximum friction force amplitudes are presented in figure 6.5 The comparison of the friction force amplitudes in both the initial and

maximum friction condition show a clear distinction between the fretting and non-fretting case. The friction force measured during the fretting period demonstrates a consistent increase over the friction force values measured during the initial period.

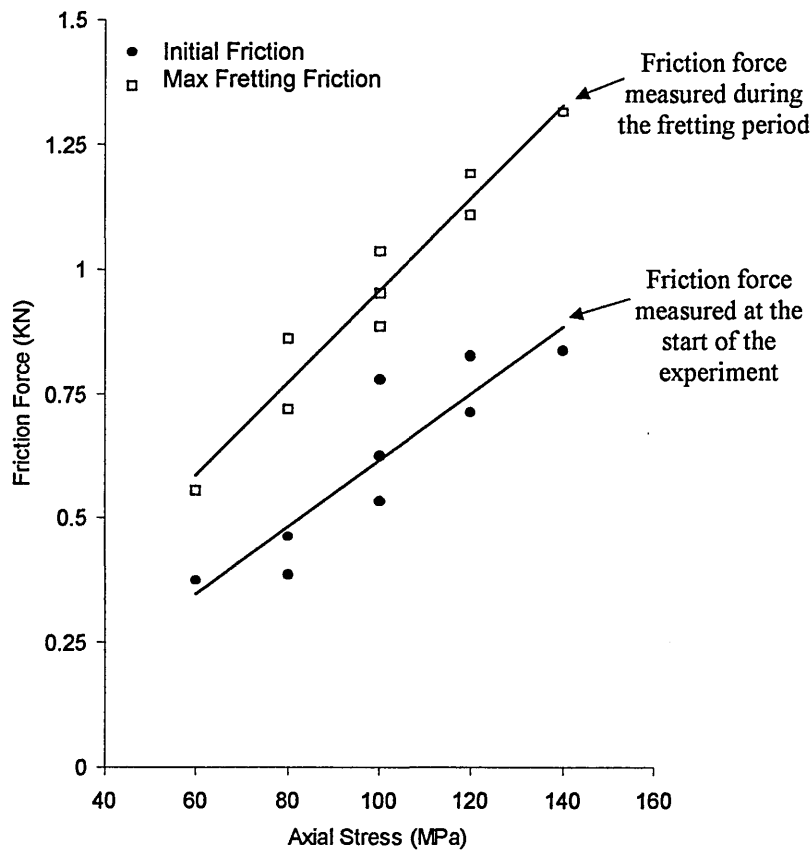


Figure 6.5 Comparison of both the initial and maximum friction force amplitudes, measured during the experimental crack initiation study.

The relationship between initial friction and fretting friction is better observed from the equivalent friction coefficients. Averaged friction forces for each load case were used to determine the effective friction coefficient from Coulomb's law. The results presented in figure 6.6 demonstrate two distinct friction coefficients, a lower coefficient for the initial condition (representing the undamaged contact interaction) and the higher fretting friction coefficient (as a result of wear and surface damage). The results show a clear distinction between the initial and fretting friction coefficients. The friction coefficient determined during fretting is significantly larger than the friction coefficient determined

during the initial test period. The results demonstrate that friction coefficients determined under non-fretting conditions are inadequate to represent the friction behaviour in fretting fatigue. However, the increase in the fretting friction coefficient does not take the full effects of friction into account as the friction was measured during micro slip. The peak frictions generated during macro slip have the potential to further increase the fretting friction coefficient.

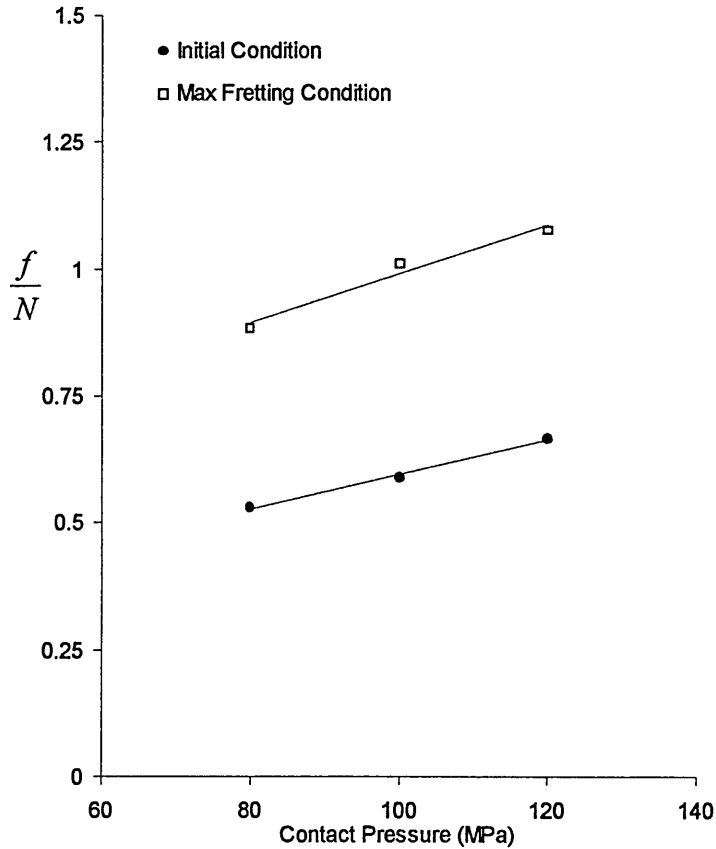


Figure 6.6 Comparison of the equivalent friction coefficients for both the initial and fretting conditions

6.2.3.2 The Effects of Contact Size on Friction Force

The experimental study of contact size on friction force was arranged to run until the specimen broke through the cross section. This provided friction results at the point of failure. The cyclic friction response adheres to the findings in section 6.2.1, the loops

exhibit the initial macro slip condition, transposing to a micro slip within the first few hundred cycles.

Study of the peak friction amplitudes throughout the life of the test show the transient increase in the peak friction force to achieve a maximum value within the first few hundred cycles. The wear and debris process then stabilises to a steady state condition for the remainder of the life. Study of the friction force response at failure is not possible for all the results due to variations in the recording increment. Failure occurs within a few hundred cycles and for the majority of cases the recording increment fails to capture this data. Due to the length of the overall life the recording increment was set to capture the friction response every five thousand cycles and as such the failure often occurred between increments. Nevertheless, some tests did measure the friction force during the failure process and these results provide an insight into the response of friction during the final phase of the fatigue life.

The friction force depreciates to a near zero value within a few hundred cycles, during the critical failure of the specimen. Study of the friction force response prior to the failure shows no indication that failure is imminent. This suggests friction is only affected once the crack has achieved a suitable length to alter the rigid body response of the specimen. Figure 6.7 shows an example (test 803) of the friction force measurement during failure.

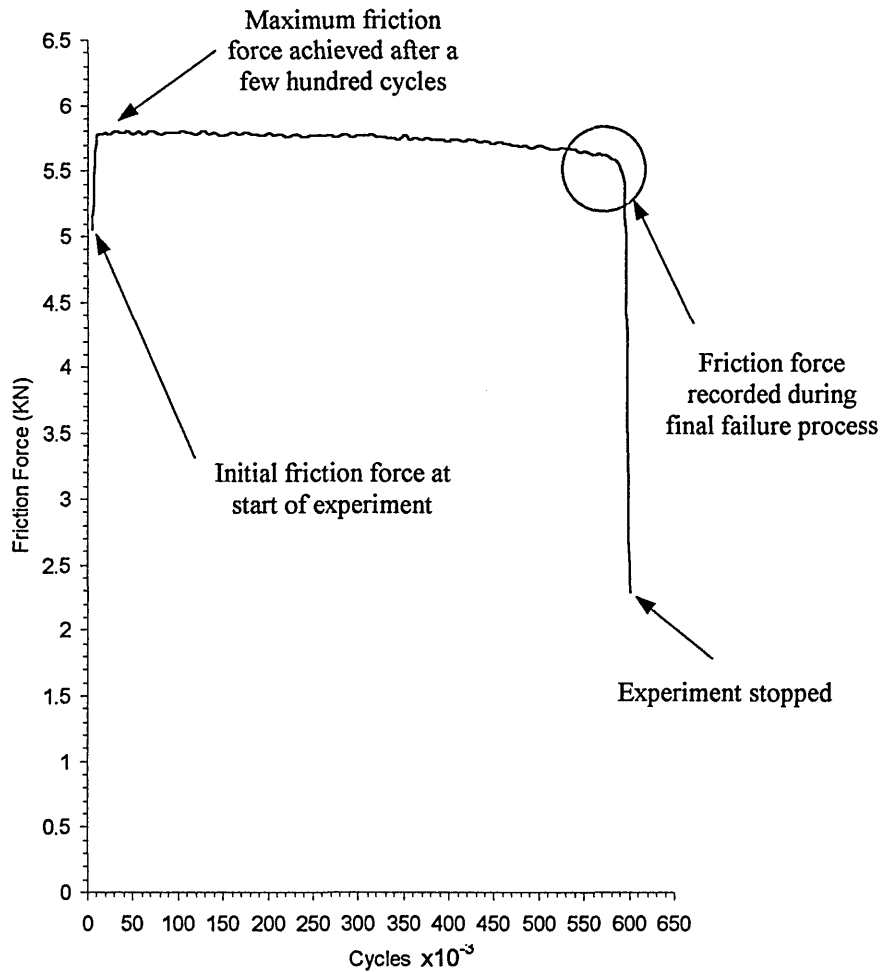


Figure 6.7 An example (Test 803) of the peak friction response during the a fretting fatigue experiment

Study of the average friction force amplitudes measured at the initial contact condition (figure 6.8a) reveals a diverse scatter in the results. This diversity can be attributed to a variation in the onset of fretting and wear as a result of each load combination. Therefore, the recording increment has measured the friction response during this initial wear period and the contact interaction has already begun to change from macro to micro slip.

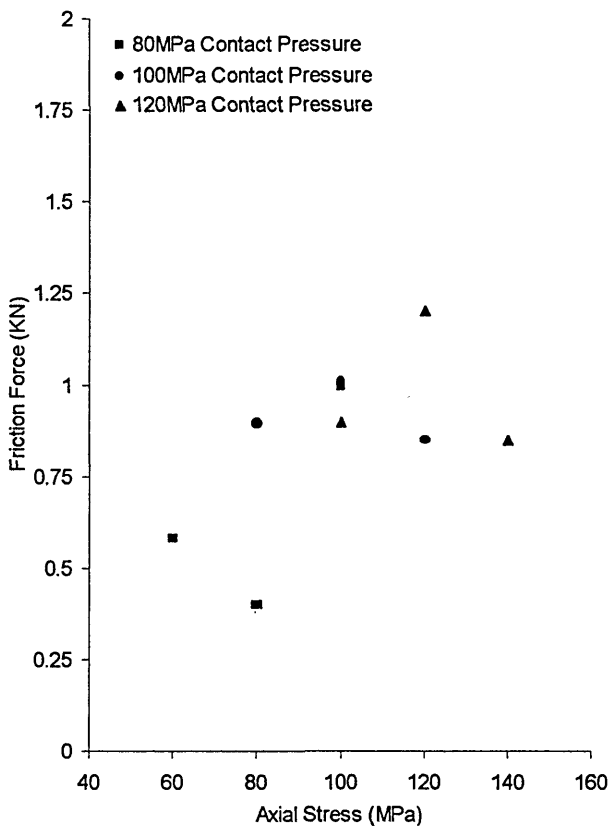


Figure 6.8a

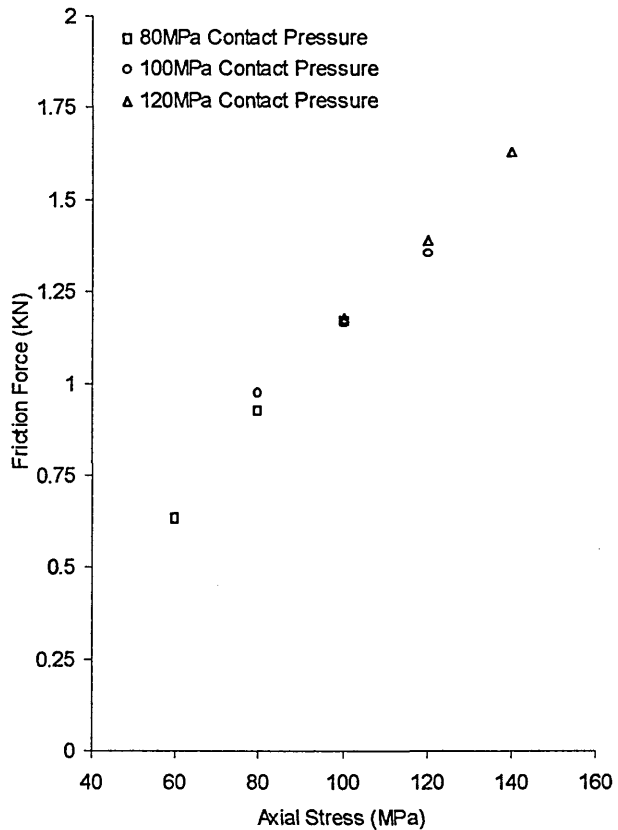


Figure 6.8b

Figure 6.8 The average friction force amplitudes for both the initial (a) and maximum (b) friction condition

A general trend is not obvious due to the range of scatter in the initial friction results. However, a progressive increase in the friction force amplitude is discernible as the axial stress increases. The influence of axial stress on the friction force signifies that the surface condition has already started to change from macro to micro slip. The influence of contact pressure is less evident in the friction results at the start of the experiment. Although, the peak friction forces measured for each contact pressure show a progressive increase with increasing contact pressure.

Study of the friction force amplitudes measured during the fretting period (figure 6.8b) reveals similar friction force behaviour to the 1.27mm results. The friction force is primarily influenced by the axial stress and the contact interaction has changed to micro

slip. The influence of contact pressure has become less apparent and is only discernible by the maximum value of friction force achieved.

Comparison of the initial and peak friction conditions exemplifies the effects of fretting on the friction response. Figure 6.9 presents a comparison between the initial and maximum fretting friction results. Although the fretting friction adheres to the findings from the 1.27mm results the diverse scatter in the initial friction results makes the differentiation between the two conditions less apparent. However, as stated the initial friction results are already undergoing the transition from macro to micro slip and so signify the friction response during the transient period within the first few hundred cycles.

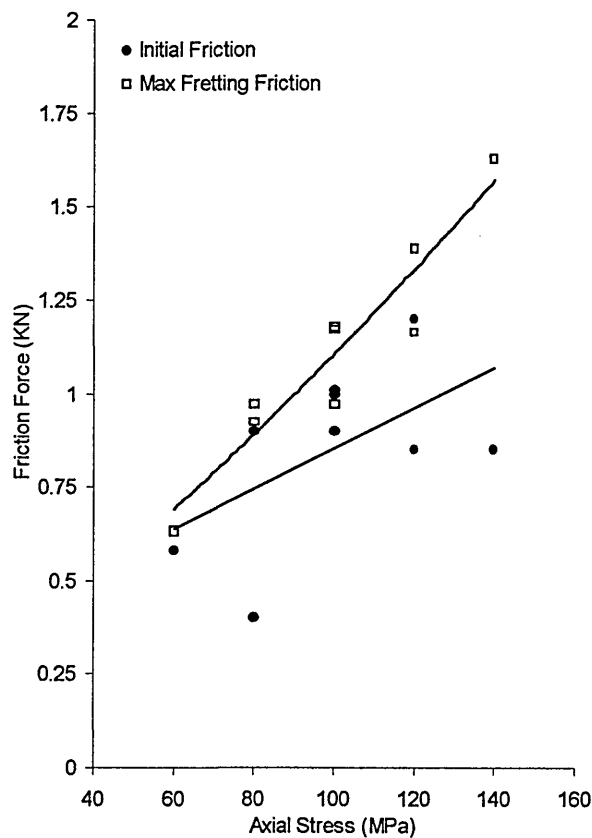


Figure 6.9 Comparison of both the initial friction forces with the maximum fretting friction forces measured during the size effect study.

The difference between the initial and fretting friction is more noticeable from the equivalent friction coefficients. Figure 6.10 shows the average friction force amplitudes at each contact pressure for both of the initial and maximum fretting conditions.

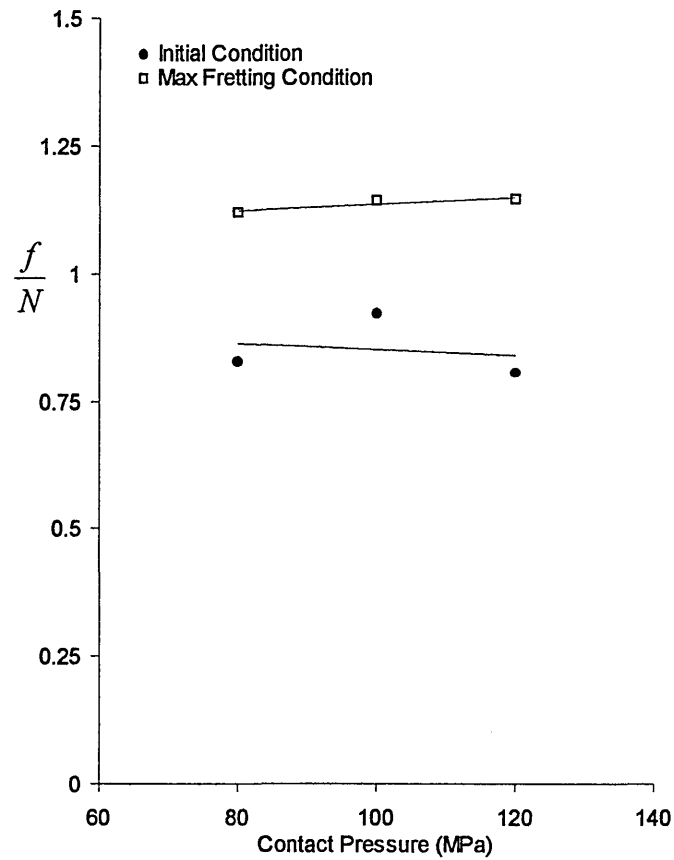


Figure 6.10 Comparison of the equivalent friction coefficient for the initial and maximum fretting condition.

The results show a distinct difference in the friction response for the initial undamaged surface when compared with the friction response from the fretted surface. The friction coefficient results reveal a consistent value for both the initial condition and the fretted condition and support the theory of a single friction to define friction behaviour in fretting fatigue. However, as already discussed in the analysis of the 1.27mm results, the magnitude of the fretting friction coefficient will increase as the results in figure 6.10 are in micro slip.

The controlled slip experimental programme demonstrates the effects of varying the magnitude of the slip displacement with the oscillatory phase angle on friction force. The phase angle of the slip is varied either in or out of phase with the axial load for the three contact pressures.

Applying a controlled slip in phase with the axial load cycle, results in the contact pad displacing with the specimen surface. Under normal conditions the friction force is generated as the contact surfaces move opposite to each other. When both surfaces move together in the same direction, the magnitude of relative surface motion is reduced, which reduces the friction force. The slip displacement controls the extent to which the contact pad moves in the same direction as the specimen surface and this controls the level of relative surface motion, which affects the magnitude of friction force generated.

This behaviour is observed for the fretting fatigue experiments that induced both 10 μm and 70 μm of slip in the direction of the axial load cycle (tests 901, 902, 904, 905, 907 and 908). Applying a 10 μm slip displacement, in phase with the axial load cycle reduces the level of slip over a nominal result for this load case (nominal results are considered as those results in which slip is not controlled). This results in the contact interaction starting in micro slip with no transition from macro to micro slip (as observed for nominal results). Macro slip did occur for a single contact pad during the 908 test however, this result is not repeated in the other tests and is considered inaccurate. The friction hysteresis results for the 10 μm slip displacement in phase with the axial load cycle are presented in Appendix C, tests 902, 905 and 908

The results demonstrate there is no transition from macro to micro slip and the hysteresis remains relatively unchanged during the fatigue life. Although the contact interaction has been affected by removing the transition from macro slip to micro slip the peak friction forces remains largely unaffected. Increases in the contact pressure do not appear to affect the friction force results. This behaviour can be explained by the contact interaction. The peak friction forces measured during micro slip are dominated by the axial load and variations in the contact pressure are not considered to be significant.

Increasing the slip displacement to $70\mu\text{m}$ results in a significant reduction in the peak friction force magnitude. In all load cases the friction force is close to zero, and although a hysteresis is present the differences in friction force are small. This suggests that this magnitude of controlled slip is approximate to the magnitude of slip displacement under nominal conditions. The $70\mu\text{m}$ of induced slip applied in phase with the axial load reduces the relative displacements at the contact surfaces to almost zero. The result is an almost zero friction force throughout the duration of the fatigue life. The effects of increasing contact pressure for this surface condition are not apparent in the friction force results. Both the friction hysteresis and the peak friction forces measured during life show no evidence to suggest the contact pressure is an influence on friction force. The friction hysteresis results for the $70\mu\text{m}$ slip displacement in phase with the axial load cycle are presented in Appendix C, tests 901, 904 and 907

Altering the phase angle to vary 90° out of phase with the axial load and applying a $20\mu\text{m}$ slip displacement, resulted in an initial friction force response in macro slip for the both the lower and higher contact pressures (80MPa and 120MPa). The results show that global sliding occurs for the majority of the load cycle and this observation

becomes more acute at the higher contact pressure (120MPa). The macro slip condition changes to micro slip as the contact surface begins to wear due to the fretting process and subsequently the peak friction force increases. The intermediate contact pressure (100MPa) does not exhibit this behaviour and the friction response begins in micro slip, which is maintained for the duration of the test. As there is no transition from macro to micro slip for the intermediate contact pressure, the peak friction forces do not vary.

The results show that variations in contact pressure have significant influence on the friction force when a 20 μ m slip displacement is induced 90⁰ out of phase with the axial load. The differences in the type of contact interaction at various contact pressures can be explained by the complex wear mechanism occurring as a result of the induced slip. The friction hysteresis results for the 20 μ m slip displacement applied 90⁰ out of phase with the axial load cycle are presented in Appendix C, tests 903, 906 and 909

The effects of the controlled slip displacement results can be seen in the friction life summary data (Chapter 5, section 5.2.3.1). The results of the forced slip displacements applied in phase with the axial load display a stable response throughout the fatigue life with little variation in the peak friction results. The 10 μ m results exhibit similar results for all three contact pressures, where the 70 μ m results exhibit no variation in the near zero friction force from the initial condition through to failure. The results of the 20 μ m slip displacement induced at 90⁰ out of phase with the axial load show that contact pressure has a significant effect of the friction response.

6.2.5 Validation of the 1.27mm Pad Size Experimental Friction Results

Comparison of the friction force results for the 1.27mm pad size experiments with existing data from the experimental work conducted by Fernando *et al* [75], is presented in figure 6.11. Direct comparisons are not possible due to variations in the loads applied during each experimental programme. The result comparison demonstrates a similarity in the friction force magnitudes, despite the differences in experimental facilities.

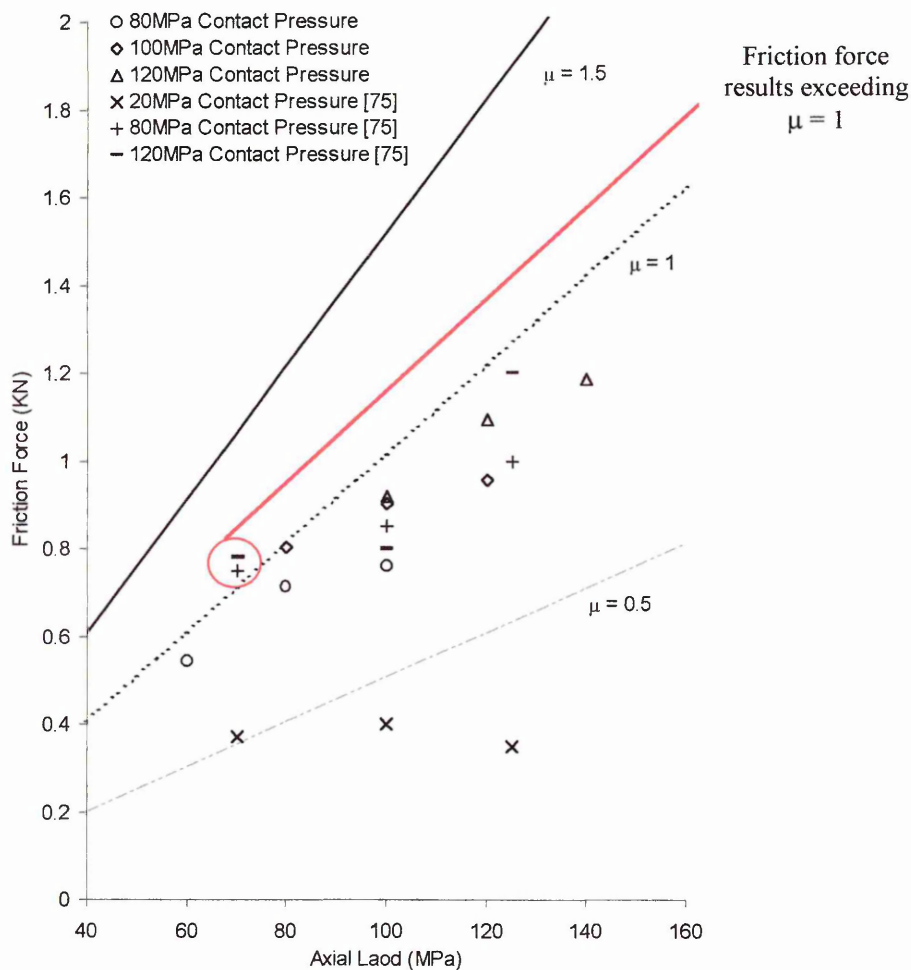


Figure 6.11 Comparison of the equivalent friction coefficient for the initial and maximum fretting condition.

The results are compared with three coefficients of friction and show that a typical friction coefficient for aluminium and steel ($\mu=0.5$) is inadequate to represent friction force during fretting fatigue. Most friction force results fall below the intermediate

friction coefficient ($\mu=1$). However, as most of these results are measured during micro slip the maximum friction force (which can only be measured during macro slip) has not been achieved. Evidence of this can be observed from figure 6.10, which demonstrates that friction forces measured either during or close to macro slip exceed the intermediate friction coefficient value ($\mu=1$) Therefore, the higher friction coefficient ($\mu=1.5$), is the most suitable value to represent friction in fretting fatigue.

Similarities in the friction response during fretting fatigue for both the current experimental arrangement and the experimental facility developed by Fernando *et al* [75] can be used to assume that similarities are also present in the stress fields and ultimately, the fatigue lives. Due to the fact that the 1.27mm experiments conducted during the initiation study of the current experimental programme were not tested to failure, the assumptions that the fatigue lives will also be comparable, provides an important basis for the estimation of the fatigue lives for the initiation study. Figure 6.12 presents the fretting fatigue lives for the 1.27mm experiment as performed by Fernando *et al* [75] and derives a trend for the purpose of estimating the fatigue lives for similar load cases.

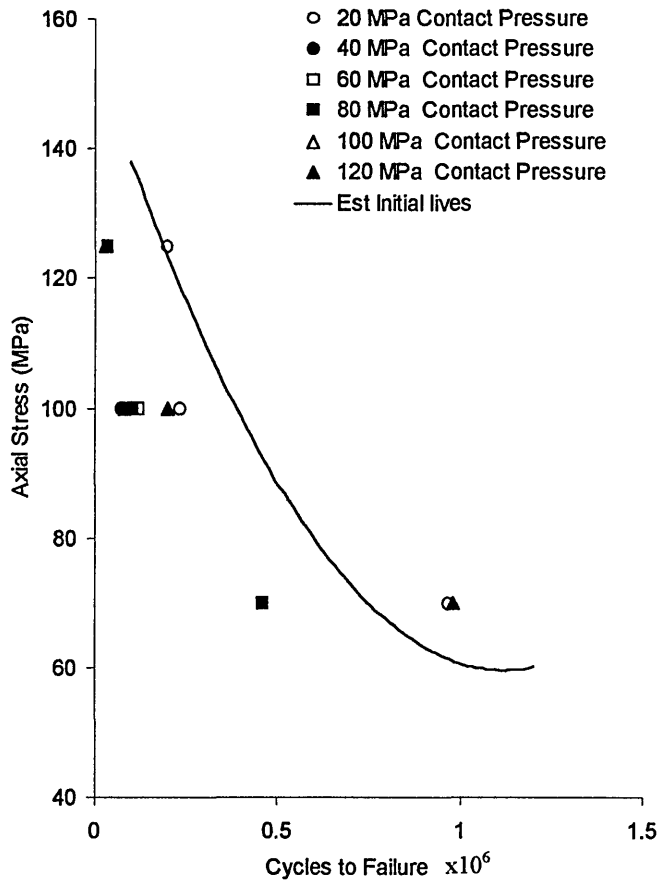


Figure 6.12 Fretting fatigue lives from the 1.27mm pad size experimental study conducted by Fernando *et al* [75]

6.2.6 Comparison of Friction Forces for Different Contact Pad Sizes

The difference between the contact pad sizes used in the experimental study is a 136% increase in contact area from the 1.27mm to the 3mm contact pads. The study investigates the effects of this increase in contact area on friction force results. Coulomb's friction law has been used to assess the friction force at the contact surfaces. However, Coulomb's friction law does not account for the contact area. Therefore, comparisons are made between the peak friction amplitudes for both the 1.27mm and 3mm pad sizes to determine if the maximum friction force is affected by the size of the contact area. Figure 6.13 presents the friction force amplitudes during the fretting period for both the 1.27mm and 3mm contact pad sizes.

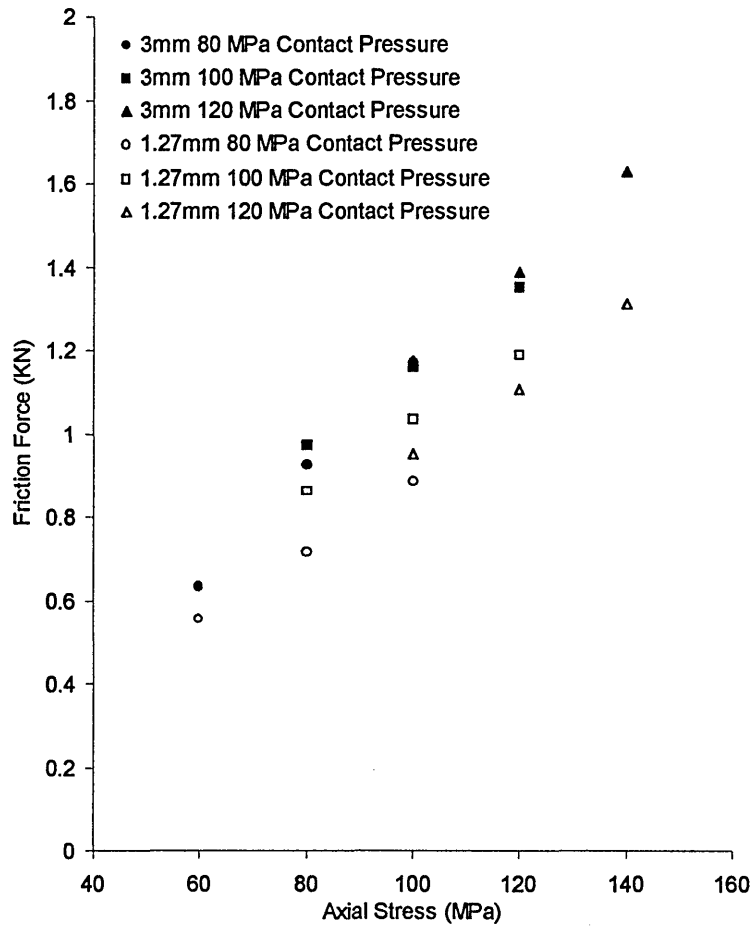


Figure 6.13 Comparison of the peak friction forces measured during the fretting period for both the 1.27mm and 3mm pad size experiments

The comparison is based on the same axial and contact load combinations for each pad size. The friction force results of the two pad sizes do exhibit differences, most noticeably the difference in the magnitudes of the friction forces. The larger pad size generates marginally higher friction forces for all three contact pressures compared to the smaller pad size results. The variations in the friction force amplitudes may be due to the variations in relative stiffness between the 3mm and 1.27mm contacting bodies. This is supported by the slight difference in gradient, which is evident when comparing similar load case results for both pad sizes. However, the differences are marginal (less than 20%) and do not reflect the significant increase in contact area (increase of 136%).

Therefore, the results suggest that friction is not significantly affected by the contact zone size during micro slip, which is contrary to the findings from Hills study on a Hertzian experimental arrangements [64]. This would imply that the area of micro slip is comparable for similar loading conditions and only affected by the total available area for slip. If the contact interaction changes from micro to macro slip the relationship between friction and load changes. Therefore, the results will be effected by the size of the contact pad only when the area of micro slip approaches the contact area and macro slip occurs. Under these conditions the peak friction force will vary relative to the contact area.

6.2.7 Numerically Predicted Friction Behaviour

The numerical analysis results provide the opportunity to study the localised friction behaviour during fretting and determine the effects of friction on the stress distribution. To investigate the effects of friction force on stress the numerically predicted friction force must be validated against the experimentally recorded friction force. Therefore, comparison of the numerically predicted friction force with the experimentally recorded friction force must be made to ascertain the accuracy of the numerical solution.

6.2.7.1 Numerically Predicted Friction Force

The finite element models predict friction based on Coulomb's friction law, which requires a single friction coefficient. The friction coefficient is input as a global value that is applicable to all node pairs along the contact surface. Friction force is then determined for each contact node pair based on the friction coefficient and the local contact pressure. The result is a friction force generated for each contact pair, which can

then be accumulated to determine the total friction force at the contact surface, or considered individually to determine localised friction response.

The finite element analysis focused on a single friction force cycle during the peak fretting condition, which occurs within the first few hundred cycles of the fretting fatigue process. It is during this period that the maximum friction forces are achieved for the fatigue life of the specimen. Therefore, it is during this period that the most severe stresses are generated in the specimen and it is likely that during this period fretting cracks nucleate. Study of the experimental result show that the friction force is then maintained for the remainder of the fatigue life, (Chapter 5 section 5.2.2.2)

Finite element analyses were conducted for both the 1.27mm and 3mm pad size experimental arrangements. The results of the analyses included the numerically predicted friction forces for an equivalent range of loads to those conducted in the experiments. The total friction force at the contact surface was used to predict the cyclic friction response, which generated the frictional hysteresis. The peak friction forces were averaged to obtain the friction force amplitudes for each load case.

6.2.7.2 The Numerically Predicted Friction for the 1.27mm Contact Pad Size

The 1.27mm pad size finite element models were based on the experimental arrangement used by Fernando *et al* [75]. The axial and normal load combinations used in this study induced both macro and micro slip conditions and the finite element models were expected to predict this behaviour. Figure 6.14 presents an example of a numerically predicted cyclic friction response in macro slip for the 1.27mm pad size

results in Appendix D and compares it against the experimentally recorded cyclic friction response from results obtained by Fernando *et al* [75]

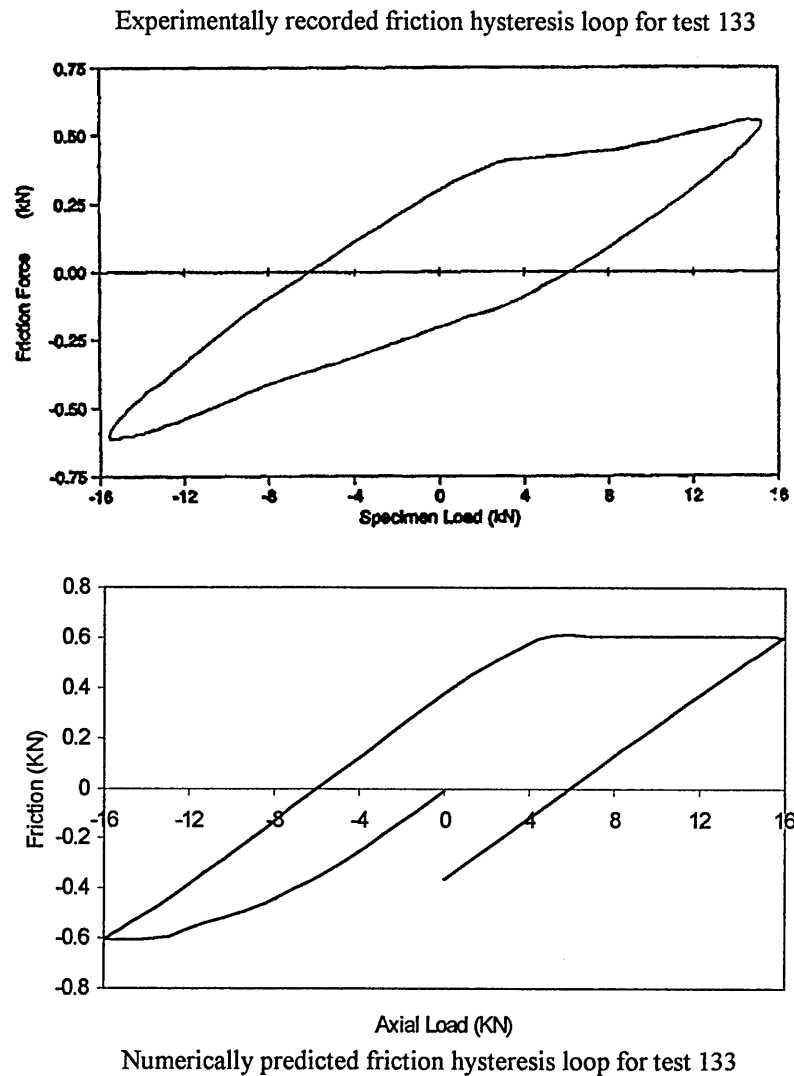
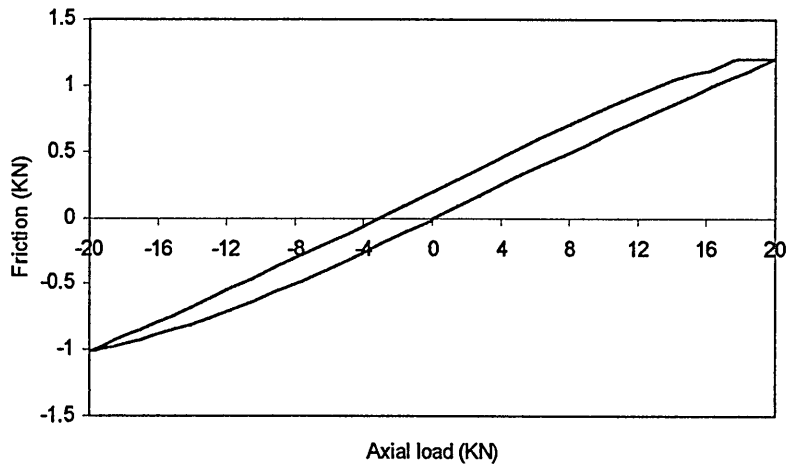
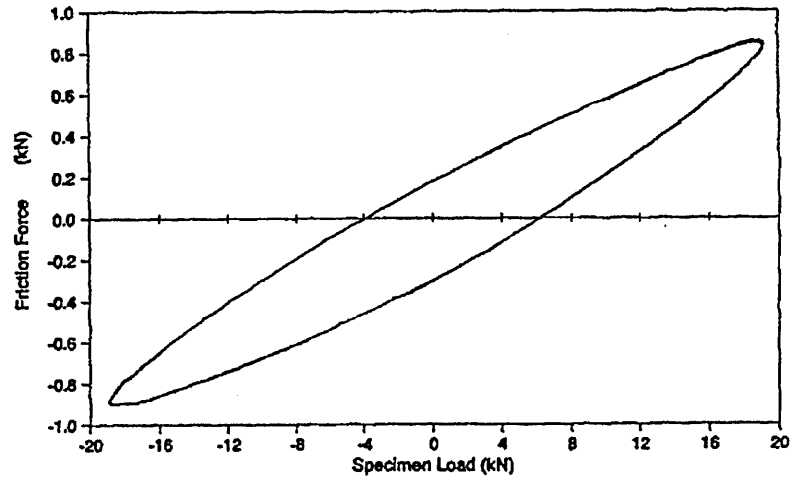


Figure 6.14 Comparison of the numerically predicted friction hysteresis loop with the experimentally recorded friction hysteresis loop for the 1.27mm contact pad size (test 133) demonstrating the numerical capability to predict macro slip

Figure 6.15 presents an example of a numerically predicted cyclic friction response in micro slip for the 1.27mm pad size results in Appendix D and compares it against the experimentally recorded cyclic friction response from results obtained by Fernando *et al* [75]

Experimentally recorded friction hysteresis loop for test 128



Numerically predicted friction hysteresis loop for test 128

Figure 6.15 Comparison of the numerically predicted friction hysteresis loop with the experimentally recorded friction hysteresis loop for the 1.27mm contact pad size (test 128) demonstrating the numerical capability to predict micro slip

Study of the cyclic friction response for the 1.27mm pad size models revealed that for the example results in figure 6.14 the numerical solutions successfully predicted macro slip, which was present for that particular load case (test 133). In figure 6.15 the numerically solution also successfully predicted the micro slip behaviour, present in the experimental results for that load case (test 128).

For the load cases that induced macro slip, the peak friction forces are predominantly influenced by the changes in contact pressure. As the contact pressure increases the maximum achievable friction force in micro slip increases. At the point where the contact interaction achieves macro slip, the friction force remains constant and does not increase with further increases in axial load. This behaviour is observed from experimental friction force results in macro slip. The increase in the peak friction force is related to the contact pressure by Coulomb's friction law. Therefore, the numerical solution successfully predicts the friction response when the contact interaction is in macro slip.

The capability of the finite element results to predicted the friction force response for partial or micro slip condition varies for each load case. For the example presented in figure 6.15, the numerical solution accurately predicts the friction force in micro slip for both the tensile and compression parts of the load cycle. The hysteresis is symmetrical and the cyclic friction force is stable within the micro slip condition. However, examinations of the numerical cyclic friction force results, which predicted micro slip (Appendix D) reveals that not all results exhibit a stable loop.

For particular results, the frictional hysteresis is not symmetrical and the slip behaviour varies between the tensile and compressive parts of the axial load cycle. This behaviour is due to an increase in the friction force during the compression part of the load cycle as a result of elastic strain energy. The elastic displacements at each node pair occur when the local friction force achieves a maximum value determined by Coulomb's friction law from the local contact pressure and the friction coefficient. As the contact pressure varies through the load cycle, elastic displacements can occur at different locations and at different points in the cycle. In the case of those results, which exhibit

non-symmetrical hysteresis, elastic displacements occur during the tensile part of the load cycle, which are then halted as the cycle reverses in compression. The resultant friction force from the compression part of the load cycle acts in the opposite direction to the friction force generated by the tensile part of the load cycle. The elastic strain energy induced by the elastic slip displacements in the tensile part of the load cycle then combines with the friction force from the compression part of the load cycle. The result is an increase in the friction force during the final reversal of the compression part of the load cycle back to zero. The friction force does not return to zero despite the fact that there is no axial load. Evidence of this behaviour is demonstrated in figure 6.16, which shows the final friction force has not returned to zero.

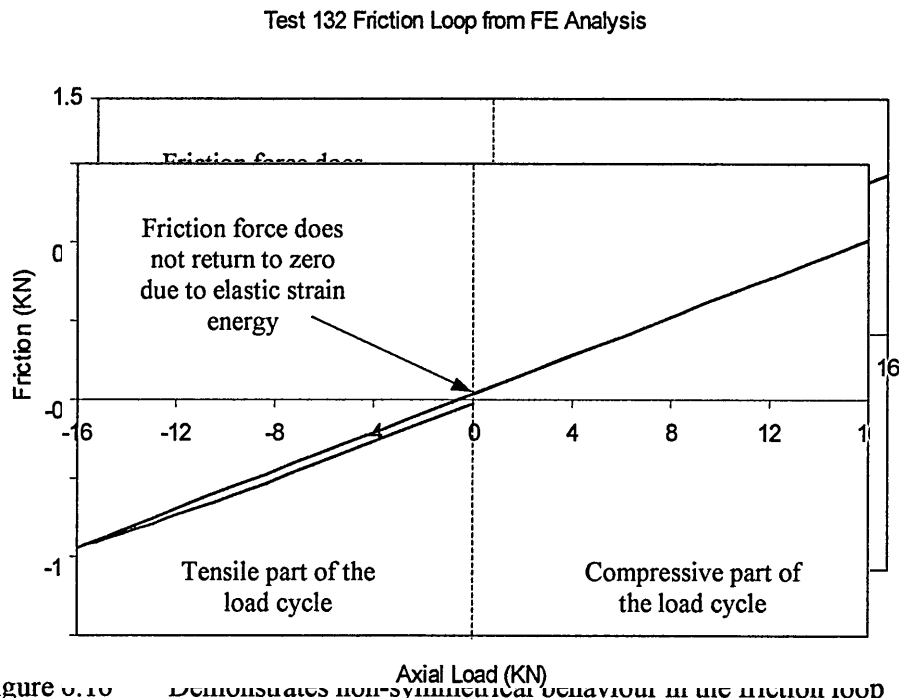


Figure 6.16 demonstrates non-symmetrical behaviour in the friction loop response, where the friction force does not return to zero when the axial load completes the cycle

However, not all results exhibit the same severity in this behaviour. Examination of the load cases reveals that this behaviour is more apparent for load combinations with high contact pressures in comparison to the axial loads. Appendix D contains the numerically predicted cyclic friction forces results for the 1.27mm pads size models.

The numerically predicted peak friction forces demonstrate both the macro and micro slip conditions for the range of load cases conducted during the experimental program. Figure 6.17 presents the peak friction force results for the 1.27mm pad size numerical analyses.

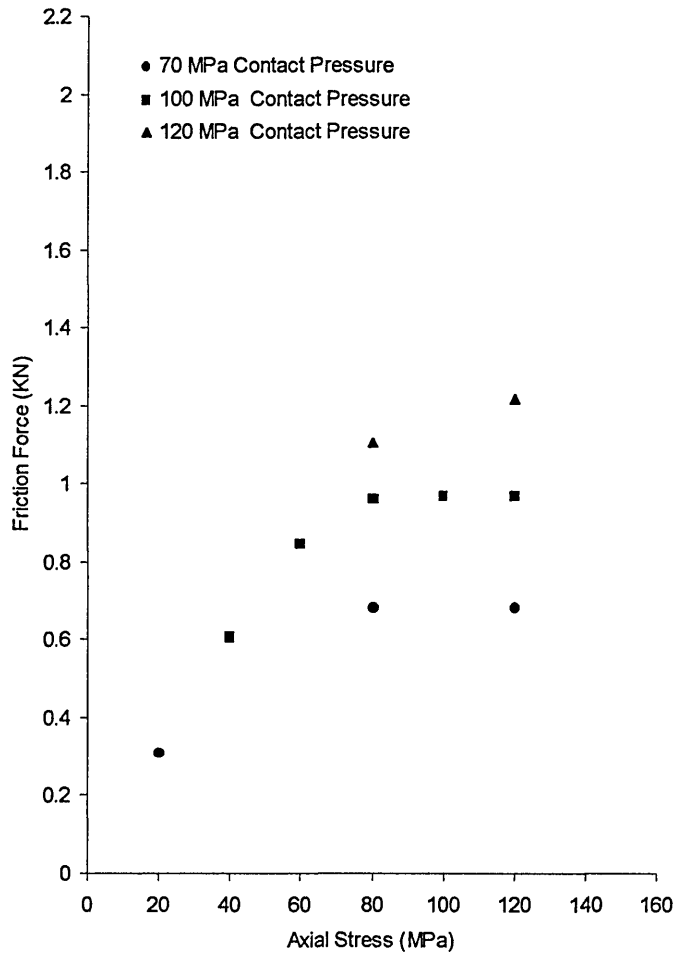


Figure 6.17 Numerically predicted friction force amplitudes for the 1.27mm pad size experiments performed by Fernando *et al* [75]

6.2.7.3 The Numerically Predicted Friction for the 3mm Contact Pad Size

The finite element models for the 3mm contact pad size were based on the current experimental arrangement. The load cases for the 800 series experimental programme were devised to induce only micro slip during fretting. The finite element (Appendix D) accurately predicted this type of slip condition. All the results for this analysis generated

a small amount of frictional hysteresis when compared with the experimental equivalent. Figure 6.18 presents an example of the numerically predicted micro slip hysteresis loop to compare against the experimental equivalent.

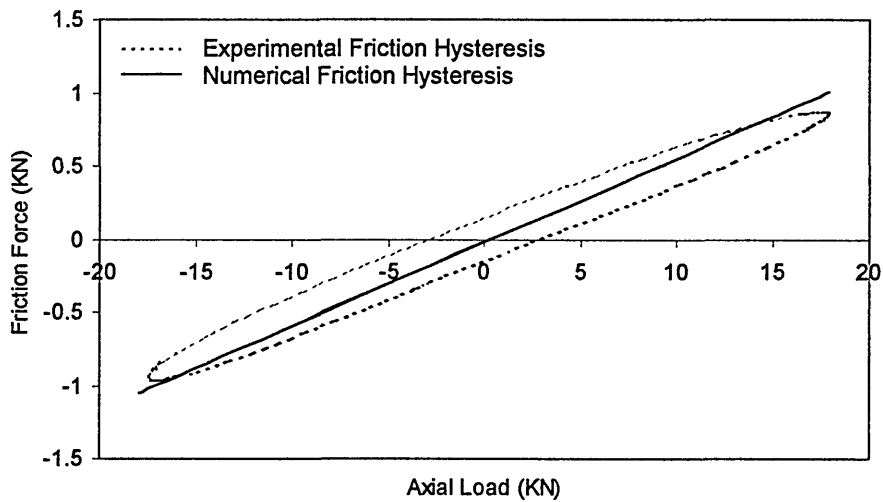


Figure 6.18 Comparison of the experimental cyclic friction response with the numerically prediction (test 803)

The numerically predicted cyclic friction force responses demonstrate a small amount of hysteresis when compared to the experimental results. The rate of change in friction force with axial load is relatively constant throughout the load cycle, generating a symmetrical hysteresis. Minor variations in the friction force are present for the same axial loads during the load cycle and although these dissimilarities are relatively small in comparison to the overall friction force (less than 5% difference), non-symmetrical behaviour is observed. The numerically predicted cyclic friction response does not support the presence of extensive slip during the load cycle. Study of the slip data and local friction maps (Appendix E) support this observation. The local friction maps show the friction force across the contact surface during the load cycle. The magnitude of the local friction force remains relatively small and only increases significantly at the edge of the contact pad during the peaks of the axial load cycle.

The numerically predicted cyclic friction response does show an increase in the peak friction forces with an increase in axial load. This behaviour is observed in experimentation for the micro slip condition. Although the contact pressure influences the friction force, the axial load determines the maximum achievable friction force during micro slip. Figure 6.19 presents the peak friction force results for the 3mm pad size numerical analyses.

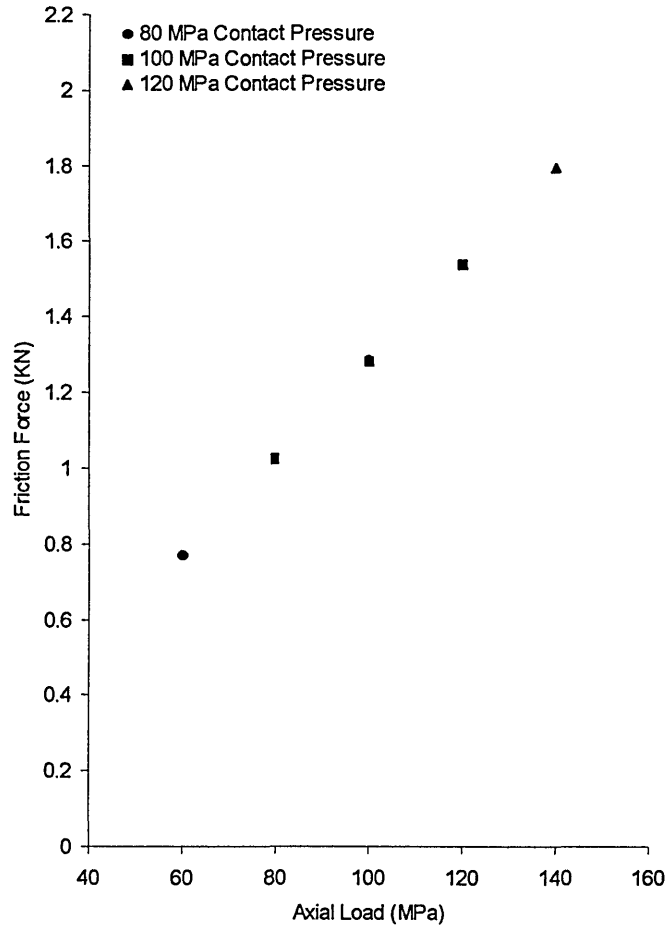


Figure 6.19 Numerically predicted friction force amplitudes for the 3mm contact pad size

6.2.8 Validation of the Numerically Predicted Friction Results

To ascertain the validity of the numerically predicted frictions the results are compared with the experimentally recorded frictions. Due to the inconsistencies between the numerical and experimental slip data, the comparisons are made using the peak friction

forces. Figure 6.20 presents a comparison between the numerical and experimental peak friction forces for both the 1.27mm and 3mm pad size results.

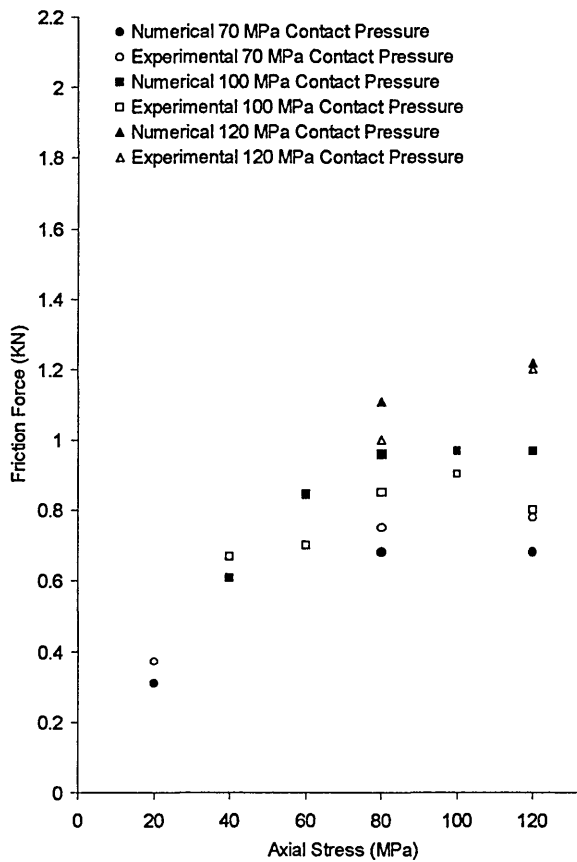


Figure 6.20a

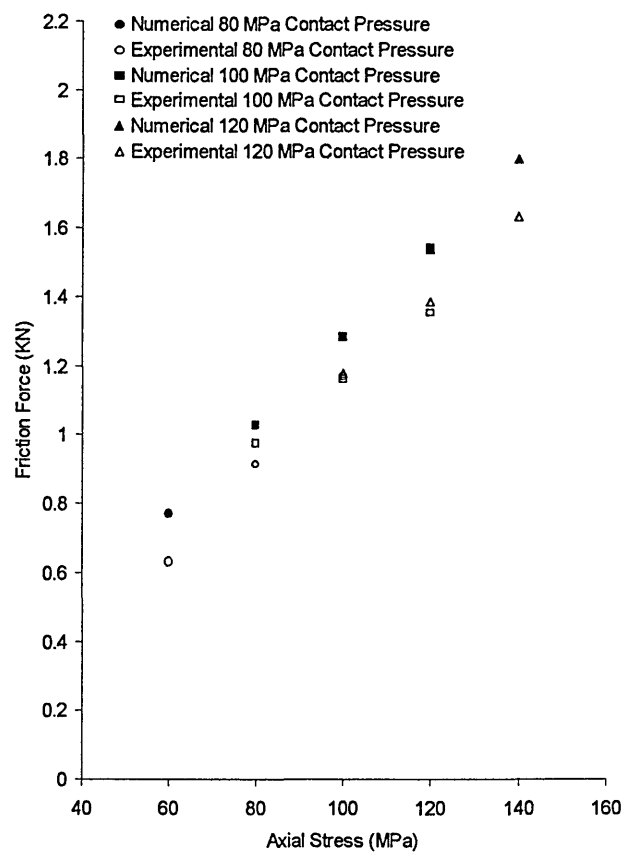


Figure 6.20b

Figure 6.20 Comparison of the numerically predicted friction force amplitudes for both the 3mm and 1.27mm contact pad size results with the experimentally recorded friction

Figure 6.20 shows that the numerically predicted peak friction force compare well with the experimentally recorded peak friction forces for both the 1.27mm and 3mm pad size results. The numerical results are capable of simulating both macro and micro slip behaviour and generate similar trends in the peak friction forces to the experimental results. However, comparisons of the hysteresis loops reveal inconsistencies between the experimental results and numerical predictions. These discrepancies signify inaccuracies in the definition of slip displacements by the finite element models.

The predicted friction forces from the finite element models have successfully demonstrated a capability to predict the peak friction forces during fretting fatigue. Therefore, the numerical models are capable of accurately simulating the friction force at the contact surface. As friction force is considered to significantly influence the stress distribution in the contact region, the numerically predicted stresses will be comparable with the actual fretting fatigue stresses.

Swalla and Neu [28] determined that the shear stress at the contact interface of the specimen (τ_{xy}) and the tangential stress (σ_{xx}) acting perpendicular to the interface, tended to exhibit the greatest sensitivity to fretting fatigue loading. Consequently, studies of the numerical predicted shear stresses and tangential or axial stresses are presented in section 6.5 to identify a suitable parameter capable of predicting fretting fatigue life.

The experimental programme incorporated both the study of initial crack growth and fretting fatigue lives for a range of contact pressures and axial loads. The study of initial crack growth was conducted using the 1.27mm contact pad size experiments. The purpose of the study was to investigate crack growth during fatigue life. Therefore, experiments were devised to run for 20%, 40% and 60% of the estimated fatigue life. The fatigue lives were estimated from the results of the experimental work conducted by Fernando *et al* [75] (figure 6.12 in section 6.2.5 presents the fatigue lives with the curve representing the estimated lives for the initial crack growth study). The purpose of running the experiments to particular percentages of the overall fatigue life was to determine at what percentage of the life fretting cracks could be identified.

Fretting fatigue lives were recorded during the larger 3mm pad size tests. In the study of the effects of contact size on friction force, the experiments were run until failure of the specimen occurred. The number of cycles to failure was considered as the fretting fatigue life for the range of axial loads and contact pressures considered. The following section will consider the results from the initial crack growth study and the fretting fatigue life study.

6.3.1 The Study of Initial Crack Growth

Visual techniques were used to determine the severity of the fretting process by examining the fretting scar and identifying cracks at different percentages of the fatigue life. A Philips XL40 scanning electron microscope was used in both the secondary electron and electron backscatter modes of imaging. Secondary electron images were

used to find cracks in the scarred surface and the electron backscatter images were used to differentiate between surface cracks and cracks that had propagated through the thickness of the surface scar into the bulk of the aluminium specimen. The electron backscatter mode provided a topographical image of the surface and made it easier to identify the dominant fretting crack.

Study of the fretting surfaces revealed networks of surface cracks, these cracks did not penetrate through the thickness of the scar and were not considered as fretting fatigue cracks that would induce critical failure. Under certain axial loads and contact pressures a surface crack initiated through the depth of the scar and became the dominant crack. The fretting fatigue process would continue to drive this crack until failure occurred. The purpose of the investigation was to identify if a dominant crack had initiated within the particular percentages of the fatigue life. Hutson *et al* [28] found that analysis of the fracture surface (using a scanning electron microscope) revealed the cracks, which induced failure, occurred within 250 μ m of the edge of the contact scar. Therefore, investigations of the contact surface were performed in the edge region of the scar.

In all cases where dominate cracks were identified, the cracks were observed to occur at the edge of the scarred region. The cracks occurred at either the trailing edge or leading edge of the contact pad, (the leading edge is seen as the edge closest to the top of the specimen where the axial load is applied and the trailing edge is seen as the opposite edge). Figure 6.21 illustrates the crack initiation site in relation to the experimental arrangement.

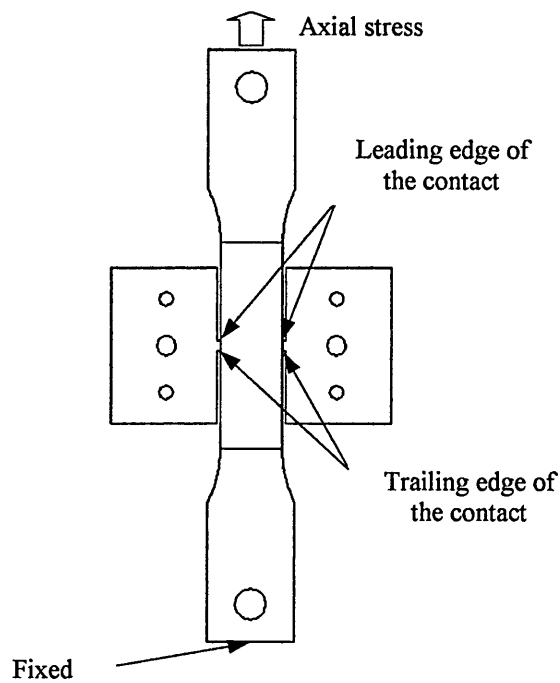


Figure 6.21 Illustrates the location of the leading edge and trailing edge of the contact pads where dominant fretting cracks initiated

This observation compared well with the numerical contact pressure distribution, which predicted that the highest contact pressures occurred at the edges of the contact pad. For a surface crack to gain dominance over other surface cracks and propagate to failure it requires a concentration of stresses. In the case of fretting, the contribution from both the stresses induced by the axial load and the stresses induced by the contact pressure, combine to form a multiaxial stress state. As the axial stress can be considered uniform throughout the cross section, the influential factor in initiating the dominant crack must be the stresses that are induced by contact. The stresses induced in the specimen from contact are shear stresses, which are influenced by friction force. As previously discussed (Section 3.4.3), the distribution of the shear stresses at the contact surface achieve a maximum value at the edges of the contact area. This is only applicable for flat contacts where there are no substantial cracks and is only relevant during the initial crack growth phase. Once cracks nucleate and begin to grow to a substantial length (several millimetres) the influence of the multiaxial loading becomes less pronounced.

6.3.1.1 Initial Crack Growth for 80MPa Contact Pressure (500 test series)

The 80MPa contact pressure was run at three axial stresses, 60MPa, 80MPa and 100MPa. Investigation of the fretting scar for the lower axial load case (60MPa) shows minor levels of surface damaged. A single dominant crack was identified for the test run to 20% of the fatigue life. However, further analysis of the surface scar revealed that the damage was not symmetrical across the entire contact area. Therefore the contact pressure distribution was concentrated towards one edge of the contact area. This distribution caused higher contact pressures at one side of the pad and the initiation of the dominant crack is not considered indicative of this load case. This observation was confirmed when the remaining tests for this load case were analysed (tests run to 40% and 60% of the fatigue life). Despite being run for more cycles the initiation of a dominant crack was not repeated and the surface scar covered the total contact area. Figure 6.22 presents an image of the fretting scar showing the uneven contact scar as a result of uneven contact pressure.

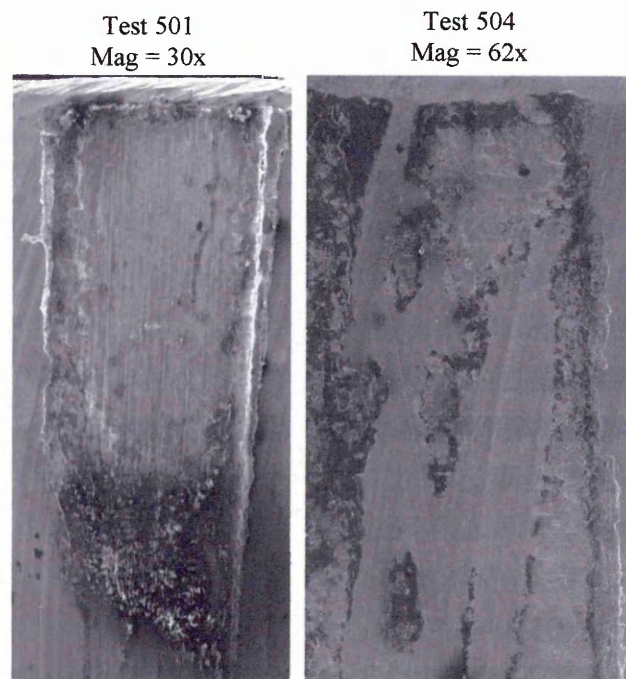


Figure 6.22 Comparison of the fretting scars for tests 501 and 504. Test 504 demonstrates the type of surface damage caused for the 80MPa contact pressure results. Test 501 demonstrates that the contact was not distributed across the entire contact surface.

The analysis of the fretting scar for the remaining tests (40% and 60% of the fatigue life) reveals that a dominant fretting crack could not be successfully identified when the specimen was subjected to a 60MPa axial stress and 80MPa contact stress.

Increasing the axial stress to 80MPa revealed more substantial surface damage in the analysis of the fretting scar. Two distinct regions could be identified within the fretting scar. A smooth inner region and a more heavily damaged outer region. Figure 6.23 presents a typical image of the fretting scar for this load case.

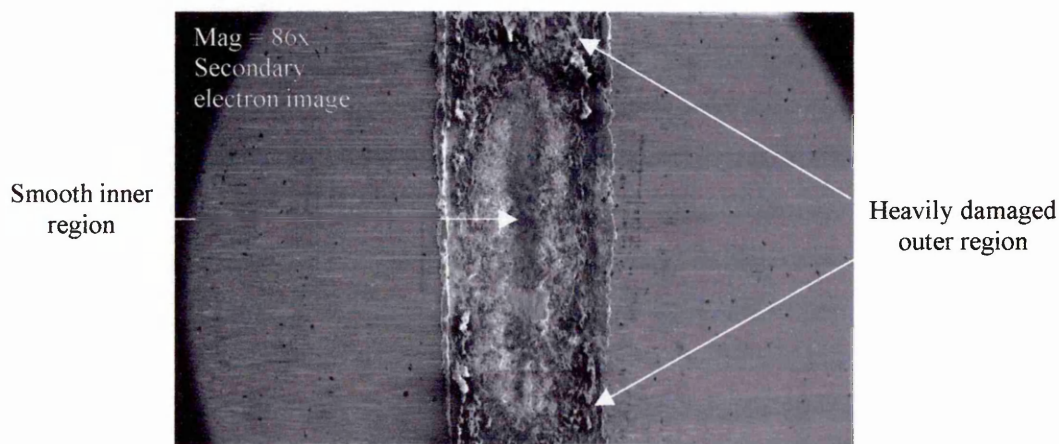


Figure 6.23 A typical fretting scar for the 80MPa axial stress and 80MPa contact pressure. The scar shows the two distinct regions of damage, a smooth inner region and a more heavily damaged outer region

Examination of this outer region revealed a dominant fretting crack had initiated along the length of the contact edge in all three of the tests run at different percentages of the fatigue life. Therefore, a dominant fretting fatigue crack was identified for the 80MPa axial stress and contact pressure load case from as early as 20% of the fatigue life. Figures 6.24a and 6.24b present examples of the dominant fretting fatigue cracks observed from the experiments run to 20% and 40% of the fatigue life.

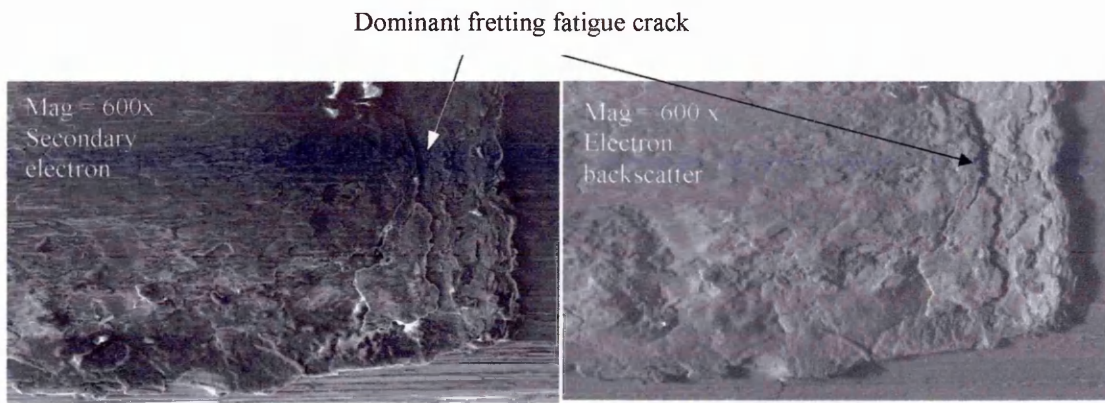


Figure 6.24a Test 504 (20% of fatigue life) showing a dominant fretting crack has initiated at the edge of the fretting scar in both the secondary electron and electron back scatter modes of imaging.

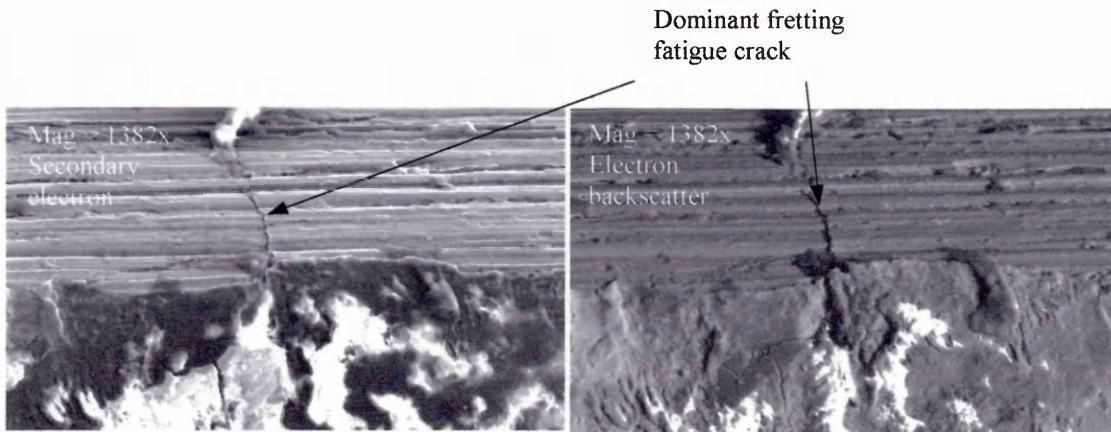


Figure 6.24b Test 505 (40% of fatigue life) showing detail of the dominant fretting crack in both the secondary electron and electron backscatter modes of imaging.

Examination of the fretting scars for the 100MPa axial stress experiments revealed more significant levels of surface damage. The fretting scars do not exhibit a smooth inner region with a more heavily damaged outer region. The fretting scars exhibit major damage across the entire contact area. Figure 6.25 presents an image of the fretting scar after 20% of the fatigue life for this load case.

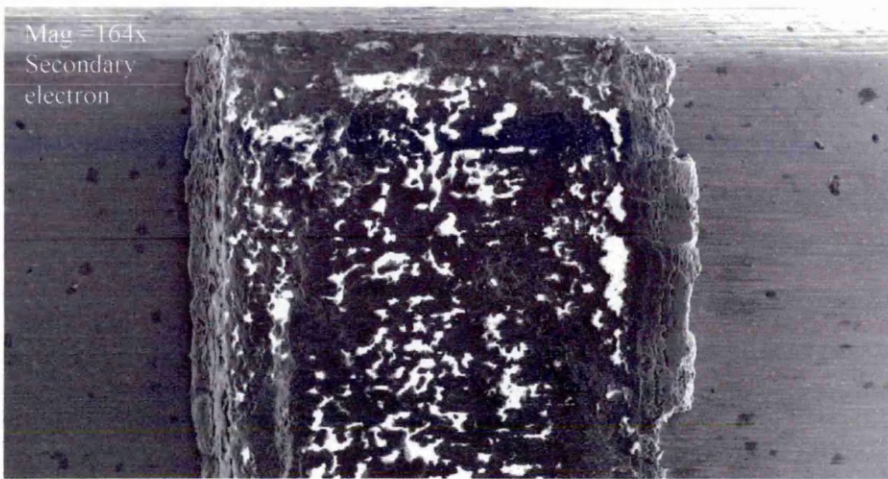


Figure 6.25 Test 507 (20% of fatigue life) shows major damage is not confined to the outer region of the fretting scar

Figure 6.25 shows a significant amount of deterioration has occurred within 20% of the fatigue life. Investigation of the fretting scars for all three of the test run at different percentages of the fatigue life reveals no visual evidence to support the existence of a dominant fretting crack. Figure 6.26 presents images of fretting scars from both the secondary electron and electron backscatter modes of imaging which show that despite extensive surface damage, a dominant fretting crack was not identified.

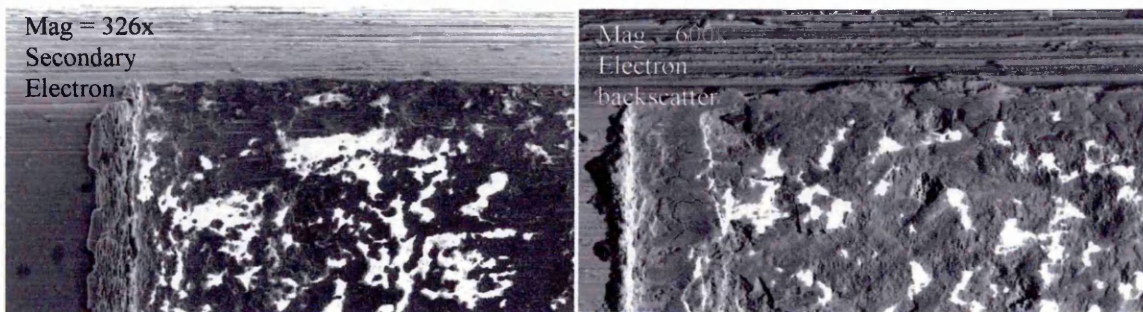


Figure 6.26 Test 509 (60% of fatigue life) both the secondary electron and backscatter modes of imaging show no evidence of a dominate fretting fatigue crack

The images of the fretting scar show that a significant amount of material has been removed from the specimen surface during the fretting process. Therefore, increasing the axial stress to 100MPa has increased the wear mechanism at the contact surface.

6.3.1.2 Initial Crack Growth for 100MPa Contact Pressure (600 test series)

The 100MPa contact pressure was run at three axial stresses, 80MPa, 100MPa and 120MPa. Investigation of the fretting scar for the lower axial load case (80MPa) revealed dominant fretting fatigue cracks were identified in all three of the test run at different percentages of the fatigue life. The fretting scars exhibited the two distinct regions of damage, a relatively smooth inner region and a heavily damaged outer region. Figure 6.27 presents a typical fretting scar for this load case.

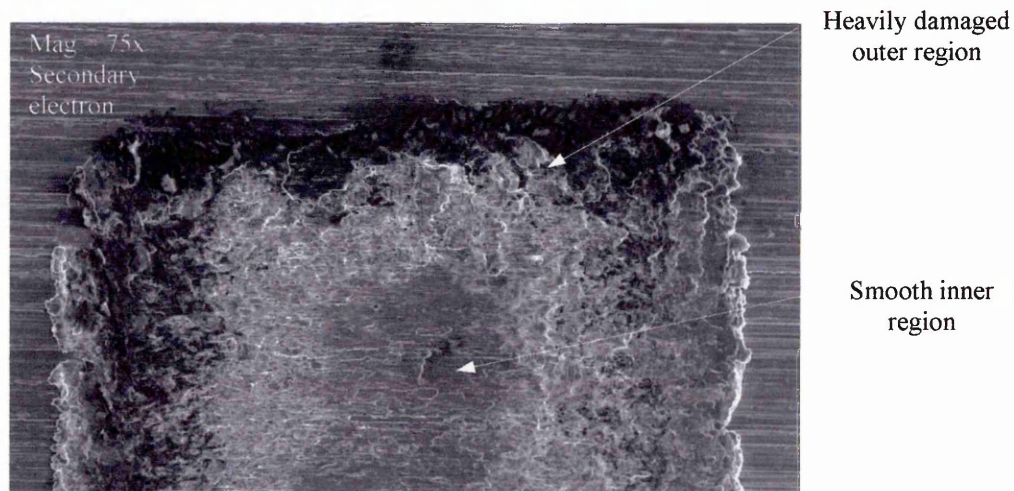


Figure 6.27 Test 601 (20% of fatigue life) typical fretting scar for the 80MPa axial stress and 100MPa contact pressure experiments. Image shows distinct boundary between the relatively smooth inner region and heavily damaged outer region of the fretting scar

Dominant fretting fatigue cracks were found to have grown substantially within 20% of the fatigue life. Figure 6.28 presents both secondary electron and electron backscatter images of fretting cracks identified during this early stage of the fatigue life

Dominate fretting fatigue crack



Figure 6.28 Test 601(20% of the fatigue life) images showing the presence of a dominant fretting crack in both secondary electron and electron backscatter modes of imaging

The dominant fretting cracks grew along the edge of the fretting scar and propagated through the depth of the scar into the bulk of the aluminium specimen. Figure 6.29 presents images of the fretting scars for the tests run to 60% of the fatigue life. The presence of a dominant fatigue crack is clearly visible.

Detail of dominant crack

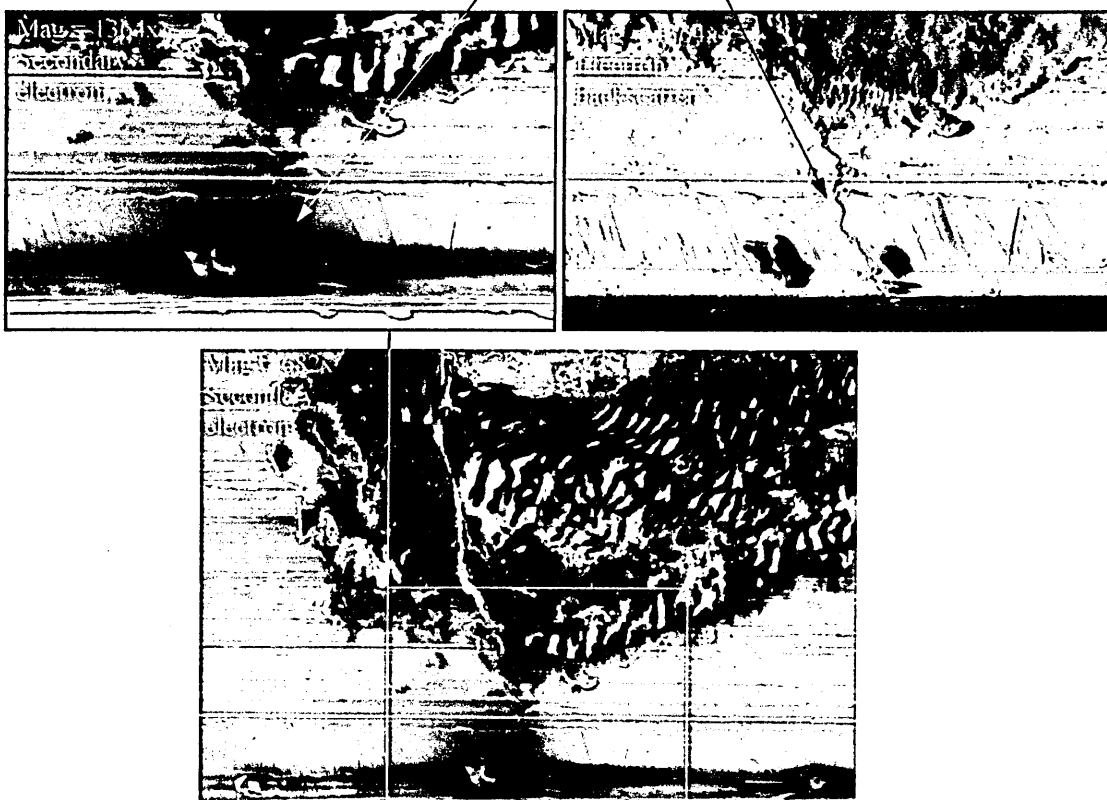


Figure 6.29 Test 603 (60% of the fatigue life) evidence of dominant fretting cracks, which have propagated from a surface crack along the edge of the fretting scar

Increasing the axial stress to 100MPa reveals little discernible difference in the fretting scar from the previous results (80MPa axial stress). Examination of the fretting scar shows the two distinct areas of damage are present. Figure 6.30 presents images of a typical fretting scar for this load case, the scar exhibits the smooth inner region and the heavily damaged outer region.

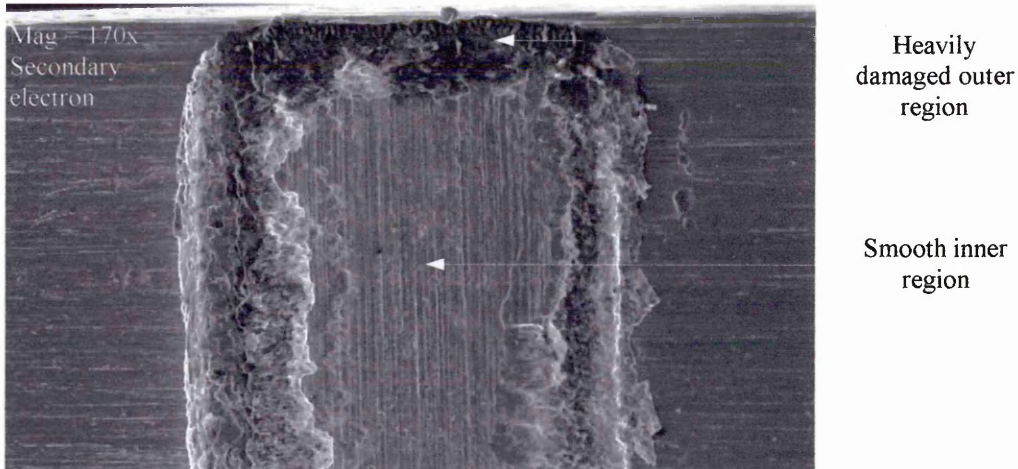
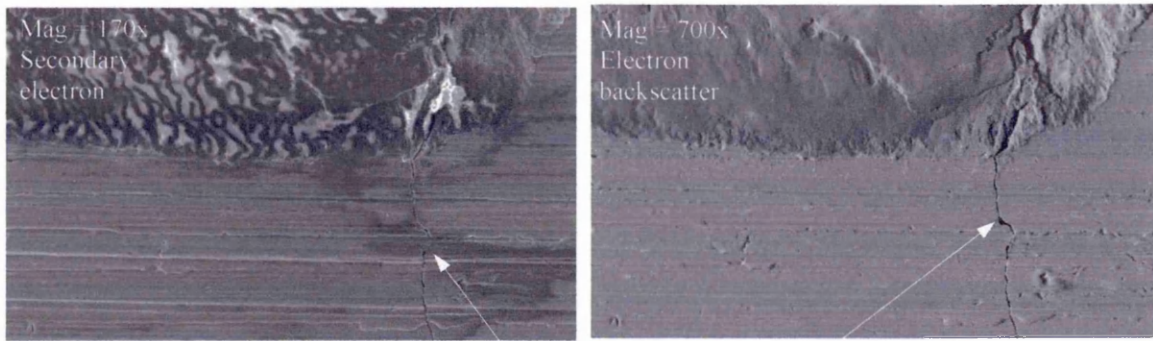


Figure 6.30 Test 604 (20% of fatigue life) shows the fretting scar exhibits the two distinct regions of scarring.

Inspection at the edge of the scarred region reveals that dominant fretting cracks were initiated for tests run at 20%, 40% and 60% of the fatigue life. The dominant crack initiated from a surface crack at the edge of the fretting scar, the crack then propagated through the depth of the scar. Figure 6.31 presents images of the fretting scar at 20% of the fatigue life and represents the type of cracks observed in the 40% and 60% of fatigue life tests.



Dominant fretting fatigue crack

Figure 6.31 Test 601 (20% of fatigue life) shows the type of dominant fretting fatigue crack observed in all test run with 100MPa axial stress and contact pressure

When the axial stress was increased to 120MPa the fretting scar changed. The two regions of damage previously seen in the 80MPa and 100MPa axial stress result were not apparent in fretting scar for the 120MPa axial stress load case. The entire contact area had severe surface damage, (similar to the fretting scar generated for the 80MPa contact pressure with 100MPa axial stress). Figure 6.32 presents images of a typical fretting scar for this load case.

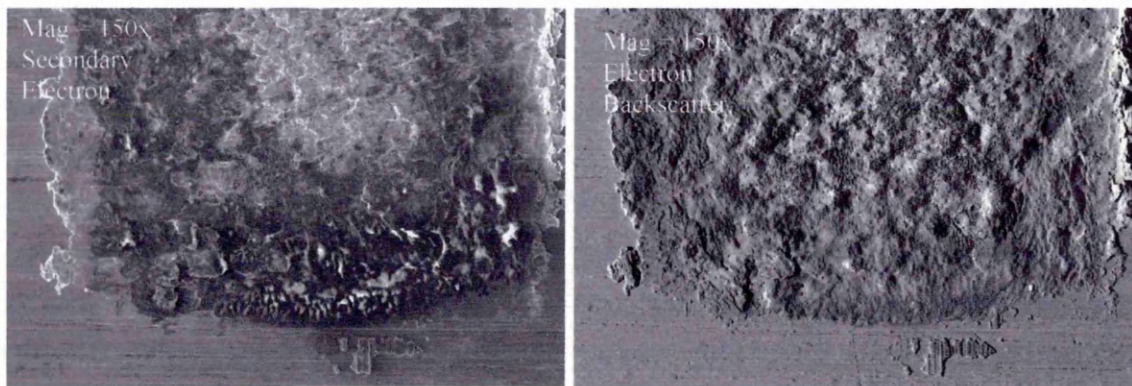


Figure 6.32 Test 607 (20% of fatigue life) shows the type of surface damage observed for experiments run at 120MPa axial stress with 100MPa contact pressure

Examination of the scarred region provided no visual evidence of a dominant fretting fatigue crack for any of the tests (20%, 40% and 60%). The extent of the surface damage implied that the load case had increased the wear mechanism.

6.3.1.3 Initial Crack Growth for 120MPa Contact Pressure (700 test series)

The 120MPa contact pressure was run with three axial stresses 100MPa, 120MPa and 140MPa. All the fretting scars for each of the three axial stresses exhibit similar results with two distinct regions of damage, the heavily damaged outer region and the relatively smooth inner region. Figure 6.33 presents the fretting scars for all three of the axial stress results.

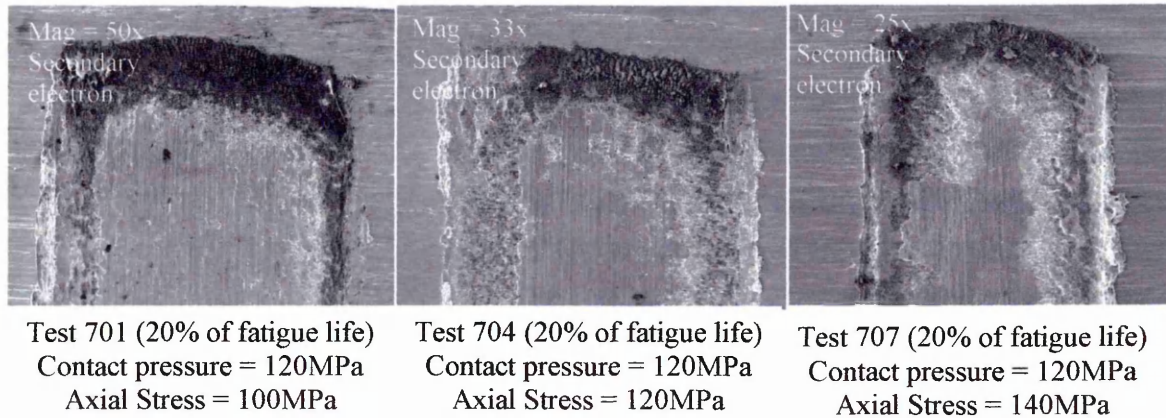


Figure 6.33 Images of the fretting scars for the tests run with 120MPa contact pressure

Examination at the edge of the fretting scar revealed that all three axial stress results provided evidence that dominant fretting fatigue cracks had initiated within 20% of the fatigue lives. The cracks initiated from surface cracks along the edge of the scar and in some cases (e.g. test 704) multiply cracks were identified. This indicates that dominance has been shared between more than one crack, resulting in two cracks growing beyond the fretting scar. Figure 6.34 presents images of the fretting scars where dominant cracks were identified.

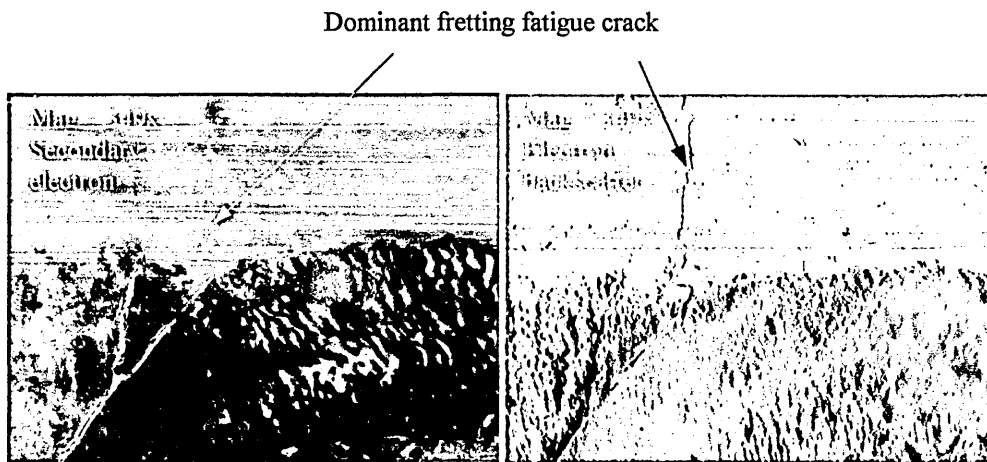


Figure 6.34a Test 701 (20% of the fatigue life) shows the presence of a dominant crack at the edge of the fretting scar

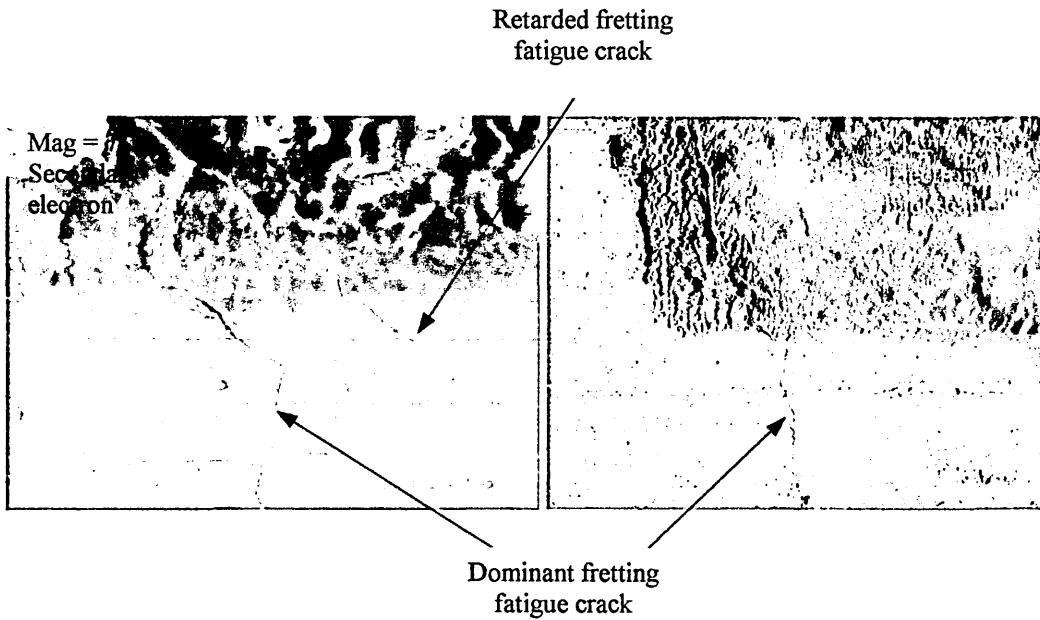


Figure 6.34b Test 704 (20% of the fatigue life) shows two dominant cracks at the edge of the fretting scar

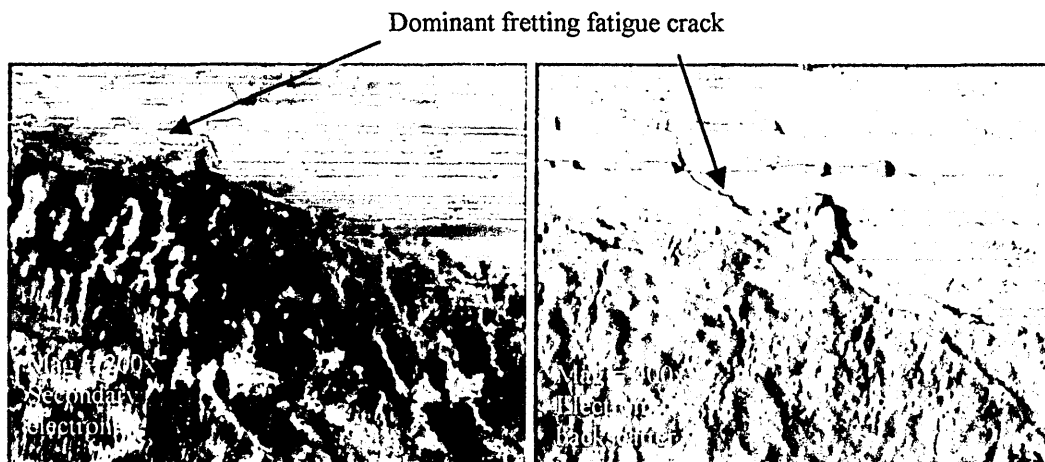


Figure 6.34c Test 707 (20% of the fatigue life) shows a dominant crack at the edge of the fretting scar

Due to the initiation of dominant fretting cracks within 20% of the fatigue life for all axial stresses used during the 120MPa contact pressure experiments, the continued experimentation run to 40% and 60% of the fatigue life was not considered necessary.

6.3.1.4 Summary of the Initial Crack Growth Study

A summary of the findings from the study of initial crack growth is presented in tables 6.1 to 6.3. The tables include the peak friction force amplitude measured during the fretting period.

Table 6.1 80MPa Contact Pressure

Axial Stress (MPa)	Friction Force (KN)	Description of Fretting Fatigue Scar	Fretting Fatigue Crack Initiation
60	0.572	Minor level of wear with no distinct pattern of damage	No (reliable) dominant fretting fatigue cracks identified
80	0.755	Fretting scar exhibits two distinct regions of damage, a heavily damaged outer region and a relatively smooth inner region	Dominant fretting fatigue cracks found to initiate in edge region of fretting scar within 20% of fatigue life
100	0.85	High levels of wear result in severe levels of surface damage, no distinct pattern of damage	No dominant fretting fatigue cracks identified

Table 6.2 100MPa Contact Pressure

Axial Stress (MPa)	Friction Force (KN)	Description of Fretting Fatigue Scar	Fretting Fatigue Crack Initiation
80	0.83	Fretting scar exhibits two distinct regions of damage, a heavily damaged outer region and a relatively smooth inner region	Dominant fretting fatigue cracks found to initiate in edge region of fretting scar within 20% of fatigue life
100	1.0	Fretting scar exhibits two distinct regions of damage, a heavily damaged outer region and a relatively smooth inner region	Dominant fretting fatigue cracks found to initiate in edge region of fretting scar within 20% of fatigue life
120	1.1	High levels of wear result in severe levels of surface damage, no distinct pattern of damage	No dominant fretting fatigue cracks identified

Table 6.3 120MPa Contact Pressure

Axial Stress (MPa)	Friction Force (KN)	Description of Fretting Fatigue Scar	Fretting Fatigue Crack Initiation
100	0.95	Fretting scar exhibits two distinct regions of damage, a heavily damaged outer region and a relatively smooth inner region	Dominant fretting fatigue cracks found to initiate in edge region of fretting scar within 20% of fatigue life
120	1.1	Fretting scar exhibits two distinct regions of damage, a heavily damaged outer region and a relatively smooth inner region	Dominant fretting fatigue cracks found to initiate in edge region of fretting scar within 20% of fatigue life
140	1.3	Fretting scar exhibits two distinct regions of damage, a heavily damaged outer region and a relatively smooth inner region	Dominant fretting fatigue cracks found to initiate in edge region of fretting scar within 20% of fatigue life

The examination of the specimen fretting surfaces has revealed that there is a relationship between the type of surface scar and the presence of dominant fretting fatigue cracks. Dominant cracks have been identified where the fretting scar has exhibited two distinct types of surface damage, with a heavily damaged outer region and a relatively smooth inner region. Other types of surface damage were found to contain no evidence of dominant fretting cracks. The absence of dominant fretting cracks occurred when the load case induce minor surface damage (as in the case of 60MPa axial stress with an 80MPa contact pressure) or major surface damage (when the magnitude of the axial stress exceeded the magnitude of the contact pressure, for the 80MPa and 100MPa contact pressure experiments).

In the case of minor surface damage, the lack of damage is indicative of the applied loads. The 80MPa contact pressure and 60MPa axial stress were not sufficient to cause enough wear to generate a significant amount of surface cracking and the friction force generated at the contact surface was not sufficient to initiate a dominant fretting crack.

In the case of major surface damage, the combinations of axial stress and contact pressure did generate a significant amount of surface cracking. The friction forces generated under these conditions were sufficient to initiate a dominant fretting crack. Therefore, the lack of dominant fretting cracks must be attributed to increases in the wear mechanism.

The process of wear removes material from the contact surface during the load cycle. The material removed from the contact surface becomes debris, which then acts as a third body solid lubricant. The amount of material removed during each load cycle is dependent on the wear mechanism and the size of freshly nucleated fretting cracks is dependent of the material properties and stress concentration at the surface. Therefore, if the amount of material removed from the contact surface by the wear mechanism is greater than the size of a freshly nucleated crack, the nucleating crack will be removed during the wear process before it can initiate further and become dominant.

It is this process that is responsible for the lack of dominant fretting cracks for the loads which induce major surface damage. This behaviour is supported by the findings in the summary tables 6.1 to 6.3. In each case where major surface damage has occurred across the entire contact area, there has been no visual evidence of dominant fretting cracks. Therefore, the probability of initiating a dominant fretting fatigue crack is dependant not only on friction force and stress distribution within the material but also on the wear mechanism at the contact surface.

6.4 THE STUDY OF FRETTING FATIGUE LIVES

Fretting fatigue lives were recorded for the 3mm contact pad size experiments for both the nominal fretting condition (800 series) and the study of controlled slip on friction force (900 series).

6.4.1 Fretting Fatigue Lives for the 3mm Contact Pad Experiments (800 Series)

The fretting fatigue lives for the 3mm pad size demonstrate the effects of varying the applied contact pressure and axial stress on the number of cycles to failure. Figures 6.35a to 6.35c presents the fatigue lives and friction forces recorded during the fretting period for each of the three contact pressures (80MPa, 100MPa and 120MPa) applied during the experiments (800 series). The fatigue lives and friction forces are the recorded values at each of the three axial loads run for each contact pressure.

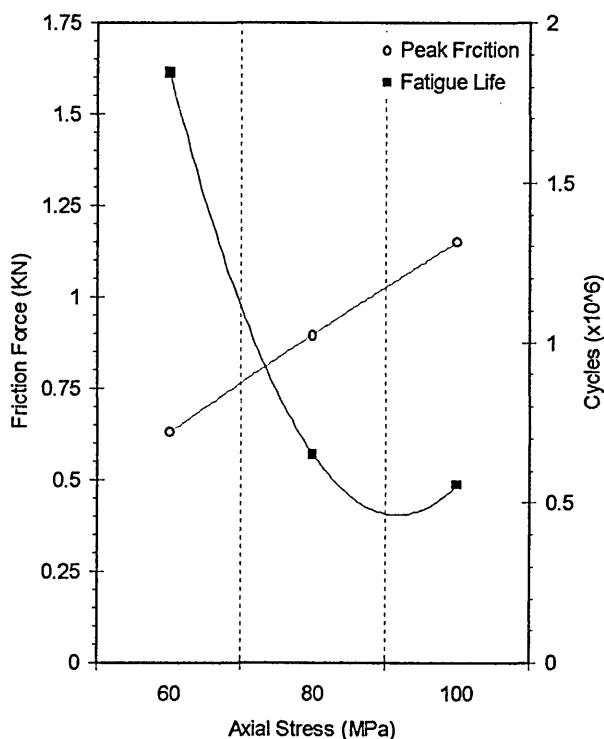


Figure 6.35a Comparison of friction force and fatigue life for the 3mm contact pad size experiments run with 80MPa contact pressure and three axial stress values

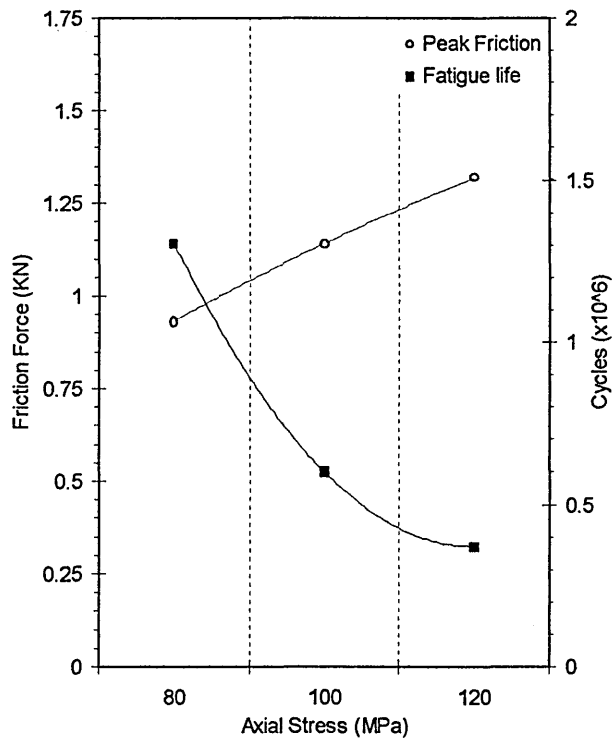


Figure 6.35b Comparison of friction force and fatigue life for the 3mm contact pad size experiments run with 100MPa contact pressure and three axial stress values

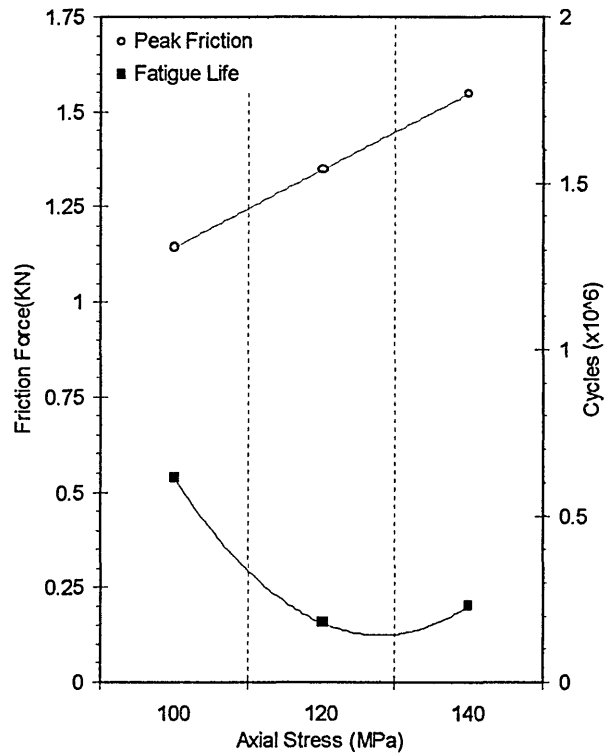


Figure 6.35c Comparison of friction force and fatigue life for the 3mm contact pad size experiments run with 120MPa contact pressure and three axial stress values

The results show that the fatigue lives decrease and the friction force increases as the contact pressure increases. The relationship between friction force and contact pressure is defined by Coulomb's friction law, when the friction coefficient achieves a stable peak value during the fretting period. Therefore, changes in the peak friction force during this period are proportional to changes in the contact pressure. Increases in the contact pressure result in increases in the friction force. The effects of this increase in friction force can be seen in the reduction in the fatigue lives.

The results also show the effect of increasing axial stress. Friction responds in micro slip for a majority of the fatigue life (the transition from macro to micro slip occurs over only a few hundred cycles). Therefore, axial stress has a significant effect on friction force when the contact interaction is in micro slip. The response of friction force to axial stress can be seen from figures 6.35a to 6.35c. Increasing the magnitude of the axial stress results in increases in the friction force. The relationship between axial stress and fatigue life changes as axial stress increases. The initial increase in axial stress results in a reduction in the fatigue lives. However, as the axial stress is increased further the fatigue life does not decrease. At higher axial stresses the fatigue lives either stabilise or in some cases increase.

This phenomena can not be attributed to the stresses generated by the loads which drive the crack, as increasing the axial stress will increase the stress concentration at the crack tip which will increase the crack growth rate and reduce the fatigue life. As this is not observed in the results, the increase or stabilisation in the fatigue life must be attributed to another mechanism, which is influenced by increasing the axial stress. As discussed in the analysis of initial crack growth (section 6.3.1), high axial stresses can increase the wear mechanism, which then acts to remove the crack nuclei before the crack can

initiate and become dominant. It is this mechanism that alters the fatigue life response at high axial stresses.

6.4.1.1 Comparison of Fretting Fatigue Lives for the 1.27mm and 3mm Contact Pad Experiments

The fretting fatigue lives from the 3mm pad size experiments are compared with the fretting fatigue lives for the 1.27mm pad size experiments conducted by Fernando *et al* [75].

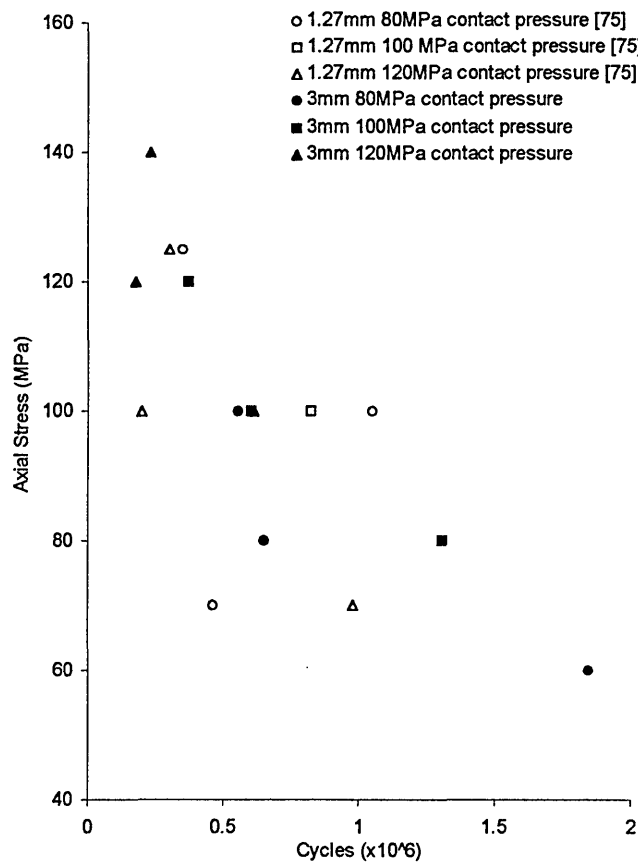


Figure 6.36 Comparison of the fretting fatigue lives for the 1.27mm [75] and 3mm contact pad size experiments

Comparison of the results for similar load cases suggests the smaller contact pad size (1.27mm) generate shorter fretting fatigue lives than the larger contact pad size. The

difference in fatigue lives can be attributed to differences between the experimental apparatus and fatigue scatter. The basis for compatibility is determined from the trend of the overall results. Both sets of results demonstrate similar behaviour in response to the axial stress. As the axial stress increases, the fatigue lives reduce until the fatigue lives either stabilise or increase at higher values of axial stress. This phenomenon has been attributed to an increase in the wear mechanism, which acts to retard initial crack growth and increase the number of cycles to failure.

6.4.2 The Effects of Controlled Slip on Fretting Fatigue Lives

Controlling slip at the contact surface has effectively controlled the friction force response. Varying both the slip displacement magnitudes and the cyclic phase angle (with the axial load cycle) the contact interactions and friction force magnitudes have responded differently to a nominal case where only the applied axial stress determines slip displacements and friction force. The consequence of controlling slip and subsequently friction force were measured in the fretting fatigue lives.

In the experiments where friction force was reduced to almost zero, (test with a $70\mu\text{m}$ slip displacement applied in phase with the axial load cycle) increasing contact pressure had a marginal affect on the peak friction force. Comparing the fatigue lives for each of the three contact pressures reveals similar behaviour, despite variations in the number of cycles to failure, the fatigue lives remained relatively constant. Figure 6.37 presents the fatigue lives for the tests and compares with the peak friction forces recorded during the tests for each contact pressure.

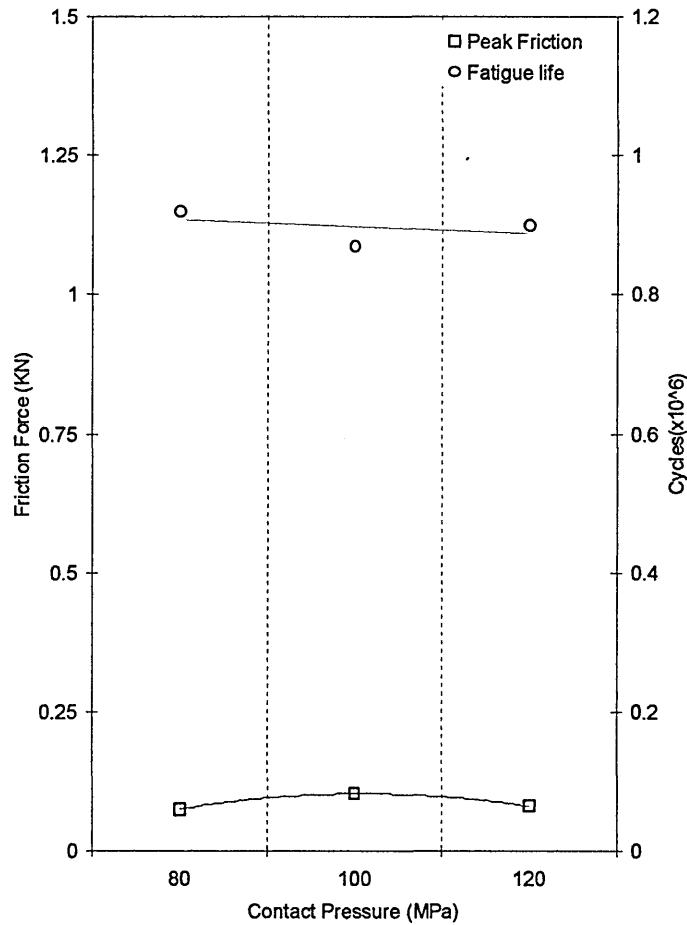


Figure 6.37 Comparison of fretting fatigue lives with friction force for experiments run with a 70 μ m slip displacement in phase ($\phi = 0$) with the axial load generating almost no friction

The results show that changes in contact pressure have little or no effect on the friction force, which has little or no effect on the fatigue lives. The induced slip has reduced the amount of relative surface motion, which has reduced the friction force and wear mechanism. Therefore, the fatigue lives remain relatively constant.

When the nominal slip displacement was reduced by 10 μ m, the effects on peak friction force values were marginal when compared to a nominal load case. However, the contact interaction was affected, in that there was no transition from macro to micro slip during the initial test period, which was previously observed under nominal conditions.

Increasing contact pressure resulted in fatigue lives increasing. Figure 6.38 presents the fatigue lives for the tests run with a 10 μ m reduction in slip displacement.

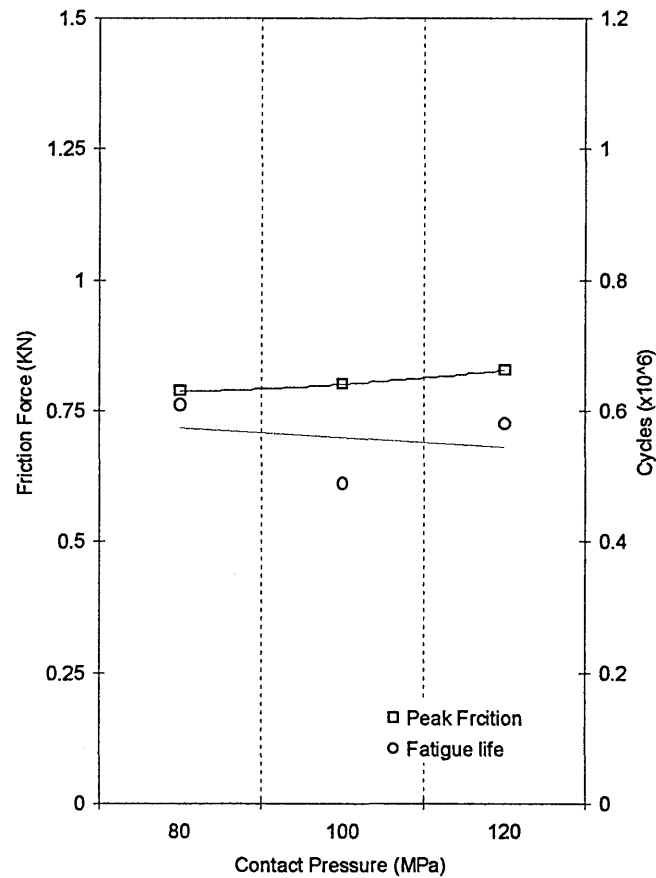


Figure 6.38 Comparison of fretting fatigue lives with friction force for experiments run with a 10 μ m slip displacement in phase ($\phi = 0$) with the axial load

The results show that increasing the contact pressure has marginally increased the friction force. The marginal increase in friction force has resulted in the fretting fatigue lives exhibiting similar behaviour to the nominal case although not to the same extent. The initial increase in contact pressure (from 80MPa to 100MPa) results in a decrease in the fretting fatigue life. However, further increases in the contact pressure result in an increase in the fretting fatigue lives. This behaviour has been observed in the nominal fretting fatigue cases (section 6.4.1) and has been attributed to wear affecting the initial growth of dominant fretting fatigue cracks. The reduction in nominal slip (by 10 μ m) has

reduced the effects of this behaviour and the differences in the fatigue lives are not as large as the differences in the fatigue lives for nominal cases (section 6.4.1)

Comparing the fatigue lives for the experiments run with two different slip displacements (10 μm and 70 μm) in phase with the axial load cycle reveals that friction force has a significant influence on fatigue life during micro slip. Comparison of the results clearly shows that the lower friction force results (70 μm slip displacement) have longer fatigue lives than the higher friction force results (10 μm slip displacements). Figure 6.39 compares the fretting fatigue lives for the two slip displacements applied in phase with the axial load cycle.

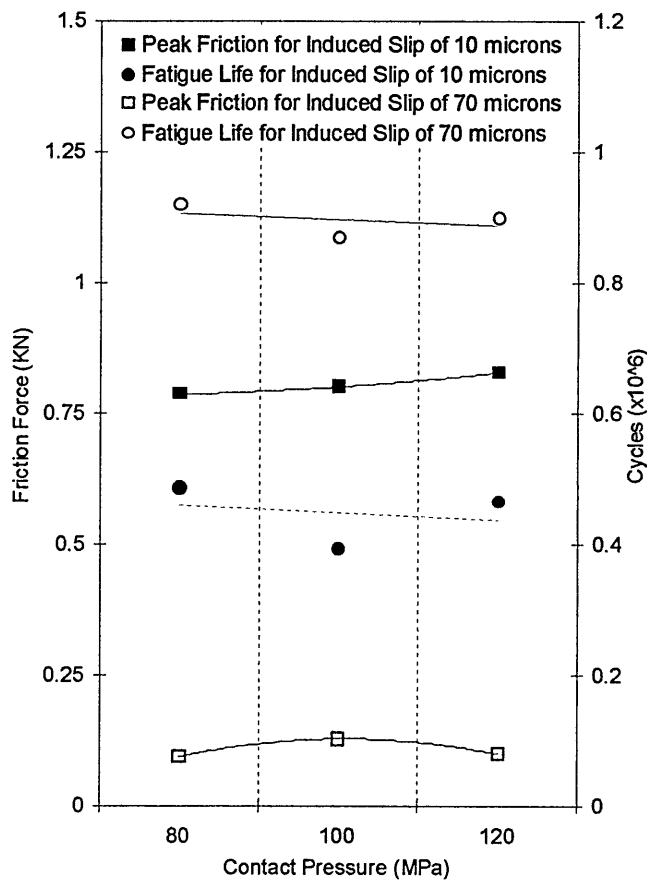


Figure 6.39 Comparison of fretting fatigue lives with friction force for experiments run at 10 μm and 70 μm slip displacements in phase ($\phi = 0$) with the axial load

Altering the phase angle to apply a 20 μ m slip displacement 90⁰ out of phase with the axial load cycle has resulted in the friction force responding initially in macro slip, translating to micro slip as fretting and wear damages the contact surface. The width of the frictional hysteresis shows a large amount of slip occurs, even when the condition changes to micro slip. The fatigue lives vary with contact pressure so that as the contact pressures increases (from 80MPa to 100MPa) the fatigue lives reduce. However, further increases in the contact pressure results in an increase in the fatigue life. Therefore, at higher contact pressures wear is responsible for the removal of initial fretting cracks, which retards the dominant crack growth process. Figure 6.40 compares friction forces and fatigue lives for experiments run at 20 μ m out of phase with the axial load cycle

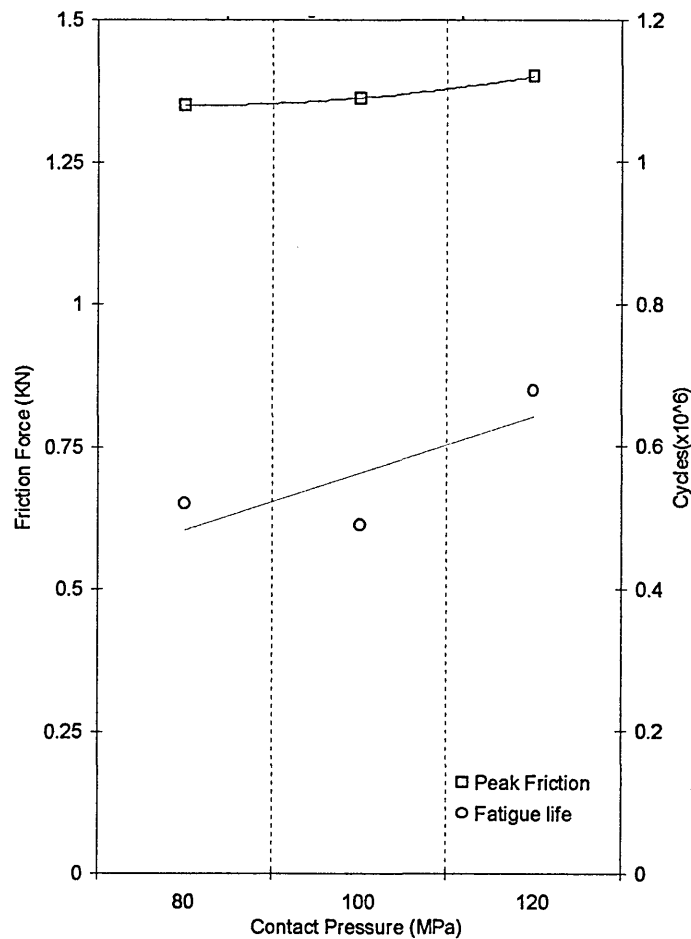


Figure 6.40 Comparison of fretting fatigue lives with friction force for experiments run at 20 μ m slip displacement out of phase ($\phi = 90^0$) with the axial load

Inducing various magnitudes of slip displacements either, in phase or 90° out of phase with the axial load cycle has affected the friction force. The friction force has a significant influence on the initial growth of dominant fretting cracks, which affects the overall fatigue life.

6.5 ANALYSIS OF THE NUMERICALLY PREDICTED STRESSES FOR FLAT CONTACTS

The finite element solution was validated by comparing the predicted friction behaviour with the experimental friction behaviour recorded during the peak fretting period. The finite element models for both contact pad sizes (1.27mm and 3mm) successfully predicted the friction force response for a range of contact pressures and applied axial stresses. The validated finite element solutions supplied the stress distributions in the region at the edge of the flat contact. The experimental study of initial crack growth and failure demonstrates that dominant fatigue cracks initiate in the edge region of the fretting scar. The initiation and continued propagation of a dominant fretting crack requires a concentration of stresses to drive crack growth. Therefore, the stresses in this region were investigated to determine the influence flat contact had on the stress distributions. Furthermore, study of the friction force distributions along the contact surface (Appendix E) reveals that the peak friction force occurs at the edge of the contact area. Therefore, an analysis of the stresses at the contact edge was conducted to determine the influence of friction force on surface stresses.

Lykins *et al* [66] reported that the crack location in fretting fatigue failure correlated well with the location of the maximum shear stress. Therefore, shear stress is considered to be influential in the initiation of dominant fretting fatigue cracks. However, at the contact surface, shear stress is influenced by friction force and that influence will depreciate as the depth beneath the contact area increases. The diminishing influence of friction force on the shear stress with increasing depth will result in a depth at which friction force has a negligible effect on shear stress. At this depth, continued crack growth must be attributed to another crack driving mechanism. Due to the orientation of the crack, the axial stress in the fretting region is considered to be the driving

mechanism for continued crack growth. Therefore, the axial and shear stress distributions are considered at both the surface and through the depth of the fretting region. Figure 6.41 illustrates the orientation of a typical dominant fretting fatigue crack with the crack driving stresses.

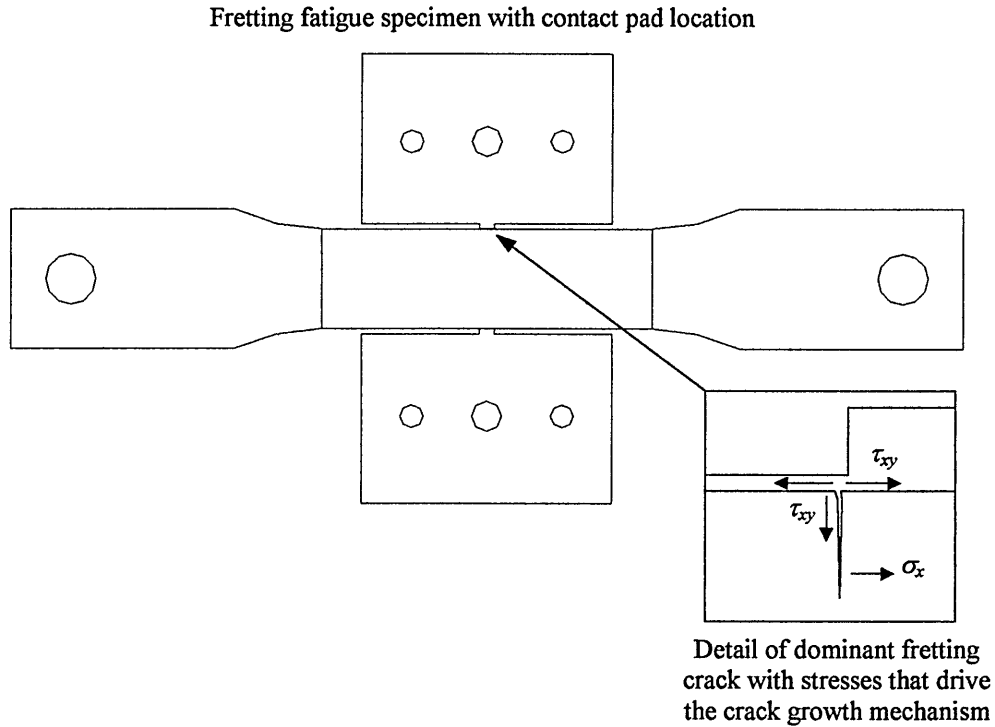


Figure 6.41 The multiaxial stress system in the fretting fatigue specimen

The axial and shear stresses incorporate both a positive and negative component (in response to the axial load cycle). The direction of the shear stress in relation to the orientation of experimentally observed fretting fatigue cracks signify that both the positive and negative components of the cyclic shear stress need to be considered, as both contribute to the crack driving mechanism. Therefore, the shear stress is assessed as a range, which accounts for both the maximum positive value and minimum negative value. However, in the case of axial stress, only the tensile component is considered. The compressive component of the axial stress is not considered to contribute to the crack driving mechanism due to the orientation of the fretting crack. In compression, the axial stress will act to close the crack and although cracks do grow in compression, it is

due to the presence of shear stresses. Therefore, compressive axial stresses do not directly contribute to the crack growth mechanism and so the maximum tensile value is used to represent axial stress.

Comparison of the results for the two contact pad sizes reveals variations in the magnitudes of the peak stresses with variations in the applied loads. The 1.27mm contact pad size results demonstrate the influence of contact pressure on the shear and axial stress distributions when the contact interaction is in micro slip. The larger 3mm contact pad size results include both the affects of axial loading and contact pressure on the stress distributions when the contact interactions in micro slip.

6.5.1 The Distribution of Stresses at the Contact Surface

Dominant fretting fatigue cracks initiate at the edges of flat contacts where the maximum friction forces occur. Study of the stress distributions at the contact surface (for both the 1.27mm and 3mm contact pad size models) reveals that friction forces significantly influence the shear stress. The shear stress distribution is similar to the friction force distribution and the peak shear stresses occur at the edges of the contact area. Friction force also affects the tensile component of the axial stress, although not to the same extent as the shear stress results. The maximum tensile stress occurs in the region near the edge of the contact area. Figure 6.42 presents an example from Appendix F, the result is typical of the surface stress distributions for both the 1.27mm and 3mm contact pad size models.

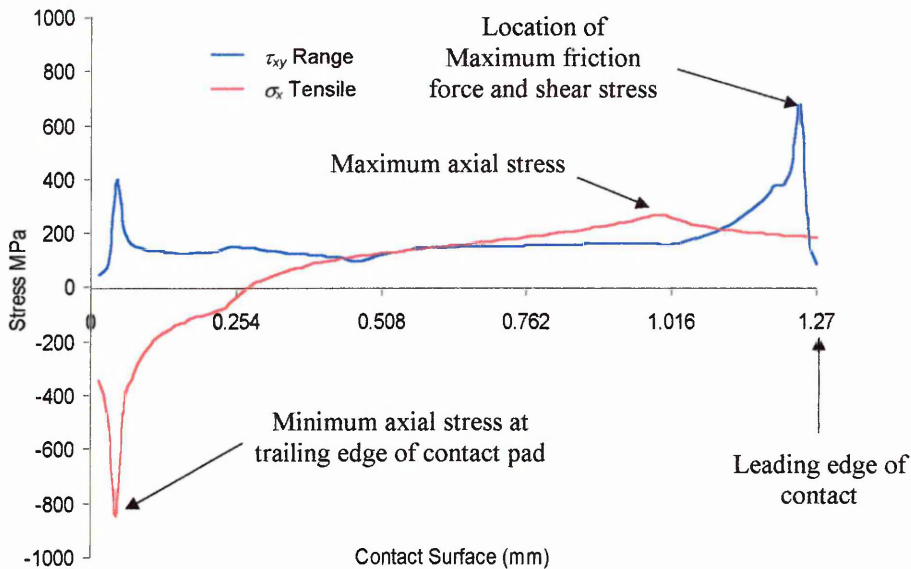


Figure 6.42 Example from Appendix F (test 124) demonstrating the shear and axial stress distributions at the contact surface

In the case of the 1.27mm contact pad size models, the peak axial stress increased in magnitude and moved closer to the leading edge of the contact area as the contact pressure increased. The axial stress at the contact surface was separated into both a tensile and compressive area. At the lower contact pressures, the area of the contact surface in compression was localised to the trailing edge of the contact pad. As the contact pressure increased the area of compression at the contact surface increased. This behaviour resulted in the contact surface being in both equal areas of compression and tension for the highest contact pressure results.

At low contact pressures, the shear stress distribution is relatively symmetrical, in that the peak shear stress at the trailing edge of the contact pad is similar in magnitude to the peak shear stress at the leading edge of the contact pad. As the contact pressure increases, the shear stress distributions concentrate towards the leading edge of the contact pad. Therefore, increasing contact pressure results in a concentration of both the axial and shear stresses within the area of the leading edge of the contact pad. Figure

6.43 demonstrates the effects of increasing contact pressure on the axial and shear stress distributions

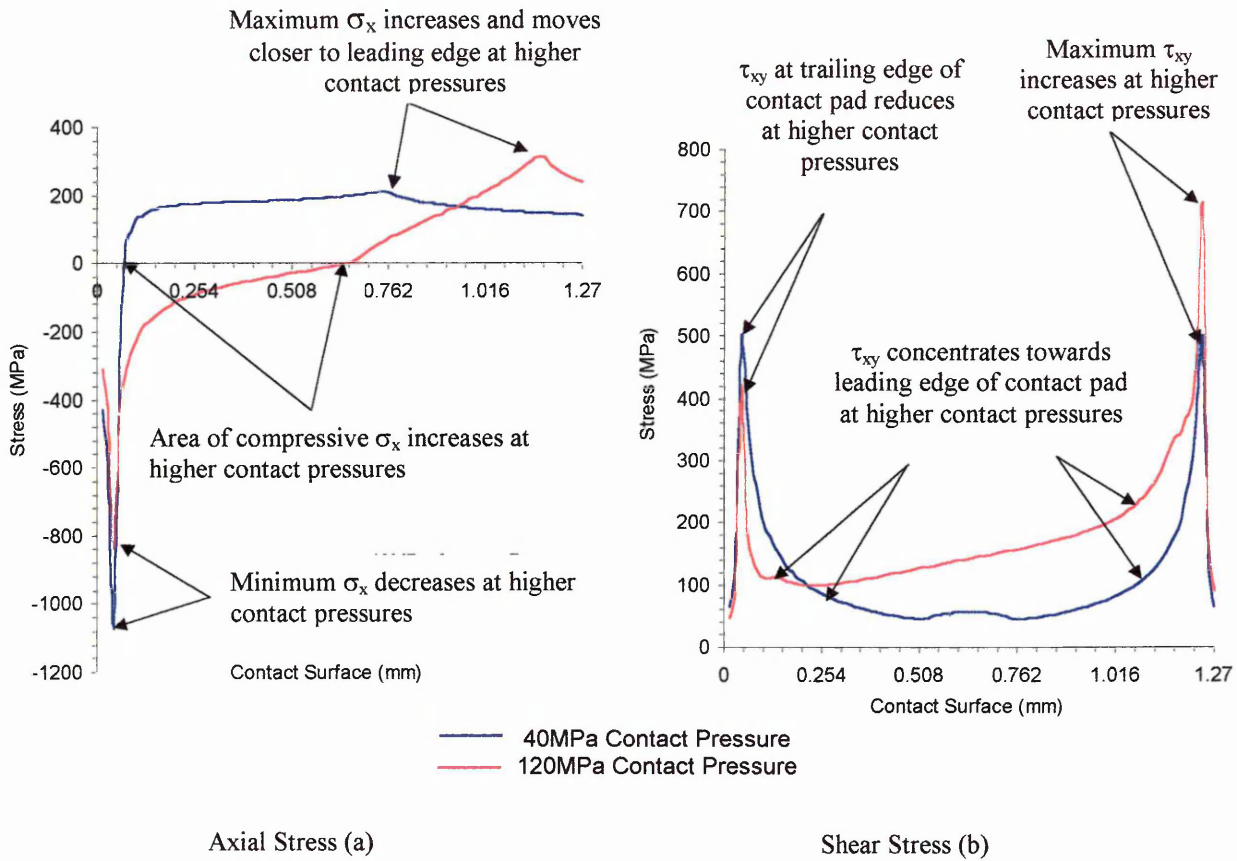


Figure 6.43 Demonstrates the effects of increasing contact pressure on the axial (a) and shear (b) stress distributions at the 1.27mm contact surface

Analysis of the surface stress distributions for the 3mm contact pad size models reveals that the axial and shear stresses behave in a similar manner to the 1.27mm stress distributions when the contact pressure varies. However, variations in the axial loads (when the contact pressure remains constant) have different effects on the axial and shear stress distributions at the contact surface. The peak axial and shear stresses occur at the leading edge of the contact pad. However, only the shear stress increases with increasing axial load, the peak axial stress remains relatively constant. Increasing the axial load has resulted in the stresses concentrating at the leading edge of the contact

pad. Figure 6.44 illustrates the effects of varying axial load on the surface stress distributions for the 3mm contact pad size results.

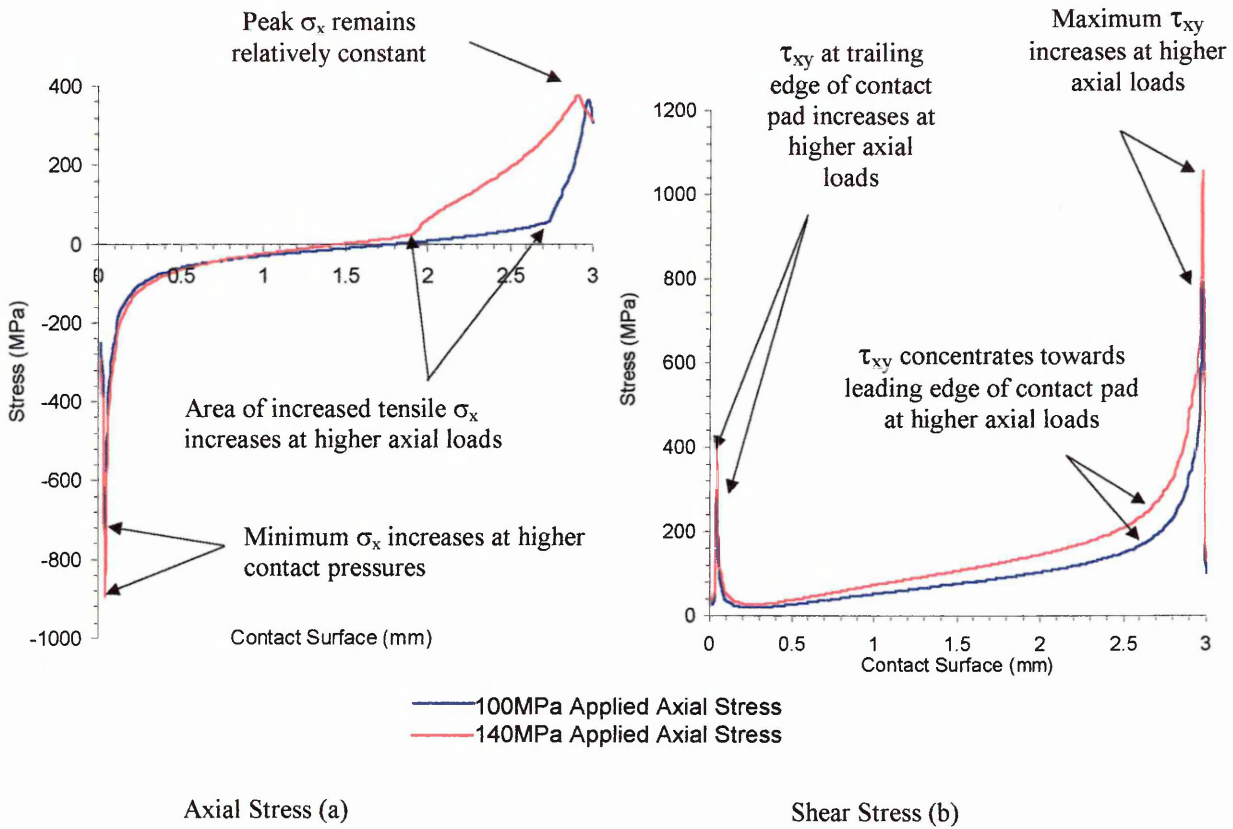


Figure 6.44 Demonstrates the effects of increasing axial load on the axial (a) and shear (b) stress distributions at the 3mm contact surface

In all the surface stress results (available in Appendix F) the shear stresses achieve a maximum peak value within 60 μ m of the leading edge of the contact pad. This behaviour demonstrates that the peak shear stress at the surface aligns with the experimentally observed location for the initiation of dominant fretting fatigue cracks. This observation agrees with the findings from the work conducted by Lykins *et al* [66]. At the surface, the shear and axial stresses are influenced by the friction force, however, friction force is generated at the contact surface and not through the depth of the material. Therefore, the sub surface axial and shear stress distributions are analysed to ascertain how the stresses develop through the depth of the fretting region.

6.5.2 The Distribution of Sub Surface Stresses

The sub surface stress distributions are defined as the stresses predicted along planes at incremental depths, which lie parallel to the contact surface. The depth increment is determined by the element size, which are approximately $15\mu\text{m}$ for both the 1.27mm and 3mm contact pad size models. Figure 6.44 illustrates the location of the sub surface stress planes in relation to the contact surface and load orientations.

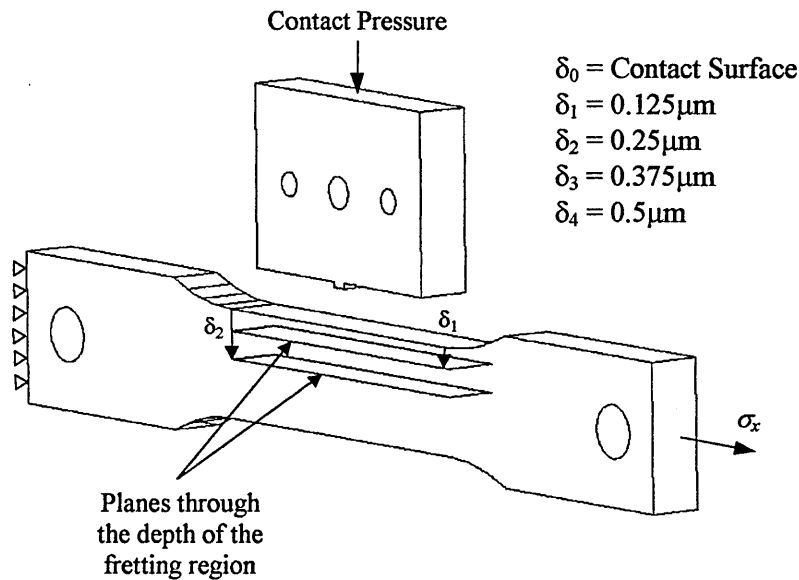


Figure 6.45 Schematic of sub surface planes where stress was measured

Analysis of the axial and shear stresses in the region beneath the contact surface reveals the magnitude of the stresses depreciates as the depth increases. This behaviour is apparent for both the 1.27mm and 3mm contact pad size results. The magnitude of the shear stress has the most significant rate of change with increasing depth. The magnitude of the axial stress also decreases as the depth increases. However, the rate of change is not as severe as the shear stress results. Figure 6.46 presents an example from Appendix H, which shows how axial and shear stresses vary with depth through the fretting region.

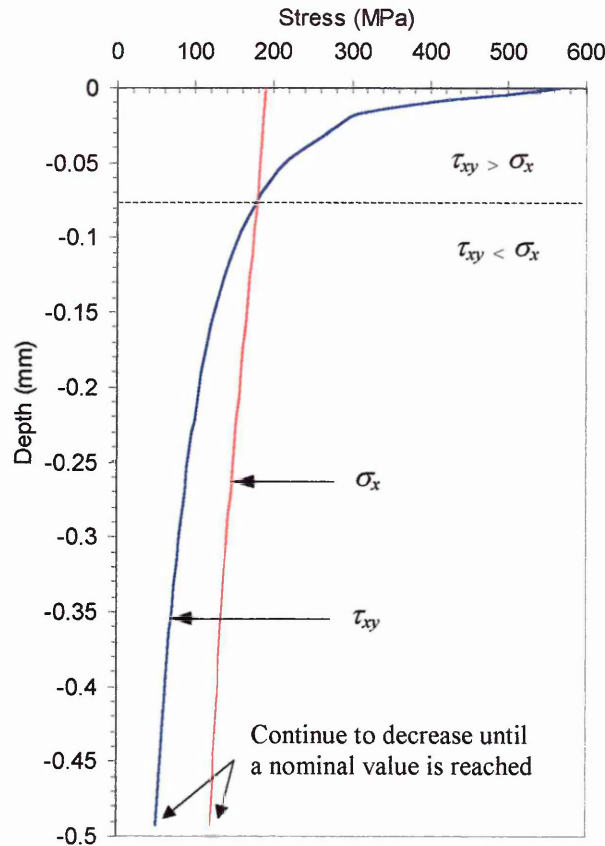


Figure 6.46 Shows how stresses vary as the depth increases through the fretting region at the edge of the contact area (Test 124)

The reduction in stress as the depth increases through the fretting region is due to the diminishing effects of friction force. Others have observed the effect of increasing depth on the sub surface stress distributions. In the analyses of sub surface stress contours associated with fretting contact, it was revealed that the contact stresses decay rapidly beneath the contact surface [14,18,25,31]. Appendix G presents the sub surface stress distributions for both the 1.27mm and 3mm contact pad size results

Comparing the axial and shear stress distributions at each incremental depth revealed that the peak stresses coincided with the leading edge of the contact pad (the critical location) in almost all the applied load cases. Exceptions did occur however, the

differences were attributed to macro slip at the contact surface. Comparing the magnitude of the axial and shear stresses at the contact surface, revealed that the shear stresses were larger than the axial stresses. This relationship was not maintained through the entire depth of the fretting region (the fretting region is defined as the sub surface volume in which the axial and shear stresses are influenced by friction). Study of the depth to which the contact parameters influenced the subsurface stress distributions revealed the influence extends to approximately 200 μ m beneath the contact surface. This observation is in agreement with the findings from the work conducted by Swalla and Neu [28].

By monitoring the axial and shear stress magnitudes through the depth of the fretting region at the edge of the contact area (the critical location), it was observed that the maximum stress changed from shear at the contact surface to axial at particular depths. The depth at which this transition occurred altered for different load cases. The significance of this change in maximum stress becomes apparent when considering the mechanism for driving crack growth. Although both the axial and shear stresses generate a multiaxial stress state that controls the crack growth process, the magnitude of each stress will dictate the influence that stress has on crack growth at particular depths. Therefore, at the surface the initial crack growth will be primarily influenced by the shear stress, as the shear stress component is significantly larger than the axial stress component at the surface. However, as the crack grows through the depth of the fretting region the maximum stress changes from shear to axial and the continued crack growth will be primarily influenced by the axial stress.

This condition will continue until the crack grows beyond the fretting region and the shear stress contribution becomes negligible. When the crack grows beyond the fretting

region the growth will be driven by the axial stresses and the effects of contact and friction no longer influence the crack growth process. Figure 6.47 presents results for the 3mm contact pad size models that demonstrate the depth at which the maximum stress changes from shear stress to axial stress (transfer depth). The results represent the change in depth for a range of applied axial stresses (axial loads) and contact pressures.

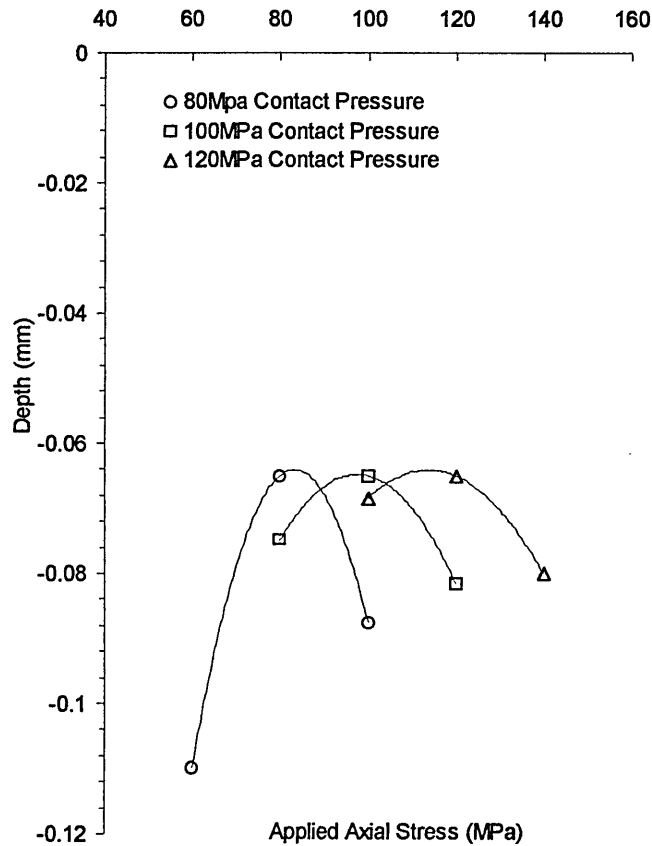


Figure 6.47 The depths at which the magnitude of the axial stress becomes larger than the shear stress for the 3mm contact pad size results. The results are taken at the critical location

Study of the depths at which the maximum stress transfers from shear to axial demonstrate that the load case has significant influence on the transfer depth. The transfer depth increases as the contact pressure increases. However, as the applied axial stress (axial load) increases the relationship changes. Increasing the axial load results in an initial reduction in the transfer depth, although further increases result in an increase in transfer depth. This behaviour is attributed to the type of surface interaction. In micro slip the friction force and subsequent shear stresses are sensitive to changes in axial

load. Therefore, a variation in transfer depth with axial load is due to the contact surface interaction being in micro slip. This non-linear behaviour has been observed for fretting fatigue lives in micro slip, where the fatigue lives reduce with increasing axial load, only to stabilise or increase at higher axial loads. The similarities between fretting fatigue lives and transfer depths at higher axial loads suggest that the increase in fatigue lives is not only influenced by the wear mechanism, but also by the distribution of the multiaxial stress system.

Study of the stress distributions through the depth of the fretting region demonstrates a complex relationship is shared between the axial and shear stresses, which influences the initiation and subsequent growth of dominant fretting fatigue cracks. Due to the combined influence of axial and shear stresses on the growth of fretting fatigue cracks, neither stress should be considered independently. Therefore, further investigation is required to determine an equivalent stress concentration parameter based on both the numerically resolved axial and shear stresses for the purpose of predicting fretting fatigue lives (section 6.6.)

6.6 THE USE OF NUMERICAL STRESSES FOR FATIGUE LIFE PREDICTION

Analyses of the sub surface stress data, at the critical location has suggested a relationship between the axial and shear stresses in the nucleation and subsequent growth of fretting fatigue cracks. An attempt to predict fretting fatigue lives using the sub surface axial and shear stresses was conducted using Neuber's Notch root hypothesis [17].

6.6.1 Notch Root Hypothesis

As the stress/strain distribution in the region of fretting is similar to that of sharp notches, it can be considered that notch fatigue analysis, proposed by Neuber [17] can be used to analyse fretting fatigue problems. Neuber developed a model based on the pre-existence of a notch or discontinuity. The presence of a notch generates a stress concentration, which can then be used to influence the overall life of the component. Taylor [73] considered that a body containing a large blunt notch could have the fatigue limit reduced by an order equivalent to the K_t value, which in the case of a large notch could be as high as three.

The stress concentration is expressed as a ratio of maximum stress at the notch root and the nominal stress (or the stress in an un-notched sample). By equating the presence of a notch to the high stresses generated as a result of contact at the critical location, it is proposed that Neuber's analysis can be employed to predict a fretting fatigue life, based on an equivalent stress concentration factor determined from sub surface axial and shear stresses.

6.6.2 Neuber's Analysis

Neuber's analysis [17] was proposed for a strain life approach, which accounts for notch root plasticity. The method requires the remote strain history and smooth specimen strain life data, or fatigue properties to be known for life prediction. Neuber's rule states that the theoretical stress concentration, K_t , is the geometric mean of the stress and strain concentrations, and although this was only proven for a single geometry, it is assumed to hold true for most notched geometries [17].

$$K_t = \sqrt{(K_\sigma K_\epsilon)}$$

$$K_t^2 = \frac{\sigma}{S} \frac{\epsilon}{e}$$

or

$$K_t^2 S e = \sigma \epsilon \quad \text{Equation 6.1}$$

Neuber's rule (equation 6.1) relates nominal elastic stresses (S) to local elastic-plastic stresses (σ) and has been developed to incorporate fatigue through the application of the fatigue notch factor, K_f . This parameter is dependent on K_t as well as material data, generally developed from empirical data. K_f relates to K_t by means of a notch sensitivity factor, q . In many cases, the effects of the notch sensitivity factor means that K_f is often smaller than K_t so that in the case of a notch sensitivity factor achieving unity ($q = 1$), K_f and K_t become equal. The significance of this means that K_t will always generate the most conservative life predictions and as such the decision to use K_t as the stress concentration factor for fretting fatigue life predictions was based on this argument.

The Neuber's rule can be expressed as follows (see Equation 6.1):

$$K_t^2 S e = \sigma \varepsilon$$

Expressing equation 6.1 in terms of stress and strain range amplitudes

$$K_t \frac{\Delta S \Delta e}{4} = \frac{\Delta \sigma \Delta \varepsilon}{4} \quad \text{Equation 6.2}$$

The nominal and local stress strain relationships can be expressed as follows

$$\frac{\Delta e}{2} = \frac{\Delta S}{2E}$$

$$\frac{\Delta \varepsilon}{2} = \frac{\Delta \sigma}{2E} + \left(\frac{\Delta \sigma}{2K} \right)^{1/n'} \quad \text{Equation 6.3}$$

Therefore amalgamating equations 6.2 and 6.3

$$K_t^2 \frac{\Delta S}{2} \left[\frac{\Delta S}{2E} \right] = \frac{\Delta \sigma}{2} \left[\frac{\Delta \sigma}{2E} + \left(\frac{\Delta \sigma}{2K'} \right)^{1/n'} \right] \quad \text{Equation 6.4}$$

The above equations have been derived in order to demonstrate the relationship between the remote and local stresses. Therefore, by determining the remote stresses from the loading history, it is possible to calculate the notch root local stress range amplitude.

By iteration the stress range amplitude at the notch can be obtained

$$\Delta \sigma$$

Therefore, using equation 6.5 it is possible to determine the notch root strain range amplitude

$$\frac{\Delta\varepsilon}{2} = \frac{\Delta\sigma}{2E} + \left(\frac{\Delta\sigma}{2K'} \right)^{1/n} \quad \text{Equation 6.5}$$

By calculating the notch root strain range amplitude, it is possible to determine the fatigue life from the strain life equation 6.6:

$$\frac{\Delta\varepsilon}{2} = \frac{\sigma'_f}{E} (2N_f)^b + \varepsilon'_f (2N_f)^c \quad \text{Equation 6.6}$$

Where σ'_f , ε'_f , b and c are material constants.

Again iterating the above expression in terms of $2N_f$ it is possible to predict the number of reversals to failure, or fatigue life.

6.6.3 Equivalent Stress Concentration Factor (K_{equ})

Neuber's method of life prediction depends largely on the acquisition of an accurate stress concentration factor at the notch root, or as in this case the critical location, at the contact surface. Due to the complexity in the collaboration of the axial and shear stresses in the initial growth of fretting cracks, it is necessary to determine an equivalent stress concentration determined from both the axial stress concentration (K_t) and the shear stress concentration (K_{ts}). Figure 6.48 considers the stress system in the fretting specimen.

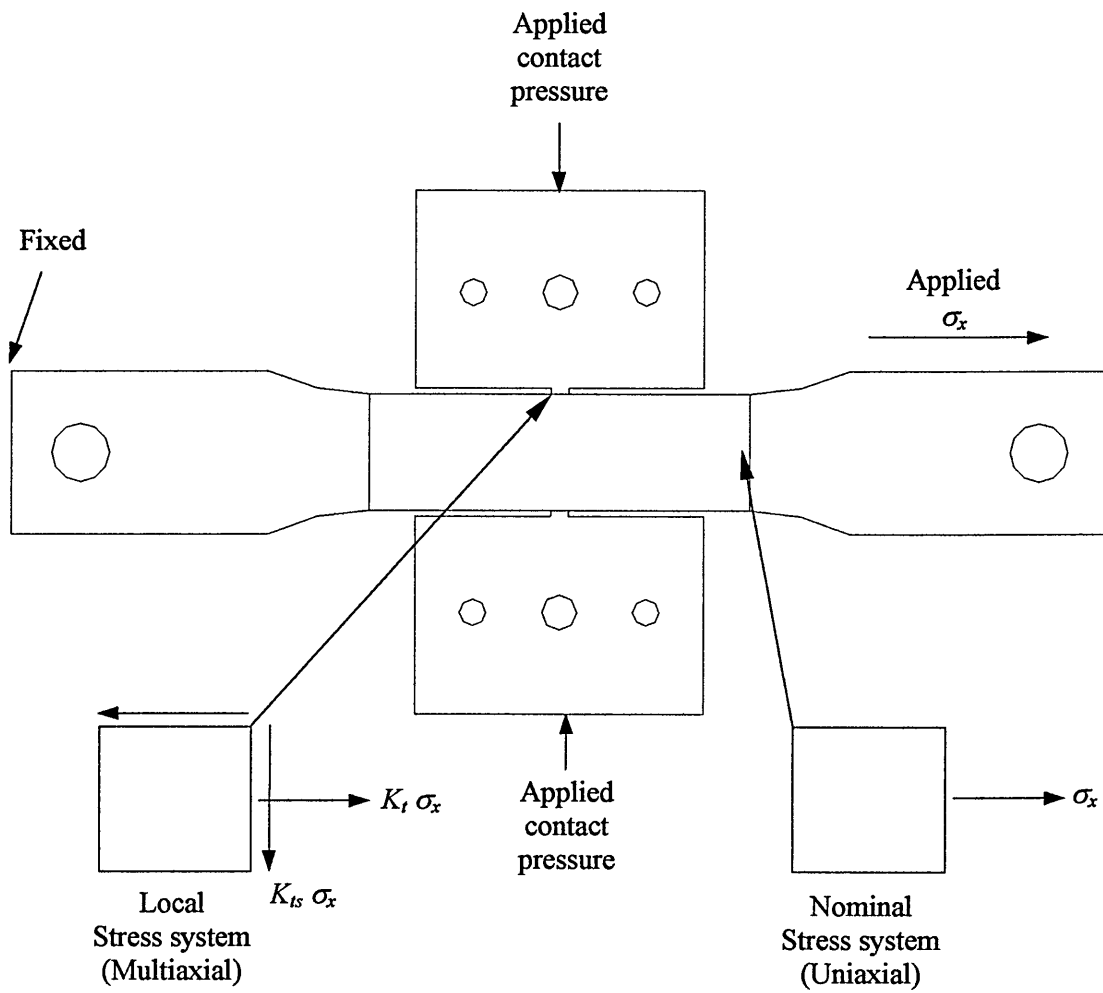


Figure 6.48 The multiaxial and uniaxial stress system in the fretting specimen

Therefore, considering the maximum shear stress at the critical location (local stress)

$$\tau_{MAX} = \sqrt{\left(\frac{K_t \sigma_x}{2}\right)^2 + (K_{ts} \cdot \sigma_x)^2}$$

$$\tau_{MAX} = \left[\sqrt{\frac{K_t^2}{4} + K_{ts}^2} \right] \sigma_x$$

$$\tau_{MAX} = K_{equ} \cdot \sigma_x$$

$$\therefore K_{equ} = \sqrt{\frac{K_t^2}{4} + K_{ts}^2}$$

Equation 6.7

The equivalent stress concentration factor can therefore be determined from the simple expression (Equation 6.7) for any given shear or axial stress concentration.

Analysis of the numerical sub surface stress data at the critical location for the 1.27mm (100MPa applied axial stress results) and 3mm pad size models has yielded stress concentration factors for both the axial stress (K_t) and the shear stress (K_{ts}) at set depths of approximately 15 μ m. Stress concentrations were acquired at each depth until unity was achieved, thereby signifying a return to the remote stress condition.

$$K_{t\delta} = \frac{\sigma_{depth}}{\sigma_{applied}} = 1$$

$$K_{ts\delta} = \frac{\tau_{depth}}{\frac{1}{2}\sigma_{applied}} \quad \text{Equation 6.8}$$

The depth at which the concentration achieved unity varied depending on load condition and contact zone size and typically occurred between 0.5 to 0.8125mm. The stress concentrations exhibited similar behaviour to the stress distributions, with steep gradient changes close to the contact surface, with more gradual changes in concentration as the effects of the contact diminished [8]. To determine a representative K_t and K_{ts} for the necessary depth, each set of concentrations were integrated over the depth to which unity occurred from the surface. The resultant concentration would therefore characterise the typical concentration at that depth. Figure 6.49 illustrates the method of determining a single value for both the shear and axial stress concentrations for each analysis.

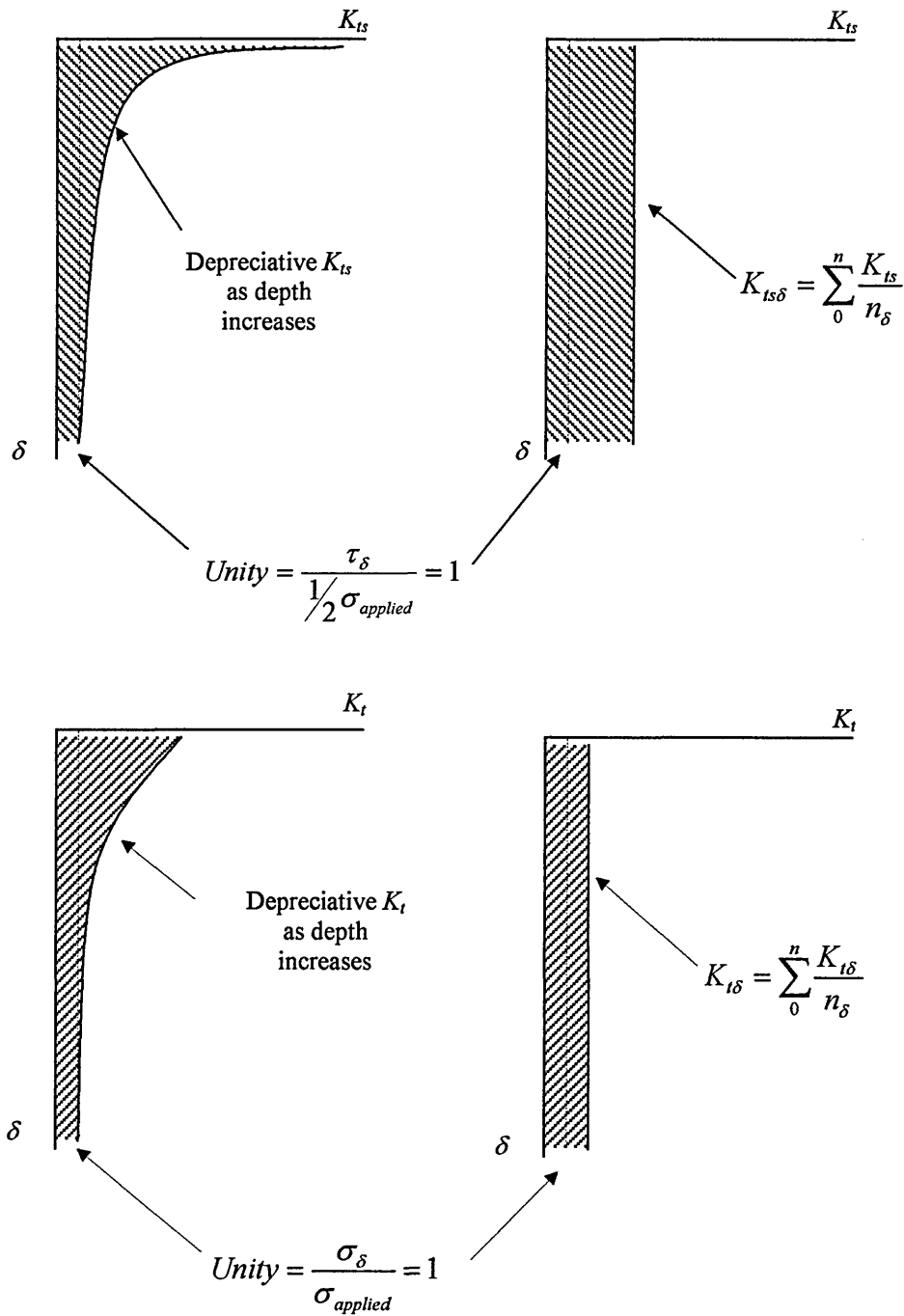


Figure 6.49 Method of determining values for both the shear and axial stress concentrations for each analysis

The integrated stress concentrations $K_{t\delta}$ and $K_{ts\delta}$ were then used to calculate an equivalent stress concentration (K_{equ}), which was used to determine fretting fatigue lives for the 3mm and 1.27mm results using Neuber's analysis

6.6.4 Results of Fretting Fatigue Life Predictions

The numerically predicted sub surface stresses in the fretting region were used to calculate equivalent stress concentration factors (K_{equ}) for both the 1.27mm and 3mm contact pad size models. The equivalent stress concentration factor calculations generated values between 2 and 2.5 for results in micro slip and values between 1.8 and 2 for results in macro slip. Figures 6.50a to 6.50c presents the analytically predicted fretting fatigue lives with the experimental fretting fatigue lives for the 3mm contact pad size results

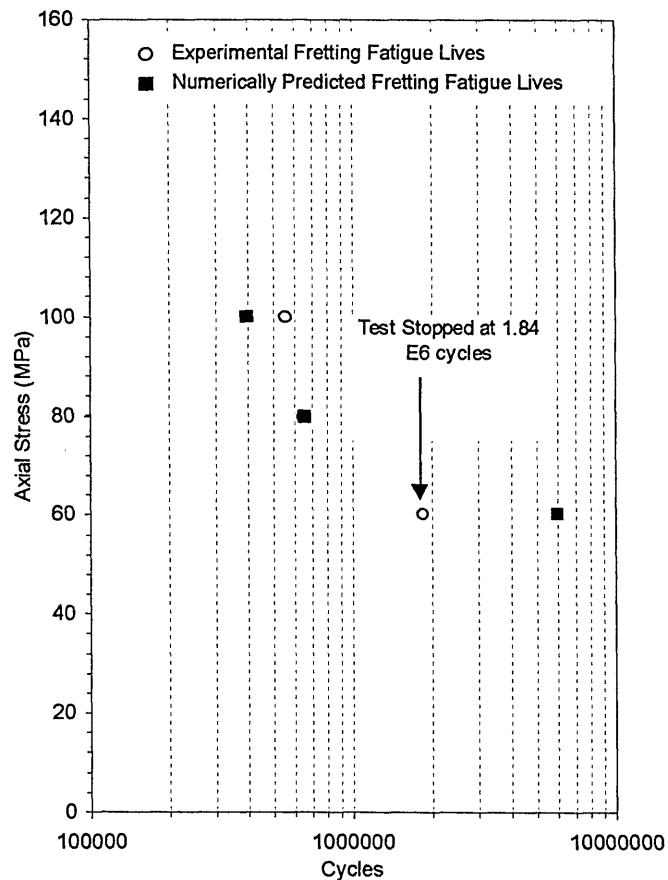


Figure 6.50a

Comparison of numerically predicted fatigue lives with experimentally recorded fatigue lives for 3mm pad size results with 80 MPa contact pressure

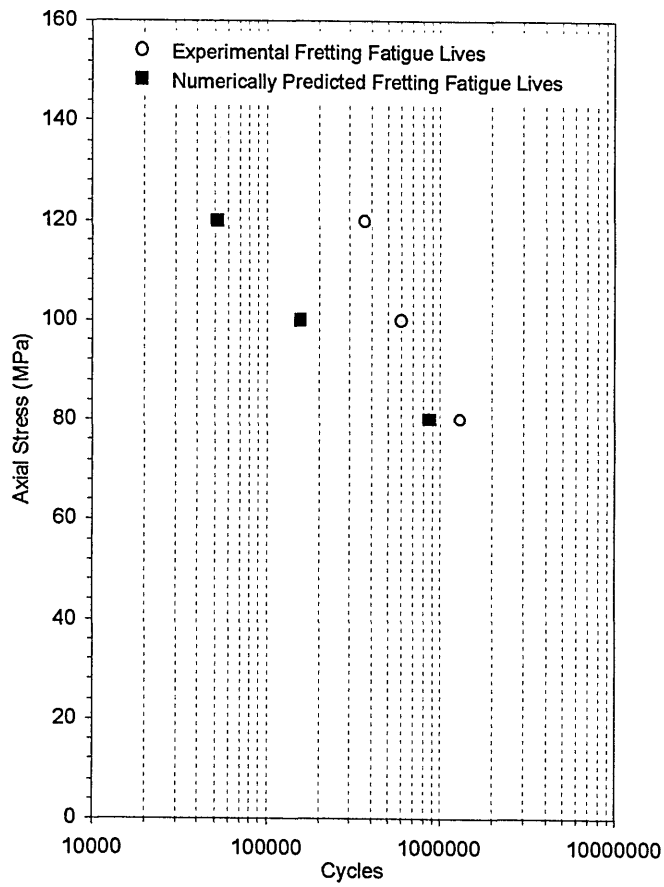


Figure 6.50b Comparison of numerically predicted fatigue lives with experimentally recorded fatigue lives for 3mm pad size results with 100 MPa contact pressure

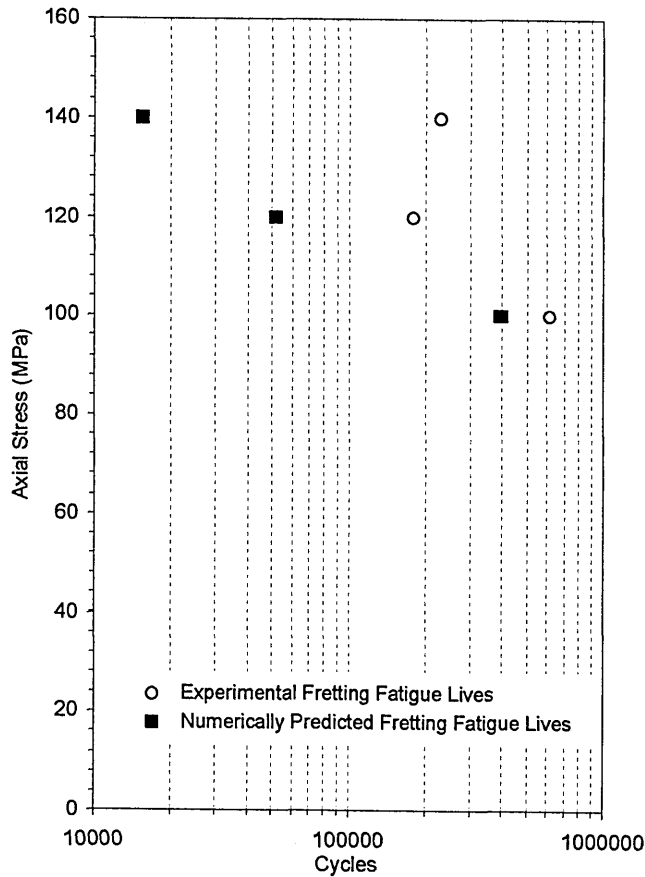


Figure 6.50c Comparison of numerically predicted fatigue lives with experimentally recorded fatigue lives for 3mm pad size results with 120 MPa contact pressure

The results demonstrate that for all but one load case (test 802) the analytical predictions do provide conservative fretting fatigue lives. In test 802, the experiment was stopped at 1.84×10^6 cycles with no indication of failure. Therefore, the experimental fretting fatigue life does not represent the potential fretting fatigue life for that load case and the actual life may be closer to the analytical prediction.

The trend of the analytically predicted fretting fatigue lives is similar to the experimental fretting fatigue lives and the experimentally observed phenomena* is observed in the trend of the analytical results. The behaviour is particularly apparent for the lower contact pressure results (tests 801, 802 & 803) where the predicted fretting fatigue lives are close to the experimentally recorded results. However, as the contact pressure increases the predicted fretting fatigue lives become more conservative and the trend becomes less accurate, until the highest contact pressure case, which demonstrates neither the trend or the accuracy observed in the lower contact pressure results.

Comparison of the analytically predicted fretting fatigue lives with the experimental fretting fatigue lives indicates that Neuber's analysis with an equivalent stress concentration factor is capable of accurately predicting fretting fatigue lives for load cases with low contact pressures. However, accuracy begins to decrease as the contact pressure increases, yielding conservative results. The increasing inaccuracy with increasing contact pressure can be attributed to the analytical method, which does not account for the effects of wear on the initial crack growth process. From the experimental study of initial crack growth and fretting fatigue lives (section 6.3 and

* Fretting Fatigue Phenomenon is the initial decrease in fatigue life as the loads increase, followed by either a stabilisation or increase in the fatigue lives at higher loads

6.4) it was observed that at high contact pressures and axial loads, the fatigue lives increased (in spite of higher stress concentrations due to the higher loads). The behaviour was attributed to the wear mechanism removing nucleating cracks before a dominant fretting crack could initiate. The analytical predictions are based on multiaxial stress concentration factors and do not consider this phenomenon. Therefore, in cases where the wear mechanism becomes a predominant feature in the initial growth of dominant fretting cracks, the analytical predictions do not account for this and the accuracy of the predicted fretting fatigue lives decreases and become more conservative.

Figure 6.51 presents a summary comparison of the predicted fretting fatigue lives with the experimental fretting fatigue lives for the 3mm contact pad size results.

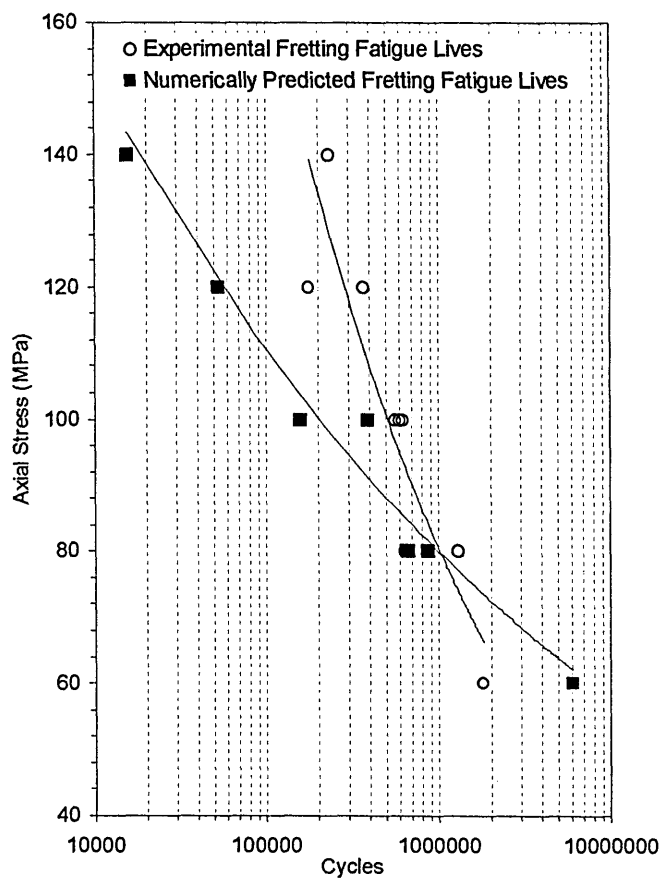


Figure 6.51 Comparison of numerically predicted life to experimentally acquired fatigue life for 3mm pad size

The comparison of the analytically predicted fretting fatigue lives with the experimental fretting fatigue lives for the 1.27mm contact pad size arrangement revealed the predicted results compared well with the experimental results [75] for all but the lowest contact pressure. The analytical results have over predicted the fretting fatigue lives in the majority of cases. However, the analytical method has successfully predicted the fretting fatigue life trend. The discrepancy in the lower contact pressure is attributed to an anomalous experimental result. The result does not follow the trend of the other fatigue lives and is therefore not considered representative of that load case. Therefore, the actual fretting fatigue may be close to the analytical prediction.

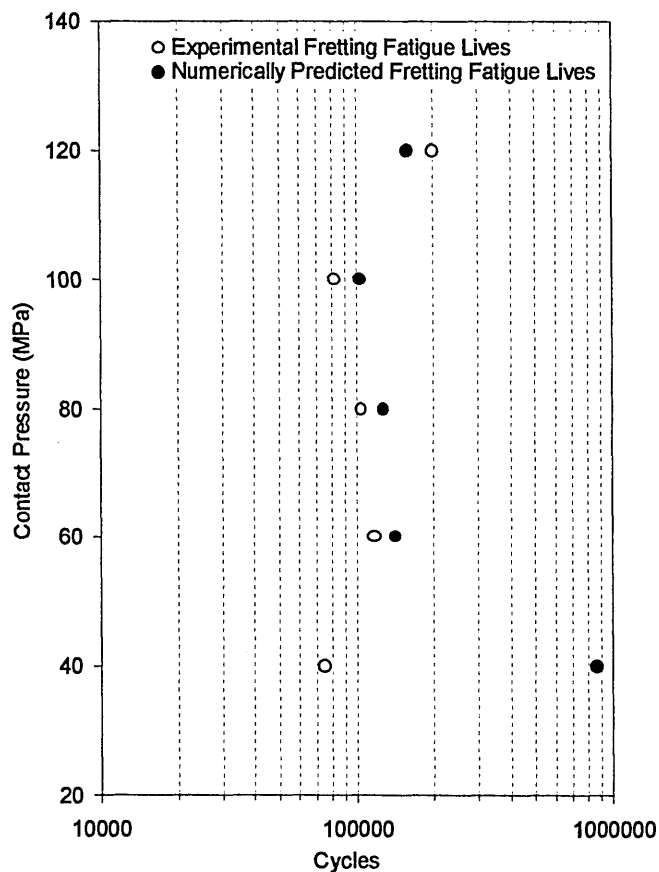


Figure 6.52 Comparison of numerically predicted life to experimentally recorded life for 1.27mm pad size experiments with 100MPa contact load

The analytical fretting fatigue life predictions demonstrate discrepancies in the continued accuracy for the full range of load cases. The inaccuracies are attributed to

the analytical method, which does not account for the effects of wear retarding the initiation of dominant fretting cracks. The fretting fatigue life is reduced by the high local multiaxial stresses however, the retarded crack growth from the wear process augments the fatigue life. The analytical model does not account for this process and the fretting fatigue lives are predicted based only on the local and nominal stresses, which result in conservative predictions.

Although, the process of retarded crack growth due to wear is not accounted for in the analytical method, the analytical method does predict the trends observed in the experimental results (for results with lower contact pressures). Therefore, the fretting fatigue life phenomenon is not only influenced by wear, but also by the sub surface stress distributions. Study of the axial and shear sub surface stresses revealed that at the contact surface the shear stress was dominant and at particular depths, the axial stress became dominant. Analysis of the transfer depths at different load cases revealed a similar trend to the trend observed in the fatigue fretting fatigue lives. Therefore, the sub surface multiaxial stress state is also an influential parameter in the accurate assessment of fretting fatigue lives.

CHAPTER 7

CONCLUSIONS

The study of the fretting fatigue phenomenon in 2024-T351 aluminium alloy has focused on the flat contact problem. An experimental analysis of friction behaviour for contacts containing sharp edges has been performed to determine the influence of friction force on the initiation of dominant fretting cracks and the fretting fatigue lives. Finite element models have been developed to predict the friction force behaviour and provide multiaxial stress data in the fretting region. The numerically predicted stresses have been used to determine an equivalent stress concentration factor (K_{equ}). The equivalent stress concentration factor was used to predict fretting fatigue lives using Neuber's analysis. The following conclusions were determined from this research programme.

- Friction force coefficients determined from simple sliding tests are insufficient to assess the behaviour of friction in fretting fatigue. The coefficient of friction determined at the beginning of the experiments ranged between 0.4 and 0.5. As fretting occurred the friction force increased in response to surface damage. The equivalent friction coefficient (determined from the maximum friction force measured during each experiment) increased and was best represented by values greater than 1. As the experiments were conducted in micro slip, the maximum fretting friction coefficient was not achieved. However, numerical analysis conducted with friction coefficients of 1.5 successfully predicted friction force amplitudes in both macro and micro slip.
- Analysis of friction behaviour during fretting fatigue revealed that friction force increased within a few hundred cycles of the start of the test to reach a peak value, which remained relatively stable for the duration of the test. Study of the hysteresis loops confirmed that the increase was related to a change in the contact interaction, which altered from macro to micro slip. This change in contact interaction was attributed to surface damage induced by the fretting process. The steady state friction force response observed after the initial transient period was attributed to debris acting as a third body solid lubricant
- Study of the distribution of friction force across the contact surface during the load cycle reveals that friction force achieves a peak value at the leading edge of the contact pad. Friction force has a significant influence on the distribution of shear and axial stresses at the contact surface and the peak shear stress coincides with the peak friction force at the contact surface. The location of the peak friction force and shear stress correlates well with the location associated with the initiation of

dominant fretting fatigue cracks. Therefore, shear stress is considered an influential parameter in the initiation of dominant fretting fatigue cracks

- During micro slip, the peak friction force is predominantly influenced by the axial load. However, during macro slip the peak friction force is predominantly influenced by contact pressure.
- Analysis of friction forces for different contact areas revealed that the peak friction was not significantly affected by contact area. This is primarily due to the distribution of friction force for flat contacts. The peak friction forces occur within a localised region at the edges of the contact pad. Therefore, the friction force distribution along the area between the edges has no significant influence on the axial and shear stress distributions. Therefore, the size of the contact area for complete contacts is not as significant as the presence of sharp edges. However, the effect of the contact area will influence the friction force distribution in cases where the total contact area is either very small (so that the peak frictions forces are close enough to share stress concentrations) or very large (so that the peak friction forces are too remote for both to influence the sub surface stress distribution)
- Study of the friction force response during the fretting fatigue life revealed that friction was not affected by the presence of dominant fretting fatigue cracks for the majority of the fatigue life and only responded when the specimen approached failure. This observation suggests that the crack did not grow to a length, which would affect the stiffness of the specimen. Therefore, the majority of the fatigue life was devoted to initiating a dominant fretting fatigue crack and the later stages of the fatigue life resulted in propagation and failure.

- Controlling the slip displacement and therefore the friction force has revealed that friction has an influential effect on fatigue life. When the friction force is constant and the contact pressure varies, the fatigue lives remain relatively constant.
- The initial growth of dominant fretting fatigue cracks was affected by the combination of contact pressures and axial loads. Combinations that induced minor surface damage did not initiate dominant surface cracks within 60% of the fatigue life (low contact pressures and axial loads). Combinations that did induce surface damage, particularly when the surface damage adhered to a characteristic type of surface scar (fretting scars that exhibited a heavily damaged outer region with a relatively smooth inner region) did initiate dominant fretting fatigue cracks. However, combinations that induced major surface damage showed no visual evidence of dominant fretting fatigue cracks after 60% of the fatigue lives
- In cases where the fretting scar exhibited major surface damage (with no distinct regions of scarring) the lack of visual evidence of dominant fretting fatigue cracks was attributed to the wear mechanism removing crack nuclei and therefore, the potential to initiate a dominant fretting fatigue crack. The process retards the growth of dominant fretting fatigue cracks, which then augmented the fatigue life.
- Investigations of the contact induced stresses have identified a critical location at which the stresses concentrate. This critical location collaborates well with experimentally observed crack initiation sites and predominately occurs towards the leading edge of the contact pad

- The surface stress distributions revealed the axial and shear stresses were influenced by friction. Continued investigation of the subsurface stresses at the critical location identified a rapid depreciation in the magnitude of stress as the subsurface depth increased. This was particularly evident for shear stress and further comparisons of the shear and axial stress distributions revealed a depth at which the shear stress (the larger of the two stresses at the contact surface) was superseded by the axial stress.
- Further analysis of the subsurface stress distributions revealed the depth of the transfer varies with contact pressure and axial load and analysis of the trends reveal a similarity between the variation in depth and the fretting fatigue life at different loads. A similar trend is observed in fretting fatigue lives, where continued increases in either contact or axial load increases the number of cycles to failure. This behaviour has been attributed to the increase in the rate of surface damage or wear and evidence of this is seen in the fretting scars for high load cases. However, examination of the subsurface stresses and transfer depths suggest that the subsurface stress fields influence this fretting fatigue phenomena and the lives based on this parameter alone show evidence of this behaviour.
- The finite element models developed using ABAQUS 5.7 [1] has successfully predicted the friction behaviour for both the 1.27mm and 3mm contact pad size in both macro and micro slip. The results confirm the assumptions made during the development of the finite element models were correct and the techniques employed to model the sharp corner contact were successful. Dissimilarities were observed between the numerically predicted friction results and the experimentally recorded friction results. The frictional hysteresis loops were not congruent due to variation in the actual slip magnitudes with the predicted slip magnitudes. This variation was

attributed to the dimensionality of the finite element model. The slip displacements were determined in only one dimension, across the length of the contact surface. Whereas the actual experimental slip displacements were determined from the two dimensional contact area. Therefore, the finite element model did not account for slip variations through the contact area.

- The equivalent stress concentration factor, determined from numerically predicted shear and axial sub surface stresses, at the critical location, provided accurate fretting fatigue life predictions. The results of the analysis showed that in most cases the equivalent stress concentration, K_{equ} , was between 2 and 2.5, for contact interactions in micro slip and 1.8 to 2 for contact interactions in macro slip. Life predictions based on these values (using Neuber's analysis) showed a good correlation with a majority of the experimentally recorded fatigue results. Inaccuracies occurred where mechanisms such as wear became a predominate feature in the failure process. As the equivalent stress concentrations are determined from the subsurface stresses, the effects of wear are not accounted for. However, the results were capable of simulating the trends observed in experimental fretting fatigue lives, where continued increases in loads do not reciprocate with a continued reduction in the number of cycles to failure. The results demonstrate the analytical method based on a numerically determined stress concentration factor was successful in predicting fretting fatigue lives.

7.1. Further Work

The research programme has provided an insight into the mechanisms, which influence fretting fatigue failure in 2024-T351 Aluminium alloys. The analytical method developed to predict fretting fatigue lives, based on a numerical determined multiaxial stress concentration factor has proved successful. The accuracy of the predicted fretting fatigue lives has varied and the following section presents further work, which is intended to improve the accuracy of the current method:

- Further experimentation to acquire data for a wider range of load cases and contact sizes is necessary to further validate the current findings.
- An in-depth experimental study of surface damage to ascertain the relationship between friction, wear and the rate at which cracks nucleate.
- An analytical model that takes account of the wear mechanism to improve the life predictions at higher load conditions.
- Further investigation of the subsurface stress fields to attain a greater understanding of the transfer depth parameter.

REFERENCES

- [1] HIBBITT, KARLSSON and SORENSON INC, (1998). *ABAQUS, 'Users Manual', Version 5.7*
- [2] R. B. WATERHOUSE (1992) *Fretting Fatigue*, International Materials Reviews, 37(2), pp. 77-97
- [3] D P DAVIES, GKN WESTLAND HELICOPTERS LTD A OLVER, R F BAKER and S MEDINA (1999) *Fretting and Wear of Spline Couplings*, Coupling and Shaft Technology for Aerospace Transmissions, I Mech E, 9 June 1999
- [4] Z R ZHOU, S FAYEULLE and L VINCENT (1992) *Cracking Behaviour of Various Aluminium Alloys during Fretting Wear*, Wear, 155, pp, 317-330
- [5] R. B. WATERHOUSE (1994) *Effects of Material and Surface Condition*

- on Fretting Fatigue*, Fretting Fatigue, ESIS 18, Mechanical Engineering Publications, London, pp. 339-349
- [6] C GERDES, H BARTSCH and G HÄRKEGÅRD (1994) *Two Dimensional Modelling of Fretting Fatigue*, Fretting Fatigue, ESIS 18, Mechanical Engineering Publications, London, pp. 111-124
- [7] J A PAPE, R W NEU (1999) *Influence of Contact Configuration in Fretting Fatigue Testing*, Wear, 225, pp. 1205-1214
- [8] JA ARAUJO, D NOWELL (1999) *Analysis of Pad Size Effects in Fretting Fatigue using Short Crack Arrest Methodologies*, International Journal of Fatigue, 21, pp. 947-956
- [9] M P SZOLWINSKI, G HARISH and T N FARRIS (1997) *Comparison of Fretting Fatigue Crack Nucleation Experiments to Multiaxial Fatigue Theory Life Predictions*, Proceedings of the ASME Aerospace Division, AD-Vol. 55, pp. 449-457
- [10] D W HOEPPNER (1994) *Mechanisms of Fretting Fatigue*, Fretting Fatigue, ESIS 18, Mechanical Engineering Publications, London, pp. 3-19
- [11] W D MILESTONE and J T JANECZKO (1971), *Friction between Steel Surface during Fretting*, Wear, 18, pp. 29-40
- [12] S SURESH (1998) *Fatigue of Materials*, Second Edition, Cambridge University Press, ISBN 0 521 57046 7
- [13] M CIAVARELLA, D DINI, G P DEMELIO *On Fretting Fatigue Damage Parameters* pp. 467-475
- [14] M P SZOLWINSKI, T N FARRIS (1998) *Observation, Analysis and Prediction of Fretting Fatigue in 2024 – T351 Aluminium Alloy*, Wear, 221, pp. 24-36

- [15] S MALKIN, D P MAJORS and T H COURTNEY (1972) *Surface Effects During Fretting Fatigue of Ti-6AL-4V*, *Wear*, 22, pp. 235-244
- [16] K HUENECKE (1997) *Jet Engines – Fundamentals of Theory, Design and Operation*, Airlife Publishing Ltd., ISBN 1 85310 834 0
- [17] J. A BANNANTINE, J J COMER and J L HANDCOCK (1990) *Fundamentals of Metal Fatigue Analysis*, Prentice – Hall, Englewood Cliffs, NJ
- [18] M A SHEIKH, U S FERNANDO, M W BROWN and K J M MILLER (1994) *Elastic Stress Intensity Factors for Fretting Cracks Using the Finite Element Method*, *Fretting Fatigue*, ESIS 18, Mechanical Engineering Publications, London, pp. 83-101
- [19] D A HILLS, D NOWELL and A SACKFIELD (1988) *Surface Fatigue Considerations in Fretting*, *Interface Dynamics*, Paper II, pp. 35-40
- [20] U S FERNANDO, G H FARRAH and M W BROWN (1994) *Fretting Fatigue Crack Growth Behaviour of BS L65 4 Percent Copper Aluminium Alloy Under Constant Normal Load*, *Fretting Fatigue*, ESIS 18, Mechanical Engineering Publications, London, pp. 183-195
- [21] J M DOBORMIRSKI, (1992) *Variables of Fretting Process: are there 50 of them?* In: M H ATTIA, R B WATERHOUSE (Eds.), *Standardization of Fretting Fatigue Test Methods and Equipment – ASTM STP 1159*, American Society for testing and Materials, Philadelphia, PA pp. 60-66
- [22] C RUIZ, P.H.B BODDINGTON and K C CHEN (1984) *An Investigation of Fatigue and Fretting in a Dovetail Joint*, *Experimental Mechanics*, 24 (3), pp. 208-217
- [23] L J FELLOWS, D NOWELL and D A HILLS (1997) *On the Initiation*

of Fretting Fatigue Cracks, Wear, 205(1-2), pp. 120-129

- [24] U SELLGREN and U OLOFSSON (1999) *Application of a Constitutive Model for Micro Slip in Finite Element Analysis*, Computer Methods in Applied Mechanics and Engineering, 170(1-2), pp. 65-77
- [25] P D NICOLAOU, T E MATIKAS and E B SHELL (1999) *Modelling Fretting Fatigue: Interface Contact Conditions Based on Profilometry Data*, Proceedings of SPIE – The International Society for Optical Engineering, 3568, pp. 28-39
- [26] U OLOFSSON (1995) *Cyclic Micro – Slip Under Unlubricated Conditions*, Tribology International, 28(4), pp. 207-217
- [27] G HUSHENG, G HAICHENG and Z HUIJIU (1991) *Effects of Slip Amplitude on Fretting Fatigue*, Wear, 148(1), pp. 15-13
- [28] D R SWALLA, R W NEU (2001) *Influence of Coefficient of Friction on Fretting Fatigue Crack Nucleation Prediction*, Tribology International 34, pp 493-503
- [28] HUTSON AL, NICHOLAS T, and GOODMAN R (1999) *Fretting Fatigue of Ti-6Al-4V under Flat-on-Flat Contact*, International Journal of Fatigue, 21, pp. 663-669
- [29] D A HILLS and D NOWELL (1994) *A Critical Analysis of Fretting Fatigue Experiments*, Fretting Fatigue, ESIS 18, Mechanical Engineering Publications, London, pp. 171-182
- [30] D A HILLS and D NOWELL (1999) *A Combined Testing and Modelling Methodology for the Prediction of Fretting Fatigue Performance of Splined Shafts*, Coupling and Shaft Technology for Aerospace Transmissions, I Mech. E, 9 June 1999
- [31] HARISH G and FARRIS TN (1998) *Effect of Fretting Contact Stresses*

- on Crack Nucleation in Riveted Lapjoints*, American Institute of Aeronautics and Astronautics, 20-23, pp. 383-391
- [32] HYUNG-KYU KIM and SOON-BOK LEE (1997) *Crack Initiation and Growth Behaviour of AL2024-T4 under Fretting Fatigue*, Int. J. Fatigue, 19(3), pp. 243-251
- [33] G P WRIGHT and J J O'CONNOR (communicated by) I SNEDDON (1971) *Finite Element Analysis of Alternating Axial Loading of an Elastic Plate Pressed Between two Elastic Rectangular Blocks with Finite Friction*, International Journal of Engineering Science, 9(6), pp. 555-570
- [34] T HATTORI and M NAKAMURA (1994) *Fretting Fatigue Evaluation using Stress Singularity Parameters at Contact Edges*, Fretting Fatigue, ESIS 18, Mechanical Engineering Publications, London, pp. 453-460
- [35] S FAARNES and G HÄRKEGÅRD (1994) *Simplified Stress Intensity Factors in Fretting Fatigue*, Fretting Fatigue, ESIS 18, Mechanical Engineering Publications, London, pp. 73-81
- [36] K SATO (1992) *Determination and Control of Contact Pressure Distribution in Fretting Fatigue*, Standardisation of Fretting Fatigue Test Methods and Equipment, ASTM STP 1159, American Society for Testing and Materials, Philadelphia, pp. 85-100
- [37] U S FERNANDO, M W BROWN, K J MILLER, R COOK and D RAYAPROLU (1994) *Fretting Fatigue Crack Growth Behaviour of BS L65 4 Percent Copper Aluminium Alloy Under Variable Normal Load*, Fretting Fatigue, ESIS 18, Mechanical Engineering Publications, London, pp. 197-209
- [38] L J FELLOWS, D NOWELL and D A HILLS (1995) *Analysis of Crack*

Initiation and Propagation in Fretting Fatigue: the Effective Flaw Size Methodology, *Fatigue and Fracture of Engineering Materials & Structures*, 20(1), pp. 61-70

- [39] K SATO and H FUJII (1986) *Crack Propagation Behaviour in Fretting Fatigue*, *Wear*, 107, pp. 245-262
- [40] K SATO, H FUJII and S KODAMA (1986) *Crack Propagation Behaviour in Fretting Fatigue of S45C Carbon Steel*, *Bulletin of JSME*, 29(256), pp. 3253-3258
- [41] R COOK and P R EDWARDS (1982) *Crack Propagation at Short Crack Lengths Under Variable Amplitude Loading*, 2nd Technical Report, Materials and Structures Department, Royal Aircraft Establishment, Farnborough, Hants, England, pp. 1-20
- [42] C D LYKINS, S MALL and V JAIN (2000) *An Evaluation of Parameters for Predicting Fretting Fatigue Crack Initiation*, *International Journal of Fatigue*, 22 pp. 703-716.
- [43] D ALDHAM and J WARBURTON (1985) *The Unlubricated Fretting Wear of Mild Steel in Air*, *Wear*, 106, pp. 177-201
- [44] L JOHANSSON (1994) *Numerical Simulation of Contact Pressure Evolution in Fretting*, *Journal of Tribology*, 116, pp. 247-254
- [45] JAFFAR MJ (2000) *Effect of Friction on Subsurface Stresses in Sliding Line Contact of Multilayered Elastic Solids*, *International Journal of Solids and Structures*, 37, pp. 6571-6575
- [46] M W MOESSER, S ADIBNAZARI and D W HOEPPNER (1994) *Finite Element Model of Fretting Fatigue with Variable Coefficient of Friction Over Time and Space*, *Fretting Fatigue*, ESIS 18, Mechanical Engineering Publications, London, pp. 103-109

- [47] J DOMINGUEZ (1998) *Cyclic Variations in Friction Forces and Contact Stresses during Fretting Fatigue*, *Wear*, 218, pp. 43-53
- [48] Z OUYANG, S PAN, Y LI and N OUYANG (1993) *Friction Coefficient in Fretting between Titanium Alloy and Stainless Steel*, *Journal of Strain Analysis*, 28(1), pp. 63-66
- [49] O VINGSBO and J SCHON (1991) *Friction Coefficient in Vibrational Sliding*, *Wear of Materials*, pp. 174-180
- [50] P R EDWARDS and R COOK (1978) *Frictional Force Measurements on Fretted Specimens under Constant Amplitude Loading*, Technical Report 78019, Royal Aircraft Establishment, pp. 1-22
- [51] B AVITZUR (1987) *Multi Disciplinary Approach to the Understanding and Modelling of the Friction Phenomenon*, Winter Annual Meeting of the American Society of Mechanical Engineers, pp. 189-199.
- [52] B FREDRIKSON, B TORSTENFELT and N ENDAHL (1984) *Numerical Solutions to Contact, Friction and Crack Problems with Applications*, *Engineering Computations*, 1(2), pp. 133-143
- [53] A BENRABAH, C LANGLADE, A B VANNES (1999) *Residual Stresses and Fretting Fatigue*, *Wear*, 224, pp. 267-273
- [54] L J FELLOWS, D NOWELL and D A HILLS (1995) *Contact Stresses in Moderately Thin Strips*, *Wear*, 185(1-2), pp. 235-238
- [55] D NOWELL and D A HILLS (1990) *Crack Initiation Criteria in Fretting Fatigue*, *Wear*, 136(2), pp. 329-343
- [56] D A HILLS (1994) *Mechanics of Fretting Fatigue*, *Wear*, 175(1-2), pp. 107-113
- [57] D A HILLS and G URRIOLAGOITIOA SOSA (1999) *Origins of Partial Slip in Fretting – A Review of Unknown and Potential Solutions*,

- [58] H GANAPATHY and T N FARRIS (1997) *Modelling of Rivet Skin Contact: Application to Fretting Fatigue*, 30th AIAA/ASME/ASCE, 4(4), pp. 2761-2771
- [59] T N FARRIS, A F GRANDT. Jr., G HARISH and H L WANG (1996) *Analysis of Widespread Fatigue Damage in Structural Joints*, 41st International SAMPE Symposium & Exhibition, SAMPE, Anaheim.
- [60] SZOLWINSKI MP, MATLIK JF, and FARRIS TN (1999) *Effects of HCF Loading on FF Crack Nucleation*, International Journal of Fatigue, 21, pp. 671-677
- [61] MP SZOLWINSKI and TN FARRIS (1996) *Mechanics of Fretting Fatigue Crack Formation*, Wear, 198, pp. 93-107
- [62] FAANES S (1996) *Distribution of Contact Stress Along a Worn Fretting Surface*, International Journal of Solids and Structure 33 (23), pergamon, pp. 3477-3489
- [63] W N FINDLEY, J J COLEMAN and B C HANLEY (1956) *Theory for Combined Bending and Torsion Fatigue with Data for SAE 4340 Steel*, Proc, International Conference on Fatigue of Metals, Institution of Mechanical Engineers, ASME, pp. 150-157
- [64] J A ARAUJO and D NOWELL *The Use of Critical Plane Approach to Predict Fretting Fatigue Initiation Life of Components Subjected to Different Contact Stress Fields*, pp. 459-466
- [65] D SOCIE (1987) *Multiaxial Fatigue Damage Models*, Journal of Engineering Materials, Technol., 109, pp. 292-298
- [66] K NISHIOSKA and K HIRAKAWA (1969) *Fundamental Investigations of Fretting Fatigue*, part 3, Bull. JSME, 12 (51) pp. 235-242

- [66] C D LYKINS, S MALL and V JAIN (2001) *Combined Experimental-Numerical Investigation of Fretting Fatigue Crack Initiation*, International Journal of Fatigue, 23, pp. 703-711
- [67] J. A ALIC, A.L HAWLEY and J M UREY (1979) *Formation of Fretting Fatigue Cracks in 7075 T7351 Aluminium Alloy*, Wear, 56, pp. 351-361
- [68] S ADIBNAZARI and D W HOEPPNER (1994) *The Role of Normal Pressure in Modelling Fretting Fatigue*, Fretting Fatigue, ESIS 18, Mechanical Engineering Publications, London, pp. 125-133
- [69] D P ROOKE (1994) *The Development of Stress Intensity Factors*, Fretting Fatigue, ESIS 18, Mechanical Engineering Publications, London, pp. 23-58
- [70] T HATTORI, M NAKAMURA, H SAKATA and T WANTANABE (1988) *Fretting Fatigue Analysis using Fracture Mechanics*, JSME International Journal, 31(1), pp. 100-107
- [71] S FAARNES and U S FERNANDO (1994) *Life Predictions in Fretting Fatigue using Fracture Mechanics*, Fretting Fatigue, ESIS 18, Mechanical Engineering Publications, London, pp. 149-159
- [72] RE PATERSON (1995) *Notch Sensitivity*, Metal Fatigue, McGraw Hill, pp. 293-306 handbook
- [73] D TAYLOR (1999) *Geometrical Effects in Fatigue: A Unifying Theoretical Model*, International Journal of Fatigue, 21, pp. 413-420
- [74] www.matweb.com (2001) Aluminium alloy – 2024 T351
- [75] SIRIUS – Structural Integrity Research Institute University of Sheffield.
U S Fernando, M A Sheikh, G H Farrahi, K J Miller and, M W Brown (1992) *An Investigation into the Fretting Fracture of BS L65 Copper*

- [76] Q Y LIU, Z R ZHOU (2000) *Observation, Analysis and Prediction of Fretting Fatigue in 2024 – T351 Aluminium Alloy*, *Wear*, 239, pp. 237-243
- [77] A VILLANUEVA – LEAL, S HINDUJA (1994) *Modelling the Characteristics of Interface Surfaces by the Finite Element Method*, *Proc Instn Engrs, IMechE*, 198C, 4, pp. 9-23
- [78] K HIRATSUKA, M GOTO (2000) *The Role of Changes in Hardness of Substrates, Transfer Particles and Wear Particles in Initial Steady Wear transition*, *Wear*, 238, pp. 70-77

BIBLIOGRAPHY

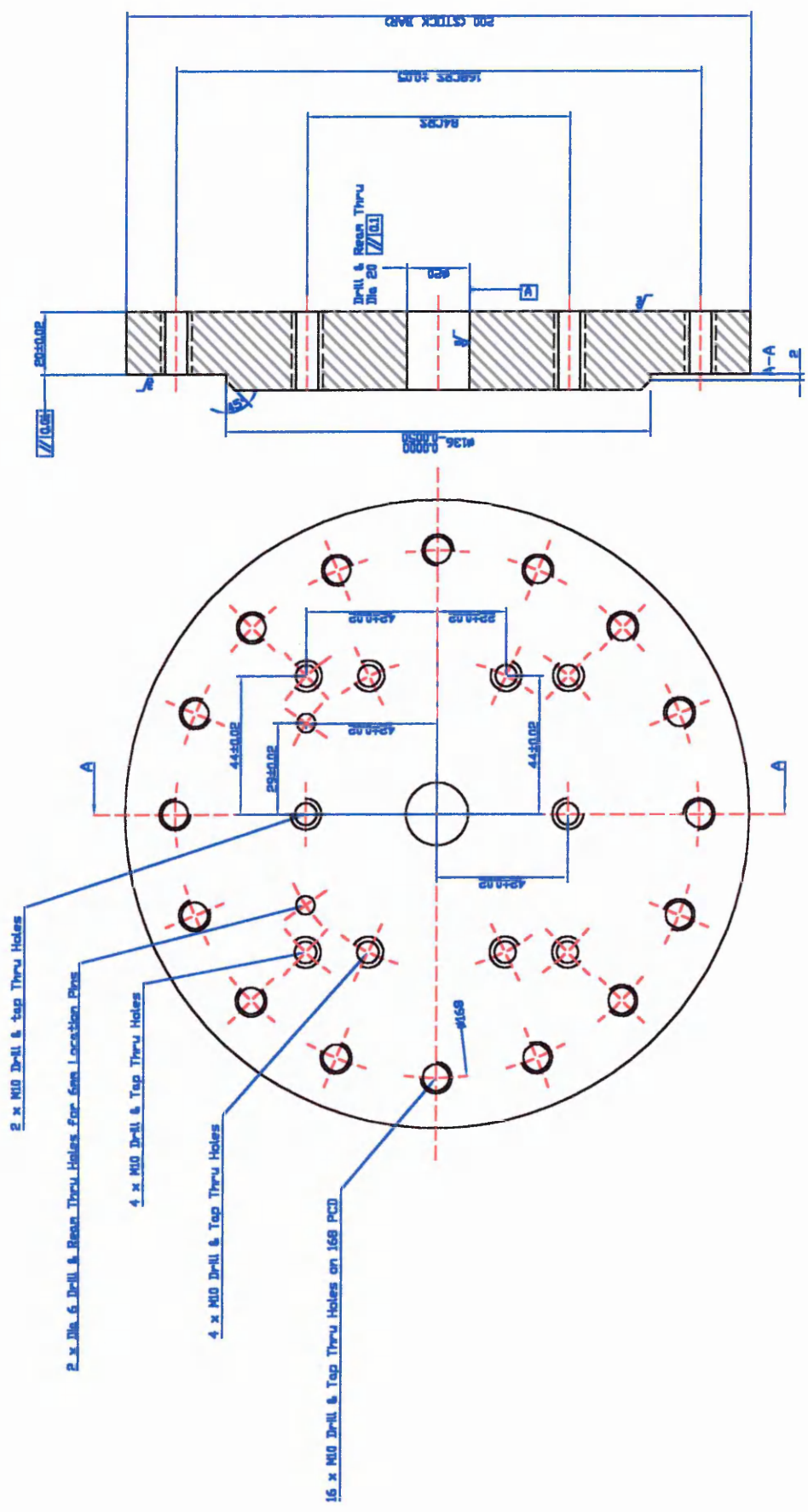
- S SURESH (1998) *Fatigue of Materials – 2nd ED*, Cambridge University Press
- E RABINOWICZ (1995) *Friction and Wear of Materials – 2nd ED*, Wiley – Interscience
- P C VARLEY (1970) *The Technology of Aluminium and its Alloys*, Butler & Tanner Ltd, Frome and London
- D BROEK (1983) *Elementary Engineering Fracture Mechanics – 3rd ED*, Kluwer Academic Publishers Group
- P P BENHAM, R J CRAWFORD and C G ARMSTRONG (1996) *Mechanics of Engineering Materials – 2nd ED*, Longman Group Ltd
- A D SAKAR (1976) *Wear of Metals*, Pergamon Press Ltd
- K A STROUD (1995) *Engineering Mathematics – 4th ED*, Macmillan Press Ltd

APPENDIX A

ENGINEERING DRAWINGS OF TEST RIG AND

SAMPLE

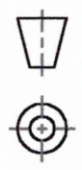
DO NOT SCALE IF IN DOUBT ASK



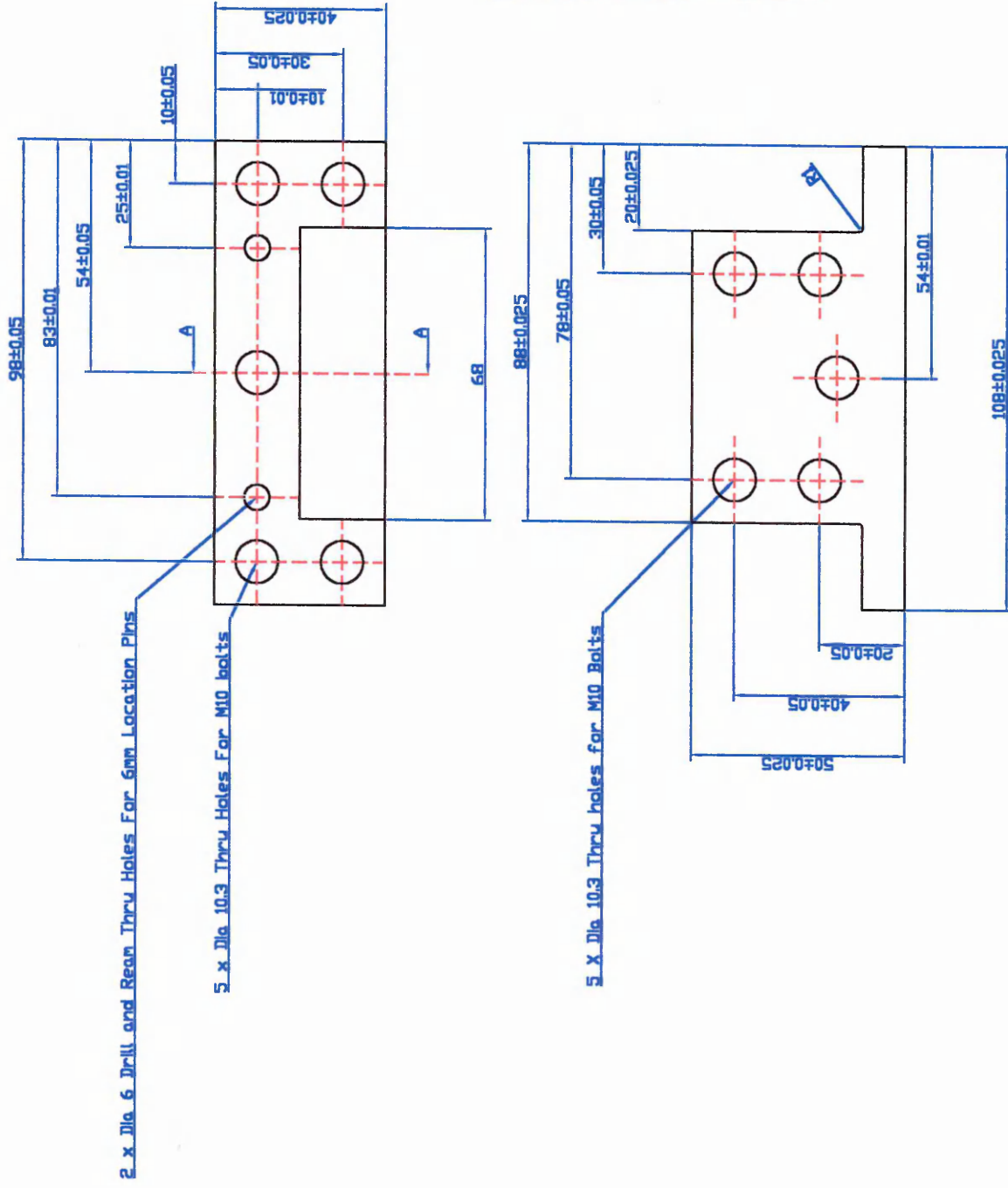
All 10 Tapped Holes to Conform Positional Tol

ALL DIMENSIONS IN MM

DRAWN BY R J Green	DATE 26/10/98	REV No 2	MODIFICATION SHEET MS00000	DATE	SIGN	CHECKED	PART CODE	Top Plate		Scale 1:1.5
CHECKED BY U S Fernando	DATE / /	QUANTITY 1	MATERIAL EN 24				00001	Date date	Edition edition	SHEET 2

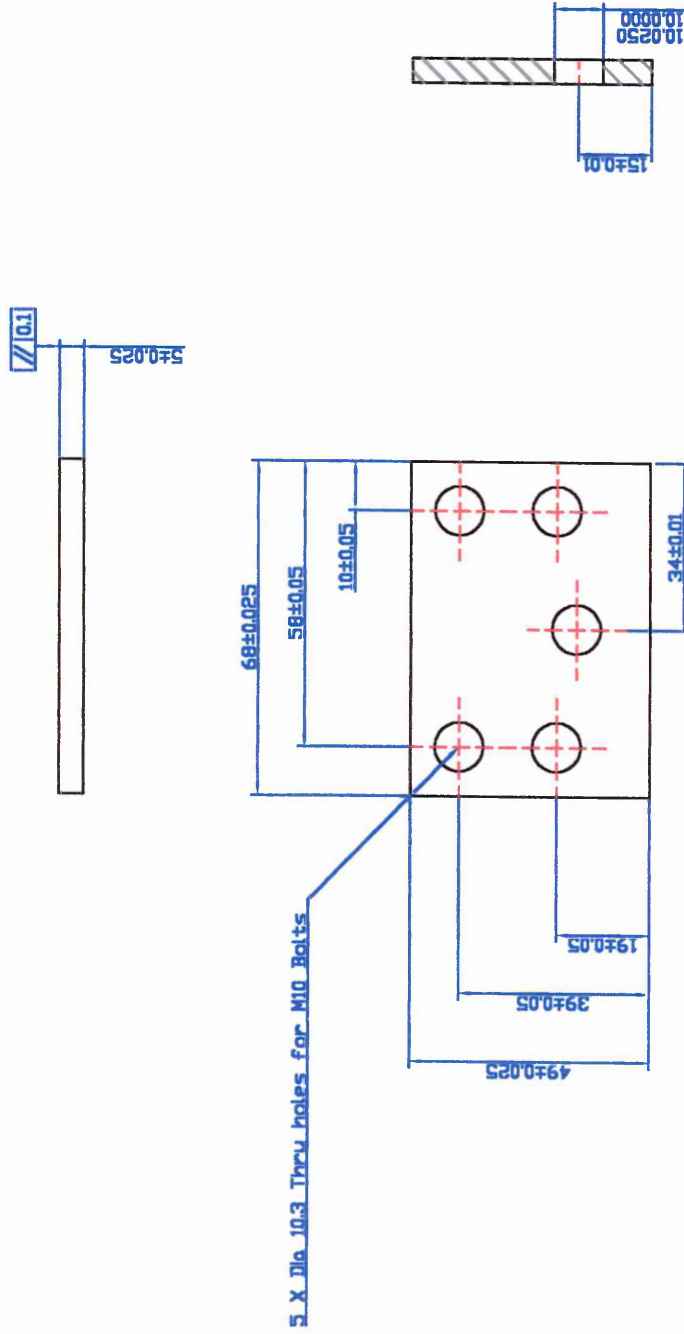


DO NOT SCALE IF IN DOUBT ASK



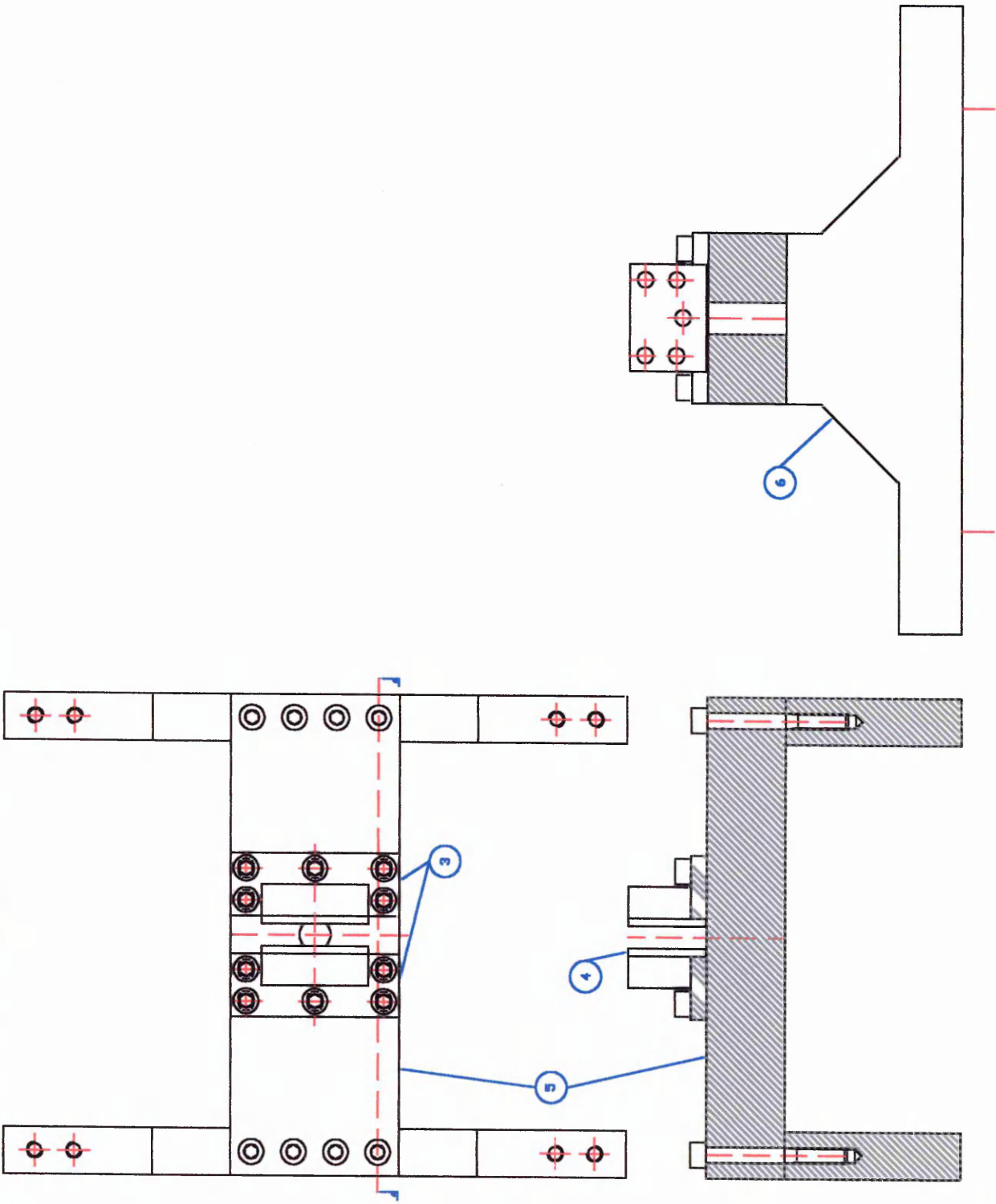
DRAWN BY R J Green	DATE 25/10/98	REV No 2	MODIFICATION SHEET MS00000	CHECKED	SIGN	DATE	PART CODE 00002	Fixed L Section		Scale 1:1
CHECKED BY U S Fernando	DATE / /	QUANTITY 1	MATERIAL EN 24					Date date	Edition edition	SHEET 3

DO NOT SCALE IF IN DOUBT ASK



ALL DIMENSIONS IN MM

DRAWN BY R J Green	DATE 2/11/98	REV No 1	MODIFICATION SHEET MS00000	DATE	SIGN	CHECKED	PART CODE 00004	Friction Plates	Scale 1:1
CHECKED BY U S Fernando	DATE / /	QUANTITY 4	MATERIAL EN 24					Date date	Edition edition SHEET 5

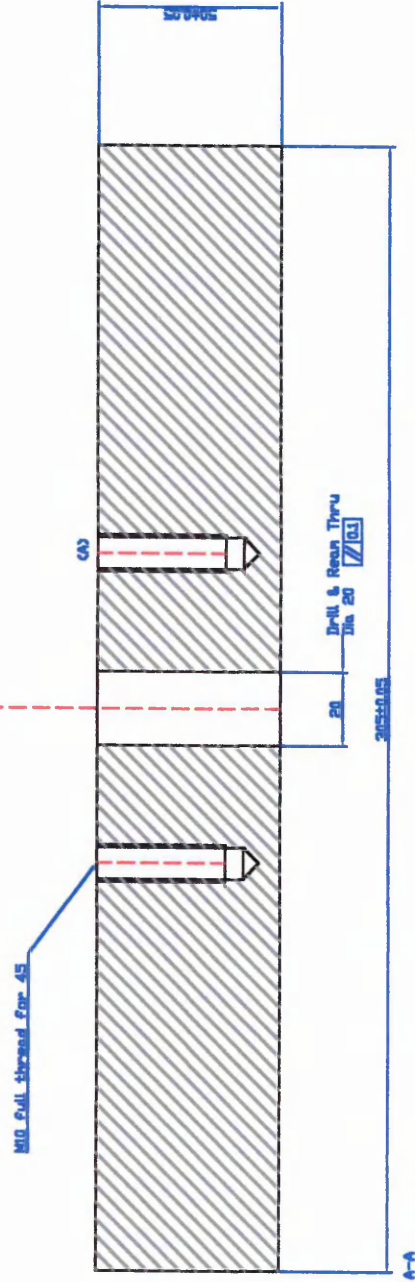
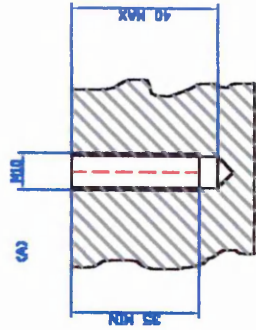
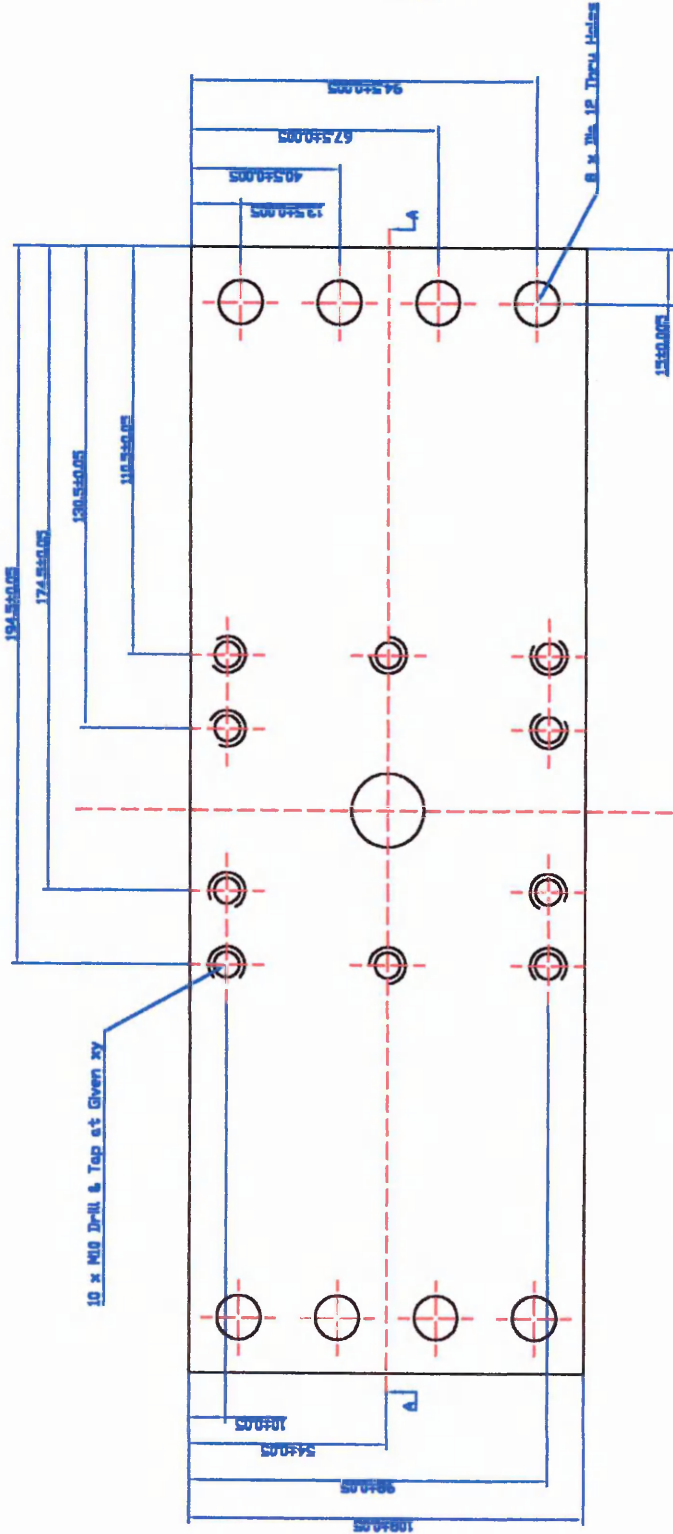


44

DRAWN BY R.J. Green	DATE 5/11/98	REV No 1	MODIFICATION SHEET MS00000	DATE	SIGN	CHECKED	Bottom Clamp Assembly		Scale 1:2.5
CHECKED BY U.S. Fernando	DATE / /	QUANTITY 1	MATERIAL As Specified					Date date	SHEET 6
							Edition edition		



DO NOT SCALE IF IN DOUBT ASK

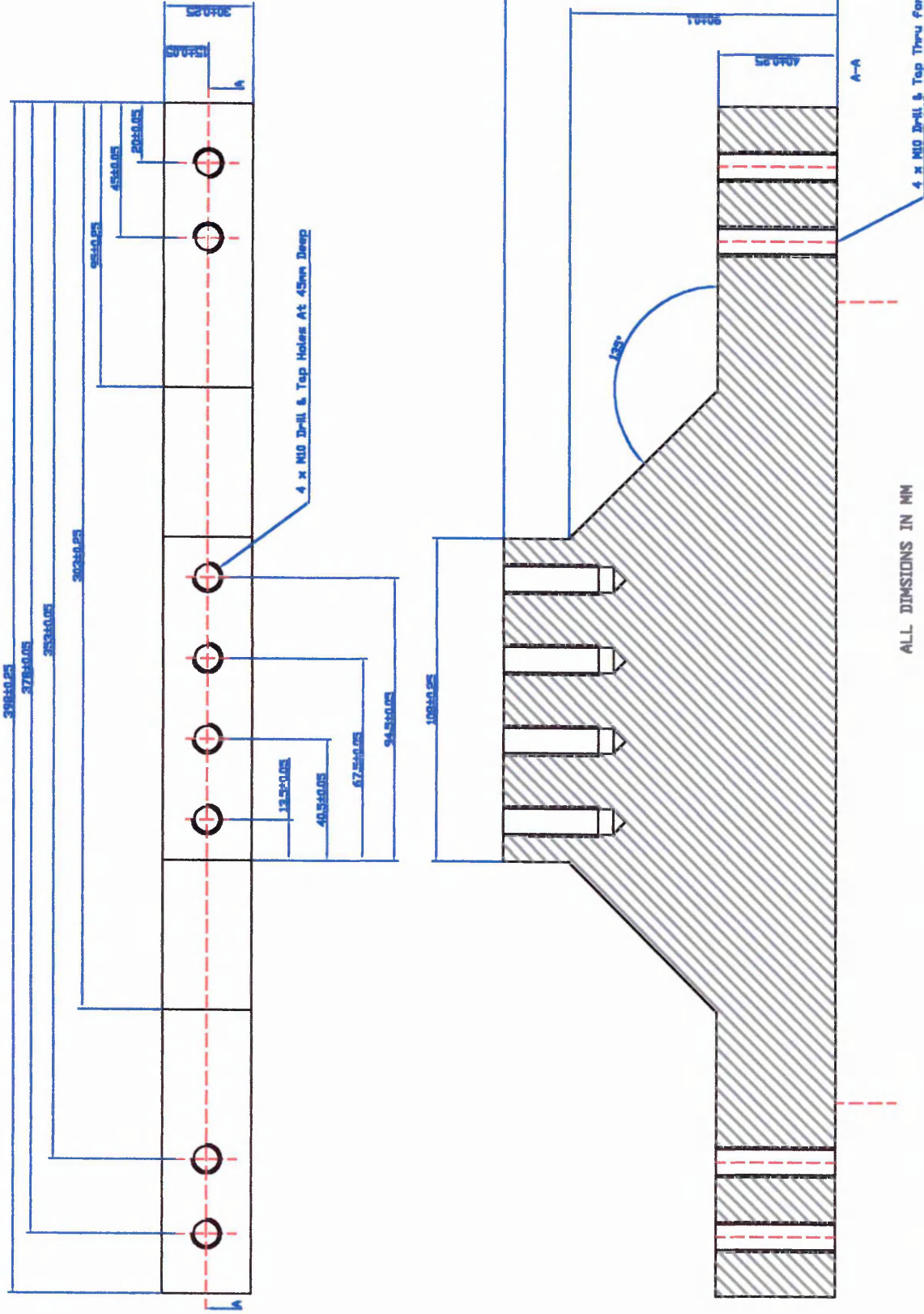


All Drilled & Taped Holes for M10 Bolts
ALL DIMENSIONS IN MM

DRAWN BY R J Green	DATE 3/11/98	REV No 1	MODIFICATION SHEET MS00000	DATE	SIGN	CHECKED	PART CODE	Date date	Scale 1:1.5
CHECKED BY U S Fernando	DATE / /	QUANTITY 1	MATERIAL EN 24	00005			Bridge	Edition edition	SHEET 7

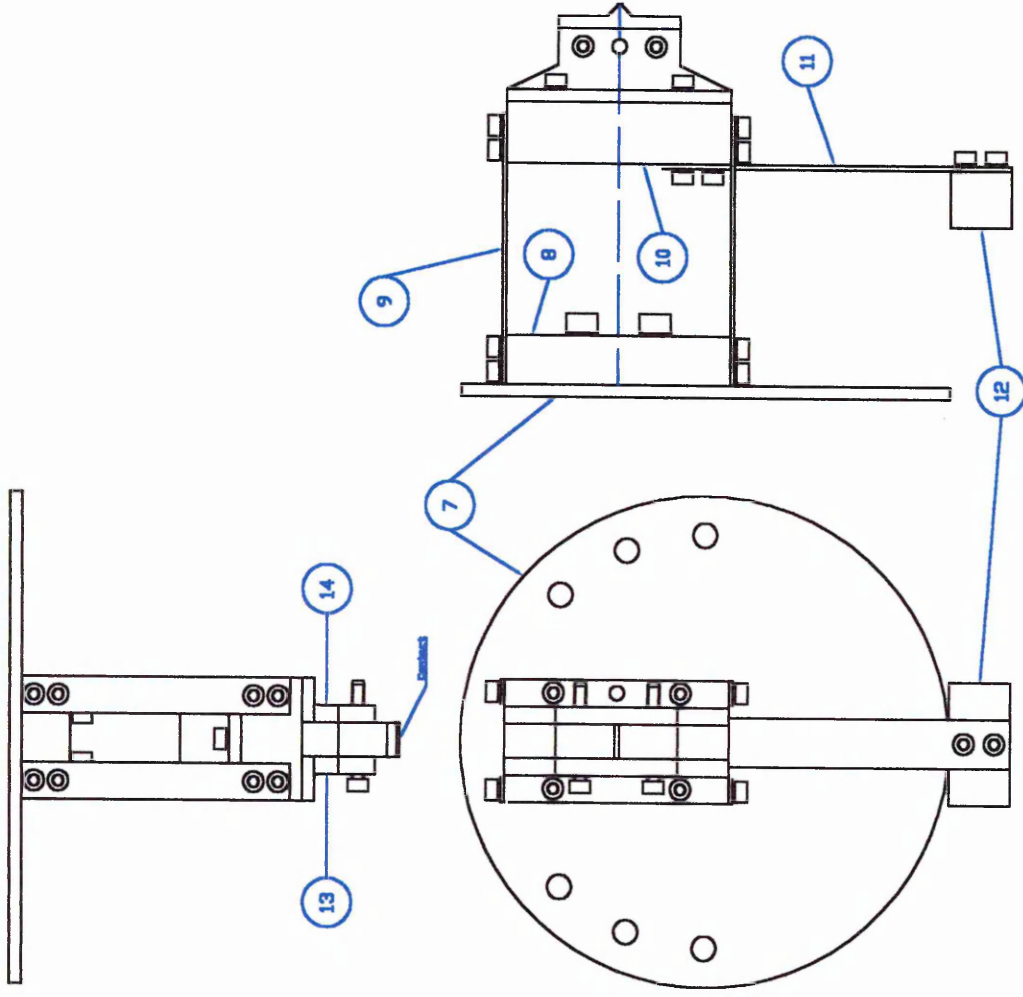


DO NOT SCALE IF
IN DOUBT ASK



DRAWN BY R J Green	DATE 4/11/98	REV No 2	MODIFICATION SHEET MS00001	25/11/98	SIGN	CHECKED	PART CODE	Date date	Support Legs	Scale 1:1.5
CHECKED BY U S Fernando	DATE / /	QUANTITY 2	MATERIAL EN 24				08006			SHEET 8

DO NOT SCALE IF IN DOUBT ASK



ALL DIMENSIONS IN MM

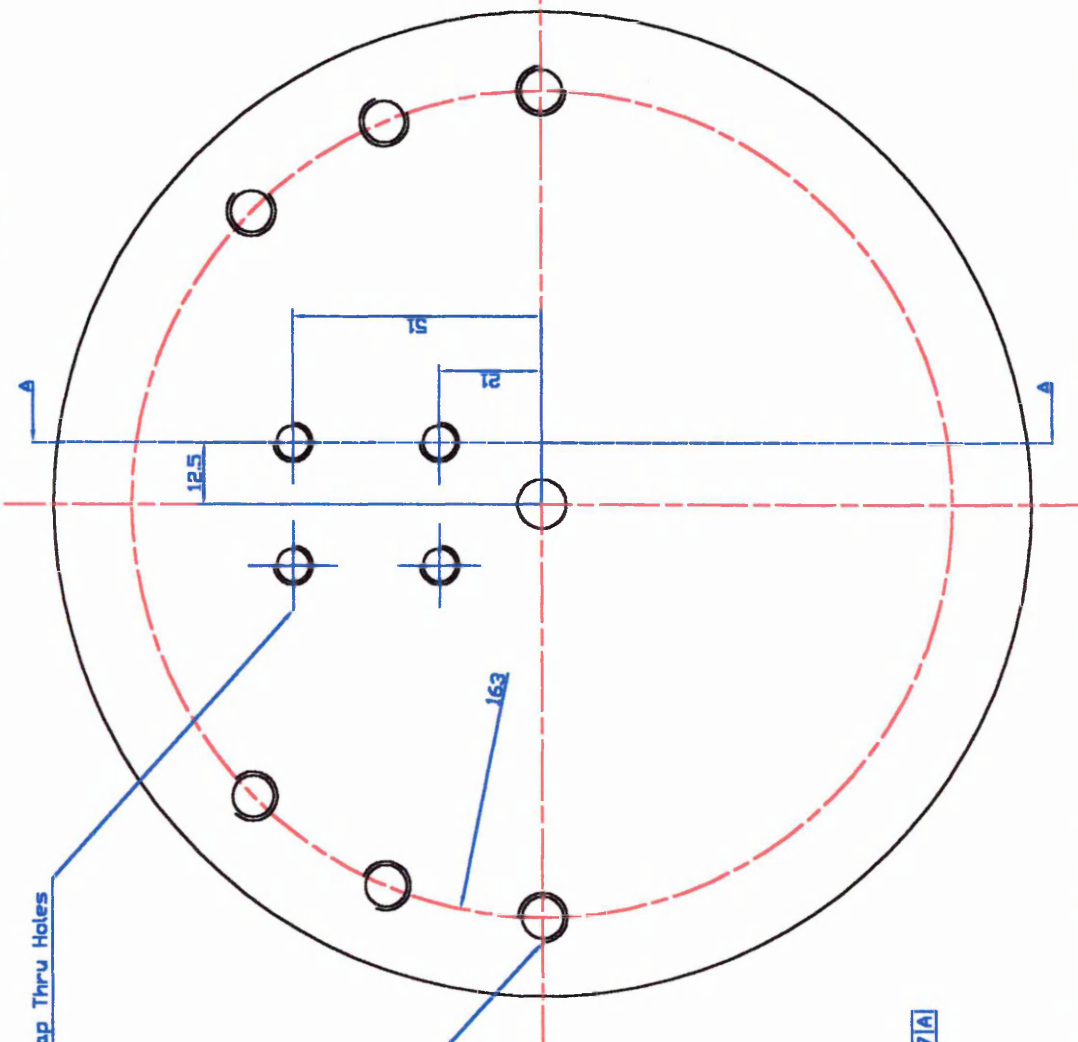
DRAWN BY R J Green	DATE 23/11/98	REV No 0	MODIFICATION SHEET	MS00000	DATE	SIGN	CHECKED	PART CODE	00000	 	Scale 1:2	SHEET 9
CHECKED BY U S Ferrnando	DATE	QUANTITY 2	MATERIAL	AS SPECIFIED	DATE	SIGN	CHECKED	SHU	Date		Side Contact Assembly	Edition 1

DO NOT SCALE IF IN DOUBT ASK



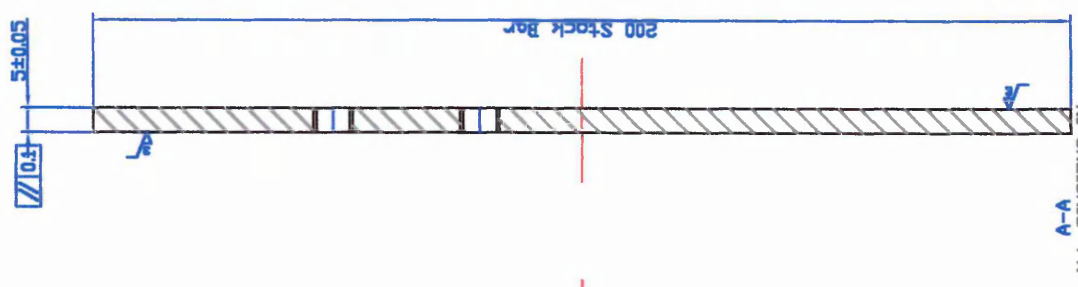
A Drill & Ream Thru
Dia. 10 $\sqrt{0.1}$

4 x M8 Drill & Tap Thru Holes



16 x M10 Drill & Tap Thru Holes on 163 PCD

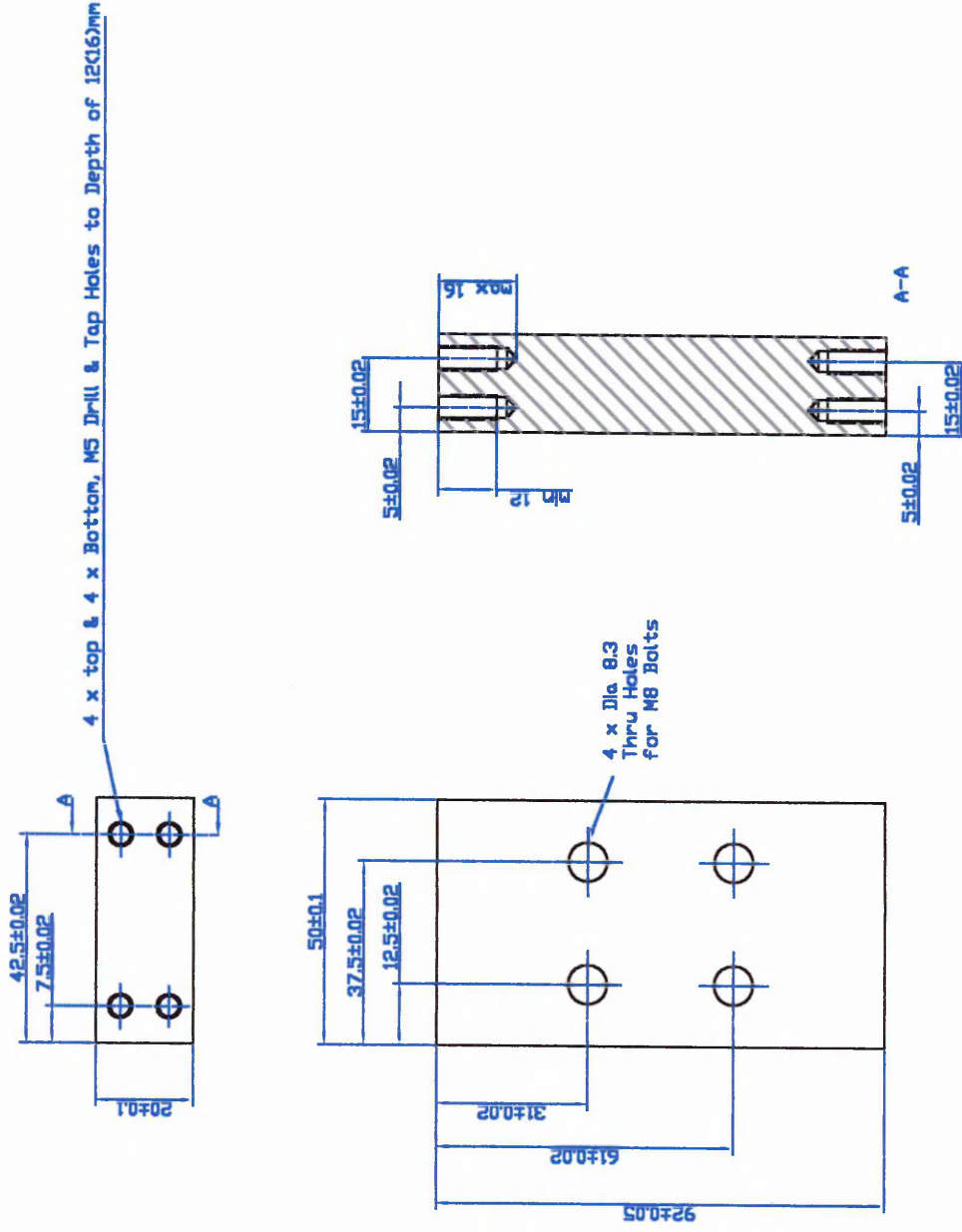
All 10 Tapped Holes
to Conform
Positional Tol. $\phi 0.071A$



A-A
ALL DIMENSIONS IN
MM

Scale 1:1	Side Plates		Sheet 10
Date	Date	Edition 1	SHU
Part Code 00007	Part Code 00007	Checked	Sign
Modification Sheet MS00000	Date	Date	Date
Rev No 1	Quantity 2	Material EN	Material
Drawn By R J Green	Checked By U S Fernando		

DO NOT SCALE IF IN DOUBT ASK

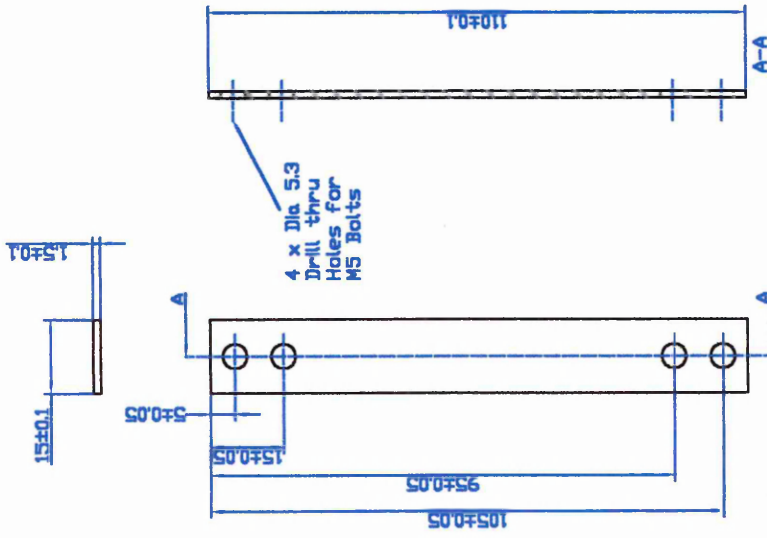


ALL DIMENSIONS IN MM

DRAWN BY R J Green	DATE 28/11/98	REV No 1	MODIFICATION SHEET	MS00000	DATE	SIGN	CHECKED	PART CODE	00008	Scale 1:1	SHEET 11
CHECKED BY U S Fernando	DATE	QUANTITY 1	MATERIAL EN							Support Block	Edition 1
										Date date	SHU



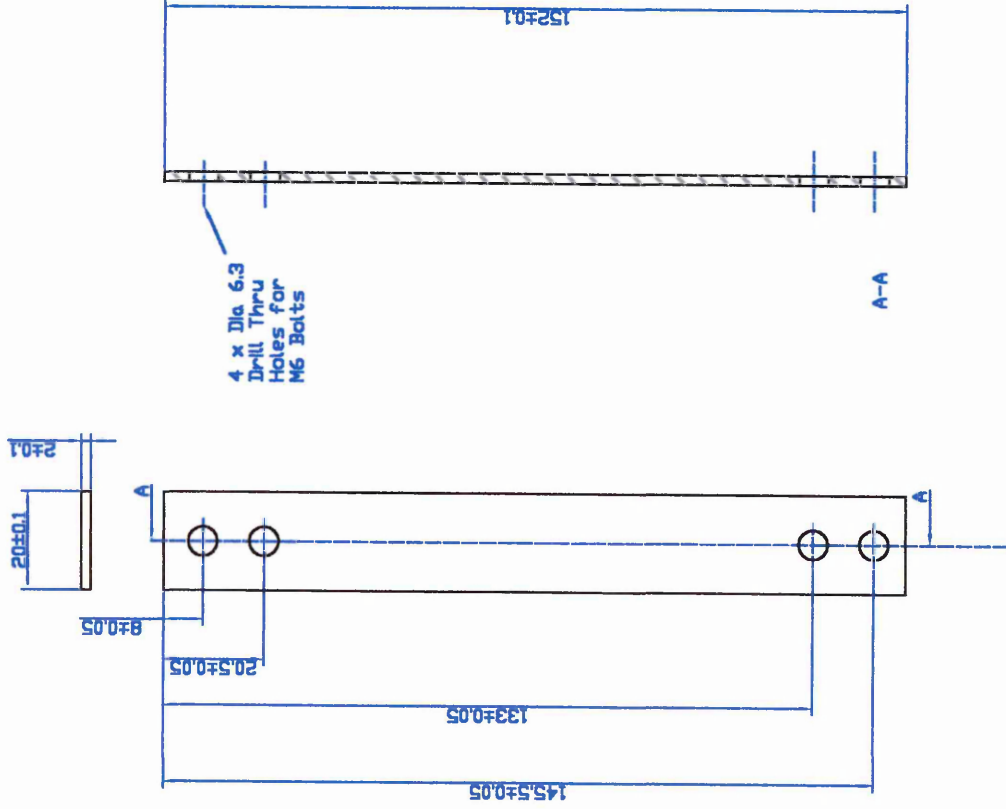
DO NOT SCALE IF IN DOUBT ASK



ALL DIMENSIONS IN MM

DRAWN BY R J Graess	DATE 19/11/98	REV No 0	MODIFICATION SHEET	MS00000	DATE	SIGN	CHECKED	PART CODE	00009	 	Parrallelogram Beams SHU	Scale 1:1	SHEET 12
	CHECKED BY U S Fernando	DATE / /	QUANTITY 4	MATERIAL	DATE date	Edition 1							

DO NOT SCALE IF IN DOUBT ASK

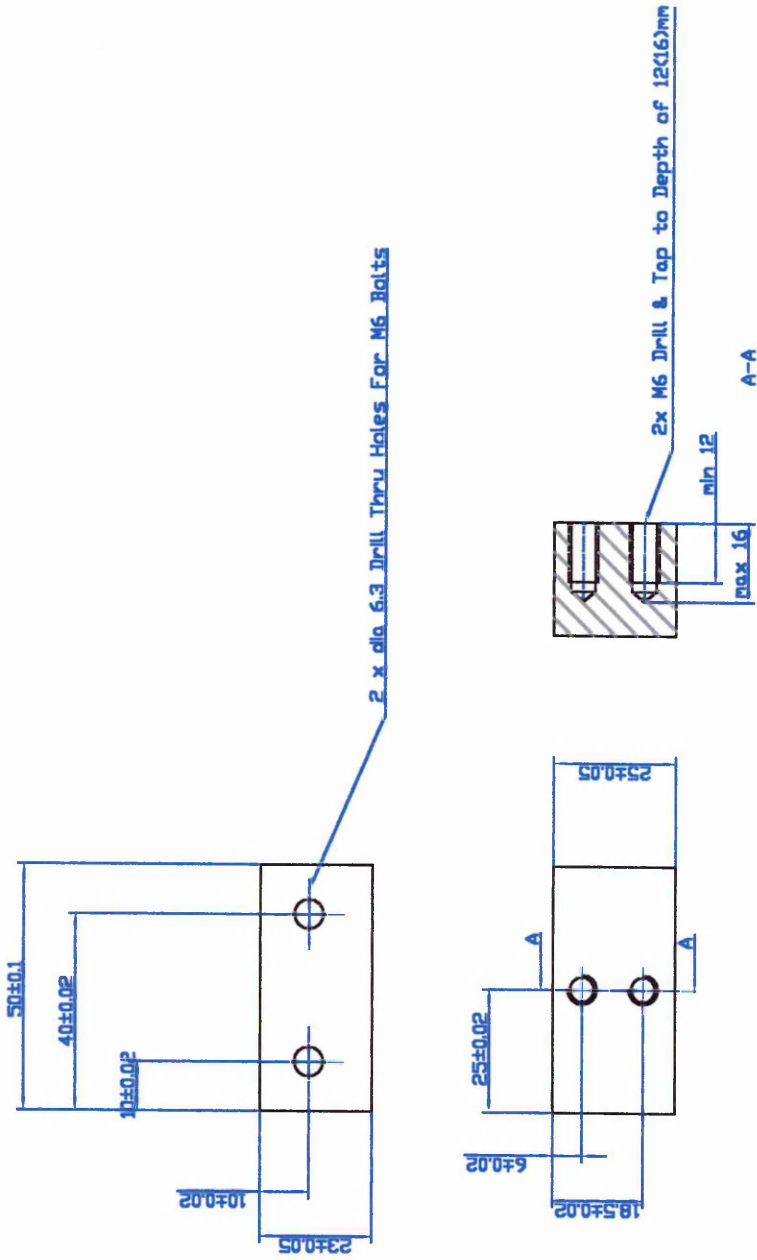


ALL DIMENSIONS IN
MM

DRAWN BY R J Green	DATE 20/11/98	REV No 1	MODIFICATION SHEET	MS00000	DATE	SIGN	CHECKED	PART CODE	00011	Scale 1:1	SHEET 1/4
CHECKED BY U S Fernando	DATE	QUANTITY 4	MATERIAL EN							Verticle Beam	SHU
										Date date	Edition 1



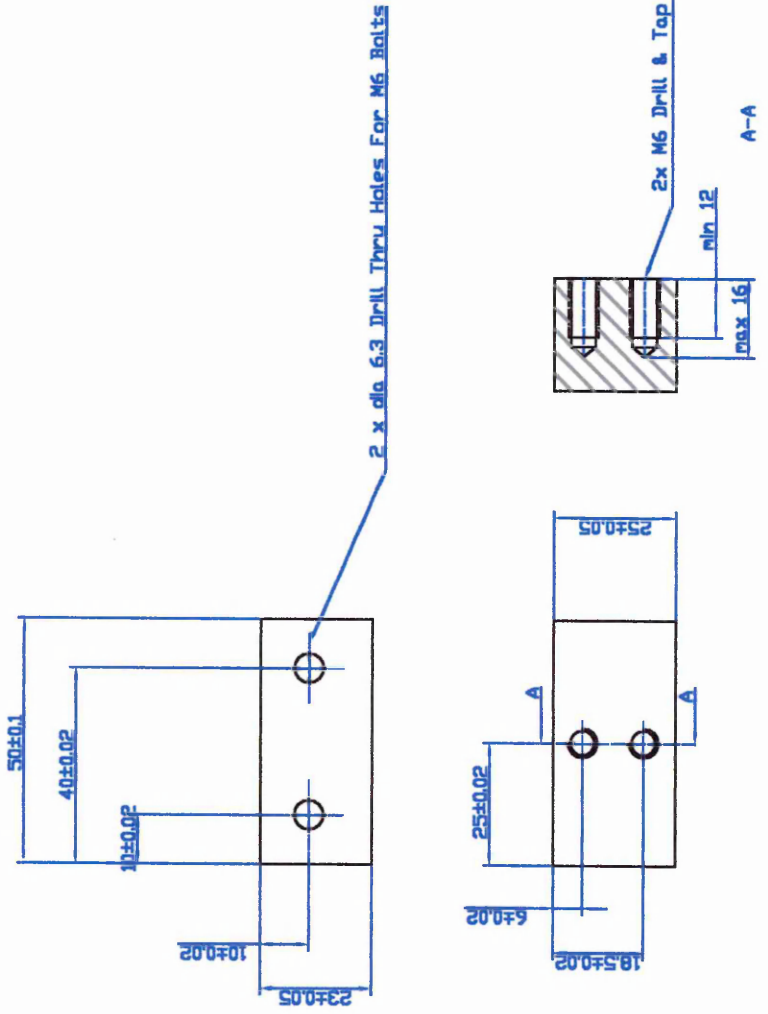
DO NOT SCALE IF IN DOUBT ASK



ALL DIMENSIONS IN MM

DRAWN BY R J Green	DATE 21/11/98	REV No 1	MODIFICATION SHEET	MS00000	DATE	SIGN	CHECKED	PART CODE	 	Verticle Beam Support	Scale 1:1
CHECKED BY U S Fernando	DATE	QUANTITY 1	MATERIAL EN	00012	DATE			Date date		SHU	Edition 1

DO NOT SCALE IF IN DOUBT ASK

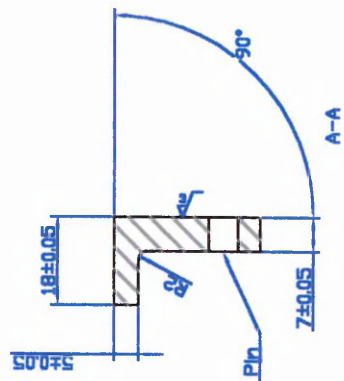


ALL DIMENSIONS IN MM

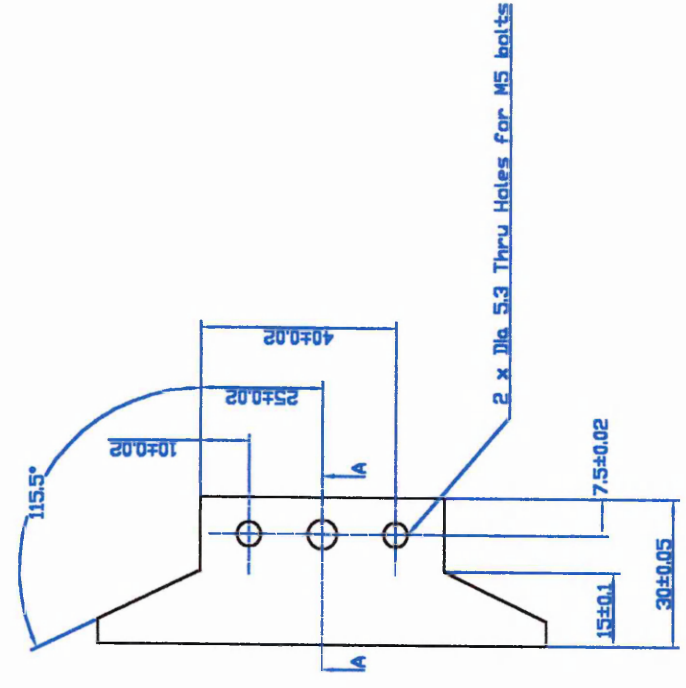
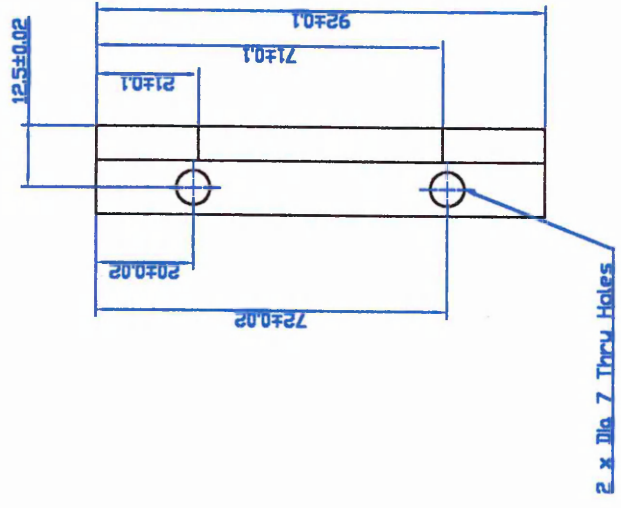
DRAWN BY R J Green	DATE 21/11/98	REV No 1	MODIFICATION SHEET	MS00000	DATE	SIGN	CHECKED	PART CODE		Verticle Beam Support	Scale 1:1
CHECKED BY U S Ferrando	DATE	QUANTITY 1	MATERIAL EN	00012	DATE			00012		Date date	Edition 1

SHU

DO NOT SCALE IF IN DOUBT ASK



Dia. 6 Drill & Ream thru Hole For 6mm Location Pin

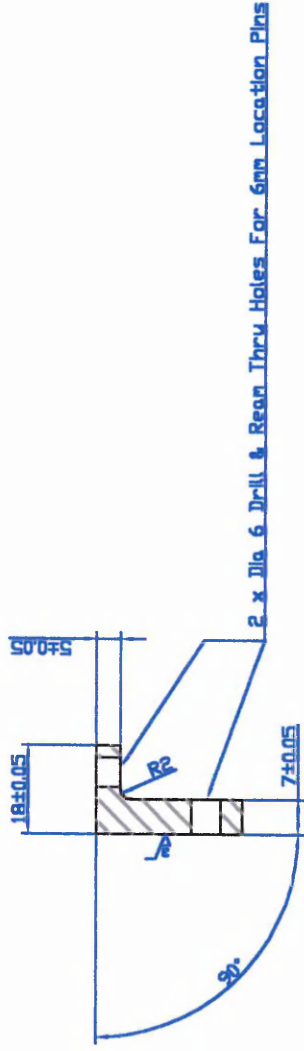


ALL DIMENSIONS IN MM

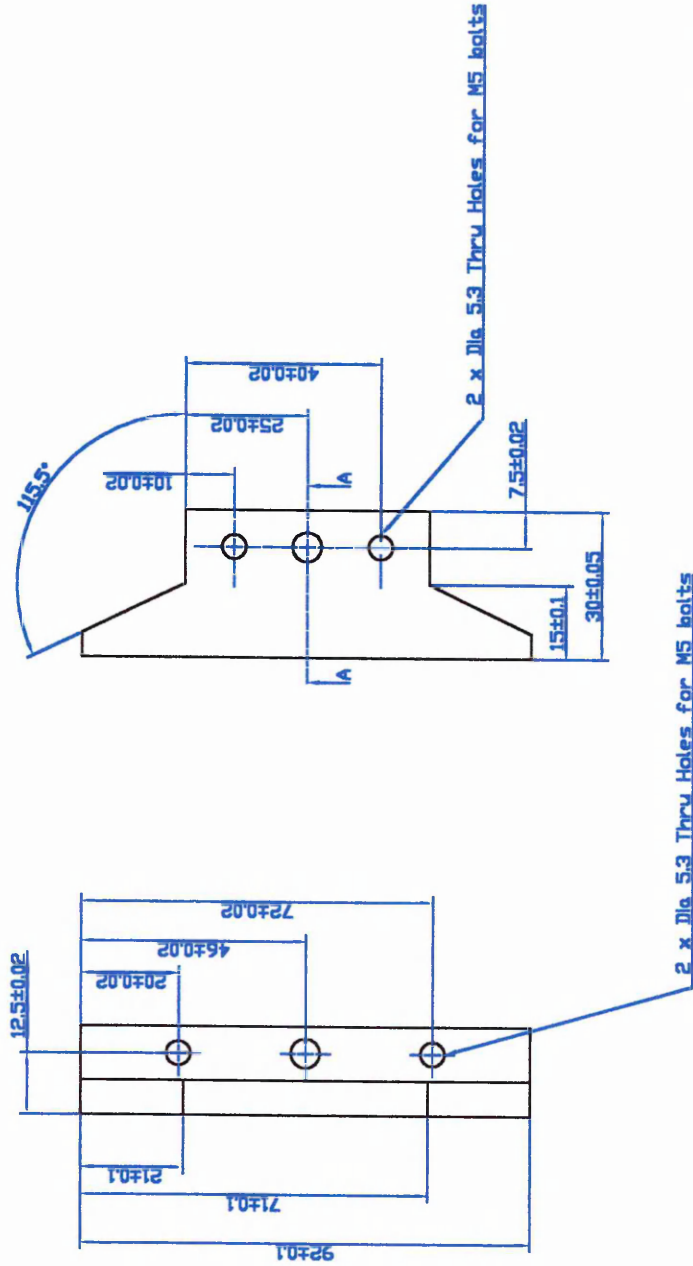
DRAWN BY R J Green	DATE 21/11/98	REV No 1	MODIFICATION SHEET MS00000	DATE	SIGN	CHECKED	PART CODE 00013	Scale 1:1
CHECKED BY U S Fernandez	DATE	QUANTITY 1	MATERIAL EN					SHEET 16
							Contact Moving L Section	Edition 1
							Date date	SHU



DO NOT SCALE IF IN DOUBT ASK



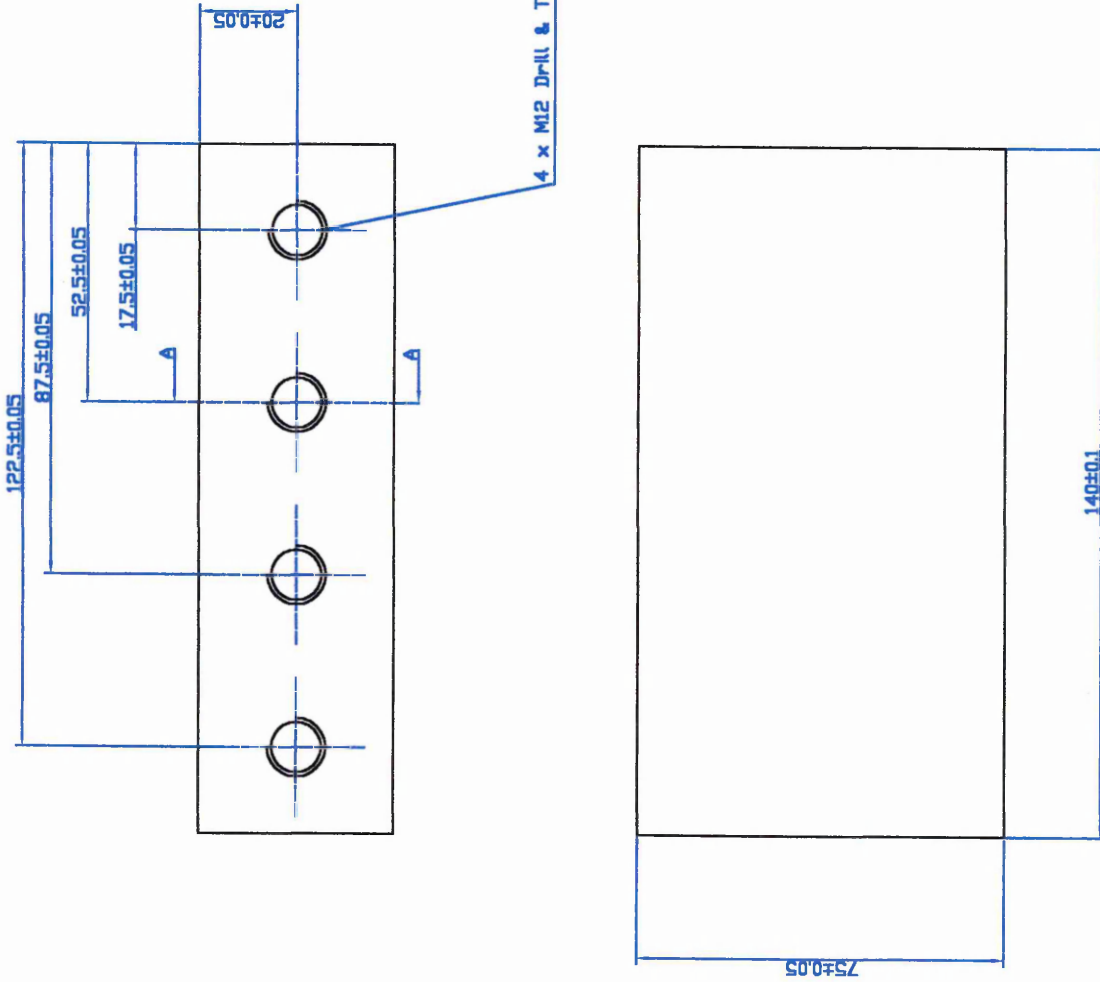
A-A



ALL DIMENSIONS IN
MM

DRAWN BY R J Green	DATE 21/11/98	REV No 1	MODIFICATION SHEET	MS00000	DATE	SIGN	CHECKED	PART CODE	0004	Scale 1:1
CHECKED BY U S Fernandez	DATE	QUANTITY 1	MATERIAL EN							SHU
Contact Fixed L Section										Edition 1
										Date date
										SHEET 17

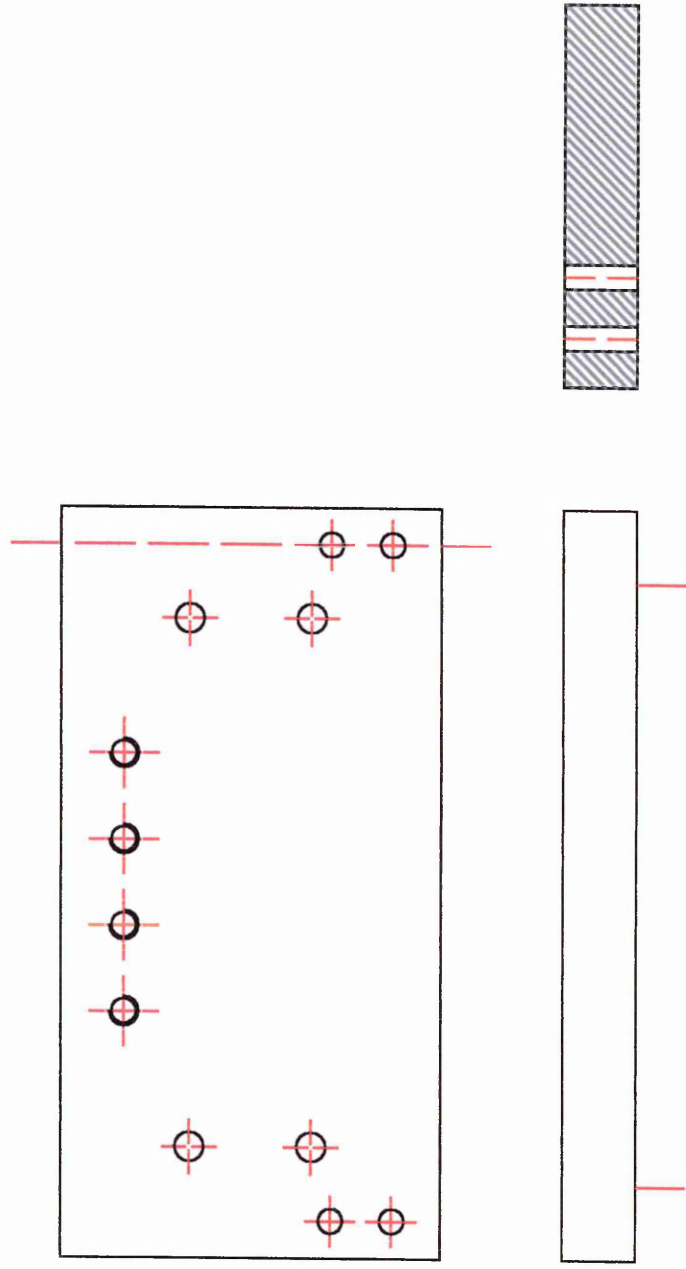
DO NOT SCALE IF IN DOUBT ASK



ALL DIMENSIONS IN
MM

DRAWN BY R J Green	DATE 19/11/98	REV No 1	MODIFICATION SHEET	MS00000	DATE	SIGN	CHECKED	PART CODE	 		Built In Beam Supports	Scale 1:1
CHECKED BY U S Ferrando	DATE / /	QUANTITY 2	MATERIAL					00016	Date date		SHU	Edition 1
											SHEET 19	

DO NOT SCALE IF IN DOUBT ASK

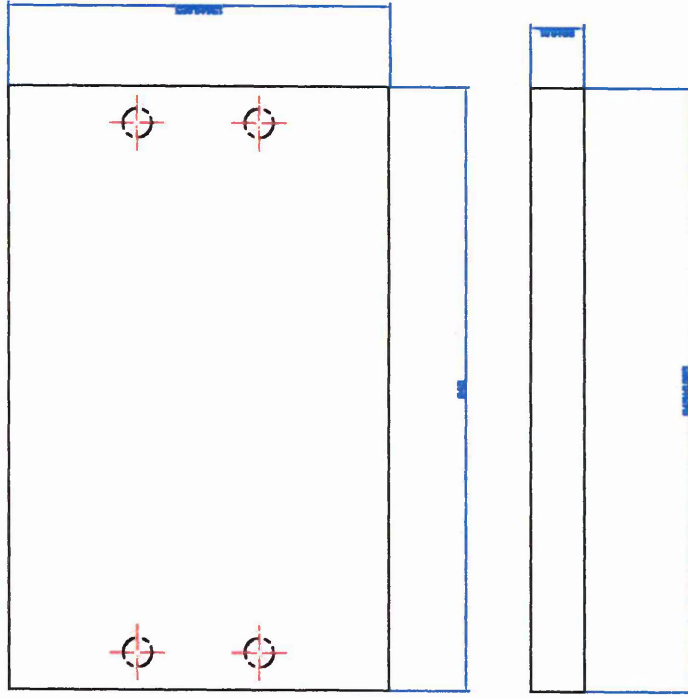


ALL DIMENSIONS IN
MM

DRAWN BY R J Green	DATE 23/11/98	REV No 0	MODIFICATION SHEET	MS00000	DATE	SIGN	CHECKED	PART CODE	 	Date date	Edition 1	Scale 1:2
	CHECKED BY U S Fernando	DATE	QUANTITY 2	MATERIAL EN	00017	SHU	SHEET 26					

Base Plates

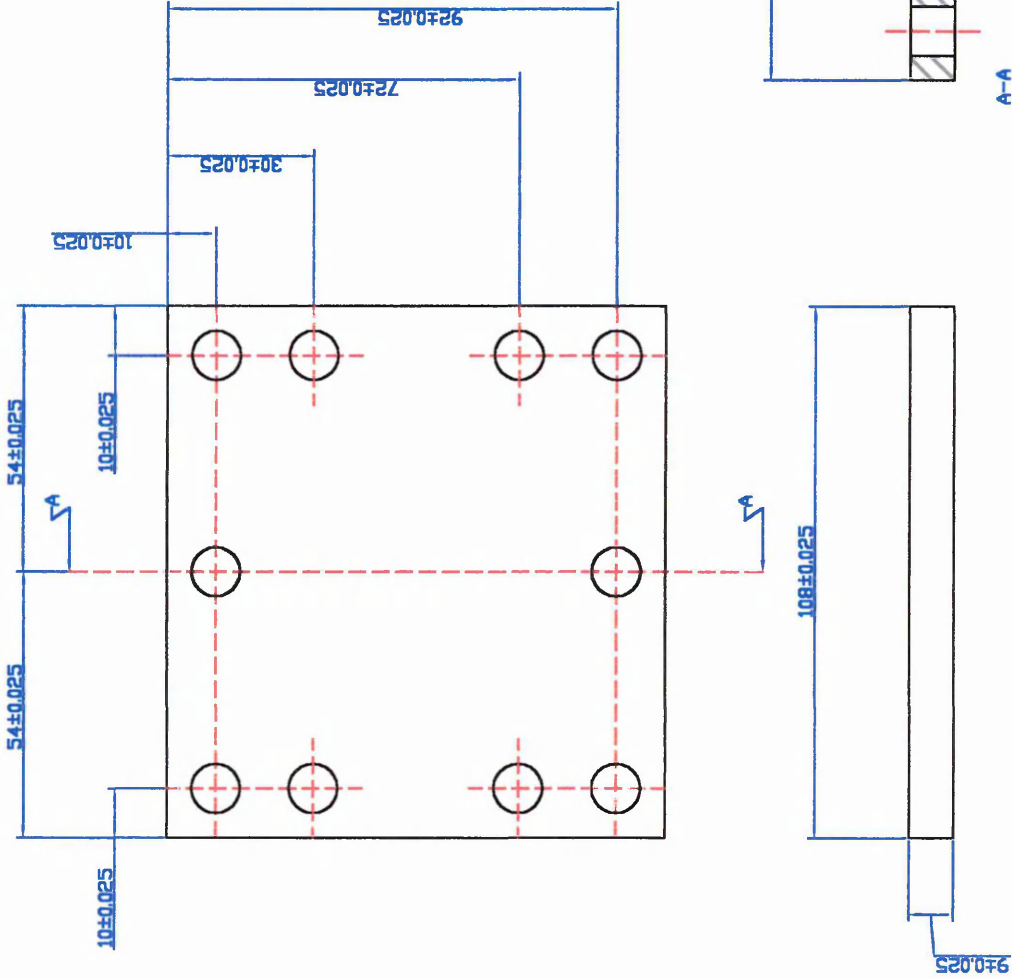
DO NOT SCALE IF IN DOUBT ASK



ALL DIMENSIONS IN
MM

DRAWN BY R J Green	DATE 23/11/98	REV No 0	MODIFICATION SHEET	MS00000	DATE	SIGN	CHECKED	PART CODE	 	Raiser Base Plates		Scale 1:2
	CHECKED BY U S Fernando	DATE	QUANTITY 2	MATERIAL	EN			00017		Date date	Edition 1	SHU

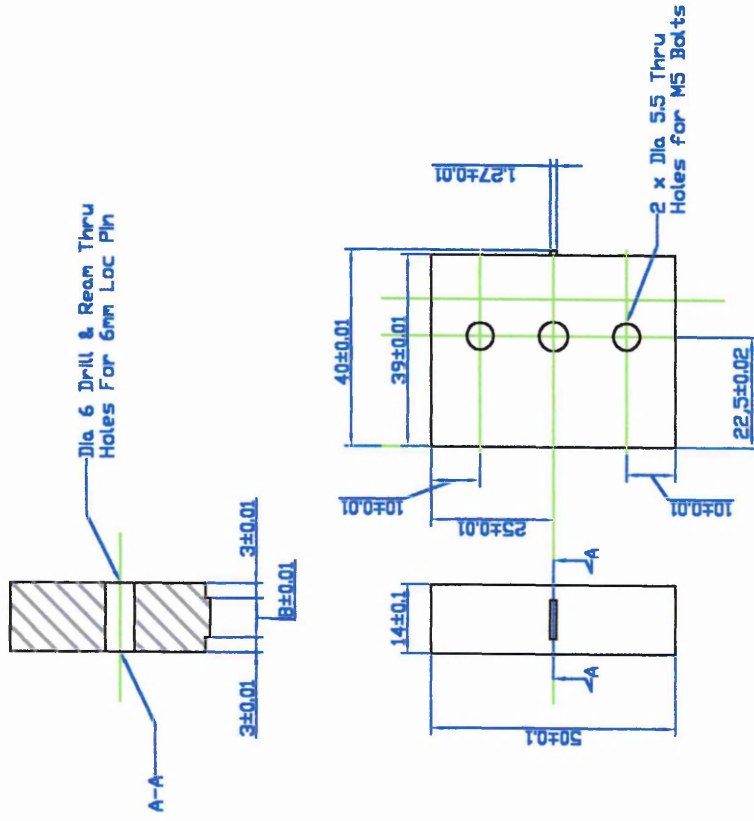
DO NOT SCALE IF IN DOUBT ASK



ALL DIMENSIONS IN MM

DRAWN BY R J Green	DATE 15/05/2000	REV No <input type="checkbox"/>	MODIFICATION SHEET MS00000	DATE	SIGN	CHECKED	PART CODE 000000		Raiser Block	Scale 1:1
CHECKED BY U S Fernando	DATE / /	QUANTITY 2	MATERIAL EN 24	DATE			Edition edition	Date date	SHEET Z1	

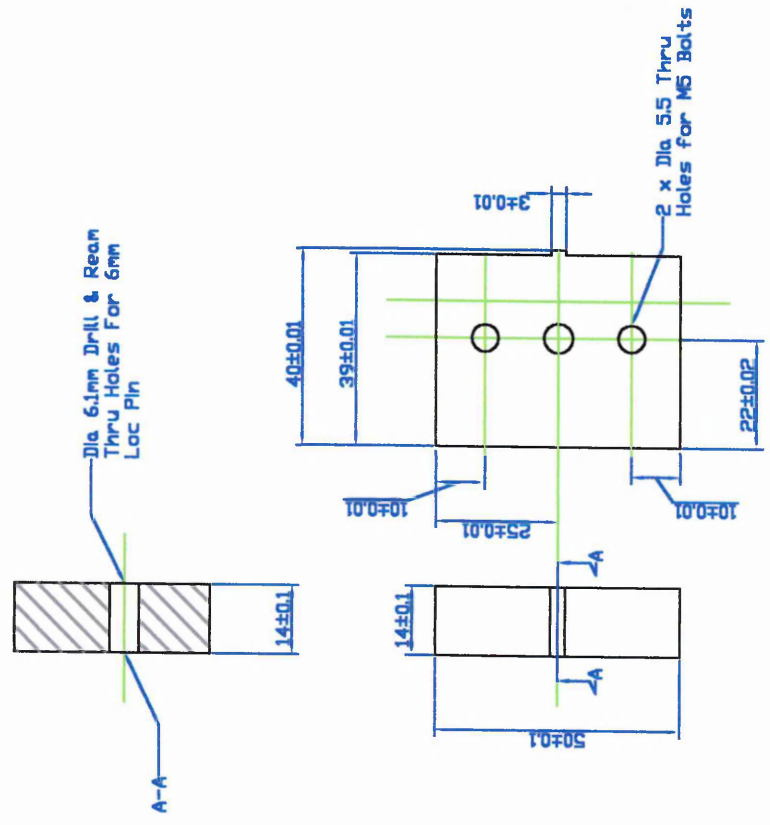
DO NOT SCALE IF IN DOUBT ASK



ALL DIMENSIONS IN MM

DRAWN BY R J Green	DATE 15/05/2000	REV No 0	MODIFICATION SHEET	MS00000	DATE	SIGN	CHECKED	PART CODE	000000		Date date	Edition edition	Scale 1:1	SHEET 22
	CHECKED BY U S Fernando	DATE / /	QUANTITY 2	MATERIAL	EN 24			000000			Contact Pads 1.27mm			

DO NOT SCALE IF IN DOUBT ASK



ALL DIMENSIONS IN MM

DRAWN BY R J Green	DATE 15/05/2000	REV No 0	MODIFICATION SHEET	MS00000	DATE	SIGN	CHECKED	PART CODE	000000	Scale 1:1	SHEET 22
CHECKED BY U S Fernando	DATE / /	QUANTITY 10	MATERIAL	DECIDED BY OPERATORS	INFINITE WISDOM					Contact Pads 3mm	Edition edition
										Date date	



APPENDIX B

SAMPLE ABAQUS INPUT FILES

Global Model

```
*HEADING
ELASTIC YEILD ZONE MODEL FOR TEST 127, A = 100, N = 80, MU = 1.5
*PREPRINT, HISTORY=no, ECHO=NO, MODEL=NO
*RESTART,WRITE,FREQ=10
**          CONTACT SECTION
*NODE
100001,0.0,1.0
100031,7.62,1.0
120031,7.62,0.0
120036,8.89,0.0
100036,8.89,1.0
100084,21.0,1.0
103108,21.0,10.0
103060,8.89,10.0
103055,7.62,10.0
103025,0.0,10.0
*NGEN, NSET=CONTOPL
103025,103055,1
*NGEN, NSET=CONTOPM
103055,103060,1
*NGEN, NSET=CONTOPR
103060,103108,1
*NGEN, NSET=CONBOTL
100001,100031,1
*NGEN, NSET=CONBOTM
100031,100036,1
*NGEN, NSET=CONBOTR
100036,100084,1
*NGEN, NSET=CENDSUF
120031,120036,1
*NFILL, NSET=CONTOTL
CONBOTL,CONTOPL,36,84
*NFILL, NSET=CONTOTM
CONBOTM,CONTOPM,36,84
*NFILL, NSET=CONTOTR
CONBOTR,CONTOPR,36,84
*NFILL, NSET=CTOTSUF
CONBOTM,CENDSUF,4,5000
*NSET, NSET=CONFIX, GENERATE
100001,103025,84
**
**          GLOBAL MODEL NSETS
**
*NSET, NSET=OUTC,GENERATE
100015, 100017, 1
100015, 101443,84
101443, 101480,1
100052, 101480,84
100050, 100052, 1
*NSET, NSET=MIDC, GENERATE
100100, 101360, 84
101360, 101395, 1
100135, 101395,84
*NSET, NSET=INNC, GENERATE
100101, 101277, 84
101277, 101310, 1
100134, 101310,84
**
*ELEMENT, TYPE=CPE4
100001, 100001,100002,100086,100085
200001,105031,105032,100032,100031
```

```

*ELGEN, ELSET=ALLELC
100001, 83,1,1, 36,84,83
200001, 5,1,1, 4,5000,5
*ELSET, ELSET=CSURF, GENERATE
100001,100030,1
200001,200016,5
200016,200020,1
200005,200020,5
100036,100083,1
*ELSET,ELSET=CONLOAD, GENERATE
102936,102940,1
**          PLATE SECTION
*NODE
1,0.0,-10.0
61,7.62,-10.0
71,8.89,-10.0
261,33.0,-10.0
20880,33.0,0.0
20690,8.89,0.0
20680,7.62,0.0
20620,0.0,0.0
*NGEN, NSET=TOPL
20620,20680,1
*NGEN, NSET=TOPM
20680,20690,1
*NGEN, NSET=TOPR
20690,20880,1
*NGEN, NSET=BOTL
1,61,1
*NGEN, NSET=BOTM
61,71,1
*NGEN, NSET=BOTR
71,261,1
*NFill, NSET=TOTL
BOTL,TOPL,79,261
*NFill, NSET=TOTM
BOTM,TOPM,79,261
*NFill, NSET=TOTR
BOTR,TOPR,79,261
*NSET,NSET=PLATFIX2, GENERATE
1,20620,261
*NSET,NSET=PLATFREE, GENERATE
261,20880,261
*NSET,NSET=PLATFIX1
BOTL,BOTM,BOTR
**
**          GLOBAL MODEL NSET
**
*NSET,NSET=OUTS, GENERATE
20649, 20651, 1
9948, 20649, 261
9948, 10020, 1
10020, 20721, 261
20719, 20721, 1
*NSET,NSET=MIDS, GENERATE
10210, 20389, 261
10210, 10280, 1
10280, 20459, 261
*NSET,NSET=INNS, GENERATE
10472,20651, 261
10472,10540,1
10540, 20719,261
**
*ELEMENT, TYPE=CPE4

```

```

1, 1,2,263,262
*ELGEN,ELSET=ALLELP
1,260,1,1, 79,261,260
*ELSET,ELSET=PSURF, GENERATE
20281,20540,1
*ELSET,ELSET=LOADSUF,GENERATE
260,20540,260
*ELSET,ELSET=FIXSUF, GENERATE
1,20281,260
**          CONTACT CONDITIONS
*SOLID SECTION, ELSET=ALLELP, MATERIAL=AL
8
*SOLID SECTION, ELSET=ALLELC, MATERIAL=STEEL
8
*MATERIAL, NAME=AL
*ELASTIC
70E3, 0.33
*MATERIAL, NAME=STEEL
*ELASTIC
209E3, 0.33
** DEFINING CONTACTS
*SURFACE DEFINITION, NAME=SPLATE
PSURF
*SURFACE DEFINITION, NAME=MCONT
CSURF
*CONTACT PAIR, INTERACTION=CONT, SMALL SLIDING
SPLATE, MCONT
*SURFACE INTERACTION, NAME=CONT
8
*SURFACE BEHAVIOR
0
*FRICTION,LAGRANGE
1.5
*NORMAL, TYPE = CONTACT SURFACE
MCONT, 120031, 0.0, -1.0, 0.0
*NORMAL, TYPE = CONTACT SURFACE
MCONT, 120036, 0.0,-1.0, 0.0
**          BOUNDARY CONDITIONS
*BOUNDARY
CONFIX,1
PLATFIX2,1
PLATFIX1,2
*AMPLITUDE, DEFINITION=PERIODIC,NAME=SINWAVE
1,6.283185307,0,0
0,1,0,0,0,0,0,0
*STEP,NLGEOM,INC=20
** APPLYING NORMAL LOAD
*STATIC
0.1,1.0
*DLOAD
CONLOAD,P3,[INPUT CONTACT LOAD]
*EL PRINT, FREQUENCY=0
*NODE PRINT, FREQUENCY=0
*CONTACT PRINT, NSET=TOPM
*CONTACT FILE
*NODE FILE, NSET=OUTC
U
*NODE FILE, NSET=MIDC
U
*NODE FILE, NSET=INNC
U
*NODE FILE, NSET=OUTS
U
*NODE FILE, NSET=MIDS

```

```
U
*NODE FILE, NSET=INNS
U
*END STEP
*STEP,NLGEOM,INC=40
** APPLYING AXIAL LOAD
*STATIC,DIRECT
0.025,1.0
*DLOAD,AMPLITUDE=SINWAVE
LOADSUF,P2, [INPUT AXIAL LOAD]
*EL PRINT, FREQUENCY=0
*CONTACT PRINT, NSET=TOPM
*CONTACT FILE
*NODE FILE, NSET=OUTC
U
*NODE FILE, NSET=MIDC
U
*NODE FILE, NSET=INNC
U
*NODE FILE, NSET=OUTS
U
*NODE FILE, NSET=MIDS
U
*NODE FILE, NSET=INNS
U
*END STEP
```

First Sub Model

```
*HEADING
TEST 1ST SUB MODEL FOR EYZMOD124
*PREPRINT, HISTORY=no, ECHO=NO, MODEL=NO
*RESTART,WRITE,FREQ=10
**          CONTACT SECTION
**
*NODE
1, 3.81, 1.0
31, 7.62,1.0
40031,7.62,0.0
40041,8.89,0.0
41, 8.89,1.0
71, 12.7, 1.0
2273, 3.81, 5.0
2303, 7.62, 5.0
2313, 8.89, 5.0
2343, 12.7, 5.0
*NGEN, NSET=CONTOPL
2273,2303,1
*NGEN, NSET=CONTOPM
2303,2313,1
*NGEN, NSET=CONTOPR
2313,2343,1
*NGEN, NSET=CONBOTL
1,31,1
*NGEN, NSET=CONBOTM
31,41,1
*NGEN, NSET=CONBOTR
41,71,1
*NGEN, NSET=CENDSUF
40031,40041,1
**
*NFILL, NSET=CONTOTL
CONBOTL,CONTOPL,32,71
*NFILL, NSET=CONTOTM
CONBOTM,CONTOPM,32,71
*NFILL, NSET=CONTOTR
CONBOTR,CONTOPR,32,71
*NFILL, NSET=CTOTSUF
CONBOTM,CENDSUF,8,5000
**
**          GLOBAL MODEL NSETS
**
*NSET, NSET=MIDC,GENERATE
1, 2273, 71
2273, 2343, 1
71, 2343,71
**
**          SUBMODEL NSETS
*NSET, NSET=SOUTC, GENERATE
20, 22, 1
20, 1227, 71
1227, 1259, 1
52, 1259,71
50, 52, 1
*NSET, NSET=SMIDC, GENERATE
92, 1157, 71
1157, 1187, 1
122, 1187, 71
*NSET,NSET=SINNC, GENERATE
93, 1087, 71
```

```

1087, 1115, 1
121, 1115, 71
**
*ELEMENT, TYPE=CPE4
1, 1,2,73,72
5001, 5031,5032,32,31
*ELGEN, ELSET=ALLELC
1, 70,1,1, 32,71,70
5001, 10,1,1, 8,5000,10
*ELSET, ELSET=CSURF, GENERATE
1,30,1
5001,5071,10
5071,5080,1
5010,5080,10
41,70,1
**          PLATE SECTION
*NODE
100001,3.81,-5.0633
100061,7.62,-5.0633
100081,8.89,-5.0633
100141,12.7,-5.0633
111421,12.7,0.0
111361,8.89,0.0
111341,7.62,0.0
111281,3.81,0.0
*NGEN, NSET=TOPL
111281,111341,1
*NGEN, NSET=TOPM
111341,111361,1
*NGEN, NSET=TOPR
111361,111421,1
*NGEN, NSET=BOTL
100001,100061,1
*NGEN, NSET=BOTM
100061,100081,1
*NGEN, NSET=BOTR
100081,100141,1
*NFILL, NSET=TOTL
BOTL, TOPL, 80, 141
*NFILL, NSET=TOTM
BOTM, TOPM, 80, 141
*NFILL, NSET=TOTR
BOTR, TOPR, 80, 141
**
**          GLOBAL MODEL NSET
**
*NSET, NSET=MIDS, GENERATE
100001, 111140, 141
100001, 100141, 1
100141, 111280, 141
**
**          SUB MODEL NSET
*NSET, NSET=SOUTS, GENERATE
111320, 111322, 1
108359, 111320, 141
108359, 108421, 1
108421, 111382, 141
111380, 111382, 1
*NSET, NSET=SMIDS, GENERATE
108501, 111180, 141
108501, 108561, 1
108561, 111240, 141
*NSET, NSET=SINNS, GENERATE
108643, 111322, 141

```

```

108643, 108701, 1
108701, 111380, 141
**
*ELEMENT, TYPE=CPE4
100001, 100001,100002,100143,100142
*ELGEN,ELSET=ALLELP
100001,140,1,1, 80,141,140
*ELSET,ELSET=PSURF, GENERATE
111061,111200,1
**          CONTACT CONDITIONS
*SOLID SECTION, ELSET=ALLELP, MATERIAL=AL
8
*SOLID SECTION, ELSET=ALLELC, MATERIAL=STEEL
8
*MATERIAL, NAME=AL
*ELASTIC
70E3, 0.33
*MATERIAL, NAME=STEEL
*ELASTIC
209E3, 0.33
** DEFINING CONTACTS
*SURFACE DEFINITION, NAME=SPLATE
PSURF
*SURFACE DEFINITION, NAME=MCONT
CSURF
*CONTACT PAIR, INTERACTION=CONT, SMALL SLIDING
SPLATE, MCONT
*SURFACE INTERACTION, NAME=CONT
8
*SURFACE BEHAVIOR
0
*FRICTION,LAGRANGE
1.5
*NORMAL, TYPE = CONTACT SURFACE
MCONT, 40031, 0.0, -1.0, 0.0
*NORMAL, TYPE = CONTACT SURFACE
MCONT, 40041, 0.0,-1.0, 0.0
**          BOUNDARY CONDITIONS
**          SUBMODEL BOUNDARY CONDITIONS
*SUBMODEL1
MIDC
MIDS
**
** APPLYING NORMAL LOAD
*STEP,NLGEOM,INC=20
*STATIC
0.1,1.0
*BOUNDARY, SUBMODEL, STEP=1
MIDC, 1,2
MIDS, 1,2
*EL PRINT, FREQUENCY=0
*NODE PRINT, FREQUENCY=0
*CONTACT PRINT, NSET=TOPM
*CONTACT FILE
*NODE FILE, NSET=SOUTC
U
*NODE FILE, NSET=SMIDC
U
*NODE FILE, NSET=SINNC
U
*NODE FILE, NSET=SOUTS
U
*NODE FILE, NSET=SMIDS
U

```

```
*NODE FILE, NSET=SINNS
U
*END STEP
** APPLYING AXIAL LOAD
*STEP,NLGEOM,INC=40
*STATIC,DIRECT
0.025,1.0
*BOUNDARY, SUBMODEL, STEP=2
MIDC, 1,2
MIDS, 1,2
*EL PRINT, FREQUENCY=0
*CONTACT PRINT, NSET=TOPM
*CONTACT FILE
*NODE FILE, NSET=SOUTC
U
*NODE FILE, NSET=SMIDC
U
*NODE FILE, NSET=SINNC
U
*NODE FILE, NSET=SOUTS
U
*NODE FILE, NSET=SMIDS
U
*NODE FILE, NSET=SINNS
U
*END STEP
```

Second Sub Model

```
*HEADING
TEST 2nd SUB MODEL FOR EYZMOD124
*PREPRINT, HISTORY=no, ECHO=NO, MODEL=NO
*RESTART,WRITE,FREQ=10
**
**           CONTACT SECTION
**
*NODE
1, 6.35, 1.0
21, 7.62,1.0
80021,7.62,0.0
80041,8.89,0.0
41, 8.89,1.0
61, 10.16, 1.0
1953, 6.35, 3.0
1973, 7.62, 3.0
1993, 8.89, 3.0
2013, 10.16, 3.0
*NGEN, NSET=CONTOPL
1953,1973,1
*NGEN, NSET=CONTOPM
1973,1993,1
*NGEN, NSET=CONTOPR
1993,2013,1
*NGEN, NSET=CONBOTL
1,21,1
*NGEN, NSET=CONBOTM
21,41,1
*NGEN, NSET=CONBOTR
41,61,1
*NGEN, NSET=CENDSUF
80021,80041,1
**
*NFill, NSET=CONTOTL
CONBOTL,CONTOPL,32,61
*NFill, NSET=CONTOTM
CONBOTM,CONTOPM,32,61
*NFill, NSET=CONTOTR
CONBOTR,CONTOPR,32,61
*NFill, NSET=CTOTSUF
CONBOTM,CENDSUF,16,5000
**
**
**           GLOBAL MODEL NSETS
**
*NSET, NSET=SMIDC,GENERATE
1, 1953, 61
1953, 2013, 1
61, 2013,61
**
**           SUB MODEL NSETS
**
*NSET, NSET=SSOUTC, GENERATE
10, 12, 1
10, 1047, 61
1047, 1089, 1
52, 1089, 61
50, 52, 1
*NSET, NSET=SSMDC, GENERATE
72, 987, 61
987, 1027, 1
```

```
112, 1027, 61
*NSET, NSET=SSINNC, GENERATE
73, 927, 61
927, 965, 1
111, 965, 61
**
*ELEMENT, TYPE=CPE4
1, 1,2,63,62
5001, 5021,5022,22,21
*ELGEN, ELSET=ALLELC
1, 60,1,1, 32,61,60
5001, 20,1,1, 16,5000,20
*ELSET, ELSET=CSURF, GENERATE
1,20,1
5001,5301,20
5301,5320,1
5020,5320,20
41,60,1
**          PLATE SECTION
*NODE
100001,6.35,-1.2658
100041,7.62,-1.2658
100081,8.89,-1.2658
100121,10.16,-1.2658
104961,10.16,0.0
104921,8.89,0.0
104881,7.62,0.0
104841,6.35,0.0
*NGEN, NSET=TOPL
104841,104881,1
*NGEN, NSET=TOPM
104881,104921,1
*NGEN, NSET=TOPR
104921,104961,1
*NGEN, NSET=BOTL
100001,100041,1
*NGEN, NSET=BOTM
100041,100081,1
*NGEN, NSET=BOTR
100081,100121,1
*NFILL, NSET=TOTL
BOTL,TOPL,40,121
*NFILL, NSET=TOTM
BOTM, TOPM, 40, 121
*NFILL, NSET=TOTR
BOTR, TOPR, 40, 121
**
**          GLOBAL MODEL NSET
**
*NSET, NSET=SMIDS, GENERATE
100001, 104720, 121
100001, 100121, 1
100121, 104840, 121
**
**          SUBMODEL NSET
**
*NSET, NSET=SSOUTS, GENERATE
104860, 104862, 1
102319, 104860, 121
102319, 102401, 1
102401, 104942, 121
104940, 104942, 1
*NSET, NSET=SSMDS, GENERATE
102441, 104740, 121
```

```

102441, 102521, 1
102521, 104820, 121
*NSET, NSET=SSINNS, GENERATE
102563, 104862, 121
102563, 102641, 1
102641, 104940, 121
**
*ELEMENT, TYPE=CPE4
100001, 100001,100002,100123,100122
*ELGEN,ELSET=ALLELP
100001,120,1,1, 40,121,120
*ELSET,ELSET=PSURF, GENERATE
104681,104800,1
**          CONTACT CONDITIONS
*SOLID SECTION, ELSET=ALLELP, MATERIAL=AL
8
*SOLID SECTION, ELSET=ALLELC, MATERIAL=STEEL
8
*MATERIAL, NAME=AL
*ELASTIC
70E3, 0.33
*MATERIAL, NAME=STEEL
*ELASTIC
209E3, 0.33
** DEFINING CONTACTS
*SURFACE DEFINITION, NAME=SPLATE
PSURF
*SURFACE DEFINITION, NAME=MCONT
CSURF
*CONTACT PAIR, INTERACTION=CONT, SMALL SLIDING
SPLATE, MCONT
*SURFACE INTERACTION, NAME=CONT
8
*SURFACE BEHAVIOR
0
*FRICTION,LAGRANGE
1.5
*NORMAL, TYPE = CONTACT SURFACE
MCONT, 80021, 0.0, -1.0, 0.0
*NORMAL, TYPE = CONTACT SURFACE
MCONT, 80041, 0.0,-1.0, 0.0
**          BOUNDARY CONDITIONS
**          SUBMODEL BOUNDARY CONDITIONS
*SUBMODEL1
SMIDC
SMIDS
**
** APPLYING NORMAL LOAD
*STEP,NLGEOM,INC=20
*STATIC
0.1,1.0
*BOUNDARY, SUBMODEL, STEP=1
SMIDC, 1,2
SMIDS, 1,2
*EL PRINT, FREQUENCY=0
*NODE PRINT, FREQUENCY=0
*CONTACT PRINT, NSET=TOPM
*CONTACT FILE
*NODE FILE, NSET=SSOUTC
U
*NODE FILE, NSET=SSMDC
U
*NODE FILE, NSET=SSINNC
U

```

```
*NODE FILE, NSET=SSOUTS
U
*NODE FILE, NSET=SSMDS
U
*NODE FILE, NSET=SSINNS
U
*END STEP
** APPLYING AXIAL LOAD
*STEP,NLGEOM,INC=40
*STATIC,DIRECT
0.025,1.0
*BOUNDARY, SUBMODEL, STEP=2
SMDC, 1,2
SMDS, 1,2
*EL PRINT, FREQUENCY=0
*CONTACT PRINT, NSET=TOPM
*CONTACT FILE
*NODE FILE, NSET=SSOUTC
U
*NODE FILE, NSET=SSMDC
U
*NODE FILE, NSET=SSINNC
U
*NODE FILE, NSET=SSOUTS
U
*NODE FILE, NSET=SSMDS
U
*NODE FILE, NSET=SSINNS
U
*END STEP
```

Third Sub Model

```
*HEADING
TEST 3rd SUB MODEL FOR EYZMOD124
*PREPRINT, HISTORY=no, ECHO=NO, MODEL=NO
*RESTART,WRITE,FREQ=10
**
**           CONTACT SECTION
**
*NODE
1, 6.985, 1.0
21, 7.62,1.0
61, 8.89,1.0
81, 9.525, 1.0
160021,7.62,0.0
160061,8.89,0.0
2593, 6.985, 2.0
2613, 7.62, 2.0
2653, 8.89, 2.0
2673, 9.525, 2.0
*NGEN, NSET=CONTOPL
2593,2613,1
*NGEN, NSET=CONTOPM
2613,2653,1
*NGEN, NSET=CONTOPR
2653,2673,1
*NGEN, NSET=CONBOTL
1,21,1
*NGEN, NSET=CONBOTM
21, 61,1
*NGEN, NSET=CONBOTR
61,81,1
*NGEN, NSET=CENDSUF
160021,160061,1
**
**
*NFILL, NSET=CONTOTL
CONBOTL,CONTOPL,32,81
*NFILL, NSET=CONTOTM
CONBOTM,CONTOPM,32,81
*NFILL, NSET=CONTOTR
CONBOTR,CONTOPR,32,81
*NFILL, NSET=CTOTSUF
CONBOTM,CENDSUF,32,5000
**
**
**           GLOBAL MODEL NSETS
**
*NSET, NSET=SSMDC, GENERATE
1, 2593, 81
2593, 2673, 1
81, 2673,81
**
**           SUB MODEL NSETS
**
**NSET, NSET=FOUTC, GENERATE
**2521, 2523, 1
**2521, 3007, 81
**3007, 3069, 1
**2583, 3069, 81
**2581, 2583, 1
**NSET, NSET=FMDC, GENERATE
**2603, 2927, 81
```

```

**2927, 2987, 1
**2663, 2987, 81
**NSET, NSET=FINNC, GENERATE
**2523, 2847, 81
**2847, 2905, 1
**2581, 2905, 81
**
*ELEMENT, TYPE=CPE4
1, 1,2,83,82
5001,5021,5022,22,21
*ELGEN, ELSET=ALLELC
1, 80,1,1, 32,81,80
5001, 40,1,1, 32,5000,40
*ELSET, ELSET=CSURF, GENERATE
1,20,1
5001,6241,40
6241,6280,1
5040,6280,40
61,80,1
**                PLATE SECTION
*NODE
200001,6.985,-0.6329
200041,7.62,-0.6329
200121,8.89,-0.6329
200161,9.525,-0.6329
206601,9.525,0.0
206561,8.89,0.0
206481,7.62,0.0
206441,6.985,0.0
*NGEN, NSET=TOPL
206441,206481,1
*NGEN, NSET=TOPM
206481,206561,1
*NGEN, NSET=TOPR
206561,206601,1
*NGEN, NSET=BOTL
200001,200041,1
*NGEN, NSET=BOTM
200041,200121,1
*NGEN, NSET=BOTR
200121,200161,1
*NFILL, NSET=TOTL
BOTL,TOPL,40,161
*NFILL, NSET=TOTM
BOTM,TOPM,40,161
*NFILL, NSET=TOTR
BOTR,TOPR,40,161
**
**                GLOBAL MODEL NSET
**
*NSET,NSET=SSMDS, GENERATE
200001, 206280, 161
200001, 200161, 1
200161, 206440, 161
**
**                SUB MODEL NSETS
**
**NSET, NSET=FOUTS, GENERATE
**10460, 10462, 1
**7079, 10460, 161
**7079, 7201, 1
**7201, 10582, 161
**10580, 10582, 1
**NSET, NSET=FMDS, GENERATE

```

```
**7241, 10300, 161
**7241, 7361, 1
**7361, 10420, 161
**NSET, NSET=FINNS, GENERATE
**7403, 10462, 161
**7403, 7521, 1
**7521, 10580, 161
**
*ELEMENT, TYPE=CPE4
200001, 200001,200002,200163,200162
*ELGEN,ELSET=ALLELP
200001,160,1,1, 40,161,160
*ELSET,ELSET=PSURF, GENERATE
206241,206400,1
**
**          SUB SURFACE STRESS ELEMENTS SETS
**
*ELSET,ELSET=SUBSURF, GENERATE
201318,201404,1
201478,201564,1
201638,201724,1
201798,201884,1
201958,202044,1
202118,202204,1
202278,202364,1
202438,202524,1
202598,202684,1
202758,202844,1
202918,203004,1
203078,203164,1
203238,203324,1
203398,203484,1
203558,203644,1
203718,203804,1
203878,203964,1
204038,204124,1
204198,204284,1
204358,204444,1
204518,204604,1
204678,204764,1
204838,204924,1
204998,205084,1
205158,205244,1
205318,205404,1
205478,205564,1
205638,205724,1
205798,205884,1
205958,206044,1
206118,206204,1
206278,206364,1
**
**          CONTACT CONDITIONS
**
*SOLID SECTION, ELSET=ALLELP, MATERIAL=AL
8
*SOLID SECTION, ELSET=ALLELC, MATERIAL=STEEL
8
*MATERIAL, NAME=AL
*ELASTIC
70E3, 0.33
*MATERIAL, NAME=STEEL
*ELASTIC
209E3, 0.33
** DEFINING CONTACTS
*SURFACE DEFINITION, NAME=SPLATE
```

```
PSURF
*SURFACE DEFINITION, NAME=MCONT
CSURF
*CONTACT PAIR, INTERACTION=CONT, SMALL SLIDING, ADJUST
SPLATE, MCONT
*SURFACE INTERACTION, NAME=CONT
8
*SURFACE BEHAVIOR
0
*FRICTION, LAGRANGE
1.5
*NORMAL, TYPE = CONTACT SURFACE
MCONT, 160021, 0.0, -1.0, 0.0
*NORMAL, TYPE = CONTACT SURFACE
MCONT, 160061, 0.0, -1.0, 0.0
**      SUBMODEL BOUNDARY CONDITIONS
*SUBMODEL
SSMDC
SSMDS
**
** APPLYING NORMAL LOAD
*STEP, NLGEOM, INC=20
*STATIC
0.1, 1.0
*BOUNDARY, SUBMODEL, STEP=1
SSMDC, 1, 2
SSMDS, 1, 2
*EL PRINT, FREQUENCY=0
*NODE PRINT, FREQUENCY=0
*CONTACT PRINT, NSET=TOPM
*CONTACT FILE
**NODE FILE, NSET=FOUTC
**U
**NODE FILE, NSET=FMDC
**U
**NODE FILE, NSET=FINNC
**U
**NODE FILE, NSET=FOUTS
**U
**NODE FILE, NSET=FMDS
**U
**NODE FILE, NSET=FINNS
**U
*END STEP
** APPLYING AXIAL LOAD
*STEP, NLGEOM, INC=40
*STATIC, DIRECT
0.025, 1.0
*BOUNDARY, SUBMODEL, STEP=2
SSMDC, 1, 2
SSMDS, 1, 2
*EL PRINT, FREQUENCY=10, ELSET=SUBSURF
S11
S12
*EL FILE
*CONTACT PRINT, NSET=TOPM
*CONTACT FILE
**NODE FILE, NSET=FOUTC
**U
**NODE FILE, NSET=FMDC
**U
**NODE FILE, NSET=FINNC
**U
**NODE FILE, NSET=FOUTS
```

Global Model

```
*HEADING
Hallam Global Model Test 801, MU = 1.5
*PREPRINT, HISTORY=no, ECHO=NO, MODEL=NO
*RESTART,WRITE,FREQ=10
**          CONTACT SECTION
*NODE
1,8.0,1.0
48,31.5,1.0
20048,31.5,0.0
20054,34.5,0.0
54,34.5,1.0
101,58.0,1.0
8181,58.0,41.0
8134,34.5,41.0
8128,31.5,41.0
8081,8.0,41.0
60001,7.5,1.0
68081,7.5,41.0
*NGEN, NSET=CONTOPL
8081,8128,1
*NGEN, NSET=CONTOPM
8128,8134,1
*NGEN, NSET=CONTOPR
8134,8181,1
*NGEN, NSET=CONBOTL
1,48,1
*NGEN, NSET=CONBOTM
48,54,1
*NGEN, NSET=CONBOTR
54,101,1
*NGEN, NSET=CENDSUF
20048,20054,1
*NGEN, NSET=BCNBOT
1,60001,60000
*NGEN,NSET=BCNTOP
8081,68081,60000
*NFILL, NSET=CONTOTL
CONBOTL,CONTOPL,80,101
*NFILL, NSET=CONTOTM
CONBOTM,CONTOPM,80,101
*NFILL, NSET=CONTOTR
CONBOTR,CONTOPR,80,101
*NFILL, NSET=CTOTSUF
CONBOTM,CENDSUF,2,10000
*NFILL, NSET=BCN
BCNBOT,BCNTOP,80,101
**
**          GLOBAL MODEL NSETS
**
*NSET, NSET=OUTC,GENERATE
23, 25, 1
23, 4063,101
4063, 4119,1
79, 4119,101
77, 79, 1
*NSET, NSET=MIDC, GENERATE
125, 3963, 101
3963, 4017, 1
179, 4017,101
*NSET, NSET=INNC, GENERATE
126, 3863, 101
```

```

3863, 3915, 1
178, 3915,101
**
*ELEMENT, TYPE=CPE4
1, 1,2,103,102
10001,10048,10049,49,48
*ELEMENT, TYPE=SPRING1
60001,1,60001,60102,102
*ELGEN, ELSET=ALLELC
1, 100,1,1, 80,101,100
10001, 6,1,1, 2,10000,6
*ELGEN, ELSET=BCSPRING
60001,1,60001,1, 80,101,1000
*ELSET, ELSET=CSURF, GENERATE
1,47,1
10001,10007,6
10007,10012,1
10006,10012,6
54,100,1
*ELSET,ELSET=CONLOAD, GENERATE
7948,7953,1
**          PLATE SECTION
*NODE
30001,0.0,-14.0
30127,31.5,-14.0
30139,34.5,-14.0
30265,66.0,-14.0
45105,66.0,0.0
44979,34.5,0.0
44967,31.5,0.0
44841,0.0,0.0
*NGEN, NSET=TOPL
44841,44967,1
*NGEN, NSET=TOPM
44967,44979,1
*NGEN, NSET=TOPR
44979,45105,1
*NGEN, NSET=BOTL
30001,30127,1
*NGEN, NSET=BOTM
30127,30139,1
*NGEN, NSET=BOTR
30139,30265,1
*NFILL, NSET=TOTL
BOTL,TOPL,56,265
*NFILL, NSET=TOTM
BOTM,TOPM,56,265
*NFILL, NSET=TOTR
BOTR,TOPR,56,265
*NSET,NSET=PLATFIX2, GENERATE
30001,44841,265
*NSET,NSET=PLATFREE, GENERATE
30265,45105,265
*NSET,NSET=PLATFIX1
BOTL,BOTM,BOTR
**
**          GLOBAL MODEL NSET
**
*NSET,NSET=OUTS, GENERATE
44918, 44920, 1
37233, 44918, 265
37233, 37343, 1
37343, 45028, 265
45026, 45028, 1

```

```

*NSET,NSET=MIDS, GENERATE
37499, 44654, 265
37499, 37607, 1
37607, 44762, 265
*NSET,NSET=INNS, GENERATE
37765,44655, 265
37765,37871,1
37871, 44761,265
**
*ELEMENT, TYPE=CPE4
30001, 30001,30002,30267,30266
*ELGEN,ELSET=ALLELP
30001,264,1,1, 56,265,264
*ELSET,ELSET=PSURF, GENERATE
44521,44784,1
*ELSET,ELSET=LOADSUF, GENERATE
30264,44784,264
*ELSET,ELSET=FIXSUF, GENERATE
30001,44521,264
**          CONTACT CONDITIONS
*SOLID SECTION, ELSET=ALLELP, MATERIAL=AL
8
*SOLID SECTION, ELSET=ALLELC, MATERIAL=STEEL
8
*SPRING, ELSET=BCSPRING
1
2250
*MATERIAL, NAME=AL
*ELASTIC
70E3, 0.33
*MATERIAL, NAME=STEEL
*ELASTIC
209E3, 0.33
** DEFINING CONTACTS
*SURFACE DEFINITION, NAME=SPLATE
PSURF
*SURFACE DEFINITION, NAME=MCONT
CSURF
*CONTACT PAIR, INTERACTION=CONT, SMALL SLIDING
SPLATE, MCONT
*SURFACE INTERACTION, NAME=CONT
8
*SURFACE BEHAVIOR
0
*FRICTION,LAGRANGE
1.5
*NORMAL, TYPE = CONTACT SURFACE
MCONT, 20048, 0.0, -1.0, 0.0
*NORMAL, TYPE = CONTACT SURFACE
MCONT, 20054, 0.0,-1.0, 0.0
**          BOUNDARY CONDITIONS
*BOUNDARY
PLATFIX2,1
PLATFIX1,2
*AMPLITUDE, DEFINITION=PERIODIC,NAME=SINWAVE
1,6.283185307,0,0
0,1,0,0,0,0,0,0
*STEP,NLGEOM,INC=20
** APPLYING NORMAL LOAD
*STATIC
0.1,1.0
*DLOAD
CONLOAD,P3,[INPUT CONTACT LOAD]
*EL PRINT, FREQUENCY=0

```

```
*NODE PRINT, FREQUENCY=0
*CONTACT PRINT, NSET=TOPM
*CONTACT FILE
*NODE FILE, NSET=OUTC
U
*NODE FILE, NSET=MIDC
U
*NODE FILE, NSET=INNC
U
*NODE FILE, NSET=OUTS
U
*NODE FILE, NSET=MIDS
U
*NODE FILE, NSET=INNS
U
*END STEP
*STEP, NLGEOM, INC=40
** APPLYING AXIAL LOAD
*STATIC, DIRECT
0.025, 1.0
*DLOAD, AMPLITUDE=SINWAVE
LOADSUF, P2, [INPUT AXIAL LOAD]
*EL PRINT, FREQUENCY=0
*NODE PRINT, NSET=CENDSUF, FREQUENCY=10
U1
*CONTACT PRINT, NSET=TOPM
*CONTACT FILE
*NODE FILE, NSET=OUTC
U
*NODE FILE, NSET=MIDC
U
*NODE FILE, NSET=INNC
U
*NODE FILE, NSET=OUTS
U
*NODE FILE, NSET=MIDS
U
*NODE FILE, NSET=INNS
U
*END STEP
```

First Sub Model

```
*HEADING
HALLAM MODEL 1ST SUB MODEL 1
*PREPRINT, HISTORY=NO, ECHO=NO, MODEL=NO
**RESTART, WRITE, FREQ=10
**          CONTACT SECTION
**
*NODE
1, 19.5, 1.0
49, 31.5, 1.0
40049, 31.5, 0.0
40061, 34.5, 0.0
61, 34.5, 1.0
109, 46.5, 1.0
8721, 19.5, 21.0
8769, 31.5, 21.0
8781, 34.5, 21.0
8829, 46.5, 21.0
*NGEN, NSET=CONTOPL
8721, 8769, 1
*NGEN, NSET=CONTOPM
8769, 8781, 1
*NGEN, NSET=CONTOPR
8781, 8829, 1
*NGEN, NSET=CONBOTL
1, 49, 1
*NGEN, NSET=CONBOTM
49, 61, 1
*NGEN, NSET=CONBOTR
61, 109, 1
*NGEN, NSET=CENDSUF
40049, 40061, 1
**
*NFILL, NSET=CONTOTL
CONBOTL, CONTOPL, 80, 109
*NFILL, NSET=CONTOTM
CONBOTM, CONTOPM, 80, 109
*NFILL, NSET=CONTOTR
CONBOTR, CONTOPR, 80, 109
*NFILL, NSET=CTOTSUF
CONBOTM, CENDSUF, 4, 10000
**
**          GLOBAL MODEL NSETS
**
*NSET, NSET=MIDC, GENERATE
1, 8721, 109
8721, 8829, 1
109, 8829, 109
**
**          SUBMODEL NSETS
*NSET, NSET=SOUTC, GENERATE
24, 26, 1
24, 4384, 109
4384, 4446, 1
86, 4446, 109
84, 86, 1
*NSET, NSET=SMIDC, GENERATE
134, 4276, 109
4276, 4336, 1
194, 4336, 109
*NSET, NSET=SINNC, GENERATE
135, 4168, 109
```

```
4168, 4226, 1
193, 4226, 109
**
*ELEMENT, TYPE=CPE4
1, 1,2,111,110
10001, 10049,10050,50,49
*ELGEN, ELSET=ALLELC
1, 108,1,1, 80,109,108
10001, 12,1,1, 4,10000,12
*ELSET, ELSET=CSURF, GENERATE
1,48,1
10001,10037,12
10037,10048,1
10012,10048,12
61,108,1
**          PLATE SECTION
*NODE
50001,19.5,-7.0
50097,31.5,-7.0
50121,34.5,-7.0
50217,46.5,-7.0
62369,46.5,0.0
62273,34.5,0.0
62249,31.5,0.0
62153,19.5,0.0
*NGEN, NSET=TOPL
62153,62249,1
*NGEN, NSET=TOPM
62249,62273,1
*NGEN, NSET=TOPR
62273,62369,1
*NGEN, NSET=BOTL
50001,50097,1
*NGEN, NSET=BOTM
50097,50121,1
*NGEN, NSET=BOTR
50121,50217,1
*NFILL, NSET=TOTL
BOTL,TOPL,56,217
*NFILL, NSET=TOTM
BOTM,TOPM,56,217
*NFILL, NSET=TOTR
BOTR,TOPR,56,217
**
**          GLOBAL MODEL NSET
**
*NSET,NSET=MIDS, GENERATE
50001, 62153, 217
50001, 50217, 1
50217, 62369, 217
**
**          SUB MODEL NSET
*NSET,NSET=SOUTS, GENERATE
62200, 62202, 1
55907, 62200, 217
55907, 56029, 1
56029, 62322, 217
62320, 62322, 1
*NSET,NSET=SMIDS, GENERATE
56125, 61984, 217
56125, 56245, 1
56245, 62104, 217
*NSET,NSET=SINNS, GENERATE
56343, 61985, 217
```

```

56343, 56461, 1
56461, 62103, 217
**
*ELEMENT, TYPE=CPE4
50001, 50001,50002,50219,50218
*ELGEN,ELSET=ALLELP
50001,216,1,1, 56,217,216
*ELSET,ELSET=PSURF, GENERATE
61881,62096,1
**          CONTACT CONDITIONS
*SOLID SECTION, ELSET=ALLELP, MATERIAL=AL
8
*SOLID SECTION, ELSET=ALLELC, MATERIAL=STEEL
8
*MATERIAL, NAME=AL
*ELASTIC
70E3, 0.33
*MATERIAL, NAME=STEEL
*ELASTIC
209E3, 0.33
** DEFINING CONTACTS
*SURFACE DEFINITION, NAME=SPLATE
PSURF
*SURFACE DEFINITION, NAME=MCONT
CSURF
*CONTACT PAIR, INTERACTION=CONT, SMALL SLIDING
SPLATE, MCONT
*SURFACE INTERACTION, NAME=CONT
8
*SURFACE BEHAVIOR
0
*FRICTION,LAGRANGE
1.5
*NORMAL, TYPE = CONTACT SURFACE
MCONT, 40049, 0.0, -1.0, 0.0
*NORMAL, TYPE = CONTACT SURFACE
MCONT, 40061, 0.0,-1.0, 0.0
**          BOUNDARY CONDITIONS
**          SUBMODEL BOUNDARY CONDITIONS
*SUBMODEL
MIDC
MIDS
**
** APPLYING NORMAL LOAD
*STEP,NLGEOM,INC=20
*STATIC
0.1,1.0
*BOUNDARY, SUBMODEL, STEP=1
MIDC, 1,2
MIDS, 1,2
*EL PRINT, FREQUENCY=0
*NODE PRINT, FREQUENCY=0
*CONTACT PRINT, NSET=TOPM
*CONTACT FILE
*NODE FILE, NSET=SOUTC
U
*NODE FILE, NSET=SMIDC
U
*NODE FILE, NSET=SINNC
U
*NODE FILE, NSET=SOUTS
U
*NODE FILE, NSET=SMIDS
U

```

```
*NODE FILE, NSET=SINNS
U
*END STEP
** APPLYING AXIAL LOAD
*STEP,NLGEOM, INC=40
*STATIC,DIRECT
0.025,1.0
*BOUNDARY, SUBMODEL, STEP=2
MIDC, 1,2
MIDS, 1,2
*EL PRINT, FREQUENCY=0
*CONTACT PRINT, NSET=TOPM
*CONTACT FILE
*NODE FILE, NSET=SOUTC
U
*NODE FILE, NSET=SMIDC
U
*NODE FILE, NSET=SINNC
U
*NODE FILE, NSET=SOUTS
U
*NODE FILE, NSET=SMIDS
U
*NODE FILE, NSET=SINNS
U
*END STEP
```

Second Sub Model

```
*HEADING
HALLAM MODEL 2nd SUB MODEL
*PREPRINT, HISTORY=NO, ECHO=NO, MODEL=NO
**RESTART,WRITE,FREQ=10
**
**          CONTACT SECTION
**
*NODE
1, 25.5, 1.0
49, 31.5,1.0
80049,31.5,0.0
80073,34.5,0.0
73, 34.5,1.0
121, 40.5, 1.0
9801, 40.5, 11.0
9753, 34.5, 11.0
9729, 31.5, 11.0
9681, 25.5, 11.0
*NGEN, NSET=CONTOPL
9681,9729,1
*NGEN, NSET=CONTOPM
9729,9753,1
*NGEN, NSET=CONTOPR
9753,9801,1
*NGEN, NSET=CONBOTL
1,49,1
*NGEN, NSET=CONBOTM
49,73,1
*NGEN, NSET=CONBOTR
73,121,1
*NGEN, NSET=CENDSUF
80049,80073,1
**
*NFILL, NSET=CONTOTL
CONBOTL,CONTOPL,80,121
*NFILL, NSET=CONTOTM
CONBOTM,CONTOPM,80,121
*NFILL, NSET=CONTOTR
CONBOTR,CONTOPR,80,121
*NFILL, NSET=CTOTSUF
CONBOTM,CENDSUF,8,10000
**
**
**          GLOBAL MODEL NSETS
**
*NSET, NSET=SMIDC, GENERATE
1, 9681, 121
9681, 9801, 1
121, 9801,121
**
**          SUB MODEL NSETS
**
*NSET, NSET=SSOUTC, GENERATE
36, 38, 1
36, 2456, 121
2456, 2506, 1
86, 2506, 121
84, 86, 1
2579,2580,1
*NSET, NSET=SSMDC, GENERATE
158, 2336, 121
```

```
2336, 2384, 1
206, 2384, 121
*NSET, NSET=SSINNC, GENERATE
159, 2216, 121
2216, 2262, 1
205, 2262, 121
**
*ELEMENT, TYPE=CPE4
1, 1,2,123,122
10001, 10049,10050,50,49
*ELGEN, ELSET=ALLELC
1, 120,1,1, 80,121,120
10001, 24,1,1, 8,10000,24
*ELSET, ELSET=CSURF, GENERATE
1,48,1
10001,10169,24
10169,10192,1
10024,10192,24
73,120,1
**          PLATE SECTION
*NODE
100001,25.5,-3.5
100097,31.5,-3.5
100145,34.5,-3.5
100241,40.5,-3.5
113737,40.5,0.0
113641,34.5,0.0
113593,31.5,0.0
113497,25.5,0.0
*NGEN, NSET=TOPL
113497,113593,1
*NGEN, NSET=TOPM
113593,113641,1
*NGEN, NSET=TOPR
113641,113737,1
*NGEN, NSET=BOTL
100001,100097,1
*NGEN, NSET=BOTM
100097,100145,1
*NGEN, NSET=BOTR
100145,100241,1
*NFILL, NSET=TOTL
BOTL,TOPL,56,241
*NFILL, NSET=TOTM
BOTM, TOPM, 56,241
*NFILL, NSET=TOTR
BOTR, TOPR, 56,241
**
**          GLOBAL MODEL NSET
**
*NSET,NSET=SMIDS, GENERATE
100001, 113497, 241
100001, 100241, 1
100241, 113737, 241
**
**          SUBMODEL NSET
**
*NSET, NSET=SSOUTS, GENERATE
113568, 113570,1
106579, 113568, 241
106579, 106677, 1
106677, 113666, 241
113664, 113666, 1
*NSET, NSET=SSMDS, GENERATE
```

```

106821, 113328, 241
106821, 106917, 1
106917, 113424, 241
*NSET, NSET=SSINNS, GENERATE
107063, 113329, 241
107063, 107157, 1
107157, 113423, 241
**
*ELEMENT, TYPE=CPE4
100001, 100001,100002,100243,100242
*ELGEN,ELSET=ALLELP
100001,240,1,1, 56,241,240
*ELSET,ELSET=PSURF, GENERATE
113201,113440,1
**          CONTACT CONDITIONS
*SOLID SECTION, ELSET=ALLELP, MATERIAL=AL
8
*SOLID SECTION, ELSET=ALLELC, MATERIAL=STEEL
8
*MATERIAL, NAME=AL
*ELASTIC
70E3, 0.33
*MATERIAL, NAME=STEEL
*ELASTIC
209E3, 0.33
** DEFINING CONTACTS
*SURFACE DEFINITION, NAME=SPLATE
PSURF
*SURFACE DEFINITION, NAME=MCONT
CSURF
*CONTACT PAIR, INTERACTION=CONT, SMALL SLIDING
SPLATE, MCONT
*SURFACE INTERACTION, NAME=CONT
8
*SURFACE BEHAVIOR
0
*FRICTION,LAGRANGE
1.5
*NORMAL, TYPE = CONTACT SURFACE
MCONT, 80049, 0.0, -1.0, 0.0
*NORMAL, TYPE = CONTACT SURFACE
MCONT, 80073, 0.0,-1.0, 0.0
**          BOUNDARY CONDITIONS
**          SUBMODEL BOUNDARY CONDITIONS
*SUBMODEL1
SMIDC
SMIDS
**
** APPLYING NORMAL LOAD
*STEP,NLGEOM,INC=20
*STATIC
0.1,1.0
*BOUNDARY, SUBMODEL, STEP=1
SMIDC, 1,2
SMIDS, 1,2
*EL PRINT, FREQUENCY=0
*NODE PRINT, FREQUENCY=0
*CONTACT PRINT, NSET=TOPM
*CONTACT FILE
*NODE FILE, NSET=SSOUTC
U
*NODE FILE, NSET=SSMDC
U
*NODE FILE, NSET=SSINNC

```

```
U
*NODE FILE, NSET=SSOUTS
U
*NODE FILE, NSET=SSMDS
U
*NODE FILE, NSET=SSINNS
U
*END STEP
** APPLYING AXIAL LOAD
*STEP,NLGEOM,INC=40
*STATIC,DIRECT
0.025,1.0
*BOUNDARY, SUBMODEL, STEP=2
SMIDC, 1,2
SMIDS, 1,2
*EL PRINT, FREQUENCY=0
*CONTACT PRINT, NSET=TOPM
*CONTACT FILE
*NODE FILE, NSET=SSOUTC
U
*NODE FILE, NSET=SSMDC
U
*NODE FILE, NSET=SSINNC
U
*NODE FILE, NSET=SSOUTS
U
*NODE FILE, NSET=SSMDS
U
*NODE FILE, NSET=SSINNS
U
*END STEP
```

Third Sub Model

```
*HEADING
HALLAM MODEL 2 SUB MODEL
*PREPRINT, HISTORY=NO, ECHO=NO, MODEL=NO
**RESTART, WRITE, FREQ=10
**
**          CONTACT SECTION
**
*NODE
1, 30.0, 1.0
25, 31.5, 1.0
73, 34.5, 1.0
97, 36, 1.0
80025, 31.5, 0.0
80073, 34.5, 0.0
3881, 30.0, 3.5
3905, 31.5, 3.5
3953, 34.5, 3.5
3977, 36, 3.5
*NGEN, NSET=CONTOPL
3881, 3905, 1
*NGEN, NSET=CONTOPM
3905, 3953, 1
*NGEN, NSET=CONTOPR
3953, 3977, 1
*NGEN, NSET=CONBOTL
1, 25, 1
*NGEN, NSET=CONBOTM
25, 73, 1
*NGEN, NSET=CONBOTR
73, 97, 1
*NGEN, NSET=CENDSUF
80025, 80073, 1
**
**
*NFILL, NSET=CONTOTL
CONBOTL, CONTOPL, 40, 97
*NFILL, NSET=CONTOTM
CONBOTM, CONTOPM, 40, 97
*NFILL, NSET=CONTOTR
CONBOTR, CONTOPR, 40, 97
*NFILL, NSET=CTOTSUF
CONBOTM, CENDSUF, 16, 5000
**
**
**          GLOBAL MODEL NSETS
**
*NSET, NSET=SSMDC, GENERATE
1, 3881, 97
3881, 3977, 1
97, 3977, 97
**
**          SUB MODEL NSETS
**
*NSET, NSET=FOUTC, GENERATE
16, 18, 1
16, 1568, 97
1568, 1634, 1
82, 1634, 97
80, 82, 1
*NSET, NSET=FMDC, GENERATE
114, 1472, 97
```

```

1472, 1536, 1
178, 1536, 97
*NSET, NSET=FINNC, GENERATE
115, 1376, 97
1376, 1438, 1
177, 1438, 97
**
*ELEMENT, TYPE=CPE4
1, 1,2,99,98
5001,5025,5026,26,25
*ELGEN, ELSET=ALLELC
1, 96,1,1, 40,97,96
5001, 48,1,1, 16,5000,48
*ELSET, ELSET=CSURF, GENERATE
1,24,1
5001,5721,48
5721,5768,1
5048,5768,48
73,96,1
**          PLATE SECTION
*NODE
100001,30.0,-1.75
100049,31.5,-1.75
100145,34.5,-1.75
100193,36.0,-1.75
111001,36.0,0.0
110953,34.5,0.0
110857,31.5,0.0
110809,30.0,0.0
*NGEN, NSET=TOPL
110809,110857,1
*NGEN, NSET=TOPM
110857,110953,1
*NGEN, NSET=TOPR
110953,111001,1
*NGEN, NSET=BOTL
100001,100049,1
*NGEN, NSET=BOTM
100049,100145,1
*NGEN, NSET=BOTR
100145,100193,1
*NFILL, NSET=TOTL
BOTL,TOPL,56,193
*NFILL, NSET=TOTM
BOTM, TOPM, 56, 193
*NFILL, NSET=TOTR
BOTR, TOPR, 56, 193
**
**          GLOBAL MODEL NSET
**
*NSET, NSET=SSMDS, GENERATE
100001, 110809, 193
100001, 100193, 1
100193, 111001, 193
**
**          SUB MODEL NSETS
**
*NSET, NSET=FOUTS, GENERATE
110840, 110842, 1
105243, 110840, 193
105243, 105373, 1
105373, 110970, 193
110968, 110970, 1
*NSET, NSET=FMDS, GENERATE

```

```

105437, 110648, 193
105437, 105565, 1
105565, 110776, 193
*NSET, NSET=FINNS, GENERATE
105631, 110649, 193
105631, 105757, 1
105757, 110775, 193
**
*ELEMENT, TYPE=CPE4
100001, 100001,100002,100195,100194
*ELGEN,ELSET=ALLELP
100001,192,1,1, 56,193,192
*ELSET,ELSET=PSURF, GENERATE
110561,110752,1
**
**
** CONTACT CONDITIONS
*SOLID SECTION, ELSET=ALLELP, MATERIAL=AL
8
*SOLID SECTION, ELSET=ALLELC, MATERIAL=STEEL
8
*MATERIAL, NAME=AL
*ELASTIC
70E3, 0.33
*MATERIAL, NAME=STEEL
*ELASTIC
209E3, 0.33
** DEFINING CONTACTS
*SURFACE DEFINITION, NAME=SPLATE
PSURF
*SURFACE DEFINITION, NAME=MCONT
CSURF
*CONTACT PAIR, INTERACTION=CONT, SMALL SLIDING, ADJUST
SPLATE, MCONT
*SURFACE INTERACTION, NAME=CONT
8
*SURFACE BEHAVIOR
0
*FRICTION,LAGRANGE
1.5
*NORMAL, TYPE = CONTACT SURFACE
MCONT, 80025, 0.0, -1.0, 0.0
*NORMAL, TYPE = CONTACT SURFACE
MCONT, 80073, 0.0,-1.0, 0.0
** SUBMODEL BOUNDARY CONDITIONS
*SUBMODEL
SSMDC
SSMDS
**
** APPLYING NORMAL LOAD
*STEP,NLGEOM,INC=20
*STATIC
0.1,1.0
*BOUNDARY, SUBMODEL, STEP=1
SSMDC, 1,2
SSMDS, 1,2
*EL PRINT, FREQUENCY=0
*NODE PRINT, FREQUENCY=0
*CONTACT PRINT, NSET=TOPM
*CONTACT FILE
*NODE FILE, NSET=FOUTC
U
*NODE FILE, NSET=FMDC
U

```

```
*NODE FILE, NSET=FINNC
U
*NODE FILE, NSET=FOUTS
U
*NODE FILE, NSET=FMDS
U
*NODE FILE, NSET=FINNS
U
*END STEP
** APPLYING AXIAL LOAD
*STEP,NLGEOM,INC=40
*STATIC,DIRECT
0.025,1.0
*BOUNDARY, SUBMODEL, STEP=2
SSMDC, 1,2
SSMDS, 1,2
*EL FILE
*CONTACT PRINT, NSET=TOPM
*CONTACT FILE
*NODE FILE, NSET=FOUTC
U
*NODE FILE, NSET=FMDC
U
*NODE FILE, NSET=FINNC
U
*NODE FILE, NSET=FOUTS
U
*NODE FILE, NSET=FMDS
U
*NODE FILE, NSET=FINNS
U
*END STEP
```

Fourth Sub Model

```
*HEADING
HALLAM MODEL 801 FINAL SUB MODEL
*PREPRINT, HISTORY=NO, ECHO=NO, MODEL=NO
*RESTART,WRITE,FREQ=10
**
**           CONTACT SECTION
**
*NODE
1, 31.0, 1.0
17, 31.5,1.0
113, 34.5,1.0
129, 35, 1.0
160017,31.5,0.0
160113,34.5,0.0
4257, 35.0, 2.0
4241, 34.5, 2.0
4145, 31.5, 2.0
4129, 31.0, 2.0
*NGEN, NSET=CONTOPL
4129,4145,1
*NGEN, NSET=CONTOPM
4145,4241,1
*NGEN, NSET=CONTOPR
4241,4257,1
*NGEN, NSET=CONBOTL
1,17,1
*NGEN, NSET=CONBOTM
17,113,1
*NGEN, NSET=CONBOTR
113,129,1
*NGEN, NSET=CENDSUF
160017,160113,1
*NFILL, NSET=CONTOTL
CONBOTL,CONTOPL,32,129
*NFILL, NSET=CONTOTM
CONBOTM,CONTOPM,32,129
*NFILL, NSET=CONTOTR
CONBOTR,CONTOPR,32,129
*NFILL, NSET=CTOTSUF
CONBOTM,CENDSUF,32,5000
**
**
**           GLOBAL MODEL NSETS
**
*NSET, NSET=FMDC, GENERATE
1, 4129, 129
4129, 4257, 1
129, 4257,129
**
*ELEMENT, TYPE=CPE4
1, 1,2,131,130
5001,5017,5018,18,17
*ELGEN, ELSET=ALLELC
1, 128,1,1, 32,129,128
5001, 96,1,1, 32,5000,96
*ELSET, ELSET=CSURF, GENERATE
1,16,1
5001,7977,96
7977,8072,1
5096,8072,96
113,128,1
```

**
** PLATE SECTION
**

*NODE
200001,31.0,-0.875
200033,31.5,-0.875
200225,34.5,-0.875
200257,35.0,-0.875
214649,35.0,0.0
214617,34.5,0.0
214425,31.5,0.0
214393,31.0,0.0
*NGEN, NSET=TOPL
214393,214425,1
*NGEN, NSET=TOPM
214425,214617,1
*NGEN, NSET=TOPR
214617,214649,1
*NGEN, NSET=BOTL
200001,200033,1
*NGEN, NSET=BOTM
200033,200225,1
*NGEN, NSET=BOTR
200225,200257,1
*NFILL, NSET=TOTL
BOTL,TOPL,56,257
*NFILL, NSET=TOTM
BOTM, TOPM, 56, 257
*NFILL, NSET=TOTR
BOTR, TOPR, 56, 257

**
** GLOBAL MODEL NSET
**

*NSET,NSET=FMDS, GENERATE
200001, 214393, 257
200001, 200257, 1
200257, 214649, 257
**
*ELEMENT, TYPE=CPE4
200001, 200001,200002,200259,200258
*ELGEN,ELSET=ALLELP
200001,256,1,1, 56,257,256
*ELSET,ELSET=PSURF, GENERATE
214080,214336,1
**

** SUB SURFACE STRESS ELEMENTS SETS
**

*ELSET,ELSET=SUBSURF, GENERATE
214110,214307,1
213854,214051,1
213598,213795,1
213342,213539,1
213086,213283,1
212830,213027,1
212574,212771,1
212318,212515,1
212062,212259,1
211806,212003,1
211550,211747,1
211294,221491,1
211038,211235,1
210782,210979,1
210526,210723,1
210270,210467,1

```

210014,210211,1
209758,209955,1
209502,209699,1
209246,209443,1
208990,209187,1
208734,208931,1
208478,208675,1
208222,208419,1
207966,208163,1
207710,207907,1
207454,207651,1
207198,207395,1
206942,207139,1
206686,206883,1
206430,206627,1
206174,206371,1
**
**           CONTACT CONDITIONS
**
**SOLID SECTION, ELSET=ALLELP, MATERIAL=AL
8
**SOLID SECTION, ELSET=ALLELC, MATERIAL=STEEL
8
**MATERIAL, NAME=AL
**ELASTIC
70E3, 0.33
**MATERIAL, NAME=STEEL
**ELASTIC
209E3, 0.33
** DEFINING CONTACTS
**SURFACE DEFINITION, NAME=SPLATE
PSURF
**SURFACE DEFINITION, NAME=MCONT
CSURF
**CONTACT PAIR, INTERACTION=CONT, SMALL SLIDING, ADJUST
SPLATE, MCONT
**SURFACE INTERACTION, NAME=CONT
8
**SURFACE BEHAVIOR
0
**FRICTION,LAGRANGE
1.5
**NORMAL, TYPE = CONTACT SURFACE
MCONT, 160017, 0.0, -1.0, 0.0
**NORMAL, TYPE = CONTACT SURFACE
MCONT, 160113, 0.0,-1.0, 0.0
**
**           SUBMODEL BOUNDARY CONDITIONS
**
**SUBMODEL
FMDC
FMDS
**
**           APPLYING NORMAL LOAD
**
**STEP,NLGEOM,INC=20
**STATIC
0.1,1.0
**BOUNDARY, SUBMODEL, STEP=1
FMDC, 1,2
FMDS, 1,2
**EL PRINT, FREQUENCY=0
**NODE PRINT, FREQUENCY=0
**CONTACT PRINT, NSET=TOPM

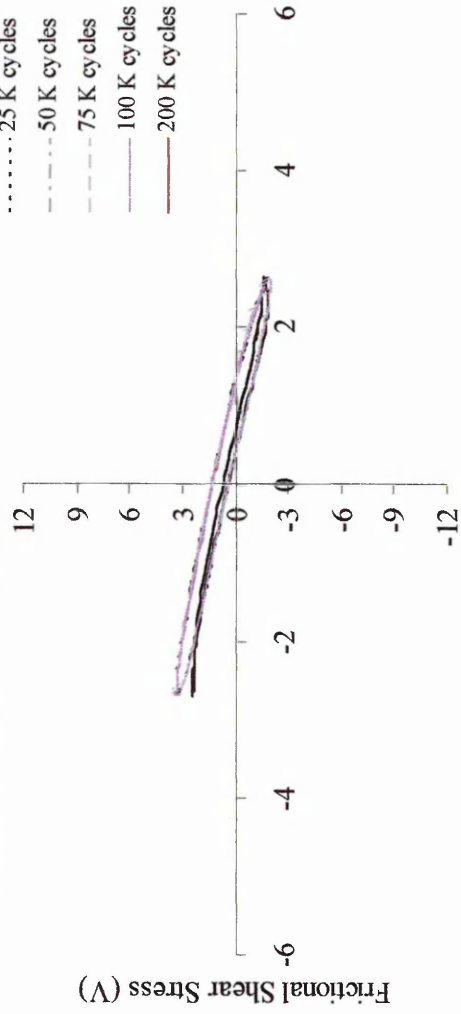
```

```
*CONTACT FILE
*END STEP
**
**           APPLYING AXIAL LOAD
**
*STEP,NLGEOM,INC=40
*STATIC,DIRECT
0.025,1.0
*BOUNDARY, SUBMODEL, STEP=2
FMDC, 1,2
FMDS, 1,2
*EL PRINT, FREQUENCY=10,ELSET=SUBSURF
S11
S12
*EL FILE
*CONTACT PRINT, NSET=TOPM
*CONTACT FILE
*END STEP
```

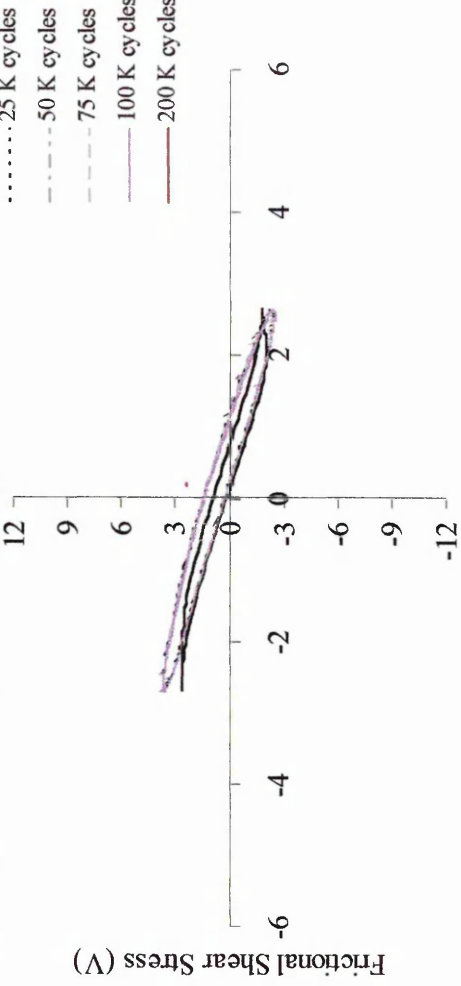
APPENDIX C

EXPERIMENTAL FRICTION HYSTERESIS LOOPS

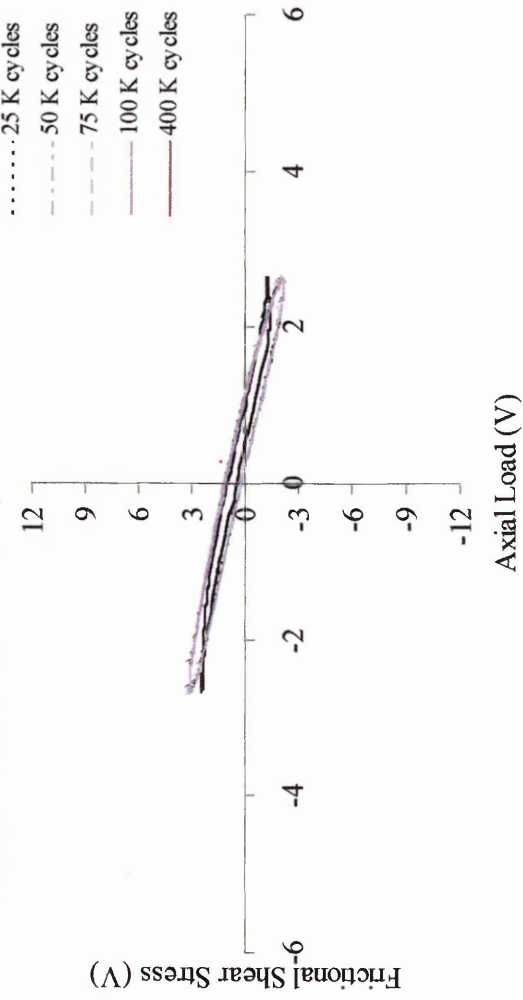
Test 501(LHS at 20% of Estimated Life)



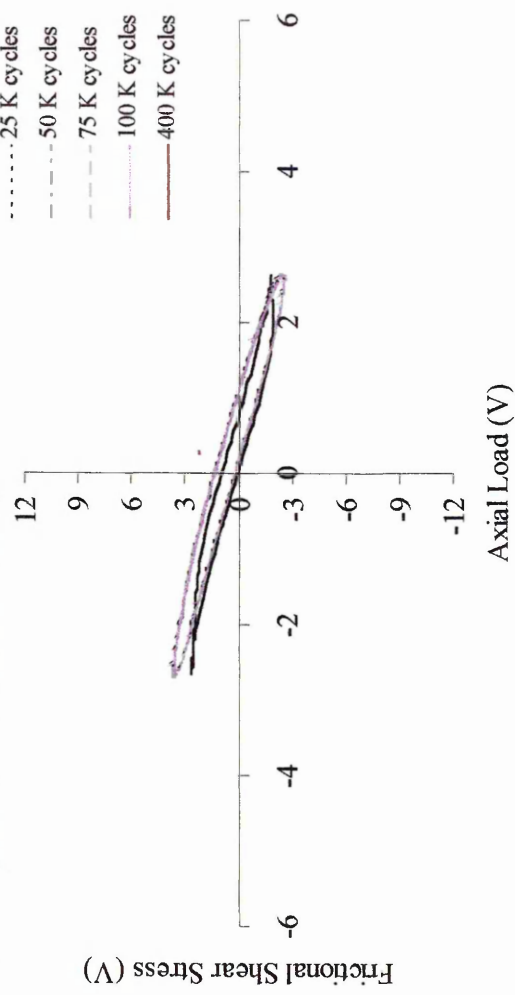
Test 501(RHS at 20% of Estimated Life)

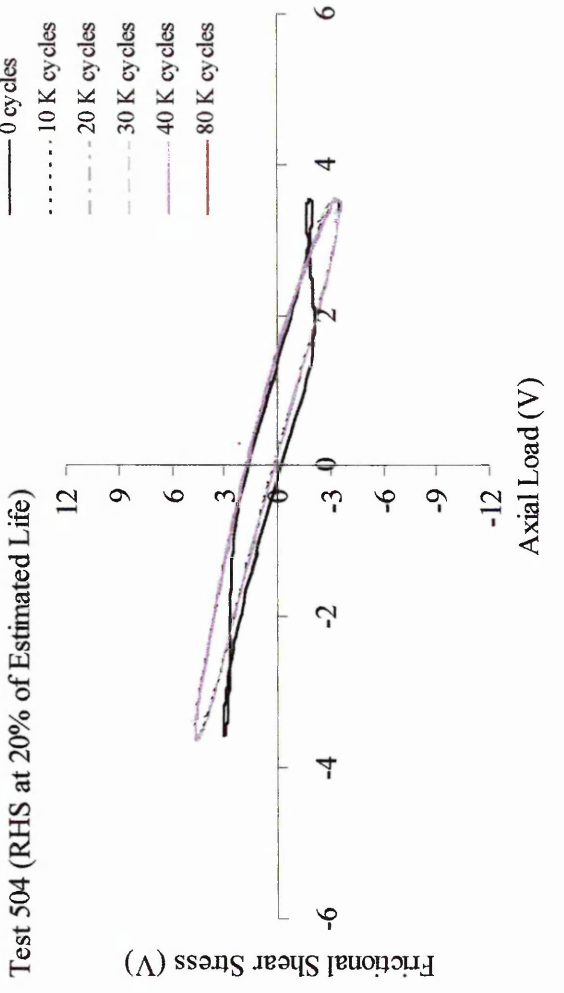
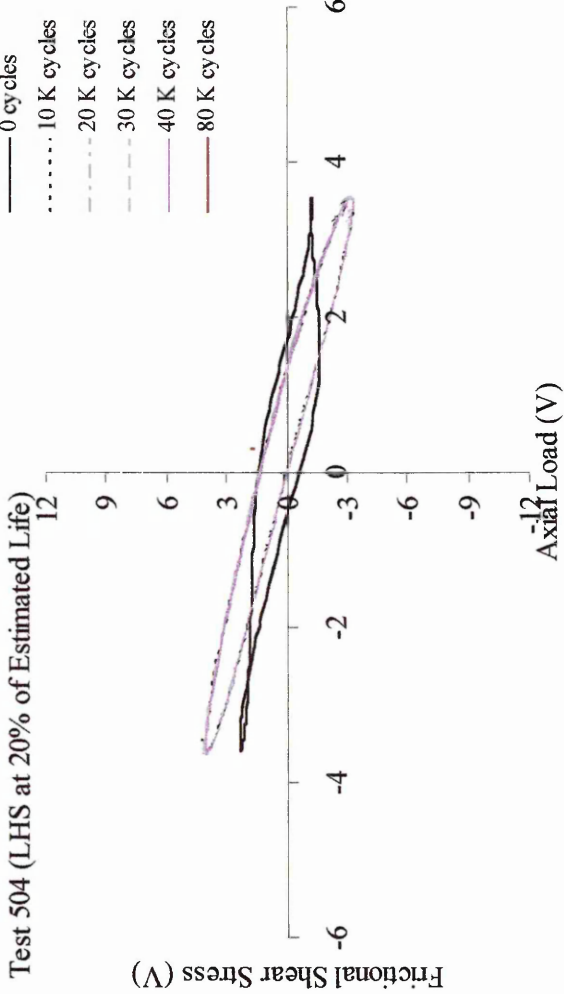
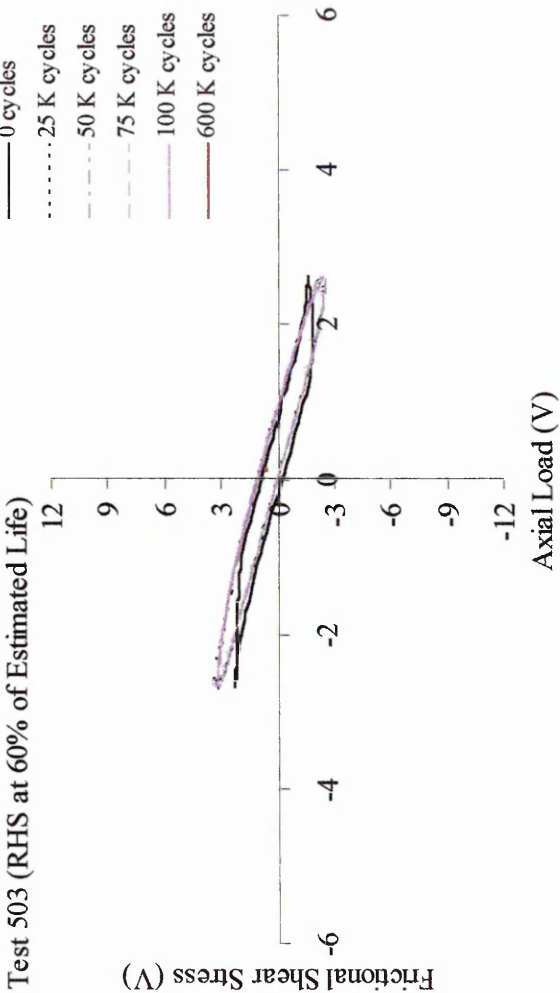
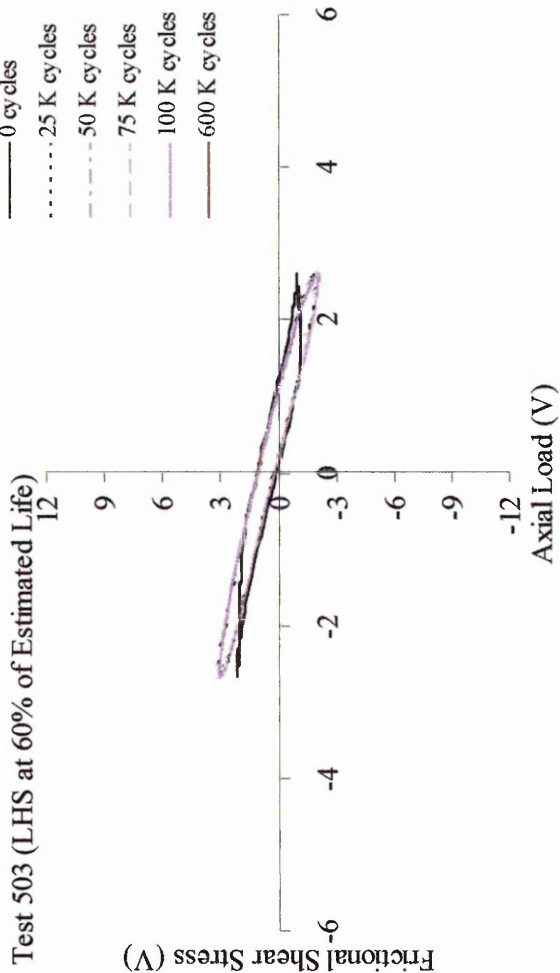


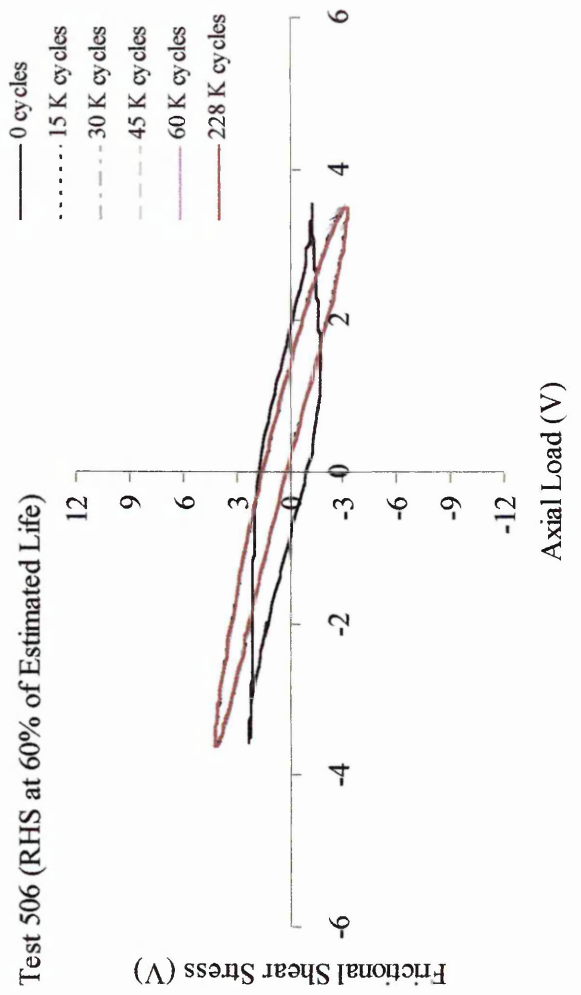
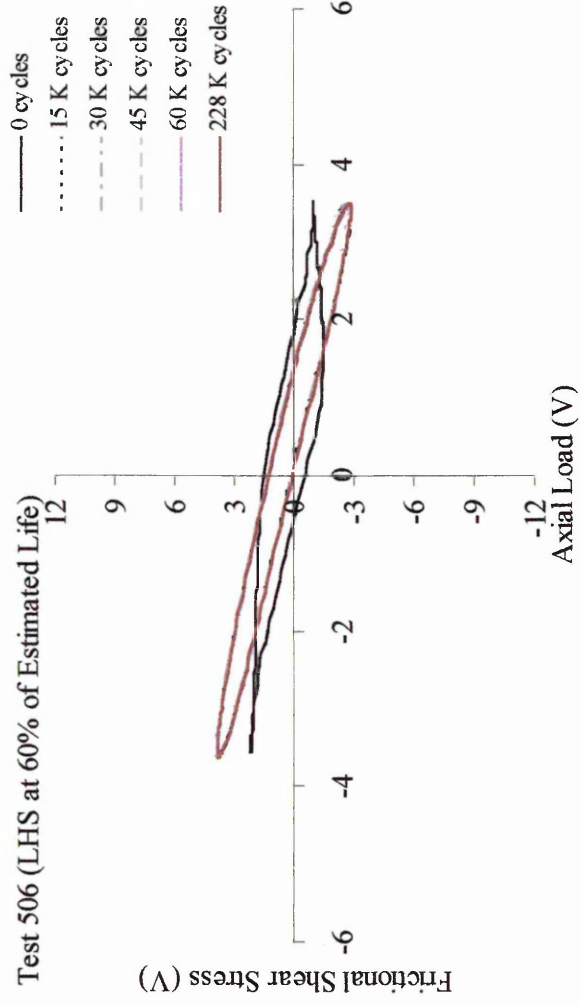
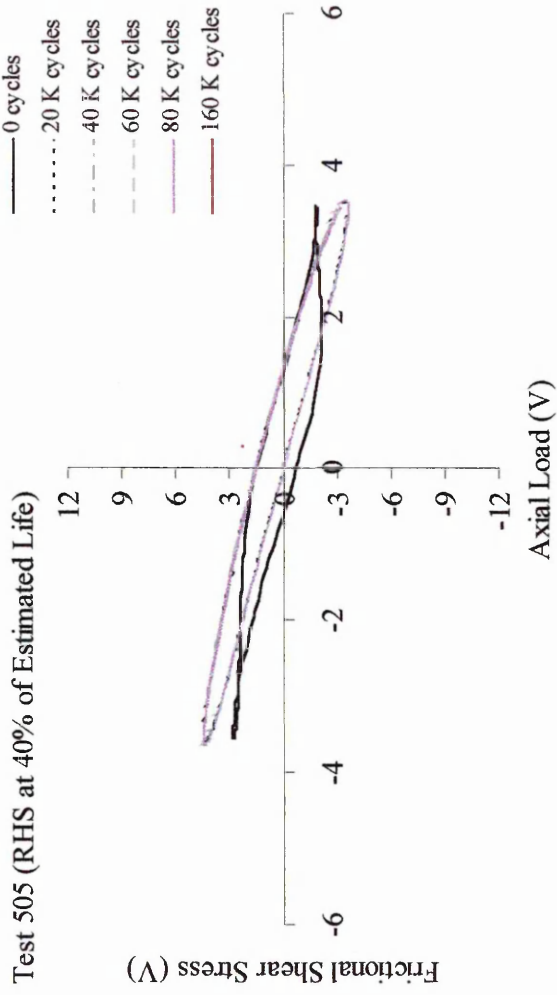
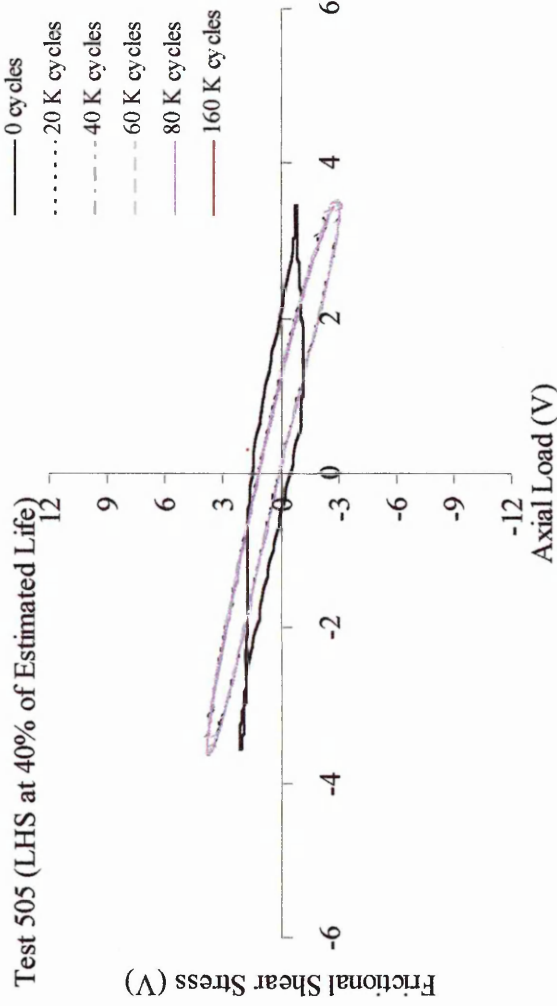
Test 502 (LHS at 40% of Estimated Life)

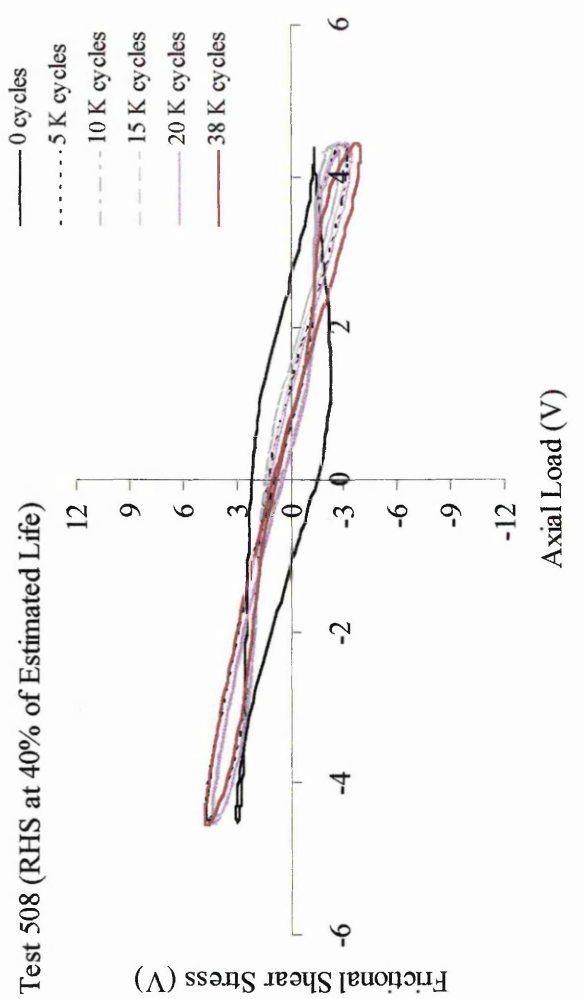
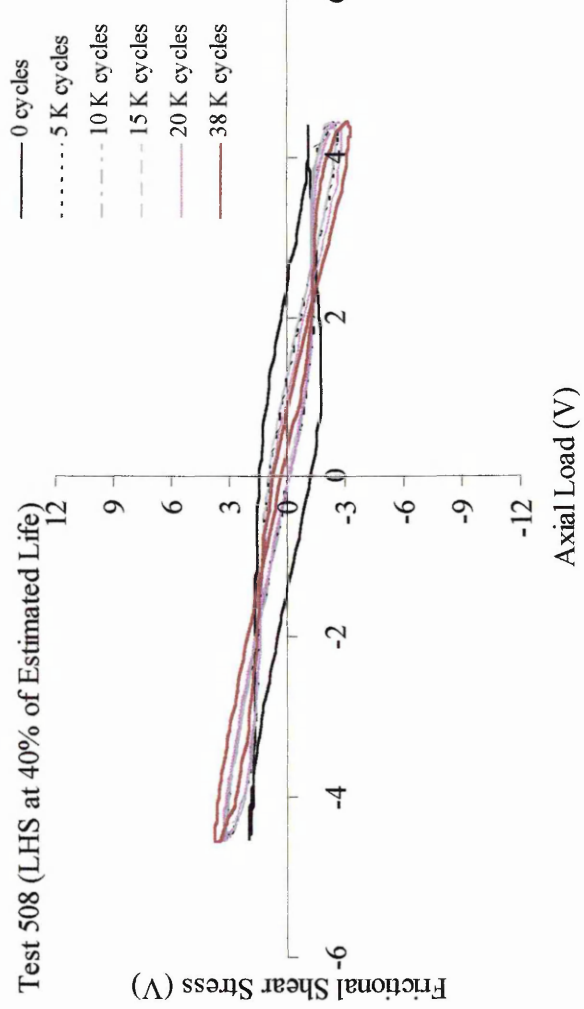
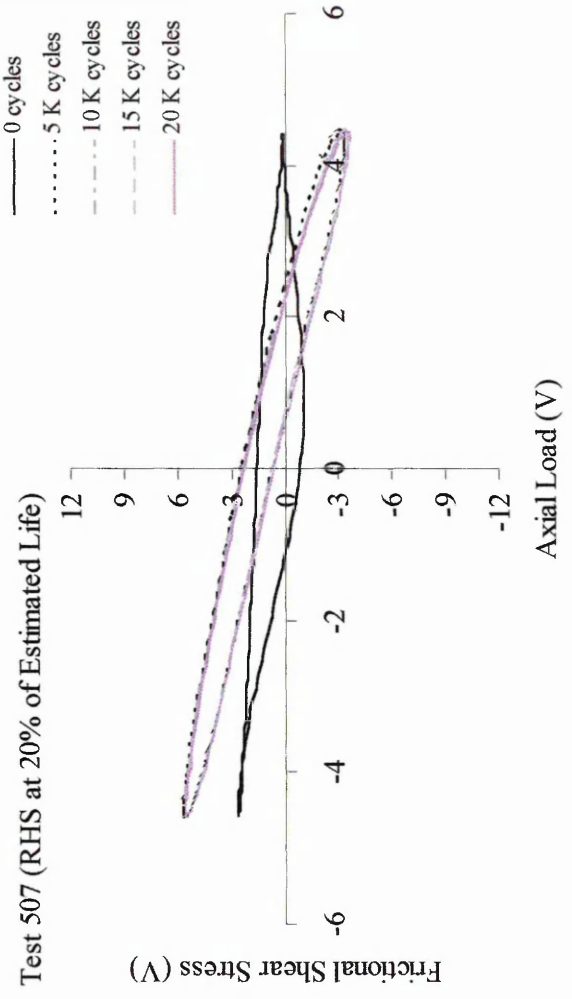
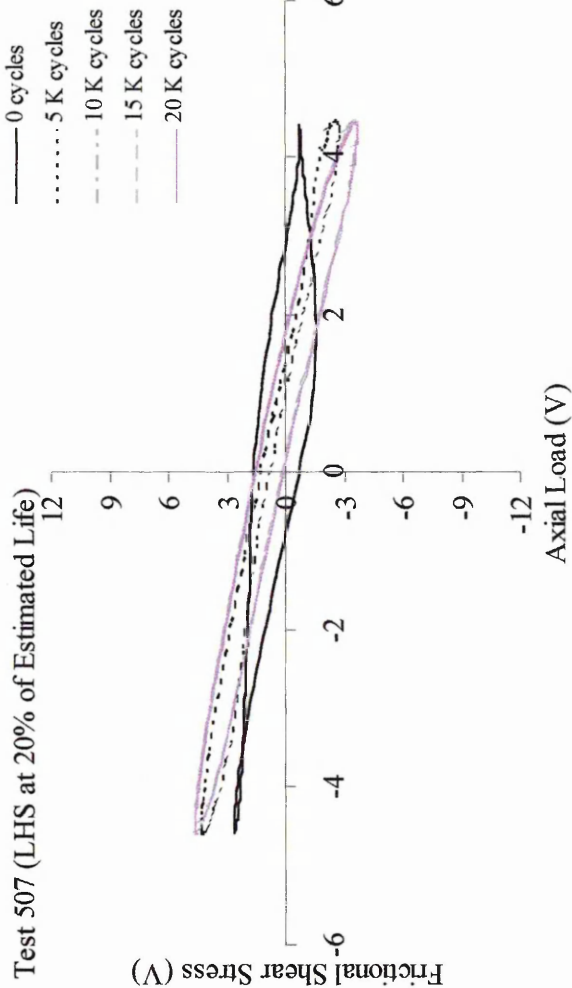


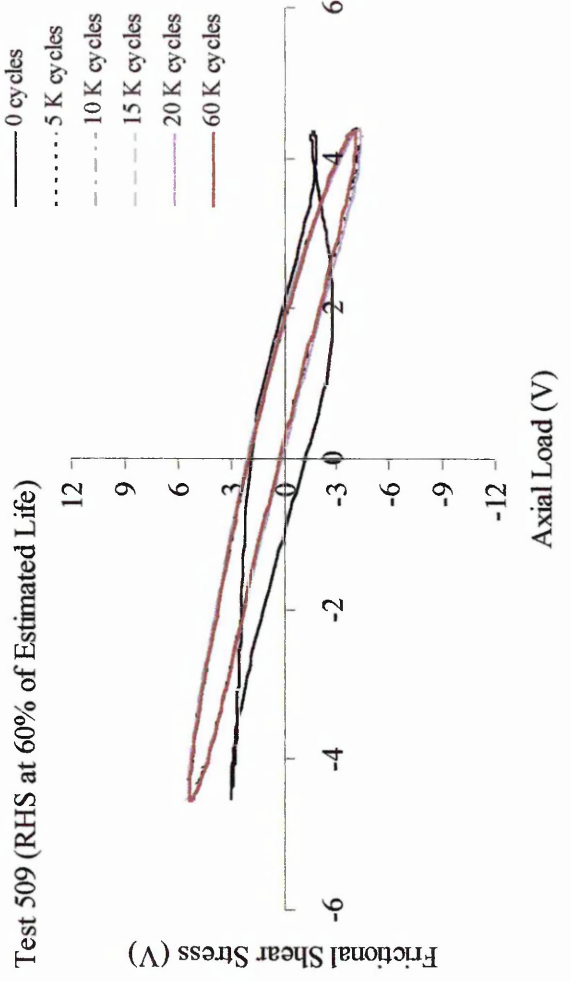
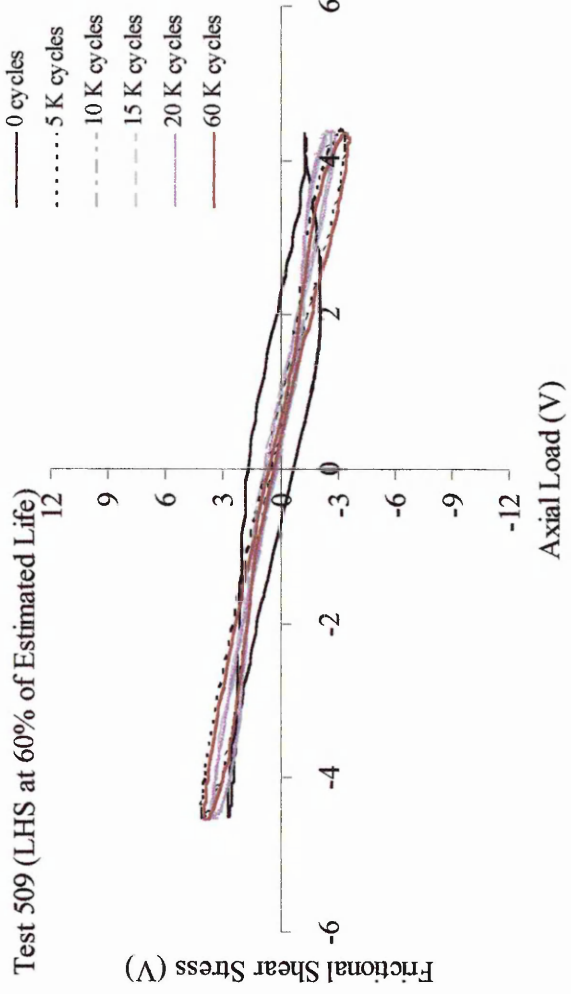
Test 502 (RHS at 40% of Estimated Life)

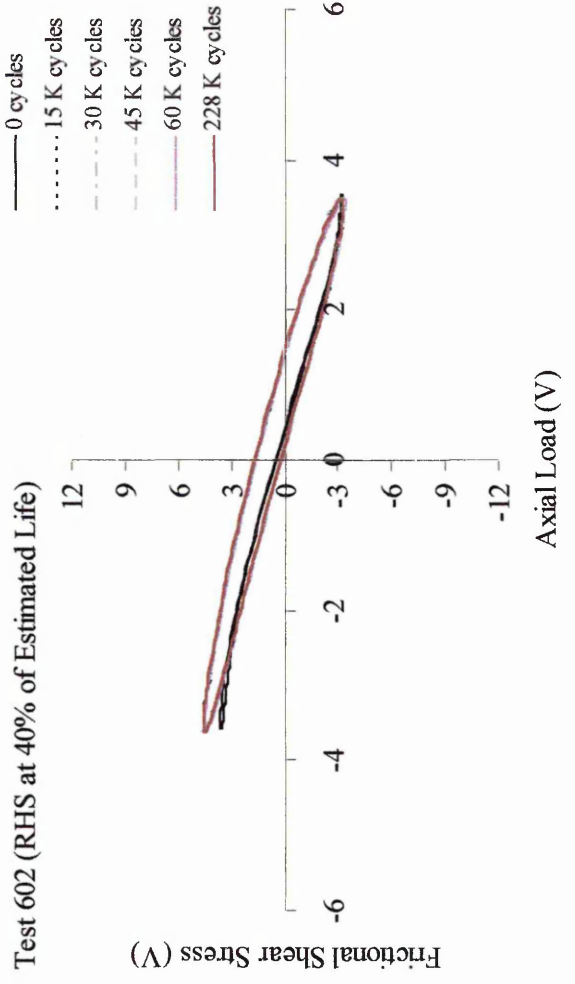
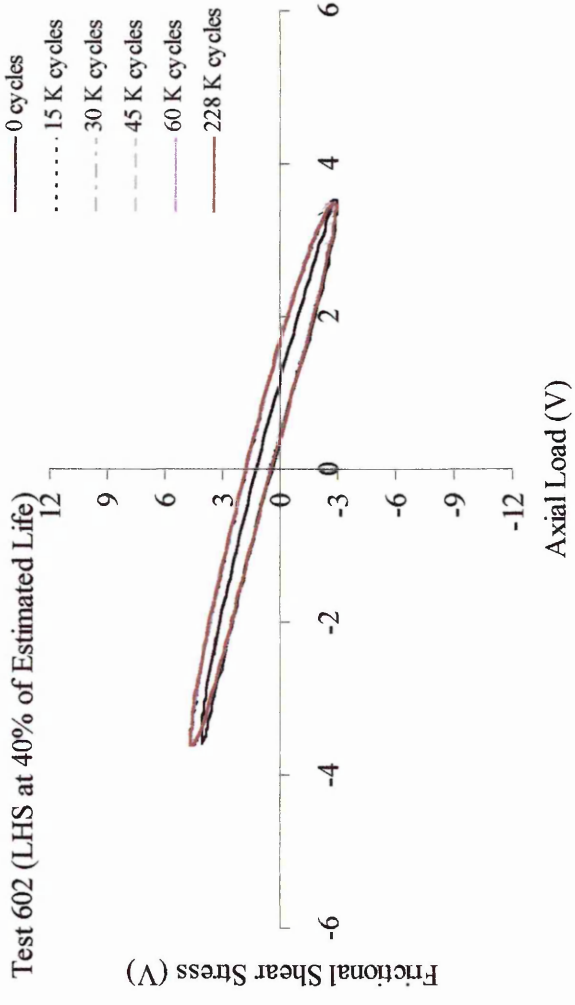
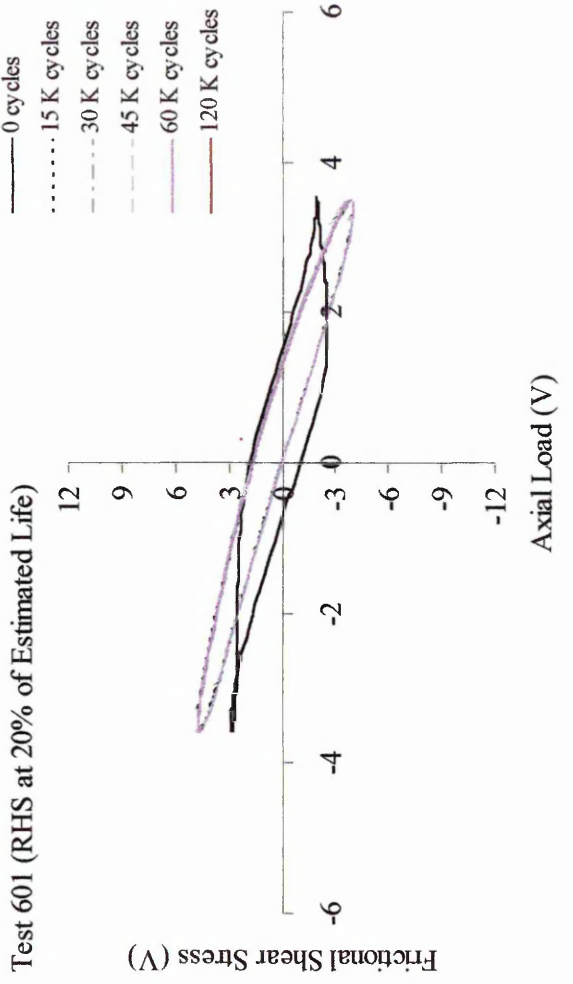
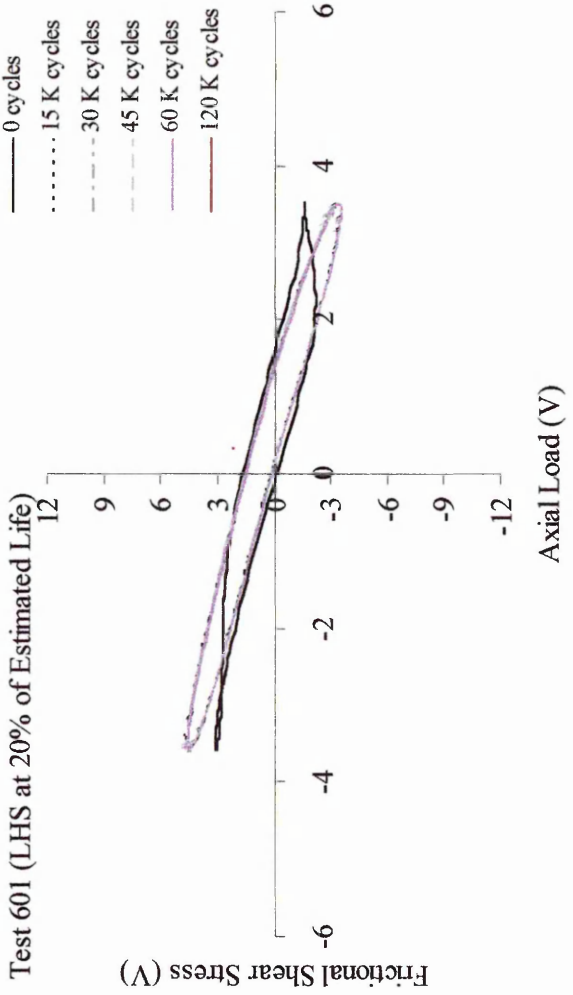


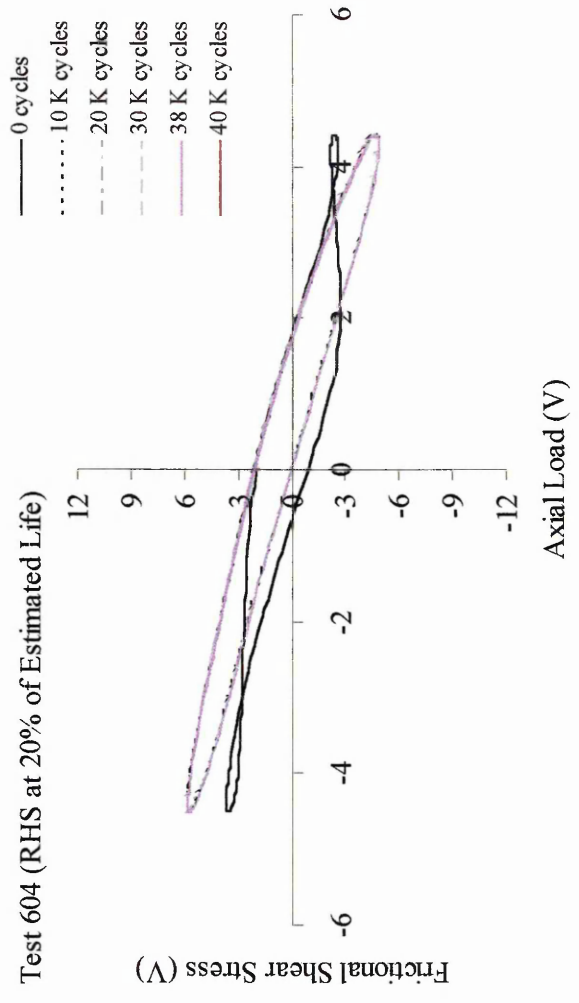
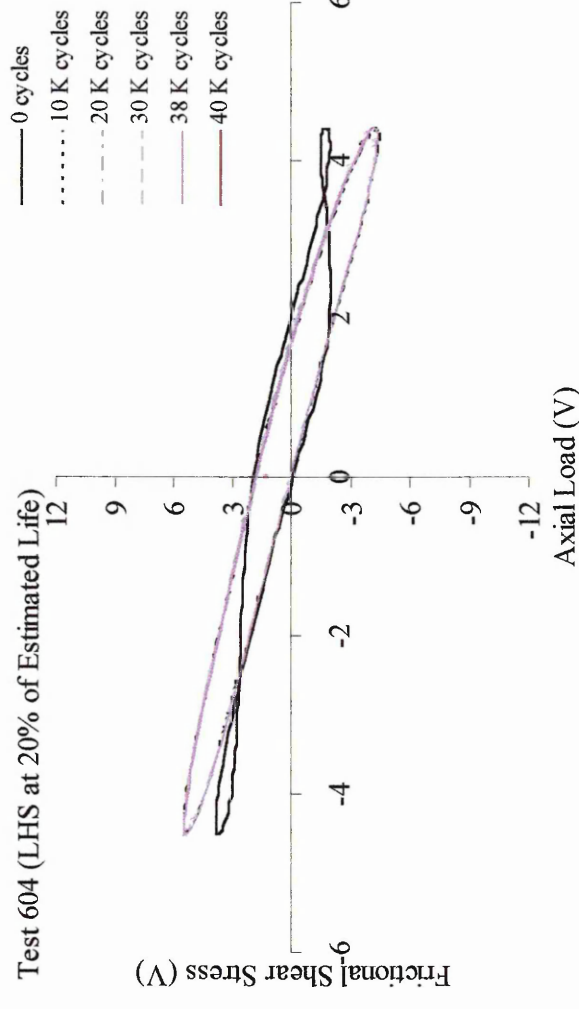
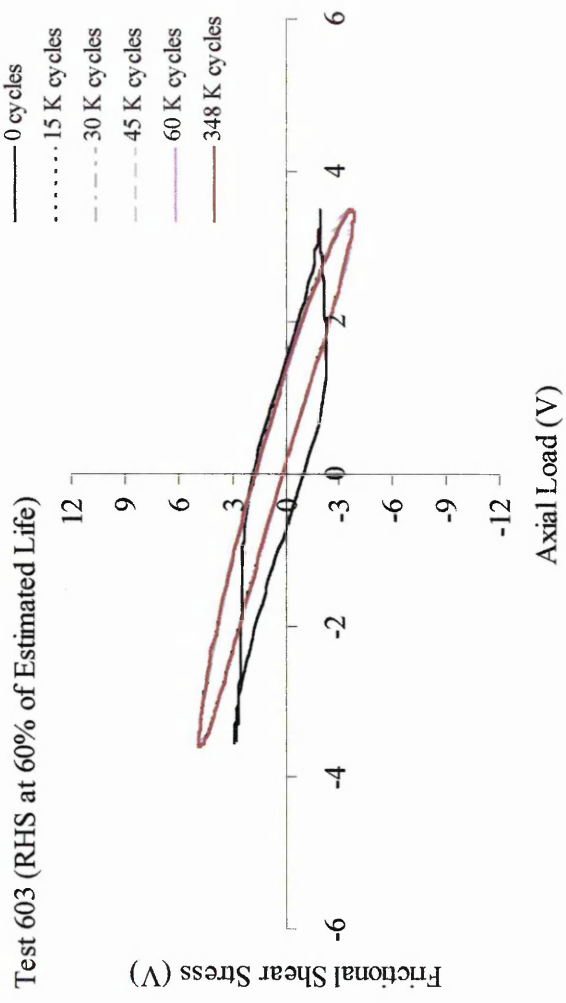
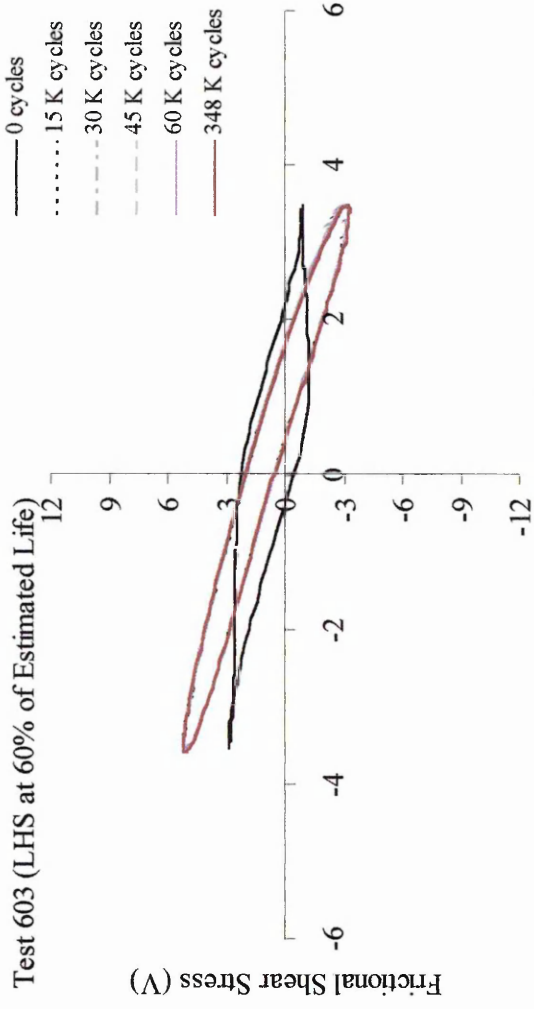


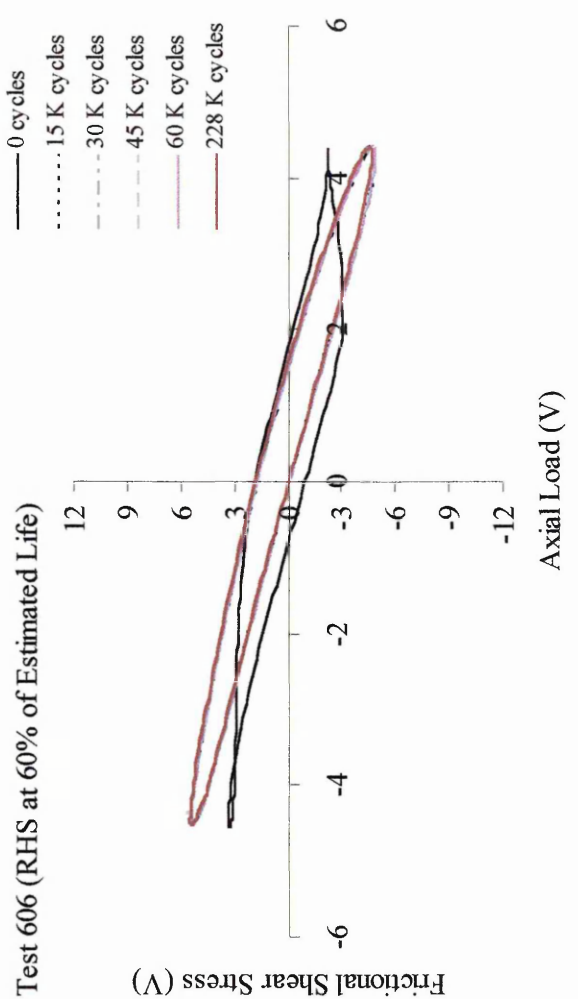
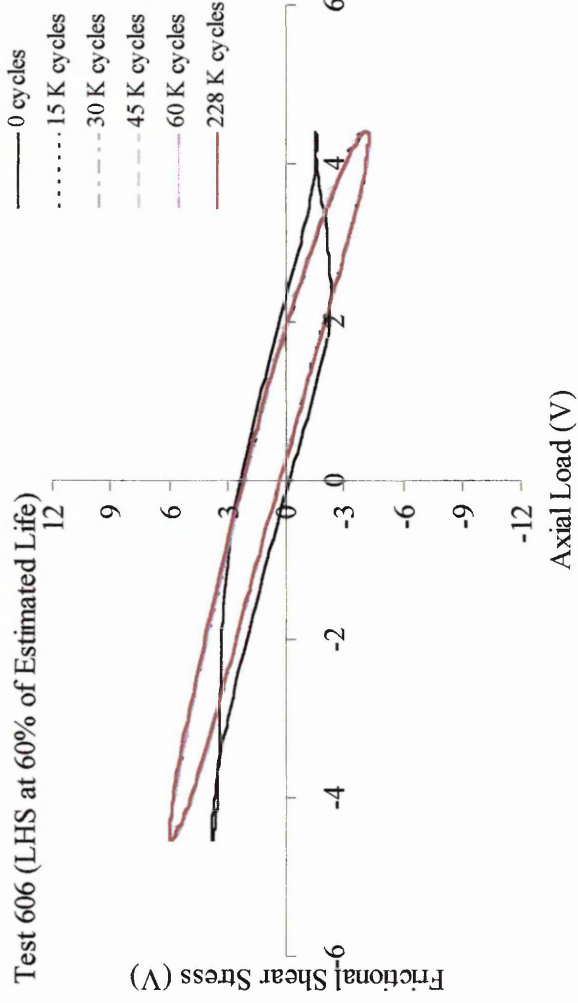
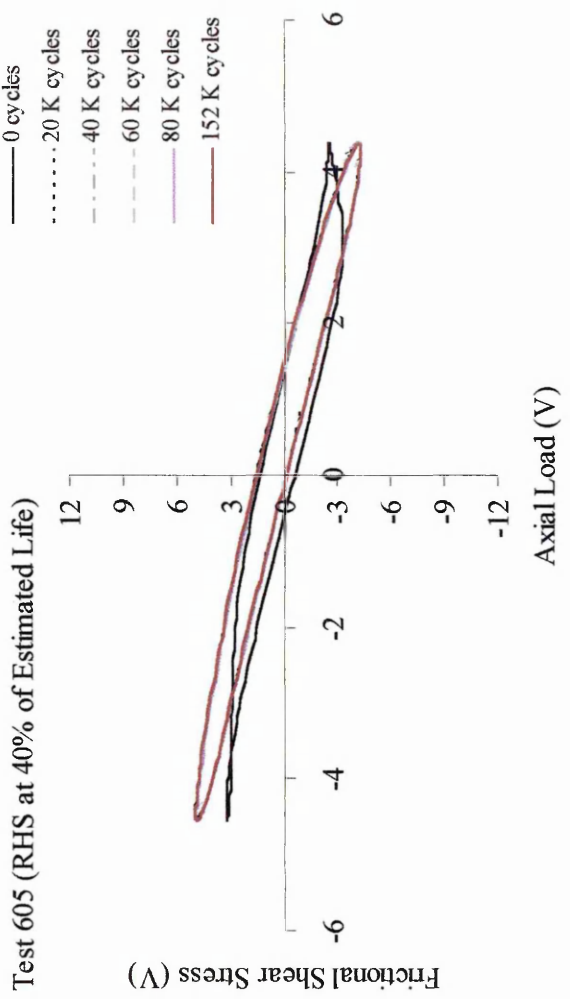
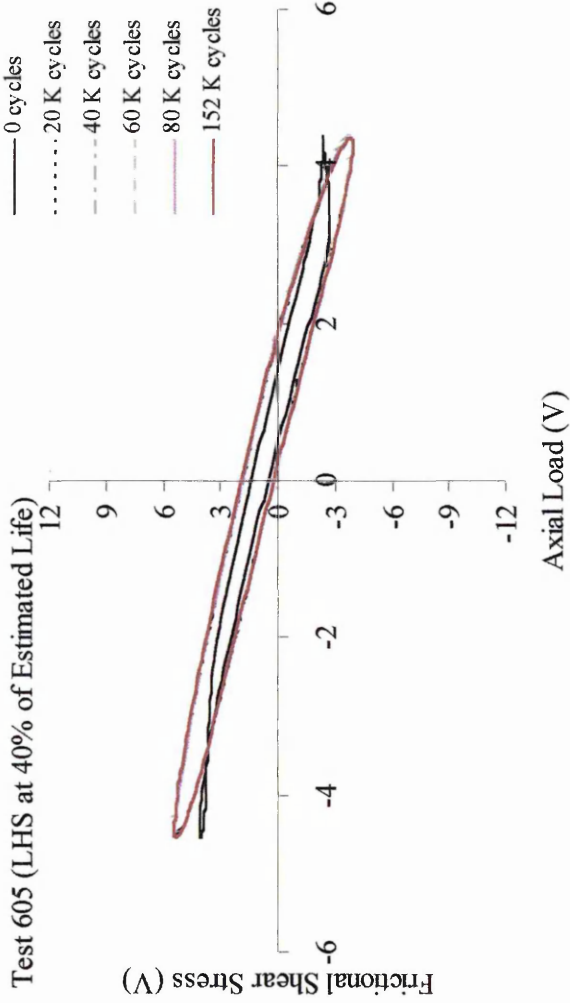


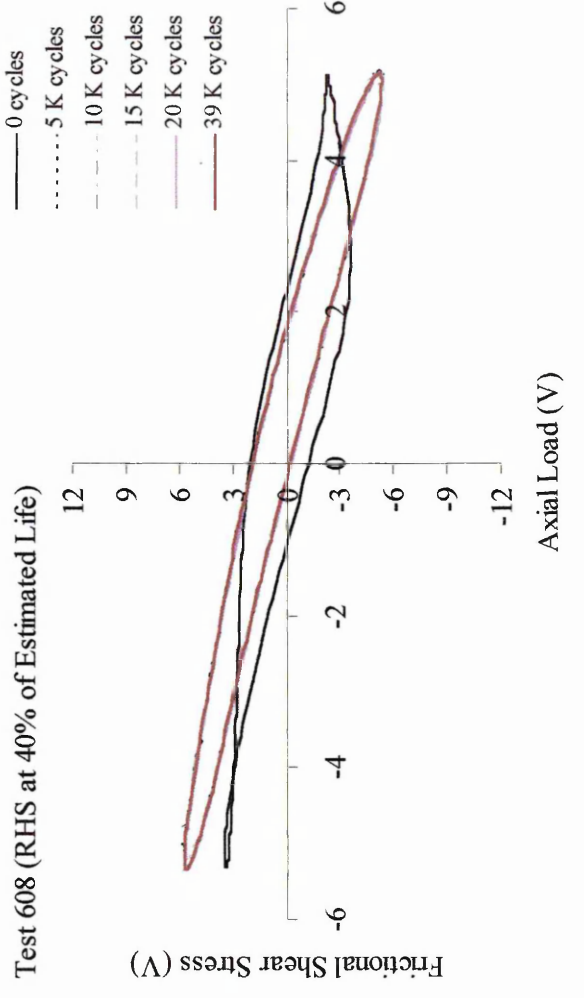
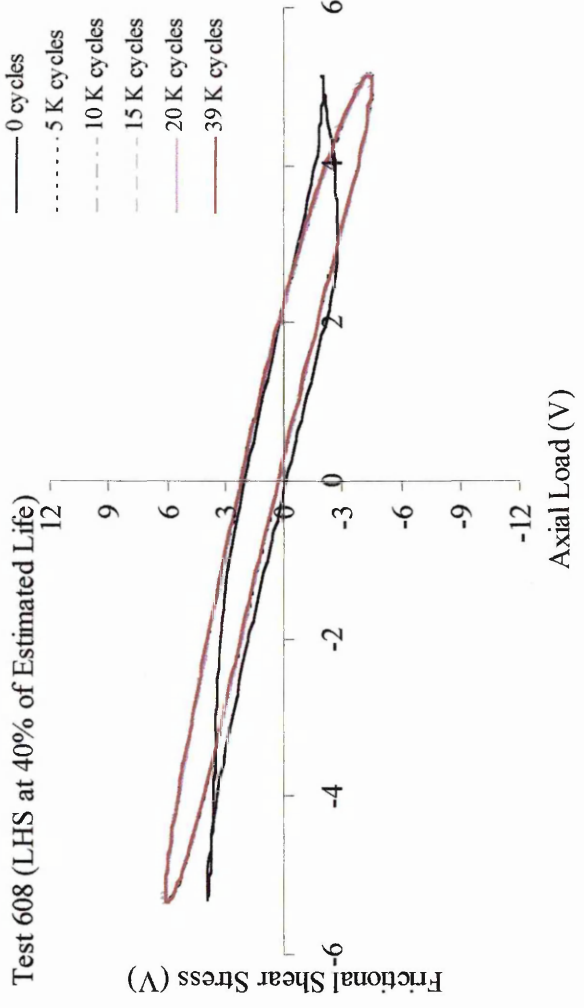
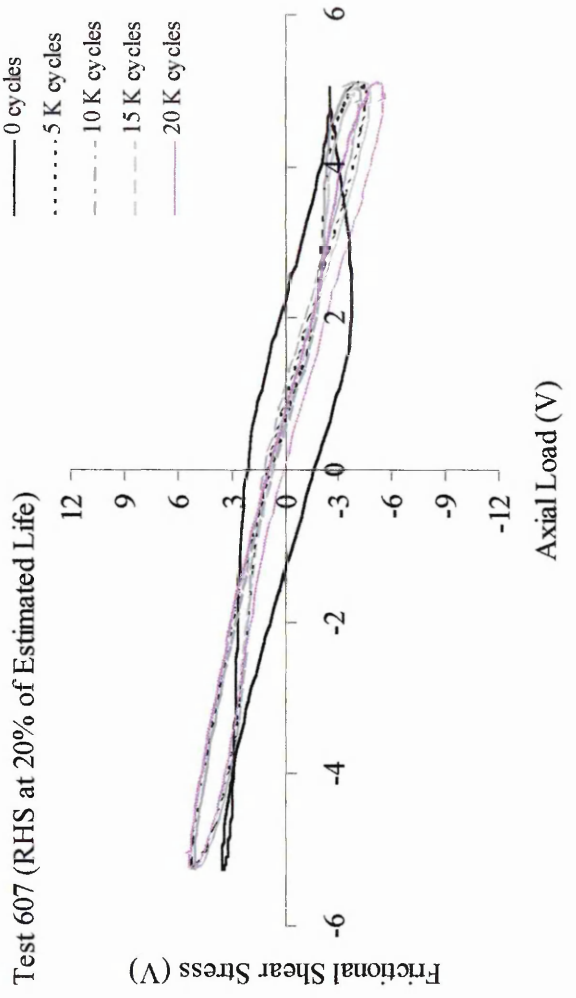
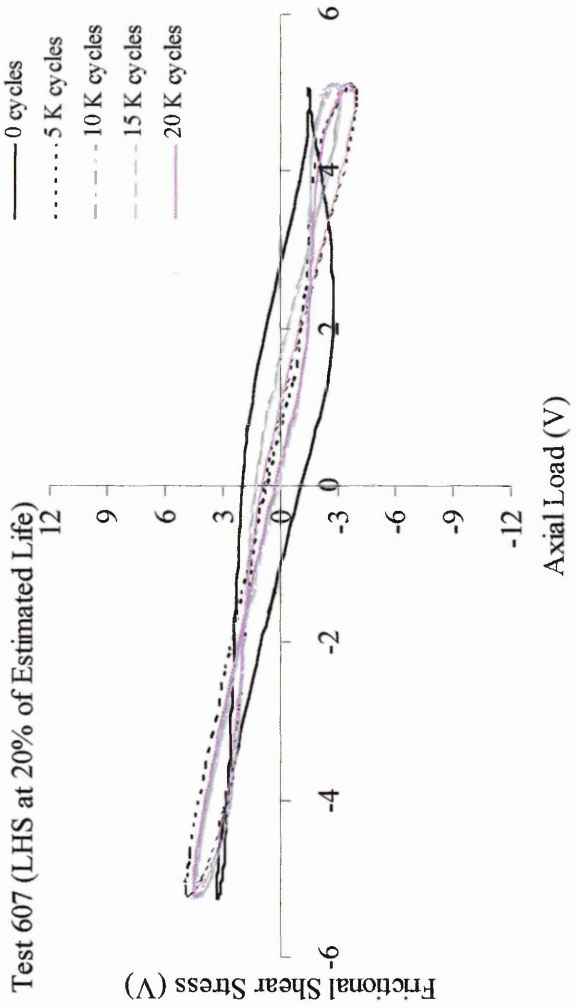


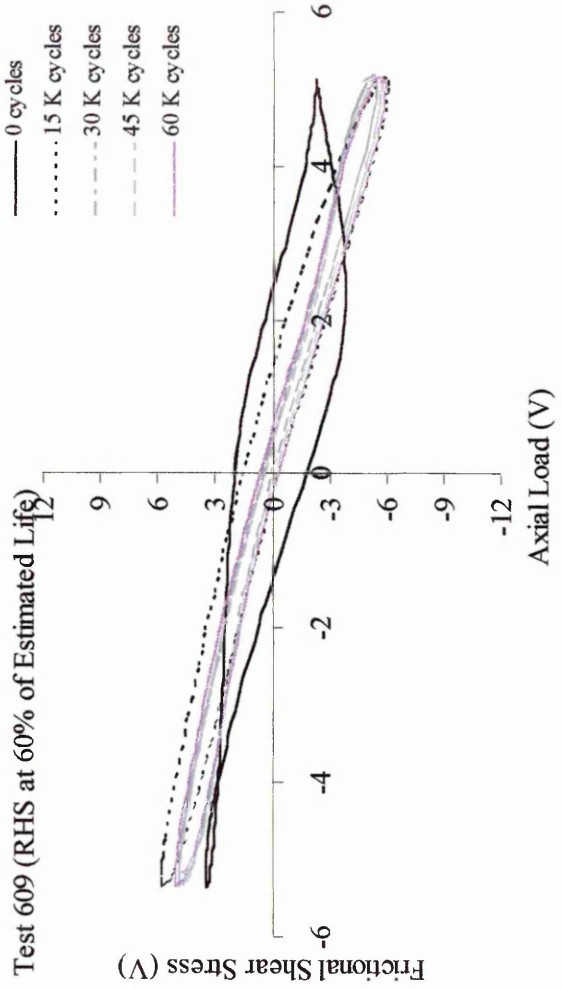
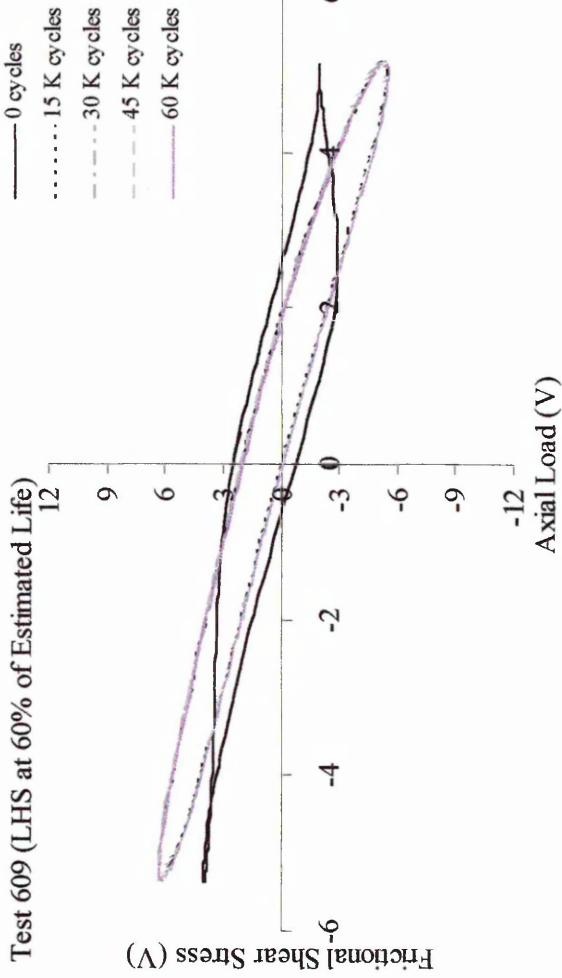


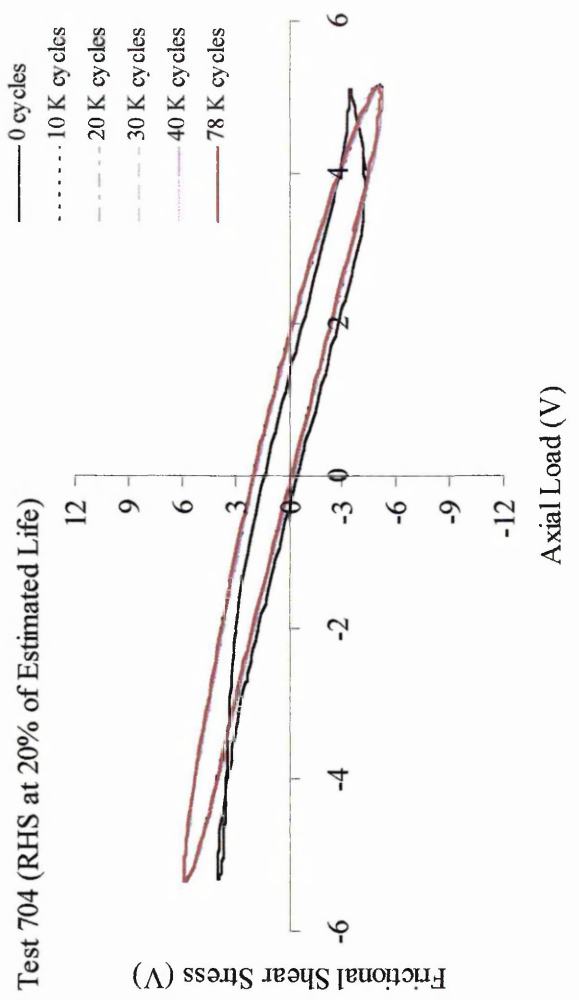
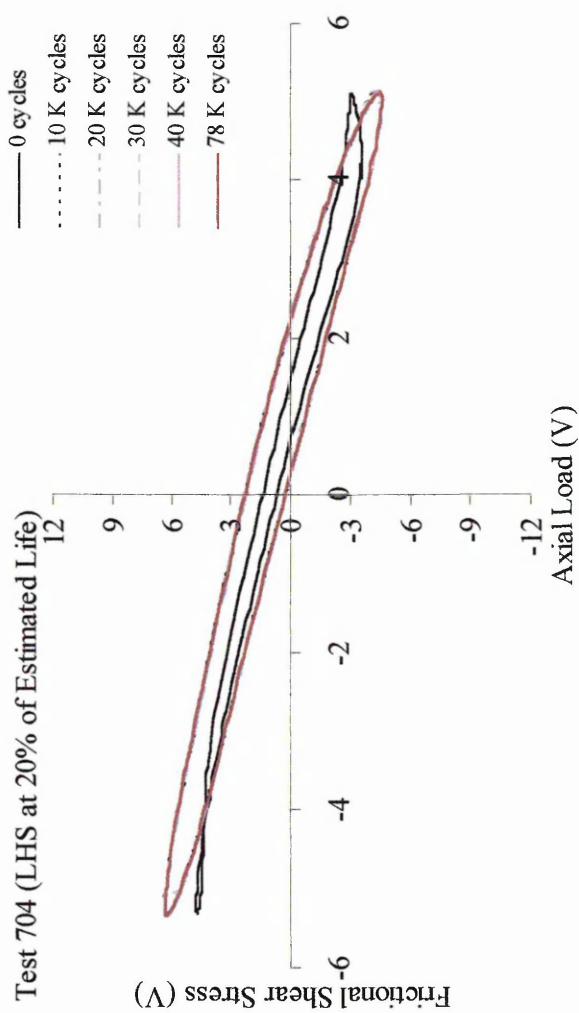
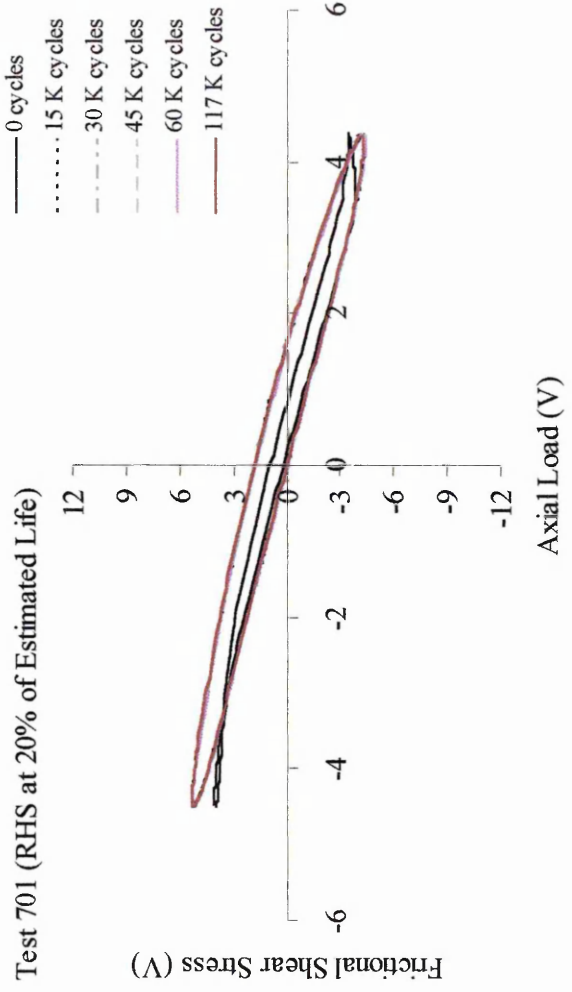
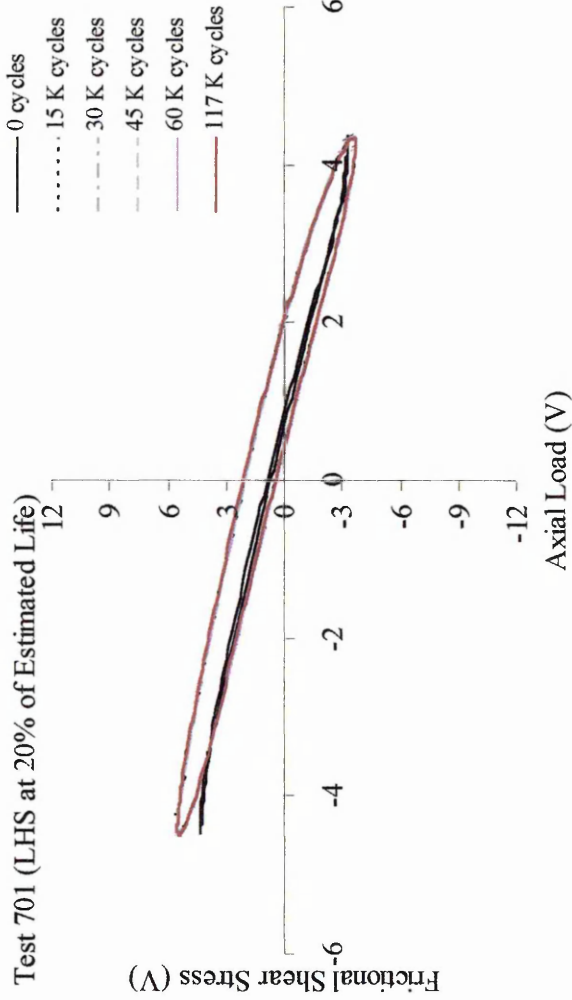


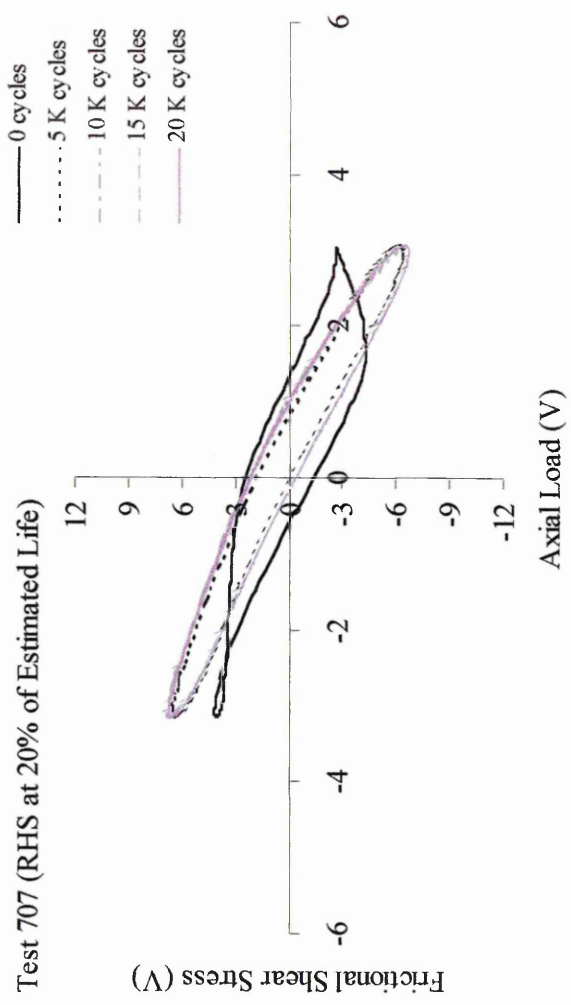
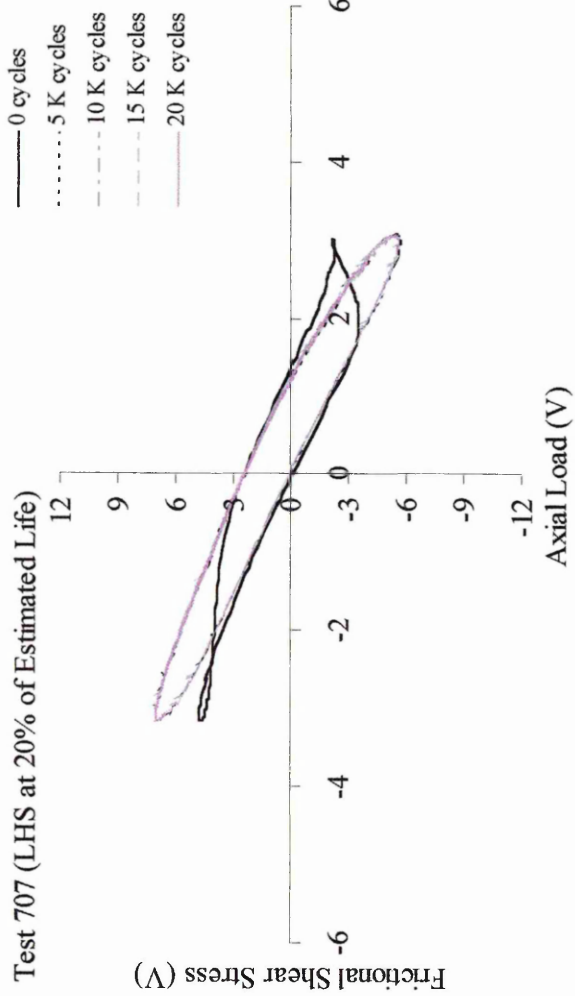




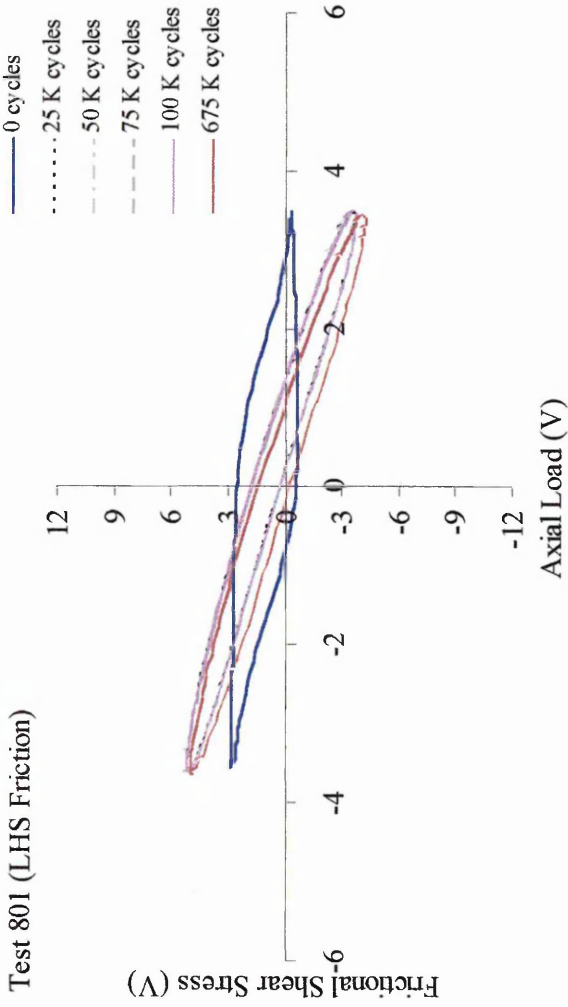




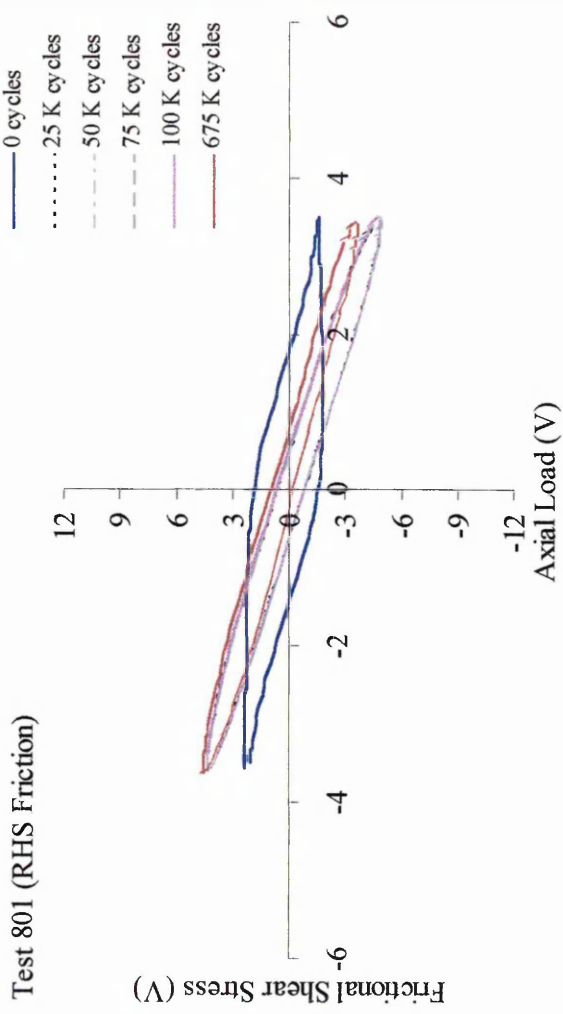




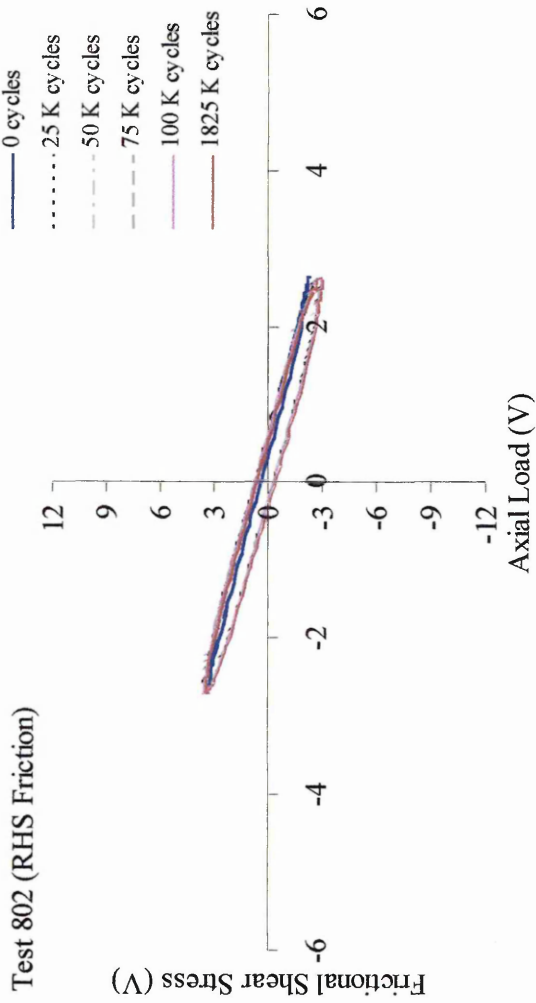
Test 801 (LHS Friction)



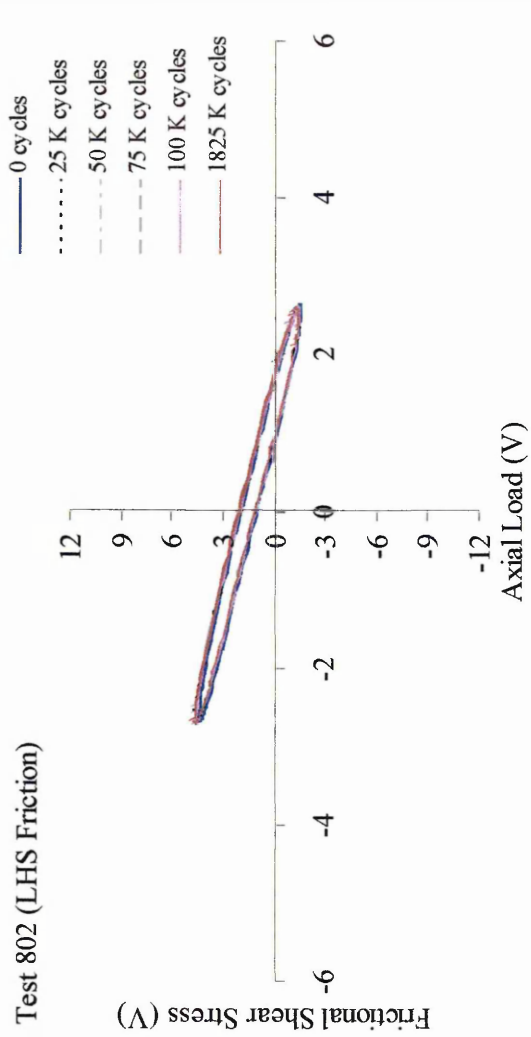
Test 801 (RHS Friction)



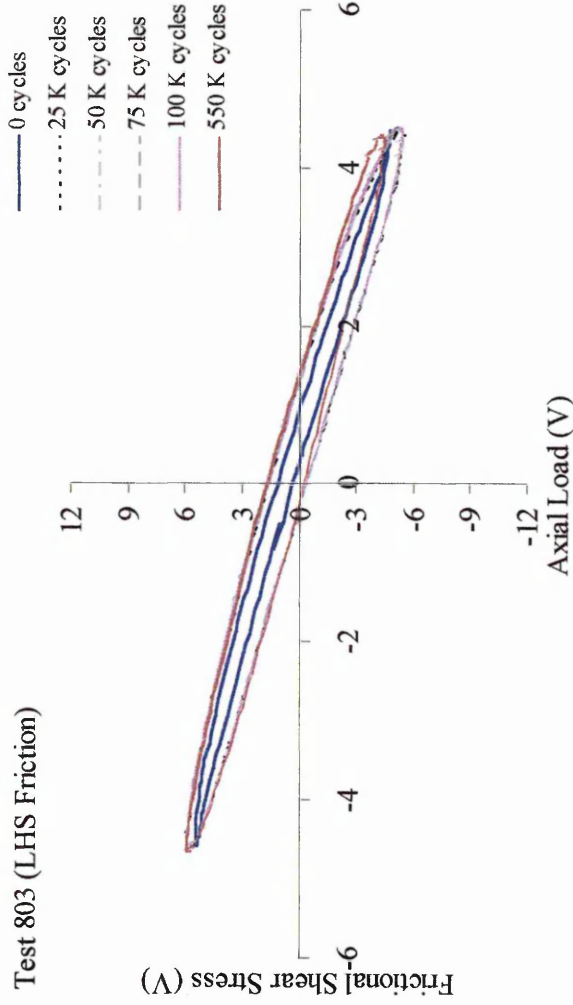
Test 802 (RHS Friction)



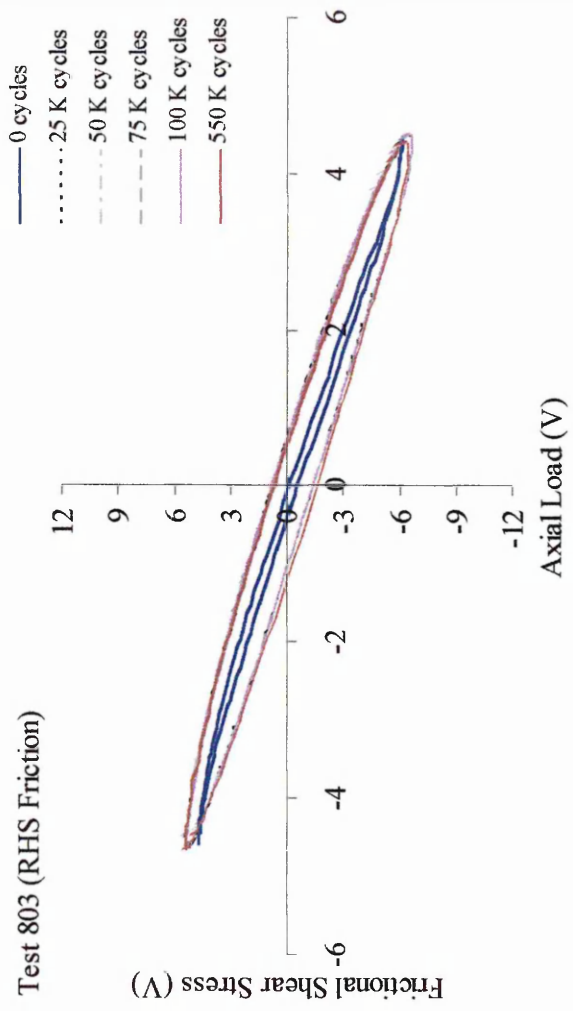
Test 802 (LHS Friction)



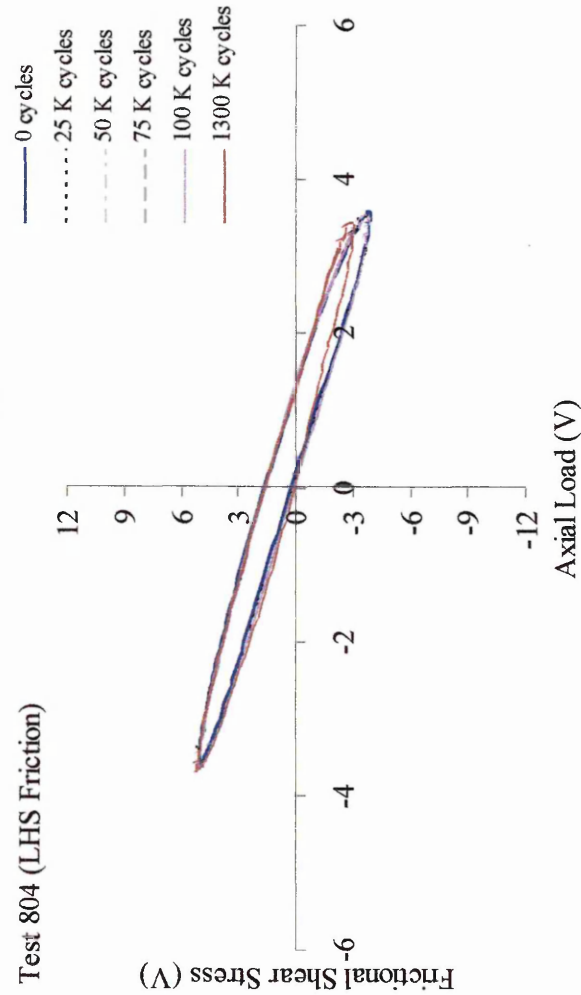
Test 803 (LHS Friction)



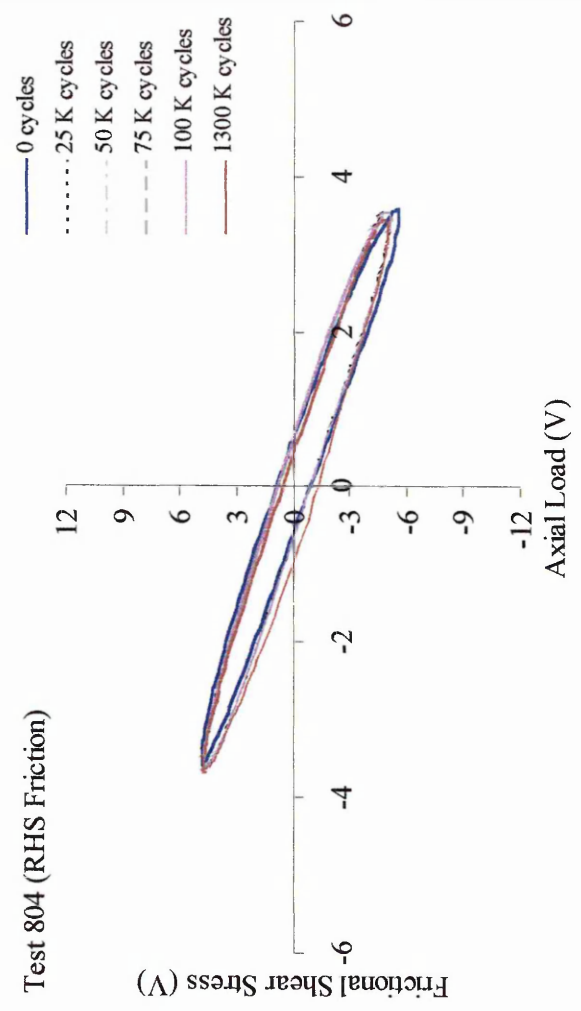
Test 803 (RHS Friction)



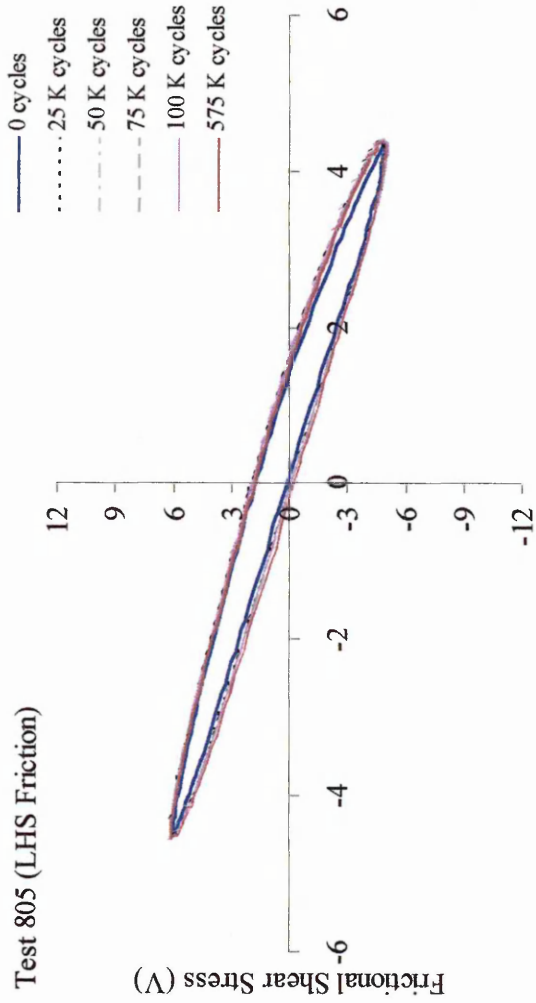
Test 804 (LHS Friction)



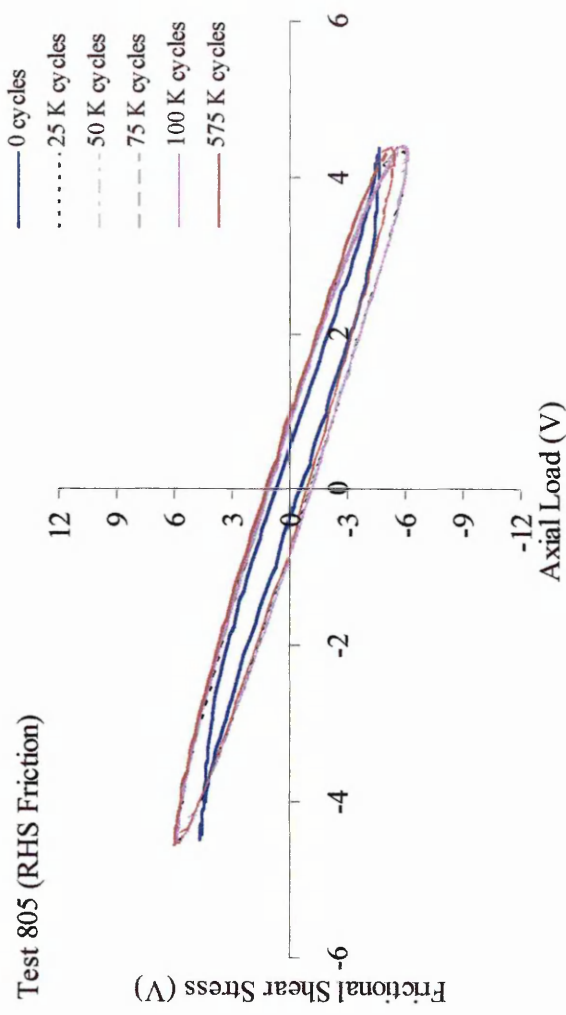
Test 804 (RHS Friction)



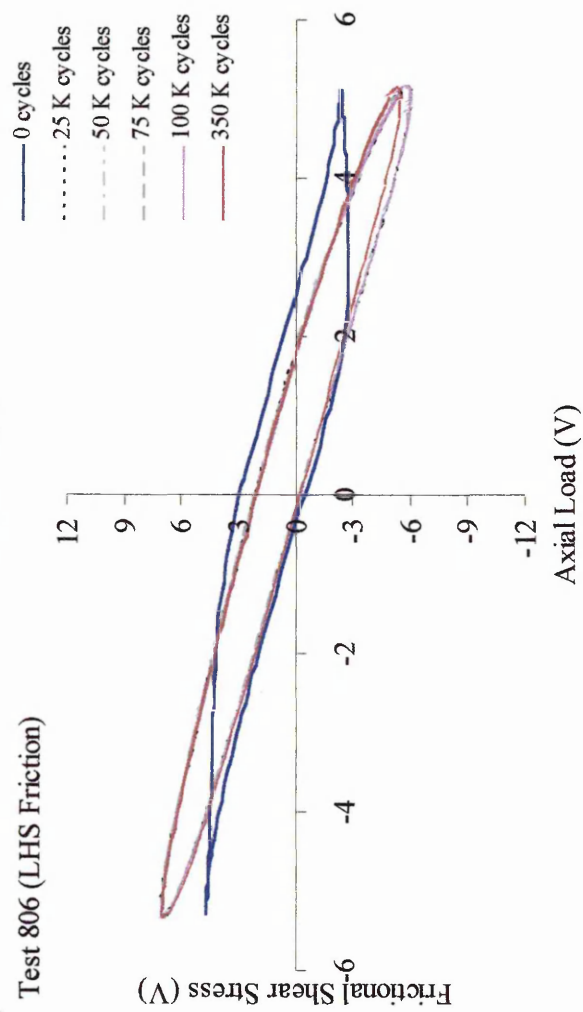
Test 805 (LHS Friction)



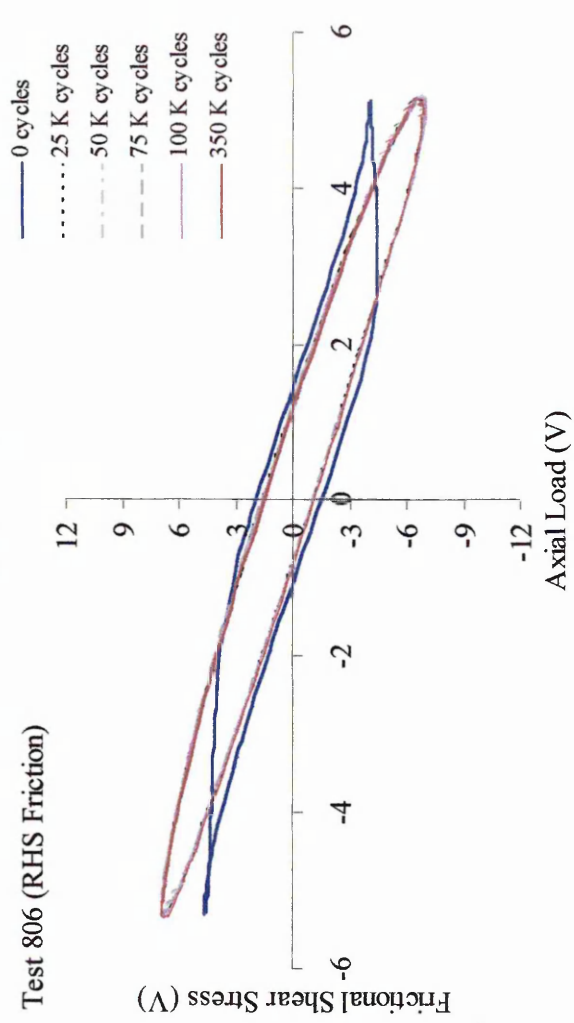
Test 805 (RHS Friction)



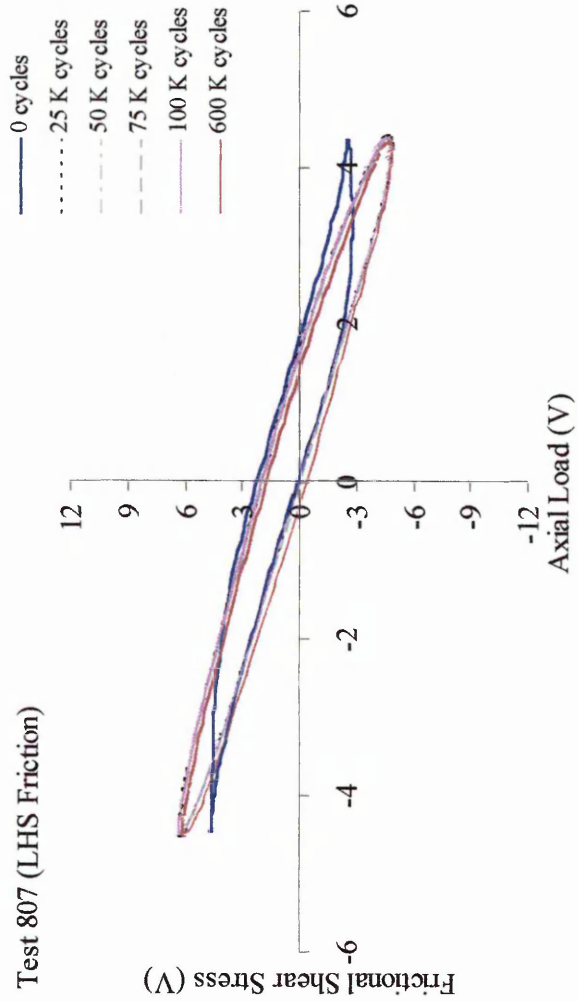
Test 806 (LHS Friction)



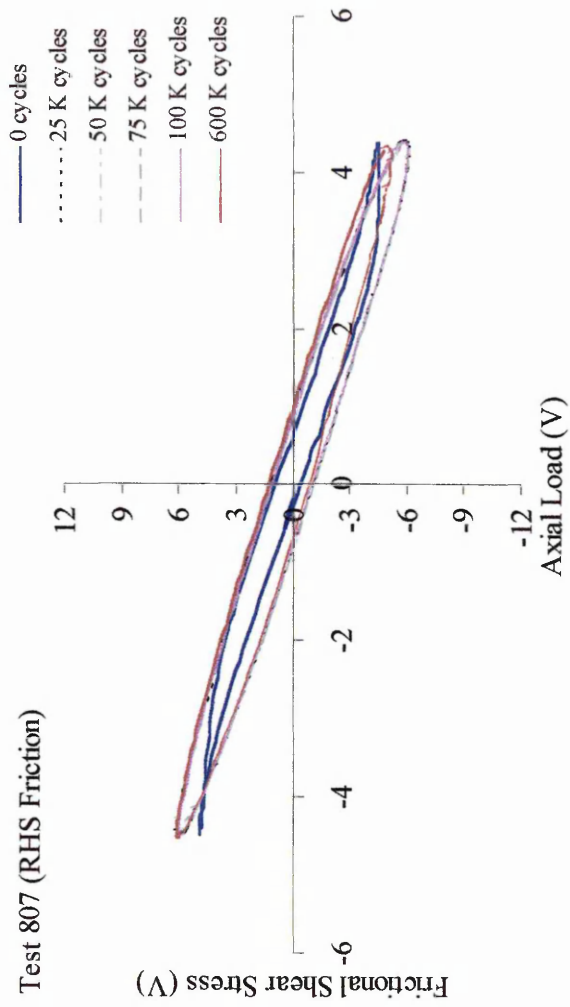
Test 806 (RHS Friction)



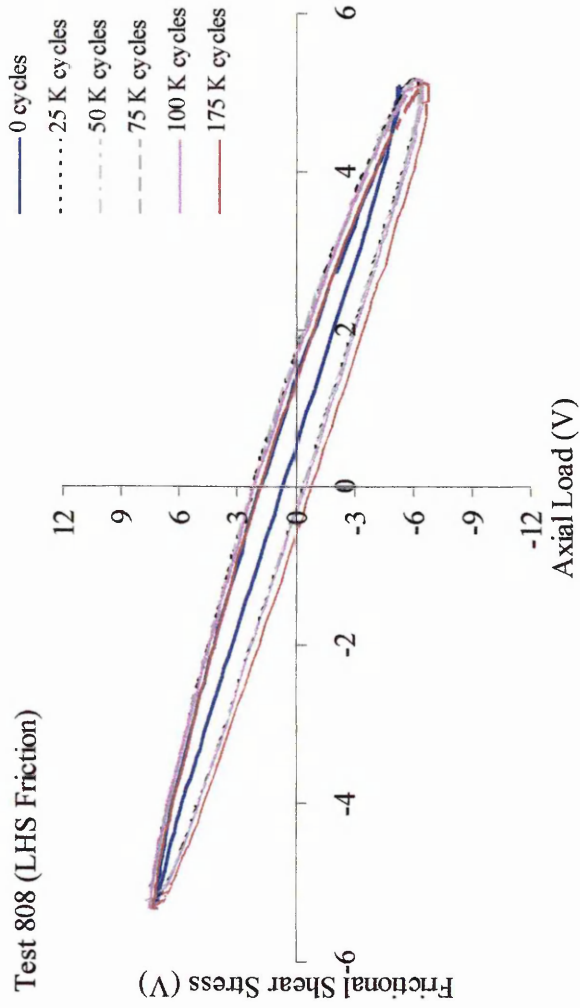
Test 807 (LHS Friction)



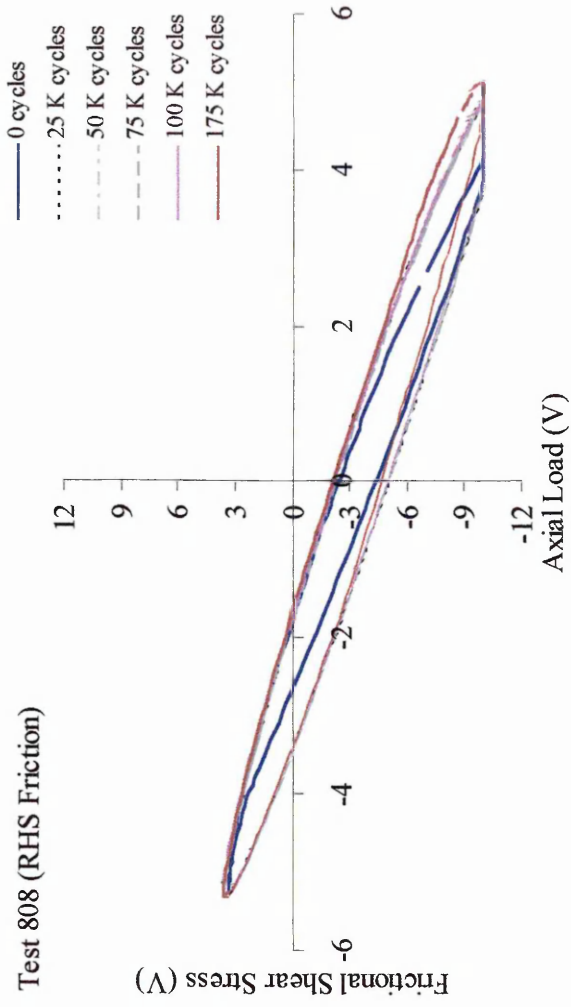
Test 807 (RHS Friction)



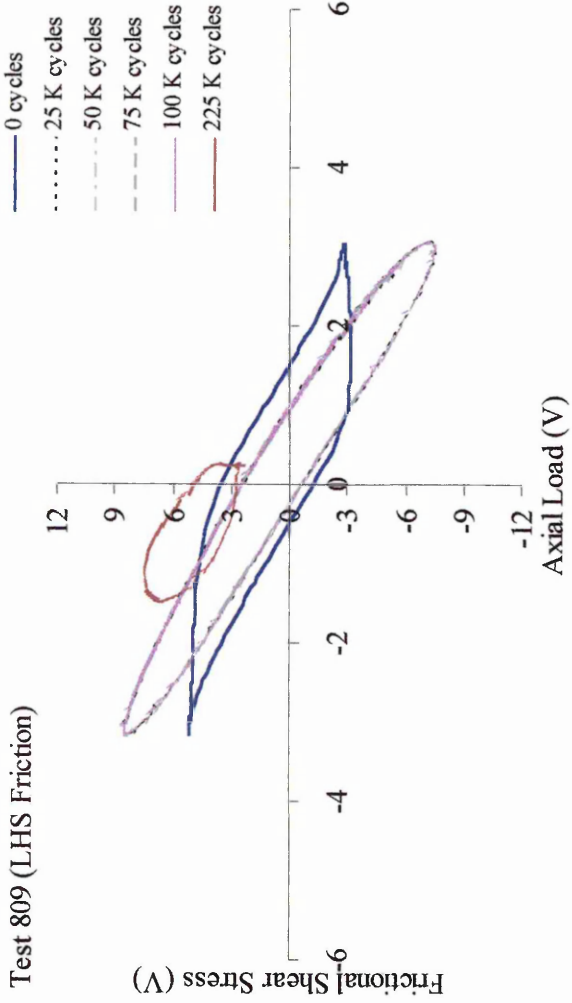
Test 808 (LHS Friction)



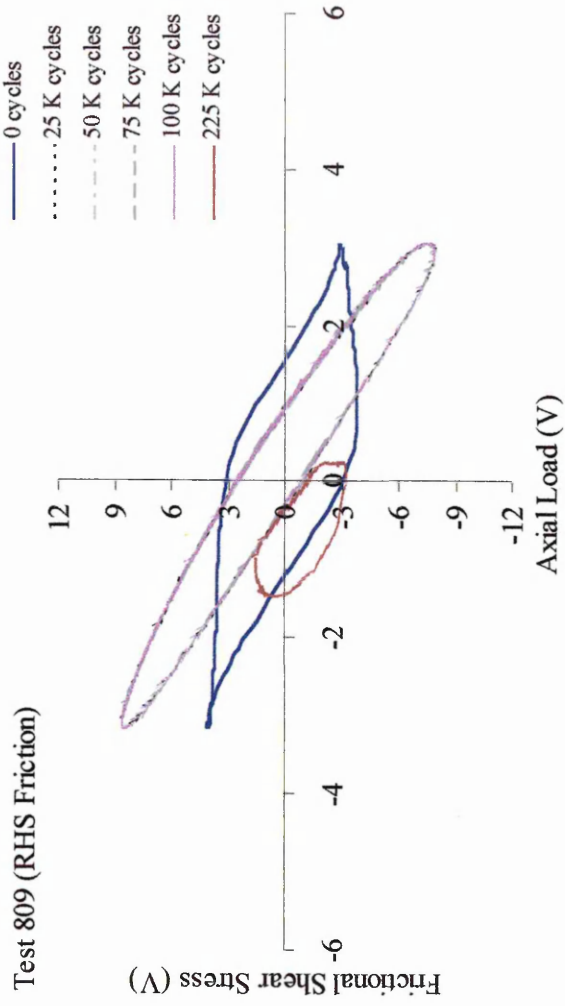
Test 808 (RHS Friction)



Test 809 (LHS Friction)

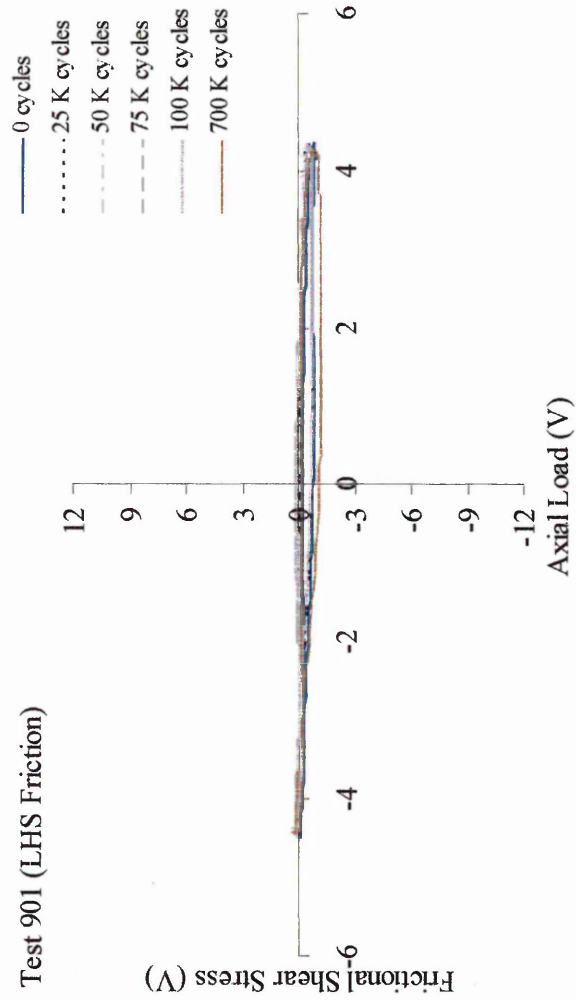


Test 809 (RHS Friction)

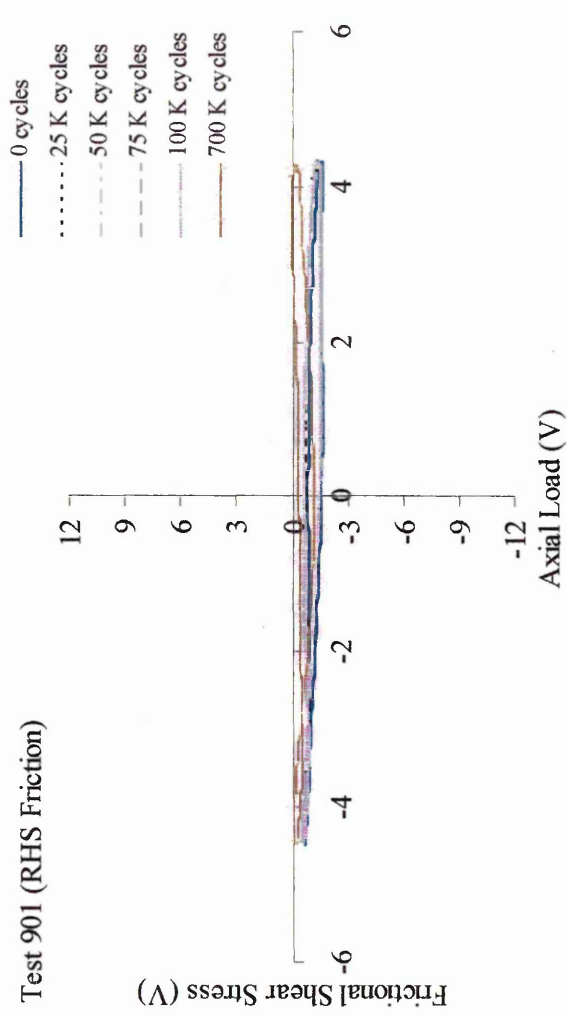


900 TEST SERIES FRICTION HYSTERESIS LOOPS

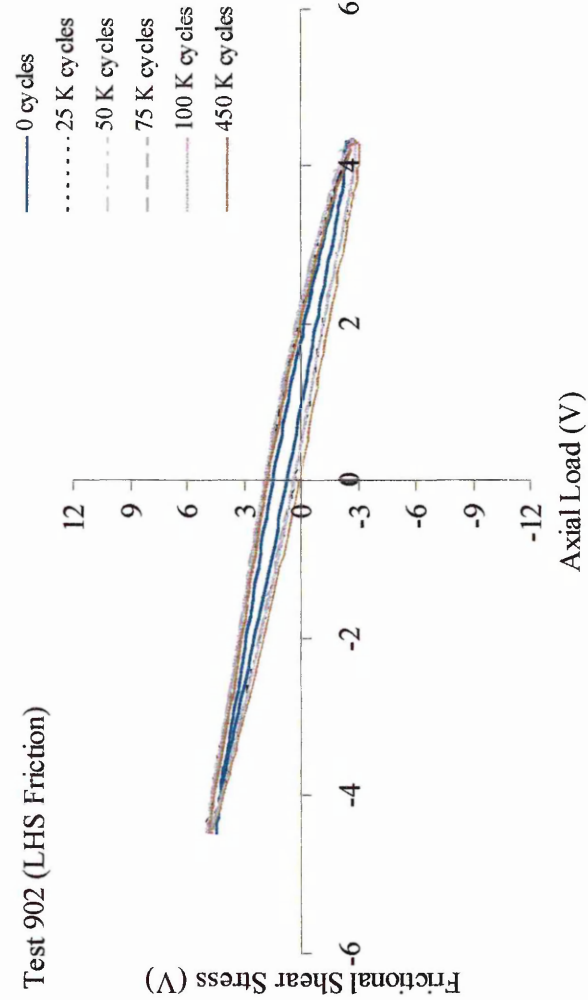
Test 901 (LHS Friction)



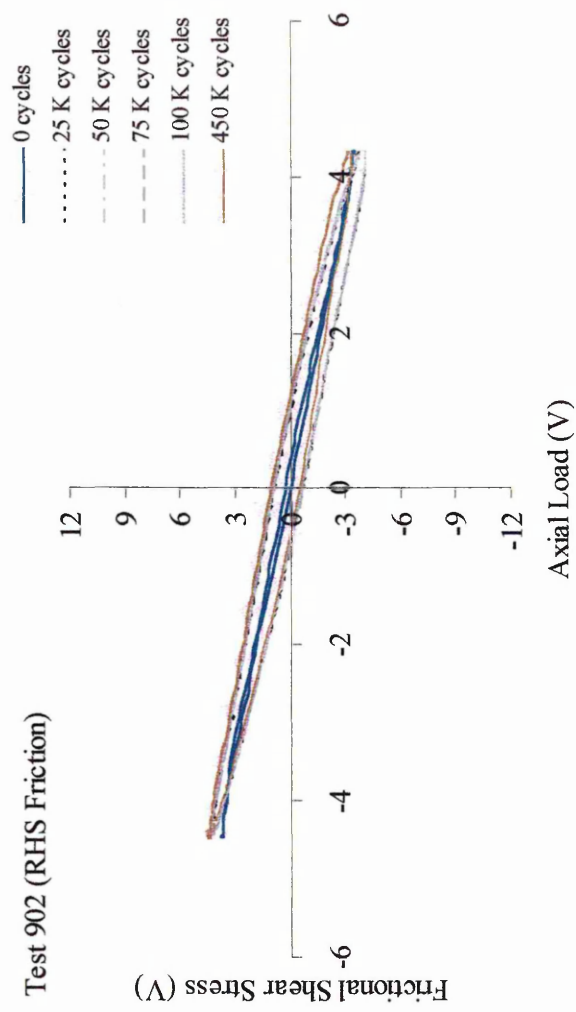
Test 901 (RHS Friction)



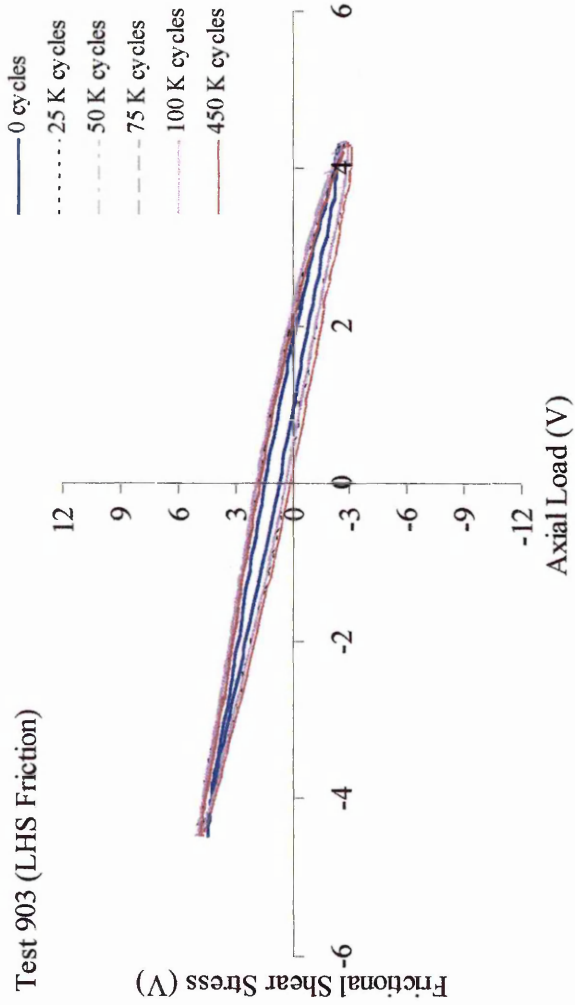
Test 902 (LHS Friction)



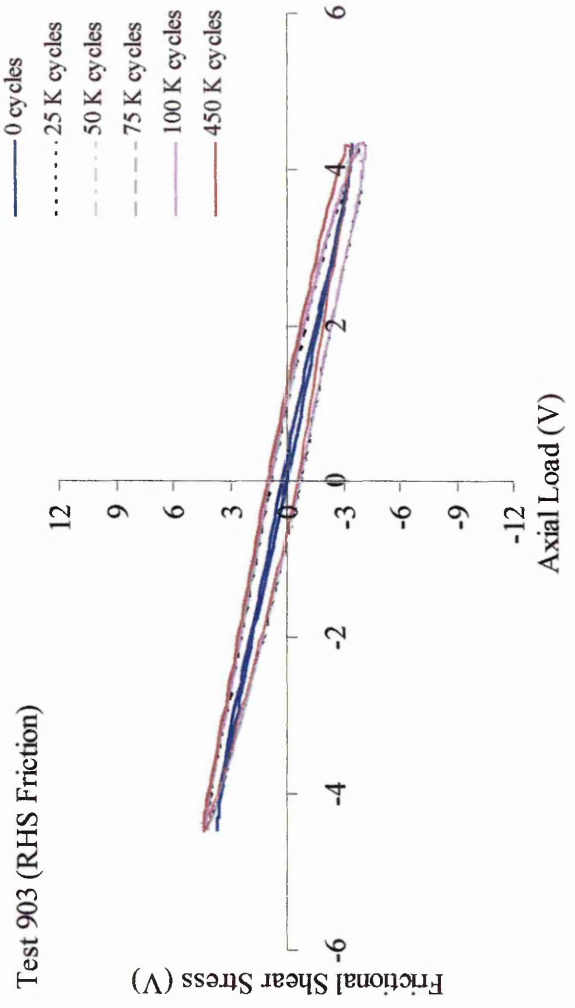
Test 902 (RHS Friction)



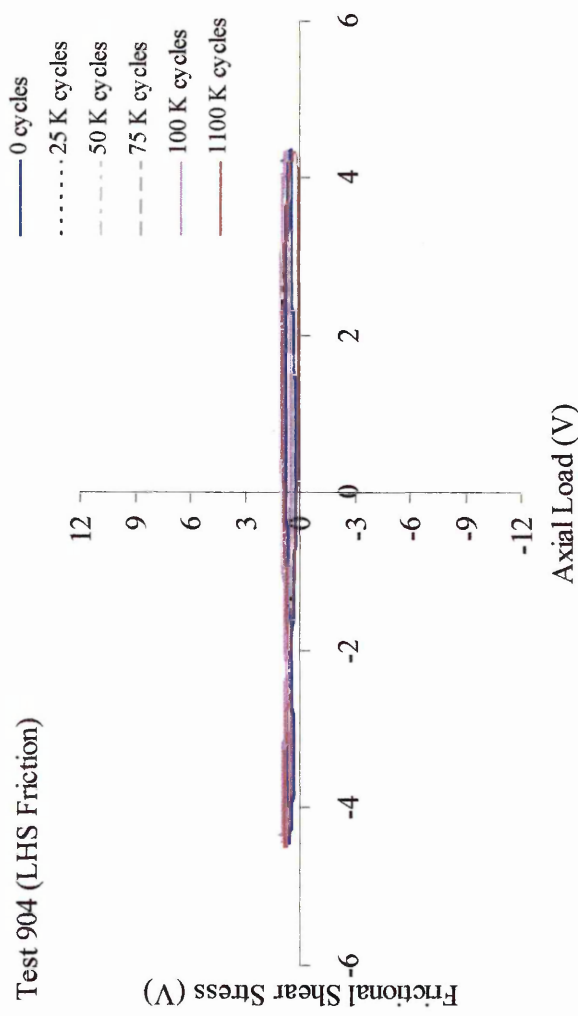
Test 903 (LHS Friction)



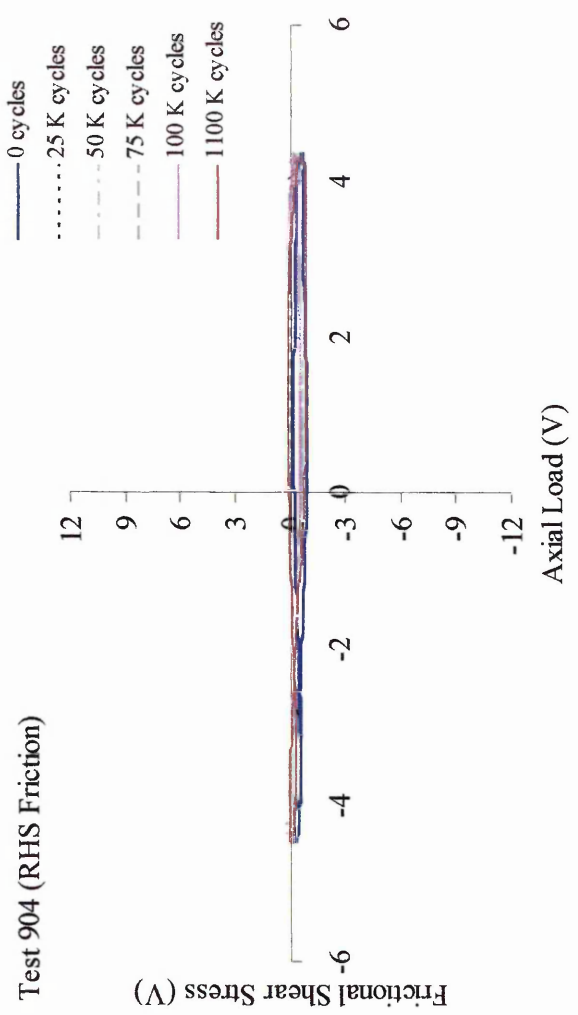
Test 903 (RHS Friction)



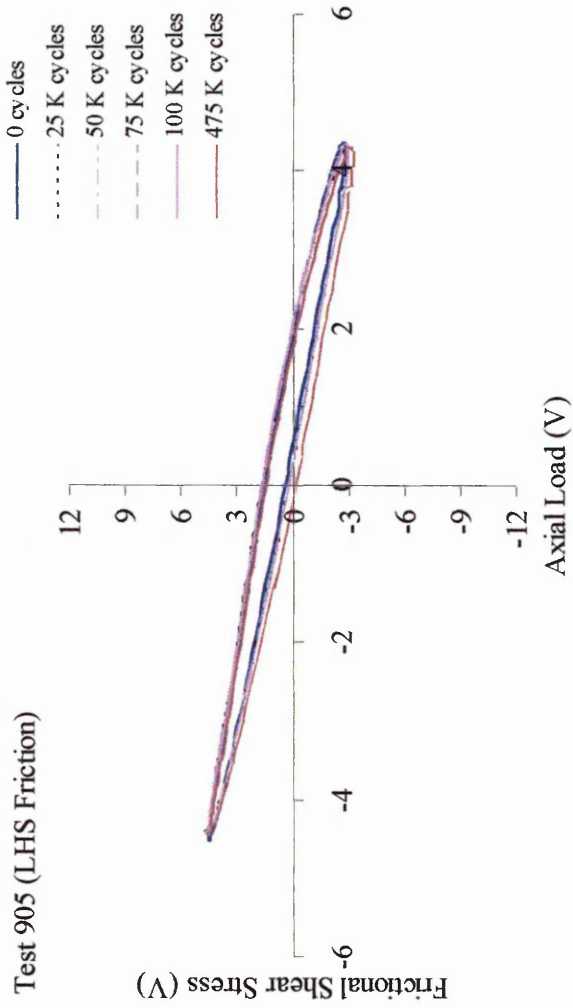
Test 904 (LHS Friction)



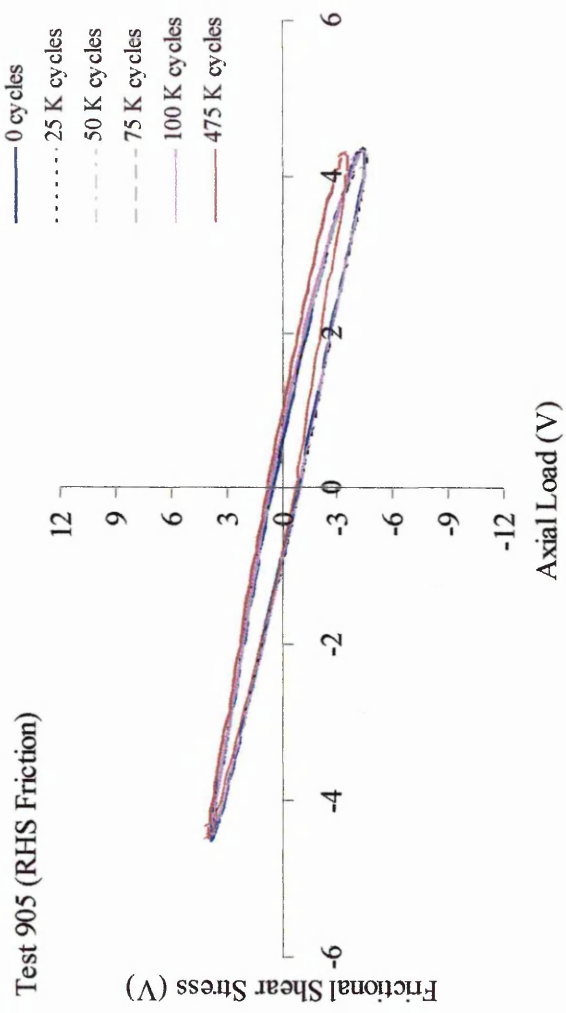
Test 904 (RHS Friction)



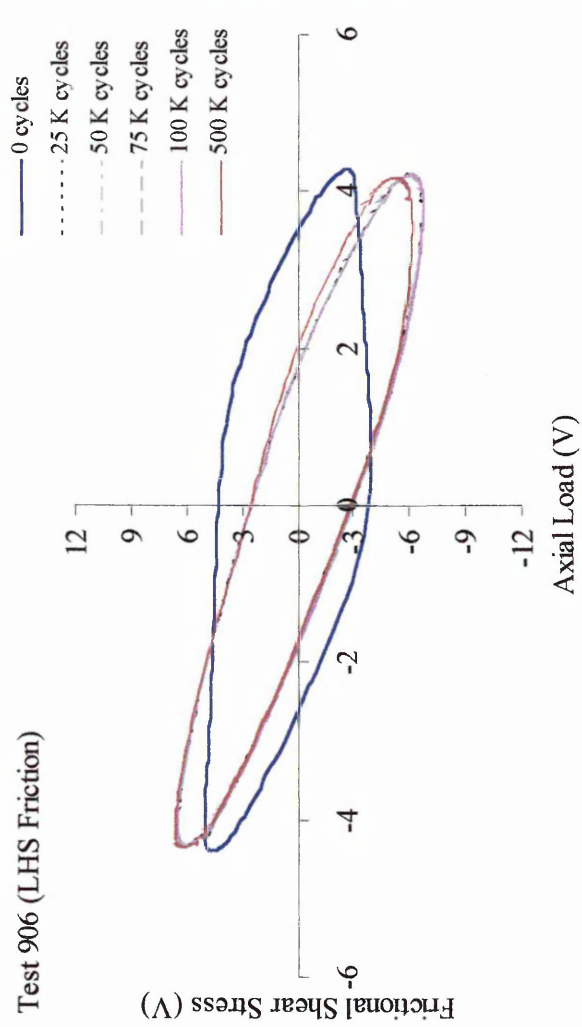
Test 905 (LHS Friction)



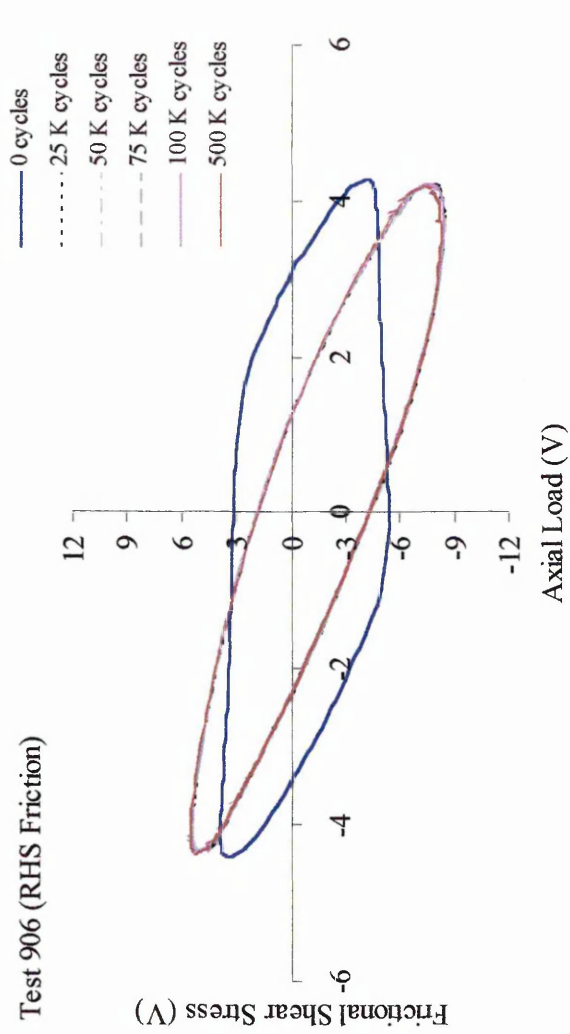
Test 905 (RHS Friction)



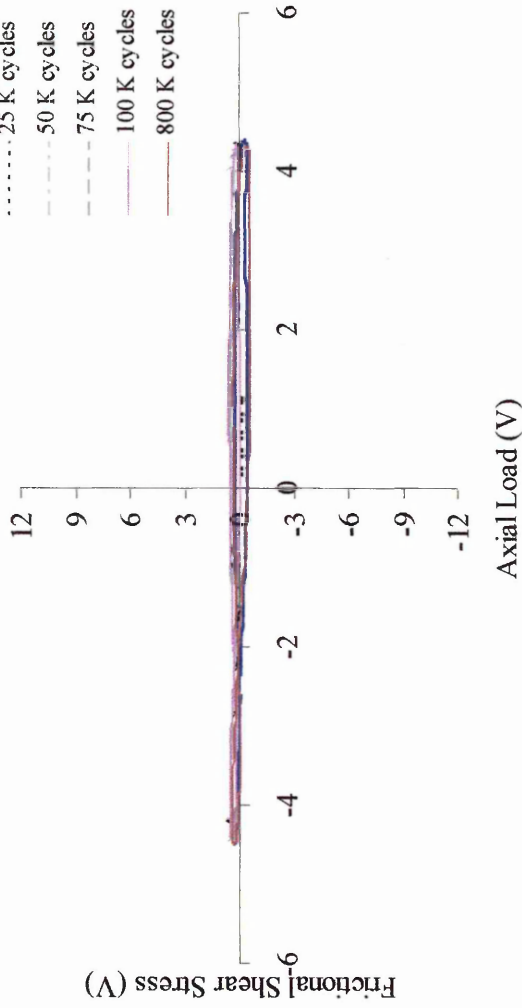
Test 906 (LHS Friction)



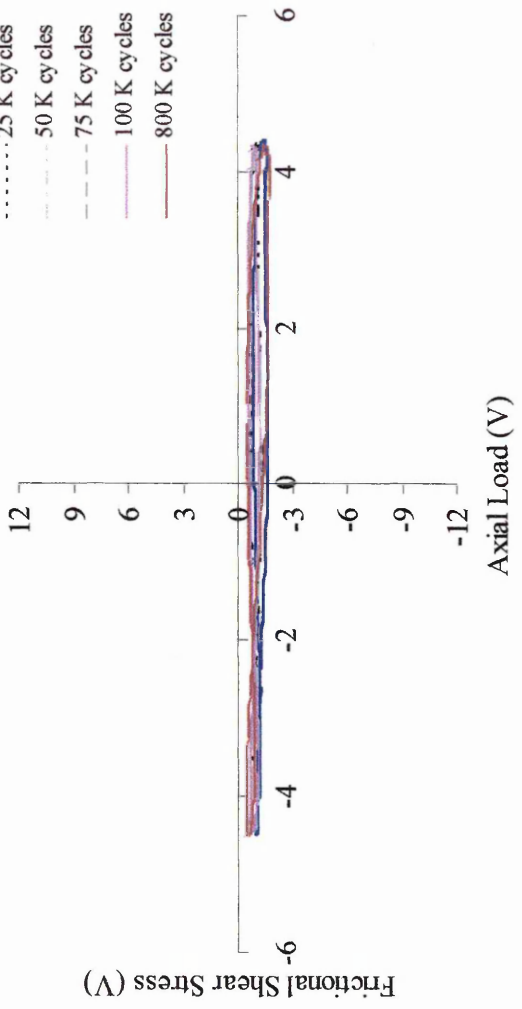
Test 906 (RHS Friction)



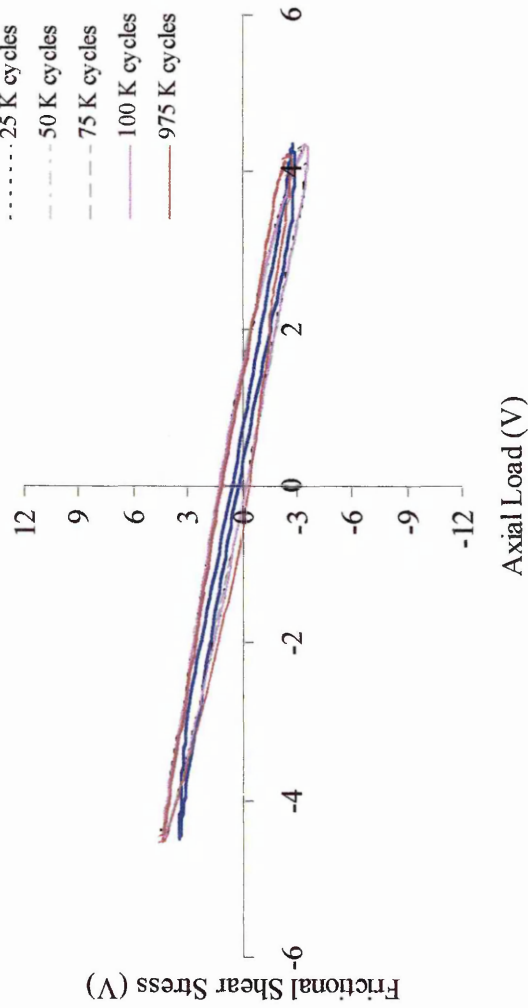
Test 907 (LHS Friction)



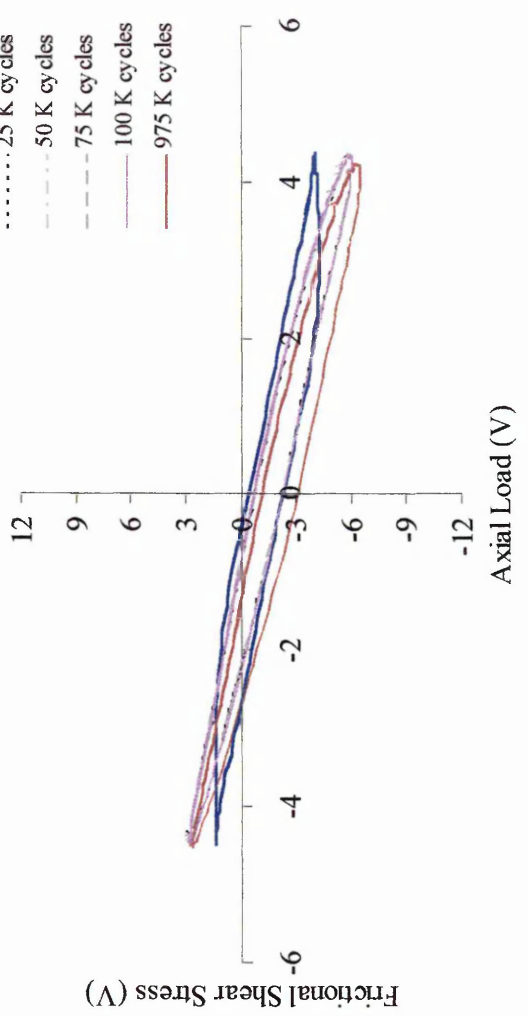
Test 907 (RHS Friction)



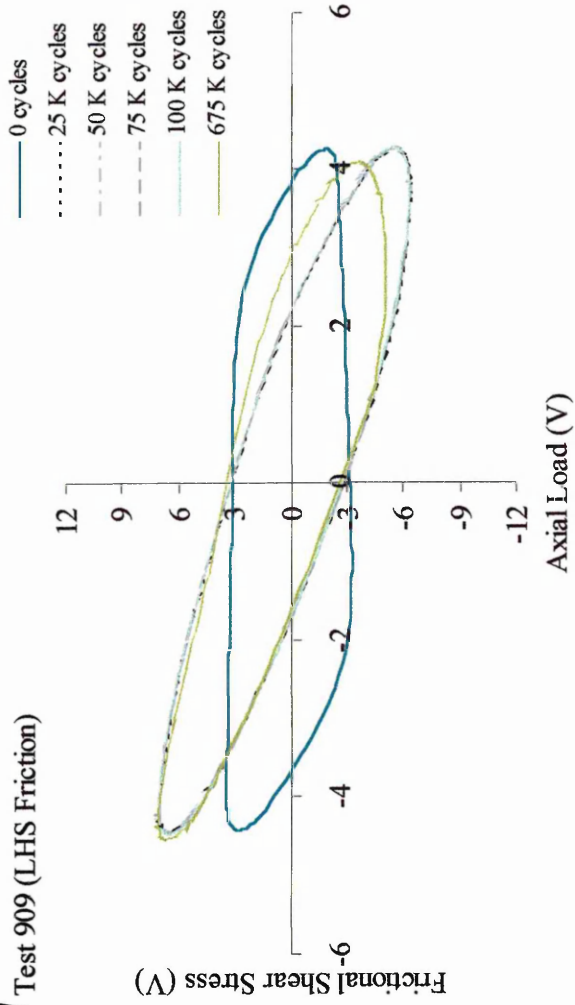
Test 908 (LHS Friction)



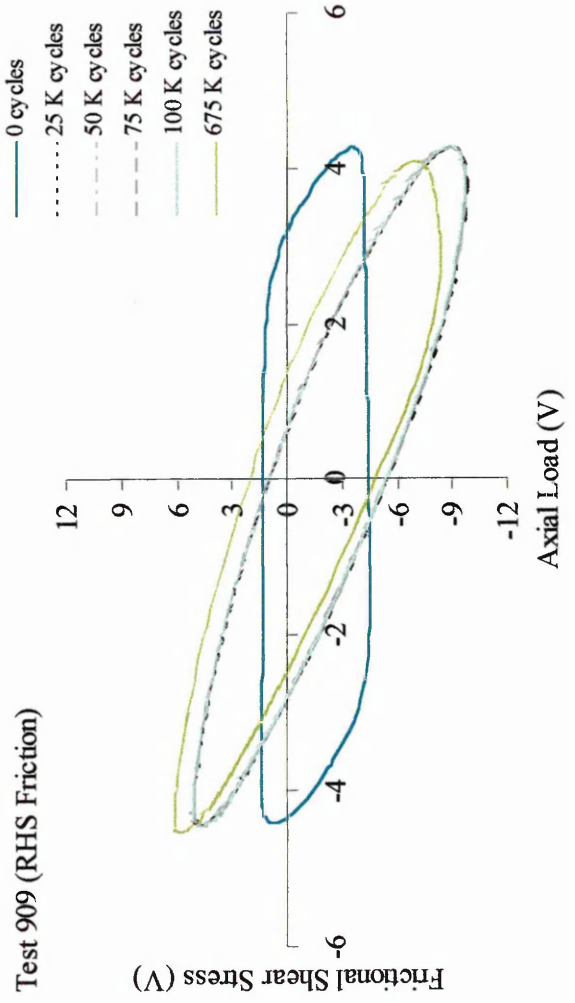
Test 908 (RHS Friction)



Test 909 (LHS Friction)



Test 909 (RHS Friction)



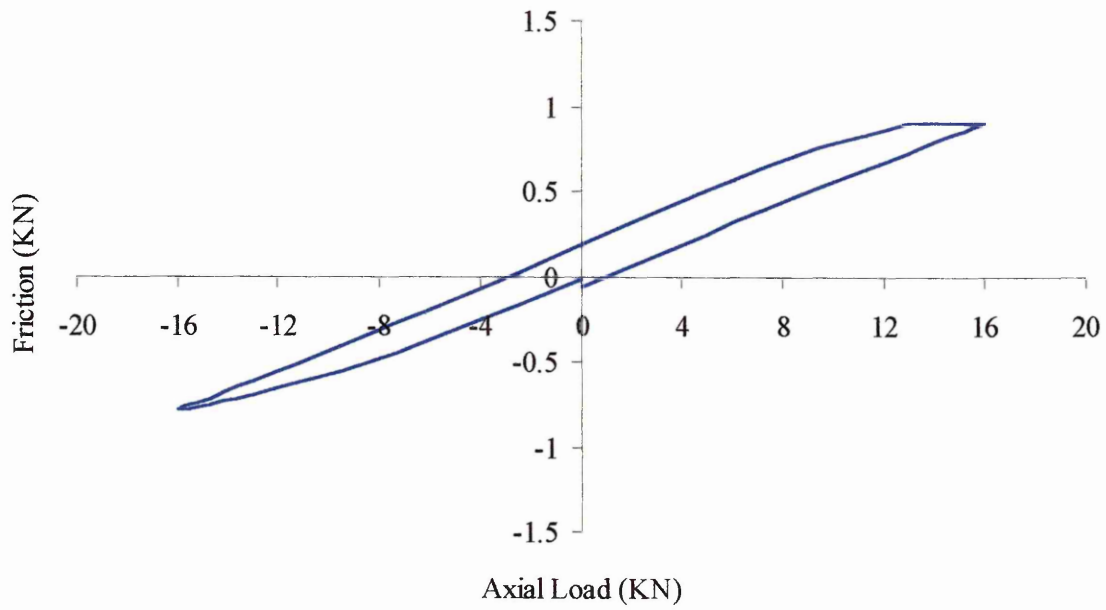
APPENDIX D

NUMERICAL FRICTION HYSTERESIS LOOPS

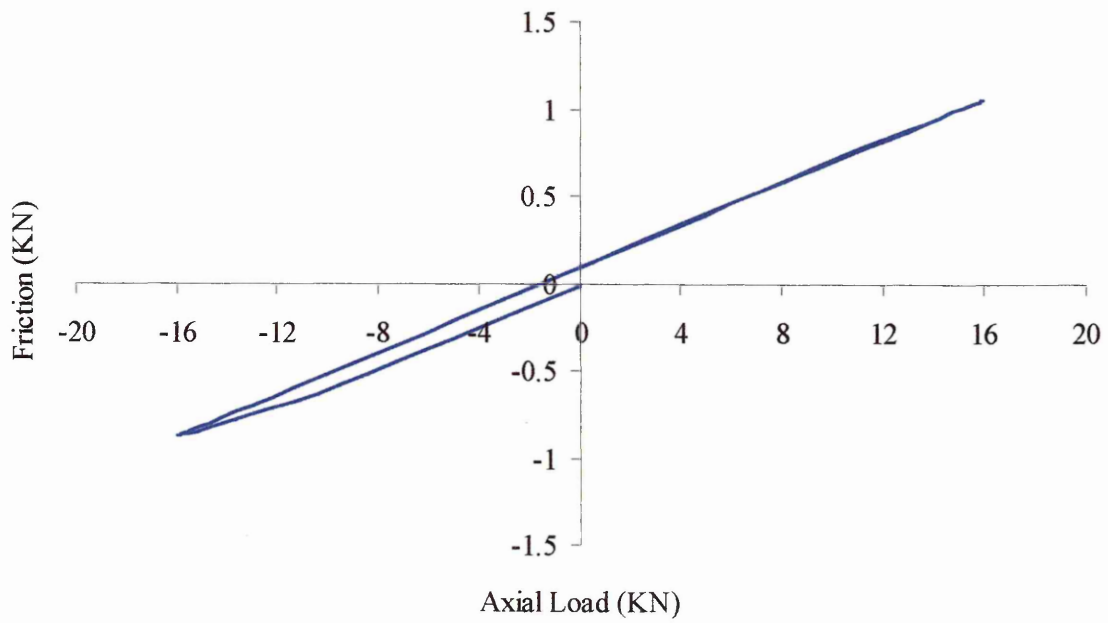
1.27MM PAD SIZE NUMERICAL FRICTION HYSTERESIS LOOPS

[75]

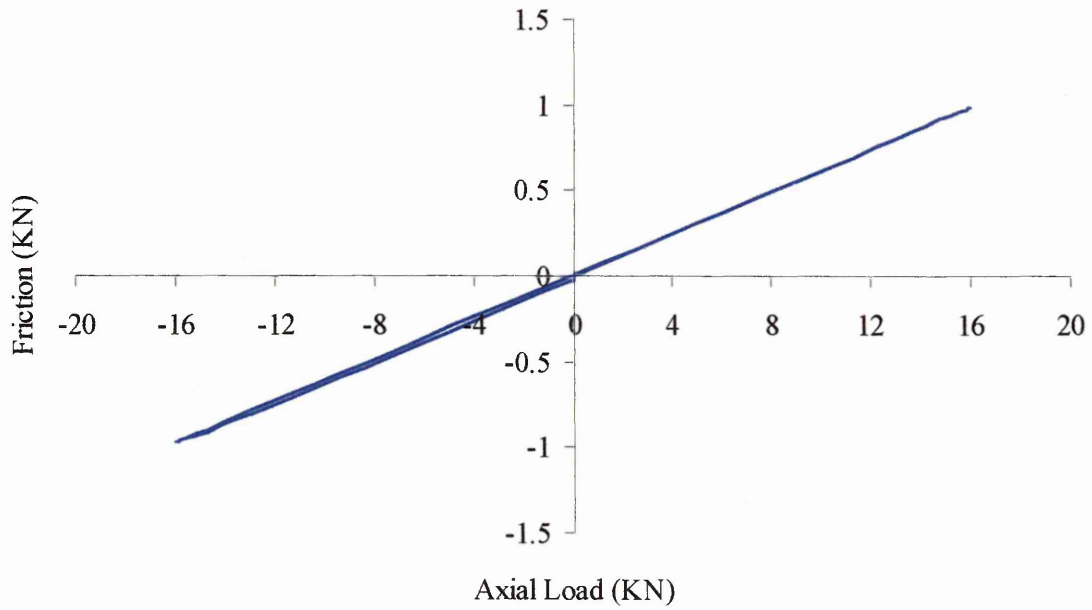
Test 122 Friction Loop from FE Analysis



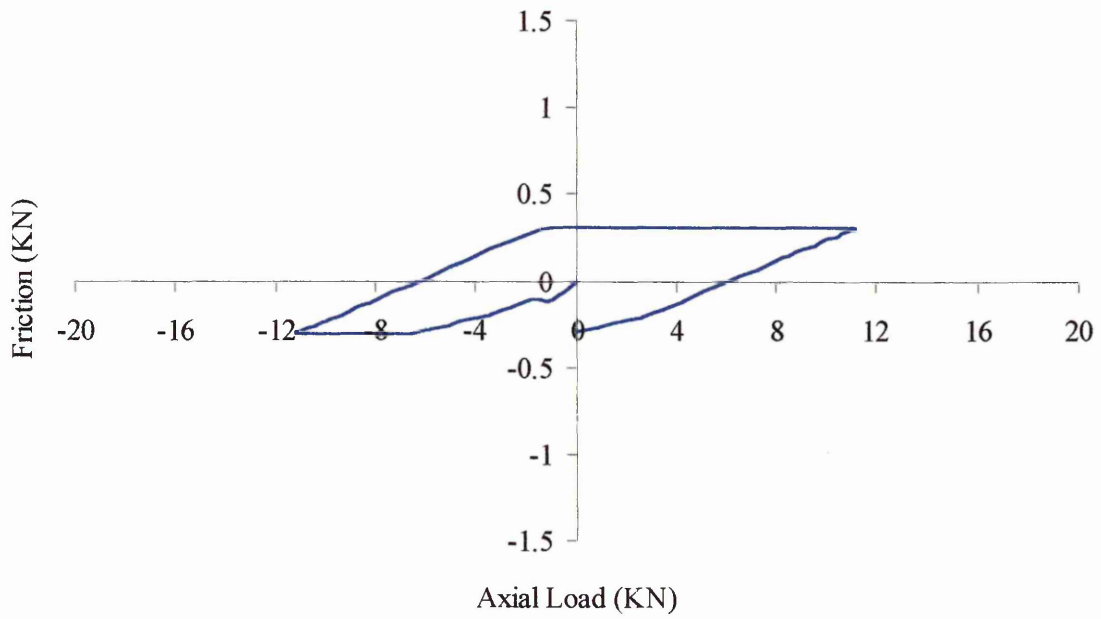
Test 124 Friction Loop from FE Analysis



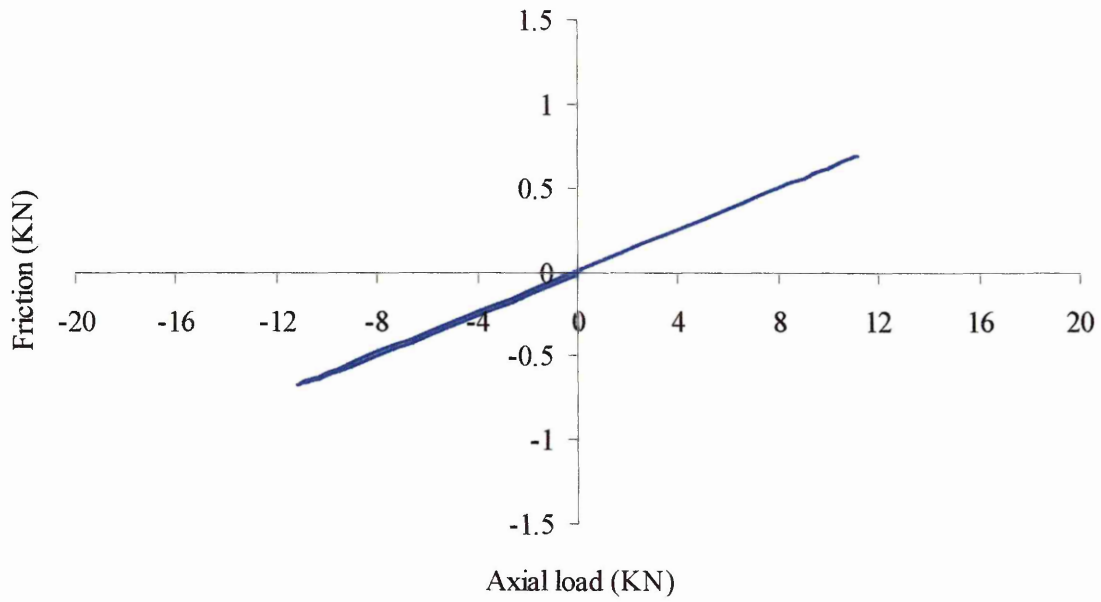
Test 125 Friction Loop from FE Analysis



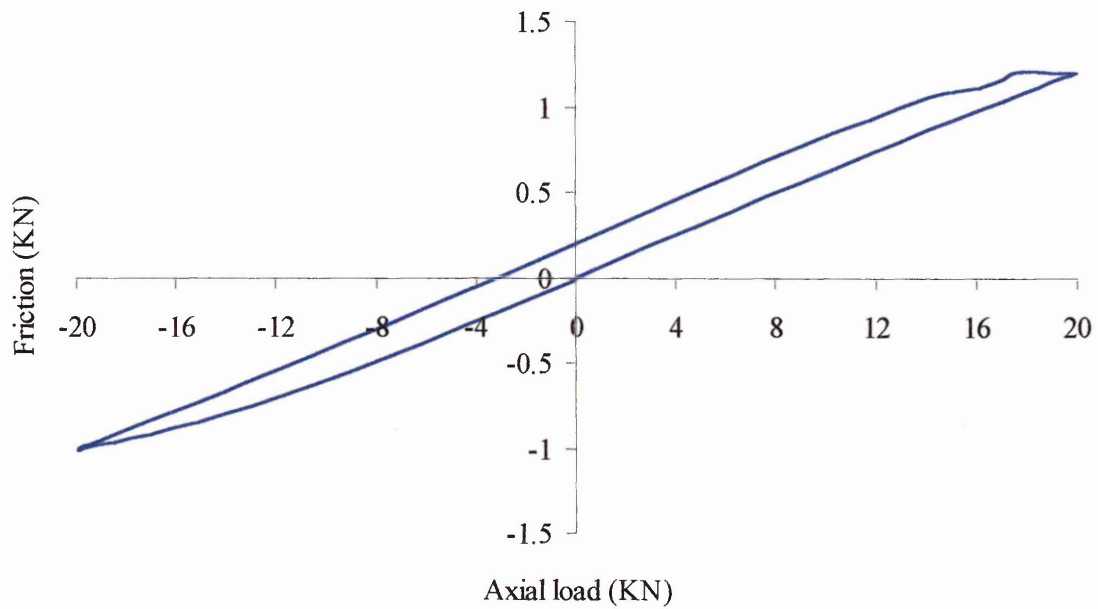
Test 126 Friction Loop form FE Analysis



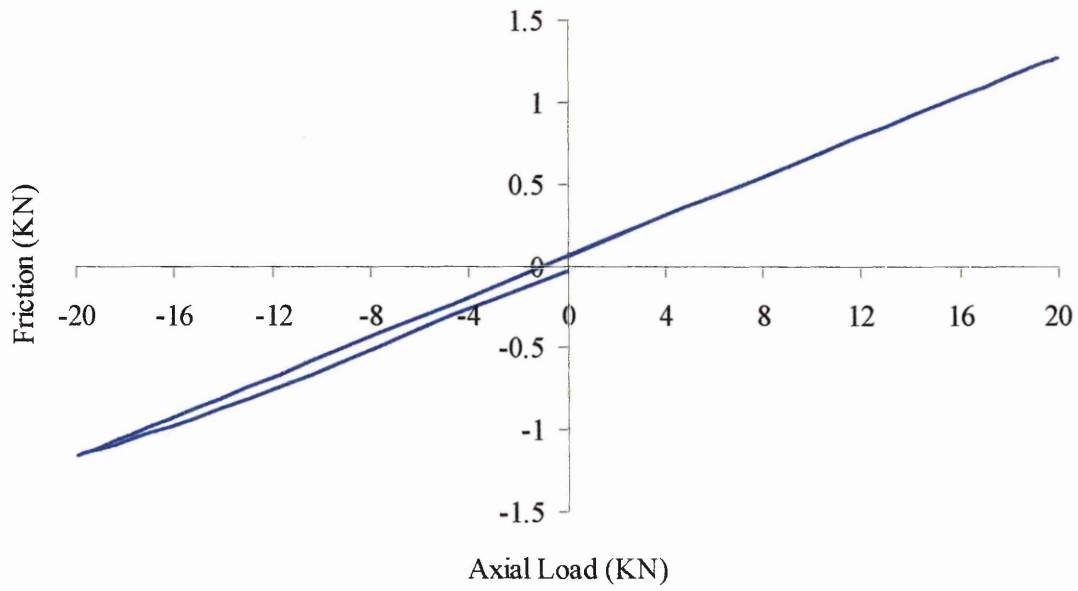
Test 127 Friction Loop from FE Analysis



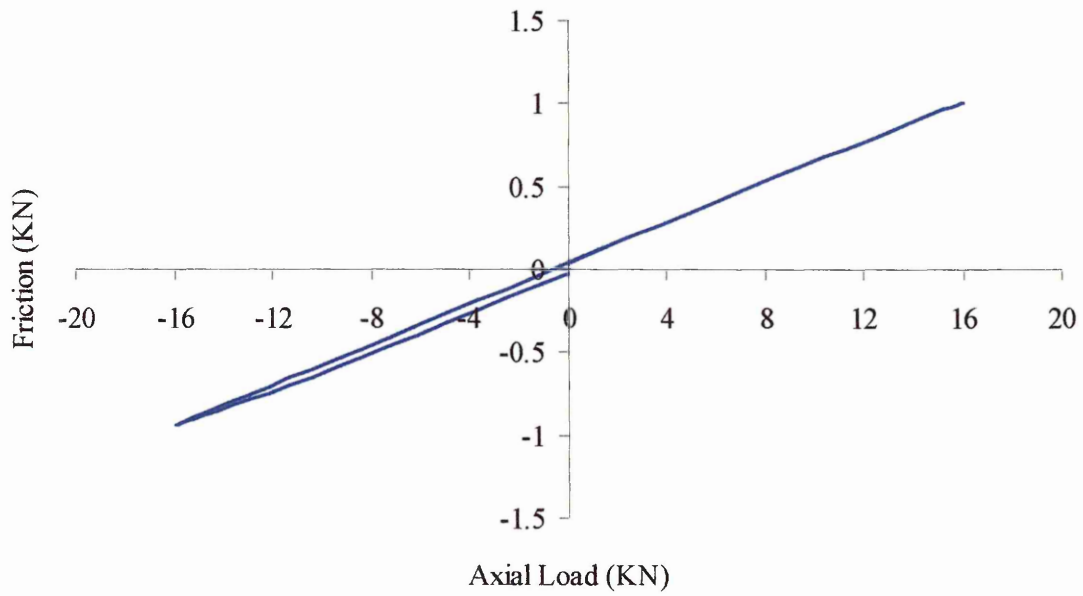
Test 128 Friction Loop from FE Analysis



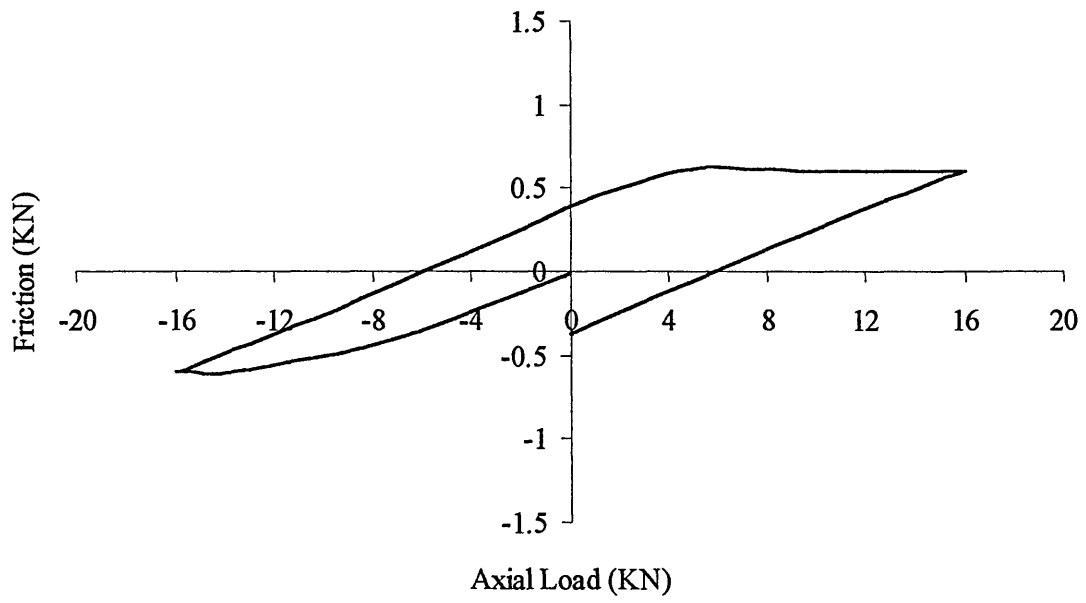
Test 130 Friction Loop from FE Analysis



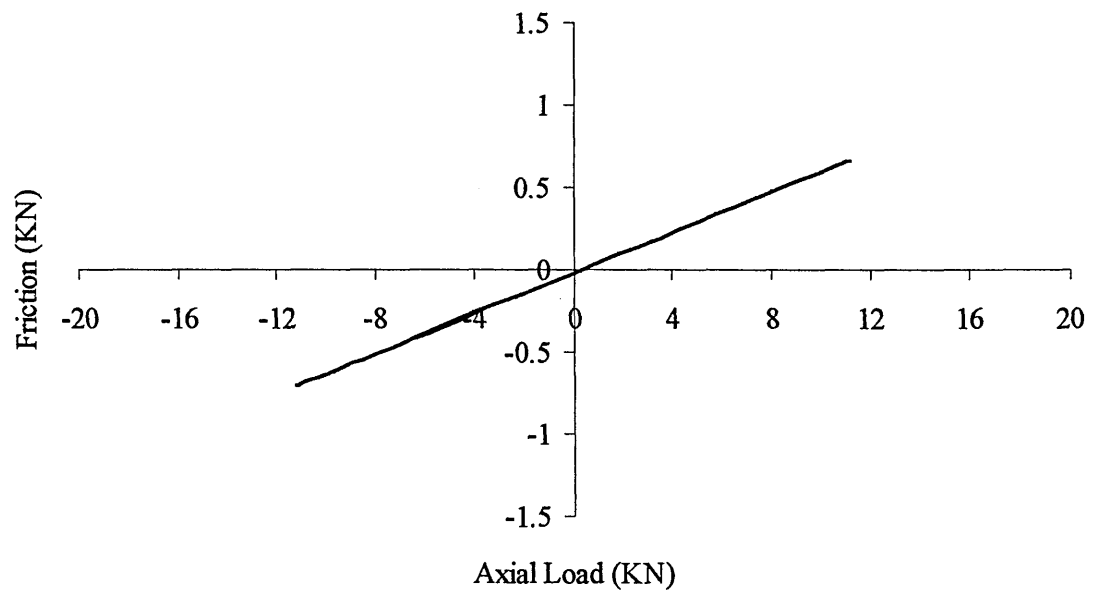
Test 132 Friction Loop from FE Analysis



Test 133 Friction Loop from FE Analysis

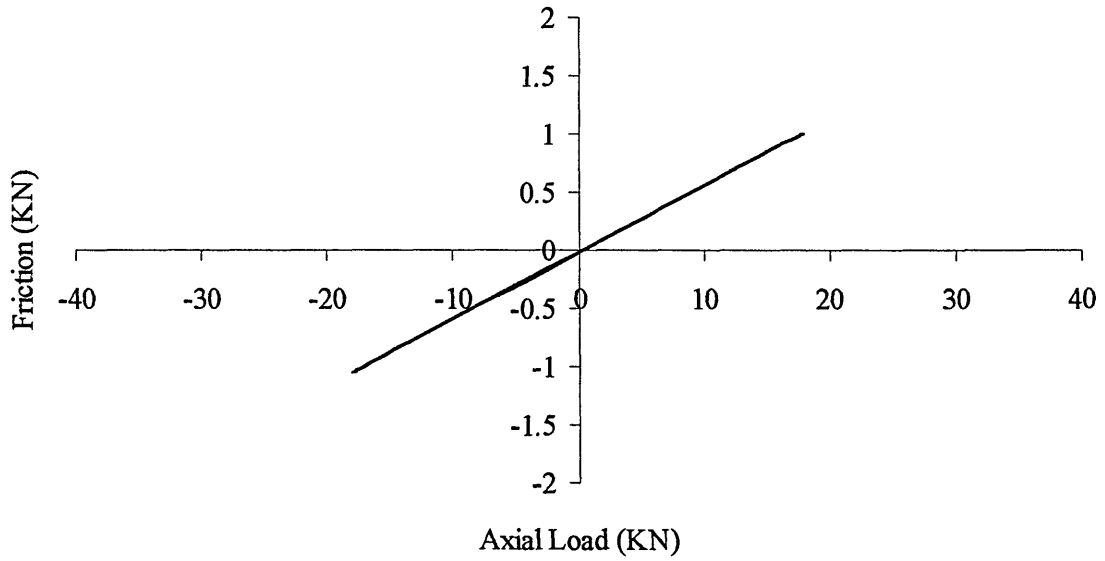


Test 134 Friction Loop from FE Analysis

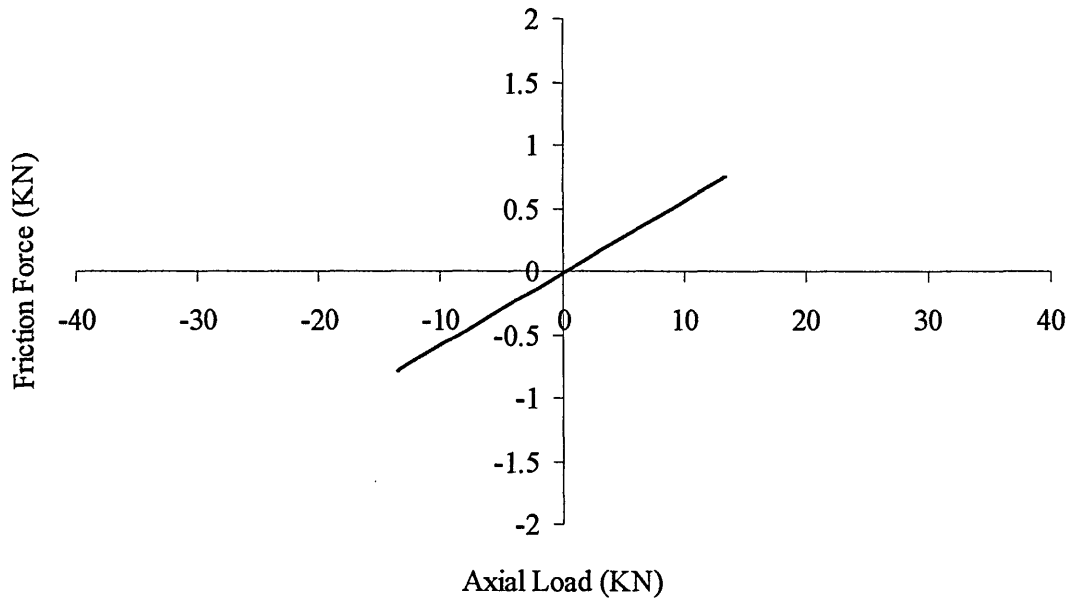


**3MM PAD SIZE NUMERICAL FRICTION HYSTERESIS LOOPS (800
TEST SERIES)**

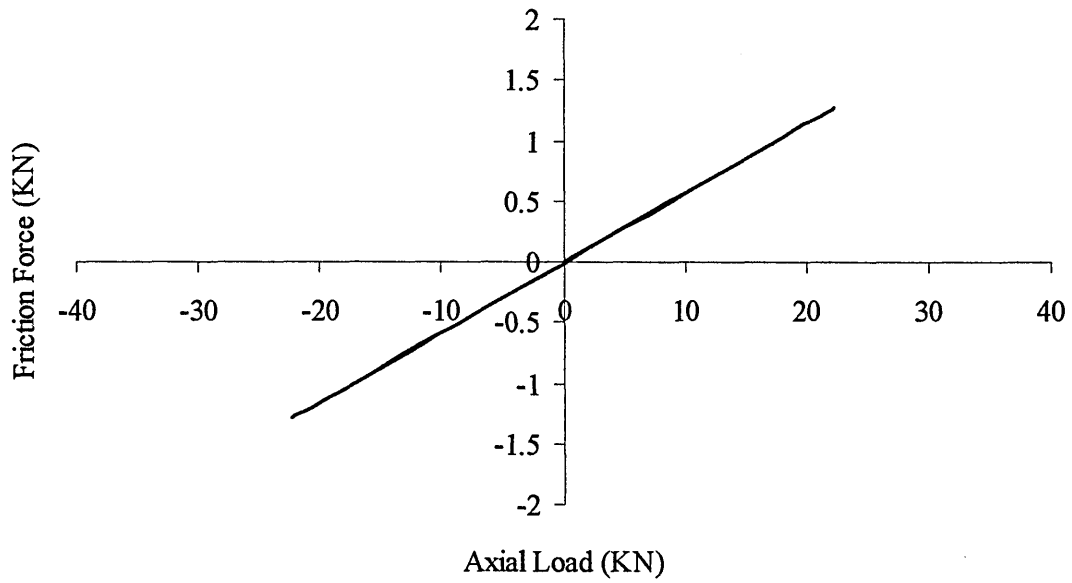
Numerical Friction Hysteresis Loop for 801



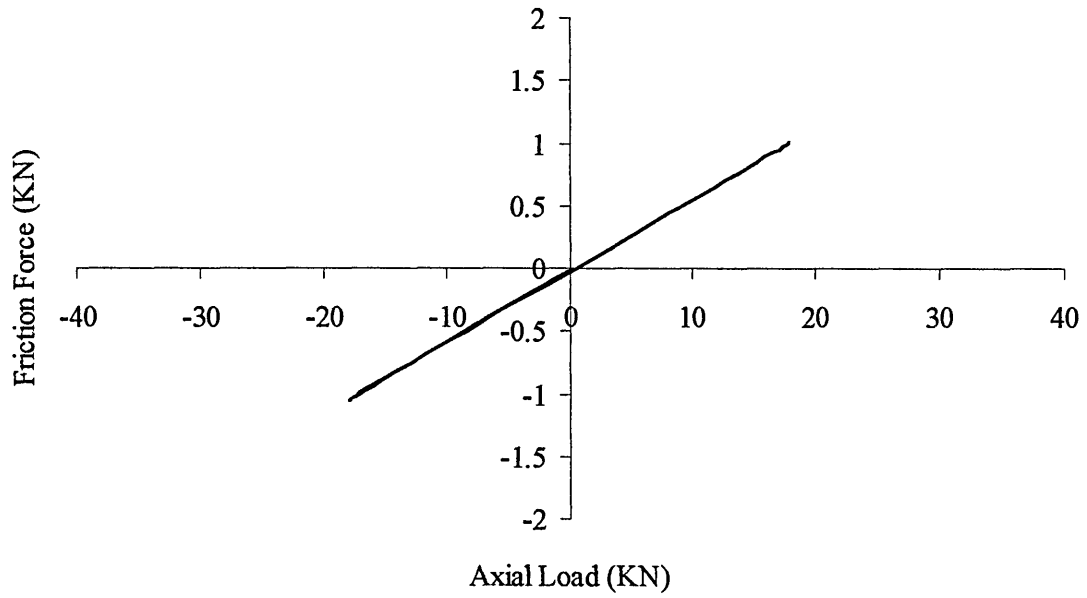
Numerical Friction Hysteresis Loop for 802



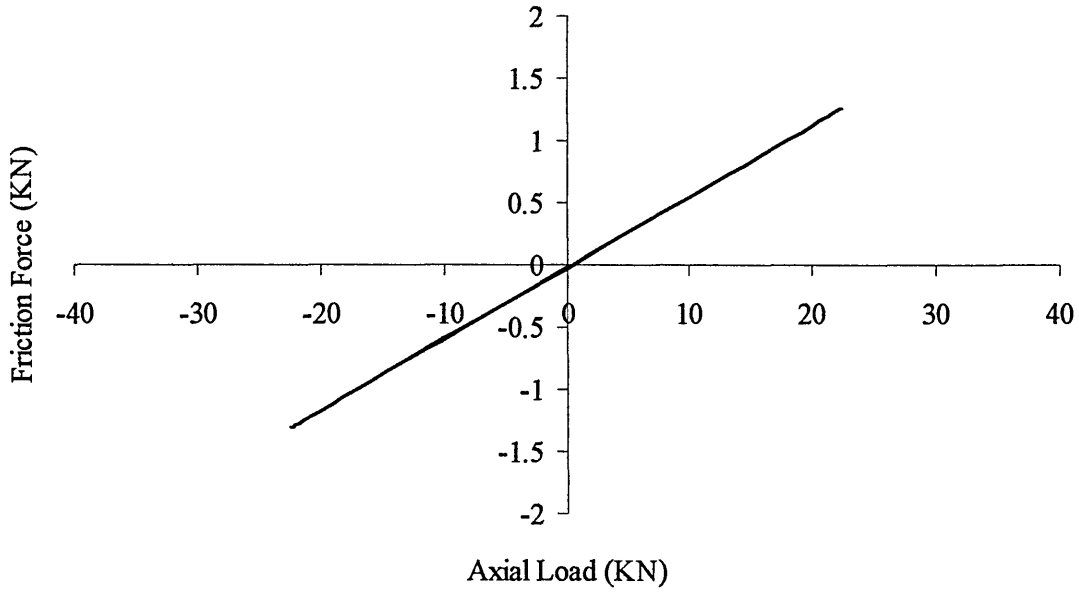
Numerical Friction Hysteresis Loop for 803



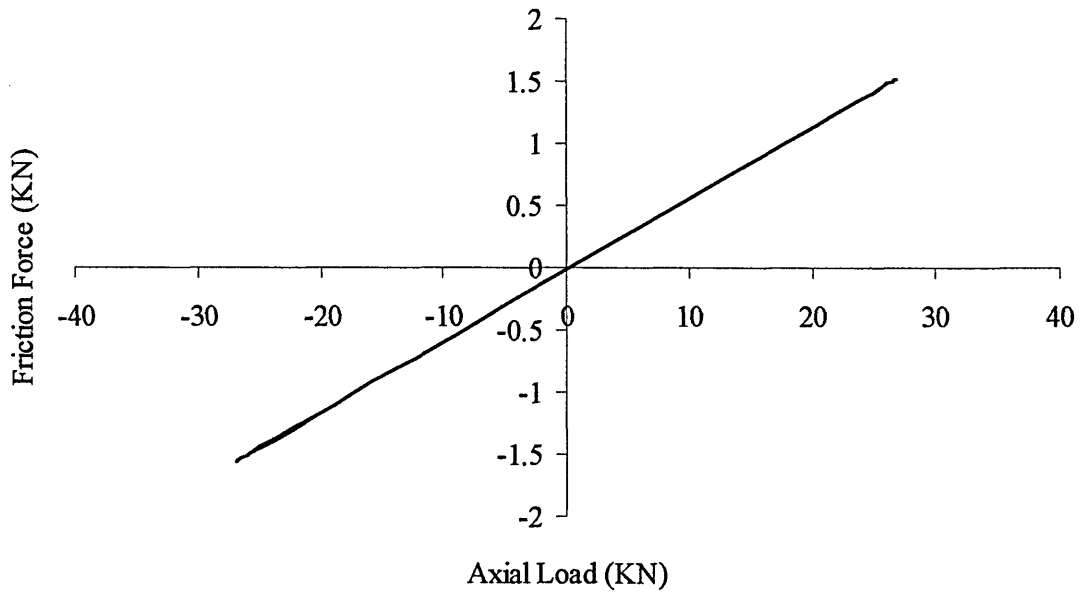
Numerical Friction Hysteresis Loop for 804



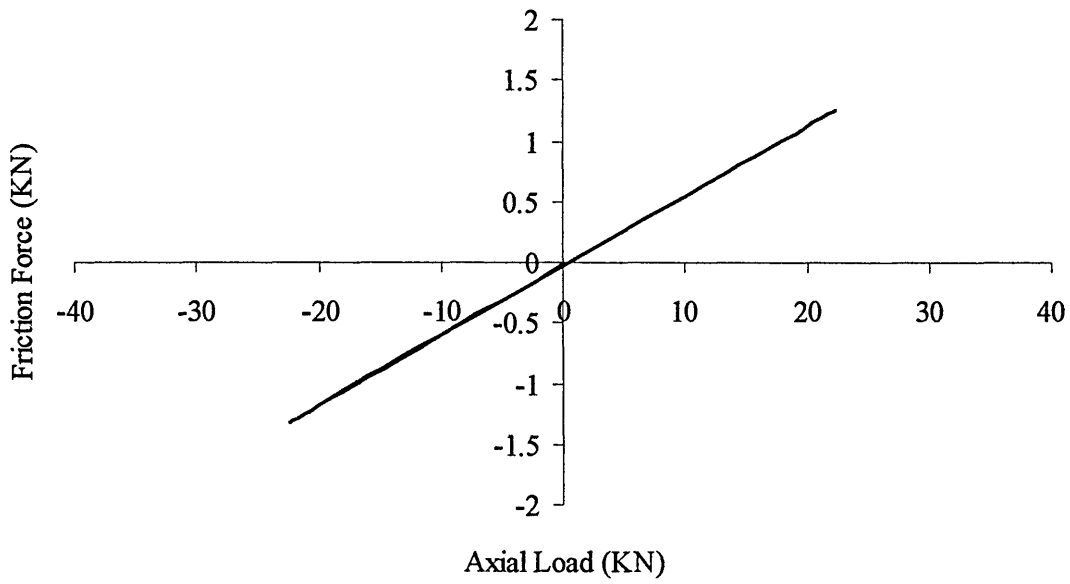
Numerical Friction Hysteresis Loop for 805



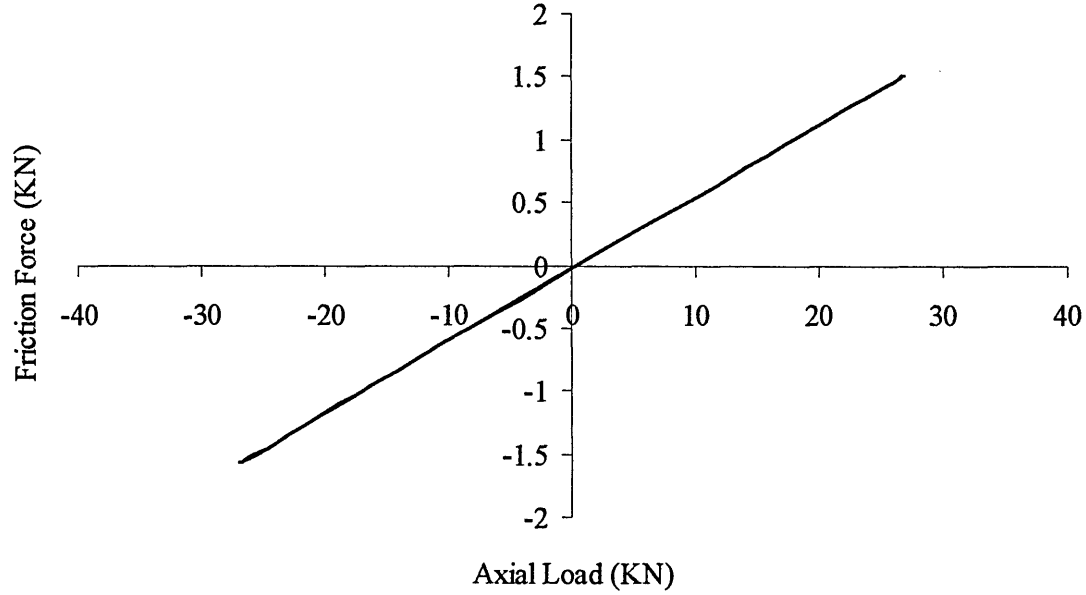
Numerical Friction Hysteresis Loop for 806



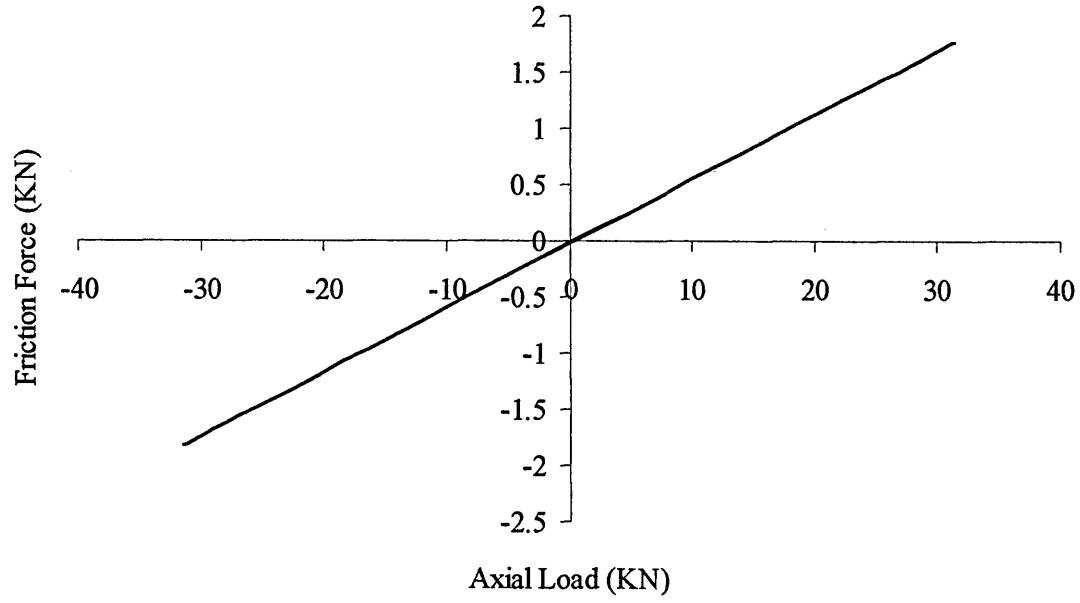
Numerical Friction Hysteresis Loop for 807



Friction Hysteresis Loop 808



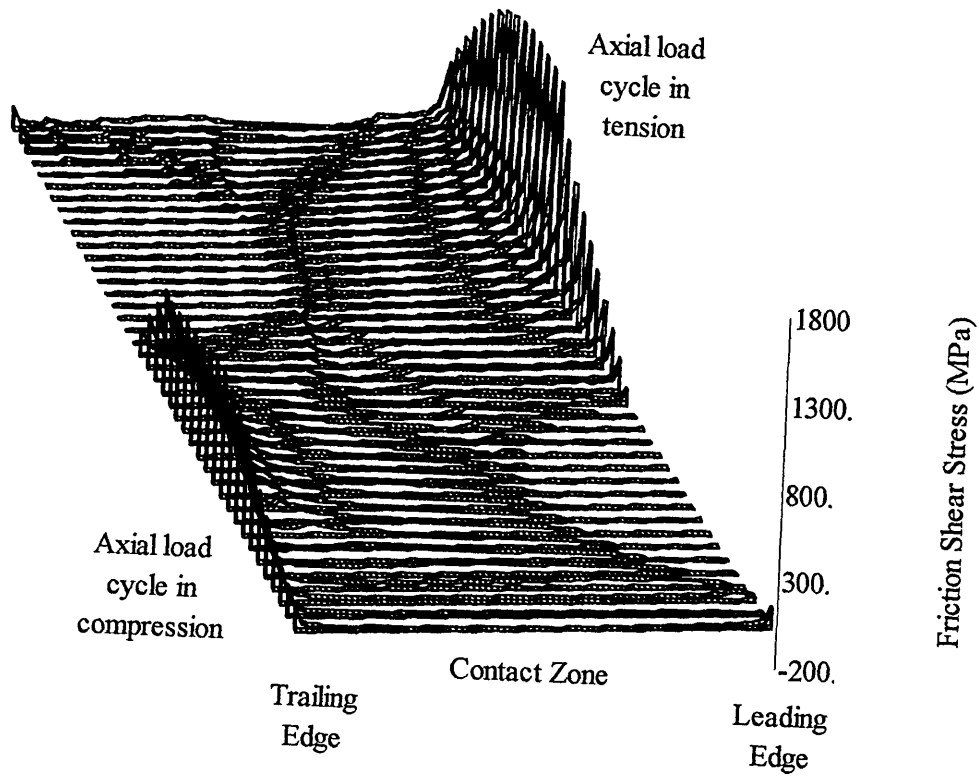
Numerical Friction Hysteresis Loop for 809



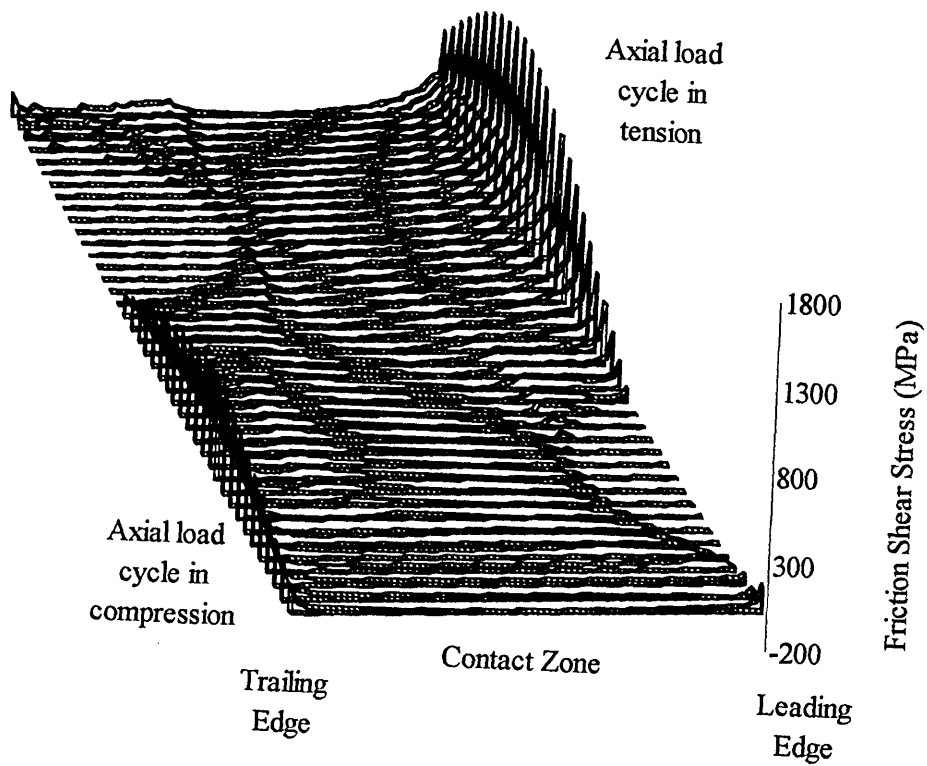
APPENDIX E

LOCALISED FRICTIONAL SHEAR STRESS MAPS

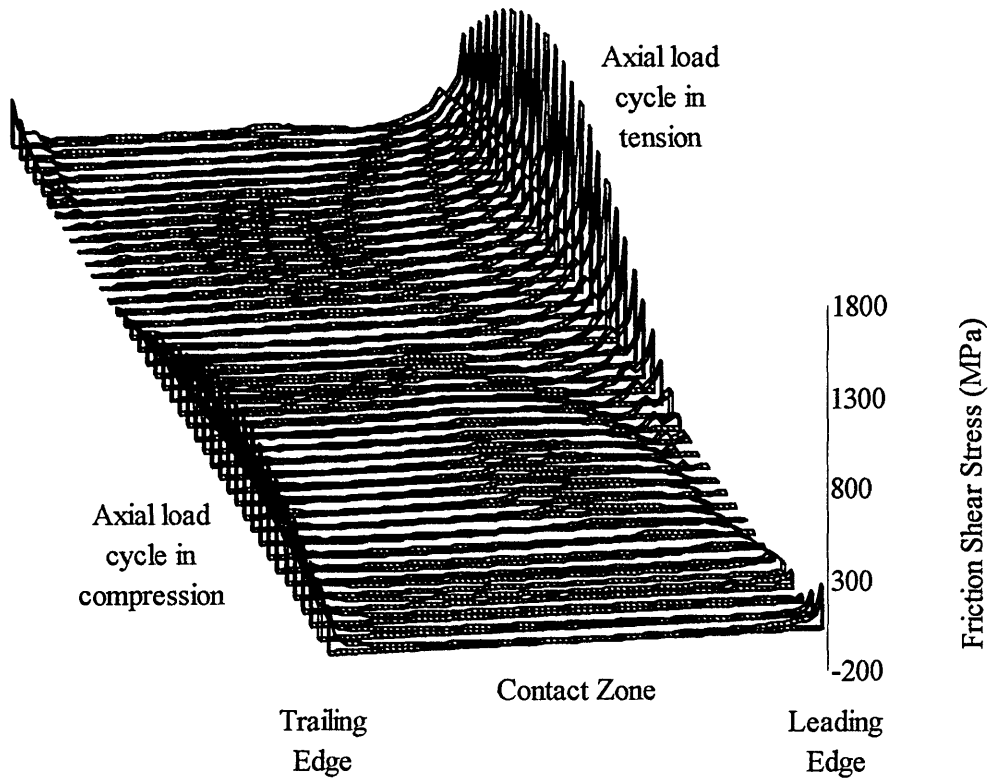
Local Frictional Shear Stress Distribution Over a Single Load Cycle for Test 122



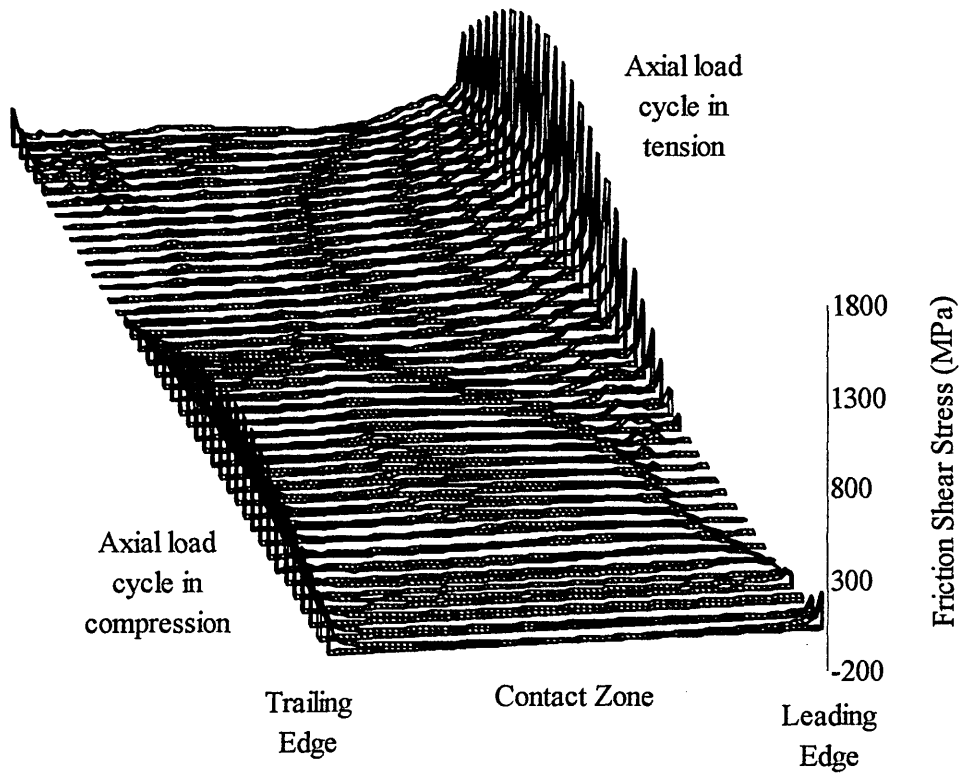
Local Frictional Shear Stress Distribution Over a Single Load Cycle for Test 124



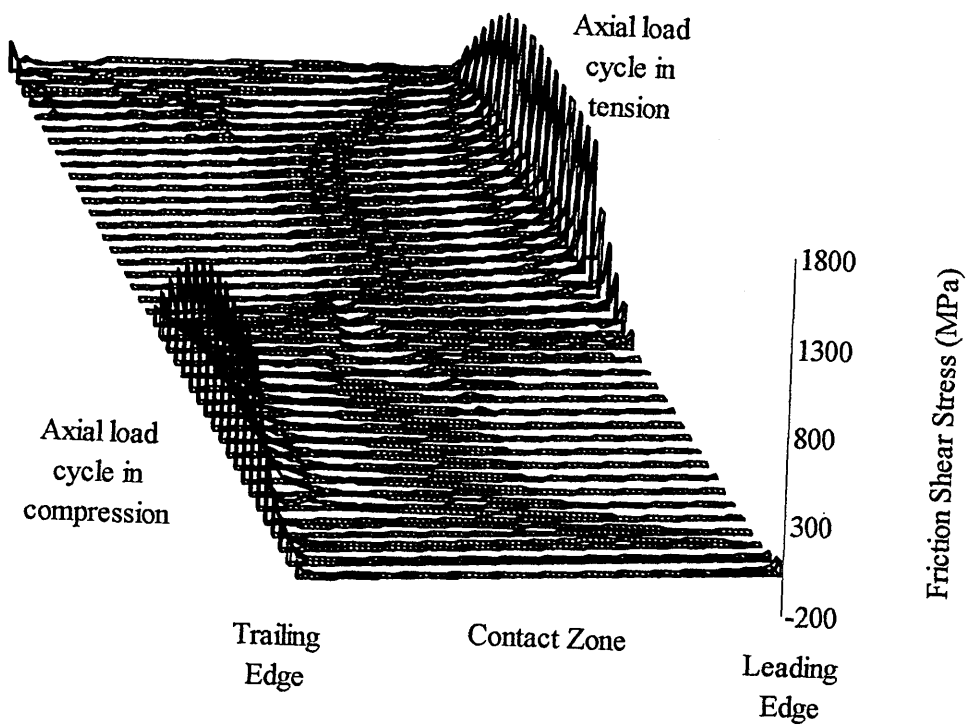
Local Frictional Shear Stress Distribution Over a Single Load Cycle for Test 125



Local Frictional Shear Stress Distribution Over a Single Load Cycle for Test 132

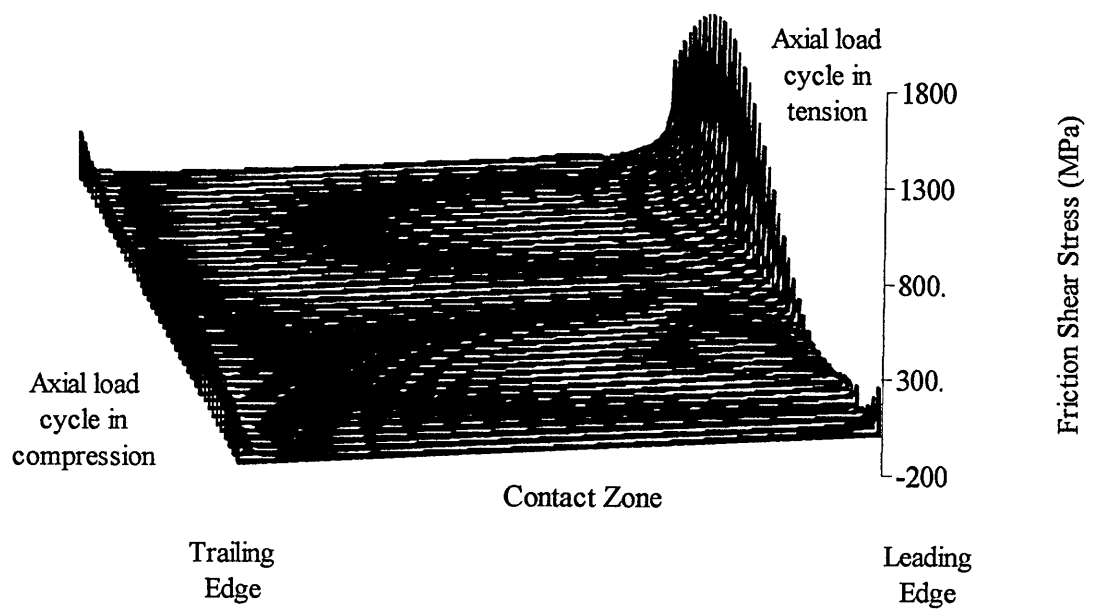


Local Frictional Shear Stress Distribution Over a Single Load Cycle for Test 133

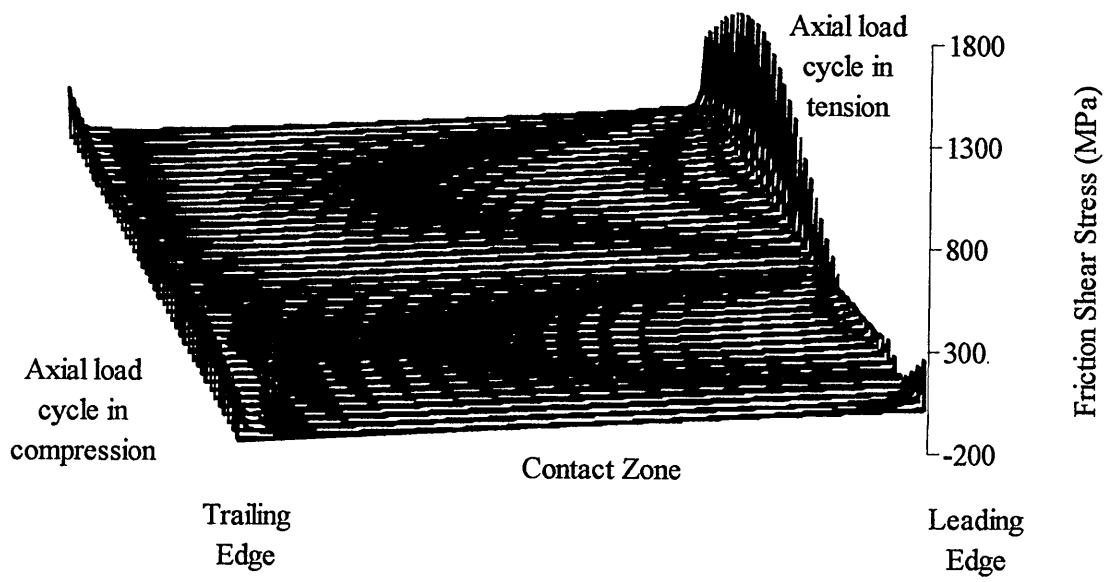


3MM NUMERICAL FRICTION MAPS (800 TEST SERIES)

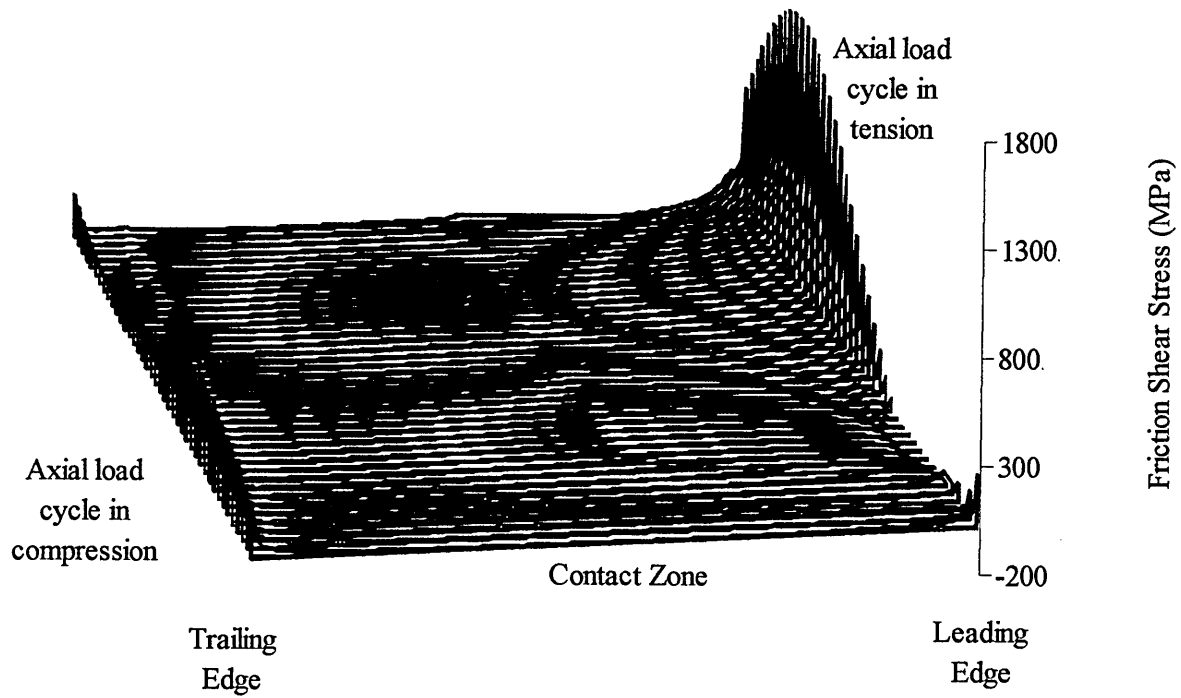
Local Frictional Shear Stress Distribution Over a Single Load Cycle for Test 801



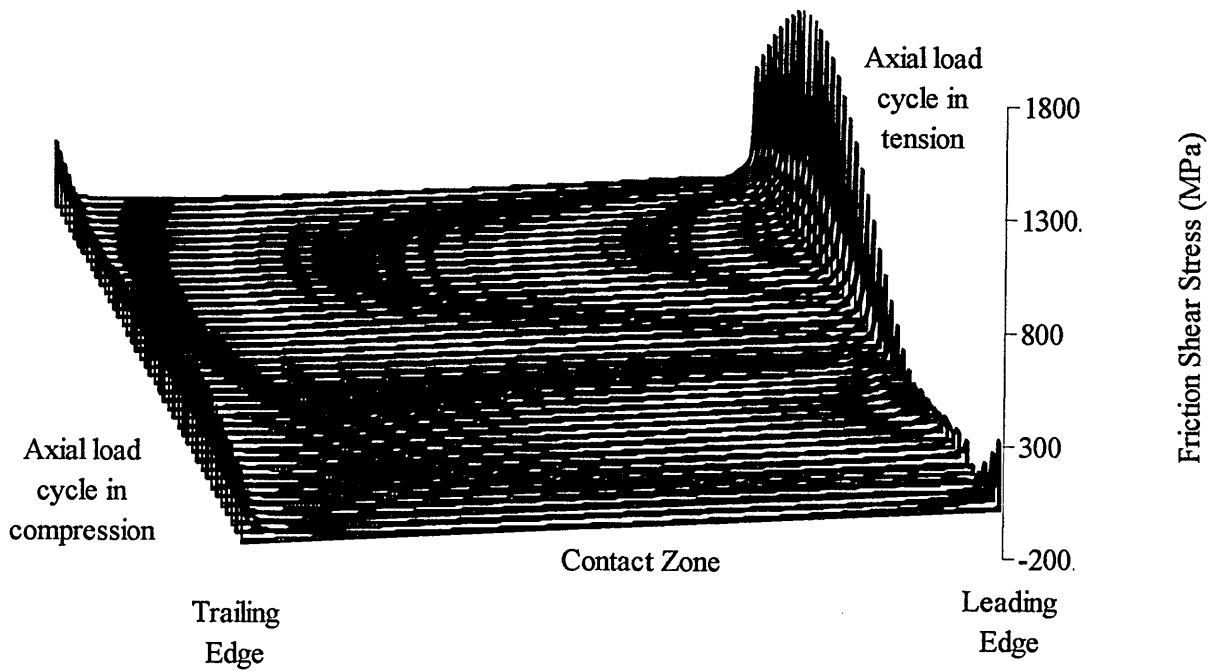
Local Frictional Shear Stress Distribution Over a Single Load Cycle for Test 802



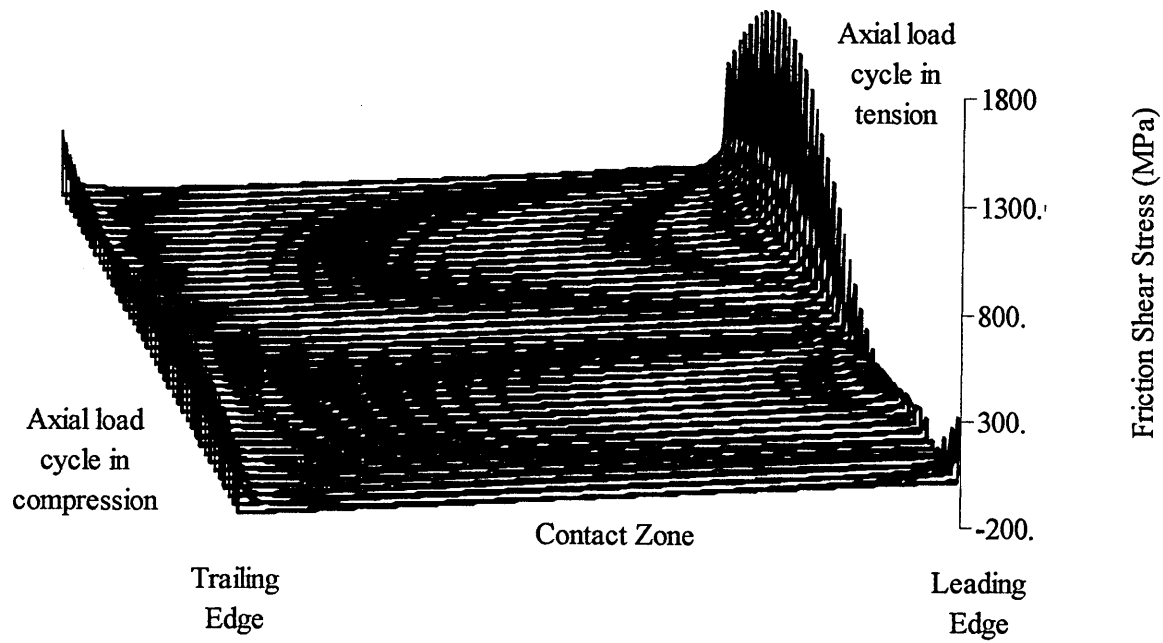
Local Frictional Shear Stress Distribution Over a Single Load Cycle for Test 803



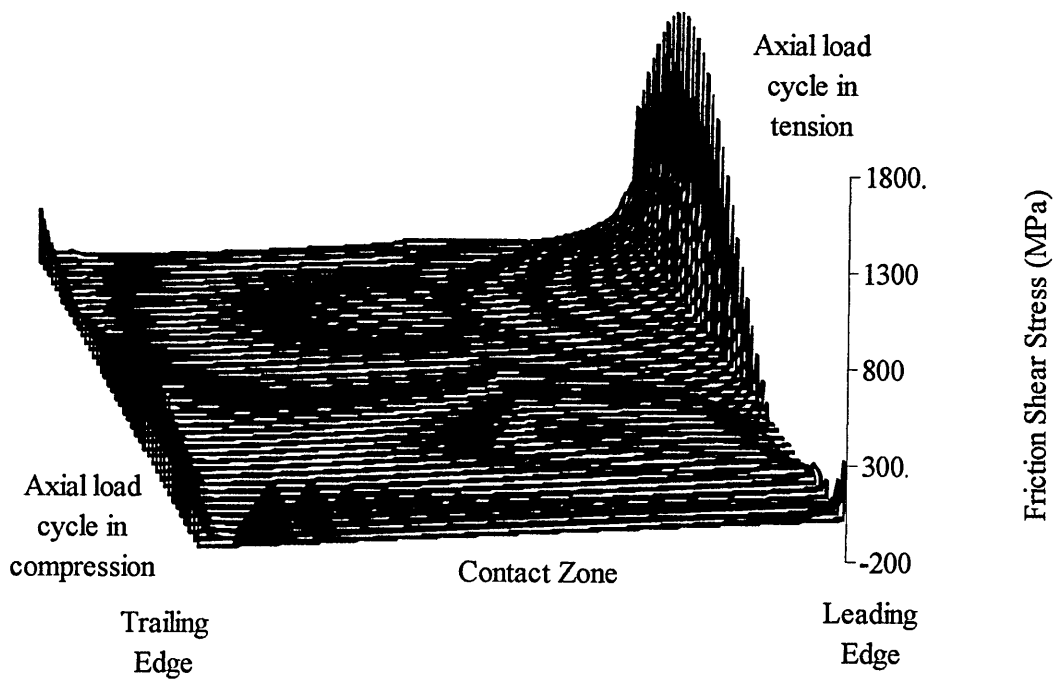
Local Frictional Shear Stress Distribution Over a Single Load Cycle for Test 804



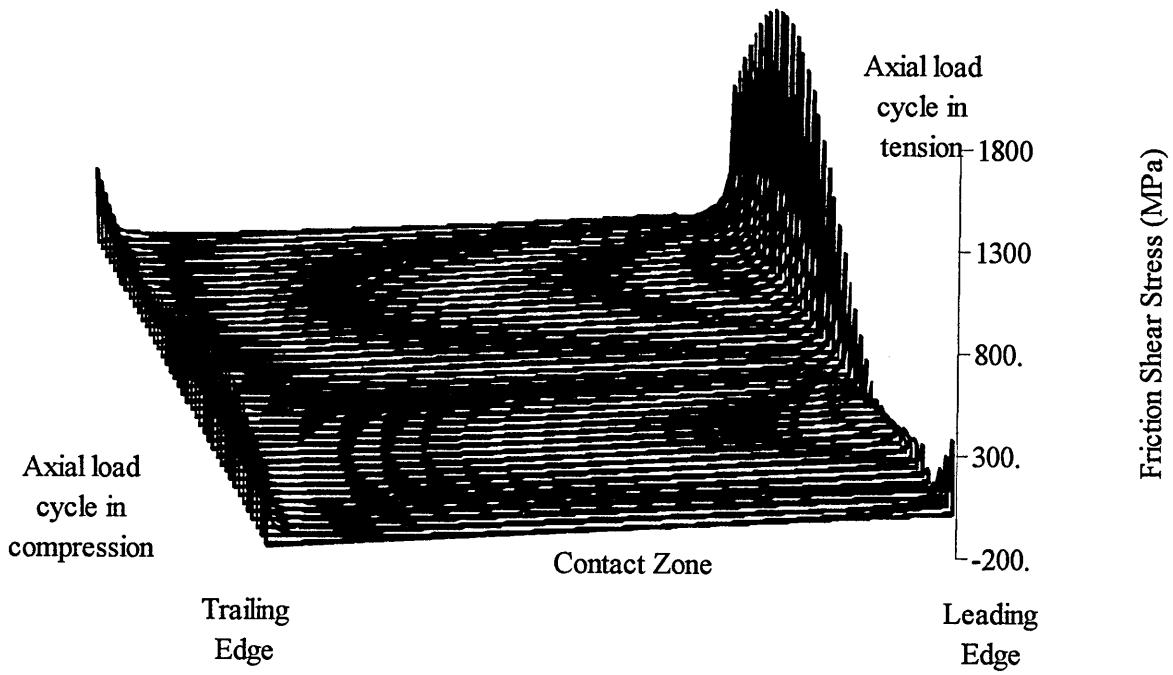
Local Frictional Shear Stress Distribution Over a Single Load Cycle for Test 805



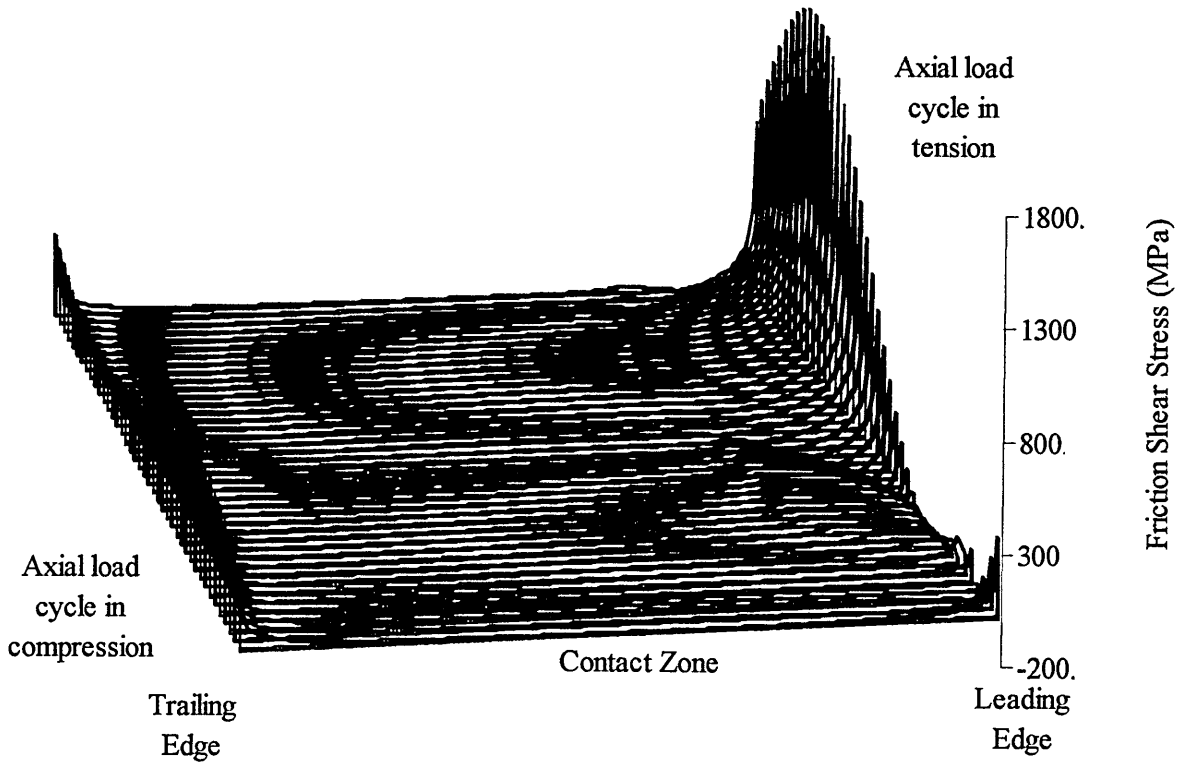
Local Frictional Shear Stress Distribution Over a Single Load Cycle for Test 806



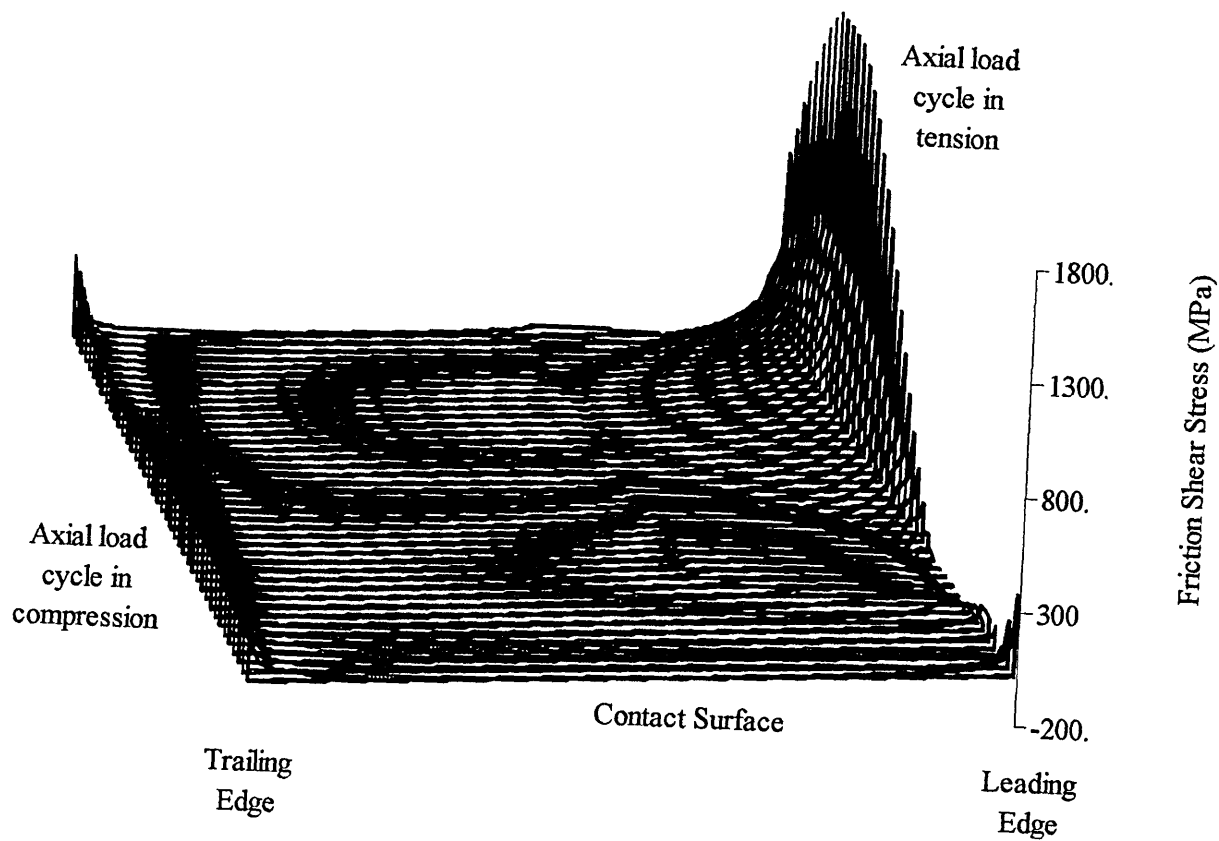
Local Frictional Shear Stress Distribution Over a Single Load Cycle for Test 807



Local Frictional Shear Stress Distribution Over a Single Load Cycle for Test 808

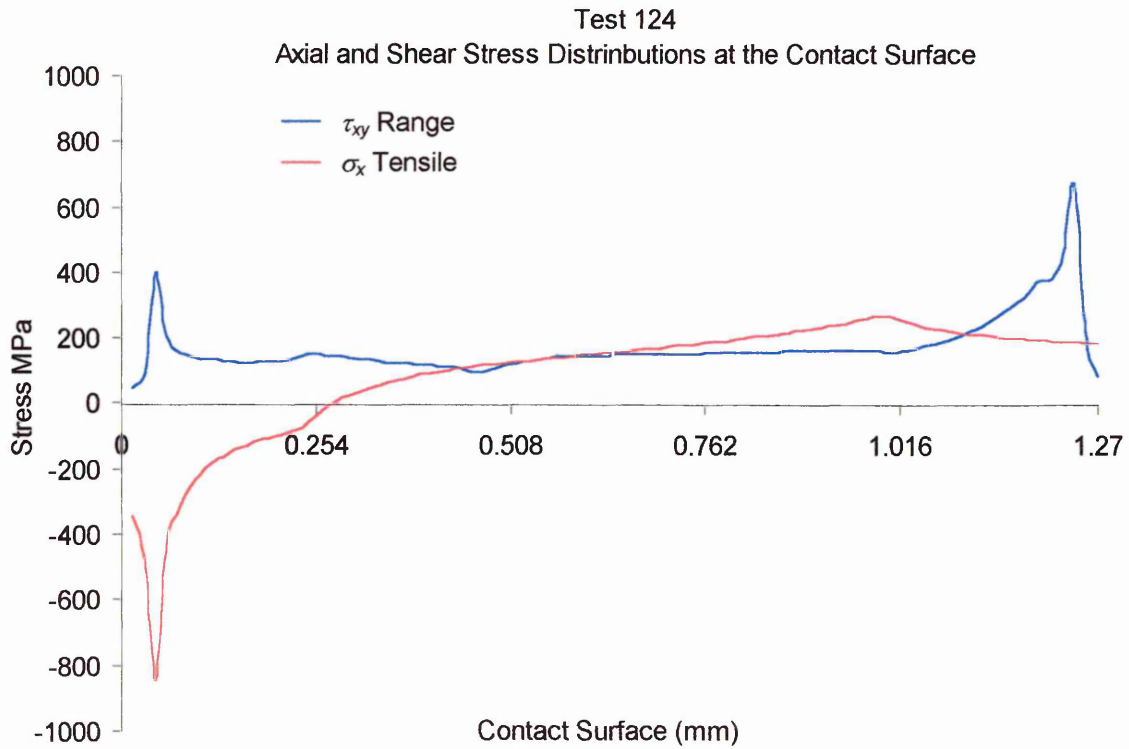
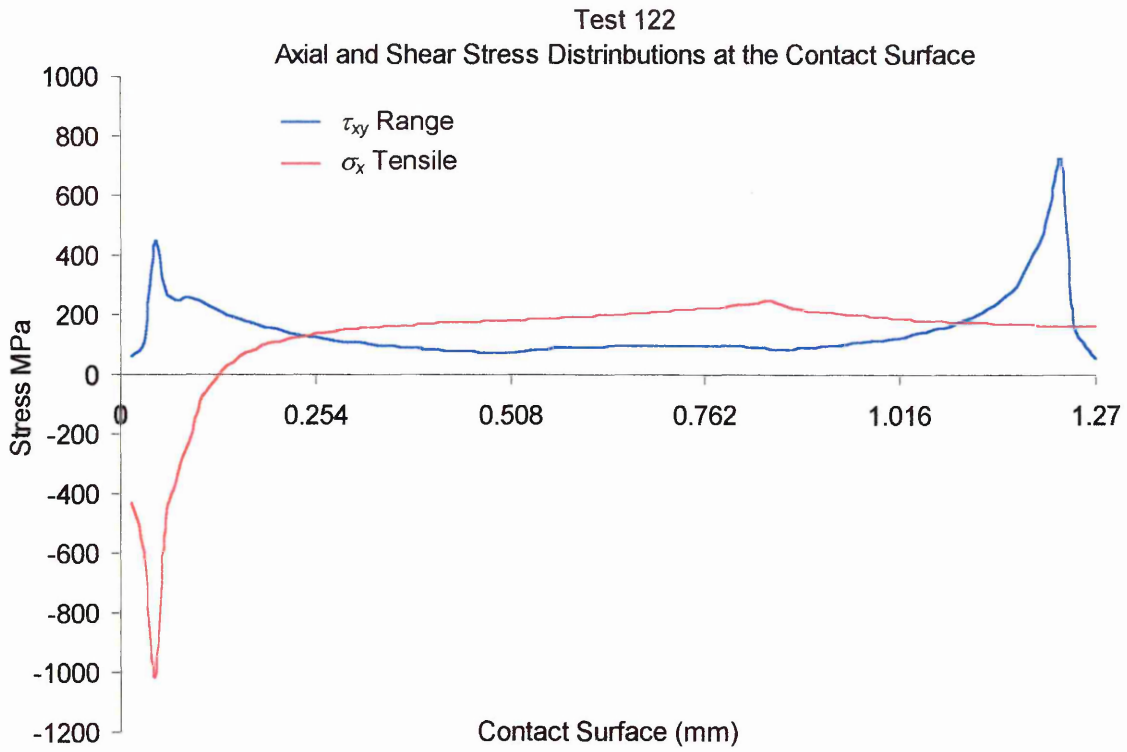


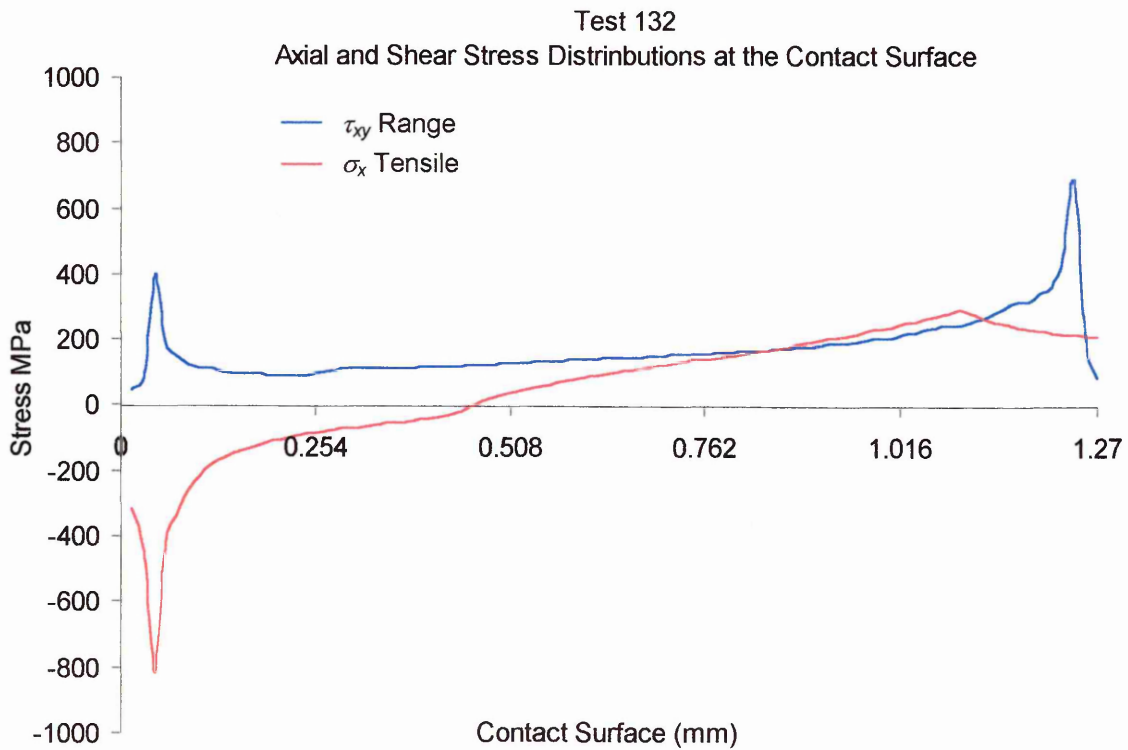
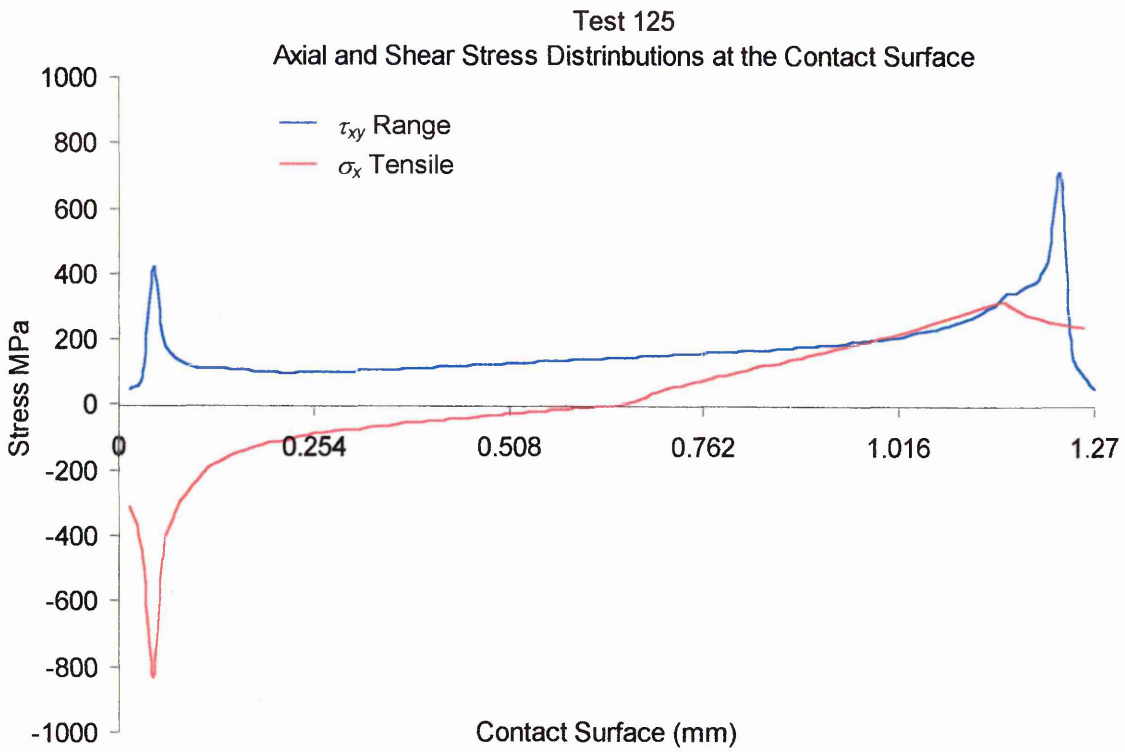
Local Frictional Shear Stress Distribution Over a Single Load Cycle for Test 809



APPENDIX F

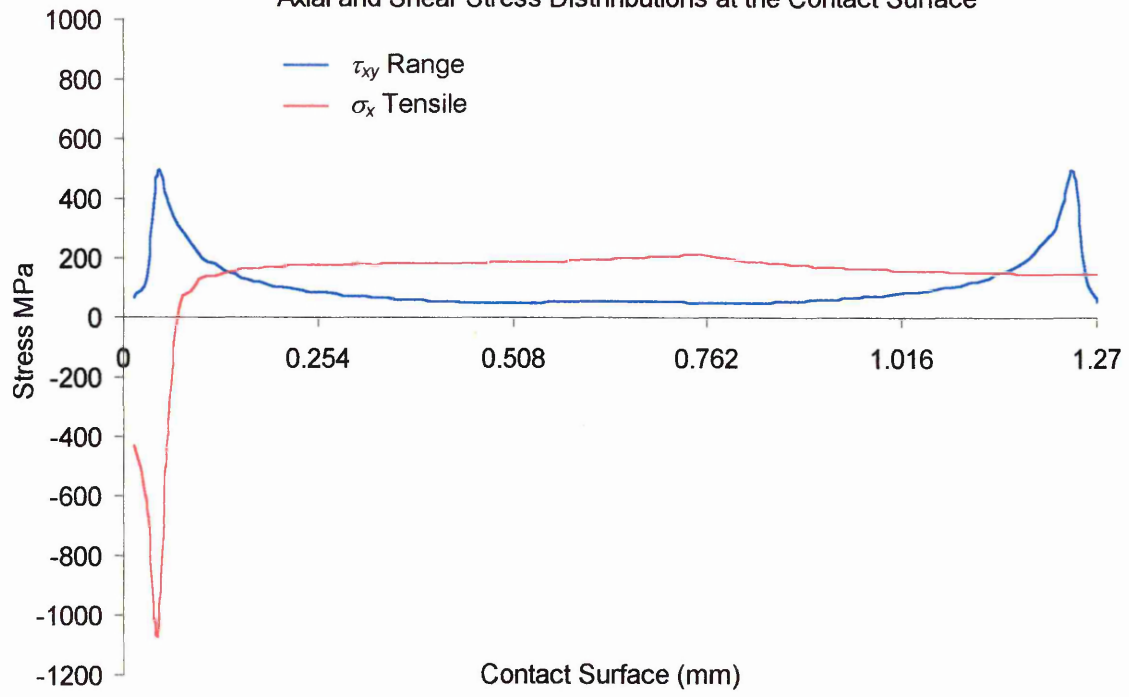
AXIAL AND SHEAR STRESS DISTRIBUTIONS AT THE CONTACT SURFACE



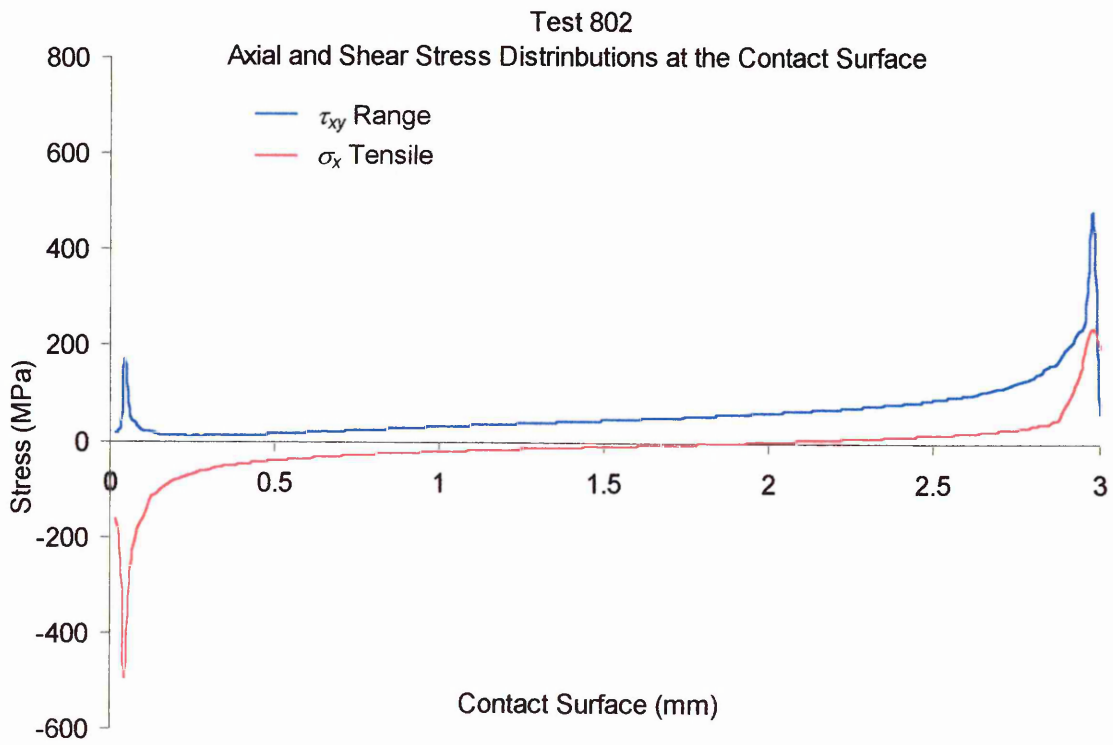
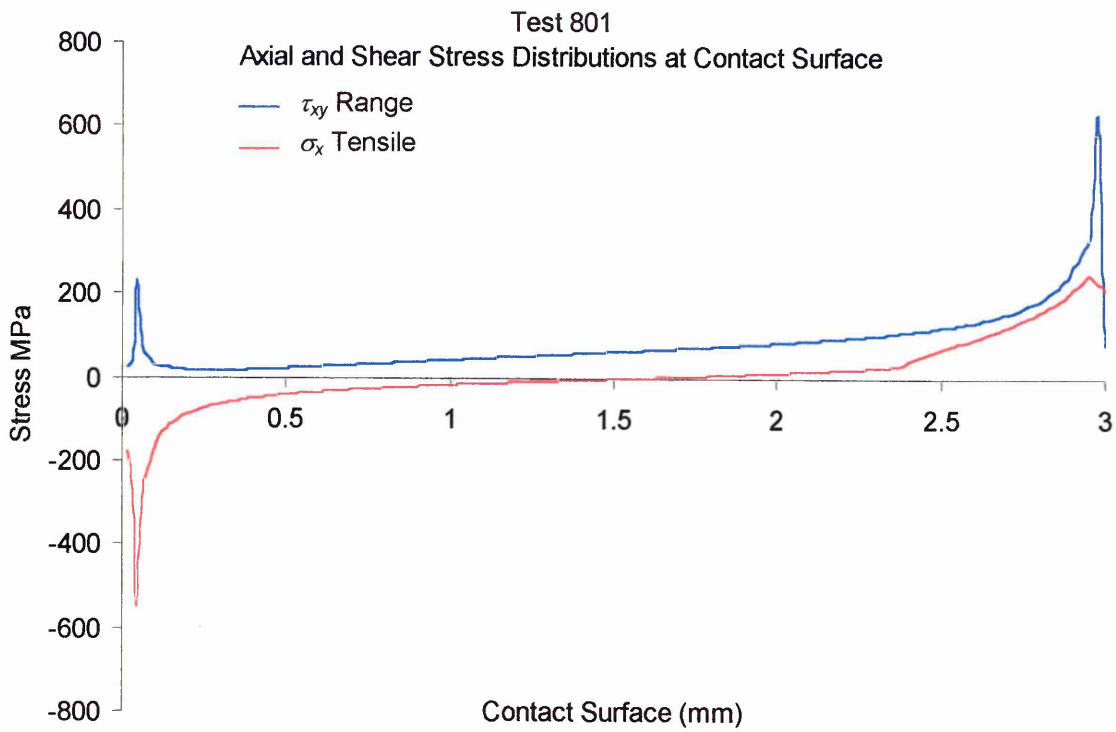


Test 133

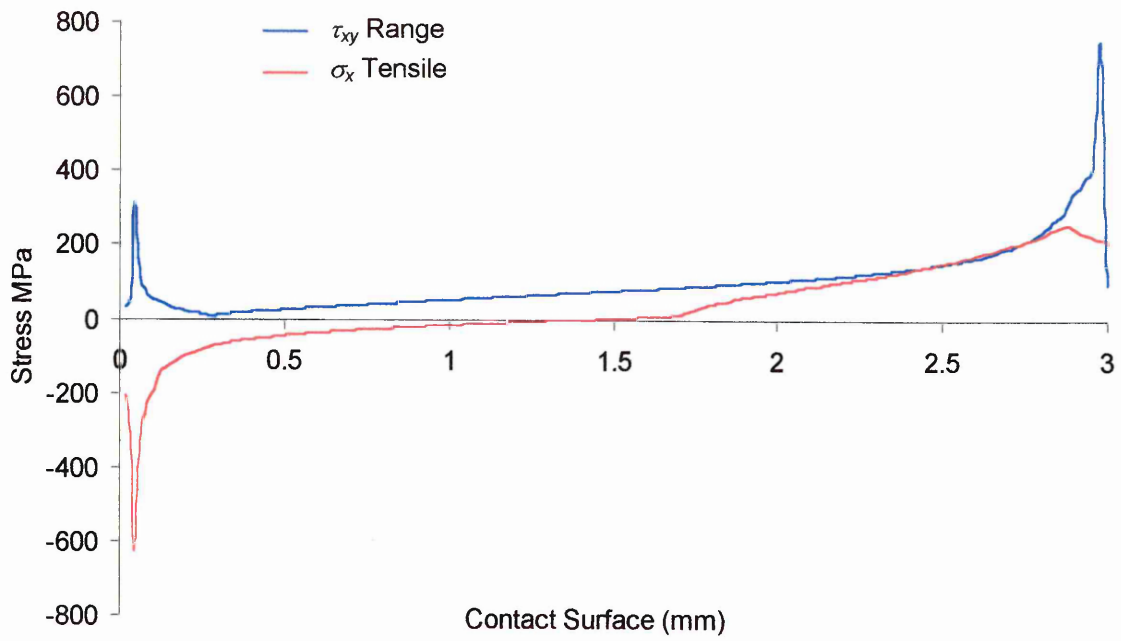
Axial and Shear Stress Distributions at the Contact Surface



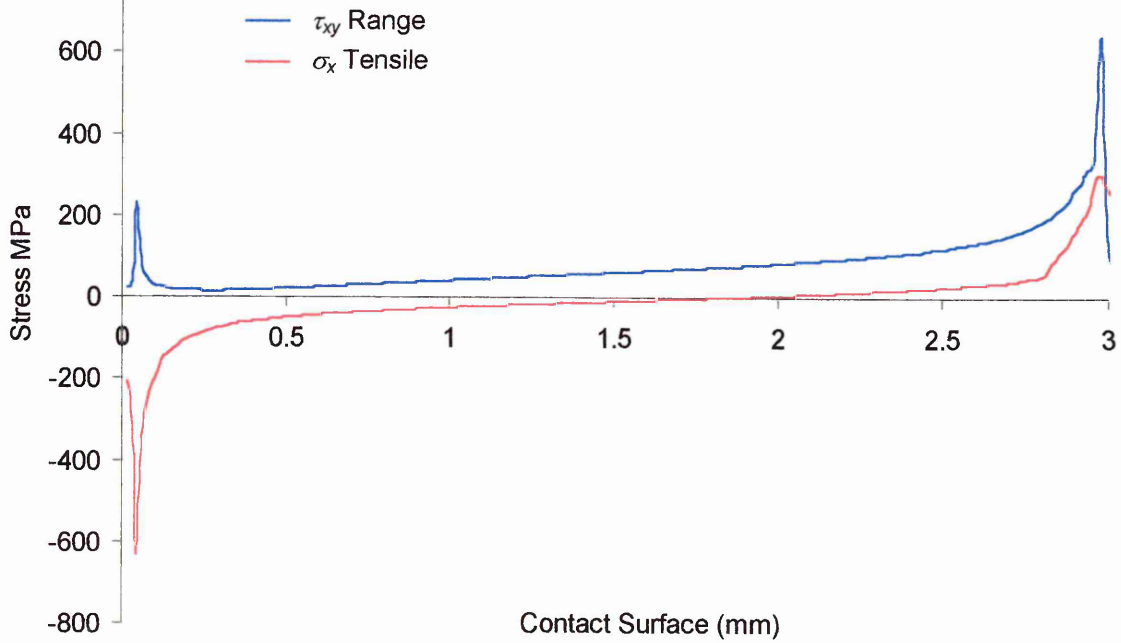
3MM CONTACT PAD SIZE RESULTS (800 TEST SERIES)

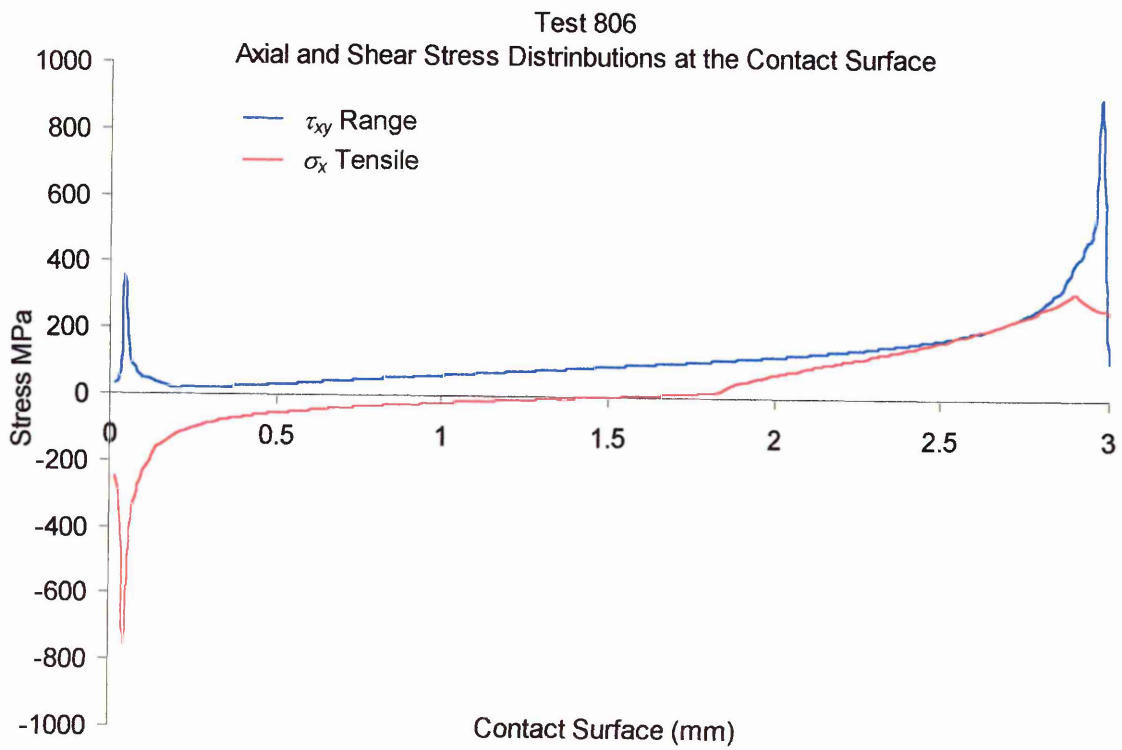
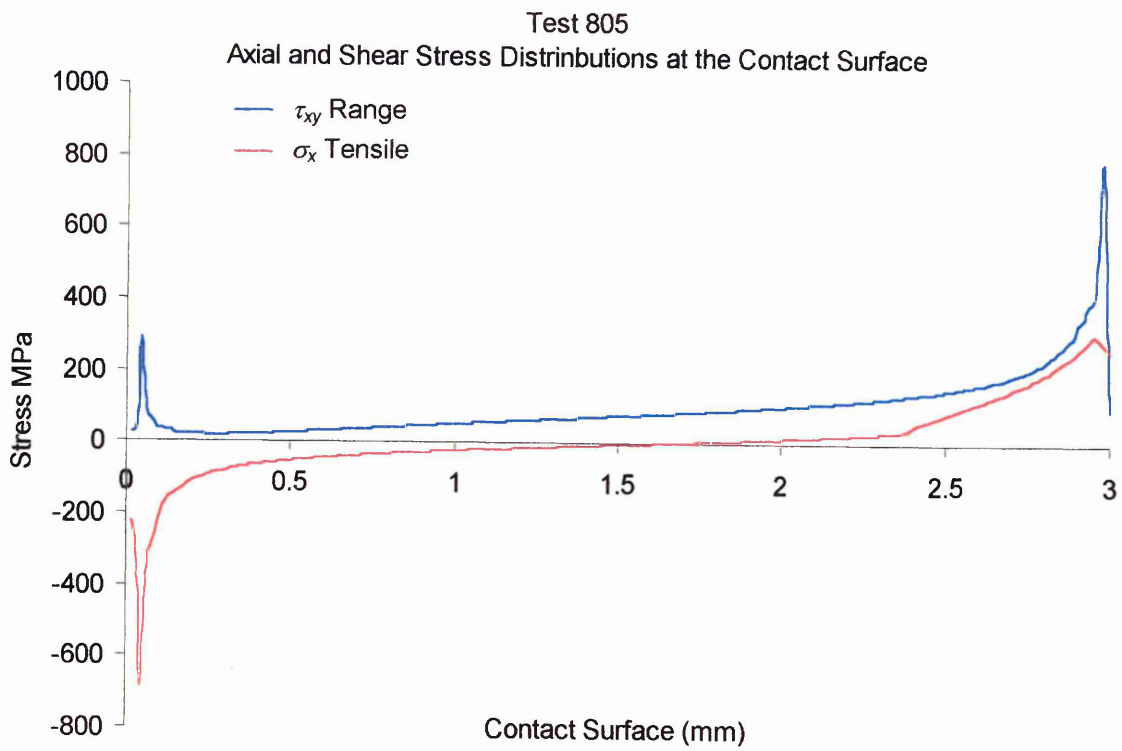


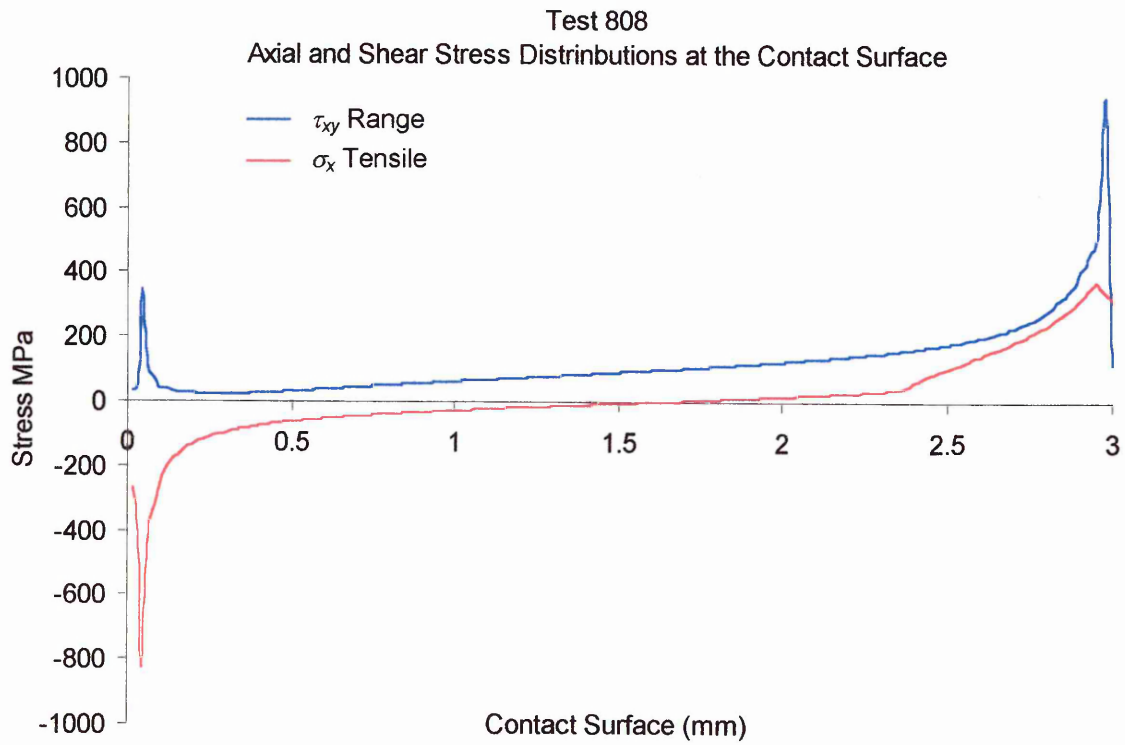
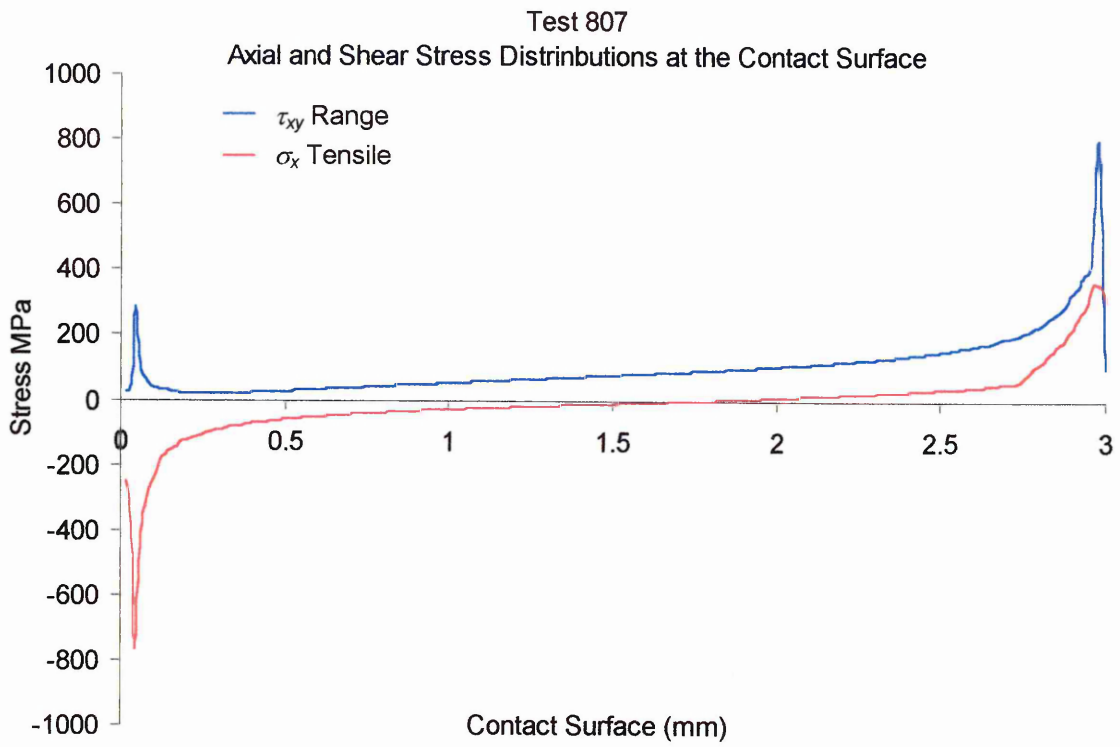
Test 803
Axial and Shear Stress Distributions at the Contact Surface



Test 804
Axial and Shear Stress Distributions at the Contact Surface

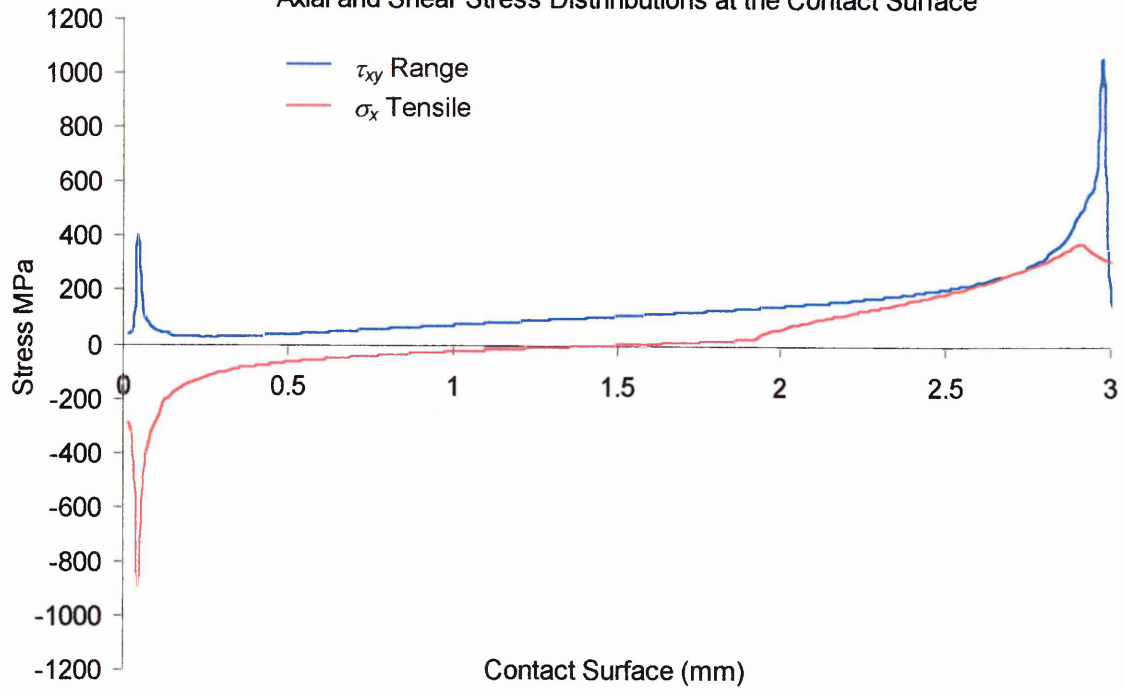






Test 809

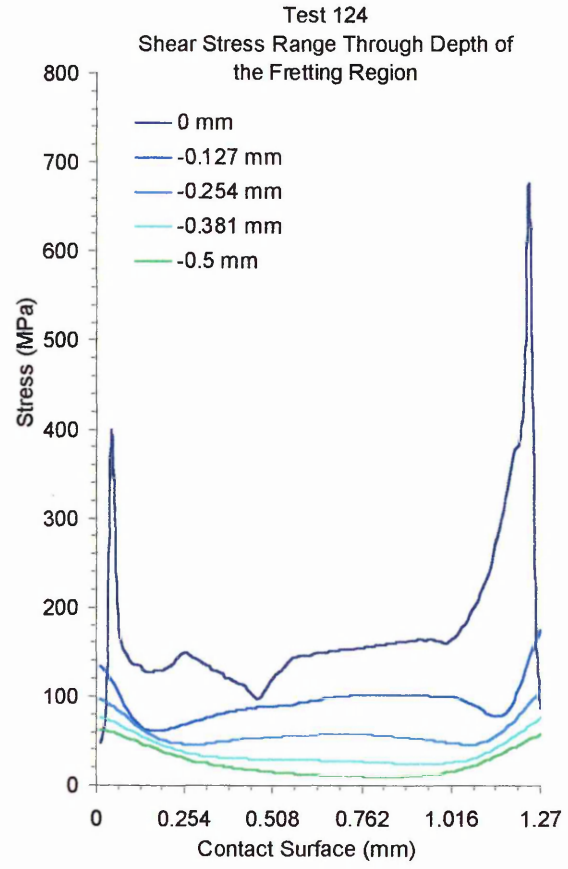
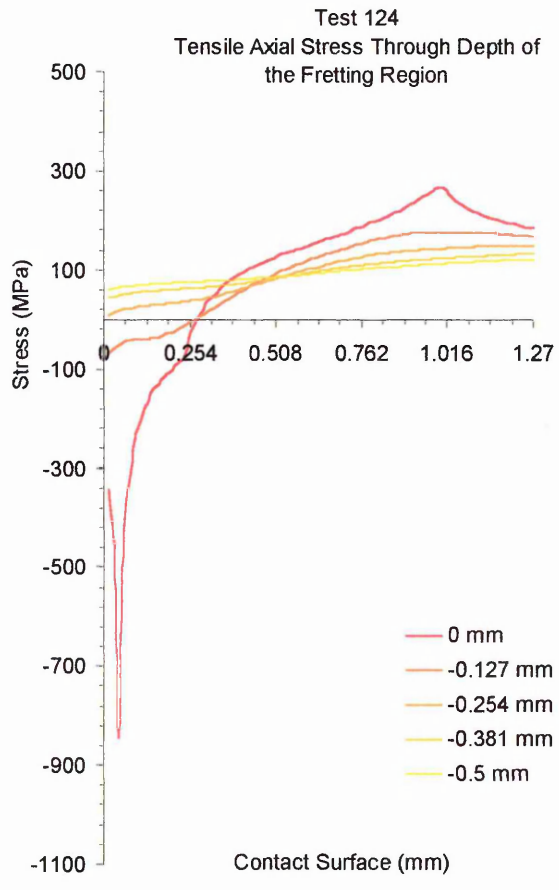
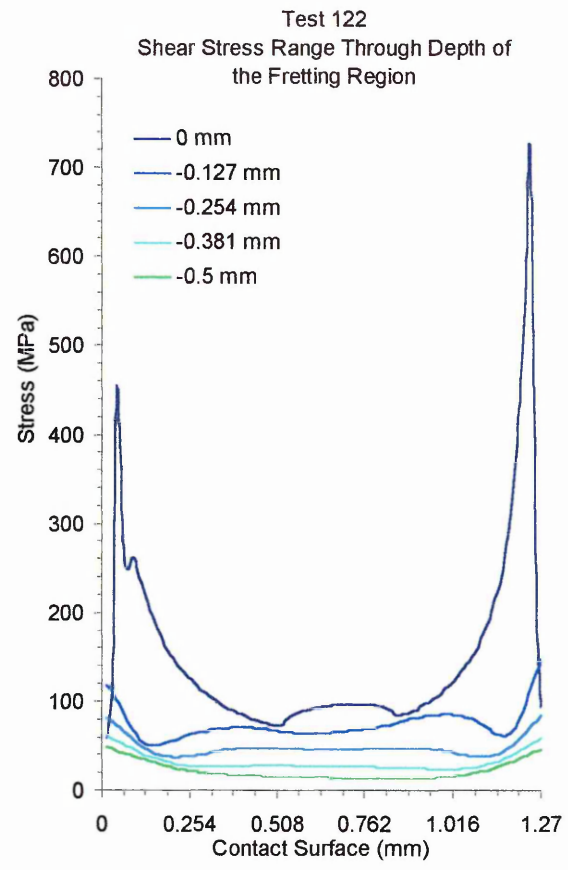
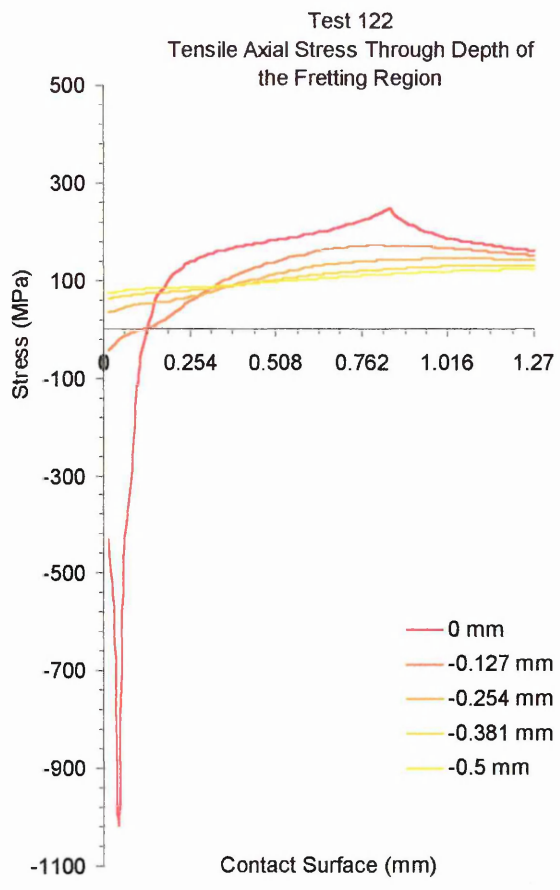
Axial and Shear Stress Distributions at the Contact Surface

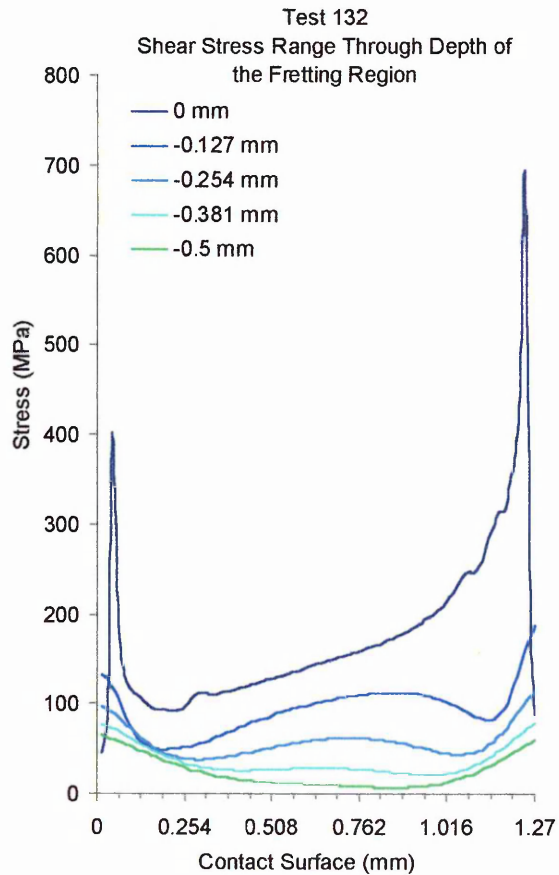
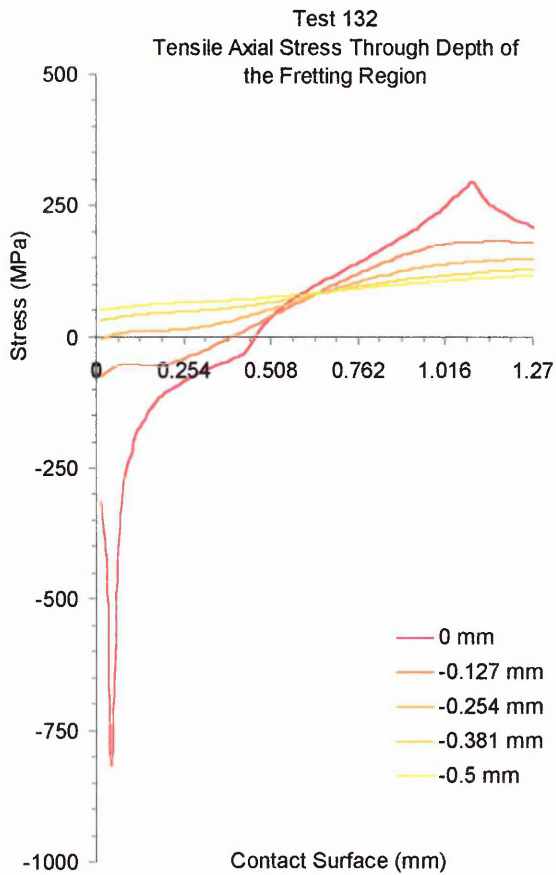
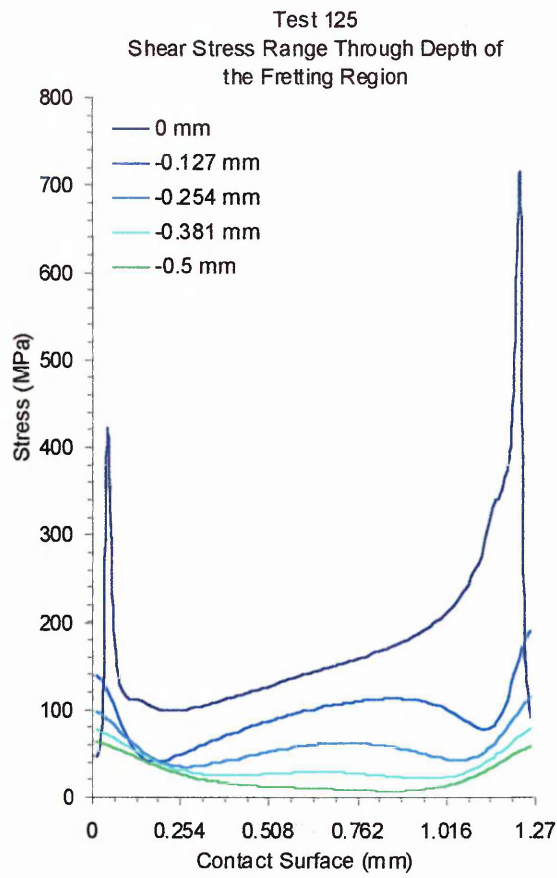
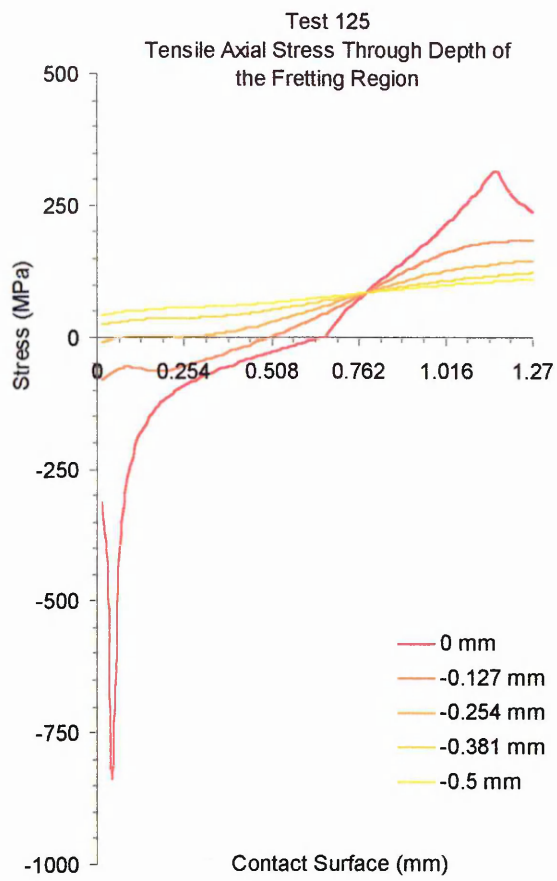


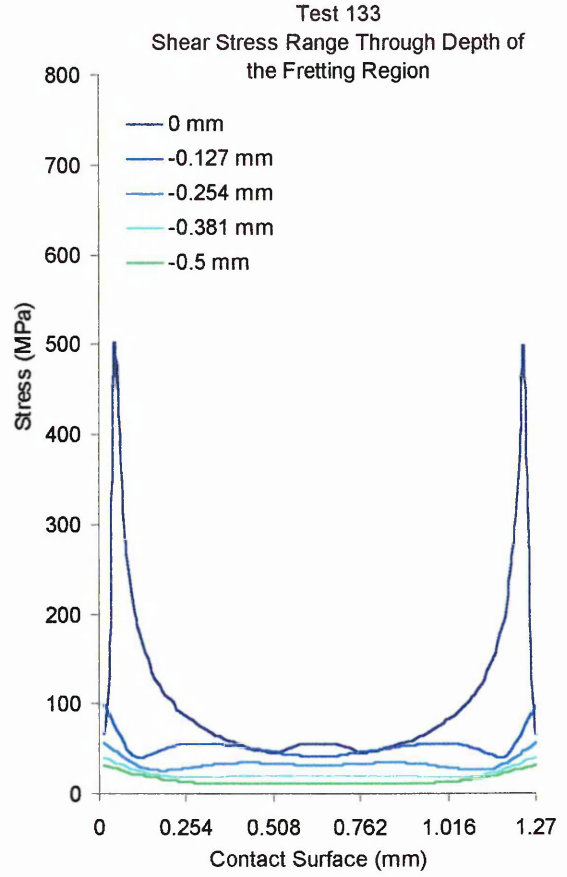
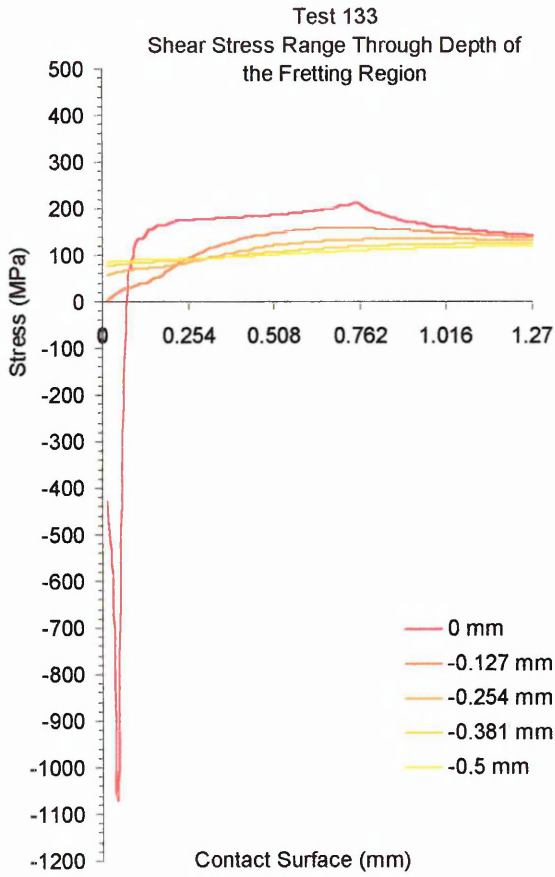
APPENDIX G

AXIAL AND SHEAR SUB SURFACE STRESS

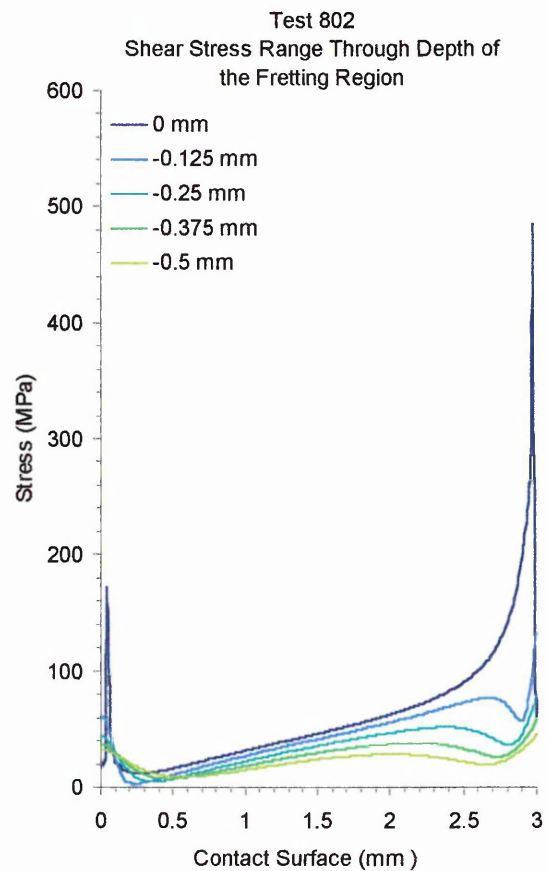
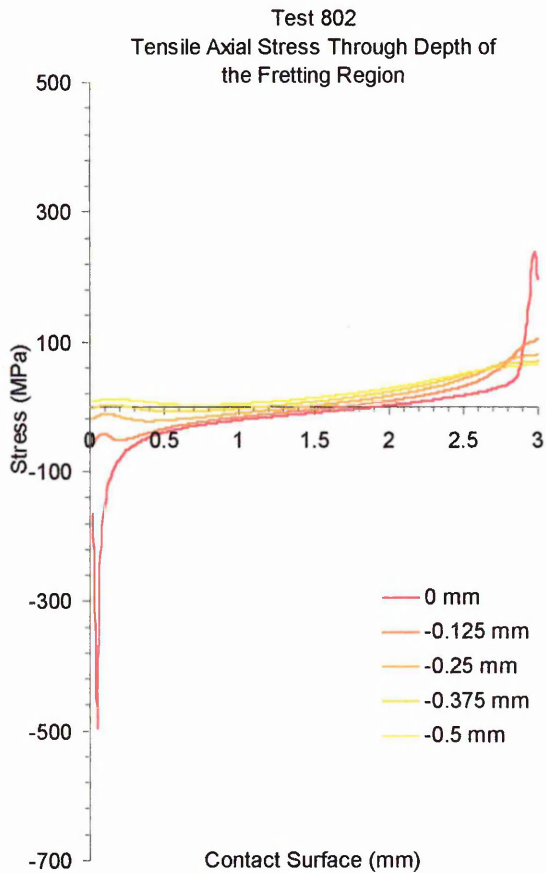
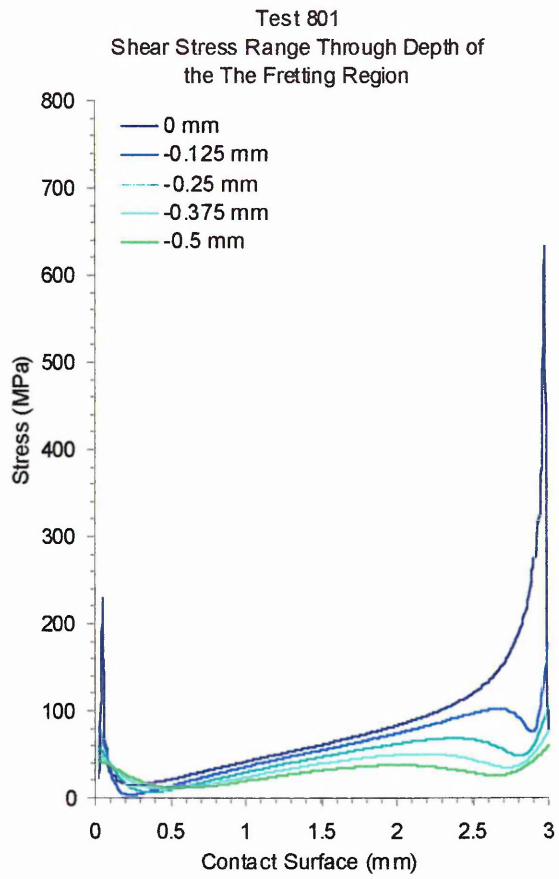
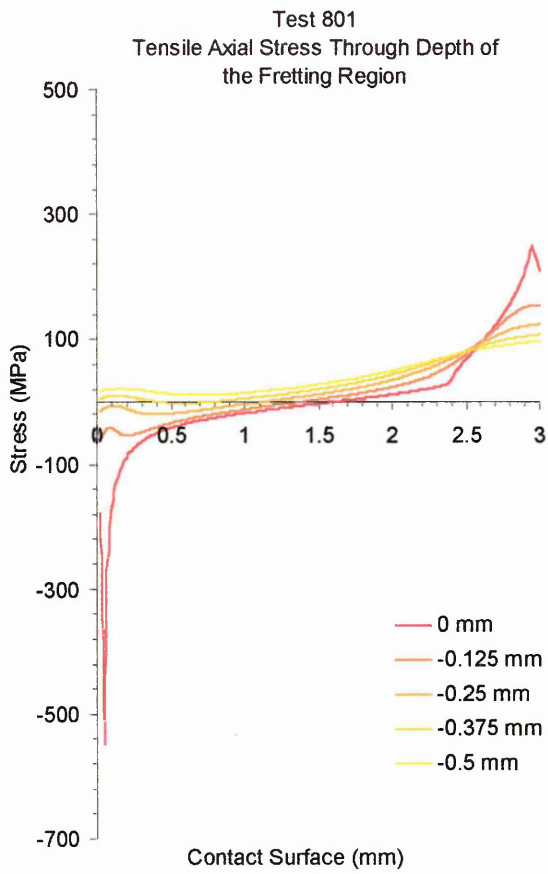
DISTRIBUTIONS THROUGH THE FRETTING REGION

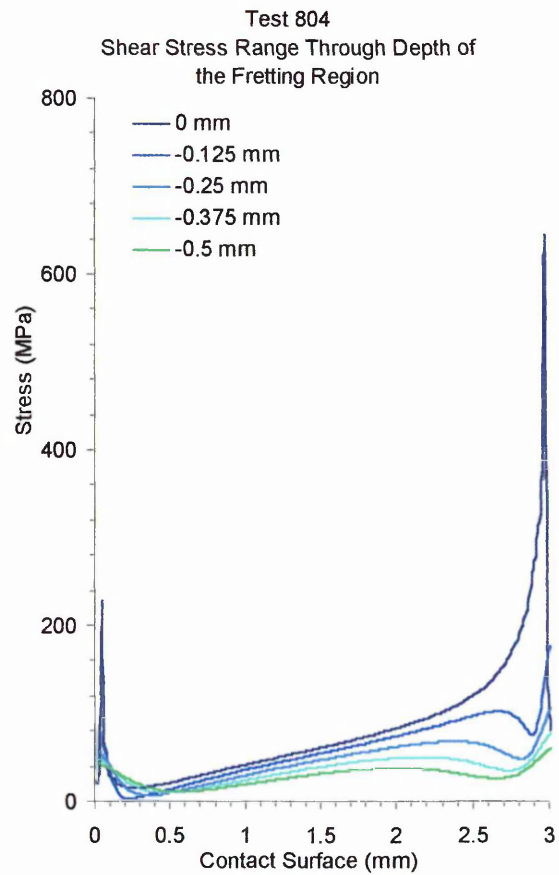
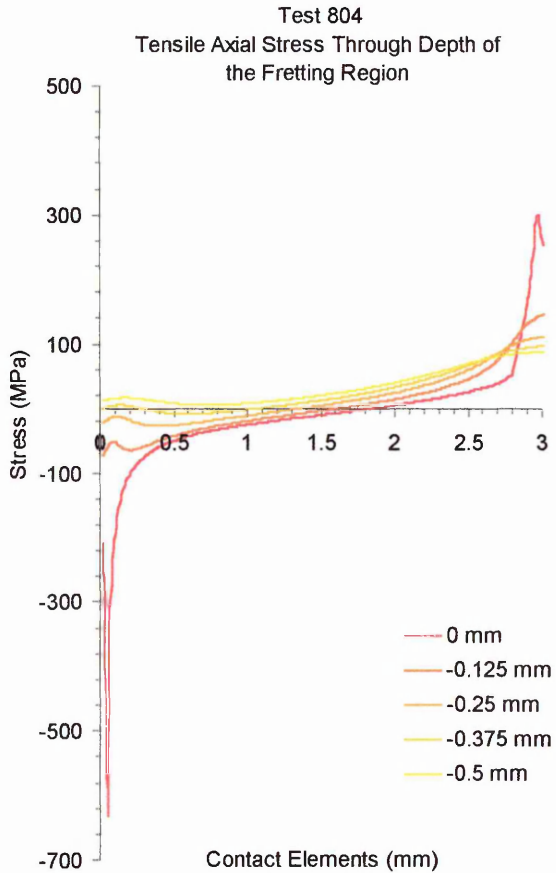
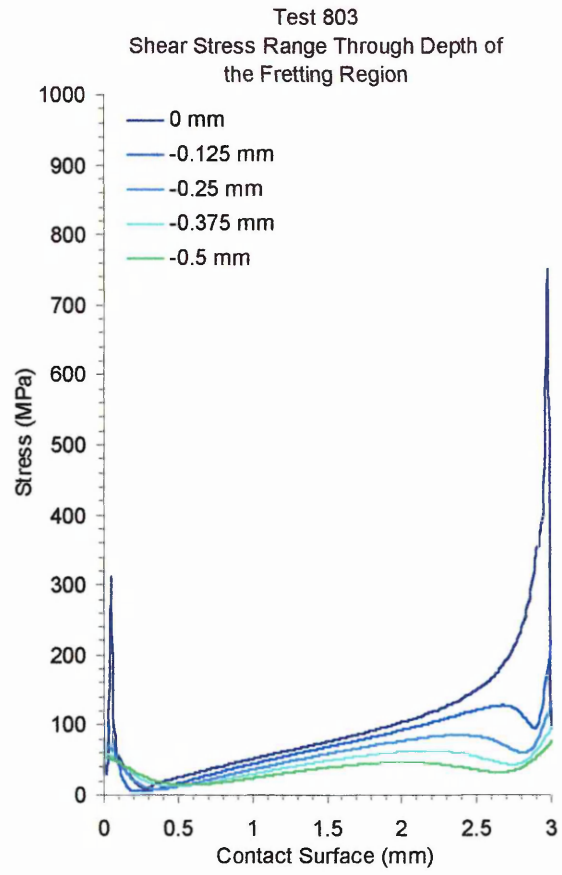
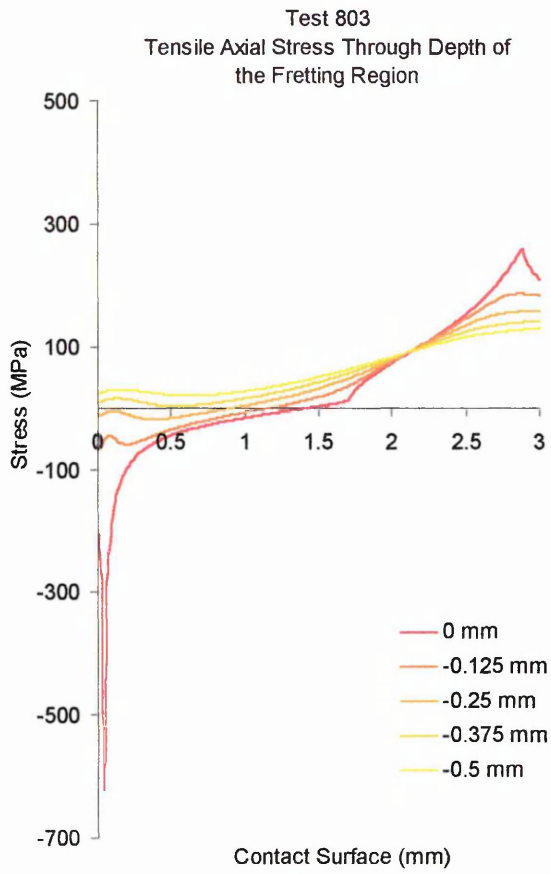


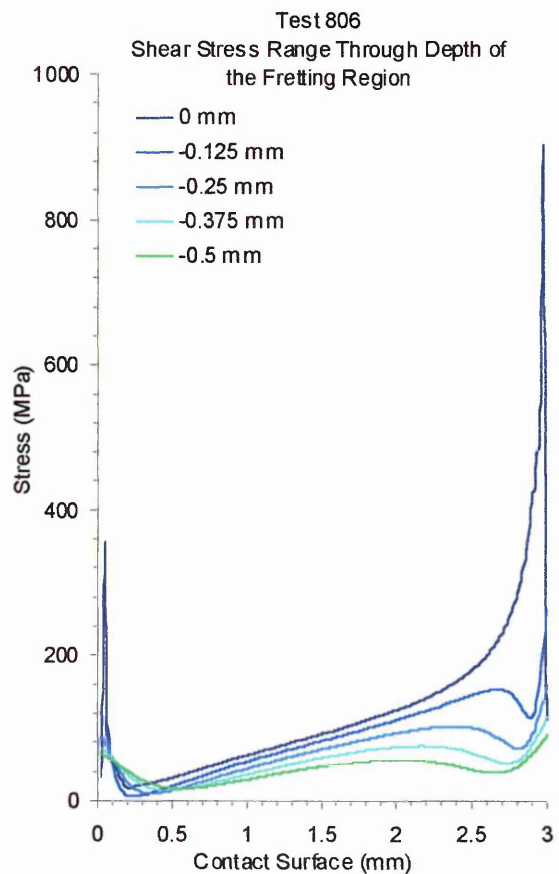
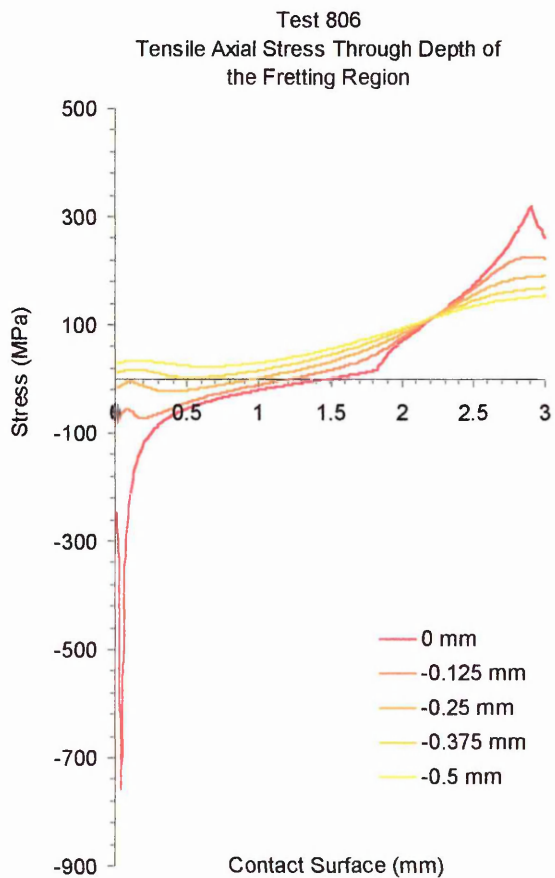
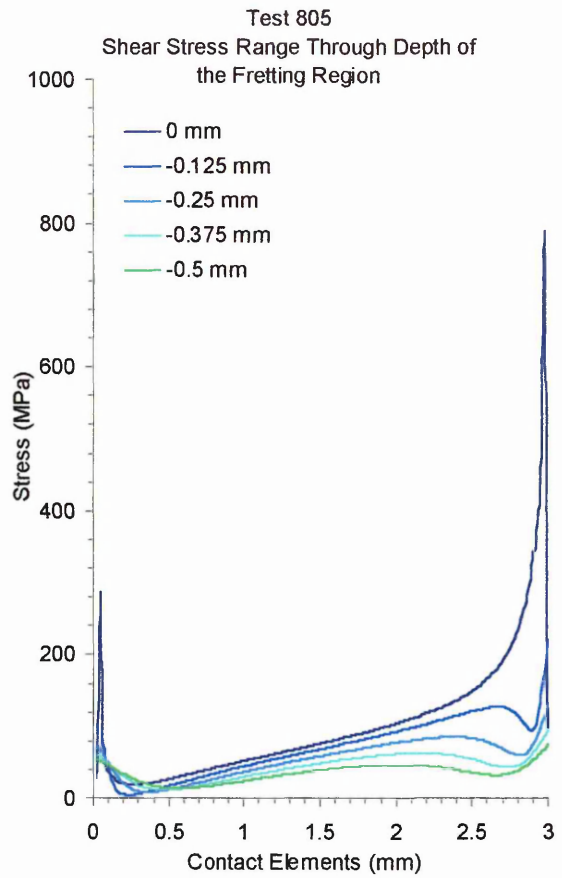
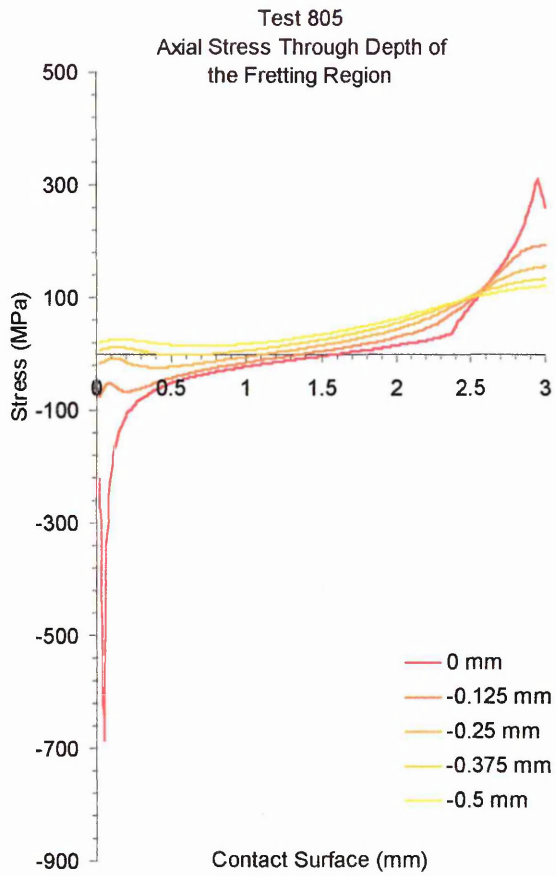


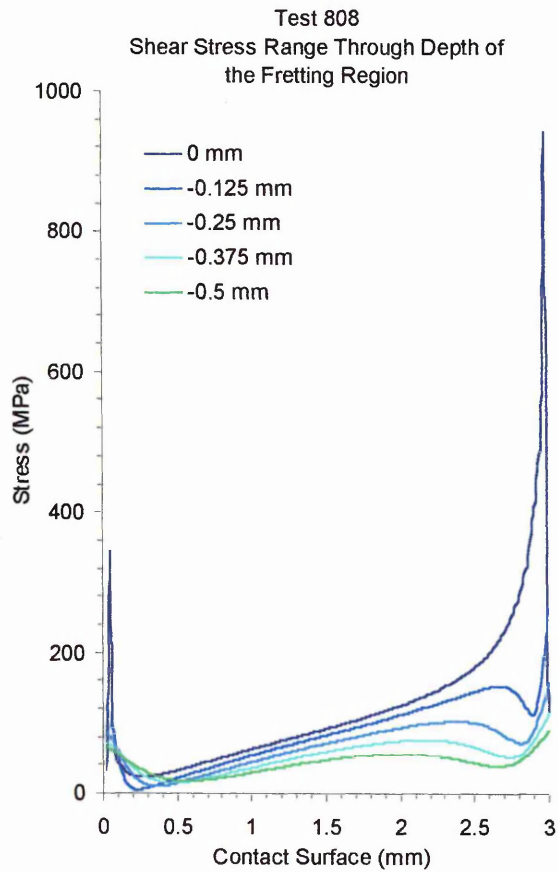
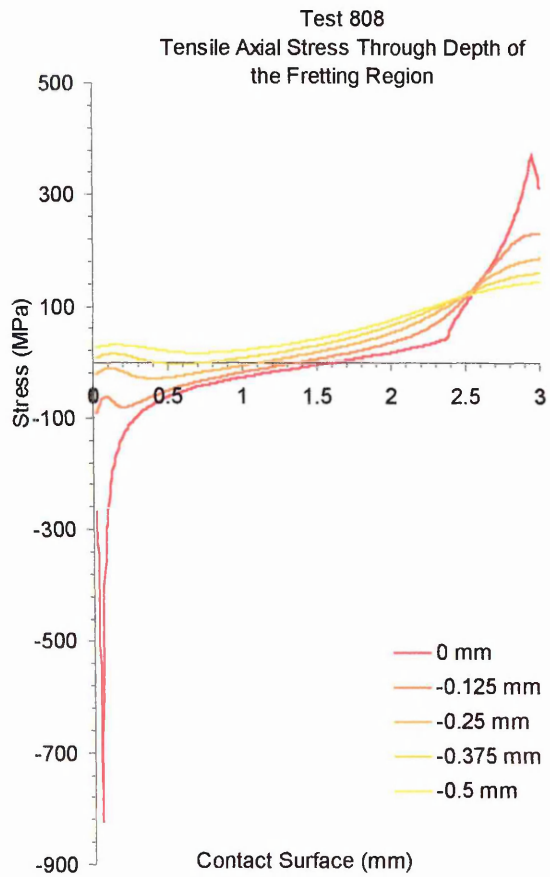
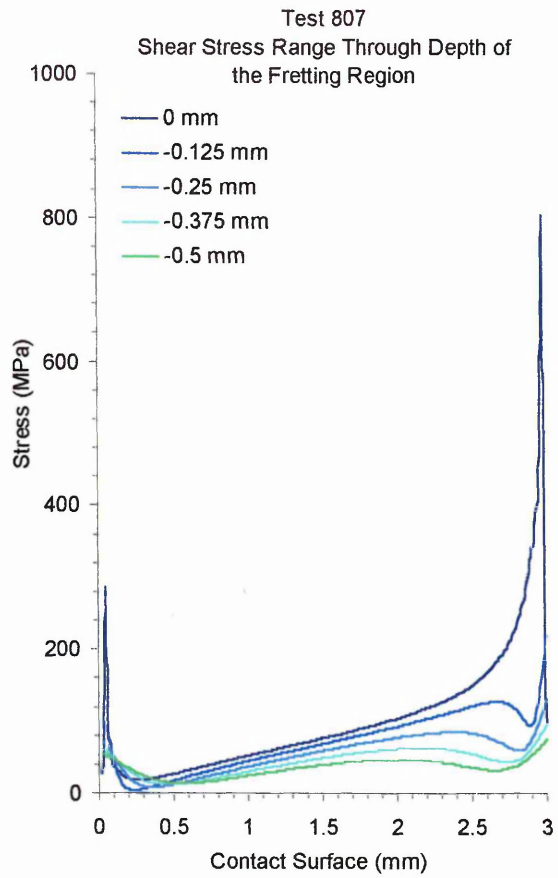
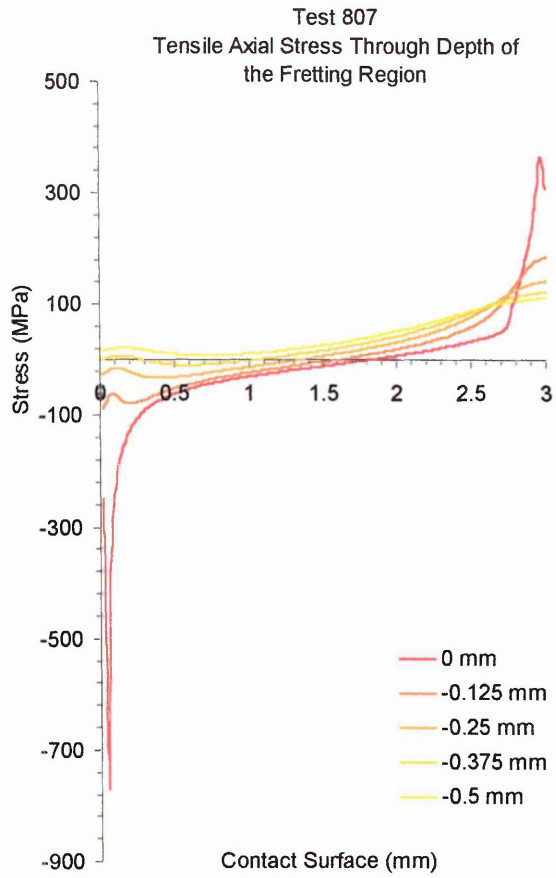


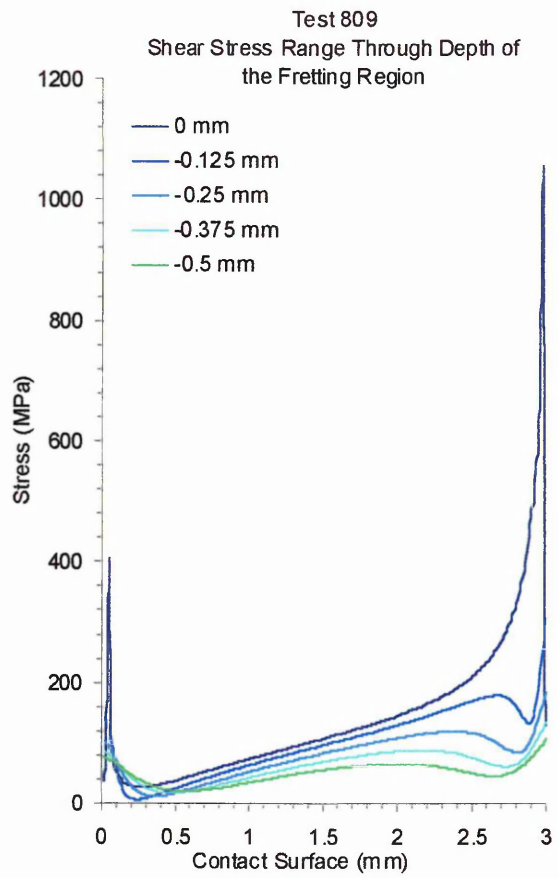
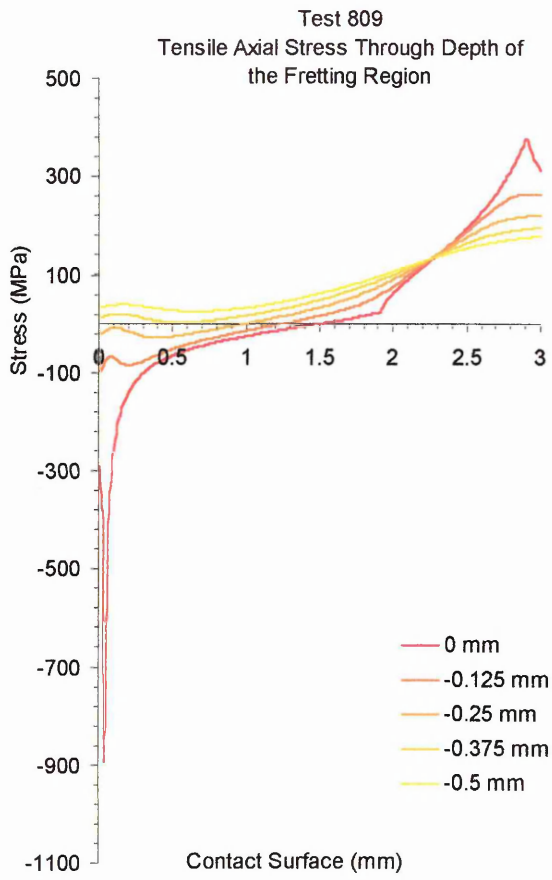
3 MM CONTACT PAD SIZE RESULTS (800 TEST SERIES)





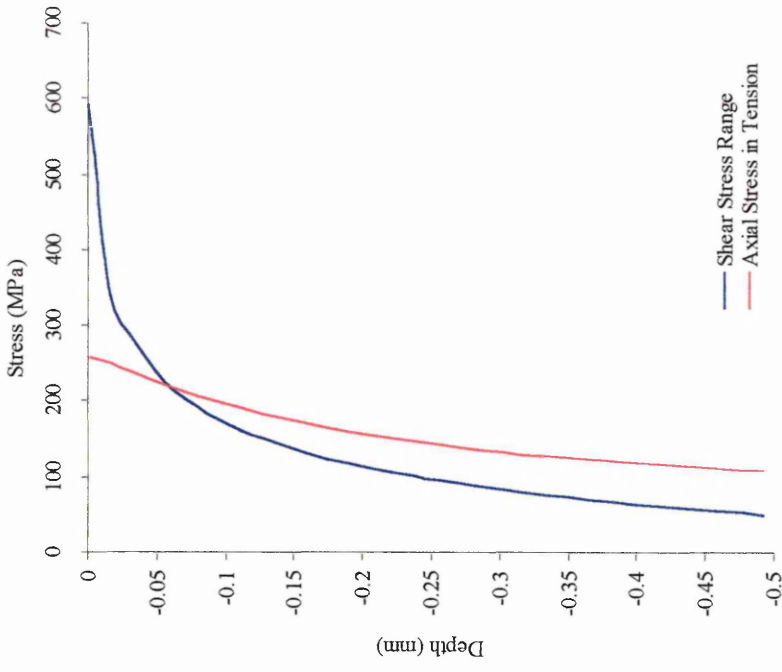




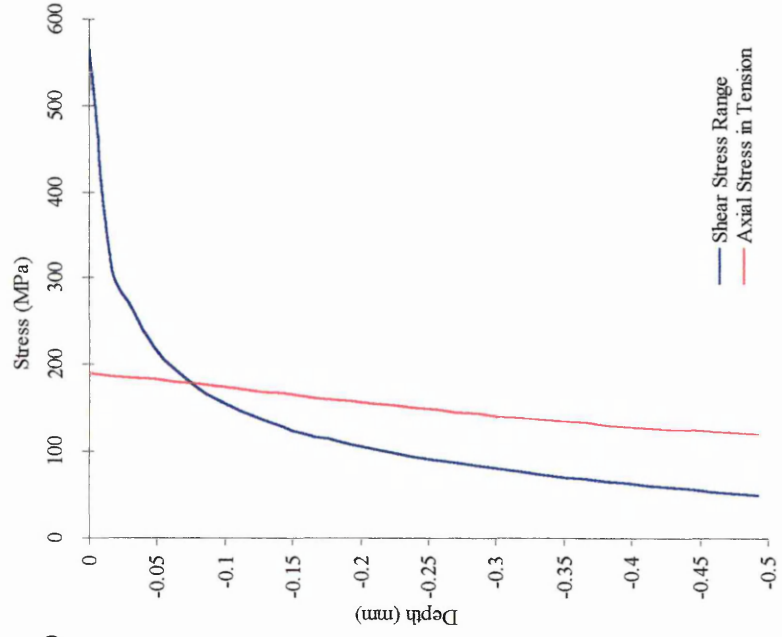


APPENDIX H

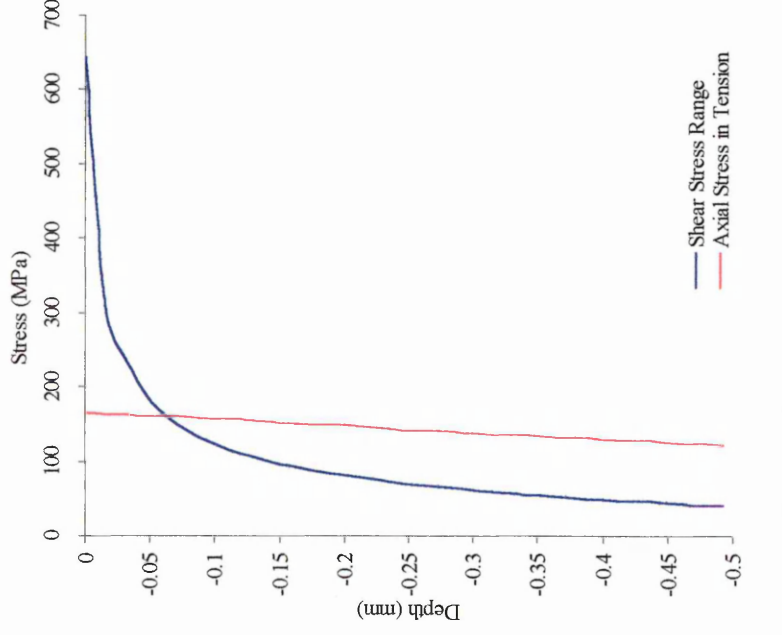
AXIAL AND SHEAR STRESS VARIATIONS THROUGH THE DEPTH OF THE FRETTING REGION AT THE CRITICAL LOCATION



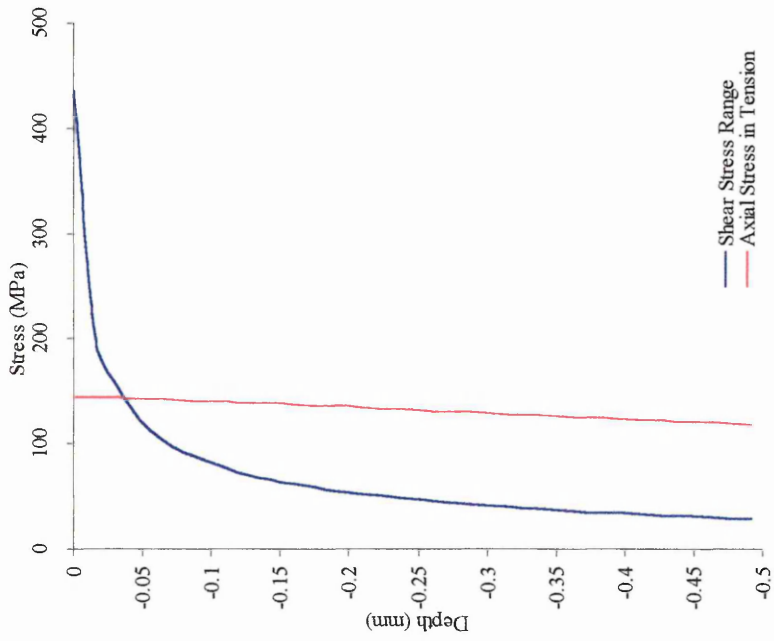
Test 125 Axial and Shear Stresses Through the Depth of the Fretting Region at the Critical Location



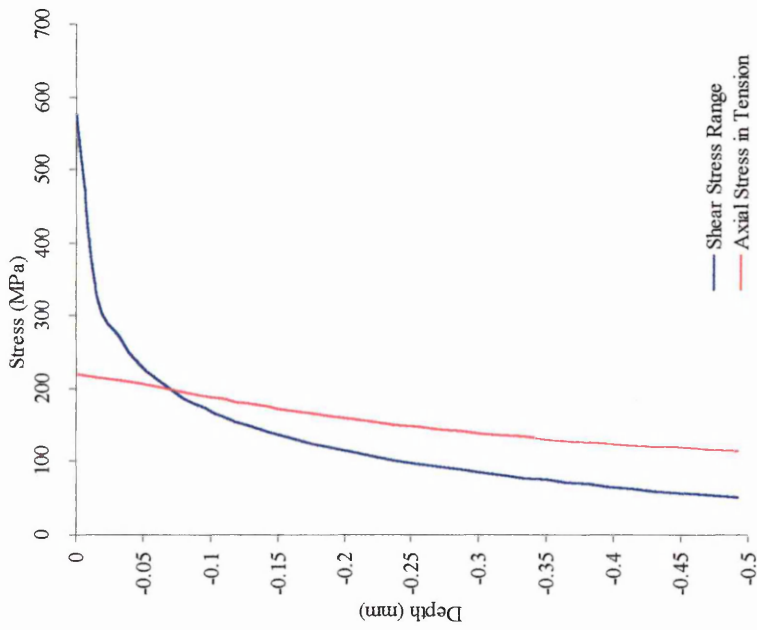
Test 124 Axial and Shear Stresses Through the Depth of the Fretting Region at the Critical Location



Test 122 Axial and Shear Stresses Through the Depth of the Fretting Region at the Critical Location

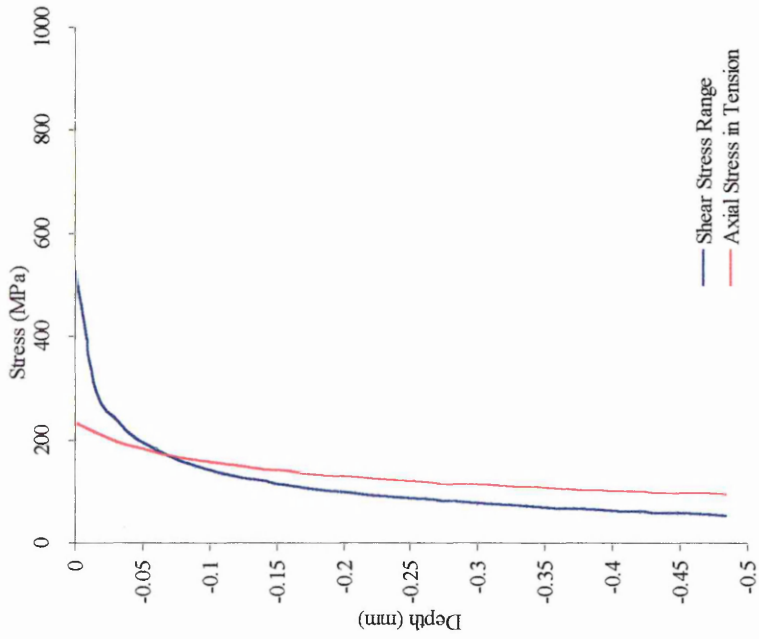


Test 133 Axial and Shear Stresses Through the Depth of the Fretting Region at the Critical Location

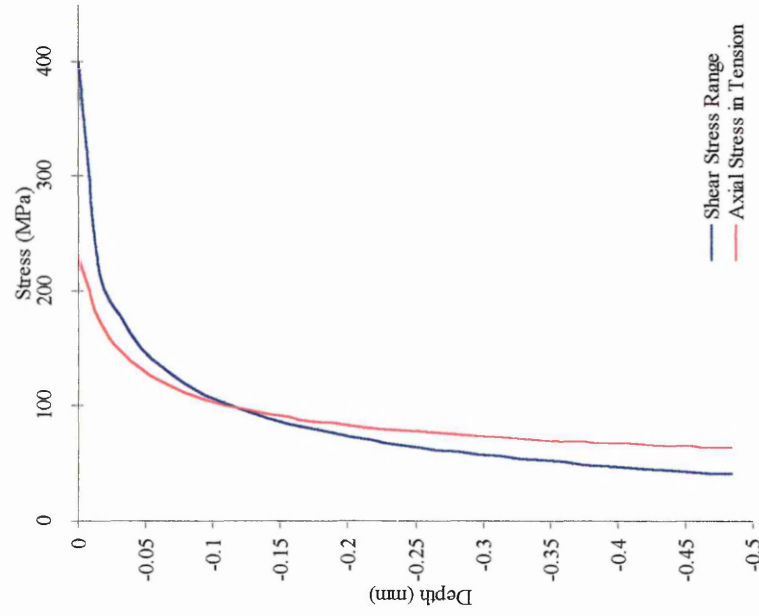


Test 132 Axial and Shear Stresses Through the Depth of the Fretting Region at the Critical Location

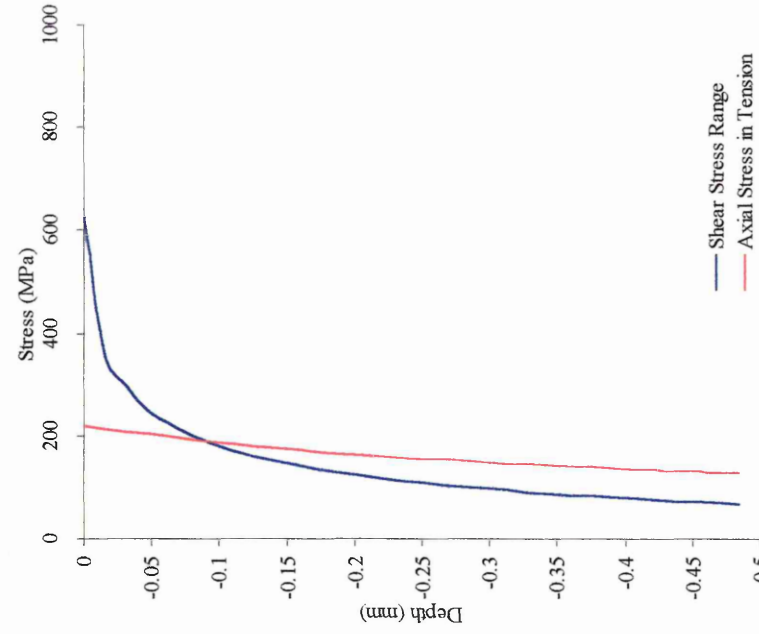
3MM CONTACT PAD SIZE RESULTS (800 TEST SERIES)



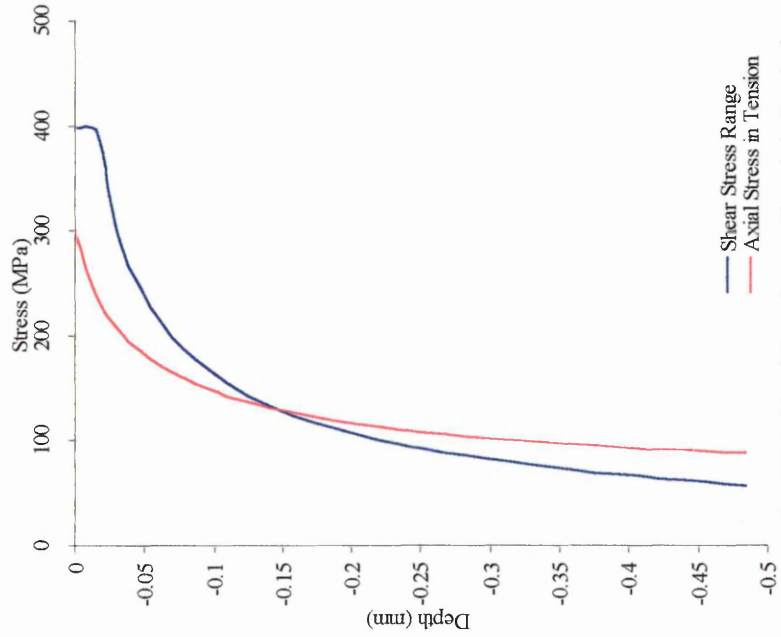
Test 801 Axial and Shear Stresses Through the Depth of the Fretting Region at the Critical Location



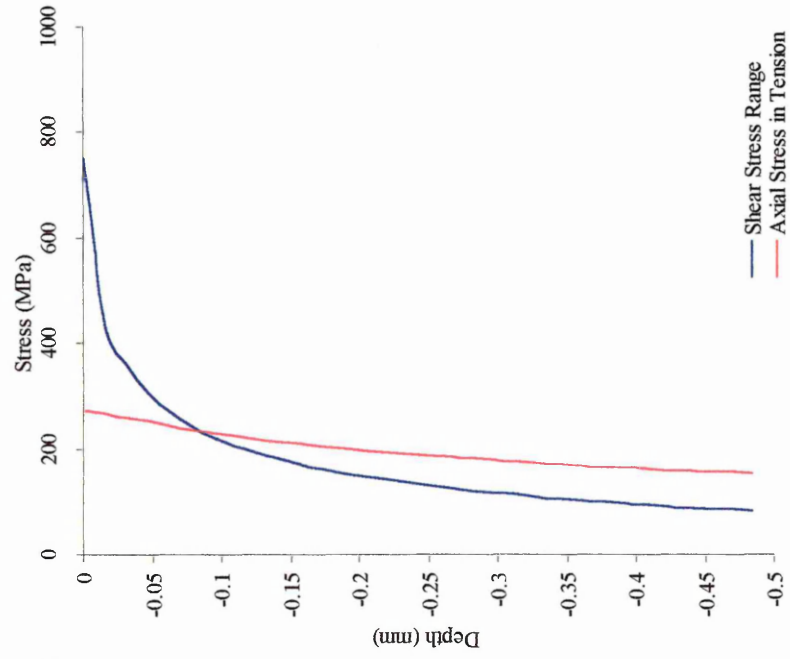
Test 802 Axial and Shear Stresses Through the Depth of the Fretting Region at the Critical Location



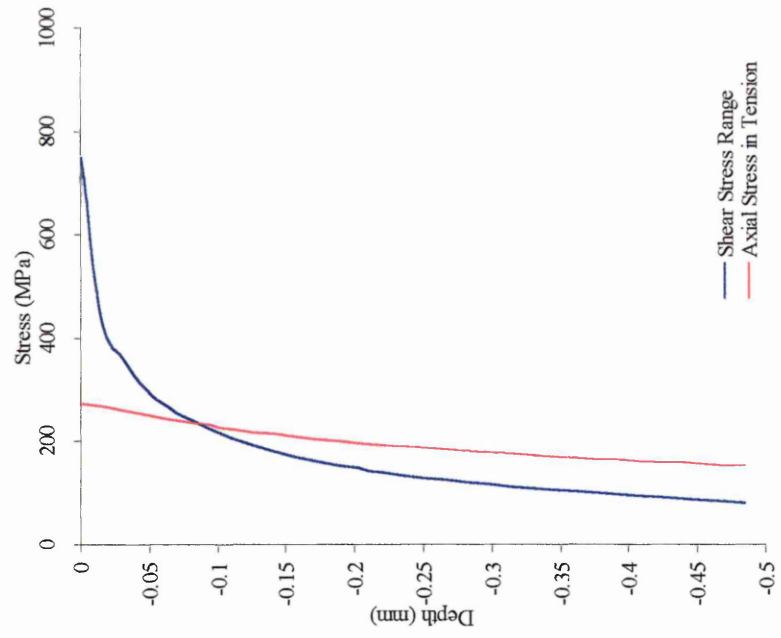
Test 803 Axial and Shear Stresses Through the Depth of the Fretting Region at the Critical Location



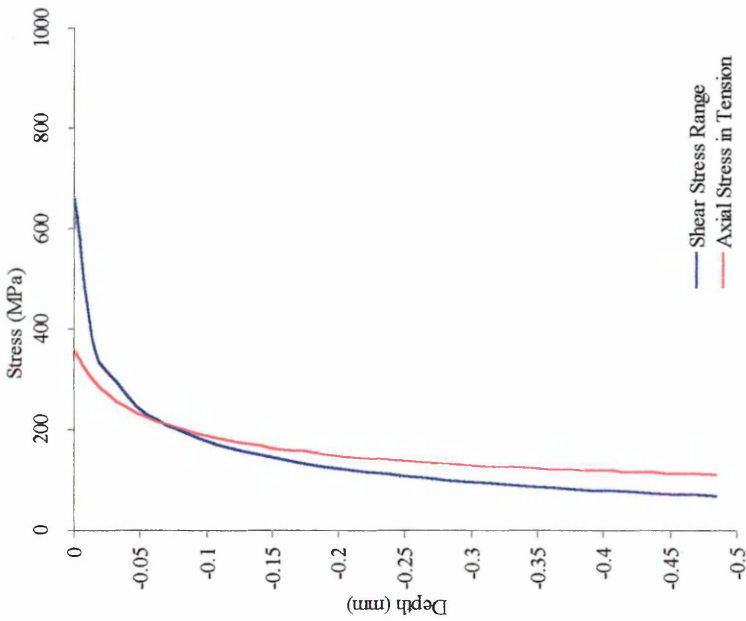
Test 804 Axial and Shear Stresses Through the Depth of the Fretting Region at the Critical Location



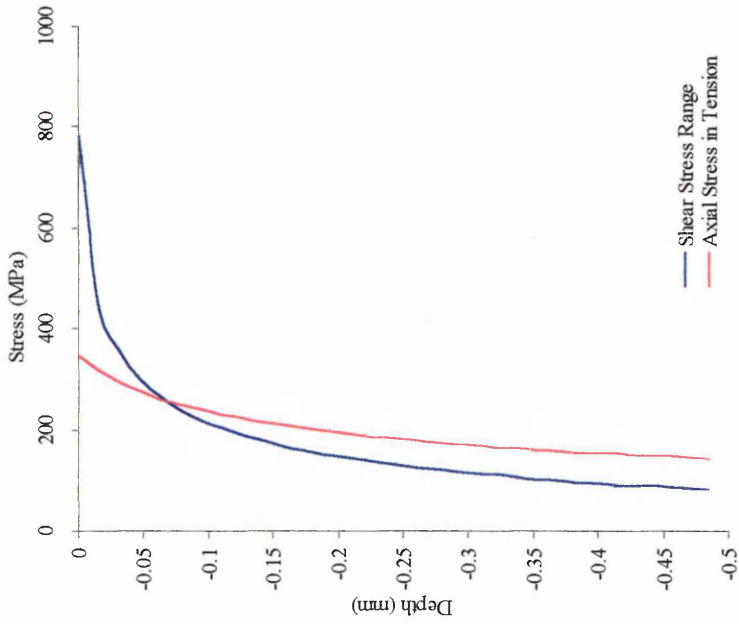
Test 805 Axial and Shear Stresses Through the Depth of the Fretting Region at the Critical Location



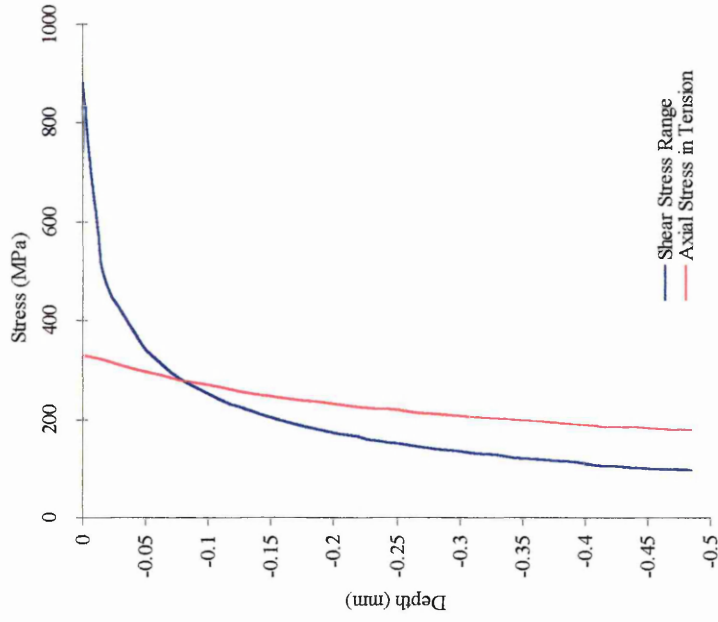
Test 806 Axial and Shear Stresses Through the Depth of the Fretting Region at the Critical Location



Test 807 Axial and Shear Stresses Through the Depth of the Fretting Region at the Critical Location



Test 808 Axial and Shear Stresses Through the Depth of the Fretting Region at the Critical Location



Test 809 Axial and Shear Stresses Through the Depth of the Fretting Region at the Critical Location